組換えアルブミン-プロトヘム錯体から成る酸素輸送合成ヘム蛋白質の創製

課題番号：１６３５００９３

平成１６年度～１８年度 科学研究費補助金
（基盤研究（B））研究成果報告書

平成１９年１１月

研究代表者：小　松　晃　之
早稲田大学・理工学術院・准教授

目　次

１．はじめに

本報告書は、日本学術振興会科学研究費補助金（基盤研究（B）、課題番号：16350093、平成16年度～18年度（3年間））の助成のもとに実施された研究課題「組換えアルブミン–プロトヘム錯体から成る酸素輸送合成ヘム蛋白質の創製」のまとめである。研究代表者は、得られた新知見が単なる学術的な貢献に留まることなく、近い将来 人工酸素運搬体など 広く社会に還元できる革新技術として具現化されることを強く願っている。

ヒト血清アルブミン（HSA、分子量: 66.5 kDa）は血漿蛋白質の約60 wt%を占める単純蛋白質であり、血流中ではコロイド浸透圧調整のほか、各種内因性物質（代謝産物）・外因性物質（薬物など）を非特異的に包接し運搬する役割を担っている。メトヘモグロビンから解離した鉄(III)プロトポルフィリン［ヘミン（hemin）］も体内ではHSAに捕捉され、肝臓へと運ばれる。我々は 2003年、HSA–hemin錯体のX線結晶構造解析に成功し、heminがHSAのSubdomain IB内にチロシン（Tyr）-161との軸配位結合により固定されていることを明らかにした（P. A. Zunszain, et al., *BMC Struct. Biol.* **2003**, *3*, 6）。hemin結合サイトは疎水性アミノ酸で囲まれているが、中心鉄を還元して酸素を吹き込んでも、ミオグロビン（Mb）やヘモグロビン（Hb）のように酸素を可逆的に吸脱着することはできない。これは軸配位子がヒスチジン（His）でないことに起因する。もしHSAのSubdomain IB内に軸塩基として作用するHisが存在すれば、HSA–heme錯体もHbのように酸素を繰り返し結合解離できるのではないか？ この着想が本研究の発端となった。

初年度は、組換えアルブミン（rHSA）の発現とrHSA–heme錯体の調製および酸素結合反応の解析を実施し、ヘム近傍分子環境が酸素結合に与える影響を明らかにした。第二年次は、酸素配位座側に遠位塩基を導入することにより、hemeの酸素親和性を18倍増大させることに成功した。さらに heme を亜鉛プロトポルフィリン（ZnPP）に変換すると、得られたrHSA–ZnPP 錯体が、水の光還元反応系における有効な増感剤として作用することも見出した。第三年次は、ヘムポケット構造の最適化を進め、最終的に ヒト Hb やヒト赤血球と同じ酸素親和性を有するrHSA–heme錯体の創製に成功した。

三年間の期間内に得られた成果は、研究報文１７報、総説・図書３件として公開され、国内外から多くの注目を集めた。英国化学会誌 *Chemistry World* にトピックスとして紹介されたほか、英国 Imperial College London の News Release、日経バイオテク誌、ドイツのSpectrumDirect誌にも取り上げられた。

日本学術振興会科学研究費補助金の支援のもとに、本研究が支障なく推進できたことはもちろん、当初の予測を超える成果が得られたことを大変光栄に思う。ここに厚く御礼申し上げるとともに、本研究展開にあたりお世話になった関係各位に深く謝意を表する。

2．研究組織

研究代表者　：　小松　晃之　（早稲田大学・理工学術院・准教授）
研究分担者　：　黄　　宇彬　（早稲田大学・理工学術院・講師）
研究分担者　：　中川　晶人　（早稲田大学・理工学術院・助手）
（海外研究協力者：　Stephen Curry　（Imperial College London・教授））

3．交付決定額（配分額）

（金額単位：円）

	直接経費	間接経費	合　計
平成１６年度	7,200,000	0	7,200,000
平成１７年度	3,200,000	0	3,200,000
平成１８年度	2,600,000	0	2,600,000
総　　計	13,000,000		13,000,000

4．研究発表

4-1）雑誌論文

1. “Exchange Transfusion with Entirely Synthetic Red-Cell Substitute Albumin-Heme into Rats: Physiological Responses and Blood Biochemical Tests”, Y. Hunag, T. Komatsu, H. Yamamoto, H. Horinouchi, K. Kobayashi, E. Tsuchida, *J. Biomed. Mater. Res.* **2004**, *71A*, 63–69.

2. “Synthesis of Protoheme IX Derivatives with a Covalently Linked Proximal-Base and Their Human Serum Albumin Hybrids as Artificial Hemoprotein”, A. Nakagawa, N. Ohmichi, T. Komatsu, E. Tsuchida, *Org. Biomol. Chem.* **2004**, *2*, 3108–3112.

3. “Dioxygenation of Human Serum Albumin Having a Prosthetic Heme Group in a Tailor-Made Heme Pocket”, T. Komatsu, N. Ohmichi, P. A. Zunszain, S. Curry, E. Tsuchida, *J. Am. Chem. Soc.* **2004**, *126*, 14304–14305.

4. “Physicochemical Characterization of Cross-Linked Human Serum Albumin Dimer and Its Synthetic Heme Hybrid as an Oxygen Carrier”, T. Komatsu, Y. Oguro, Y. Teramura, S. Takeoka, J. Okai, M. Anraku, M. Otagiri, E. Tsuchida, *Biochim. Biophys. Acta* **2004**, *1675*, 21–31.

5. “Exchange Transfusion with Synthetic Oxygen-Carrying Plasma Protein “Albumin-Heme” into an Acute Anemia Rat Model after Seventy-Percent Hemodilution”, T. Komatsu, H. Yamamoto, Y. Huang, H. Horinouchi, K. Kobayashi, E. Tsuchida, *J. Biomed. Mater. Res.* **2004**, *71A*, 644–651.

6. "Human Serum Albumin Bearing Covalently Attached Iron(II) Porphyrins as O_2-Binding Sites", R.-M. Wang, T. Komatsu, A. Nakagawa, E. Tsuchida, *Bioconjugate Chem.* **2005**, *16*, 23–26.

7. "Heat-Resistant Oxygen-Carrying Hemoproteins Consist of Recombinant Xylanases and Synthetic Iron(II) Porphyrin", T. Komatsu, S. Ishihara, E. Tsuchida, H. Nishide, C. Inokuma, S. Nakamura, *Biomacromolecules* **2005**, *6*, 1489–1494.

8. "O_2 and CO Binding Properties of Artificial Hemoproteins Formed by Complexing Iron Protoporphyrin IX with Human Serum Albumin Mutants", T. Komatsu, N. Ohmichi, A. Nakagawa, P. A. Zunszain, S. Curry, E. Tsuchida, *J. Am. Chem. Soc.* **2005**, *127*, 15933–15942.

9. "Albumin Clusters: Structurally Defined Protein Tetramer and Oxygen Carrier Including Thirty-Two Iron(II) Porphyrins", T. Komatsu, Y. Oguro, A. Nakagawa, E. Tsuchida, *Biomacromolecules* **2005**, *6*, 3397–3403.

10. "Human Serum Albumin Hybrid Incorporating Tailed Porphyrinatoiron(II) in the α,α,α,β-Conformer as an O_2-Binding Site", A. Nakagawa, T. Komatsu, M. Iizuka, E. Tsuchida, *Bioconjugate Chem.* **2006**, *17*, 146–151.

11. "Poly(ethylene glycol)-Conjugated Human Serum Albumin Including Iron Porphyrins: Surface Modification Improves the O_2-Transporting Ability", Y. Huang, T. Komatsu, R.-M. Wang, A. Nakagawa, E. Tsuchida, *Bioconjugate Chem.* **2006**, *17*, 393–398.

12. "PEGylated Albumin-Heme as an Oxygen-Carrying Plasma Expander: Exchange Transfusion into Acute Anemia Rat Model", Y. Huang, T. Komatsu, H. Yamamoto, H. Horinouchi, K. Kobayashi, E. Tsuchida, *Biomaterials* **2006** *27*, 4477–4483.

13. "Photosensitized Reduction of Water to Hydrogen using Human Serum Albumin Complexed with Zinc Protoporphyrin IX", T. Komatsu, R.-M. Wang, P. A. Zunszain, S. Curry, E. Tsuchida, *J. Am. Chem. Soc.* **2006**, *128*, 16297–16301.

14. "*meso*-Tetrakis(*α,α,α,α-o*-amidophenyl)porphinatoiron(II) Bearing a Proximal Histidyl Group at the β-pyrrolic Position via an Acyl Bond: Synthesis and O_2 Coordination in Aqueous Media", A. Nakagawa, T. Komatsu, E. Tsuchida, *Chem. Lett.* **2007**, *36*. 640–641.

15. "Induced Long-Range Attractive Potentials of Human Serum Albumin by Ligand Binding", T. Sato, T. Komatsu, A. Nakagawa, E. Tsuchida, *Phys. Rev. Lett.* **2007**, *98*, 208101-1–4.

16. "O_2-Binding Albumin Thin Films: Solid Membranes of Poly(ethylene glycol)-Conjugated Human Serum Albumin Incorporating Iron Porphyrin", A. Nakagawa, T. Komatsu, Y. Huang, G. Lu, E. Tsuchida, *Bioconjugate Chem.* **2007**, *18*, 1673–1677.

17. "Genetic Engineering of the Heme Pocket in Human Serum Albumin: Modulation of O_2 Binding of Iron Protoporphyrin IX by Variation of Distal Amino Acids", T. Komatsu, A. Nakagawa, P. A. Zunszain, S. Curry, E. Tsuchida, *J. Am. Chem. Soc.* **2007**, *129*, 11286–11295.

4-2) 総説・図書

1. "Oxygen Infusions (Hemoglobin-Vesicles and Albumin-Hemes) Based on Nano-Molecular Sciences", E. Tsuchida, H. Sakai, T. Komatsu, S. Takeoka, Y. Huang, K. Sou, A. Nakagawa, Y. Teramura, K. Kobayashi, *Polym. Adv. Technol.* **2005**, *16*, 73–83.

2. "Oxygen-Carrying Plasma Hemoprotein Including Synthetic Heme", T. Komatsu, E. Tsuchida, *Artificial Oxygen Carrier. Its Front Line*, Ed. K. Kobayashi, E. Tsuchida, H. Horinouchi, p. 193–204, Springer-Verlag (Tokyo, 2005).

3. "Albumin-Heme: A Synthetic Heme-Based Oxygen Carrier", T. Komatsu, Y. Huang, H. Yamamoto, H. Horinouchi, K. Kobayashi, E. Tsuchida, *Blood Substitutes,* Ed. R. Winslow, p. 532–539 (Chapter 46), Elsevier (London, 2006).

4-3) 研究紹介記事

1. "Albumin Engineered for Artificial Blood" *Chemistry World* (Royal Society), Dec. **2005**, p. 18.

2. "Genetically engineered blood protein can be used to produce hydrogen gas from water" Imperial College London News Release, 1st December, **2006**.

3. "Grüner Treibstoff –blutrot" *Spectrum Direct* (Germany), 19th Dec. **2006**.

4. "血液由来のヘモグロビンを使わない次世代人工酸素運搬体を提案"、日経バイオテク、**2007**, *7-2*, 25.

4-4) 学会発表

(招待講演)

1. 小松晃之, 酸素輸送アルブミン:完全合成系人工酸素運搬体"アルブミン-ヘム"の創製と利用(招待講演), 第 32 回日本集中治療医学会学術集会, 東京, 2005 年 2 月

2. 小松晃之,「組換えアルブミン-ヘム」:酸素輸送ヘム蛋白質の創製と生体利用(依頼講演), 2005-01 高分子錯体研究会, 東京, 2005 年 5 月

3. Tsuchida, E.; Komatsu, T. "PEG Conjugated Albumin-Heme as a Blood Substitute and Its Medical Applications", 4th International Conference on Porphyrins and Phthalocyanines, Rome (Italy), 2–7 July 2006. (Invited Lecture)

4. 小松晃之、土田英俊, アルブミンを用いた全合成系人工酸素運搬体の創製(依頼講演), 第 14 回日本血液代替物学会年次大会, 東京, 2007 年 6 月

5. T. Komatsu, A. Nakagawa, E. Tsuchida, "Genetically Engineered Hemepocket in Human Serum Albumin: Modulation of O_2 Binding to Iron Protoporphyrin IX", 12th International Symposium on MacroMolecular Complexes, Fukuoka, 27–31 August 2007. (Invited Lecture)

(国内学会)

1. 大道直美、中川晶人、小松晃之、西出宏之、Stephen Curry、土田英俊／アルブミン-ヘム錯体の構造と物理化学的特徴／第 53 回高分子学会年次大会、神戸、2004 年 5 月

2. 小黒有希子、中川晶人、小松晃之、武岡真司、土田英俊／アルブミン-プロトヘム複合体の酸素、一酸化炭素結合反応／第 53 回高分子学会年次大会、神戸、2004 年 5 月

3. 小松晃之、土田英俊／アルブミン-ヘムの安全性試験に関する検討／第 11 回日本血液代替物学会、札幌、2004 年 7 月

4. 中川晶人、小松晃之、土田英俊／$\alpha^3\beta$ 置換ヘム誘導体とアルブミン-ヘム複合体の酸素結合／第 11 回日本血液代替物学会、札幌、2004 年 7 月

5. 大道直美、小松晃之、西出宏之、土田英俊／ヘムポケットを有する組換えアルブミンに結合させたヘム錯体の酸素結合／第 53 回高分子討論会、札幌、2004 年 9 月

6. 王　栄民、小松晃之、土田英俊／酸素結合サイトとして鉄(II)ポルフィリンを共有結合したヒト血清アルブミン／第 53 回高分子討論会、札幌、2004 年 9 月

7. 中川晶人、小松晃之、小黒有希子、土田英俊／$\alpha^3\beta$ 置換ヘム誘導体を包接したアルブミン－ヘム複合体の合成と酸素結合／第 53 回高分子討論会、札幌、2004 年 9 月

8. 小松晃之、大道直美、土田英俊／ヘムポケットを有する組換えアルブミンの合成とヘム錯体の酸素結合／第 53 回高分子討論会、札幌、2004 年 9 月

9. 飯塚　誠、中川晶人、小松晃之、武岡真司、土田英俊／$\alpha^3\beta$ 置換テトラフェニルポルフィリン鉄錯体の合成と酸素結合に及ぼす置換基構造の効果／第 85 日本化学会春季年会、横浜、2005 年 3 月

10. 黄　宇彬、中川晶人、小松晃之、土田英俊／ポリオキシエチレン修飾アルブミン-ヘムの構造・物性と酸素結合能／第 85 日本化学会春季年会、横浜、2005 年 3 月

11. 中川晶人、飯塚　誠、小松晃之、土田英俊／$\alpha^3\beta$ 置換ヘム誘導体を包接したアルブミン複合体の酸素結合能／第 54 回高分子学会年次大会、横浜、2005 年 5 月

12. 黄　宇彬、中川晶人、小松晃之、土田英俊／アルブミン-ヘムの表面修飾と物性・酸素結合の相関／第 54 回高分子学会年次大会、横浜、2005 年 5 月

13. 小松晃之、土田英俊／部位特異的アミノ酸置換を利用した新しいアルブミン-ヘムの合成と酸素結合／第 12 回日本血液代替物学会、東京、2005 年 6 月

14. 浦田由紀乃、安楽　誠、小松晃之、土田英俊／組換えアルブミン二量体の体内動態特性について／第 12 回日本血液代替物学会、東京、2005 年 6 月

15. 黄　宇彬、小松晃之、中川晶人、王　栄民、土田英俊／ポリエチレングリコール鎖で表面修飾したアルブミン-ヘムの合成とその構造および溶液物性／第 12 回日本血液代替物学会、東京、2005 年 6 月

16. 中川晶人、王　永民、黄　宇彬、小松晃之、土田英俊／ポリエチレングリコール鎖で表面修飾したアルブミン-ヘムの酸素結合／第 12 回日本血液代替物学会、東京、2005 年 6 月

17. 王　栄民、小松晃之、土田英俊／Synthesis and O_2-Binding Properties of Albumin-Heme Covalently Linked GluFePs as O_2-Coordination Site／第 12 回日本血液代替物学会、東京、2005 年 6 月

18. 飯塚　誠、武岡真司、中川晶人、小松晃之、土田英俊／新規な酸素結合サイト $\alpha^3\beta$ 型ヘムの合成とアルブミン-ヘムの酸素結合／第 12 回日本血液代替物学会、東京、2005 年 6 月

19. 佐藤高彰、中川晶人、小松晃之、土田英俊／アルブミン-ヘムの静的構造とダイナミクス／第 12 回日本血液代替物学会、東京、2005 年 6 月

20. 中川晶人、小松晃之、土田英俊／遺伝子組換えアルブミン-プロトヘム複合体の酸素結合能／第 54 回高分子討論会、山形、2005 年 9 月

21. 飯塚　誠、中川晶人、小松晃之、武岡真司、土田英俊／アルブミン-ヘム複合体の酸素結合に及ぼすポルフィリン構造の効果／第 86 日本化学会春季年会、千葉、2006 年 3 月

22. 黄　宇彬、王　栄民、小松晃之、中川晶人、土田英俊／ポリエチレングリコール鎖で表面修飾したアルブミン-ヘムの特徴と酸素結合／第 86 日本化学会春季年会、千葉、2006 年 3 月

23. 小松晃之、中川晶人、土田英俊／組換えアルブミン-プロトヘムにおけるヘムポケット構造と酸素結合能の相関／第 55 回高分子学会年次大会、名古屋、2006 年 5 月

24. 小松晃之、中川晶人、土田英俊／遺伝子組換えアルブミン-プロトヘム錯体からなる新しい酸素輸送ヘム蛋白質の創製／第 13 回日本血液代替物学会、東京、2006 年 8 月

25. 中川晶人、黄　宇彬、王　栄民、小松晃之、土田英俊／ポリ(エチレングリコール)修飾アルブミン-ヘムの酸素結合能と新しい特徴／第 13 回日本血液代替物学会、東京、2006 年 8 月

26. 中川晶人、飯塚　誠、小松晃之、武岡真司、土田英俊／ヒスチジン誘導体結合ヘムを包接したアルブミン複合体の酸素結合反応／第 55 回高分子討論会、富山、2006 年 9 月

27. 中川晶人、小松晃之、土田英俊／組換えヒト血清アルブミン-プロトヘム複合体のヘムポケット構造と酸素結合能／第 56 回高分子学会年次大会、京都、2007 年 5 月

28. 中川晶人、小松晃之、土田英俊／組換えヒト血清アルブミン-プロトヘム錯体におけるヘムポケット構造と酸素結合能の相関／第 14 回日本血液代替物学会年次大会、東京、2007 年 6 月

29. 中川晶人、小松晃之、盧 剛、土田英俊／PEG 修飾アルブミン-ヘム薄膜の酸素結合能／第 56 回高分子討論会、名古屋、2007 年 9 月

（国際会議）

1. T. Komatsu, E. Tsuchida, "Human Serum Albumin Having a Prosthetic Heme Group in a Tailor-Made Heme Pocket", 10th International Symposium on Blood Substitutes, Providence (USA), 12–15 June 2005.

2. A. Nakagawa, T. Komatsu, E. Tsuchida, "O_2-Binding Properties of Albumin-Heme Hybrid Incorporating $\alpha^3\beta$-Substituted Heme Derivative", 10th International Symposium on Blood Substitutes, Providence (USA), 12–15 June 2005.

3. Y. Huang, T. Komatsu, R.-M. Wang, E. Tsuchida, "Polyoxyethylene-Modified Albumin-Heme Hybrid: Synthesis, Property, Oxygen-Binding Ability", 10th International Symposium on Blood Substitutes, Providence (USA), 12–15 June 2005.

4. R.-M. Wang, T. Komatsu, E. Tsuchida, "Albumin-Heme Conjugate Covalently Attached Heme Sites", 10th International Symposium on Blood Substitutes, Providence (USA), 12–15 June 2005.

5. T. Komatsu, E. Tsuchida, "Dioxygenation of Human Serum Albumin Having a Prosthetic Heme Group in a Tailor-Made Heme Pocket", IUPAC 11th International Symposium on Macromolecule-Metal Complexes, Pisa (Italy), 10–13 Sept. 2005.

6. T. Komatsu, E. Tsuchida, "O_2 and CO Binding Ability of Human Serum Albumin Having a Prosthetic Heme Group", 8th International Symposium on Polymers for Advanced Technologies, Budapest (Hungary), 12–16 Sept. 2005.

7. T. Komatsu, A. Nakagawa, E. Tsuchida, "Oxygen Binding Properties of Artificial Hemoproteins formed by Complexing Iron Protoporphyrin IX with Human Serum Albumin", 4th International Conference on Porphyrins and Phthalocyanines, Rome (Italy), 2–7 July 2006.

8. A. Nakagawa, T. Komatsu, E. Tsuchida, "Human Serum Albumin Hybrid Incorporating Tailed Porphyrinatoiron(II) in the $\alpha,\alpha,\alpha,\beta$-Conformer as an O_2-Binding Site", 4th International Conference on Porphyrins and Phthalocyanines, Rome (Italy), 2–7 July 2006.

9. A. Nakagawa, T. Komatsu, E. Tsuchida, "Synthesis of Tetraphenylporphinatoiron(II) Derivative Bearing a Proximal Histidyl Group via Acyl Bond and Its O_2-Binding Properties in Aqueous Media", 12th International Symposium on MacroMolecular Complexes, Fukuoka, 27–31 August 2007.

10. T. Komatsu, A. Nakagawa, E. Tsuchida, "Genetic Engineering of the Heme Pocket in Human Serum Albumin: Modulation of O_2 Binding of Iron Protoporphyrin IX", 11th International Symposium on Blood Substitutes, Beijing, 18–21 October 2007.

11. A. Nakagawa, T. Komatsu, G. Lu, E. Tsuchida, "O_2-Binding Ability of Membrane of PEG-Modified Albumin-Heme", 11th International Symposium on Blood Substitutes, Beijing, 18–21 October 2007.

12. Y. Huang, T. Komatsu, E. Tsuchida, "Polyoxyethylene-Modified Albumin-Heme Hybrid –Synthesis, Property and Oxygen-Binding Ability", 11th International Symposium on Blood Substitutes, Beijing, 18–21 October 2007.

13. T. Komatsu, A. Nakagawa, E. Tsuchida, "Genetic Engineering of the Heme Pocket in Human Serum Albumin: Modulation of O_2 Binding of Iron Protoporphyrin IX", 9th International Symposium on Polymers for Advanced Technologies, Shanghai, 22–25 October 2007.

5）研究成果

5-1）研究目的

ヒト血清アルブミンのヘムポケット内部にヒスチジン（His）を導入した組換えアルブミン（rHSA）を合成し、鉄プロトポルフィリンIX［プロトヘム：heme］を軸配位により固定、従来に類例のない酸素輸送合成ヘム蛋白質［組換えアルブミン–プロトヘム（rHSA–heme）錯体］を創製することを目的とする。酸素配位平衡を制御できる人工ヘムポケットの分子環境構造を明確にしたい。

具体的には、①近位塩基の役割を果たすHisを導入したrHSAを合成、hemeを配位結合させることにより新しい合成ヘム蛋白質を構築する。②得られたrHSA–heme錯体の酸素結合定数（酸素親和性）、酸素結合解離速度定数をパラメーターとして酸素結合能を評価、ヘモグロビン（Hb）やミオグロビン（Mb）と比較する。③さらに酸素配位座近傍に位置するアミノ酸配列に変異を加え、酸素錯体とヘムポケット構造の相関を解明、安定な酸素錯体を形成できるヘム近傍分子環境を決定する。

5-2）近位塩基を導入した組換えアルブミンの合成

まず Subdomain IB 内のヒスチジン（His）導入位置について検討した。第一候補となるのは軸配位しているチロシン (Tyr) -161 であるが、これを His に変換した場合、中心鉄－His 間

の距離が 4Å～となり、Mb の 2.18 Å に比べかなり長くなってしまう。最適位置をシミュレーションにより模索し、最終的にポルフィリン環直下にあるイソロイシン (Ile) -142 を選定、そこへ His を導入することとした（**Fig. 1**）。一方、Tyr-161 は疎水性のロイシン（Leu）またはフェニルアラニン（Phe）に変換、組換えアルブミン二重変異体［rHSA(I142H/Y161L)（以下、rHSA(HL)と表記）、rHSA(I142H/Y161F)（以下 rHSA(HF)と表記）］を設計した。

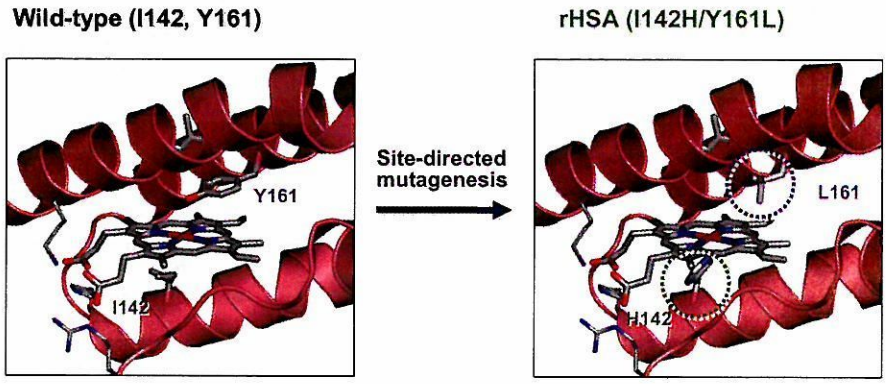

Fig. 1 Structural models of the effect of site-directed mutagenesis in subdomain IB of HSA to construct a tailor-made heme pocket, which allows O_2 binding to the heme group.

プラスミド（PHIL-D2 HSA）の His-142 および Tyr-161 相当箇所にに QuikChange を用いて変異を挿入し、シークエンス解析後、ピキア酵母（GS115）内へ導入した。rHSA は BMGY、BMMY 溶液中、30°C で培養した。精製は、透析、Blue Sepharose カラム処理、FPLC により行い、所望の rHSA を単離した。得られた rHSA は SDS-PAGE により単一バンドであることを確認した。

5-3）組換えアルブミン－プロトヘム錯体の軸配位構造と酸素配位

rHSA に hemin を 1:1 のモル比で包接し、茶褐色の rHSA–hemin 水溶液（リン酸緩衝液（pH 7.0、50 mM））を調製した。得られた rHSA(HL)–hemin 錯体水溶液の磁気円偏光二色性（MCD）スペクトルを **Fig. 2** に示す。スペクトルパターンが酸化型 Mb と非常に良く似ていることから、rHSA(HL)–hemin 錯体の場合も中心鉄には His が軸配位し、第 6 配位座には水が弱く配位しているものと推測される。

rHSA(HL)–hemin 錯体水溶液の可視吸収スペクトルを **Fig. 3** に示す。Ar 雰囲気下で中心鉄を鉄 (II) に還元すると、最大吸収波長が 426, 559 nm に現れ、これは heme が鉄 (II) 5 配位高スピン錯体を形成していることを示す。そこへ酸素を通気すると、スペクトルパターンは速やかにシフトし、λ_{max} がオキシ Hb やオキシ Mb の値と一致したことから、酸素錯体が形成されていることがわかった。さらに一酸化炭素を吹き込むと、きわめて安定なカルボニル体

が得られた。同じように、rHSA(HF)–heme も室温で酸素、一酸化炭素錯体を形成した。これは、プロトヘムが水中・室温で酸素錯体を生成した初めての例となった。

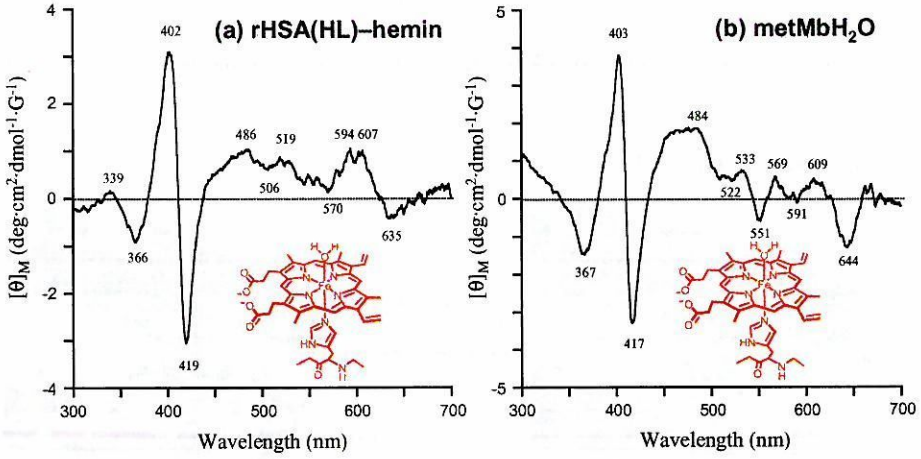

Fig. 2 MCD spectra of (a) rHSA(HL)–hemin and (b) metMb in phosphate buffered solution (pH 7.0, 50 mM) at 25°C. Magnetic field = 1.5T.

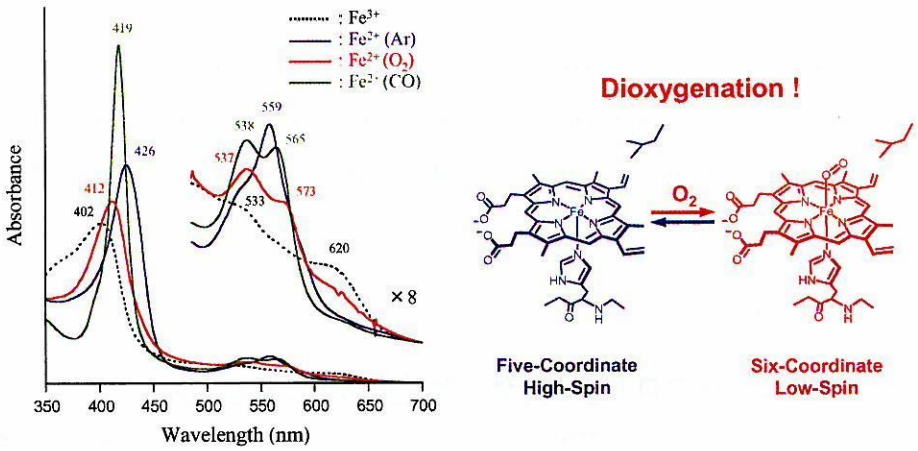

Fig. 3 UV-vis. absorption spectral changes of rHSA(HL)–heme in phosphate buffered solution (pH 7.0, 50 mM).

5-4）組換えアルブミン－プロトヘム錯体の酸素結合能

レーザーフラッシュホトリシス法を用いて酸素結合パラメーターを決定した。酸素親和性の指標である $P_{1/2}$ はヘム全体の 50%に酸素が結合した時の酸素分圧である。また、酸素結合速度定数（k_{on}）、解離速度定数（k_{off}）も決定した。

rHSA(HL)–heme の $P_{1/2}$ は 18 Torr であり、Hb、Mb、赤血球に比べ高い（**Table 1**）（酸素親和性は低い）。二つの $P_{1/2}$ 値は、ヘムの配行が二種類（Species I と II）存在することを示

唆している（詳細は発表論文 *J. Am. Chem. Soc.* **2005**, *127*, 15933 を参照）。速度論的に見ると、rHSA(HL)–heme の低い酸素親和性は、高い解離速度定数（k_{off}）に起因することがわかる。アルブミンの中では、ヘムを取り巻く分子環境が非常に疎水的であるため k_{off} が大きく、酸素親和性が低くなるものと推察される。

Table 1 O_2-Binding parameters of rHSA(mutant)-heme in phosphate buffered solution (pH 7.0, 50 mM) at 22°C.[a]

Hemoprotein	$P_{1/2}^{O_2}$ (Torr) (I)	(II)	$k_{on}^{O_2}$ ($\mu M^{-1}s^{-1}$)	$k_{off}^{O_2}$ (ms^{-1}) (I)	(II)
rHSA(HL)–heme	**18**	134	7.5	**0.22**	1.70
rHSA(HL/L185N)–heme	**1**	14	14	**0.02**	0.29
rHSA(HL/R186L)–heme	**10**	209	25	**0.41**	8.59
rHSA(HL/R186F)–heme	**9**	203	21	**0.29**	7.01
Hbα (R-state)[b]	0.24		33[c]	0.013[d]	
Mb[e]	0.51		14	0.012	
RBC	8				

[a] Number I or II indicates species I or II. [b] Humant Hb α-subunit. 20 °C; [c] At 21.5°C; Q. H. Gibson et al., *J. Biol. Chem.* **1970**, *245*, 3285. [d] At 20°C. J. S. Olson et al., *J. Biol. Chem.* **1971**, *246*, 5919. [e] Sperm whale Mb. At 20°C. R. Rohlfs et al., *J. Biol. Chem.* **1990**, *265*, 3168.

5-5）近位・遠位塩基を有する三重変異体の酸素結合能

実際に rHSA–heme 錯体を人工酸素運搬体として利用するためには、酸素親和性を Hb や赤血球の値に近づけなければならない。そこで、第三の変異を導入することにより、酸素親和性を上昇させる検討を行った。Mb のヘムポケット内には、酸素配位座側に His-64 が遠位塩基として存在し、酸素親和性の増大に大きく寄与している（**Fig. 4**）。我々は、アルブミンの場合も酸素配位座側の適当な位置に遠位塩基を挿入すれば、酸素親和性が増大するはずであると考え、配位酸素直上の Leu-185 を選定し、遠位塩基を導入した。

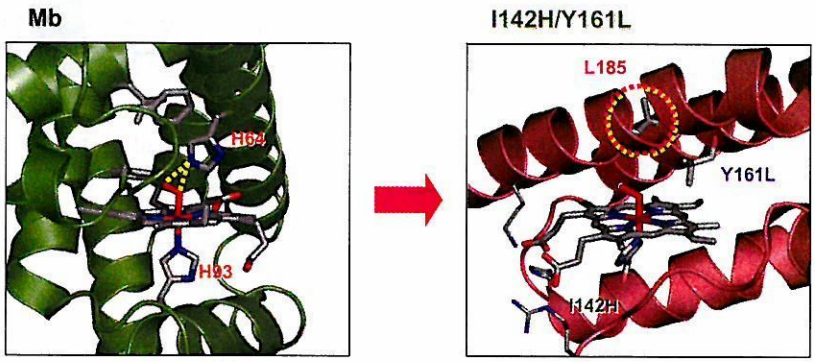

Fig. 4 Introduction of distal-base into the heme pocket of HSA.

具体的には、Leu-185 をアスパラギン（Asn）、グルタミン（Gln）、そして His に変換した（**Fig. 5**）。二重変異体にさらに一つ置換が加わることにより、三重変異体となる。

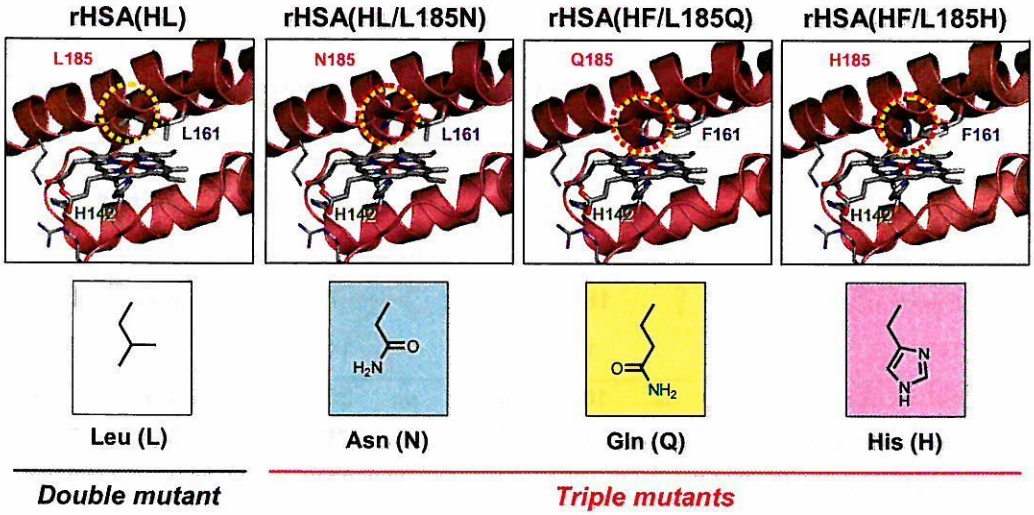

Fig. 5 The rHSA–heme triple mutants having a distal base at the Leu-185 position.

185 位置に Asn が入った三重変異体－ヘム［rHSA(HL/L185N)–heme］錯体水溶液の可視吸収スペクトルを **Fig. 6** に示す。二重変異体 rHSA(HL)–heme 同様、Ar 雰囲気下で heme は鉄(II) 5 配位高スピン錯体を形成し、そこへ酸素を通気すると酸素錯体、一酸化炭素を通気すると安定なカルボニル体が得られた。一方、メチレン鎖の一つ長い Gln や His を導入した三重変異体は、Ar 雰囲気下で弱い鉄 (II) 6 配位低スピン錯体を形成し、酸素を吹き込んでも酸素錯体は得られなかった。

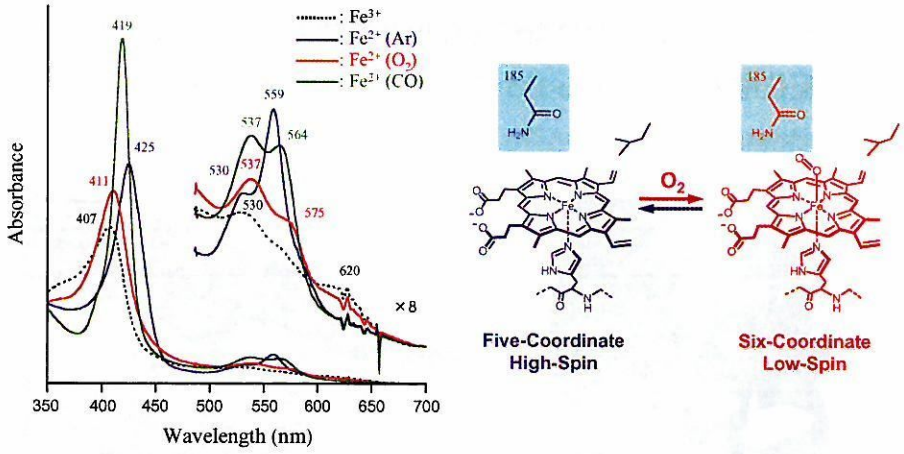

Fig. 6 UV-vis. absorption spectral changes of rHSA(HL/L185N)–heme in phosphate buffered solution (pH 7.0, 50 mM).

そこで、rHSA(HL/L185N)–heme と rHSA(HL)–heme の酸素結合パラメーターを比較した。rHSA(HL/L185N)–heme の $P_{1/2}$ は 1 Torr で、導入前の二重変異体に比べ 酸素親和性は 18 倍上昇した（**Table 1**）。Asn の導入により、ヘムポケットの極性が増大し k_{off} が減少、酸素親和性が上昇したものと考えられる。高い酸素親和性を有するこの rHSA(HL/L185N)–heme 錯体は、Hb のよいモデルといえる。

5-6）ヘムポケット構造の最適化

生体内で肺から末梢へと効率よく酸素を輸送するためには、酸素親和性を赤血球の値（8 Torr）と同等にしなければならない。我々は、185 位置に隣接するアルギニン (Arg) -186 もきわめて重要なアミノ酸であることを見出した。186 位置はヘムポケットの入口にあたり、そこへ疎水性の Leu や Phe を導入すると（**Fig. 7**）、酸素親和性が赤血球と同じ 9～10Torr に調節できることを明らかにした（**Table 1**）。

その他、182、186 位置に遠位塩基を導入したモデルなど 計 9 種類の rHSA–heme 三重変異体を合成し、詳細な物理化学的解析から ヘムポケット構造と酸素結合能について系統的な知見を得た（詳細は発表論文 *J. Am. Chem. Soc.* **129**, 11286 参照）。

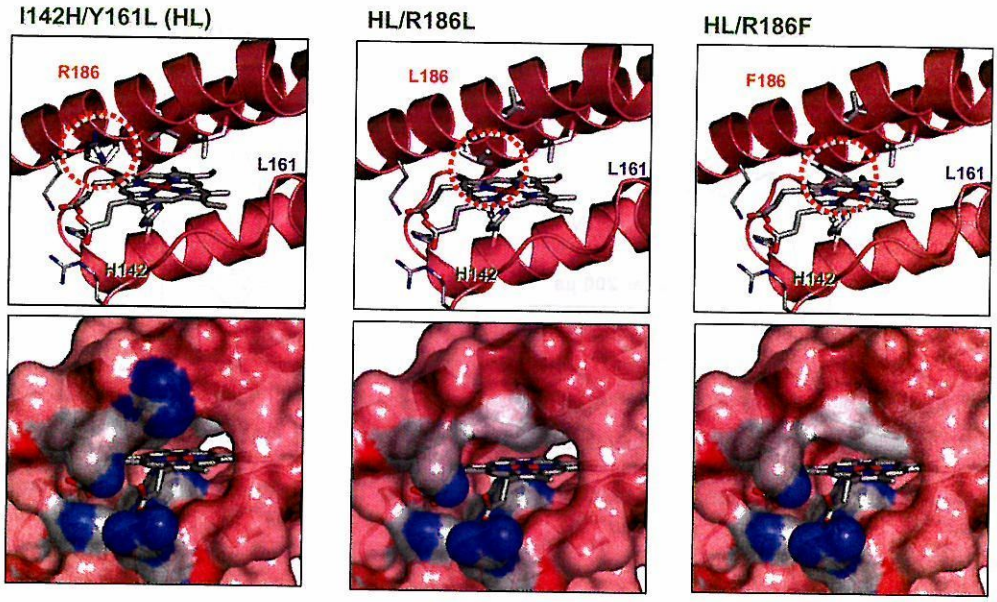

Fig. 7 The key amino acid Arg-186 and its mutants R186L and R186F.

以上の結果より、我々は 本来補欠分子族すらもたない単純蛋白質のアルブミンに酸素結合能を付与することに成功したばかりでなく、ヘムポケット構造の微調整により酸素親和性の制御が可能となることを示した。現在、臨床利用可能な人工酸素運搬体の開発を目指し、さらなる研究を継続している。

5-7）アルブミン－亜鉛プロトポルフィリン錯体（水素発生反応の光増感剤）

水の光還元による水素発生反応系としては、Pt／メチルビオロゲン（MV^{2+}）／Zn (II) テトラメチルピリジルポルフィリン（$ZnTMPyP^{4+}$）／EDTA 系が知られている。我々は heme の亜鉛置換体である Zn (II) プロトポルフィリン IX（ZnPP）を rHSA に包接させた rHSA–ZnPP 錯体を調製し、その光物理化学的特徴を明らかにするとともに、水の光還元反応における光増感作用について検討した。ZnPP は heme と同様に HSA の Subdomain IB 内に位置し、中心亜鉛には Tyr-161 が軸配位している。rHSA–ZnPP 水溶液に窒素雰囲気下でレーザー照射すると、ZnPP の励起三重項吸収が観測された（**Fig. 8**）。光励起三重項寿命（τ_T）は 11 ms で、$ZnTMPyP^{4+}$より長い。そこへ MV^{2+}を添加するとτ_Tが減少するとともに、メチルビオロゲンカチオンラジカル（$MV^{+\cdot}$）にもとづく吸収が現れたことから、rHSA–^{3}ZnPP*から MV^{2+}への電子移動が示唆された。Stern-Volmer プロットより算出した電子移動速度定数（k_q）は $1.4 \times 10^7\ M^{-1}s^{-1}$であった。

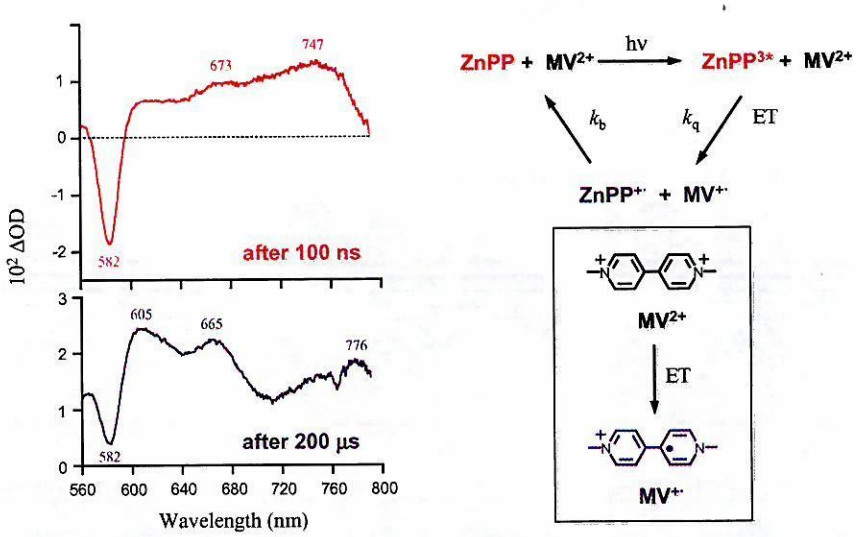

Fig. 8 Transient absorption spectrum of HSA(wt)–ZnPP (10 mM) with MV^{2+} (1 mM) in phosphate buffered solution (pH 7.0, 10 mM) after the laser flash excitation (λ=532 nm) at 25°C.

続いて、白金コロイド、犠牲試薬としてのトリエタノールアミンを溶液内へ添加し、可視光照射することにより、水の光還元反応を行った。発生する水素を経時的に定量したところ、水素発生効率は同条件の $ZnTMPyP^{4+}$系より高かった（**Fig. 9**）。つまり、rHSA–ZnPP 錯体が水の光還元反応における有効な光増感剤として機能することが明らかとなった（詳細は発表論文 *J. Am. Chem. Soc.* **2006**, *128*, 16297 を参照）。

この結果は、アルブミン－ポルフィリン錯体において、ポルフィリンの中心金属を変換す

ことにより、様々な機能を有する人工の機能蛋白質が創製できる可能性を示している。

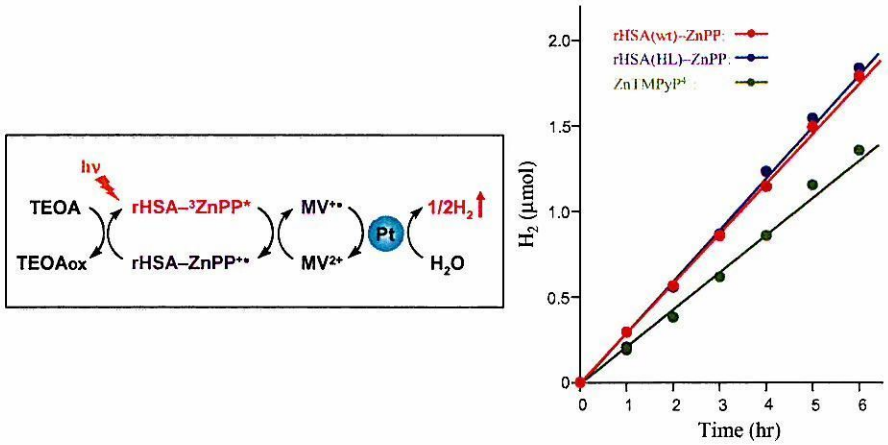

Fig. 9 Time dependence of the H_2 production from water in the phosphate buffered solution (pH 5.4, 50 mM) of HSA–ZnPP (10 mM), MV^{2+} (2 mM), TEOA (0.19 M), colloidal PVA-Pt (20 mM) at 25°C upon exposure to a 450-W xenon arc-lamp with HA30 filter (330–700 nm).

6．研究報文など

- Y. Hunag, T. Komatsu, H. Yamamoto, H. Horinouchi, K. Kobayashi, E. Tsuchida, *J. Biomed. Mater. Res.* **2004**, *71A*, 63–69.
- A. Nakagawa, N. Ohmichi, T. Komatsu, E. Tsuchida, *Org. Biomol. Chem.* **2004**, *2*, 3108–3112.
- T. Komatsu, N. Ohmichi, P. A. Zunszain, S. Curry, E. Tsuchida, *J. Am. Chem. Soc.* **2004**, *126*, 14304–14305.
- T. Komatsu, Y. Oguro, Y. Teramura, S. Takeoka, J. Okai, M. Anraku, M. Otagiri, E. Tsuchida, *Biochim. Biophys. Acta* **2004**, *1675*, 21–31.
- T. Komatsu, H. Yamamoto, Y. Huang, H. Horinouchi, K. Kobayashi, E. Tsuchida, *J. Biomed. Mater. Res.* **2004**, *71A*, 644–651.
- R.-M. Wang, T. Komatsu, A. Nakagawa, E. Tsuchida, *Bioconjugate Chem.* **2005**, *16*, 23–26.
- T. Komatsu, S. Ishihara, E. Tsuchida, H. Nishide, C. Inokuma, S. Nakamura, *Biomacromolecules* **2005**, *6*, 1489–1494.
- T. Komatsu, N. Ohmichi, A. Nakagawa, P. A. Zunszain, S. Curry, E. Tsuchida, *J. Am. Chem. Soc.* **2005**, *127*, 15933–15942.
- T. Komatsu, Y. Oguro, A. Nakagawa, E. Tsuchida, *Biomacromolecules* **2005**, *6*, 3397–3403.
- A. Nakagawa, T. Komatsu, M. Iizuka, E. Tsuchida, *Bioconjugate Chem.* **2006**, *17*, 146–151.
- Y. Huang, T. Komatsu, R.-M. Wang, A. Nakagawa, E. Tsuchida, *Bioconjugate Chem.* **2006**, *17*, 393–398.
- Y. Huang, T. Komatsu, H. Yamamoto, H. Horinouchi, K. Kobayashi, E. Tsuchida, *Biomaterials* **2006** *27*, 4477–4483.
- T. Komatsu, R.-M. Wang, P. A. Zunszain, S. Curry, E. Tsuchida, *J. Am. Chem. Soc.* **2006**, *128*, 16297–16301.
- A. Nakagawa, T. Komatsu, E. Tsuchida, *Chem. Lett.* **2007**, *36*. 640–641.
- T. Sato, T. Komatsu, A. Nakagawa, E. Tsuchida, *Phys. Rev. Lett.* **2007**, *98*, 208101-1–4.
- A. Nakagawa, T. Komatsu, Y. Huang, G. Lu, E. Tsuchida, *Bioconjugate Chem.* **2007**, *18*, 1673–1677.
- T. Komatsu, A. Nakagawa, P. A. Zunszain, S. Curry, E. Tsuchida, *J. Am. Chem. Soc.* **2007**, *129*, 11286–11295.
- E. Tsuchida, H. Sakai, T. Komatsu, S. Takeoka, Y. Huang, K. Sou, A. Nakagawa, Y. Teramura, K. Kobayashi, *Polym. Adv. Technol.* **2005**, *16*, 73–83.
- T. Komatsu, E. Tsuchida, *Artificial Oxygen Carrier. Its Front Line*, Ed. K. Kobayashi, E. Tsuchida, H. Horinouchi, p. 193–204, Springer-Verlag (Tokyo, 2005).
- T. Komatsu, Y. Huang, H. Yamamoto, H. Horinouchi, K. Kobayashi, E. Tsuchida, *Blood Substitutes,* Ed. R. Winslow, p. 532–539 (Chapter 46), Elsevier (London, 2006).
- *Chemistry World* (Royal Society), Dec. **2005**, p. 18.
- Imperial College London News Release, 1st December, **2006**.
- *Spectrum Direct* (Germany), 19th Dec. **2006**.
- 日経バイオテク、**2007**, *7-2*, 25.

Exchange transfusion with entirely synthetic red-cell substitute albumin-heme into rats: Physiological responses and blood biochemical tests

Yubin Huang,[1] Teruyuki Komatsu,[1] Hisashi Yamamoto,[2] Hirohisa Horinouchi,[3] Koichi Kobayashi,[3] Eishun Tsuchida[1]

[1]*Advanced Research Institute for Science and Engineering, Waseda University,3-4-1 Okubo, Shinjuku, Tokyo 169-8555, Japan*

[2]*Pharmaceutical Research Center, NIPRO Corporation, 3023 Nojimachi, Kusatsu, Shiga 525-0055, Japan*

[3]*Department of General Thoracic Surgery, School of Medicine, Keio University,35 Shinanomachi, Shinjuku, Tokyo 160-8582, Japan*

Received 24 October 2003; revised 13 May 2004; accepted 2 June 2004
Published online 5 August 2004 in Wiley InterScience (www.interscience.wiley.com). DOI: 10.1002/jbm.a.30127

Abstract: Recombinant human serum albumin (rHSA) incorporating 2-[8-{*N*-(2-methylimidazolyl)}octanoyloxymethyl]-5,10,15,20-[tetrakis{α,α,α,α-*o*-(1-methylcyclohexanoyl)amino}-phenyl]porphinatoiron(II) [albumin-heme (rHSA-heme)] is an artificial hemoprotein which has the capability to transport O_2 *in vitro* and *in vivo*. A 20% exchange transfusion with rHSA-heme into anesthetized rats has been performed to evaluate its clinical safety by monitoring the circulation parameters and blood parameters for 6 h after the infusion. Time course changes in all parameters essentially showed the same features as those of the control group (without infusion) and rHSA group (with administration of the same amount of rHSA). Blood biochemical tests of the withdrawn plasma at 6 h after the exchange transfusion have also been carried out. No significant difference was found between the rHSA-heme and rHSA groups, suggesting the initial clinical safety of this entirely synthetic O_2-carrier as a red-cell substitute. © 2004 Wiley Periodicals, Inc. J Biomed Mater Res 71A: 63–69, 2004

Key words: exchange transfusion; entirely synthetic red-cell substitute; albumin-heme; blood biochemical tests; O_2 carrier.

INTRODUCTION

Although hemoglobin (Hb)-based O_2 carriers are currently undergoing clinical trials as red-cell substitutes or oxygen therapeutics, there are still some concerns about new infectious pathogens in Hb and unresolved side effects such as vasoconstriction.[1–4] Recombinant human serum albumin (rHSA) incorporating the synthetic heme albumin-heme is an artificial hemoprotein that has the potential to bind and release O_2 under physiological conditions in the same manner as Hb and myoglobin.[5–7] In fact, the albumin-heme can transport O_2 through the body and release O_2 to tissues as a red-cell substitute without any acute side effects.[8,9] For example, rHSA including four molecules of 2-[8-{*N*-(2-methylimidazolyl)}-octanoyloxymethyl]-5,10,15,20-[tetrakis{α,α,α,α-*o*-(1-methylcyclohexanoyl)amino}phenyl]porphinatoiron(II) (Scheme 1) is one of the promising materials.[7] Recent study on the 30% exchange transfusion with rHSA-heme after 70% hemodilution with 5 wt % rHSA with the use of anesthetized rats demonstrated that the administration of this material improved the circulatory volume and resuscitated the hemorrhagic shock state.[10] The declined MAP and the mixed venous partial O_2 pressure immediately recovered, and the lowered renal cortical O_2-pressure also significantly increased.

In order to evaluate the initial clinical safety of this albumin-based O_2-carrier, a 20% exchange transfusion with rHSA-heme into anesthetized rats was performed, and the time courses of the circulation parameters (MAP, HR, respiration rate) and blood parameters (paO_2, pvO_2, pH, blood cell numbers) were measured for 6 h, which is adequate time to determine acute toxicity. Blood biochemical tests of the withdrawn plasma were also been carried out.

MATERIALS AND METHODS

Preparation of rHSA-heme

Recombinant human serum albumin (rHSA, Albrec®, 25 wt %) was obtained from the NIPRO Corp. (Osaka). The 5

Correspondence to: E. Tsuchida; e-mail: eishun@waseda.jp
Contract grant sponsor: MHLW
Contract grant sponsor: JSPS; contract grant number: 16350093
Contract grant sponsor: MEXT; contract grant number: 16655049

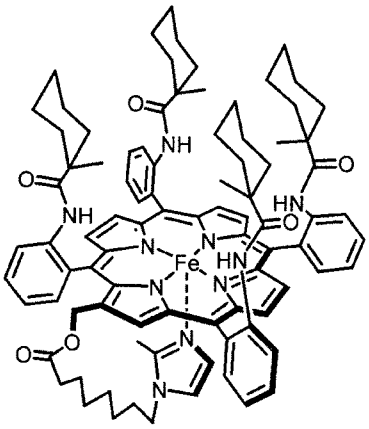

Scheme 1

g/dL rHSA was made by diluting Albrec® with saline solution (Otsuka Pharmaceutical Co., Ltd.). The rHSA-heme solution ([rHSA]: 4.9 g/dL, pH 7.45, [heme]: 2.8 m*M*, O_2-binding affinity ($p_{1/2}O_2$): 37 Torr) used for the experiments was prepared according to a previously reported procedure.[11] The red-colored rHSA-heme solution was filtered with the use of DISMIC 25CS045AS just before use.

Exchange transfusion

The investigations were carried out with 18 male Wister rats (305±3.6 g). The animals were placed on the heating pad under an inhalation anesthesia with sevofluran; its concentration was kept 2.0% for the operations and 1.5% for the experiments. After incision was made in the neck, the heparinized catheter (Natsume Seisakusho SP-55) was introduced into the right common carotid artery for blood withdrawal. Other catheters (SP-31) were inserted into the left femoral artery for a continuous MAP monitoring, and the right femoral vein for sample injection.

After stabilization of the animal condition, the 20% exchange transfusion (total blood volume of rat was estimated to be 64 mL/kg weight) was performed by 1 mL blood withdrawal via the common carotid artery and 1 mL rHSA-heme infusion from the femoral vein (each 1 mL/min) with four repeating cycles (n = 6, rHSA-heme group). Blood was taken from the artery (0.3 mL) and vein (0.2 mL) at the following five points; (i) before, (ii) immediately after, (iii) 1 h after, (iv) 3 h after, and (v) 6 h after the exchange transfusion. MAP and HR were recorded with the use of a polygraph system (NIHON KODEN LEG-1000 Ver. 01-02 or PEG-1000 Ver. 01-01) at the same time point as stated above. Withdrawn blood was rapidly applied to a blood gas system (Radio Meter Trading ABL555) to obtain the O_2-pressure (paO_2) and pH for the arterial blood, and the O_2-pressure (pvO_2) for the venous blood. The blood cell numbers were counted by a multisystem automatic blood cell counter (Sysmex KX-21). After 6 h, 4 mL of the venous blood was taken for each animal before sacrifice by sodium pentobarbital overdose. The blood samples were centrifuged at 4°C (Beckman Coulter Co., Optima LE-80K for 3500 × rpm, 10 min), and the plasma phase was frozen (−20°C) for blood biochemical tests. As a reference group, the 5 g/dL rHSA solution was administered similarly into rats (n = 6, rHSA group). Furthermore, six rats without infusion (operation only) were also set as a control group.

All animal handling and care was in accordance with the NIH guidelines. The protocol details were approved by the Animal Care and Use Committee of Keio University.

Blood biochemical tests

A total of 30 analytes, that is, total protein (TP), albumin (Alb), albumin/globulin ratio (A/G), aspartate aminotransferase (AST), alanine aminotransferase (ALT), lactate dehydrogenase (LDH), alkaline phosphatase (ALP), γ-glutamyltransferase (γ-GTP), leucine aminopeptidase (LAP), choline esterase (ChE), total bilirubin (TBil), direct bililubin (DBil), creatinine (CRN), blood urea nitrogen (BUN), uric acid (UA), amylase, lipase, creatine phosphokinase (CPK), total cholesterol (TCho), free cholesterol (FCho), cholesterol ester (ECho), β-lipoprotein (β-LP), high-density lipoprotein (HDL)-cholesterol, neutral fat (triglyceride, TG), total lipid, free fatty acid (FFA), phospholipids (PhL), K^+, Ca^{2+} and Fe^{3+}, were measured by Kyoto Microorganism Institute (Kyoto).

Data analysis

MAP, HR, respiration rate, paO_2 and pvO_2 were represented as percent ratios of the basal values with mean ± standard error of mean (SEM). Body temperature, pH, blood cell numbers and the data of blood biochemical tests were shown as mean ± SEM.

Statistical analysis were performed by repeated-analysis measures of variance (ANOVA) followed by the paired t-test for comparison with a basal value (body temperature), by the Bartlett test followed by the Tukey-Kramer multiple comparison test for pH, blood cell numbers, and the results of the blood biochemical tests, and by the Kruskal-Wallis test followed by the Tukey-Kramer multiple comparison test for more than three groups (MAP, HR, respiration rate, paO_2, and pvO_2). Values of $p < 0.05$ were considered significant. The statistical analytical software used was StatView (SAS Institute, Inc.).

RESULTS

Circulation parameters

The basal values of some measurements, the data values of which are represented by percent ratios, are summarized in Table I. There are no significant differences between the three groups (control, rHSA, and rHSA-heme groups).

The body temperature of each group was constantly

TABLE I
Basal Values of Each Group

	Control	rHSA	rHSA-heme
MAP (mmHg)	99 ± 2.8	101 ± 2.8	100 ± 6.1
HR (beats/min)	404 ± 19	435 ± 19	420 ± 13
Respiration rate (breaths/min)	66 ± 0.7	75 ± 4.0	70 ± 2.1
paO_2 (mmHg)	84.7 ± 3.1	84.9 ± 3.7	80.8 ± 2.2
pvO_2 (mmHg)	51.0 ± 1.5	45.7 ± 1.1	51.0 ± 1.7
Body weight (g)	305 ± 4.0	304 ± 2.8	305 ± 4.1

maintained within 36.9–37.4°C during the experiments [Fig. 1(a)].

The MAP time course in the control group demonstrated only a small deviation within 83.8–100.0% for 6 h. In the rHSA and rHSA-heme groups, the observed changes in MAP were almost the same as those of the control group. They ranged within 93.2–100 and 89.3–100%, respectively. It is remarkable that no vasoactive reaction was seen after the infusion of rHSA-heme [Fig. 1(b)].

The HR of the control, rHSA, and rHSA-heme groups remained unaltered for 6 h. The values of the control, rHSA, and rHSA-heme groups were in the range of 98.3–103.9, 96.9–108.8, and 85.7–100.0%, respectively [Fig. 1(c)].

The respiration rates also remained stable during the measurements. No significant difference was recognized among the three groups [Fig. 1(d)].

Blood-gas parameters

No difference in the pH changes was observed in the three groups. The pH values of the control, rHSA, and rHSA-heme groups were constant in the narrow ranges of 7.42–7.45, 7.42–7.44, and 7.42–7.44, respectively [Fig. 2(a)].

The paO_2 values of the control, rHSA, and rHSA-heme groups were also constant in the range of 100–108.1, 100–109.1, and 100–110.8%, respectively, by the end of measurements [Fig. 2(b)].

The pvO_2 of the control, rHSA and rHSA-heme groups demonstrated only small changes within 81.5–100.0, 84.9–108.4, and 81.9–100.0%, respectively [Fig. 2(c)].

Blood cell numbers

The Hct values of the control group were unchanged from 34.8–37.0% during the experiment. On the other hand, the 20% exchange transfusion with the

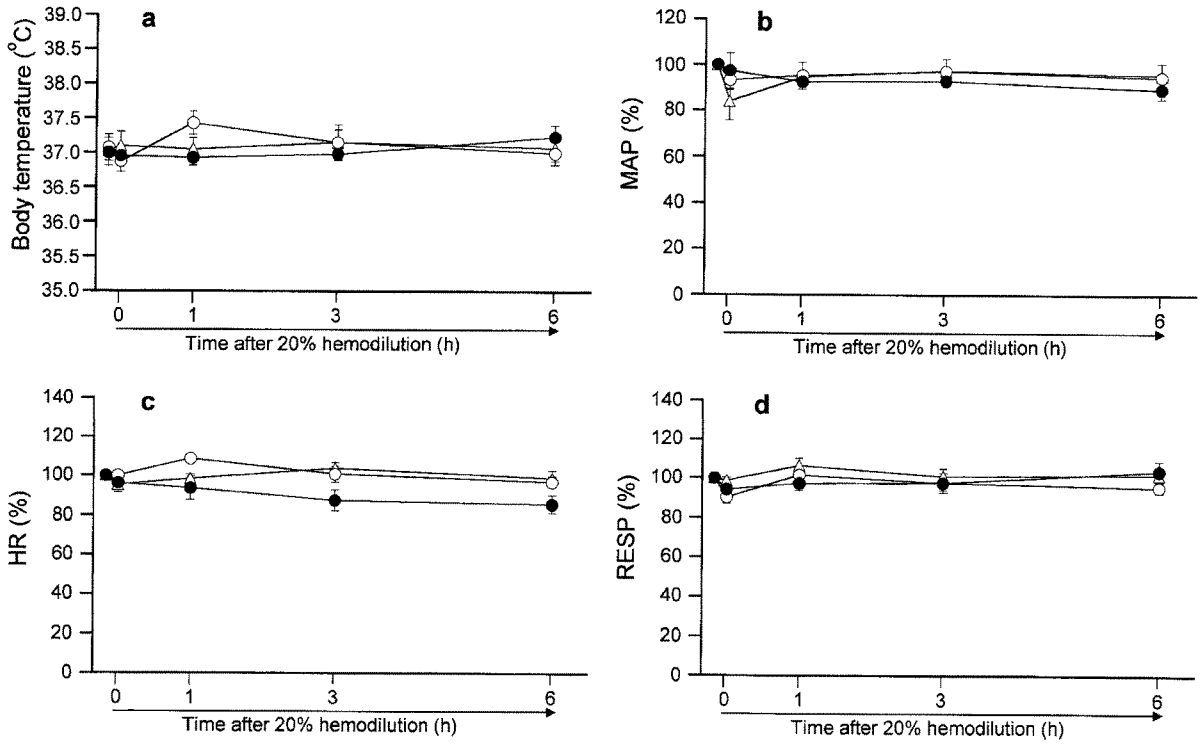

Figure 1. (a) Time courses of body temperature, (b) mean arterial pressure (MAP), (c) heart rate (HR), and (d) respiration rate (RESP) in anesthetized rats after 20% exchange transfusion with rHSA-heme or rHSA solution. Each value represents the mean ± SEM of six rats (triangles, control group without infusion; open circles, rHSA group; solid circles, rHSA-heme group).

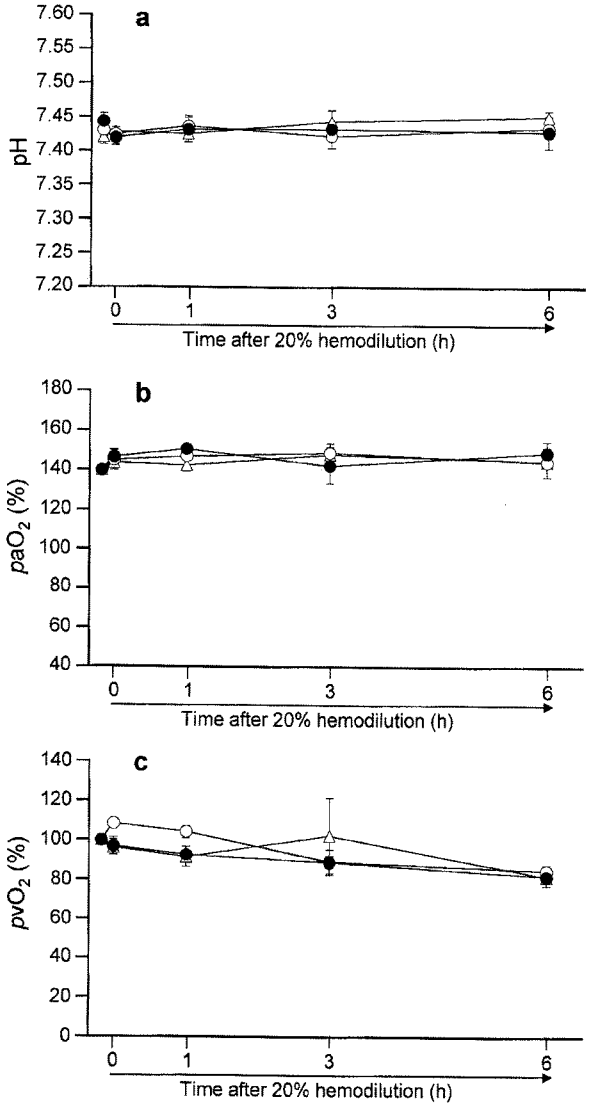

Figure 2. Time courses of (a) blood pH, (b) arterial blood O_2 pressure (paO_2), and (c) venous blood O_2-pressure (pvO_2) in anesthetized rats after 20% exchange transfusion with rHSA-heme or rHSA solution. Each value represents the mean ± SEM of six rats (triangles, control group without infusion; open circles, rHSA group; solid circles, rHSA-heme group).

rHSA or rHSA-heme solution led to rapid decreases in the Hct from 39.0 to 31.7% or from 42.2 to 33.8%, respectively. These declined values were constant for 6 h [Fig. 3(a)]. Concomitantly, the RBC numbers in the rHSA and rHSA-heme groups decreased from 634.8×10^4 to $512.8\times10^4/\mu L$ and from 620.3×10^4 to $497.7\times10^4/\mu L$ by the exchange transfusion. They did not recover for 6 h [Fig. 3(b)].

The WBC numbers in the rHSA and rHSA-heme groups also showed similar declines; however, they appeared to be relatively slow with some deviations [Fig. 3(c)]. The PLT numbers of the rHSA and rHSA-heme groups changed in the range of 57.1–76.9 × $10^4/\mu L$ and 58.4–65.6 × $10^4/\mu L$, respectively [Fig. 3(d)].

Blood biochemical tests

In order to evaluate liver function, kidney function and electrolyte balance after the infusion of rHSA-heme, total 30 analytes of the blood biochemical tests were selected for rat plasma (Fig. 4). In the rHSA group, the A/G ratio increased, and TCho, Echo, and HDL-C decreased compared to the control group.

In the rHSA-heme group, the A/G ratio and fatty acid increased, and LDH, ALP, TCho, Echo, HDL-C, and PhL decreased in comparison to the control group. However, the other analytes showed almost the same values as those of the control group. With respect to the rHSA group, no significant difference was found except for the increases in the amylase, free fatty acid, and iron concentration, and the decrease of ALP and ECho.

DISCUSSION

After the 20% exchange transfusion with the 5 g/dL rHSA solution, the Hct and RBC numbers decreased approximately 80% of their basal values. This was only because of the 20% dilution and did not imply any acute toxicity of rHSA. The significant increase in the A/G ratio was caused by the slightly high rHSA concentration of 5 g/dL. Because the albumin concentration in rat plasma is generally 3–4 g/dL, the exchange transfusion with this sample led to the increase in the albumin concentration and decrease in the globulin concentration, thus resulting in the elevated A/G ratio. The hemodilution by the 20% replacement of the animal's blood volume could reduce the level of the analytes immediately after the infusion; however, the majority of the data in the rHSA group recovered within 6 h; only LDH, TCho, Echo, and HDL-C showed values that were about 80% of the corresponding ones in the control group.

Because FCho was almost the same as that in the control group, the decreases in TCho, ECho, and HDL-C were presumably caused by the decreasing of ECho, which might come from the depressed synthetic function in the livers by administration of the external protein. The circulation parameters and blood gas parameters in the rHSA group moved within the narrow range for 6 h—almost the same as those observed in the control group. Based on these data, the authors are certain that the administration of rHSA

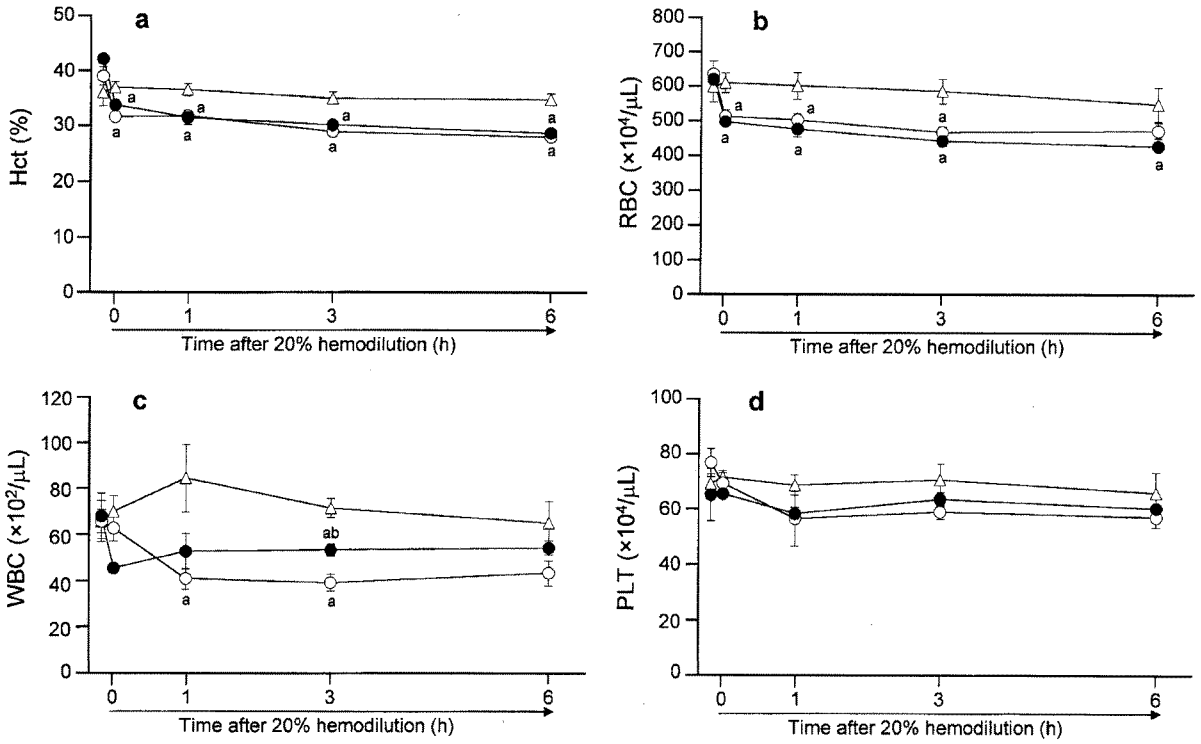

Figure 3. Time courses of hematocrit (Hct) value (a), red blood cell (RBC) numbers (b), white blood cell (WBC) numbers (c) and platelet (PLT) numbers (d) in whole blood of anesthetized rats after 20% exchange transfusion with rHSA-heme or rHSA solution. Each value represents the mean ± SEM of 6 rats (triangles, control group without infusion; open circles, rHSA group; solid circles, rHSA-heme group). $^{a}p < 0.05$ versus control group (Tukey-Kramer test).

into anesthetized rats did not induce any toxic reaction under the present experimental conditions.

After the exchange transfusion with the rHSA-heme solution, no significant difference was seen in the circulation parameters and blood gas parameters. Previous studies to elucidate the influence of albumin-heme on the MAP changes and microcirculation in the capillaries demonstrated that neither vasoconstriction nor hypertension occurred, because of the low permeability of the albumin vehicle through the vascular endothelium.[9] The latest exchange transfusion experiment with rHSA-heme after isovolemic hemodilution also supported this hypothesis.[10]

By careful inspection of the results from the blood biochemical tests, it was found that the rHSA-heme group showed higher values of amylase and free fatty acid, and lower values of ALP and ECho compared to those of the rHSA group. In general, amylase has two isozymes, which are secreted by the pancreatic parenchyma and salivary gland. When the concentrations of the amylase and lipase (pancreatic parenchyma enzyme) simultaneously increase, it may be a sign of pancreatitis and other pancreas disorders.[12–14] However, the slight increase in the lipase concentration in the current protocol was not significant. Therefore, the possibility of pancreas disorders caused by the rHSA-heme infusion is considered negligible. The high amylase value is probably due to the isozyme secreted by the salivary gland.

With the increase in the free fatty acid, the TG concentration also tended to elevate to some degree. The increase in TG may activate the lipase, which acts as its decomposition enzyme, and results in the increasing free fatty acid as a metabolite. The relation between rHSA-heme and the TG increase is still not clear.

CONCLUSIONS

The appearance of the all animals showed absolutely no change for 6 h after the 20% exchange transfusion with albumin-heme. The physiological responses of the blood circulation, gas equilibria, and blood cell numbers in the rHSA-heme group were almost the same as those of the control and rHSA groups. MAP and HR did remain constant after the injection of the rHSA-heme, suggesting again that the albumin-based O_2-carrier does not induce the vasoconstriction. The blood biochemical tests of the withdrawn plasma of rHSA-heme group showed results similar to those of the control and rHSA groups, implying no acute toxicity by the exchange transfusion

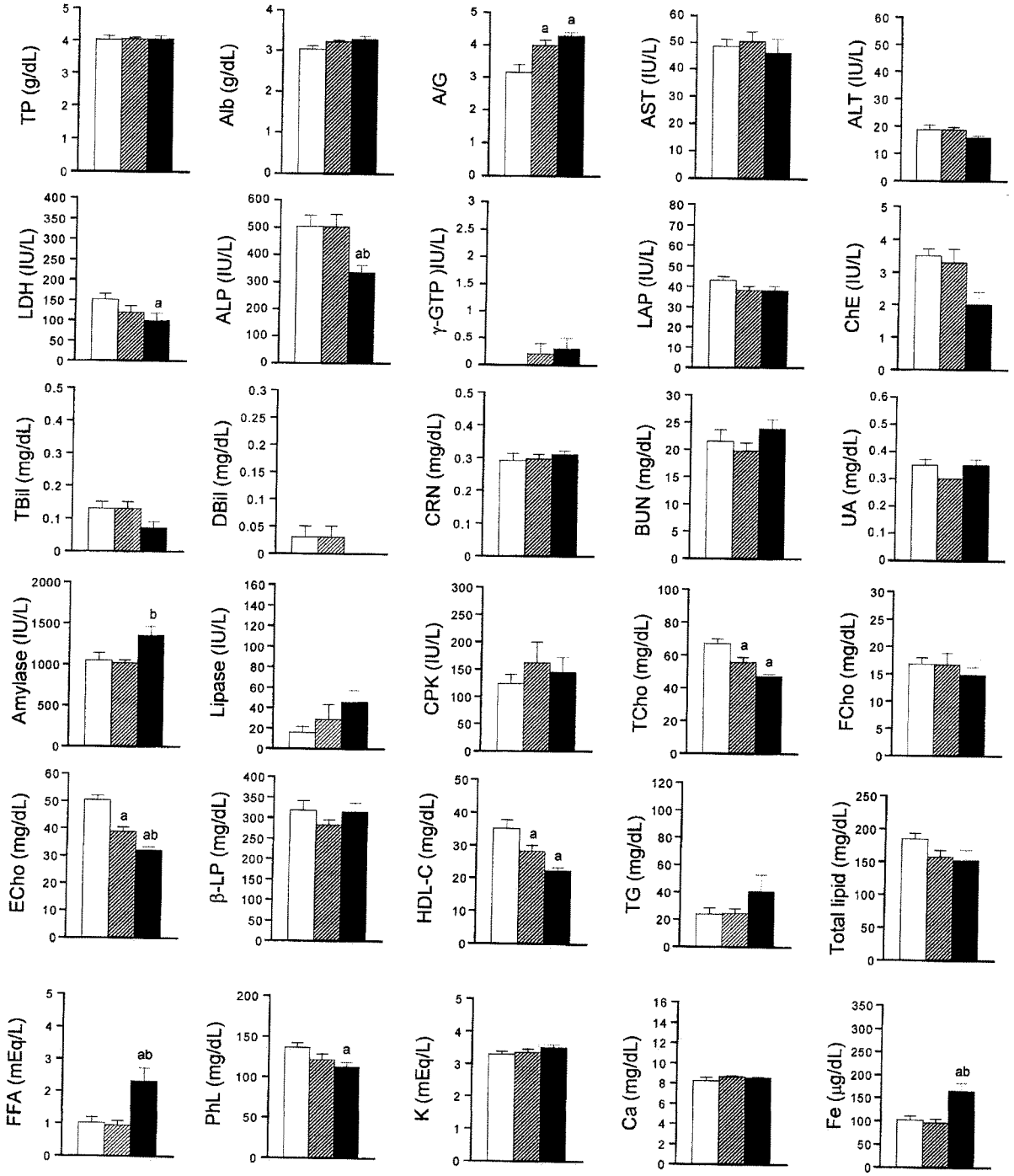

Figure 4. Blood biochemical tests of rat plasma after 20% exchange transfusion with rHSA-heme or rHSA solution. Each value represents the mean ± SEM of six rats (white bar, control group without infusion; diagonal bar, rHSA group; black bar, rHSA-heme group). $^{a}p < 0.05$ versus control group (Tukey-Kramer test); $^{b}p < 0.05$ versus rHSA group (Tukey-Kramer test).

with rHSA-heme. These results showed the initial clinical safety of the rHSA-heme solution, which allows us to undergo further advanced preclinical testing of this synthetic O_2-carrying hemoprotein as a new class of red-cell substitutes. Biochemical tests and histopathological observations for 7 days after the exchange transfusion with rHSA-heme will be reported in a forthcoming article.

The authors are grateful to Dr. Toshiya Kai (NIPRO Corp.) for preparation and characterizations of the albumin-heme solutions. They also thank Dr. Ichiro Hirotsu

(NIPRO Corp.) for his useful discussions and valuable suggestions on the experimental results. This work was partially supported by Health Science Research Grants (Research on Pharmaceutical and Medical Safety) of the MHLW, Grant-in-Aid for Scientific Research (No. 16350093) from JSPS, and Grant-in-Aid for Exploratory Research (No. 16655049) from MEXT.

References

1. Chang TMS. Recent and future developments in modified hemoglobin and microencapsulated hemoglobin as red blood cell substitutes. Artif Cells Blood Substit Immobil Biotechnol 1997;25:1–24.
2. Tsuchida E. Perspectives of blood substitutes. In: Tsuchida E, editor. Blood substitutes: Present and future perspectives. Lausanne: Elsevier; 1998. p 1–14.
3. Winslow RM. New transfusion strategies: red cell substitutes. Annu Rev Med 1999;50:337–353.
4. Squires JE. Artificial blood. Science 2002;295:1002–1005.
5. Komatsu T, Hamamatsu K, Wu J, Tsuchida E. Physicochemical properties and O_2-coordination structure of human serum albumin incorporating tetrakis(*o*-pivamido)phenylporphyrinatoiron(II) Derivatives. Bioconjug Chem 1999;10:82–86.
6. Tsuchida E, Komatsu T, Matsukawa Y, Hamamatsu K, Wu J. Human serum albumin incorporating tetrakis(*o*-pivalamido-)phenylporphinatoiron(II) derivative as a totally synthetic O_2-carrying hemoprotein. Bioconjug Chem 1999;10:797–802.
7. Komatsu T, Matsukawa Y, Tsuchida E. Effect of heme structure on O_2-binding properties of human serum albumin–heme hybrids: intramolecular histidine coordination provides a stable O_2-adduct complex. Bioconjug Chem 2002;13:397–402.
8. Tsuchida E, Komatsu T, Hamamatsu K, Matsukawa Y, Tajima A, Yoshizu A, Izumi Y, Kobayashi K. Exchange transfusion of albumin-heme as an artificial O_2-infusion into anesthetized rats: physiological responses, O_2-delivery and reduction of the oxidized hemin sites by red blood cells. Bioconjug Chem 2000;11:46–50.
9. Tsuchida E, Komatsu T, Matsukawa Y, Nakagawa A, Sakai H, Kobayashi K, Suematsu M. Human serum albumin incorporating synthetic heme: red blood cell substitute without hypertension by nitric oxide scavenging. J Biomed Mater Res 2003; 64A:257–261.
10. Komatsu T, Yamamoto H, Huang Y, Horinouchi H, Kobayashi K, Tsuchida E. Physiological responses to exchange transfusion with synthetic oxygen-carrier "albumin-heme" in acute anemia after 70% hemodilution. J Biomed Mater Res. Submitted for publication.
11. Huang Y, Komatsu T, Nakagawa A, Tsuchida E, Kobayashi S. Compatibility *in vitro* of albumin-heme (O_2-carrier) with blood cell components. J Biomed Mater Res 2003;66A:292–297.
12. Gorelick FS. Acute pancreatitis. In: Yamada T, editor. Textbook of gastroenterology (2nd ed.). Philadelphia: Lippincott; 1955. p 2064–2091.
13. Agarwal N, Pitchumoni CS, Sivaprasad AV. Evaluating tests for acute pancreatitis. Am J Gastroenterol 1990;85:356–361.
14. Clavin PA, Burgan S, Moossa AR. Serum enzyme and other laboratory tests in acute pancreatitis. Br J Surg 1989;76:1234–1238.

ARTICLE

OBC

www.rsc.org/obc

Synthesis of protoheme IX derivatives with a covalently linked proximal base and their human serum albumin hybrids as artificial hemoprotein

Akito Nakagawa, Naomi Ohmichi, Teruyuki Komatsu and Eishun Tsuchida*

Advanced Research Institute for Science and Engineering, Waseda University, 3-4-1 Ohkubo, Shinjuku-ku, Tokyo 169-8555, Japan. E-mail: eishun@waseda.jp; Fax: +81 3-3205-4740; Tel: +81 3-5286-3120

Received 15th June 2004, Accepted 3rd September 2004
First published as an Advance Article on the web 27th September 2004

The simple one-pot reaction of protoporphyrin IX and ω-(*N*-imidazolyl)alkylamine or *O*-methyl-L-histidyl-glycine with benzotriazol-1-yl-oxytris(dimethylamino)phosphonium hexafluorophosphate at room temperature produced a series of protoporphyrin IX species with a covalently linked proximal base at the propionate side-chain. The central iron was inserted by the general $FeCl_2$ method, converting the free-base porphyrins to the corresponding protoheme IX derivatives. Mesoporphyrin IX and diacetyldeuteroporphyrin IX analogues were also prepared by the same procedure. The Fe(II) complexes formed dioxygen (O_2) adducts in dimethylformamide at 25 °C. Some of them were incorporated into the hydrophobic domain of recombinant human serum albumin (rHSA), providing albumin–heme hybrids (rHSA–heme), which can bind and release O_2 in aqueous media (pH 7.3, 25 °C). The oxidation process of converting the dioxygenated heme in rHSA to the inactive Fe(III) state obeyed first-order kinetics, indicating that the μ-oxo dimer formation was prevented by the immobilization of heme in the albumin scaffold. The rHSA–heme, in which the histidylglycyl tail coordinates to the Fe(II) center, showed the most stable O_2 adduct complexes.

Introduction

Numerous model compounds of hemoglobin (Hb) and myoglobin (Mb) have already been prepared and their O_2-binding equilibria and kinetics were extensively studied.[1] In particular, synthetic hemes having a sterically encumbered porphyrin platform can form stable O_2 adducts in organic solvent at room temperature. If we are to reproduce or mimic any biochemical reaction, the aqueous medium is particularly important. The dioxygenated complexes of highly-modified hemes are unfortunately oxidized to the ferric state in water. Human serum albumin (HSA) is the most abundant plasma protein in our circulatory system and solubilizes hydrophobic small molecules.[2] We have found that synthetic hemes are also spontaneously incorporated into HSA, which provides unique albumin–heme hybrids (HSA–hemes) and allows their Fe(II) states to remain stable in aqueous solution.[3] Actually, recombinant HSA[4] (rHSA) including tetrakis(α,α,α,α-*o*-pivalamidophenyl)porphinatoiron(II) with a covalently linked proximal base can reversibly bind and release O_2 under physiological conditions, and acts as an artificial O_2 transporter in the blood stream.[5] Our next target is to realize O_2 coordination to rHSA–heme involving protoheme IX in the same manner as natural Hb and Mb. The dioxygenation of protoheme IX has several advantages. (1) Synthetic procedures are rather simplified with respect to the highly modified tetraphenylporphyrin. (2) It has the same structure and thus the same spectra as do hemoproteins; this makes possible the study of subtle changes in the protein nanostructure. (3) Its metabolism process has been clarified,[6] which is an advantage for medical use as an artificial O_2 carrier.

We report herein the simple synthetic methodology of protoheme IX derivatives with a covalently-linked proximal imidazolyl arm and the O_2-binding properties of the obtained rHSA–hemes.

Results and discussion

Synthesis

The free-base porphyrins with a covalently linked proximal base (**1a–8a**, Scheme 1) were synthesized by the one-pot reaction of protoporphyrin IX, ω-(*N*-imidazolyl)alkylamine [R_2H; 3-(*N*-imidazolyl)propylamine, 4-(*N*-(2-methylimidazolyl))-butylamine or *O*-methyl-L-histidyl-glycine] for one propionic acid group, and a capping alcohol or amine on the other side (R_3H; MeOH, EtOH or $MeNH_2$) in the presence of benzotriazol-1-yl-oxytris(dimethylamino)phosphonium hexafluorophosphate (BOP) at 25 °C in pyridine [or dimethylformamide (DMF)] (Scheme 2). The carbonyl attachment was made through either an ester or an amide function. After the reaction, the mixture was poured into 10% NaCl solution, which led to the precipitation of the crude porphyrin. Centrifugation at 7000 g for 30 min gave a purple pellet. The pyridine (or DMF), BOP, R_2H and R_3H in the supernatant were all discarded at this point. The obtained precipitate was dissolved in $CHCl_3$ and showed several spots on a thin layer chromatograph. The anpolar band corresponds to the double R_3-substituted component (ex. protoporphyrin IX diethyl ester in the cases of **2**, **5**, **6**) and the second band is the desired porphyrin, which is purified by a silica gel chromatographic separation (yield: 20–30%). The iron was then inserted by the general $FeCl_2$ method with 2,6-lutidine in DMF solution, giving the corresponding hemins. Mesoporphyrin IX and diacetyldeuteroporphyrin IX also gave similar analogues (**7b** and **8b**). We obtained a mixture of two isomeric compounds that we were unable to separate.

Traylor and co-workers reported many pioneering studies on "chelated hemes".[7] They synthesized compound **1b**, for instance, using an acid anhydride procedure directly from protohemin chloride.[7e] First, the protohemin dimethyl ester was partially hydrolyzed and, after purification, the mono acid was coupled to a 3-(*N*-imidazolyl)propylamine by the pivaloyl chloride method. Nevertheless, reaction mixtures involving the diacid and monoacid are normally insoluble in common organic solvents, therefore, the yield of this reaction largely depends on the separation techniques. In contrast, our simple procedure makes it possible to synthesize a series of new protoporphyrins with a wide variety of proximal bases and end-capping groups of the other propionic acid.

Dioxygenation of heme in DMF solution

The obtained hemin complexes **1b–8b** in DMF solution were reduced to the corresponding Fe(II) complexes using a solution

DOI: 10.1039/b409017a

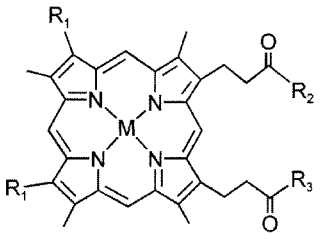

R_1	R_2	R_3	
			1
			2
		-OH	3
			4
			5
			6
			7
			8

Scheme 1

of the crown ether-dithionite as reducing agent.[8] The UV-vis absorption spectrum of **2c** [Fe(II) complex] under a nitrogen (N_2) atmosphere showed a single broad band in the α,β region around 520–580 nm. This indicates the formation of a typical five-*N*-coordinate high-spin complex,[7] in which the proximal imidazole group intramolecularly coordinates to the central Fe(II) ion in the non-coordinating solvent (DMF) (Fig. 1). Because 2-methyl-imidazole significantly inhibits a sixth ligand binding to the *trans*-position, **6c** also demonstrated a similar 5-coordinated spectrum in DMF solution. Upon bubbling of the O_2 gas through the solution of **2c**, the spectral pattern immediately changed to that of the O_2 adduct complex. After adding carbon monoxide (CO) gas, the heme changed to a very stable carbonyl complex. Similar absorption changes were observed for all the heme derivatives, **1c–8c**. The absorption maxima (λ_{max}) of compounds **1c–8c** in DMF solution under N_2, O_2 and CO atmospheres are summarized in Table 1.

The positions and the relative intensities of all peaks were independent of the temperature changes from 5 to 25 °C. In general, the electron density of the porphyrin ring systematically changes the λ_{max} of the B-band and Q-band.[9] The replacement of the vinyl groups at the 3,8-positions of protoheme IX with ethyl groups (from **2c** to **7c**) produced a hypsochromic shift. In contrast, changing the vinyl groups to electron withdrawing acetyl groups (from **2c** to **8c**) produced a bathochromic shift.

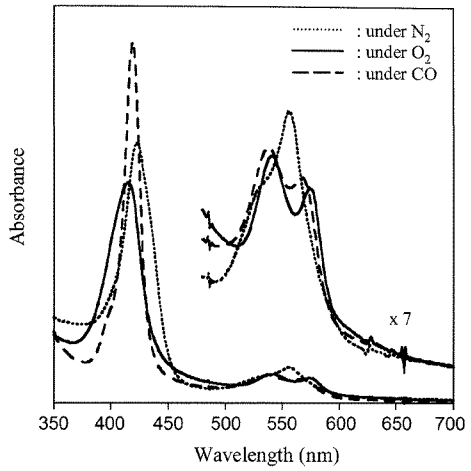

Fig. 1 UV-vis spectra of **2c** in DMF at 25 °C.

Table 1 Absorption maxima (λ_{max}) of heme derivatives in DMF under various conditions

	λ_{max}/nm		
Compound	Under N_2	Under O_2	Under CO
1c (15 °C)	427, 530, 558	414, 543, 575	420, 540, 569
1c (25 °C)	424, 532, 559	412, 542, 575	420, 539, 567
2c (5 °C)	422, 531, 556	415, 541, 574	419, 537, 567
2c (25 °C)	421, 533, 557	409, 539, 571	418, 537, 565
3c (25 °C)	426, 537, 559	415, 543, 575	420, 539, 567
4c (5 °C)	421, 527, 555	413, 540, 572	417, 536, 564
5c (5 °C)	419, 529, 551	406, 537, 569	412, 534, 562
5c (25 °C)	423, 533, 557	408, 539, 573	419, 538, 567
6c (5 °C)	430, 555	413, 547, 576	418, 538, 561
7c (25 °C)	414, 523, 548	407, 531, 563	409, 529, 556
8c (5 °C)	440, 541, 571	432, 552, 579	434, 549, 576
8c (25 °C)	439, 545, 569	431, 552, 580	433, 548, 577

We could not find any significant difference in the absorption maxima of **1c–6c**, because modification of the propionic acids did not affect the electron density of the porphyrin macrocycle.

Preparation of rHSA–heme

Aqueous solutions of rHSA–heme were prepared by injecting an ethanol solution of the carbonylated heme into an aqueous solution of rHSA. The inclusion of heme into rHSA was confirmed by the following results: (1) Sepharose gel column chromatography showed the elution peaks of heme and rHSA coincided at the same position, (2) during dialysis of the rHSA–heme solution against phosphate buffer, the outer aqueous phase did not contain the heme component. The UV-vis absorption spectra of the obtained solution showed that the heme was retained as a CO adduct complex.

The binding number of heme in one rHSA was determined to be 0.9–1.1 (mol/mol) by assaying the iron and rHSA concentrations. The binding constant of **1b** for rHSA was estimated to be *ca.* 4×10^6 M^{-1}, which is approximately 1/25 of that for protohemin IX itself to albumin (*ca.* 1×10^8 M^{-1}).[10] Polar heme derivatives **3c** with monopropionic acid and **4c** with a methyl-

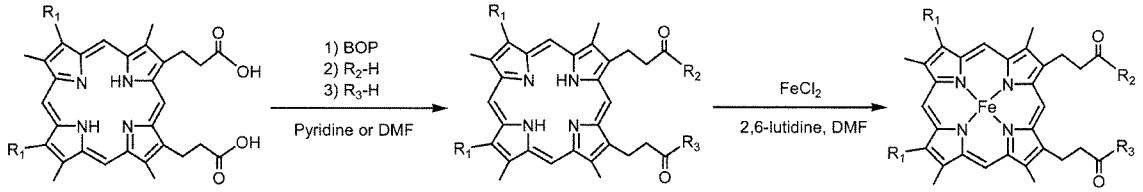

BOP: benzotriazol-1-yl-oxytris(dimethylamino)phosphonium hexafluorophosphate

Scheme 2 Synthesis of protoheme IX derivatives.

Table 2 Absorption maxima (λ_{max}) of rHSA–hemes in phosphate buffer solution (pH 7.3) at 25 °C

Compounds	λ_{max}/nm		
	Under N_2	Under O_2	Under CO
rHSA–**1c**	420, 536, 561	414, 540, 567	419, 541, 566
rHSA–**2c**	420, 538, 561	416, 540, 567	421, 543, 567
rHSA–**5c**	422, 539, 561	418, 540, 571	422, 541, 569
rHSA–**8c**	444, 549, 571	432, 551, 580	440, 555, 578

amide capping group at the porphyrin periphery were partially oxidized to the Fe(III) state during the inclusion process. Since the binding force of the heme derivative to rHSA is a hydrophobic interaction,[11] relatively polar porphyrins may not be incorporated into a certain domain of rHSA and easily oxidized compared to more apolar ones.

The circular dichroism spectra of the rHSA–hemes (rHSA–**1c**, –**2c**, –**5c**, –**7c** and –**8c**) are almost identical to that of rHSA itself (not shown). This suggests that the secondary structure of the albumin host molecule did not change after incorporation of the hemes. Furthermore, the isoelectric points of these rHSA–hemes were all 4.8, which is the original value of rHSA. The surface net charges of rHSA remained unaltered after heme incorporation.

Dioxygenation of rHSA–heme in aqueous solution

Light irradiation of the CO adduct complex of rHSA–heme (rHSA–**1c**, –**2c**, –**5c**, –**6c**, –**7c** and –**8c**) under an N_2 atmosphere led to CO dissociation and demonstrated new spectral patterns with well-defined α and β bands. For example, the typical absorption spectral changes of rHSA–**2c** are shown in Fig. 2.

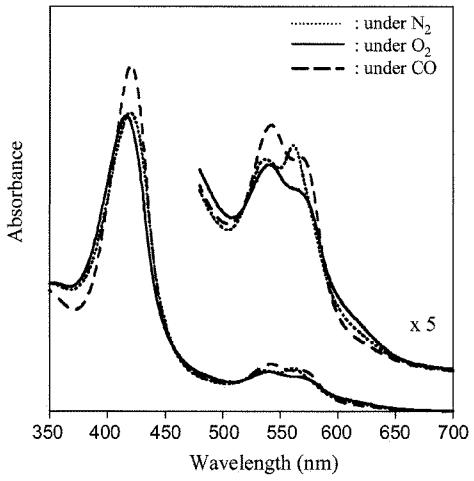

Fig. 2 UV-vis spectra of rHSA–**2c** in phosphate buffer solution (pH 7.3) at 25 °C.

From the nature of these spectra, we concluded that the obtained Fe(II) complexes are a mixture of Fe(II) 5-coordinated (high-spin) and 6-coordinated (low spin) species. It implies that the sixth coordinate position of the heme might be partially occupied by some amino acid residue of the protein scaffold. Upon exposure of O_2 to the Fe(II) complex of rHSA–**1c**, the spectrum changed to that of the O_2 adduct species. Although the aqueous micelle solution of **1c** with 5% surfactant (cetyltrimethylammonium bromide) forms a CO adduct complex, dioxygenation was not stable enough to measure the spectrum at 25 °C.[7e] In contrast, rHSA–**1c**, –**2c**, –**5c**, and –**8c** formed O_2 adduct complexes at 25 °C (pH 7.3) except for rHSA–**6c** and –**7c** (Table 2). The introduction of a methyl group to the 2-position of the imidazole ring is widely recognized to reduce the O_2 and CO binding affinities.[1] In this case, the strength of the imidazole coordination to the Fe(II) center is too weak to produce a stable O_2 adduct complex.

Table 3 Half-life ($\tau_{1/2}$) and O_2 binding affinity ($P_{1/2}$) of rHSA–hemes in phosphate buffer solution (pH 7.3) at 25 °C

Compounds	$\tau_{1/2}$/min	$P_{1/2}$/Torr
rHSA–**1c**	20	0.1
rHSA–**2c**	50	0.1
rHSA–**5c**	90	0.1
rHSA–**8c**	50	0.4

The oxidation process of dioxygenated rHSA–heme to the inactive Fe(III) state obeyed first-order kinetics. This indicates that the μ-oxo dimer formation was prevented by the immobilization of heme in the albumin structure. The half-life of the O_2 adduct complexes ($\tau_{1/2}$) and the O_2 binding affinities ($P_{1/2}$) of rHSA–hemes are summarized in Table 3. The histidylglycyl tail coordinated protoheme (**5c**) in rHSA showed the most stable O_2 adduct complex ($\tau_{1/2}$: 90 min) with respect to the imidazole bound ones. The more hydrophobic ethylpropionate (**2c**) also contributed to prolong the stability of the O_2 adduct complex relative to the methylpropionate protoheme (**1c**).

The $P_{1/2}$ values of rHSA–**1c**, –**2c** and –**5c** are 0.1 Torr at 25 °C. On the other hand, rHSA–**8c** showed a higher $P_{1/2}$ value (low O_2-binding affinity) compared to the others. The acetyl groups at the 3,8-positions of **8c** decrease the electron density of the porphyrin macrocycle, therefore $P_{1/2}$ could be significantly reduced. Traylor and co-workers found that the O_2 binding affinity of the chelated heme was sensitive to the electron density at Fe(II) and thus to the substituents at the heme periphery. The O_2 binding constant decreased by 1/6 upon changing the substituent from a vinyl to an acetyl group.[12] Our experimental data of hemes in rHSA are quite consistent with their observations.

Conclusion

A convenient one-pot synthesis of protoporphyrin IX derivatives with a covalently linked proximal base has been described. rHSA successfully incorporates the protoheme derivatives, providing an artificial hemoprotein, which can form an O_2 adduct complex at 25 °C. The rHSA–heme, in which the histidylglycil tail intramolecularly coordinates to the Fe(II) center, showed the most stable O_2 adduct complex with the relatively high O_2 binding affinity of 0.1 Torr.

Experimental

Materials and apparatus

All reagents were used as supplied commercially unless otherwise noted. All solvents were normally purified by distillation before use. DMF was distilled under reduced pressure in N_2. Pyridine was refluxed over and distilled from P_2O_5. The water was deionized using an ADVANTEC GS-200 system. The rHSA (Albrec®, 25 wt%) was obtained from NIPRO Corp. (Osaka).

Thin-layer chromatography was carried out on 0.2 mm precoated plates of silica gel 60 F254 (Merck). Purification was performed by silica gel 60 (Merck) column chromatography. The infrared spectra were measured with a JASCO FT/IR-410 spectrometer. The UV-vis absorption spectra were recorded by a JASCO V-570 spectrophotometer. The ^{1}H-NMR spectra were recorded using a JEOL Lambda 500 spectrometer. Chemical shifts were expressed in parts per million downfield from Me_4Si as the internal standard. The FAB-MS spectra were obtained using a JEOL JMS-SX102A spectrometer.

Synthesis of porphyrin derivatives

O-Methyl-L-histidyl-glycine[13] and 4-(*N*-(2-methylimidazolyl))-butylamine[14] were synthesized according to the reported procedures.

3,18-Divinyl-8-(3-methoxycarbonyl)ethyl-12-(3-(*N*-imidazolyl)propylamido)ethyl-2,7,13,17-tetramethylporphyrin (1a). A pyridine (7 mL) solution of 3-(*N*-imidazolyl)propylamine (35 μL, 0.29 mmol) was added dropwise to protoporphyrin IX (200 mg, 0.36 mmol) and benzotriazol-1-yloxytris-(dimethylamino)phosphonium hexafluorophosphate (411 mg, 0.93 mmol) in pyridine (20 mL) and stirred for 30 min at room temperature. The mixture was reacted for 4 h at 40 °C. After the addition of methanol (10 mL), the solution was stirred for another 12 h at 40 °C. The mixture was then poured into a 10% NaCl solution (1 L, 4 °C) and the suspension was centrifuged for 30 min at 7000*g*. The supernatant was discarded and the precipitate was collected and dried *in vacuo*. The residue was chromatographed on a silica gel column using $CHCl_3/CH_3OH$ = 8/1 (v/v) as the eluent. The main band was collected and dried at room temperature for several hours *in vacuo*, giving compound **1a** as a purple solid (75 mg, 20%). R_f = 0.3 ($CHCl_3/CH_3OH$ = 8/1 (v/v)); IR (NaCl) ν = 1731 (C=O, ester), 1646 (C=O, amide) cm^{-1}; UV-vis ($CHCl_3$) λ_{max} = 408, 506, 542, 575, 630 nm; ^{1}H-NMR ($CDCl_3$) δ: −4.0 (s, 2H, inner), 1.8–2.4 (m, 4H, –(CH_2)$_2$–Im), 2.7 (m, 4H, –CH_2–COO–, NH–CH_2–), 3.2 (t, 2H, –CONH–CH_2–), 3.3–3.7 (m, 18H, por–CH_3, –CH_2–CO–, –$COOCH_3$), 4.2 (d, 4H, por–CH_2–), 5.4 (s, 1H, Im), 6.0–6.3 (m, 4H, =CH_2 (vinyl)), 6.4 (d, 1H, Im), 6.6 (d, 1H, Im), 8.0–8.4 (m, 2H, –CH= (vinyl)), 9.7 (m, 4H, *meso*); MS *m/z*: 681.67.

Fe(III) complex of 1a (1b). Iron(II) chloride tetrahydrate (106 mg, 0.53 mmol) was added to a dry DMF (10 mL) solution of **1a** (36 mg, 53 μmol) and 2,6-lutidine (30 μL, 0.27 mmol) under an N_2 atmosphere. The reaction mixture was stirred at 70 °C for 3 h. After confirming the disappearance of the porphyrin's fluorescence (600–800 nm, ex. 400 nm), the solution was cooled to room temperature and poured into 10% NaCl solution (1 L, 4 °C). The suspension was centrifuged for 30 min at 7000*g* and the supernatant was discarded. The precipitate was dried *in vacuo* and chromatographed on a silica gel column using $CHCl_3/CH_3OH$ = 8/1 (v/v) as the eluent. The main band was collected and dried at room temperature for several hours *in vacuo* to give compound **1b** as a brown solid (27 mg, 68%). R_f = 0.3 ($CHCl_3/CH_3OH$ = 8/1); IR (NaCl) ν = 1728 (C=O, ester), 1646 (C=O, amide) cm^{-1}; UV-vis ($CHCl_3$) λ_{max} = 389, 513, 641 nm; HR-MS *m/z*: calcd for $C_{41}H_{43}O_3N_7Fe$: 737.2777, found: 737.2778 [M^+].

3,18-Divinyl-8-(3-ethoxycarbonyl)ethyl-12-(3-(*N*-imidazolyl)-propylamido)ethyl-2,7,13,17-tetramethylporphyrin (2a). The synthetic procedure of compound **2a** was the same as that used for **1a** except for using ethanol instead of methanol. Yield 30%; R_f = 0.4 ($CHCl_3/CH_3OH$ = 10/1); IR (NaCl) ν = 1650 (C=O, amide), 1732 (C=O, ester) cm^{-1}; UV-vis ($CHCl_3$) λ_{max} = 409, 544, 580, 633 nm; ^{1}H-NMR ($CDCl_3$) δ: −4.1 (s, 2H, inner-NH), 0.8–0.9 (t, 3H, –COO–CH_2–CH_3), 1.3–1.5 (t, 2H, –CONH–CH_2–CH_2–), 3.0–3.1 (t, 2H, –CH_2–Im), 3.1–3.3 (m, 4H, –CH_2–COO), 3.5–3.7 (m, 12H, por–CH_3), 3.8–3.9 (m, 2H, –COO–CH_2–CH_3), 4.2–4.4 (d, 4H, por–CH_2–), 6.1 (s, 1H, Im), 6.1–6.4 (q, 5H, =CH_2 (vinyl), Im), 6.6–6.7 (d, 1H, Im), 6.9–7.0 (d, 1H, Im), 8.1–8.3 (m, 2H, –CH= (vinyl)), 9.8–10.2 (m, 4H, *meso*); MS *m/z*: 695.29.

Fe(III) complex of 2a (2b). Iron insertion to **2a** was carried out by the same procedure as in the **1b** preparation. Yield 80%; R_f = 0.3 ($CHCl_3/CH_3OH$ = 8/1); IR (NaCl) ν = 1651 (C=O, amide), 1725 (C=O, ester) cm^{-1}, UV-vis ($CHCl_3$) λ_{max} = 406, 520, 578 nm; HR-MS *m/z*: calcd. for $C_{42}H_{45}O_3N_7Fe$: 751.2933, found: 751.2953 [M^+].

3,18-Divinyl-8-(3-carboxy)ethyl-12-(3-(*N*-imidazolyl)propyl-amido)ethyl-2,7,13,17-tetramethylporphyrin (3a). Sodium hydroxide (2 N, 4.5 mL) was added to the methanol (10 mL) solution of **2a** (266 mg, 0.38 mmol) and the mixture was stirred for 12 h at room temperature. It was brought to dryness *in vacuo*. Methanol was added to the residue and the mixture was added dropwise to 10% NaCl solution (pH 2, 4 °C). It was centrifuged for 30 min at 7000*g* and the precipitate was collected and dried *in vacuo*, affording compound **3a** as a brown solid (187 mg, 78%), IR (KBr) ν = 1652 (C=O, amide), 1707 (C=O, –COOH) cm^{-1}; UV-vis (DMSO) λ_{max} = 409, 508, 543, 578, 631 nm; ^{1}H-NMR (d_6-DMSO) δ: −3.5 (s, 2H, inner-NH), 1.6–1.7 (t, 2H, –CONH–CH_2–CH_2–), 2.8–2.9 (t, 2H, –CH_2–Im), 3.1–3.3 (m, 2H, –CONH–CH_2–), 3.5–3.9 (m, 12H, por–CH_3), 4.2–4.4 (d, 4H, por–CH_2–), 6.1 (s, 1H, Im), 6.1–6.4 (q, 5H, =CH_2 (vinyl), Im), 6.6–6.7 (d, 1H, Im), 6.9–7.0 (d, 1H, Im), 8.5–8.6 (m, 2H, –CH= (vinyl)), 10.2–10.4 (m, 4H, *meso*); MS *m/z*: 670.41.

Fe(III) complex of 3a (3b). Iron insertion to **3a** was carried out by the same procedure as in the **1b** preparation. Yield 80%; IR (KBr) ν = 1646 (C=O, amide), 1707 (C=O, –COOH) cm^{-1}; UV-vis (DMSO) λ_{max} = 403, 508, 631 nm; HR-MS *m/z*: calcd. for $C_{40}H_{41}O_3N_7Fe$: 723.2620, found: 724.2668 [M + H^+].

3,18-Divinyl-8-(3-methylamido)ethyl-12-(3-(*N*-imidazolyl)-propylamido)ethyl-2,7,13,17-tetramethylporphyrin (4a). Compound **4a** was synthesized according to the same procedure as for **1a** except for using methyl amine instead of methanol. Yield 20%; R_f = 0.5 ($CHCl_3/CH_3OH$ = 3/1); IR (NaCl) ν = 1631 (C=O, amide) cm^{-1}; UV-vis ($CHCl_3$) λ_{max} = 409, 509, 543, 579, 632 nm; ^{1}H-NMR (CD_3OD, $CDCl_3$) δ: −4.0 (s, 2H, inner), 1.8–2.4 (m, 4H, –(CH_2)$_2$–Im), 2.5 (t, 3H, –CONH–CH_3), 2.9 (m, 2H, –CONH–CH_2–), 3.3 (m, 4H, –CH_2–CONH–), 3.4–3.6 (m,12H, por–CH_3), 5.5 (s, 1H, Im), 6.0 (s, 1H, Im), 6.1–6.4 (m, 4H, =CH_2 (vinyl)), 6.8 (m, 1H, Im), 8.1–8.3 (m, 2H, –CH= (vinyl)), 9.7–9.9 (q, 4H, *meso*); MS *m/z*: 680.69.

Fe(III) complex of 4a (4b). Iron insertion to **4a** was carried out by the same procedure as in the **1b** preparation. Yield 67%; R_f = 0.3 ($CHCl_3/CH_3OH$ = 5/1); IR (NaCl) ν = 1646 (C=O, amide) cm^{-1}; UV-vis ($CHCl_3$) λ_{max} = 408, 521, 565 nm; HR-MS *m/z*: calcd. for $C_{41}H_{44}O_3N_7Fe$: 736.2937, found: 736.2938 [M^+].

3,18-Divinyl-8-(3-ethoxycarbonyl)ethyl-12-(((3-*N*-glycyl-L-histidinyl)-9-oxymethyl)carbonyl)ethyl-2,7,13,17-tetramethyl-porphyrin (5a). The synthetic procedure of compound **5a** was same as that used for **1a**. DMF was used instead of pyridine, because it dissolves *O*-methyl-L-histidyl-glycine. Yield 15%; R_f = 0.4 ($CHCl_3/CH_3OH$ = 15/1); IR (NaCl) ν = 1635 (C=O, amide), 1725 (C=O, ester) cm^{-1}; UV-vis ($CHCl_3$) λ_{max} = 405, 505, 541, 577, 627 nm; ^{1}H-NMR ($CDCl_3$) δ: −4.6 (s, 2H, inner-NH), 2.7–2.9 (m, 2H, Im–CH_2–), 3.0–3.5 (m, 18H, por–CH_3, –CH_2–CH_2–CO–NH–, –CH_2–CH_2–COO–CH_2–CH_3), 3.6 (s, 2H, –CONH–CH_2–CONH–), 3.8 (s, 3H,–OCH_3), 4.0–4.3 (d, 4H, por–CH_2–), 4.3–4.5 (m, 1H, α-CH), 6.0–6.4 (m, 4H, =CH_2 (vinyl)), 7.4 (s, 1H, Im–H), 8.0–8.3 (m, 5H, –CH= (vinyl), Im–H), 9.8–10.0 (m, 4H, *meso*-H); MS *m/z*: 782.68.

Fe(III) complex of 5a (5b). Iron insertion to **5a** was carried out by the same procedure as in the **1b** preparation. Yield 75%; R_f = 0.5 ($CHCl_3/CH_3OH$ = 8/1); IR (NaCl) ν = 1660 (C=O, amide), 1734 (C=O, ester) cm^{-1}; UV-vis ($CHCl_3$) λ_{max} = 388, 508, 637 nm; HR-MS *m/z*: calcd. for $C_{44}H_{46}O_6N_8Fe$: 838.2890, found: 839.2929 [M + H^+].

3,18-Divinyl-8-(3-ethoxycarbonyl)ethyl-12-(4-(*N*-(2-methyl-imidazolyl))butylamido)ethyl-2,7,13,17-tetramethylporphyrin (6a). Compound **6a** was synthesized by the same procedure as for **1a** except for using 4-(*N*-(2-methylimidazolyl))butylamine instead of 3-imidazolylpropylamine. Yield 20%; R_f: 0.1 ($CHCl_3/CH_3OH$ = 8/1); IR (NaCl) ν = 1732 (C=O, ester), 1651 (C=O, amide) cm^{-1}; UV-vis ($CHCl_3$) λ_{max} = 408, 506, 542, 576, 630 nm; ^{1}H-NMR ($CDCl_3$) δ: −4.2 (s, 2H, inner-H), 0.4–0.6 (m, 4H, CONH–CH_2–(CH_2)$_2$–), 1.4–1.5 (d, 3H, Im–CH_3), 2.2–2.4 (m,

2H, –CONH–CH_2–), 2.8–3.1 (m, 4H, por–CH_2–CH_2–), 3.2–3.3 (t, 2H, –CH_2–Im), 3.4 (s, 3H, –COO–CH_3), 3.5–3.8 (m, 12H, por–CH_3), 4.2–4.4 (t, 4H, por–CH_2–), 5.6–5.7 (d, 1H, Im), 5.8 (m, 1H, Im), 6.1–6.4 (q, 4H, =CH_2 (vinyl)), 8.1–8.2 (m, 2H, –CH= (vinyl)), 9.8–10.1 (m, 4H, *meso*); MS *m/z*: 709.72.

Fe(III) complex of 6a (6b). Iron insertion to **6a** was carried out by the same procedure as in the **1b** preparation. Yield 64%; R_f = 0.2 ($CHCl_3$/CH_3OH = 8/1); IR (NaCl) ν = 1732 (C=O, ester), 1652 (C=O, amide) cm^{-1}; UV-vis ($CHCl_3$) λ_{max} = 401, 580, 630 nm; HR-MS *m/z*: calcd. for $C_{43}H_{47}O_3N_7Fe$: 765.3090, found: 766.3184 [M + H^+].

3,18-Diethyl-8-(3-carboxy)ethyl-12-(3-(*N*-imidazolyl)propyl-amido)ethyl-2,7,13,17-tetramethylporphyrin (7a). Compound **7a** was synthesized by the same procedure as for **1a** except for using mesoporphyrin IX instead of protoporphyrin IX. Yield 10%; R_f: 0.4 ($CHCl_3$/CH_3OH = 20/1); IR (NaCl) ν = 1732 (C=O, ester), 1651 (C=O, amide) cm^{-1}; UV-vis ($CHCl_3$) λ_{max} = 408, 506, 542, 576, 630 nm; ^{1}H-NMR ($CDCl_3$) δ: 0.8 (m, 3H, CH_3–CH_2–O–), 1.6 (m, 2H,–CH_2–CH_2–Im), 1.8 (t, 6H, CH_3–CH_2–Por), 2.9 (m, 2H, CH_3–CH_2–O–), 3.1 (m, 4H, –CH_2–COO–), 3.2 (m, 2H, –NH–CH_2–), 3.6 (m, 12H, CH_3–Por), 3.8 (m, 2H,–CH_2–Im), 4.1 (m, 4H,CH_3–CH_2–Por), 4.4 (m, 4H, Por–CH_2–), 6.6 (s, 1H, –NHCO–), 6.0–6.8 (d, 3H, Im), 10.0 (m, 4H, *meso*); MS *m/z*: 699.32.

Fe(III) complex of 7a (7b). Iron insertion to **7a** was carried out by the same procedure as in the **1b** preparation. Yield 62%; R_f: 0.2 ($CHCl_3$/CH_3OH = 6/1); IR (NaCl) ν = 1732 (C=O, ester), 1668 (C=O, amide) cm^{-1}; UV-vis (DMF) λ_{max} = 394, 566, 591 nm; MS *m/z*: calcd for $C_{42}H_{49}O_3N_7Fe$: 755.3292, found 755.3246 [M^+].

3,18-Diacetyl-8-(3-carboxy)ethyl-12-(3-(*N*-imidazolyl)propyl-amido)ethyl-2,7,13,17-tetramethylporphyrin (8a). Compound **8a** was synthesized by the same procedure as for **1a** except for using diacetyldeuteroporphyrin IX instead of protoporphyrin IX. Yield 27%; R_f: 0.1 ($CHCl_3$/CH_3OH = 6/1); IR (NaCl) ν = 1735 (C=O, ester), 1651 (C=O, amide, ketone) cm^{-1}; UV-vis ($CHCl_3$) λ_{max} = 423, 516, 551, 586, 640 nm; ^{1}H-NMR ($CDCl_3$) δ: 1.5 (m, 2H, –CH_2–CH_2–Im), 2.9–3.1 (M, 4H, –CH_2–Im, –NH–CH_2–), 3.2–3.3 (m, 16H, –CH_2–COO, CH_3–Por), 3.4 (m, 6H, CH_3–CO–), 3.6 (m, 3H, CH_3–OCO–), 4.1 (m, 4H, Por–CH_2–), 6.0 (d, 1H, Im), 6.6 (m, 1H, Im), 6.9 (m, 1H, Im), 10 (m, 4H, *meso*); MS *m/z*: 712.

Fe(III) complex of 8a (8b). Iron insertion to **8a** was carried out by the same procedure as in the **1b** preparation. Yield 64%; R_f: 0.1 ($CHCl_3$/CH_3OH = 6/1); IR (NaCl) ν = 1735 (C=O, ester), 1651 (C=O, amide, ketone) cm^{-1}; UV-vis (DMF) λ_{max} = 418, 550, 578 nm; HR-MS *m/z*: calcd. for $C_{41}H_{43}O_5N_7Fe$: 769.2675, found 769.2697 [M^+].

Preparation of ferrous complex in DMF solution

The central Fe(III) ion of the porphyrin derivatives were reduced to the Fe(II) state using the complex of 18-crown-6 ether with $Na_2S_2O_4$ in DMF under aerobic conditions as previously reported.[8]

Preparation of rHSA–heme

Aqueous ascorbic acid (0.2 M, 10 μL) was added to an ethanol solution of the hemin derivative (2 mM, 1 mL) under a CO atmosphere. After complete reduction of the central Fe(III) ion, the ethanol solution (2 mM, 25 μL) was injected into the phosphate buffer solution (1 mM, pH 7.3, 2.5 mL) of rHSA (20 μM) under an Ar atmosphere. The formation of carbonyl rHSA–heme was confirmed by its UV-vis spectrum. The binding ratio of heme to rHSA was estimated by each concentration. The heme concentration was measured by the assay of iron ion using inductively coupled plasma spectrometry (Seiko, SPS7000A). The rHSA concentration was determined by bromocresol green along with the Albumin Test Wako kit (Wako Pure Chemical Industries).

Measurement of O_2 binding ability

The half-life of the O_2 adduct complex was determined by the time course of spectral changes, and the O_2 binding affinity ($P_{1/2}$) was determined by spectral changes at various partial pressures of O_2 according to previous reports.[2,15] rHSA–heme concentrations of 20 μM were normally used for UV-vis absorption spectroscopy. The spectra were recorded within the range of 350–700 nm.

Acknowledgements

This work was partially supported by a Grant-in-Aid for Scientific Research (No. 16350093) from JSPS, a Grant-in-Aid for Exploratory Research (No. 16655049) from MEXT Japan, and Health Science Research Grants from MHLW Japan.

References

1 (*a*) J. P. Collman, R. Boulatov, C. J. Sunderland and L. Fu, *Chem. Rev.*, 2004, **104**, 561; (*b*) M. Momenteau and C. A. Reed, *Chem. Rev.*, 1994, **94**, 659, and references therein.
2 T. Peters, Jr., *All about Albumin, Biochemistry, Genetics, and Medical Applications*, Academic Press, New York, 1996.
3 (*a*) T. Komatsu, K. Ando, N. Kawai, H. Nishide and E. Tsuchida, *Chem. Lett.*, 1995, 812; (*b*) T. Komatsu, K. Hamamatsu, J. Wu and E. Tsuchida, *Bioconjugate Chem.*, 1999, **10**, 82; (*c*) E. Tsuchida, T. Komatsu, Y. Mastukawa, K. Hamamatsu and J. Wu, *Bioconjugate Chem.*, 1999, **10**, 797; (*d*) T. Komatsu, T. Okada, M. Moritake and E. Tsuchida, *Bull. Chem. Soc. Jpn.*, 2001, **74**, 1695; (*e*) T. Komatsu, Y. Matsukawa and E. Tsuchida, *Bioconjugate Chem.*, 2002, **13**, 397; (*f*) A. Nakagawa, T. Komatsu, N. Ohmichi and E. Tsuchida, *Chem. Lett.*, 2003, **32**, 504.
4 A. Sumi, W. Ohtani, K. Kobayashi, T. Ohmura, K. Tokoyama, M. Nishida and T. Suyama, *Biotechnol. Blood Proteins*, 1993, **227**, 293.
5 (*a*) E. Tsuchida, T. Komatsu, Y. Matsukawa, A. Nakagawa, H. Sakai, K. Kobayashi and M. Suematsu, *J. Biomed. Mater. Res.*, 2003, **64A**, 257; (*b*) Y. Huang, T. Komatsu, A. Nakagawa, E. Tsuchida and S. Kobayashi, *J. Biomed. Mater. Res.*, 2003, **66A**, 292; (*c*) E. Tsuchida, T. Komatsu, K. Hamamatsu, Y. Matsukawa, A. Tajima, A. Yoshizu, Y. Izumi and K. Kobayashi, *Bioconjugate Chem.*, 2000, **11**, 46.
6 (*a*) P. R. Oritz de Montellano, *Curr. Opin. Chem. Biol.*, 2000, **4**, 221; (*b*) R. B. Frydman and B. Frydman, *Acc. Chem. Res.*, 1987, **20**, 250.
7 (*a*) C. K. Chang and T. G. Traylor, *J. Am. Chem. Soc.*, 1973, **95**, 8475; (*b*) C. K. Chang and T. G. Traylor, *J. Am. Chem. Soc.*, 1973, **95**, 8477; (*c*) C. K. Chang and T. G. Traylor, *Proc. Natl. Acad. Sci. USA*, 1975, **72**, 1975; (*d*) T. G. Traylor, C. K. Chang, J. Geibel, A. Berzinis, T. Mincey and J. Cannon, *J. Am. Chem. Soc.*, 1979, **101**, 6716; (*e*) J. Geibel, J. Cannon, D. Cambell and T. G. Traylor, *J. Am. Chem. Soc.*, 1978, **100**, 3575.
8 T. Mincey and T. G. Traylor, *Bioinorg. Chem.*, 1978, **9**, 409.
9 (*a*) *Porphyrins and Metalloporphyrins*, ed. K. M. Smith, Elsevier, Amsterdam, 1975; (*b*) M. Brunori, U. Saggese, G. C. Rotilio, E. Antonini and J. Wyman, *Biochemistry*, 1971, **10**, 1604.
10 G. H. Beaven, S.-H. Chen, A. D'albis and W. B. Gratzer, *Eur. J. Biochem.*, 1974, **41**, 539.
11 M. Rotenberg, S. Cohen and R. Margalit, *Photochem. Photobiol.*, 1987, **46**, 689.
12 T. G. Traylor, D. K. White, D. W. Cambell and A. P. Berzinis, *J. Am. Chem. Soc.*, 1982, **103**, 4932.
13 E. Monzani, L. Linati, L. Casella, L. D. Gioia, M. Favretto, M. Gullotti and F. Chillemi, *Inorg. Chim. Acta*, 1998, **273**, 339.
14 (*a*) E. Tsuchida, H. Nishide, Y. Sato and M. Kaneda, *Bull. Chem. Soc. Jpn.*, 1982, **55**, 1890; (*b*) K. Soai, A. Ookawa and K. Kato, *Bull. Chem. Soc. Jpn.*, 1982, **55**, 1671.
15 J. P. Collman, J. I. Brauman, B. L. Iverson, J. L. Sessler, R. M. Morris and Q. H. Gibson, *J. Am. Chem. Soc.*, 1983, **105**, 3052.

J|A|C|S
COMMUNICATIONS

Published on Web 10/19/2004

Dioxygenation of Human Serum Albumin Having a Prosthetic Heme Group in a Tailor-Made Heme Pocket

Teruyuki Komatsu,*,† Naomi Ohmichi,† Patricia A. Zunszain,‡ Stephen Curry,‡ and Eishun Tsuchida*,†

Advanced Research Institute for Science and Engineering, Waseda University, 3-4-1 Okubo, Shinjuku-ku, Tokyo 169-8555, Japan, and Department of Biological Sciences, Imperial College London, Huxley Building, South Kensington Campus, London SW7 2AZ, United Kingdom

Received July 4, 2004; E-mail: eishun@waseda.jp

Human serum albumin (HSA, MW = 66.5 kD) is the most abundant plasma protein in our bloodstream and serves as a transporter for small hydrophobic molecules such as fatty acids, bilirubin, and steroids.[1,2] Hemin dissociated from methemoglobin is also bound within a narrow D-shaped cavity in subdomain IB of HSA with an axial coordination of Tyr-161 and electrostatic interactions between the porphyrin propionates and a triad of basic amino acid residues (Figure 1).[3,4] In terms of the general hydrophobicity of the α-helical pocket, HSA potentially has features similar to the heme-binding site of myoglobin (Mb) or hemoglobin (Hb). However, even if one reduces the ferric HSA−hemin to obtain a ferrous complex, it is immediately oxidized by O_2. This is due to the fact that HSA lacks a proximal histidine, which enables the heme group to bind O_2.[3−5] We have shown that HSA incorporating tetraphenylporphinatoiron derivatives having a covalently linked axial-base can absorb O_2 under physiological conditions with a O_2 binding affinity similar to that of Hb.[6]

In this paper, we report for the first time the introduction of a proximal histidine into the subdomain IB of HSA by site-directed mutagenesis to construct a tailor-made heme pocket, which allows a reversible O_2 binding to the prosthetic heme group. Laser flash photolysis experiments revealed that this artificial hemoprotein appears to have two different geometries of the axial-imidazole coordination and shows rather low O_2 binding affinity.

We designed two recombinant HSA (rHSA) mutants, in which single or double mutations were introduced into subdomain IB: I142H [rHSA(A)] and I142H/Y161L [rHSA(B)] (Figure 1). Replacement of Y161 by histidine was not done because modeling experiments indicated that the distance from N_ϵ(H142) to Fe(heme) would be too great (>4 Å). In our mutants, the N_ϵ(H142)−Fe distance was estimated to be 2.31 Å (compared to 2.18 Å in Mb). The specific mutations were introduced into the HSA coding region in a plasmid vector (pHIL-D2 HSA) using the QuikChange (Stratagene) mutagenesis kit, and the mutants were expressed in the yeast species *Pichia pastoris*.[7] The rHSA(wild-type or mutants)−hemin complexes were prepared essentially according to our previously reported procedures, except that myristate was not added.[4] The resulting hemoproteins exhibited only a single band in SDS-PAGE.

In the absorption spectrum of the rHSA(wt)−hemin solution, the distinct charge-transfer (CT) band of Fe^{3+}−phenolate appeared at 625 nm.[8] A magnetic circular dichroism (MCD) spectrum showed a W-shaped feature in the Soret-band region.[9] These results imply the formation of a high-spin Fe^{3+} complex with the phenolate oxygen ligand of Y161, which is quite consistent with that found in the crystal structure.[3,4]

rHSA(B)−hemin did not exhibit the CT band because of the Y161L mutation and was easily reduced to the corresponding ferrous complex by adding a small molar excess amount of aqueous $Na_2S_2O_4$ under an Ar atmosphere. A single broad absorption band (λ_{max} = 559 nm) in the α,β region was very similar to that of deoxy Mb and indicated the formation of a five-N-coordinate Fe^{2+} complex (Figure 2).[10] The spectral pattern was unaltered in the temperature range of 0−25 °C. The shape of the asymmetric MCD spectrum also resembled that of deoxy Mb.[11] This suggests that the heme is accommodated into the tailor-made heme pocket with an axial coordination involving His-142.

Upon exposure of the rHSA(B)−heme solution to O_2 gas, the UV−vis absorption changed to that of the dioxygenated complex (λ_{max} = 412, 537, 573 nm) at 0−25 °C[10] (lifetime of the O_2−adduct: ca. 10 min). After exposure to flowing CO, the heme produced a typical carbonyl complex (λ_{max} = 419, 538, 565 nm).

On the contrary, rHSA(A)−heme could not bind O_2 even at low temperature (~0 °C). It can be thought that the polar phenolate residue at the top of the porphyrin platform is likely to accelerate the proton-driven oxidation of the Fe^{2+} center. Replacing Y161 by

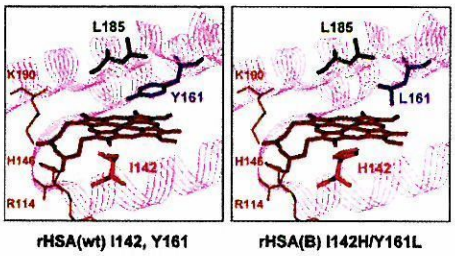

Figure 1. Prosthetic heme group complexed within the heme pocket in subdomain IB of rHSA(wt) and rHSA(B) mutant produced on the basis of the crystal structure coordinate of the rHSA−hemin complex (ref 4).

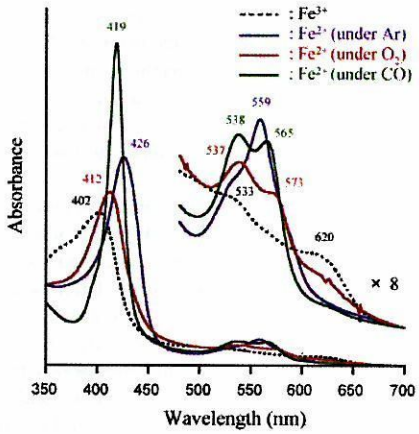

Figure 2. UV−vis absorption spectral changes of rHSA(B)−heme in phosphate buffered solution (pH 7.0, 50 mM) at 8 °C.

† Waseda University.
‡ Imperial College London.

10.1021/ja046022t CCC: $27.50

Table 1. O_2 and CO binding Parameters of rHSA(B)−heme in Phosphate Buffered Solution (pH 7.0, 50 mM) at 22 °C

hemoprotein	k_{on}^{CO} (M^{-1} s^{-1})	$k_{on}^{O_2}$ (M^{-1} s^{-1})	$k_{off}^{O_2}$ (s^{-1})	$P_{1/2}^{O_2}$ (Torr)
rHSA(B)−heme[a]	2.0×10^6 (I), 2.7×10^5 (II)	7.5×10^6 (I and II)	221 (I), 1.7×10^3 (II)	18 (I), 134 (II)
Mb[b]	5.1×10^5	1.4×10^7	12	0.51
Hb (*R*-state)[c]	4.6×10^6	3.3×10^7	13	0.24

[a] Number in parentheses (I or II) indicates species I or II. [b] At 20 °C; ref 17. [c] At 20−21.5 °C; ref 18.

hydrophobic leucine greatly enhanced the stabilization of the O_2−adduct complex.

We then employed laser flash photolysis (Nd:YAG SHG; λ = 532 nm; 6 ns pulse width) to evaluate the kinetics of O_2 and CO bindings to rHSA(B)−heme.[12−14] Interestingly, the time dependence of the absorption change accompanying the CO recombination showed double-exponential profiles; the ratio of the amplitude of the fast and slow phases was always 3:2. On the other hand, the rebinding process of O_2 obeyed monophasic decay. On the basis of studies on synthetic model hemes, it has been shown that the proximal-side steric effect is the only primary factor that influences the association rate for CO but not for O_2.[12−14] One possible explanation is that there may be two different geometries of the axial His-142 coordination and that each one shows the individual kinetics of the CO rebinding. Marden and co-workers also found a similar behavior in CO association with HSA−heme and interpreted it as indicating that there are two orientations of the heme plane in the albumin scaffold.[5] In our case, the alternative geometries may arise because the heme molecule binds into the pocket of subdomain IB in two orientations related by a 2-fold rotation about its center (180° rotational isomers). Asymmetric 3,8-divinyl groups at the porphyrin periphery, in particular, would occupy different positions that result in a small divergence of the porphyrin ring and its iron center. The crystal structure analyses could not resolve this ambiguity, because the two configurations exist as a mixture.[3,4]

Our hypothesis is consistent with infrared spectroscopy data. The CO coordinated with rHSA(B)−heme showed a broad ν_{CO} at 1962 cm^{-1} with a shoulder at 1942 cm^{-1}. We therefore suggest that there are two different modes of π-back-donation from the central Fe^{2+} to the bound CO. It is remarkable that the lower stretching frequency is very close to that of Mb (ν_{CO} = 1943 cm^{-1}).[15] Attempts to determine the ratio of the two hemin orientations by ^1H NMR spectroscopy unfortunately failed.[16] The downfield spectra of rHSA(B)−hemin in met and met-azido forms did not show sharp resonances of the four porphyrin CH_3 groups.

The two geometries of the His-142 ligation in rHSA(B)−heme should yield two different O_2 binding affinities. By analyzing CO/O_2 competitive binding following laser flash photolysis, we obtained the association and dissociation rate constants for O_2 ($k_{on}^{O_2}$, $k_{off}^{O_2}$), and the O_2 binding affinities ($P_{1/2}^{O_2}$) for these two species (I and II) (Table 1).[12−14] The $P_{1/2}^{O_2}$ values were determined to be 18 and 134 Torr, respectively; this means that the O_2 binding affinities were 2.8 and 0.4%, respectively, of that observed for Mb.[17,18] Kinetically, for species I with $P_{1/2}^{O_2}$ of 18 Torr, an 18-fold increase in the $k_{off}^{O_2}$ value leads to the low affinity for O_2. Repeated studies with synthetic model hemes and engineered mutants of Mb or Hb have shown that low polarity of the microenvironment around the heme site decreases the O_2-binding affinity by increasing the dissociation rate constant.[12−14,17] In this albumin-based hemoprotein, the porphyrin ring is buried in the core of the pocket entirely made of hydrophobic residues. Therefore, the O_2 binding affinity becomes significantly lower than those of Mb and Hb. In species II with $P_{1/2}^{O_2}$ of 134 Torr, the proximal pull effect could further increase the $k_{off}^{O_2}$ value and may cause a large decline in the O_2 binding affinity.

We have recently found that heme is accommodated into the different architecture of a tailor-made heme pocket in rHSA (Y161L/L185H) [rHSA(C)] and that the rHSA(C)−heme complex also binds O_2 as well. In this case, the proximal histidine coordinates with the heme plane from the roof side, and the O_2 molecule binds from the floor side (Figure 1). Our combined structural and mutagenic approach allows us to significantly enhance the O_2 binding properties of rHSA−heme complexes and thereby mimic the diverse biological reactivities of natural hemoproteins. From the viewpoint of clinical applications, "O_2-carrying plasma albumin" could be of extreme medical importance not only for red blood cell substitutes but also for O_2-therapeutic reagents. The crystal structure analysis of this new class of artificial hemoproteins is now underway.

Acknowledgment. This work was partially supported by a Grant-in-Aid for Scientific Research (No. 16350093) from JSPS, a Grant-in-Aid for Exploratory Research (No. 16655049) from MEXT Japan, Health Science Research Grants (Regulatory Science) from MHLW Japan, and the Wellcome Trust (UK).

Supporting Information Available: Time dependence of the absorption change accompanying the CO or O_2 rebinding to rHSA(B)−heme after the laser flash photolysis (PDF). This material is available free of charge via the Internet at http://pubs.acs.org.

References

(1) Peters, T. *All about Albumin: Biochemistry, Genetics and Medical Applications*; Academic Press: San Diego, 1996.
(2) Curry, S.; Madelkow, H.; Brick, P.; Franks, N. *Nat. Struct. Biol.* **1998**, *5*, 827.
(3) Wardell, M.; Wang, Z.; Ho, J. X.; Robert, J.; Ruker, F.; Rubel, J.; Carter, D. C. *Biochem. Biophys. Res. Commun.* **2002**, *291*, 813.
(4) Zunszain, P. A.; Ghuman, J.; Komatsu, T.; Tsuchida, E.; Curry, S. *BMC Struct. Biol.* **2003**, *3*, 6.
(5) Marden, M. C.; Hazard, E. S.; Leclerc, L.; Gibson, Q. H. *Biochemistry* **1989**, *28*, 4422.
(6) Komatsu, T.; Matsukawa, Y.; Tsuchida, E. *Bioconjugate Chem.* **2002**, *13*, 397.
(7) Peterson, C. E.; Ha, C. E.; Harohalli, K.; Park, D.; Bhagavan, N. V. *Biochemistry* **1997**, *36*, 7012.
(8) Adachi, S.; Nagano, S.; Watanabe, Y.; Ishimori, K.; Morishima, I. *Biochem. Biophys. Res. Commun.* **1991**, *180*, 138.
(9) Pond, A. E.; Roach, M. P.; Sono, M.; Rux, A. H.; Franzen, S.; Hu, R.; Thomas, M. T.; Eilks, A.; Dou, Y.; Ikeda-Saito, M.; Oritz de Montellano, P. R.; Woodruff, W. H.; Boxer, S. G.; Dawson, J. H. *Biochemistry* **1999**, *38*, 7601.
(10) Antonini, E.; Brunori, M. In *Hemoglobin and Myoglobin in Their Reactions with Ligands*; North-Holland Publishing: Amsterdam, 1971; p 18.
(11) Vickrey, L.; Nozawa, T.; Sauer, K. *J. Am. Chem. Soc.* **1976**, *98*, 343.
(12) Collman, J. P.; Brauman, J. I.; Iverson, B. L.; Sessler, J. L.; Moris, R. M.; Gibson, Q. H. *J. Am. Chem. Soc.* **1983**, *105*, 3052.
(13) Traylor, T. G.; Tsuchiya, S.; Campbell, D.; Mitchel, M.; Stynes, D.; Koga, N. *J. Am. Chem. Soc.* **1985**, *107*, 604.
(14) Komatsu, T.; Arai, K.; Nishide, H.; Tsuchida, E. *J. Chem. Soc., Dalton Trans.* **1993**, 1734.
(15) Maxwell, J. C.; Volpe, J. A.; Barlow, C. H.; Caughey, W. S. *Biochem. Biophys. Res. Commun.* **1974**, *58*, 166.
(16) (a) Jue, T.; Krishnamoorthi, R.; La Mar, G. N. *J. Am. Chem. Soc.* **1983**, *105*, 5701. (b) Yamamoto, Y.; La Mar, G. N. *Biochemistry* **1986**, *25*, 5288.
(17) Olson, J. S.; Mathews, A. J.; Rohlfs, R. J.; Springer, B. A.; Egeberg, K. D.; Sliger, S. G.; Tame, J.; Renaud, J.-P.; Nagai, K. *Nature* **1988**, *336*, 265.
(18) (a) Gibson, Q. H. *J. Biol. Chem.* **1970**, *245*, 1564. (b) Olson, J. S.; Melvin, E.; Andersen, E.; Gibson, Q. H. *J. Biol. Chem.* **1971**, *246*, 5919. (c) Steinmeier, R. C.; Parkhurst, L. J. *Biochemistry* **1975**, *14*, 1564.

JA046022T

Available online at www.sciencedirect.com

SCIENCE DIRECT®

Biochimica et Biophysica Acta 1675 (2004) 21–31

BIOCHIMICA ET BIOPHYSICA ACTA

BBA

http://www.elsevier.com/locate/bba

Physicochemical characterization of cross-linked human serum albumin dimer and its synthetic heme hybrid as an oxygen carrier

Teruyuki Komatsu[a], Yukiko Oguro[a], Yuji Teramura[a], Shinji Takeoka[a], Junpei Okai[b], Makoto Anraku[b], Masaki Otagiri[b], Eishun Tsuchida[a,*]

[a]*Advanced Research Institute for Science and Engineering, Waseda University, 3-4-1 Okubo, Shinjuku-ku, Tokyo 169-8555, Japan*
[b]*Department of Pharmaceutics, Faculty of Pharmaceutical Sciences, Kumamoto University, 5-1 Oe-honmachi, Kumamoto 862-0973, Japan*

Received 13 May 2004; received in revised form 9 August 2004; accepted 10 August 2004
Available online 11 September 2004

Abstract

The recombinant human serum albumin (rHSA) dimer, which was cross-linked by a thiol group of Cys-34 with 1,6-bis(maleimido)hexane, has been physicochemically characterized. Reduction of the inert mixed-disulfide of Cys-34 beforehand improved the efficiency of the cross-linking reaction. The purified dimer showed a double mass and absorption coefficient, but unaltered molar ellipticity, isoelectric point (p*I*: 4.8) and denaturing temperature (65 °C). The concentration dependence of the colloid osmotic pressure (COP) demonstrated that the 8.5 g dL^{-1} dimer solution has the same COP with the physiological 5 g dL^{-1} rHSA. The antigenic epitopes of the albumin units are preserved after bridging the Cys-34, and the circulation lifetime of the ^{125}I-labeled variant in rat was 18 h. A total of 16 molecules of the tetrakis{(1-methylcyclohexanamido)phenyl}porphinatoiron(II) derivative (FecycP) is incorporated into the hydrophobic cavities of the HSA dimer, giving an albumin–heme hybrid in dimeric form. It can reversibly bind and release O_2 under physiological conditions (37 °C, pH 7.3) like hemoglobin or myoglobin. Magnetic circular dichroism (CD) revealed the formation of an O_2–adduct complex and laser flash photolysis experiments showed the three-component kinetics of the O_2-recombination reaction. The O_2-binding affinity and the O_2-association and -dissociation rate constants of this synthetic hemoprotein have also been evaluated.

Keywords: Human serum albumin dimer; Cross-linking; Colloid osmotic pressure; Synthetic heme; Albumin–heme dimer; Oxygen carrier

1. Introduction

Human serum albumin (HSA) is the most abundant plasma protein and contains 35 cysteines, of which 17 couples form intramolecular disulfide bonds to fold a single polypeptide as a unique heart-shape structure [1–4]. Only the first thiol residue in the chain, namely Cys-34, does not participate in the S–S bonding and functions as a binding site for the SH-involving ligands (cysteine, glutathione, and captopril), as well as for the various metal ions and nitric oxide [1,5]. Interestingly, two albumin molecules can associate to produce a dimer through an intermolecular disulfide bridge of Cys-34; approximately 5% of HSA is actually in a dimeric form in our bloodstream [6]. Hughes [7] initially prepared the HSA dimer by the addition of bifunctional $HgCl_2$, which causes Cys-34 to connect through mercury. Subsequent oxidation of this mercury dimer by treatment with iodine gave a disulfide-linked HSA [8]. It can also be directly prepared by oxidation of HSA with ferricyanide [9]. However, electron spin resonance measurements of HSA and the latest crystal structural analysis of the recombinant HSA (rHSA) revealed that Cys-34 locates in a hydrophobic crevice at a depth of 9.5 Å from the surface [2–4,10]. This implies that the intermolecular Cys-34 disulfide bridging might lead to flattening of the pocket. We have linked two rHSA molecules with a flexible bola-shape spacer, 1,6-bis(maleimido)hexane (BMH), which is long (16 Å) enough to connect the Cys-34 residues, to produce a new type of rHSA dimer (Fig. 1) [11].

* Corresponding author. Tel.: +81 3 5286 3120; fax: +81 3 3205 4740.
E-mail address: eishun@waseda.jp (E. Tsuchida).

0304-4165/$ - see front matter © 2004 Elsevier B.V. All rights reserved.
doi:10.1016/j.bbagen.2004.08.010

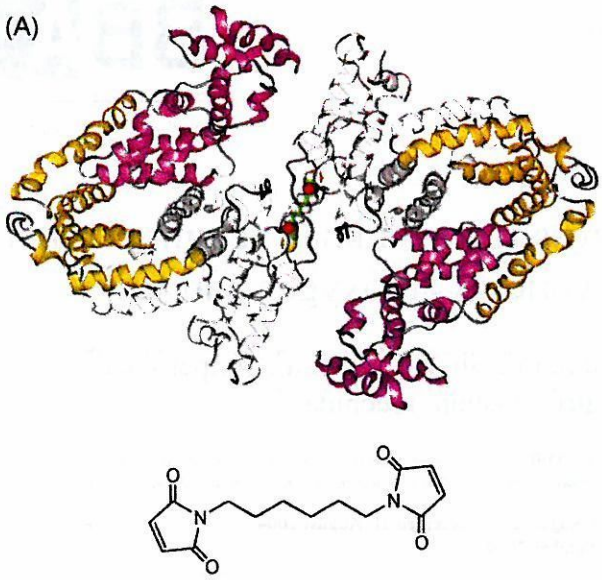

Fig. 1. (A) Simulated structure of rHSA dimer cross-linked by Cys-34 with 1,6-bis(maleimido)hexane (BMH). The domains I, II, and III of each rHSA unit are colored white, yellow, and pink, respectively. The cross-linking agent (BMH) is shown in a space-filling representation and colored by atom type (carbon: green, nitrogen: blue, oxygen: red). The figure was made with insight II (Molecular Simulations) on the basis of the 1e78 available at the Brookhaven PDB. (B) Formula of synthetic heme, FecycP.

On the other hand, a maximum of eight molecules of synthetic heme with a covalently bound proximal base is incorporated into the hydrophobic cavities of rHSA, giving an albumin–heme hybrid, which can reversibly bind and release O_2 under physiological conditions (pH 7.3, 37 °C) like hemoglobin (Hb) or myoglobin (Mb) [12]. We have shown that this O_2-carrying plasma protein acts as a red blood cell (RBC) substitute in vitro and in vivo [13]. The only fault of this system is its relatively low heme concentration, which reflects the O_2 solubility in the medium. For instance, the albumin–heme solution with a physiological HSA concentration (≈0.75 mM) involves 6 mM of heme, which corresponds to only 65% of the amount in human blood ([heme]=9.2 mM). A highly condensed solution can dissolve more heme, however, the colloid osmotic pressure (COP) increases in proportion to the albumin concentration. We have found that a total of 16 molecules of 2-[8-{*N*-(2-methylimidazolyl)}octanoyloxymethyl]-5,10,15,20-tetrakis{α,α,α,α-*o*-(pivalamido)phenyl}porphinatoiron(II) (FepivP) was incorporated into the BMH-bridged HSA dimer, and this solution with 0.75 mM HSA includes 12 mM of heme [11]. The tertiary structures of the two protein-units might be intact after the cross-linking, and the ligand-binding capacity of the dimer became twofold in excess relative to that of the monomer. Consequently, the saline solution of the albumin–heme dimer can transport a large volume of O_2 in comparison to the human blood while maintaining its COP on a physiological level. A long persistence in circulation due to the large molecular size is also expected. In this paper, we report the efficient synthesis, physicochemical characterization, and preliminary pharmacokinetics of the BMH-bridged rHSA dimer. Furthermore, the O_2-binding properties of the albumin-heme dimer incorporating the FepivP analogue, 2-[8-{*N*-(2-methylimidazolyl)}octanoyloxymethyl]-5,10,15,20-tetrakis{α,α,α,α-*o*-(1-methylcyclohexanamido)phenyl}porphinatoiron(II) (FecycP, Fig. 1), are evaluated by magnetic circular dichroism and laser flash photolysis.

2. Material and methods

2.1. Materials

An rHSA (Albrec®, 25 wt.%) was provided from the NIPRO (Osaka). Ethanol, dithiothreitol (DTT), 2,2′ -dithiopyridine, and warfarin (all high-purity grades) were purchased from Kanto Chemical, (Tokyo) and used without further purification. 1,6-Bis(maleimido)hexane was purchased from Pierce Biotechnology (Rockford, USA). Diazepam was purchased from Wako Pure Chemical Ind., (Tokyo). 2-[8-{*N*-(2-Methylimidazolyl)}octanoyloxymethyl]-5,10,15,20-tetrakis{α,α,α,α-*o*-(1-methylcyclohexanamido)phenyl}porphinatoiron(II) (FecycP) was prepared according to our previously reported procedure [14].

2.2. Synthesis of rHSA dimer

Aqueous DTT (1.0 M, 0.24 mL) was added to the phosphate buffer solution (pH 7.0, 10 mM) of rHSA (0.75 mM, 80 mL) under nitrogen, and the solution was quickly mixed by a vortex mixer, followed by an incubation for 30 min at room temperature. The obtained rHSA in reduced form was washed with a total of 880-mL phosphate buffer (pH 7.0, 2.25 mM) using an ADVANTEC UHP-76K ultrafiltration system with a Q0500 076E membrane (cutoff Mw 50 kDa) and finally condensed to 26.7 mL ([rHSA]=2.25 mM). The mercapto-ratio of the Cys-34

was confirmed by the reaction with 2,2′ -ditiopyridine (2,2′ -DTP), which immediately coupled with the free thiol group to give 2-thiopyridinone (2-TP) with an absorption at 343 nm [molar absorption coefficient (ε_{343}): 8.1×10^3 M^{-1} cm^{-1}]. Quantitative assay of the produced 2-TP showed that the mercapto-ratio of Cys-34 was 100%. Ethanolic BMH (6.38 mM, 4.76 mL) divided into three portions was then slowly added dropwise into the rHSA solution within 1 h under an N_2 atmosphere, and gently stirred overnight at room temperature. The reaction kinetics was observed by the HPLC measurements. The HPLC system consisted of a Shimadzu LC-8A pump and a Shimadzu SPD-10A UV detector. A Shodex Protein KW-803 column was used and the mobile phase was phosphate buffered saline (PBS, pH 7.4) at 25 °C (1.0 mL min^{-1}). The dimer was purified by gel column chromatography with Sephacryl S-200 HR (Pharmacia, 5 cmϕ×40 cm) and PBS (pH 7.4) as the eluant (5.0 mL min^{-1}). These separations were performed using a BIO-RAD EGP Combo Rec system. The elution was monitored by absorption at 280 nm. The purity of the dimer was measured by the HPLC technique described above. The albumin concentrations were assayed by general bromcresol green (BCG) methods using a Wako AlbuminB-Test [15].

2.3. Physicochemical properties

The UV–Vis absorption spectra were recorded on a JASCO V-570 spectrophotometer. The measurements were normally carried out at 25 °C. Circular dichroism (CD) spectra were obtained using a JASCO J-725 spectropolarimeter. The rHSA samples' concentration was 2 μM in PBS, and quartz cuvettes with a 1-mm thickness were used for the measurements over the range of 195–250 nm. The matrix associated laser desorption ionization time-of-flight mass spectra (MALDI-TOF MS) were obtained using a Shimadzu AXIMA-CFR Kompact MALDI, which was calibrated by BSA (Sigma A-0281) and HSA (Sigma A-3782). The specimens were prepared by mixing the aqueous sample solution (10 μM, 1 μL) and matrix (10 mg mL^{-1} sinapinic acid in 40% aqueous CH_3CN, 1 μL) on the measuring plate and drying in air. The viscosity and density of the rHSA solutions (PBS, pH 7.4) were obtained using an Anton PAAR DSC 300 capillary viscometer at 37 °C. The isoelectric points and molecular weights were obtained by a Pharmacia Phastsystem using isoelectric focusing (IEF) in Phast Gel IEF 3-9 and Native-PAGE in Phast Gel Gradient 8–25, respectively. The colloid osmotic pressures of the rHSA solutions (PBS, pH 7.4) were measured by a WESCOR 4420 Colloid Osmometer at 25 °C. A membrane filter with a 30-kDa cutoff was used. Differential scanning calorimetry (DSC) was measured on a SEIKO Instruments DCS120 differential scanning calorimeter at the scan rate of 1 °C min^{-1} in the temperature range between 10 and 95 °C. The concentrations of the rHSA samples were 75 μM in PBS (pH 7.4).

2.4. Ligand binding constants

The PBS solution of ligand (warfarin or diazepam, 20 μM, 2 mL) was mixed with the rHSA sample in PBS (20 μM, 2 mL), and the unbound ligand fractions were separated by centrifugation (2000 rpm, 25 °C, 20 min) using a Millipore Centriplus YM-50. Adsorption of the ligand molecules onto the filtration membranes was negligible. The unbound ligand concentrations were determined by UV–Vis spectroscopic measurements.

2.5. Compatibility with blood components in vitro

Fresh whole blood was obtained from Wistar rats (300 g, male, Saitama Experimental Animals Supply, Japan) and stored in heparinized glass tubes. The rHSA samples (PBS, pH 7.4) were then slowly added to the blood at 50 vol.% concentrations (whole volume 2 mL). After 30 min, 30 μL of the sample was mixed with 100 μL of a Terumo ACD-A solution, which was diluted in advance with pure water by 1:10 (v/v). The blood cell numbers of the obtained samples were counted using a Sysmex KX-21 blood cell counting device. Furthermore, one drop of the incubated sample of the blood with the rHSA dimer was microscopically observed using an Olympus IX50 microscope with an IX70 CCD camera.

2.6. Immunogenicity

The Tris–HCl buffer solutions (TBS, pH 7.4, 50 mM, 50 μL) of the rHSA samples (10 μg mL^{-1}) were injected into a Nunc immunoplate and incubated at 4 °C overnight. The rHSA solutions in the wells were washed with TBS, and 2% skimmed milk was added to avoid the nonspecific binding of the antibody. After washing with TBS including 0.1% Tween 20 (Tween 20–TBS), anti-HSA polyclonal antibody (50 μL per well) was added and incubated for 2 h at 25 °C. The antibody was removed by aspiration, and 50 μL of horseradish peroxidase-labelled rabbit anti-IgG polyclonal antibody diluted 1/5000 by Tween 20–TBS was injected, following an incubation for 1 h at 25 °C. Finally, 100 μL of *o*-phenylenediamine substrate solution (400 mg mL^{-1} in 0.15 M citrate-phosphate buffer (pH 5.0) involving 0.1% H_2O_2) was put into each well. H_2SO_4 (2 M; 50 μL) was then added to stop the reaction. The resulting absorbance in each well was measured at 490 nm using a Japan InterMed Imunomini NJ-2300.

2.7. Circulation lifetime in vivo

The 125-Iodinated rHSA monomer and dimer were prepared by our previously reported procedures, and purified using a Pharmacia Bio-Gel PD-10 column [16]. The recovered ^{125}I-albumin had a specific activity of 2.0×10^7 cpm μg^{-1}, and was diluted by non-labeled albumin before intracardial administration into anesthetized Wistar rats

(200–210 g, male). The kinetics of the albumin clearance from the circulation was monitored by measuring the radioactivity in the plasma phase of blood taken from the lateral tail veins using an Aloka ARC 2000 Autowell Gamma Counter. Acid precipitability of the recovered radioactivity was also measured. The aqueous trichloroacetic acid (TCA, 25%, 0.1 mL) was first added to the plasma (20 μL) diluted with 5 g dL^{-1} rHSA (80 μL), followed by centrifugation (3000 rpm, 10 min). The precipitate was then washed with 12.5% TCA (0.2 mL) and the radioactivity of the pellet was measured. The rats were sacrificed at the end of the experiments by hemorrhage. The radioactivity of the excised organs was also measured as well. The care and handling of the animals were in accordance with NIH guidelines.

2.8. Preparation of albumin–heme dimer

The preparation of rHSA–FecycP dimer was carried out by mixing the EtOH solution of carbonyl-FecycP and an aqueous phosphate buffer solution of rHSA according to our previously reported procedures ([FecycP]/[rHSA]=16:1 (mol/mol)) [13]. The albumin concentrations were assayed by the general BCG methods described above, and the amount of FecycP was determined by the assay of the iron ion concentration using inductively coupled plasma spectrometry (ICP) with a Seiko Instruments SPS 7000A spectrometer.

2.9. Magnetic circular dichroism (MCD)

MCD spectra for the phosphate buffer solution of the rHSA–FecycP dimer (10 μM) under N_2, CO, and O_2 atmospheres were measured using a JASCO J-820 circular dichrometer fitted with a 1.5-T electromagnet. The accumulation times were normally three, and from each data point was subtracted the spectra without an electromagnetic (at 0 T) as the baseline.

2.10. O_2-Binding equilibrium and kinetics

O_2-Binding to FecycP was expressed by Eq. (1).

$$\text{FecycP} + O_2 \underset{k_{off}}{\overset{k_{on}}{\rightleftharpoons}} \text{FecycP}(O_2) \quad (K = k_{on}/k_{off}) \tag{1}$$

The O_2-binding affinity (gaseous pressure at half O_2-binding for heme, $P_{1/2}=1/K$) was determined by spectral changes at various partial pressure of O_2 as in previous reports [12,a,d,14]. The FecycP concentrations of 20 μM were normally used for the UV–Vis absorption spectroscopy. The spectra were recorded within the range of 350–700 nm. The half lifetime of the dioxygenated species of the rHSA–FecycP dimer was determined by the time dependence of the absorption intensity at 549 nm, which is based on the O_2–adduct complex. The association and dissociation rate constants for O_2 (k_{on}, k_{off}) were measured by a competitive rebinding technique using a Unisoku TSP-600 laser flash photolysis apparatus [12,17–19]. The absorption decays accompanying the O_2 association to the rHSA–FecycP dimer obeyed three-component kinetics. We employed triple-exponentials to analyze the absorption decays; $\Delta A(t)$ [12,a,b,],

$$\Delta A(t) = C_1\exp(-k_1 t) + C_2\exp(-k_2 t) + C_3\exp(-k_3 t) \tag{2}$$

where k_1, k_2, k_3 are apparent rate constants for the each reaction. The data were fit to this equation using a Solver in Excel 2003.

3. Results and discussion

3.1. Synthesis of rHSA dimer

In the neutral pH range (5.0–7.0), DTT selectively reduces the mixed-disulfide of Cys-34 in HSA or BSA [20–22]. In fact, the addition of the small molar excess DTT into the rHSA solution (phosphate buffer, pH 7.0, 10 mM) under an N_2 atmosphere led to complete reduction of Cys-34 (mercapto-ratio became 100%). After removing DTT, ethanolic BMH was dropwise added to the reduced rHSA to initiate the cross-linking reaction. The pretreatment with DTT significantly increased the yield of the dimer, and the rHSA concentration of 15 g dL^{-1} gave the highest yield of 45%, which is significantly improved from our previous result (Fig. 2) [11]. Several attempts to facilitate the dimerization

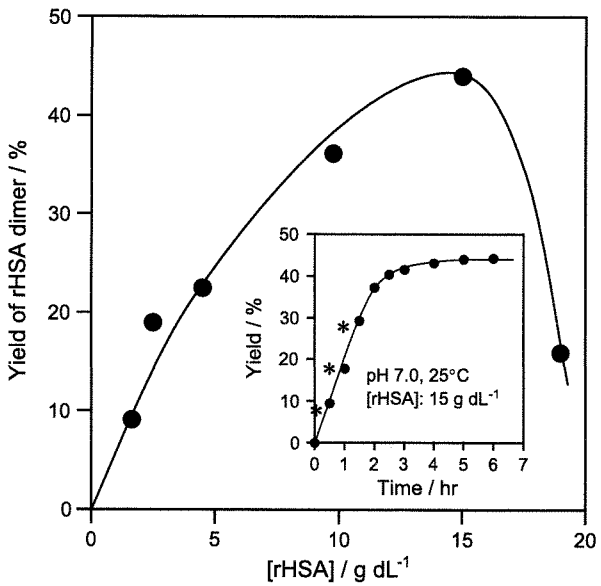

Fig. 2. The relationship between the rHSA concentration and yield of the rHSA dimer. The yields were determined based on the peak area in the HPLC elution curves. Inset shows the time course of the dimerization yield when the rHSA concentration was set at 15 g dL^{-1}. The asterisks indicate the time points when the EtOH solution of BMH was dropwise added. The total EtOH content in the reaction mixture was 15 vol.%.

unfortunately failed: (i) gentle heating (25–50 °C), (ii) changing the co-solvent from EtOH to DMF for dissolving the BMH, and molar ratio [BMH]/[rHSA]: 0.5–1.5, (iii) increasing the concentrations of co-solvents (<30%), and (iv) the further addition of the reactive rHSA monomer.

The HPLC elution curve of the reactant demonstrated only two peaks (rHSA monomer and dimer), which means that the bifunctional BMH was successfully bound to Cys-34 which led to dimer formation and not polymerization (Fig. 3). The yield reached a peak within 4 h (Fig. 2 inset). The addition of EtOH to the mixture (40 vol.%) immediately formed a white precipitate; this is similar to the well-known Cohn's methods [1,23]. However, the precipitate still contained the monomer component. In contrast, separation using gel column chromatography with Sephacryl S-200 HR gave the dimer with 99% purity and 80% recovery. Native-PAGE showed a single band in the molecular weight range of 13 kDa (Fig. 3, above). We could not detect the free thiol in the isolated rHSA dimer (mercapto-ratio: 0%), which is now available in gram quantities. The appearance of the obtained dimer solution (in PBS, 20 g dL^{-1}) did not change over 1 year at room temperature and underwent no aggregation and precipitation.

3.2. Physicochemical properties

The matrix associated laser desorption ionization time-of-flight mass spectroscopy (MALDI-TOF MS) of the BMH-bridged rHSA dimer showed a distinct sharp signal at *m/z* 132,741.3, which is in good agreement with the calculated mass (Mw. 133,179.6); the difference was only 0.3% (Table 1). The magnitudes of its UV–Vis absorption (λ_{max}: 280 nm) significantly increased compared to that of

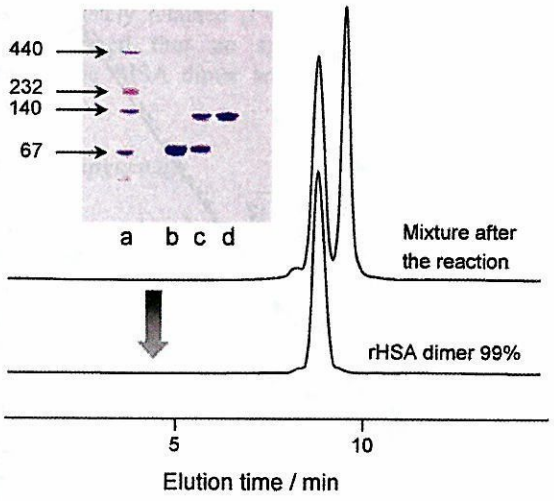

Fig. 3. HPLC elution curves of the rHSA dimer at 25 °C. The upper profile after the reaction indicated that the reactant consists of only the monomer and dimer. After gel column chromatography, the rHSA dimer was isolated with the purity of 99%. The left upper pattern is the native-PAGE electrophoresis of the rHSA dimer. a: markers, b: rHSA, c: mixture after the reaction, d: purified rHSA dimer.

Table 1
Physicochemical properties of rHSA dimer

	rHSA	rHSA dimer
Mw (Da)	66,331[a]	132,741[a]
	66×10^3 [b]	136×10^3 [b]
[calculated value]	66,451	133,180
Cys-34 mercapto ratio (%)	17	0
p*I*	4.8	4.8
ε_{280} (cm^{-1} M^{-1})	3.4×10^4	6.8×10^4
$[\theta]_{208}$ (deg cm^2 $dmol^{-1}$)	1.9×10^4	1.9×10^4
$[\theta]_{222}$ (deg cm^2 $dmol^{-1}$)	1.8×10^4	1.8×10^4

[a] Determined by MALDI-TOF/MS.
[b] Determined by [C] vs. COP/[C] (Fig. 5, inset).

rHSA with the same molar concentrations (Fig. 4(A)). The concentration of the albumin was carefully assayed by (i) BCG method [15] and (ii) weighing method with the weight of the freeze-dried sample and its molecular weight. While the molar absorption coefficient at 280 nm (ε_{280}: 6.8×10^4 M^{-1} cm^{-1}) became exactly twice the monomer's value (3.4×10^4 M^{-1} cm^{-1}), the CD spectral pattern (λ_{min}: 208, 222 nm) and the molar ellipticities at 208 and 222 nm ($[\theta]_{208}$: 1.9×10^4 deg cm^2 $dmol^{-1}$, $[\theta]_{222}$: 1.8×10^4 deg cm^2 $dmol^{-1}$) were identical to those of the monomer (Fig. 4(B), Table 1) [24,25]. It is appropriate to consider that the α-helix content of the each rHSA unit (67%) was unaltered [1–4]. The isoelectric point of the dimer (*p*I: 4.8) was also the same as that of rHSA. All these observations suggested that the secondary/tertiary structure and surface net charges of the rHSA units in the dimer did not change after the S–S disulfide bridging of Cys-34.

The DSC thermogram of this rHSA dimer showed an exothermic peak at 65 °C, which corresponds to its denaturing temperature (T_d). It has been shown that the T_d of HSA is largely dependent on the content of the

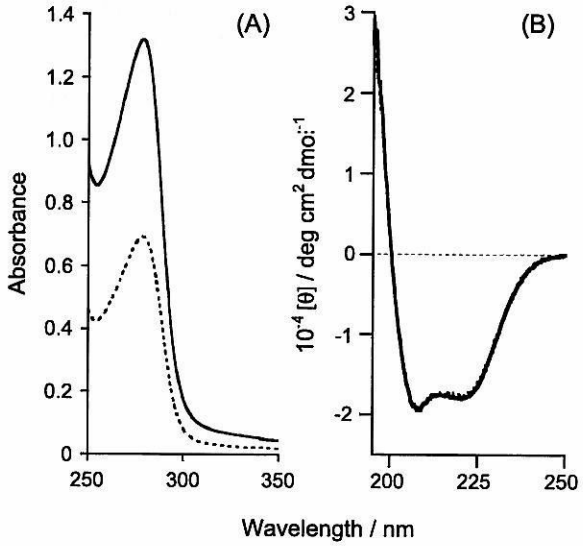

Fig. 4. (A) UV–Vis absorption spectra and (B) CD spectra of rHSA monomer (dotted line) and rHSA dimer (solid line) in PBS solution (pH 7.4) at 25 °C.

incorporated fatty acid, pH, and ionic strength [26,27]. In general, pasteurization for plasma HSA is performed at 60 °C for 10 h to eliminate the contaminations, e.g., hepatitis, HIV, and herpes virus [1]. Sodium caprylate and sodium *N*-acetyl-L-tryptophanate are commonly added to stabilize the albumin structure during the heat treatment [26]. Since the thermogram of the rHSA monomer under our sample conditions (PBS, pH 7.4) showed the T_d at 63 °C, we concluded that the rHSA dimer has the same thermodynamic stability with the monomer. Only the enthalpy change during the denaturation (ΔH) was slightly lower than the twice the monomer's value.

HSA acts as a carrier for many endogenous and exogenous substances in the blood circulation, and has two major specific drug binding sites, namely the warfarin site (Site I) and the indole and benzodiazepine site (Site II) [1,28]. We then determined the binding constants of typical ligands, warfarin (Site I-ligand) and diazepam (Site II-ligand), for the rHSA dimer using the ultracentrifugation method. In contrast to the results of the control experiments with rHSA, the amount of unbound ligand decreased to nearly half. The equilibria are expressed by following equations:

$$D + L \overset{K_1}{\rightleftharpoons} D\text{-}L \quad (3)$$

$$D\text{-}L + L \overset{K_2}{\rightleftharpoons} D\text{-}L_2 \quad (4)$$

$$D + 2L \overset{K_1K_2}{\rightleftharpoons} D\text{-}L_2 \quad (5)$$

where D is the rHSA dimer and L represents the ligand. The apparent binding constants (K_1K_2) of the warfarin and diazepam to the dimer were calculated to be 9.2×10^{10} and 3.0×10^{10} M^{-2}, respectively. If the each albumin unit independently accommodates one ligand, we estimated K_1 ($=K_2$) of each ligand as the square root of these values; 3.0×10^5 and 1.7×10^5 M^{-1}, respectively. They are almost in the same range as the binding constants for the monomeric rHSA (K_1), 3.8×10^5 and 1.4×10^5 M^{-1}, which means that neither the prevention nor the cooperation of the second ligand binding occurred in the dimer.

The attempt to prepare single crystals of the rHSA dimer for X-ray structural analysis failed, probably because it is likely to be very flexible at the BMH moiety. Transmission electron microscopy of the negatively stained samples showed homogeneous round particles with a diameter of 15–20 nm (not shown), however, the image is too small to obtain precise morphological information about the molecule.

The primary physiological function of HSA is the maintenance of COP within the blood vessels. Although HSA accounts for only 60% of the mass of the plasma protein, it contributes 80% of the COP. Two-thirds of this COP is simply the van't Hoff pressure and the other third arises from the Donnan effect of the negative charges of the plasma proteins, which is essentially due to albumin [1]. The relationship between the protein concentration and COP was observed for the rHSA and rHSA dimer solutions (Fig. 5). Both lines deviated upward from the linear correlation, because of the relatively larger value of the second virial coefficient, which is an index of the COP capacity, of the albumin molecule compared to those of the other plasma proteins. The measured rHSA monomer's curve coincided well to the previously reported result of Scatchard and co-workers (dotted line) [29]. The physiological concentration (5 g dL^{-1}) of rHSA represented the COP of 19 Torr. The careful inspections of their COP curves revealed that the 8.5 g dL^{-1} dimer solution has the same COP as the 5 g dL^{-1} rHSA. The plots of [C] versus COP/[C] gave a straight line, and the extrapolations to the y intercept afford the molecular weights of the monomer and dimer of 66×10^3 and 136×10^3 Da, respectively.

3.3. Viscosity and compatibility with blood components

Viscosity is a characteristic of proteins related to their size, shape, and conformation. The PBS solution of 8.5 g dL^{-1} rHSA dimer exhibited a Newtonian flow similar to the 5.0 g dL^{-1} rHSA, and showed a viscosity of 1.2 cP at a shear rate of 230 s^{-1} (Fig. 6). The dimer solution was then mixed with freshly drawn whole blood (1:1, v/v). The obtained suspension did not show any coagulation or precipitation for 6 h at 37 °C (after 6 h, hemolysis gradually took place even in the control experiment with saline or rHSA), and its viscosity profile was again Newtonian (1.8 cP at 230 s^{-1}). This result demonstrated good compatibility of the rHSA dimer with blood.

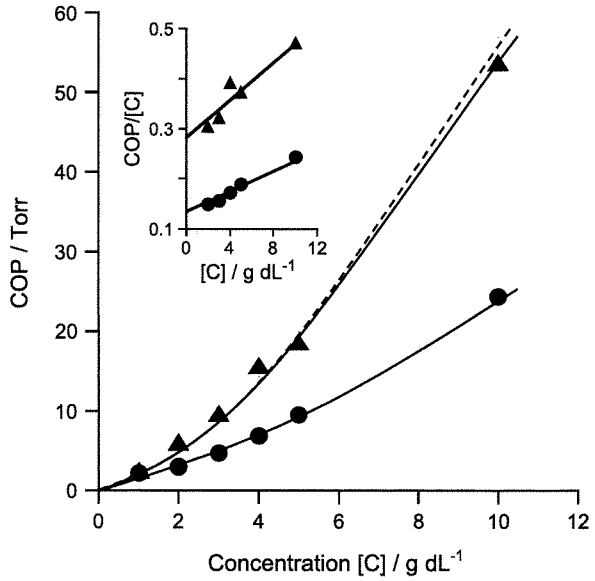

Fig. 5. Concentration [C] dependence of COP of rHSA monomer (▲) and rHSA dimer (●) in PBS (pH 7.4) at 22 °C. The dotted line represents the plasma HSA results taken from Ref. [29]. Inset shows relationship between [C] and COP/[C] for rHSA monomer (▲) and rHSA dimer (●).

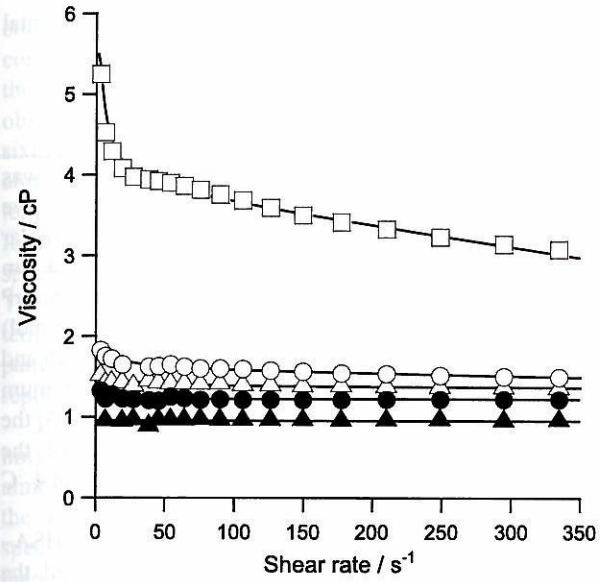

Fig. 6. Changes in the viscosity of rHSA monomer and rHSA dimer at various shear rates at 37 °C [□: whole blood, ●: 8.5 g dL^{-1} rHSA dimer, ▲: 5.0 g dL^{-1} rHSA, ○: 8.5 g dL^{-1} rHSA dimer plus whole blood (1:1, v/v), △: 5.0 g dL^{-1} rHSA plus whole blood (1:1, v/v)].

In order to evaluate the blood compatibility of the 8.5 g dL^{-1} rHSA dimer solution in detail, the changes in the number of blood cell components [RBC, white blood cells (WBC), and platelets (PLT)] have been counted after the mixture (1:1, v/v). The numbers just after the addition of the rHSA dimer to the whole blood were reasonably reduced to half the basal values; the same behavior was observed in the control experiments with the saline or 5 g dL^{-1} rHSA [Fig. 7(A)]. Optical microscopic observations revealed that the homogeneous round shape of the RBCs was completely retained [Fig. 7(B)(C)]. Therefore, it can be considered that no specific interaction occurred between the rHSA dimer and the blood cell components in vitro.

3.4. Immunogenicity

We then analyzed the immunological reactivity of the rHSA dimer against the anti-HSA polyclonal antibody. The absorption intensity of the reactant plate with the dimer showed clear concentration dependence in the same manner as those of the rHSA and plasma HSA groups (Fig. 8). It is known that HSA has five major antigenic sites by analysis using synthetic peptides [30,31]. The sites are nearly α-helical regions in the HSA molecule and include charged and/or aromatic residues which are important for the presentation of antigenic determinations. We previously reported that the cross-reactivity of the anti-HSA polyclonal antibody to BSA was extremely low, despite their homologies of the sequences over 70% and its antigenic sites in the same regions [32]. The antigenic epitopes of rHSA are preserved after bridging the Cys-34.

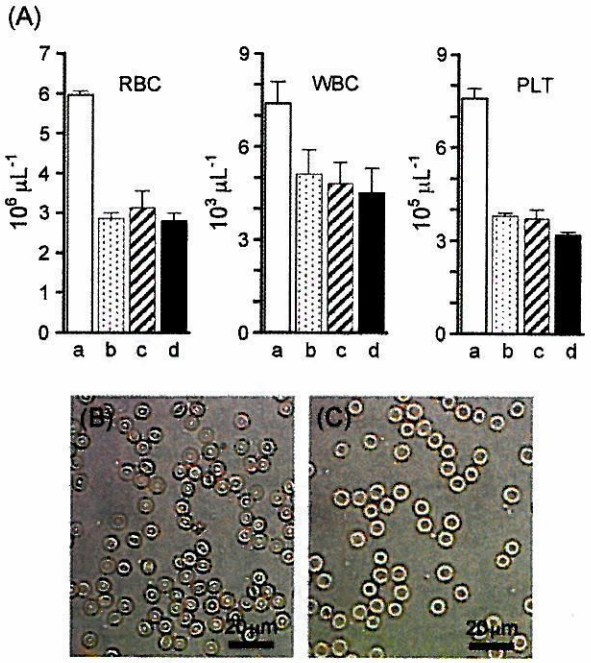

Fig. 7. (A) The blood cell (RBC, WRC, PLT) numbers in the blood suspension with the rHSA samples (1:1, v/v) at 25 °C [a: whole blood (basal value), b: with saline, c: with 5.0 g dL^{-1} rHSA, d: with 8.5 g dL^{-1} rHSA dimer]. Optical microscopic observations of (B) whole blood and (C) the blood suspension with the 8.5 g dL^{-1} rHSA dimer (1:1, v/v) (bar: 20 μm). The shape of the RBC with a diameter of ca. 8 μm did not change.

3.5. Circulation lifetime of ^{125}I-labeled rHSA dimer in rats

The rHSA and rHSA dimer labeled with ^{125}I were injected into rats to determine their blood circulation

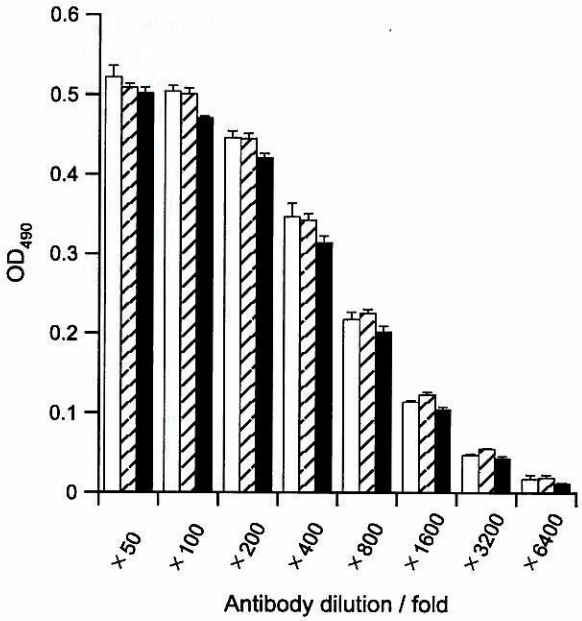

Fig. 8. Cross-reactivity of the anti-HSA polyclonal antibody with rHSA monomer and rHSA dimer [white bar: plasma HSA, diagonal bar: rHSA monomer, black bar: rHSA dimer]. All values are mean±S.D. (n=3).

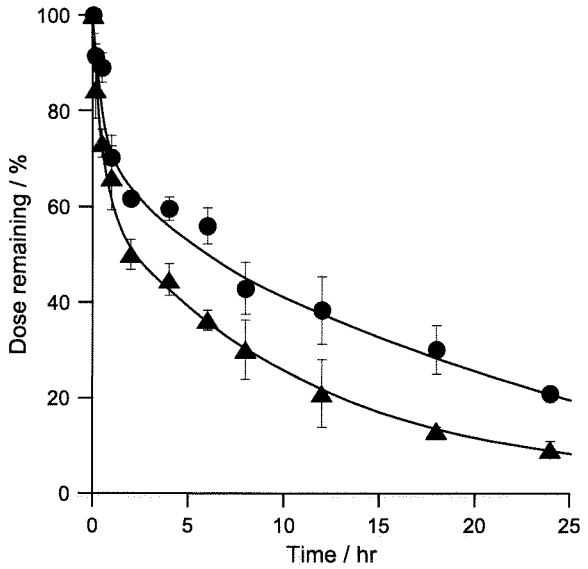

Fig. 9. Plasma levels of ^{125}I-rHSA monomer and dimer (1.0×10^7 cpm, 1.0 mg kg^{-1}) after intracardial administration into Wistar rats. All values are mean±S.D. (n=3).

lifetimes. The time courses of the radioactivity clearly showed two-phase kinetics, and significant differences between these two samples (Fig. 9). The half lifetimes ($\tau_{1/2}$) determined from the disappearance phase (β-phase) were 8.9 and 16.2 h for the monomer and dimer, respectively. The enlargement of the molecular size definitely led to retardation of extravasation through the vascular endothelium and produced a longer lifetime in the bloodstream. Radioactivity of the trichloroacetic acid precipitates recovered up to 95% the intensity, which means ^{125}I did not dissociate from the proteins. The tissue distributions of the rHSA dimer were in the skin, liver, kidney, and spleen (not shown), which took up most of the radioactivity, and we could not find any differences to that of the rHSA monomer.

More recently, McCurdy et al. [33] reported that a reiterated form of recombinant rabbit serum albumin (rRSA), in which two copies of the C34A rRSA mutant were joined with the C-terminus and N-terminus by a hexaglycine spacer, was more rapidly cleared ($\tau_{1/2}$: 3.0 days) in vivo (rabbit) than the corresponding monomer, C34A rRSA ($\tau_{1/2}$: 4.9 days). They postulated that the mechanism of this quick clearance of the dimer appears to involve the reticuloendothelial system (two binding sites on a dimer molecule to phagocytic cells may underlie the increased rate); and also suggested that the albumin dimerization through Cys-34 probably does not substantially contribute to the albumin metabolism. However, our results clearly showed that the Cys-34 BMH-bridged rHSA dimer has the longer circulation lifetime relative to that of the rHSA monomer. This opposite conclusion presumably arises from the differences in the chemical structure of the cross-linking agents, highly-ordered structure of the albumin dimer itself, and mammal species in the experimental protocol.

3.6. Albumin–heme dimer and its O_2-binding

Since a maximum of eight FecycPs (Fig. 1) was incorporated into certain domains of rHSA [12,d,], we postulated that the rHSA dimer can capture a twofold molar excess of FecycP molecules relative to the monomer. From the quantitative analyses of the amount of rHSA and FecycP in the hemoprotein, the ratio of the FecycP/rHSA (mol/mol) was determined to be 15.7 for the mixing ratio (m) of 16 and 16.4 for the m of 20. Thus, we concluded that the maximum binding numbers of FecycP to an rHSA dimer were 16, the same as FepivP [11]. The obtained red-solution of the rHSA–FecycP dimer was stored for more than 1 year at 4 °C without any aggregation and precipitation.

The UV–Vis absorption spectrum of the aqueous rHSA–FecycP dimer solution in an N_2 atmosphere showed the formation of a typical five-N-coordinate high-spin complex of porphyrinatoiron(II) (λ_{max}: 444, 539, 565 nm) [12,14,17,19]. Upon exposure of this solution to O_2, the absorption spectral pattern immediately changed to that of a dioxygenated species (λ_{max}: 426, 549 nm). This O_2-binding reaction was reversible and kinetically stable under physiological conditions (pH 7.3, 37 °C). After admitting the CO gas, the O_2–addcut complex moved to the very stable carbonyl low-spin complex (λ_{max}: 427, 539 nm) (Fig. 10).

We then employed MCD spectroscopy to characterize the coordination structure of the FecycP in the rHSA dimer. Under an N_2 atmosphere, the MCD showed a well-characterized spectrum of a mono-imidazole ligated five-

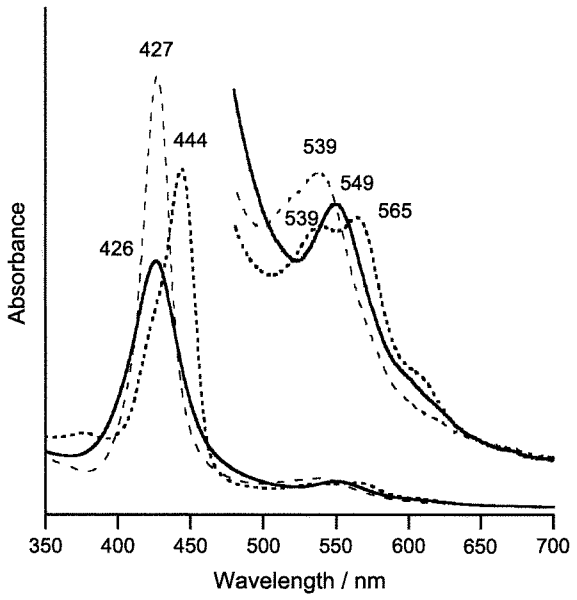

Fig. 10. UV–Vis absorption spectral changes of the rHSA–FecycP dimer in phosphate buffer solution (pH 7.3) at various conditions (25 °C) (dotted line: under N_2; solid line: under O_2; broken line: under CO).

coordinate high-spin porphyrinatoiron(II), which is in contrast to that of the six-coordinate low-spin state with the bis-imidazole ligated complex (Fig. 11) [34]. This observation indicates that no amino acid residue binds to the sixth position of FecycP in the rHSA structure under an N_2 atmosphere. The admission of O_2 gas yields an S-shaped A-term MCD in the Soret-band region, which shows the formation of an O_2–adduct complex as observed in the spectra of the other dioxygenated porphyrinatoiron(II) [34]. The CO adduct is also low spin and showed a similar A-term MCD band with a strong intensity. In all cases, the pattern in the Q-band regions coincided well with those reported previously [34].

The autooxidation reaction of the oxy state (λ_{max}: 549 nm) slowly occurred and the absorption intensity of 549 nm almost disappeared after 36 h, leading to the formation of the inactive Fe(III)cycP. The half-life of the dioxygenated species ($\tau_{1/2}$) was 6 h at 37 °C, which is significantly longer than that of our previous results for the rHSA–FepivP dimer ($\tau_{1/2}$: 2 h) [11]. The hydrophobic cyclohexanoyl fences on the porphyrin ring plane could effectively retard the autooxidation through the proton-driven process.

3.7. O_2-Binding kinetics and equilibrium of albumin–heme dimer

The association and dissociation rate constants for O_2 (k_{on}, k_{off}) were explored by laser flash photolysis. The absorption decays accompanying the O_2 recombination were composed of three-component kinetics, and the curves were fit by a triple-exponential equation [12,a,b,14]. The minor (less than 12%) component k_1, which is the fastest rate constant, is presumably correlated with a base elimination reaction [35]. From the slope of the linear plots of k_2 and k_3 versus the O_2 concentration, two association rate constants for the fast O_2 rebinding (k_{on}) and the slow O_2 rebinding were obtained (Table 2). The k_{on} values are 5.8-fold grater than k'_{on}, and the amplitude ratio of the fast and slow reactions was approximately 5/3. The O_2 association to FecycPs incorporated in the certain domains of the rHSA dimer is largely influenced by the protein environments surrounding each iron center of FecycP, for example, steric hindrance by the amino acid residues and/or difference in polarity. Six of the 16 sites of FecycP in the rHSA dimer are estimated to be the slow sites for the O_2 association.

Table 2
O_2-Binding parameters of the rHSA–FecycP dimer in phosphate buffer solution (pH 7.3) at 25 °C

	k_{on} (M^{-1} s^{-1})	k'_{on} (M^{-1} s^{-1})	k_{off} (s^{-1})	k'_{off} (s^{-1})	$P_{1/2}$ (Torr)[a]
rHSA–FecycP dimer	2.8×10^7	4.8×10^6	6.7×10^2	1.2×10^2	38
rHSA–FecycP	4.6×10^7	7.3×10^6	9.8×10^2	1.6×10^2	35
Hb (T-state)[b]	2.9×10^6		1.8×10^2		40

[a] At 37 °C. [b]pH 7.0, 20 °C, from Ref. [36].

The O_2-binding affinity ($P_{1/2}$) of the rHSA–FecycP dimer was determined to be 38 Torr at 37 °C on the basis of the UV–Vis spectral changes by O_2 titration [12,14,17–19]. The obtained $P_{1/2}$ is very close to that of rHSA–FecycP in the monomeric form and T-state Hb (Table 2) [12,d,35]. The O_2-dissociation rate constants were also calculated by k_{on}/K.

The rHSA–FecycP dimer did not show a cooperative O_2-binding profile like that seen in RBC; the Hill coefficient was 1.0 (Fig. 12). Although $P_{1/2}$ is slightly lower than that of RBC, the O_2-transporting efficiency (OTE) of the rHSA–FecycP dimer between the lungs (P_{O_2}: 110 Torr) and muscle

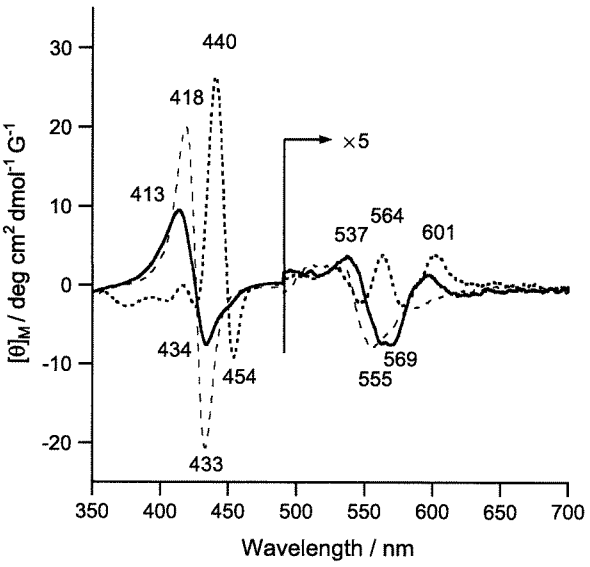

Fig. 11. MCD spectral changes of the rHSA–FecycP dimer in phosphate buffer solution (pH 7.3) at various conditions (25 °C) (dotted line: under N_2; solid line: under O_2; broken line: under CO).

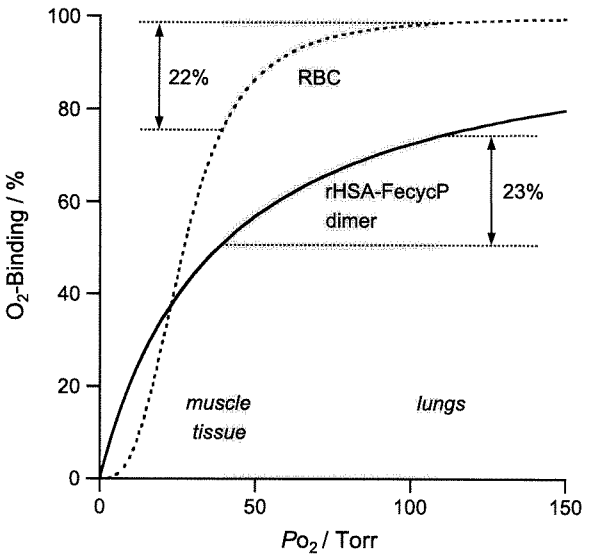

Fig. 12. OEC curve of the rHSA–FecycP dimer at 37 °C.

tissue (P_{O_2}: 40 Torr) (23%) becomes slightly higher than that of the human RBC (22%).

4. Conclusions

The obvious characteristics of the rHSA dimer cross-linked with the bola-shaped bismaleimide are as follows: (i) unaltered essential properties of the albumin units (the secondary/tertiary structure, surface net charges, thermostability), (ii) excess ligand-binding capacity relative to the monomer while maintaining its COP at the physiological value, (iii) good blood compatibility and identical antigenic epitopes with the monomer, and (iv) longer half-life in the bloodstream and similar tissue distributions with rHSA. Furthermore, (v) one molecule of the rHSA dimer incorporates 16 FecycPs, which is exactly twice the amount compared to that of the monomeric rHSA, and the obtained hemoprotein can reversibly bind and release O_2 under physiological conditions. (vi) The 8.5 g dL^{-1} rHSA–FecycP dimer solution satisfies the initial clinical requirements for the O_2-carrier as an RBC substitute, which transports 10 mM O_2 (compared to 9.2 mM in the human blood) while maintaining the COP at a constant 19 Torr.

Acknowledgements

This work was partially supported by Grant-in-Aid for Scientific Research (no. 16350093) from JSPS, and Grant-in-Aid for Exploratory Research (no. 16655049) from MEXT Japan, and Health Science Research Grants (Regulatory Science) from MHLW Japan.

References

[1] T. Peters Jr., All about Albumin. Biochemistry, Genetics, and Medical Applications, Academic Press, San Diego, 1996, and reference therein.
[2] D.C. Carter, J.X. Ho, Structure of serum albumin, Adv. Protein Chem. 45 (1994) 153–203.
[3] S. Curry, P. Brick, N.P. Franks, Fatty acid binding to human serum albumin: new insights from crystallographic studies, Biochim. Biophys. Acta 1441 (1999) 131–140.
[4] S. Sugio, A. Kashima, S. Mochizuki, M. Noda, K. Kobayashi, Crystal structure of human serum albumin at 2.5 Å resolution, Protein Eng. 12 (1999) 439–446.
[5] DJ. Meyer, H. Kramer, N. Özer, B. Coles, B. Ketterer, Kinetics and equiliburia of *S*-nitrosothiol–thiol exchange between glutathione, cysteine, penicillamines and serum-albumin, FEBS Lett. 345 (1994) 177–180.
[6] T. Peters Jr., Serum albumin, Adv. Protein Chem. 37 (1985) 161–245.
[7] a W.L. Hughes, The proteins of blood plasma, in: H. Neurath, K. Bailey (Eds.), The Proteins, vol. IIB, Academic Press, New York, 1954, pp. 663–734;
b W.L. Hughes, H.M. Dintzis, Crystallization of the mercury dimers of human and bovine mercaptalbumin, J. Biol. Chem. 239 (1964) 845–849.
[8] R. Straessle, A disulfide dimer of human mercaptalbumin, J. Am. Chem. Soc. 76 (1954) 3138–3142.
[9] L.-O. Anderson, Hydrolysis of disulfide bonds in weakly alkaline media II. Bovine serum albumin dimer, Biochim. Biophys. Acta 117 (1966) 115–133.
[10] C.N. Cornell, R. Chang, L.J. Kaplan, The environment of the sulfhydryl group in human plasma albumin as determined by spin labeling, Arch. Biochem. Biophys. 209 (1981) 1–6.
[11] T. Komatsu, K. Hamamatsu, E. Tsuchida, Cross-linked human serum albumin dimer incorporating sixteen (tetraphenylporphinato)iron(II) derivatives: synthesis, characterization, and O_2-binding property, Macromolecules 32 (1999) 8388–8391.
[12] (a) E. Tsuchida, T. Komatsu, Y. Matsukawa, K. Hamamatsu, J. Wu, Human serum albumin incorporating tetrakis(*o*-pivalamido)phenylporphinatoiron(II) derivative as a totally synthetic O_2-carrying hemoprotein, Bioconj. Chem. 10 (1999) 797–802;
(b) T. Komatsu, Y. Matsukawa, E. Tsuchida, Kinetics of CO and O_2 binding to human serum albumin–heme hybrid, Bioconj. Chem. 11 (2000) 772–776;
(c) T. Komatsu, Y. Matsukawa, E. Tsuchida, Reaction of nitric oxide with synthetic hemoprotein, human serum albumin incorporating tetraphenylporphinatoiron(II) derivatives, Bioconj. Chem. 12 (2001) 71–75;
(d) T. Komatsu, Y. Matsukawa, E. Tsuchida, Effect of heme structure on O_2-binding properties of human serum albumin–heme hybrids: intramolecular histidine coordination provides a stable O_2–adduct complex, Bioconj. Chem. 13 (2002) 397–402.
[13] (a) E. Tsuchida, T. Komatsu, K. Hamamatsu, Y. Matsukawa, A. Tajima, A. Yoshizu, Y. Izumi, K. Kobayashi, Exchange transfusion of albumin–heme as an artificial O_2-infusion into anesthetized rats: physiological responses, O_2-delivery and reduction of the oxidized hemin sites by red blood cells, Bioconj. Chem. 11 (2000) 46–50;
(b) Y. Huang, T. Komatsu, A. Nakagawa, E. Tsuchida, S. Kobayashi, Compatibility in vitro of albumin–heme (O_2-carrier) with blood cell components, J. Biomed. Mater. Res. 66A (2003) 292–297;
(c) E. Tsuchida, T. Komatsu, Y. Matsukawa, A. Nakagawa, H. Sakai, K. Kobayashi, M. Suematsu, Human serum albumin incorporating synthetic heme: red blood cell substitute without hypertension by nitric oxide scavenging, J. Biomed. Mater. Res. 64A (2003) 257–261.
[14] E. Tsuchida, T. Komatsu, K. Arai, H. Nishide, Synthesis and O_2-binding properties of tetraphenylporphyrinatoiron(II) derivatives bearing a proximal imidazole covalently bound at the β-pyrrolic position, J. Chem. Soc., Perkin Trans. 2 1995 (1995) 747–753.
[15] B.T. Doumas, W.A. Watson, H.G. Biggs, Albumin standards and measurement of serum albumin with bromcresol green, Clin. Chim. Acta 31 (1971) 87–96.
[16] H. Watanabe, K. Yamasaki, U. Kragh-Hansen, S. Tanase, K. Harada, A. Suenaga, M. Otagiri, In vivo and in vitro properties of recombinant human serum albumin from *Pichia pastoris* purified by a method of short processing time, Pharm. Res. 18 (2001) 1775–1781.
[17] J.P. Collman, J.I. Brauman, B.L. Iverson, J.L. Sessler, R.M. Morris, Q.H. Gibson, O_2 and CO Binding to iron(II) porphyrins: a comparison of the "picket fence" and "pocket" porphyrins, J. Am. Chem. Soc. 105 (1983) 3052–3064.
[18] T.G. Traylor, S. Tsuchiya, D. Campbell, M. Mitchell, D. Stynes, N. Koga, Anthracene heme cyclophanes: steric effects in CO, O_2, and RNC binding, J. Am. Chem. Soc. 107 (1985) 604–614.
[19] E. Tsuchida, T. Komatsu, K. Arai, H. Nishide, Synthesis and dioxygen-binding properties of double-sided porphyrinatoiron(II) complexes bearing covalently bound axial imidazole, J. Chem. Soc., Dalton Trans. 1993 (1993) 2465–2469.
[20] E. Katchalski, G.S. Benjamin, V. Gross, The availability of the disulfide bonds of human and bovine serum albumin and of bovine g-globulin to reduction by thioglycolic acid, J. Am. Chem. Soc. 79 (1957) 4096–4099.

[21] D.R. Grassetti, J.F. Murray Jr., Determination of sulfhydryl groups with 2,2′ - or 4,4′ -dithiopyridine, Arch. Biochem. Biophys. 119 (1967) 41–49.
[22] A.O. Pedersen, J. Jacobsen, Reactivity of the thiol group in human and bovine albumin at pH 3–9, as measured by exchange with 2,2′ - dithiodipyridine, Eur. J. Biochem. 106 (1980) 291–295.
[23] E.J. Cohn, The properties and functions of the plasma proteins, with a consideration of the methods for their separation and purification, Chem. Rev. 28 (1941) 395–417.
[24] I. Sjöholm, I. Ljungstedt, Studies on the tryptophan and drug-binding properties of human serum albumin fragments by affinity chromatography and circular dichroism measurements, J. Biol. Chem. 248 (1973) 8434–8441.
[25] A. Sumi, W. Ohtani, K. Kobayashi, T. Ohmura, K. Yokoyama, N. Nishida, T. Suyama, Purification and physicochemical properties of recombinant human serum albumin, in: C. Rivat, J.-F. Stoltz (Eds.), Biotechnology of Blood Proteins, vol. 227, John Libbey Eurotext, Montrouge, 1993, pp. 293–298.
[26] S. Gumpen, P.O. Hegg, H. Martens, Thermal stability of fatty acid–serum albumin complexes studies by differential scanning calorimetry, Biochim. Biophys. Acta 574 (1979) 189–196.
[27] T. Kosa, M. Maruyama, M. Otagiri, Species differences of serum albumins: II. Chemical and thermal stability, Pharm. Res. 15 (1998) 449–454.
[28] a G. Sudlow, D.J. Birkett, D.N. Wade, The Characterization of two specific drug binding sites on human serum albumin, Mol. Pharmacol. 11 (1975) 824–832;
b G. Sudlow, D.J. Birkett, D.N. Wade, Further characterization of specific drug binding sites on human serum albumin, Mol. Pharmacol. 12 (1976) 1052–1061.
[29] G. Scatchard, A.C. Batchelder, A. Brown, Chemical, clinical, and immunological studies on the products of human plasma fractionation: VI. The osmotic pressure of plasma and of serum albumin, J. Clin. Invest. 23 (1944) 165–170.
[30] S. Sakata, M.Z. Atassi, Immunochemistry of serum albumin. X. Five major antigenic sites of human serum albumin are extrapolated from bovine albumin and confirmed by synthetic peptides, Mol. Immunol. 17 (1980) 139–142.
[31] C. Lapresle, N. Doyen, Studies of an antigenic site of human-serum albumin with monoclonal-antibodies, Mol. Immunol. 20 (1983) 549–555.
[32] W. Ohtani, Y. Nawa, K. Takeshima, H. Kamuro, K. Kobayashi, T. Ohmura, Physicochemical and immunochemical properties of recombinant human serum albumin from *Pichia pastoris*, Anal. Biochem. 256 (1998) 56–62.
[33] T.R. McCurdy, S. Gataiance, L.J. Eltringham-Smith, WP. Sheffield, A covalently linked recombinant albumin dimer is more rapidly cleared in vivo than are wild-type and mutant C34A albumin, J. Lab. Clin. Med. 143 (2004) 115–124.
[34] a J.P. Collman, J.I. Brauman, K.M. Doxsee, T.R. Halbert, E. Bunnenberg, R.E. Linder, G.N. LaMar, J.D. Guadio, G. Lang, K. Spartalian, Synthesis and characterization of "tailed picket fence" porphyrins, J. Am. Chem. Soc. 102 (1980) 4182–4192;
b J.P. Collman, F. Basolo, E. Bunnenberg, T.C. Collins, J.H. Dawson, P.E. Ellis Jr., M.L. Marrocco, A. Moscowitz, J.L. Sessler, T. Szymanski, Use of magnetic circular dichroism to determine axial ligation for some sterically encumbered iron(II) porphyrin complexes, J. Am. Chem. Soc. 103 (1981) 5636–5648;
c J.P. Collman, J.I. Brauman, T.J. Collins, B.L. Iverson, G. Lang, R.B. Pettman, J.L. Sessler, M.A. Walters, Synthesis and characterization of the "pocket" porphyrins, J. Am. Chem. Soc. 105 (1983) 3038–3052.
[35] J. Geibel, J. Cannon, D. Campbell, T.G. Traylor, Model compounds for R-state and T-state hemoglobins, J. Am. Chem. Soc. 100 (1978) 3575–3585.
[36] C.A. Sawicki, Q.H. Gibson, Properties of the T state of human oxyhemoglobin studied by laser photolysis, J. Biol. Chem. Soc. 252 (1977) 7538–7547.

Exchange transfusion with synthetic oxygen-carrying plasma protein "albumin-heme" into an acute anemia rat model after seventy-percent hemodilution

Teruyuki Komatsu,[1] Hisashi Yamamoto,[2] Yubin Huang,[1] Hirohisa Horinouchi,[3] Koichi Kobayashi,[3] Eishun Tsuchida[1]

[1]*Advanced Research Institute for Science and Engineering, Waseda University, 3-4-1 Okubo, Shinjuku-ku, Tokyo 169-8555, Japan*

[2]*Pharmaceutical Research Center, NIPRO Corporation, 3023 Nojimachi, Kusatsu-shi, Shiga 525-0055, Japan*

[3]*Department of General Thoracic Surgery, School of Medicine, Keio University, 35 Shinanomachi, Shinjuku-ku, Tokyo 160-8582, Japan*

Received 22 July 2004; Accepted 5 August 2004
Published online 27 October 2004 in Wiley InterScience (www.interscience.wiley.com). DOI: 10.1002/jbm.a.30200

Abstract: Recombinant human serum albumin (rHSA) incorporating the synthetic heme "albumin-heme" is an oxygen-carrying plasma protein that has the potential to be a red blood cell substitute. The physiological responses to a 30% exchange transfusion with two types of albumin-heme (rHSA-FecycP, rHSA-FepivP) solutions after 70% isovolemic hemodilution with 5 g/dL rHSA were investigated using anesthetized rats. The circulation parameters, blood parameters, renal cortical oxygen pressure (pO_2), and muscle tissue pO_2 were carefully monitored for 60 min after the injection. The declined mean arterial pressure and the mixed venous partial pO_2 significantly recovered to 70.8 and 91.9% of the basal values by intravenous infusion of albumin-hemes, respectively. The lowered renal cortical pO_2 also increased, indicating oxygen transport by this synthetic hemoprotein. The administration of albumin-heme into the acute anemia rat model after hemorrhage improved the circulatory volume and resuscitated the shock state. Both rHSA-FecycP and rHSA-FepivP transported oxygen through the body. © 2004 Wiley Periodicals, Inc. J Biomed Mater Res 71A: 644–651, 2004

Key words: exchange transfusion; entirely synthetic oxygen-carrier; hemoprotein; albumin-heme; red blood cell substitute

INTRODUCTION

Because the risk of transmission of viral illness by transfused blood has become extremely low, transfusion of donor blood has nowadays become a routine procedure. However, this level of safety has been achieved at great cost, and the hepatitis virus or unknown infectious pathogens cannot be completely excluded by the nucleic acid test system. Furthermore, (i) the transfusion of donor blood requires cross-matching and compatibility tests to avoid the consequences of a hemolytic reaction in the recipient, and (ii) the purified red blood cells (RBCs) should be stored at 4°C. These requirements substantially limit the availability of blood in a disaster or emergency. Under this background, several types of hemoglobin (Hb)-based oxygen carriers have been studied as an RBC substitute or oxygen therapeutic agent.[1–4] Nevertheless, these materials do not fulfill all the requirements of blood replacement compositions. The first concern is the source of human Hb, which is limited by the availability of outdated human blood. Animal blood will raise anxiety of transmission of animal pathogens; for instance, bovine Hb may harbor prions. The Hb products potentially carry risks because of the biological origin of the raw materials. Additional problems of Hb-based oxygen carriers (i.e., modified Hb) are the high colloid osmotic pressure[5] and its vasopressor effect, which increase blood pressure and decrease cardiac output.[6–8] Although diaspirin intramolecularly crosslinked Hb is no longer developed, half of the products in advanced clinical trials still showed vasoconstriction.[4] The precise mechanism of

Correspondence to: E. Tsuchida; e-mail: eishun@waseda.jp
Contract grant sponsor: Health Science Research Grants (Regulatory Science) of the MHLW
Contract grant sponsor: JSPS Grant-in-Aid for Scientific Research; contract grant number: 16350093
Contract grant sponsor: MEXT Grant-in-Aid for Exploratory Research; contract grant number: 16655049

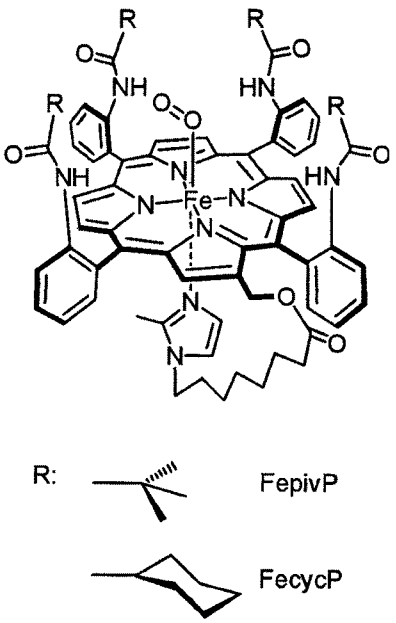

Chart 1

this hypertension is controversial, but many investigators suspect that the small Hb molecules penetrate the vascular endothelium and capture the endothelial-derived relaxing factor, namely, nitric oxide. In fact, glutaraldehyde crosslinked human polyHb does not show vasoactivity.[9] Others believe that the excessive delivery of oxygen to arteriolar vascular walls induces autoregulatory vasoconstriction.[10–13]

We have prepared entirely synthetic oxygen carriers without Hb. The incorporation of synthetic heme, 2-[8-{*N*-(2-methylimidazolyl)}octanoyloxymethyl]-5,10,15,20-tetrakis(α,α,α,α-*o*-pivalamidophenyl)porphinatoiron(II) (FepivP, Chart 1), into recombinant human serum albumin (rHSA) provides an artificial hemoprotein (rHSA-heme; rHSA-FepivP) that can reversibly bind and release oxygen under physiological conditions (pH 7.3, 37°C) like Hb.[14–19] An FepivP analog, 2-[8-{*N*-(2-methylimidazolyl)}-octanoyloxymethyl]-5,10,15,20-tetrakis{α,α,α,α-*o*-(1-methylcyclohexanamido)phenyl}porphinatoiron(II) (FecycP, Chart 1), which contains more hydrophobic 1-methylcyclohexanoyl fences, is also included into rHSA as well and the obtained rHSA-FecycP hybrid showed the same oxygen-binding equilibrium and a longer lifetime ($\tau_{1/2}$) of the oxy species compared with that of rHSA-FepivP.[20] The physicochemical properties and oxygen-transporting ability of these rHSA-based oxygen carriers, which are free of infectious pathogens, satisfy the initial clinical requirements as an RBC substitute. It is remarkable that the colloid osmotic pressure of 5 g/dL rHSA, rHSA-FecycP, and rHSA-FepivP are all the same.[15] We herein report the systematic evaluations of the physiological responses to exchange transfusions with two types of albumin-heme solutions, rHSA-FecycP and rHSA-FepivP, in anesthetized rats. The animals were first placed into an acute anemia induced by 70% hemodilution and then underwent a 30% exchange transfusion with albumin-hemes. Circulation parameters and blood parameters were monitored for 60 min after the injection. The *in vivo* oxygen deliveries to the renal cortex and the muscle tissue were also measured.

MATERIALS AND METHODS

Preparation of rHSA-heme solutions

The rHSA (Albrec®, 25 wt %) was obtained from NIPRO Corp. (Osaka, Japan). The 5 g/dL rHSA was made by diluting Albrec® with saline solution (Otsuka Pharmaceutical Co., Ltd.). Two types of albumin-hemes (rHSA-FecycP and rHSA-FepivP [rHSA]: approximately 5 g/dL) used for the exchange transfusions were prepared according to our previously reported procedure with some modifications.[19] The characteristics of these oxygen-carrying fluids are almost identical (Table I) except for the stability of the oxygenated species; oxy rHSA-FecycP showed a 4.5-fold longer lifetime against autooxidation than that of oxy rHSA-FepivP at 37°C *in vitro*. These red-colored albumin-heme solutions were filtered using a DISMIC 25CS045AS just before use.

Hemodilution and exchange transfusion

The investigations were performed according to our previously reported experimental protocols with 24 male Wistar rats (312 ± 2.9 g) (Scheme 1).[21] All animal handling and care were in accordance with the National Institutes of Health guidelines. The protocol details were approved by the Animal Care and Use Committee of Keio University.

The animals were placed on a heating pad under an inhalation anesthesia with sevoflurane; its concentration was kept at 2.0% for the operations and 1.5% for the experiments. After an incision was made in the neck, the heparinized catheter (Natume Seisakusho SP-55) was introduced into the right common carotid artery for blood withdrawal. Other catheters (SP-31) were also inserted into the left femoral artery for continuous mean arterial pressure (MAP) monitoring, and the right femoral vein for sample injection.

TABLE I
Characteristics of the Albumin-Heme Solutions

	rHSA-FecycP	rHSA-FepivP
pH	7.45	7.46
Viscosity (cP)	1.1	1.1
Heme (m*M*)	2.8	2.7
Met-heme content (%)	0	0
rHSA (%)	4.9	4.9
*p*50 (mmHg) at 37°C	37	32

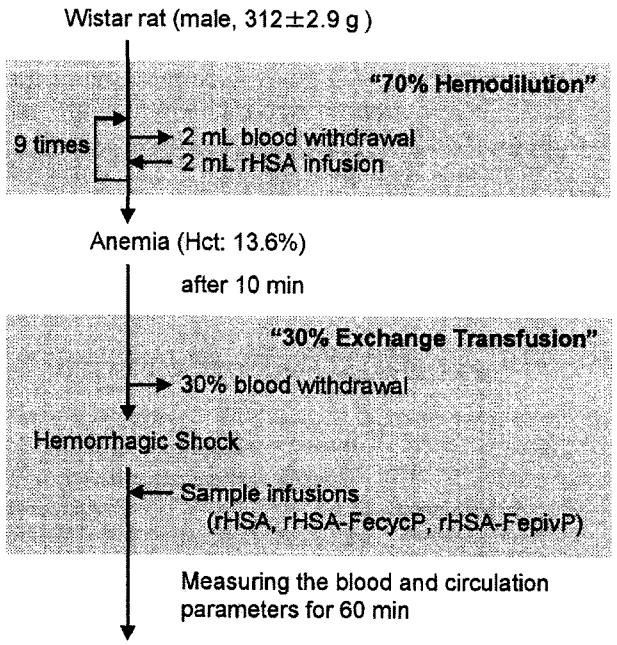

Scheme 1. Diagram illustrating the exchange, bleeding procedures, and materials.

Polarographic oxygen-electrodes (Intermedical POE-10N and POE-40PS) were inserted into the left renal cortex and muscle in the abdomen. Core temperature was measured with a rectal thermometer (Technol Seven D617-1).

After stabilization of the animal's condition, isovolemic 70% hemodilution was performed using 5 g/dL rHSA solution. Blood withdrawal via the common carotid artery (2 mL) and rHSA infusion from the femoral vein (2 mL) (each 1 mL/min) were repeated for nine cycles until the hematocrit (Hct) was reduced to 13.6% (32% of the initial Hct value: 42.6%). After 10 min, a 30% volume of the circulatory blood was withdrawn, producing a severe hemorrhagic shock state. The same volume of the samples (rHSA-FecycP and rHSA-FepivP) was then intravenously (iv) injected (n = 6 each). As negative- or positive-control groups, rats were infused with the 5 g/dL rHSA solution or the shed rat blood ([heme] = 5.3 mM) (rHSA group and whole blood group, n = 6 each). A blood-taking from the artery (0.3 mL) and vein (0.2 mL) was performed at the following six points: (i) before the 70% hemodilution, (ii) immediately after the hemodilution, and (iii) 10 min after the hemodilution, (iv) immediately after the 30% bleeding, (v) immediately after the sample infusion, and (vi) 60 min after the sample infusion. The animals were sacrificed after the experiments by sodium pentobarbital overdose. MAP was monitored through the femoral artery catheter connected to a transducer (NIHON KODEN TP-400 T or Becton Dickinson P23XL) with a pressure coupler and an amplifier (NIHON KODEN PP-101H and AP-100H). An electrocardiogram was measured using a bioelectric coupler and an amplifier (NIHON KODEN PC-101H and AC-100H), and heart rate (HR) was obtained from its R wave. MAP and HR were recorded by a Polygraph System (NIHON KODEN LEG-1000 version 01-02 or PEG-1000 version 01-01) at the following eight points: (i) before the 70% hemodilution, (ii) immediately after the hemodilution, (iii) 10 min after the hemodilution, (iv) immediately after the 30% bleeding, (v) immediately after the sample infusion, (vi) 5 min, (vii) 30 min, and (viii) 60 min after the sample infusion. The renal cortical oxygen-tension [ptO_2(R)] and muscle tissue oxygen-tension [ptO_2(M)] were simultaneously measured with a tissue oxygen-pressure monitor (Inter Medical PO_2-100DW) using an oxygen electrode (described above). Withdrawn blood was rapidly applied to a blood gas system (Radio Meter Trading ABL555) to measure the oxygen pressure (paO_2), pH and carbon dioxide pressure ($paCO_2$) of the arterial blood, and the oxygen pressure (pvO_2) of the venous blood. The RBC numbers were counted for the mixture of arterial blood (30 μL) and ACD-A solution using a multisystem automatic blood cell counter (Sysmex KX-21).

Data analysis

MAP, HR, respiration rate, paO_2, pvO_2, ptO_2(R), ptO_2(M), and $paCO_2$ are represented by percent ratios of the basal values as mean ± standard error of mean (SEM). Body temperature, pH, RBC numbers, and body weight are denoted by mean ± SEM.

Statistical analyses were performed using the Tukey-Kramer multiple comparison test for more than three groups [pH, RBC numbers, body weight, MAP, HR, respiration rate, paO_2, pvO_2, ptO_2(R), ptO_2(M), and $paCO_2$], and by repeated-measures analysis of variance followed by paired t test for comparison with a basal value (body temperature). Values of $p < 0.05$ were considered significant. The statistical analytic software used was StatView (SAS Institute Inc.).

RESULTS

Blood parameters

The basal values of several measurements, for which data are shown in percent ratios, are summarized in Table II. There are no significant differences in the four groups.

The 70% hemodilution decreased the Hct to 12.8–14.3% and RBC numbers to 202.2–223.2 × 10^4/μL, leading to acute anemia [Fig. 1(a,b)]. By a further 30% exchange transfusion with the whole blood of rat, both parameters slightly increased to 14.3% and 229.7 × 10^4/μL, respectively. They remained constant during the experimental period. In the rHSA-FecycP and rHSA-FepivP groups, both parameters decreased to 7.8–9.6% and 129.2–149.2 × 10^4/μL by the sample replacement. They corresponded well to the calculated values.

Survival time

After the exchange transfusion with the 5 g/dL rHSA solution (rHSA group), all animals died within 32 min;

TABLE II
Basal Values of Each Group

	rHSA	Whole blood	rHSA-FecycP	rHSA-FepivP
MAP (mmHg)	110 ± 2.9	115 ± 3.4	101 ± 7.3	107 ± 4.8
HR (beats/min)	371 ± 14	379 ± 17	380 ± 22	349 ± 10
Respiration rate (breaths/min)	66 ± 3.2	67 ± 4.4	60 ± 2.3	64 ± 1.7
ptO_2(R) (mmHg)	29.2 ± 2.8	38.5 ± 2.6	31.7 ± 3.6	30.2 ± 4.3
ptO_2(M) (mmHg)	39.8 ± 3.6	38.5 ± 3.7	44.2 ± 4.6	42.7 ± 3.9
paO_2 (mmHg)	83.8 ± 2.3	84.2 ± 2.3	87.8 ± 2.6	81.7 ± 2.2
pvO_2 (mmHg)	47.9 ± 1.6	46.8 ± 1.9	48.2 ± 3.1	47.4 ± 1.1
$paCO_2$ (mmHg)	42.0 ± 0.9	40.2 ± 0.8	39.6 ± 1.2	41.7 ± 1.0
Body weight (g)	312 ± 3.5	312 ± 3.9	311 ± 3.4	314 ± 0.8

the average survival time was 14.9 ± 4.3 min. However, all animals survived >60 min in the rHSA-FecycP, rHSA-FepivP, and whole blood groups. The body temperatures remained constant throughout the measurements (rHSA-FecycP group: 36.1°–36.6°C; rHSA-FepivP group: 36.3°–36.7°C; whole blood groups: 36.2°–36.8°C).

MAP, HR, and respiration rate

The 70% hemodilution decreased MAP to 77.4–81.9% of the basal value, and the further 30% bleeding decreased it to 24.9–37.7% of the baseline [Fig. 2(a)]. In contrast to the fact that no recovery was observed by the iv administration of 5 g/dL rHSA, the lowered MAP was increased to 85.6% of the baseline by the whole blood injection. In the rHSA-FecycP and rHSA-FepivP groups, the decreased MAP was elevated to 70.1 and 71.4% of the basal values (80.7 and 87.1% of the values before the bleedings).

The HR and respiration rate had decreased to 88.6–97.4 and 76.5–82.5% of the baselines by the 30% bleeding [Fig. 2(b,c)]. Both parameters returned to the initial levels by the injection of rHSA-FecycP, rHSA-FepivP, and whole blood within 30 min.

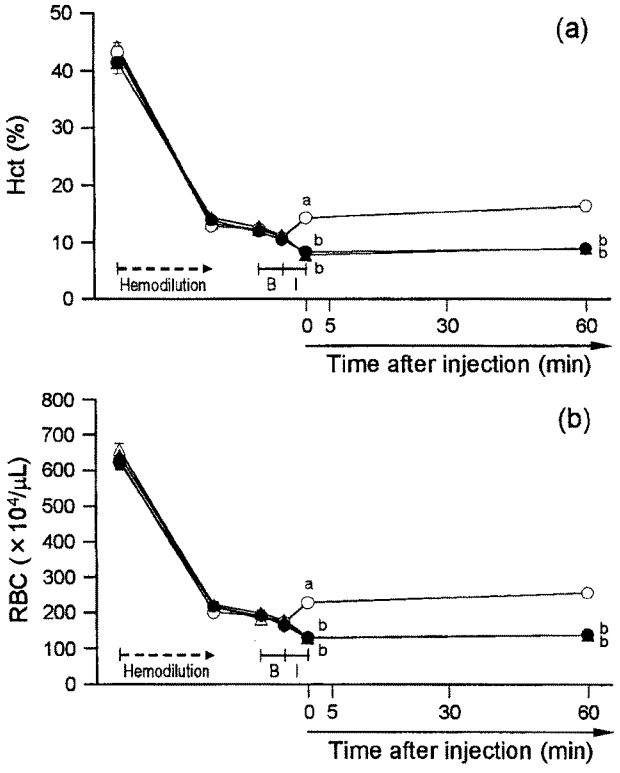

Figure 1. Effect of rHSA-heme solutions on Hct (a), and RBC numbers (b) in anesthetized rats subjected to hemodilution and hemorrhage. Each value represents the mean ± SEM of six rats (●, rHSA-FecycP group; ▲, rHSA-FepivP group; ○, whole blood group; and △, rHSA group). B, bleeding; I, sample injection. $^{a}p < 0.05$ versus rHSA group. $^{b}p < 0.05$ versus whole blood group.

ptO_2(R) and ptO_2(M)

After the 30% bleeding, ptO_2(R) decreased to 59.9–77.3% of the baseline [Fig. 3(a)]. Whereas the iv administrations of rHSA solution did not show restoration, the injection of the rHSA-FecycP, rHSA-FepivP, or whole blood immediately increased the ptO_2(R) level to 84.1–94.8% of the baselines (102.1–112.3% of the values before the bleeding). They remained unaltered by the end of the measurements.

The ptO_2(M) had also decreased to 49.4–52.9% of the basal value after the isovolemic hemodilution, and further decreased to 12.1–26.7% because of the 30% bleeding [Fig. 3(b)]. The iv administration of the whole blood increased the ptO_2(M) to 62.8% of the baseline after 60 min. In the rHSA-FecycP and rHSA-FepivP groups, the increasing ratios were relatively small: 34.2 and 36.9% of the baselines (76.2 and 66.8% of the values before the bleedings).

Blood gas parameters

The paO_2 increased to 111.3–123.2% of the baseline after the isovolemic hemodilution, and reached 148.0–153.6% after the 30% bleeding [Fig. 4(a)]. The injection of the whole blood showed a significant effect for restoration. Nonetheless, the recoveries by the albu-

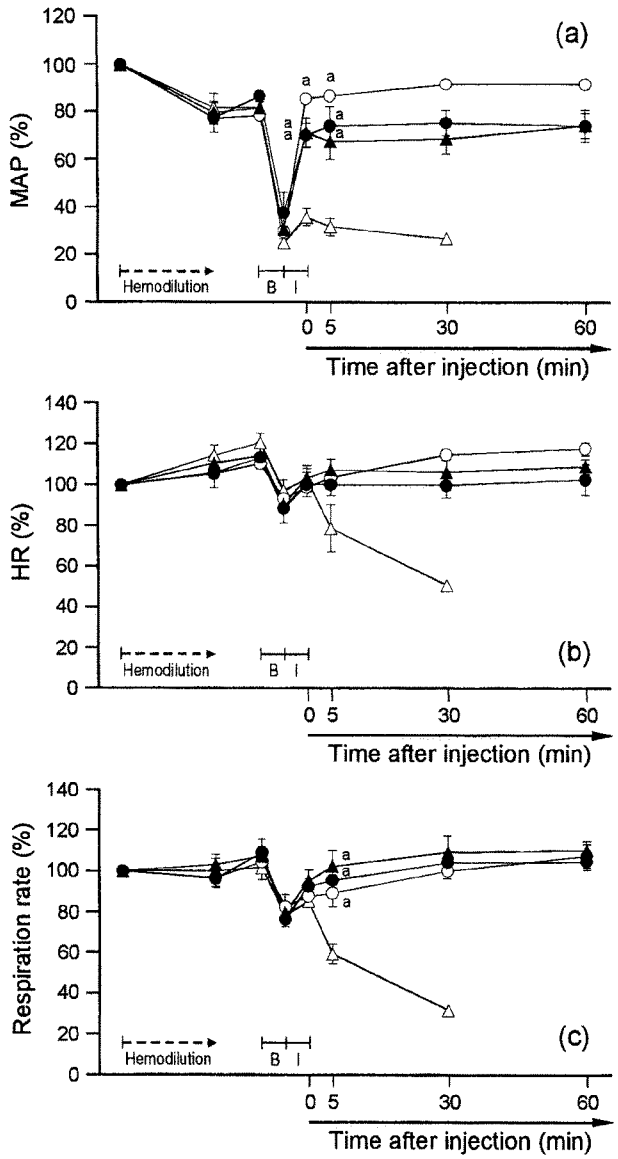

Figure 2. Effect of rHSA-heme solutions on MAP (a), HR (b), and respiration rate (c) in anesthetized rats subjected to hemodilution and hemorrhage. Each value represents the mean ± SEM of six rats (●, rHSA-FecycP group; ▲, rHSA-FepivP group; ○, whole blood group; and △, rHSA group). B, bleeding; I, sample injection. $^{a}p < 0.05$ versus rHSA group.

min-heme solutions were almost to the same extent as that seen in the rHSA group.

The pvO_2 decreased to 56.5–69.8% of the basal value after the 30% bleeding. The low value was not improved by the iv administration of 5 g/dL rHSA [Fig. 4(b)]. In contrast, the infusions of rHSA-FecycP, rHSA-FepivP, and whole blood immediately increased pvO_2 to 88.9–94.8%.

The changes in pH showed the same profile in all groups until 60 min after injection [Fig. 4(c)]. The pH of 7.39–7.42 was slightly increased to 7.47–7.49 after the bleeding and reduced to 7.34–7.37 by the administration of the samples, which slowly returned close to the initial level except for the rHSA-FecycP group.

The $paCO_2$ decreased to 66.3–73.9% of the basal value after the 30% bleeding. The iv administration of whole blood immediately increased it to 95.1% [Fig. 4(d)]. The recovery by the infusion of the rHSA-FecycP or rHSA-FepivP solution was relatively small (80.9–88.0%).

DISCUSSION

In this study, animals were anesthetized with sevoflurane, which is widely used in clinical situations. We had evaluated the oxygen-transporting ability of rHSA-FepivP using a similar acute anemia model with pentobarbital as an anesthesia.[21] Most of the parameter changes showed the same extent as those observed in the former experiment, except for the small degree of $ptO_2(R)$ reduction after the bleeding (32%) (50% decrease in the former study). It is probably attributable to the difference in the blood exchanging ratio.

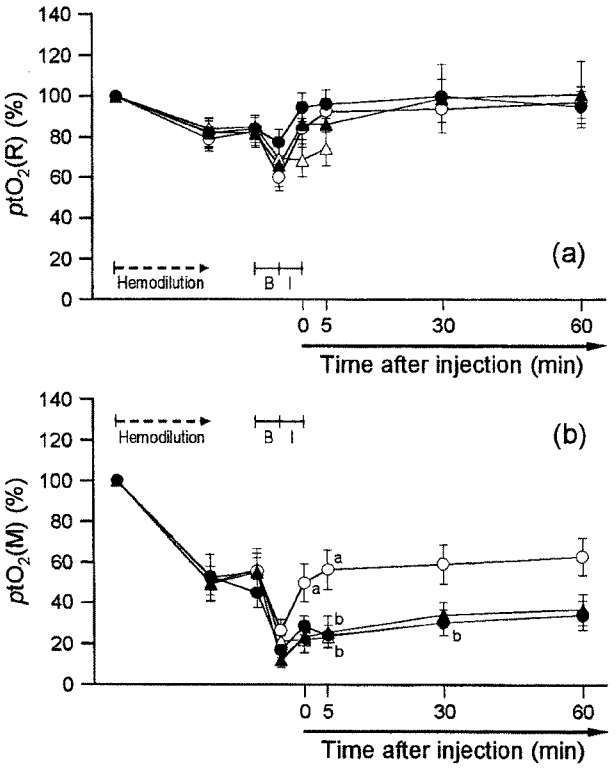

Figure 3. Effect of rHSA-heme solutions on the $ptO_2(R)$ (a) and $ptO_2(M)$ (b) in anesthetized rats subjected to hemodilution and hemorrhage. Each value represents the mean ± SEM of six rats (●, rHSA-FecycP group; ▲, rHSA-FepivP group; ○, whole blood group; and △, rHSA group). B, bleeding; I, sample injection. $^{a}p < 0.05$ versus rHSA group. $^{b}p < 0.05$ versus whole blood group.

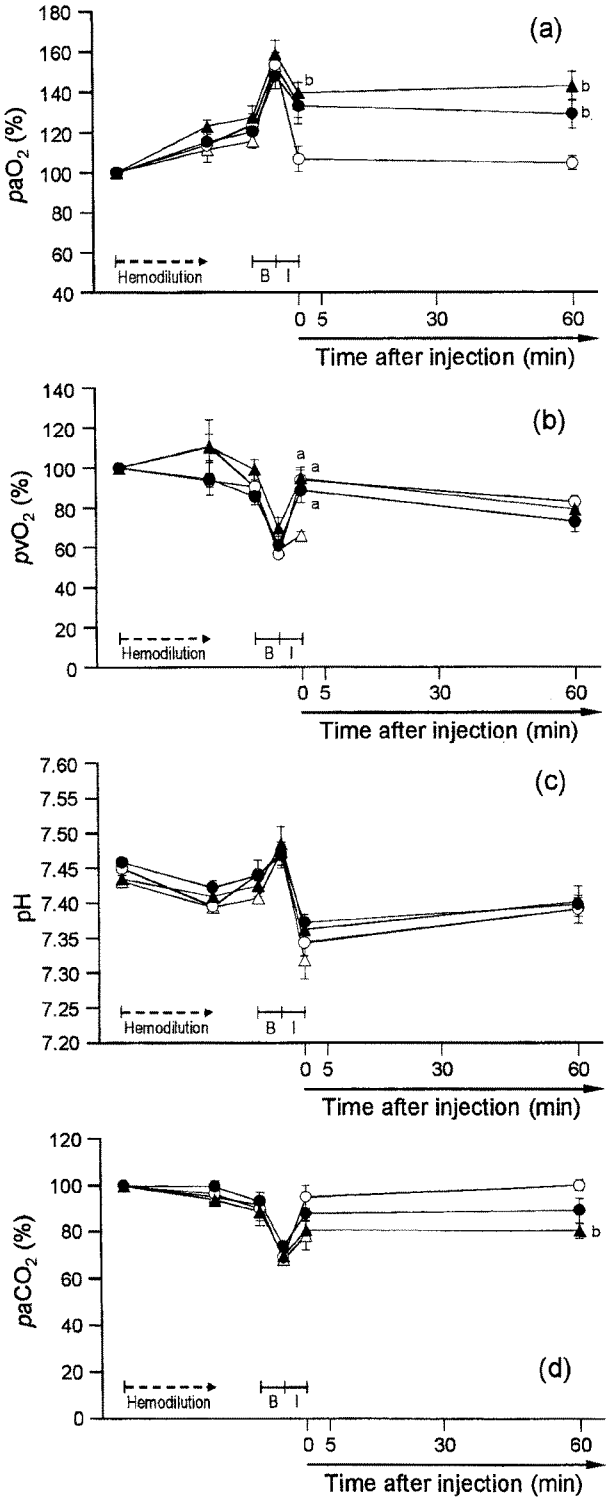

Figure 4. Effect of rHSA-heme solutions on paO_2 (a), pvO_2 (b), pH (c), and $paCO_2$ (d) in anesthetized rats subjected to hemodilution and hemorrhage. Each value represents the mean ± SEM of six rats (●, rHSA-FecycP group; ▲, rHSA-FepivP group; ○, whole blood group; and △, rHSA group). B, bleeding; I, sample injection. $^{b}p < 0.05$ versus whole blood group. $^{a}p < 0.05$ versus rHSA group.

In the glass capillaries for the Hct determinations, the supernatant after centrifugation (12 kG, 5 min) was colored red by the homogeneously dispersed albumin-heme molecules without any aggregation. This indicates that the albumin-heme fluids have a good solubility with the blood components.

Acute anemia after 70% hemodilution

The quantitative changes in Hct and RBC numbers showed that the 70% hemodilution and 30% exchange transfusion were precisely controlled. In acute anemia, the oxygen supply centralizes in vital organs, and the muscle tissues become hypoxic by peripheral vasoconstriction. In fact, the ratio of ptO_2 reduction in the muscle tissues after hemodilution was significant compared with that observed in the renal cortex.

Hemorrhagic shock by 30% bleeding

Decreasing the circulation blood volume induced a significant reduction of MAP, ptO_2(R), ptO_2(M), pvO_2, and $paCO_2$. Among the vital organs, renal perfusion is first impaired because of redistribution of the systemic blood flow; therefore, ptO_2(R) is sensitive to a subtle change in the blood circulation and oxygen delivery. The decreased pvO_2 after the 30% bleeding implies a low oxygen saturation of Hb and increased oxygen extraction. The HR and respiration rate had also decreased from the initial values. However, paO_2 was increased to 153.6% (129.6 mmHg) of the baseline, which could be attributable to hyperventilation. The $paCO_2$ decreased to 70.3% of the baseline and the pH was increased to 7.48. A respiratory alkalosis by hyperventilation might overcome the metabolic acidosis effect.

Responses to administration with albumin-heme

In all groups, the pH levels decreased to 7.35 just after sample injections. The rapid increase in blood volume could improve the circulatory flows and wash out the lactate in the tissues.

By administration of the 5 g/dL rHSA solution, the MAP, HR, respiration rate, ptO_2(R), ptO_2(M), paO_2, pvO_2, and $paCO_2$ did not recover, leading to death within 32 min. In contrast, the infusion of whole blood improved these values to their initial levels except for ptO_2(M). In the rHSA-FecycP and rHSA-FepivP groups, the animals survived >60 min after the infusion, and the HR, respiration rate, ptO_2(R), and pvO_2 showed similar recoveries as observed in the whole

blood group. MAP, $ptO_2(M)$, paO_2, pH, and $paCO_2$ also returned, but not adequate relative to the whole blood group. We are certain that the albumin-heme solutions have the potential to (i) resuscitate the hemorrhagic shock, (ii) stabilize the blood circulation, and (iii) transport oxygen throughout the body. Nevertheless, the oxygen delivery to the peripheral tissues is still insufficient. The possible reasons were considered from the viewpoints of the physicochemical properties of albumin-heme.

Oxygen-binding affinity (p_{50}) (oxygen partial pressure in which 50% of Hb or albumin-heme is oxygenated)

It is known that an allosteric effect observed in the oxygen binding to Hb [the Hill coefficient (n) = 3.0] has implications for physiological use; the oxygen-transporting efficacy of RBCs between lungs [oxygen pressure (pO_2): 110 mmHg] and muscle tissues (pO_2: 40 mmHg) is estimated to be 22% at 37°C. The oxygen-equilibrium curve of albumin-heme does not show cooperativity; n is 1.0. However, the oxygen-binding affinity of albumin-hemes are adjusted somewhat low (rHSA-FecycP: p_{50} = 37 mmHg; rHSA-FepivP: p_{50} = 32 mmHg, respectively), so that they are able to show a similar oxygen-transporting efficacy of 22–23%.

Some investigators reported that a low p_{50} value is important to avoid the hypertensive effect; that is, the constrictive response is caused by excessive oxygen delivery to the arterioles.[10–13] McCarthy et al.[22] suggested that the increased oxygen delivery can be limited by increasing the molecular size, oxygen-binding affinity, and viscosity. Indeed, the PEG-conjugated Hb with a molecular weight of 90 kDa had no effect on the MAP.[23] However, Doherty et al.[24] denied this hypothesis based on their systematic experiments using recombinant Hbs (rHbs) with various p_{50} values; the small differences in the oxygen-equilibrium curves of the rHbs did not affect the magnitude of the pressor response. Our previous top-loading experiments using the albumin-heme solution (p_{50}: 32 mmHg) on the MAP changes and microcirculatory observations of the capillaries also showed that neither vasoconstriction nor hypertension occurred, because of its low permeability through the vascular endothelium.[18] Thus, the differences in p_{50} may not be essential.

Heme concentration

The heme concentration of the shed blood to use the exchange transfusion in the whole blood group was 5.3 m*M*. In contrast, the concentrations of the FecycP or FepivP in the rHSA-FecycP or rHSA-FepivP solutions were 2.7–2.8 m*M*. The low heme concentration of albumin-heme is probably related to insufficient oxygen delivery, which may result in the low recovery of $ptO_2(M)$.

Viscosity

It has been reported that an endothelial-derived relaxing factor (nitric oxide) is generated in response to the shear stress on the capillary wall.[25] Recently, maintenance of the plasma viscosity has been proposed as a crucial mechanism to preserve the shear force during microcirculation.[26] The prompt flow by the injection of the albumin-heme solution with low viscosity (1.1 cP) compared with blood (4.4 cP) may reduce the peripheral resistance and induce partial vasoconstriction, which would reduce the blood flow. The correct measurement of the cardiac output is necessary to interpret the pO_2 data and to assay the oxygen delivery.

In conclusion, all physiological responses to the exchange transfusion with albumin-heme in acute anemia reveal that this synthetic RBC substitute has the capability to resuscitate the hemorrhagic shock. A significant difference could not be found between the two types of albumin-hemes, rHSA-FecycP and rHSA-FepivP. This rHSA-based oxygen-carrying plasma expander will become a promising material for a new class of RBC substitutes. The safety and oxygen delivery of albumin-heme will be reported in a forthcoming article.

The authors are grateful to NIPRO Corp., for their supporting the oxygen-infusion project.

References

1. Chang TMS. Recent and future developments in modified hemoglobin and microencapsulated hemoglobin as red blood cell substitutes. Artif Cells Blood Substit Immobil Biotechnol 1997;25:1–24.
2. Tsuchida E. Perspectives of blood substitutes. In: Tsuchida E, editor. Blood substitutes: present and future perspectives. Lausanne, Switzerland: Elsevier Science; 1998. p 1–14.
3. Winslow RM. New transfusion strategies: red cell substitutes. Annu Rev Med 1999;50:337–353.
4. Squires JE. Artificial blood. Science 2002;295:1002–1005.
5. Keipert P, Chang T. Pyridoxylated-polyhemoglobin solution: a low viscosity oxygen-delivery blood replacement fluid with normal oncotic pressure and long term storage feasibility. Biomater Artif Cells Artif Organs 1988;16:185–196.
6. Schultz SC, Grady B, Cole F, Hamilton I, Burhop K, Malcolm DS. A role for endothelin and nitric oxide in the pressor response to diaspirin cross-linked hemoglobin. J Lab Clin Med 1993;122:301–308.
7. Moisan S, Drapeau G, Burhop KE, Rioux F. Mechanism of the acute pressor effect and bradycardia elicited by diaspirin crosslinked hemoglobin in anesthetized rats. Can J Physiol Pharmacol 1998;76:434–442.

8. Abassi Z, Kotob S, Pieruzzi F, Abouassali M, Keiser HR, Fratantoni JC, Alayash AI. Effects of polymerization on the hypertensive action of diaspirin cross-linked hemoglobin in rats. J Lab Clin Med 1997;129:603–610.
9. Gould SA, Moore EE, Moore FA, Haenel JB, Burch JM, Sehgal H, Sehgal L, DeWoskin R, Moss GS. Clinical utility of human polymerized hemoglobin as a blood substitute after acute trauma and urgent surgery. J Trauma 1997;43:325–332.
10. Guyton AC, Ross JM, Carrier O, Walker JR. Evidence for tissue oxygen demand as the major factor causing autoregulation. Circ Res 1964;14:1–60.
11. Tsai AG, Kerger H, Intaglietta M. Microcirculatory consequences of blood substitution with αα-hemoglobin. In: Winslow RM, Vandegriff KD, Intaglietta M, editors. Blood substitutes: physiological basis of efficiency. Boston, MA: Birkhäuser; 1995. p 155–174.
12. Rohlfs RJ, Bruner E, Chiu A, Gonzales ML, Magde D. Arterial blood pressure responses to cell-free hemoglobin solutions and the reaction with nitric oxide. J Biol Chem 1998;273:12128–12134.
13. Winslow RM. αα-Crosslinked hemoglobin: was failure predicted by preclinical testing? Vox Sang 2000;79:1–20.
14. Komatsu T, Hamamatsu K, Wu J, Tsuchida E. Physicochemical properties and O_2-coordination structure of human serum albumin incorporating tetrakis(*o*-pivamido)phenylporphyrinatoiron(II) derivatives. Bioconjug Chem 1999;10:82–86.
15. Tsuchida E, Komatsu T, Matsukawa Y, Hamamatsu K, Wu J. Human serum albumin incorporating tetrakis(*o*-pivalamido)-phenylporphinatoiron(II) derivative as a totally synthetic O_2-carrying hemoprotein. Bioconjug Chem 1999;10:797–802.
16. Komatsu T, Matsukawa Y, Tsuchida E. Kinetics of CO- and O_2-binding to human serum albumin-heme hybrid. Bioconjug Chem 2000;11:772–776.
17. Komatsu T, Matsukawa Y, Tsuchida E. Reaction of nitric oxide with synthetic hemoprotein, human serum albumin incorporating tetraphenylporphinatoiron(II) derivatives. Bioconjug Chem 2001;12:71–75.
18. Tsuchida E, Komatsu T, Matsukawa Y, Nakagawa A, Sakai H, Kobayashi K, Suematsu M. Human serum albumin incorporating synthetic heme: red blood cell substitute without hypertension by nitric oxide scavenging. J Biomed Mater Res 2003; 64A:257–261.
19. Huang Y, Komatsu T, Nakagawa A, Tsuchida E, Kobayashi S. Compatibility *in vitro* of albumin-heme (O_2 carrier) with blood cell components. J Biomed Mater Res 2003;66A:292–297.
20. Komatsu T, Matsukawa Y, Tsuchida E. Effect of heme structure on O_2-binding properties of human serum albumin-heme hybrids: intramolecular histidine coordination provides a stable O_2-adduct complex. Bioconjug Chem 2002;13:397–402.
21. Tsuchida E, Komatsu T, Hamamatsu K, Matsukawa Y, Tajima A, Yoshizu A, Izumi Y, Kobayashi K. Exchange transfusion of albumin-heme as an artificial O_2-infusion into anesthetized rats: physiological responses, O_2-delivery and reduction of the oxidized hemin sites by red blood cells. Bioconjug Chem 2000; 11:46–50.
22. McCarthy MR, Vandegriff KD, Winslow RM. The role of facilitated diffusion in oxygen transport by cell-free hemoglobin: implication for the design of hemoglobin-based oxygen carriers. Biophys Chem 2001;92:103–117.
23. Vandegriff KD, Malavalli A, Wooldbridge J, Lohman J, Winslow RM. MP4, a new nonvasoactive PEG-Hb conjugate. Transfusion 2003;43:509–516.
24. Doherty DH, Doyle MP, Curry SR, Vali RJ, Fattor TJ, Olson JS, Lemon DD. Rate of reaction with nitric oxide determines the hypertensive effect of cell-free hemoglobin. Nat Biotechnol 1998;16:672–676.
25. Malek AM, Izumo S. Control of endothelial cell gene expression by flow. J Biomech 1995;28:1515–1528.
26. Tsai AG, Friesenecker B, McCarthy M, Sakai H, Intaglietta M. Plasma viscosity regulates capillary perfusion during extreme hemodilution in hamster skinfold model. Am J Physiol 1998: 275;H2170–H2180.

Human Serum Albumin Bearing Covalently Attached Iron(II) Porphyrins as O_2-Coordination Sites

Rong-Min Wang,[†,‡] Teruyuki Komatsu,[†] Akito Nakagawa,[†] and Eishun Tsuchida*[,†]

Advanced Research Institute for Science and Engineering, Waseda University, 3-4-1 Okubo, Shinjuku-ku, Tokyo 169-8555, Japan, and Institute of Polymer, Northwest Normal University, Lanzhou 730070, China . Received June 17, 2004; Revised Manuscript Received September 25, 2004

Tetrakis{(α,α,α,α-*o*-pivalamido)phenyl}porphinatoiron(II) with a bifunctional tail possessing an axially coordinated imidazolyl group and a protein attachable succinimidyl(glutamyl) group (FeP-GluSu) has been synthesized. It can efficiently react with the lysine residues of recombinant human serum albumin (rHSA), giving a new albumin–heme conjugate [rHSA(FeP-Glu)]. MALDI-TOFMS showed a distinct molecular ion peak at *m/z* 70 643, which indicates that three FeP-Glu molecules were covalently linked to the rHSA scaffold. The binding number of FeP-Glu is approximately three (mol/mol) and independent of the mixing ratio. The CD spectrum and Native PAGE revealed that the albumin structure remained unaltered after the covalent bonding of the hemes. This rHSA(FeP-Glu) conjugate can bind and release O_2 reversibly under physiological conditions (pH 7.3, 37 °C) in the same manner as hemoglobin and myoglobin. The O_2-adduct complex had a remarkably long lifetime ($\tau_{1/2}$: 5 h). The O_2-binding affinity [$P_{1/2}^{O_2}$: 27 Torr] was identical to that of human red cells. Laser flash photolysis experiments gave the O_2- and CO-association rate constants and suggested that there are two different geometries of the imidazole binding to the central ion.

Human serum albumin (HSA), which is the major plasma protein component in our bloodstream, has no prosthetic group; however it nonspecifically captures many endogenous and exogenous compounds by weak interactions, *e.g.*, H-bond, ionic attraction, and hydrophobic interaction, namely noncovalent bonds (*1*–*3*). Synthetic heme, 2-[{8-*N*-(2-methylimidazolyl)octanoyl}-oxy]methyl-5,10,15,20-tetrakis{(α,α,α,α-*o*-pivalamido)-phenyl}porphinatoiron(II) (FeP, Chart 1 a) is also incorporated into recombinant HSA (rHSA), and the obtained albumin–heme (rHSA-FeP) hybrid can reversibly coordinate O_2 under physiological conditions (pH 7.3, 37 °C) (*4*). This O_2-carrying plasma hemoprotein could be of medical importance as a blood replacement composition (*4e*–*g*). Nevertheless, the major driving force of the heme-binding to albumin is a hydrophobic interaction; therefore, its binding constants (10^4–10^6 M^{-1}) are not high enough to maintain the heme concentration in the circulatory system for a long period (*4a*). The administration of the albumin–heme hybrid solution into rats demonstrated that the lifetimes of the heme was less than 6 h (*4e*, *5*). To immobilize the heme group to the albumin scaffold more tightly and retain its O_2-transport efficacy, we have combined the O_2-coordination site FeP to the rHSA structure through a covalent bond. In this communication, we report, for the first time, the synthesis of a novel FeP analogue with a bifunctional branched-tail including an axially coordinated imidazolyl group and a protein-attachable succinimidyl(glutamyl) group (FeP-GluSu, Chart 1 a), and the properties of the rHSA conjugate bearing covalently linked FeP-Glu as a new O_2-carrying hemoprotein.

Chart 1. (a) 5,10,15,20-Tetrakis{(α,α,α,α-*o*-pivalamido)-phenyl}porphinatoiron Derivatives with a Bifunctional Tail Group. (b) Space-Filling Representation of the Oxygenated FeP-GluSu by Insight II (see ref 11)

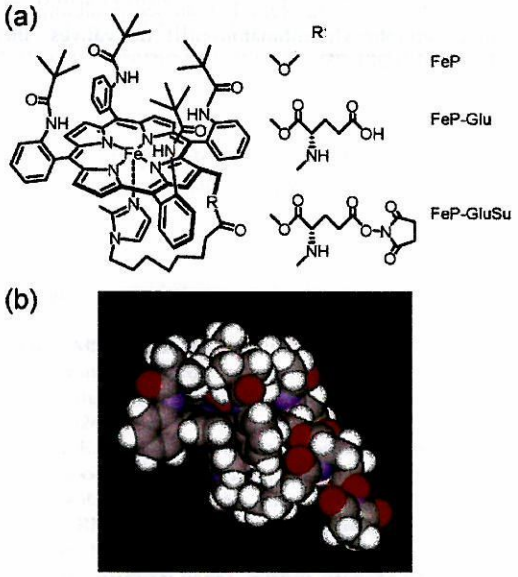

As a functional side-chain of FeP, which directly makes a covalent bond to rHSA, we selected the succinimidyl group, because it selectively reacts with the NH_2 group of lysine in the range of pH 6.3–8.6 with high yield. The branched tail that includes the imidazolyl and succnimidyl groups via a glutamate junction was introduced into the parent porphyrin **1** (*6*) as shown in Scheme 1 (*7*).

* Corresponding author. Phone: +81 3-5286-3120. Fax: +81-3-3205-4740. E-mail: eishun@waseda.jp.
† Waseda University.
‡ Northwest Normal University.

10.1021/bc049859m CCC: $30.25
Published on Web 11/12/2004

Scheme 1. Synthetic Scheme of FeP-GluSu

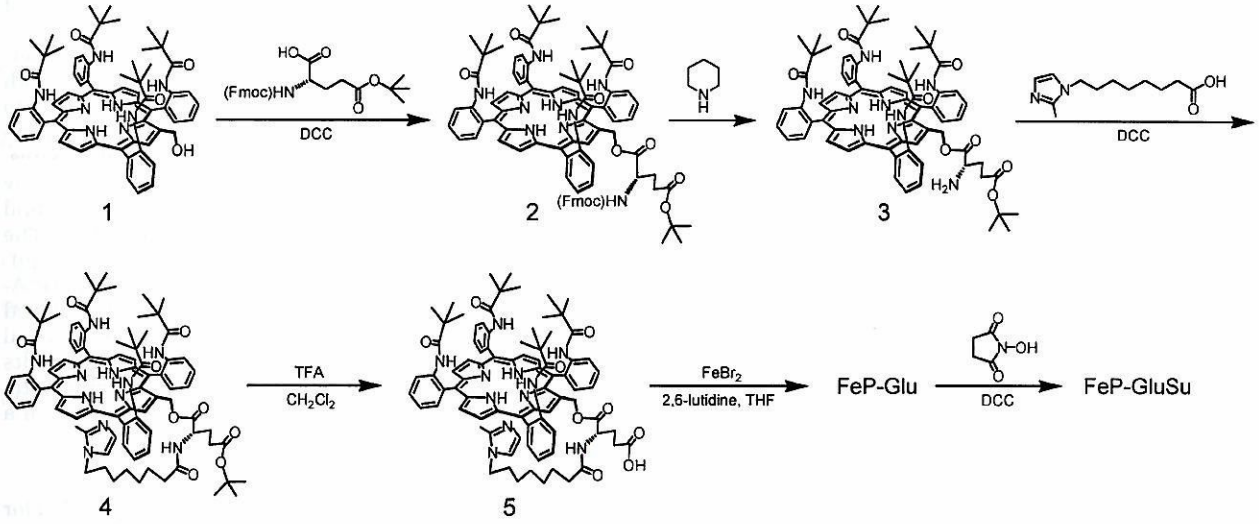

Table 1. CO-and O_2-Binding Parameters of rHSA(FeP-Glu) Conjugate in Phosphate–Buffered Solution (pH 7.3) at 25 °C

	$10^{-6}\,k_{on}^{CO}(M^{-1}\,s^{-1})$		$10^{-7}\,k_{on}^{O_2}(M^{-1}\,s^{-1})$		$10^{-2}\,k_{off}^{O_2}(s^{-1})$		$P_{1/2}^{O_2}$(Torr)[a]
system	fast	slow	fast	slow	fast	slow	
rHSA(FeP-Glu) conjugate	6.2	1.1	2.8	–	3.3	–	9 (27)
rHSA-FeP hybrid[b]	4.7	0.66	3.2	1.0	7.2	2.2	13 (35)
Hb(T-state)α[c]	0.22	–	0.29	–	1.8	–	40

[a] At 37 °C in parenthesis. [b] From ref 4c. [c] From refs 13–15.

First, Fmoc-L-Glu(g-*tert*-butyl ester) was bound to the OH group at the β-pyrrolic position of the porphyrin **1** by DCC. After removal of the Fmoc protecting group with piperidine, 8-*N*-(2-methylimidazolyl)octanoic acid was reacted with the obtained compound **3** in CH_2Cl_2, giving the imidazolyl-tailed porphyrin (**4**). The *tert*-butyl group was then removed by TFA, and the central iron insertion was carried out by the general $FeBr_2$ method to afford the iron-porphryin FeP-Glu. Finally, the reaction of *N*-hydroxysuccinimide with DCC gave the FeP-GluSu. All reactions can be performed at room temperature with high yields. The analytical data of all compounds described above were satisfactory obtained (*7*).

The FeP-Glu was converted to the ferrous complex by reduction in a heterogeneous two-phase system (toluene/aqueous $Na_2S_2O_4$) under an N_2 atmosphere (*6, 8*). The UV–vis absorption spectrum of the orange solution showed five-*N*-coordinated Fe(II) species (λ_{max}: 440, 531, 563 nm) via intramolecular imidazole binding (*6, 8, 9*). Upon exposure to CO, its UV–vis absorption immediately moved to that of the CO adduct complex. On the other hand, the dioxygenation was unstable at 25 °C, which is likely due to the presence of the neighboring glutamic acid proton.

The EtOH solution of the carbonyl FeP-GluSu (2 mL) was then injected into the phosphate-buffered solution of rHSA (8 mL, pH 7.3) (molar ratio 4/1), and the mixture was gently stirred for 1 h at room temperature. The solution was dialyzed against phosphate buffer (pH 7.3) to remove EtOH. The MALDI-TOFMS demonstrated a single molecular ion peak at *m/z* 70 643 (Figure 1). Attempts to measure the molecular weight of the rHSA-FeP hybrid, in which the FePs are noncovalently accommodated, failed using MALDI- and ESI-TOFMS; the molecular ion peak of rHSA (65 500) was only observable because the FePs are dissociated from the albumin during the ionization process (*10*). Therefore, we can conclude that the FeP-Glu is conjugated with rHSA through amide bond formation. The average number of FeP-Glu in an rHSA was estimated to be 2.9–3.5, and this number is not dependent on the mixing molar ratio of FeP-GluSu/rHSA that ranged from 4 to 10. There are a total of 59 NH_2 groups in the rHSA structure, but only three of them are presumably active for the FeP-GluSu binding.

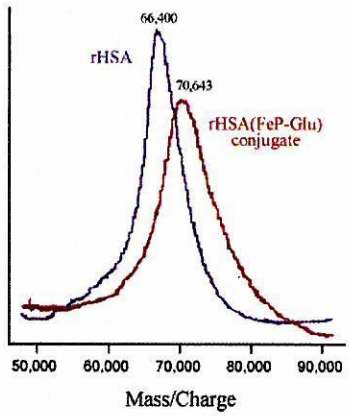

Figure 1. MALDI-TOFMS of the rHSA(FeP-Glu) conjugate. Matrix: 2,5-dihydroxybenzoic acid.

The conjugation of FeP-GluSu did not induce any change in the circular dichroism spectrum of rHSA in the 200–250 nm region. The Native PAGE of rHSA(FeP-Glu) also showed a single band with same migration distance of rHSA. Both results suggested that the secondary structure, molecular shape, and surface charge of albumin remained unaltered after the covalent binding of the hemes.

The UV–vis absorption spectrum of the rHSA(FeP-Glu) conjugate under an N_2 atmosphere showed a typical five-*N*-coordinated complex as seen in the toluene solution of FeP-Glu (Figure 2) (*4a,b, 6, 8, 9*). Upon exposure

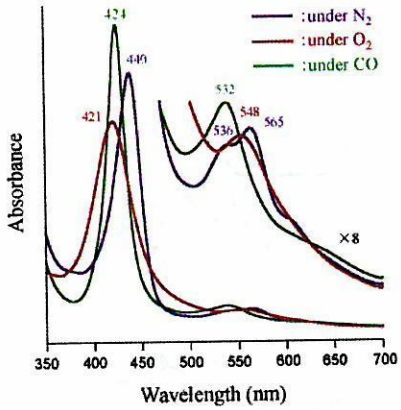

Figure 2. UV–vis absorption spectral changes of the rHSA-(FeP-Glu) conjugate in phosphate-buffered solution (pH 7.3) at 25 °C.

of this solution to O_2, the spectrum changed to that of the O_2-adduct complex under physiological conditions (pH 7.3, 37 °C) (*4a–c*). This dioxygenation was reversibly observed to be dependent on the O_2 partial pressure in the same manner as hemoglobin (Hb) and myoglobin. The half-lifetime of the O_2 adduct (ca. 5 h at 37 °C) was significantly longer than that of the noncovalent rHSA-FeP hybrid ($\tau_{1/2}$: 2 h) (*4d*). The covalent linkages of FeP-Glu to the protein scaffold obviously retarded the oxidation process of the central ferrous ion. Molecular simulation of the structure of FeP-GluSu revealed that the geometry of the imidazole ring against the porphyrin platform was perpendicular, which suggests that the spacer moiety between the imidazole and the porphyrin periphery does not produce an unfavorable distortion of the axial coordination and will not influence the O_2-binding behavior (see Chart 1b) (*11*).

The O_2-binding affinity [$P_{1/2}{}^{O_2}$] of the rHSA(FeP-Glu) conjugate was determined to be 27 Torr at 37 °C (*3b,c, 6, 7, 9, 10*), which is almost the same as that of the rHSA-FeP hybrid [$P_{1/2}{}^{O_2}$: 33 Torr] (*3b–d*) and identical to that of human red cells (*12*). The laser flash photolysis experiments provided the association rate constants of the O_2- and CO-bindings ($k_{on}{}^{O_2}$, $k_{on}{}^{CO}$) (*6, 8, 9a*). The absorption decays accompanying the O_2- and CO-recombination to the noncovalent rHSA-FeP hybrid were composed of two phases of the first-order kinetics, and the curves were fit by a double-exponential equation to determine k_{on} (fast) and k_{on} (slow) (Table 1) (*4c*). We supposed that the O_2- and CO-association to the FeP in the hydrophobic domains of the albumin was influenced by the molecular microenvironments around each O_2-coordination site, e.g., steric hindrance of the amino acid residue and difference in polarity (*4b–d*). The time dependence of the absorption change in the CO recombination to the rHSA(FeP-Glu) conjugate also showed double-exponential profile, but the rebinding process of O_2 obeyed monophasic decay. On the basis of studies on synthetic model hemes, it has been known that the proximal-side effect is the only primary factor which influences the association rate for CO but not for O_2 (*8, 9a*). We assume that there are two different geometries of the imidazole coordination and that each one shows the individual kinetics of the CO association. The covalent linkages between the axially coordinated imidazolyl side-chain and the albumin structure may provide an additional strain of the Fe–N(imidazole) bond and gives two conformations of the proximal-base binding. Since the $k_{on}{}^{O_2}$ value of rHSA(FeP-Glu) was nearly the same as the $k_{on}{}^{O_2}$ (fast) of the rHSA-FeP hybrid (Table 1), the FeP-Glu molecules are likely to locate on the surface of rHSA.

In conclusion, reaction of the newly synthesized tetrakis{(α,α,α,α-*o*-pivalamido)phenyl}porphinatoiron(II) with a proximal base and succinimidyl(glutamyl) group to rHSA produced a novel albumin conjugate bearing covalently attached heme groups as O_2-coordination sites. The molecular weight of rHSA(FeP-Glu) was directly measured by MALDI-TOF MS. In nature, one can find unique heme-linked proteins, e.g., cyctochrome *c*. The rHSA(FeP-Glu) conjugate presumably becomes a valuable model of these hemoproteins. The obtained rHSA-(FeP-Glu) can reversibly absorb O_2 under physiological conditions, and its O_2-binding affinity showed an identical value to that for human erythrocytes. These results suggest that this novel plasma protein may efficiently transport O_2 in the bloodstream as an O_2-carrier with a long circulation time.

ACKNOWLEDGMENT

This work was partially supported by Grant-in-Aid for Scientific Research (No. 16350093) from JSPS, Grant-in-Aid for Exploratory Research (No. 16655049) from MEXT Japan, and Health Science Research Grants (Regulatory Science) from MHLW Japan. R.M.W. acknowledges NNSFC (No. 20274034). The authors are grateful to NIPRO Corp. for their supporting the oxygen-infusion project.

Supporting Information Available: Experimental details of the compounds **2**, **3**, **4**, **5**, FeP-Glu, and FeP-GluSu and their spectroscopic data. This material is available free of charge via the Internet at http://pubs.acs.org.

LITERATURE CITED

(1) Peters, T., Jr. (1996) All about albumin. *Biochemistry, Genetics, and Medical Applications*, Academic Press, San Diego; and reference therein.

(2) Kragh-Hansen, U. (1981) Molecular aspects of ligand binding to serum albumin. *Pharmacol. Rev. 33*, 17–53.

(3) Curry, S., Brick, P., and Franks, N. P. (1999) Fatty acid binding to human serum albumin: new insights from crystallographic studies. *Biochim. Biphys. Acta 1441*, 131–140.

(4) (a) Komatsu, T., Hamamatsu, K., Wu, J., and Tsuchida, E. (1999) Physicochemical properties and O_2-coordination structure of human serum albumin incorporating tetrakis(*o*-pivamido)phenylporphyrinatoiron(II) Derivatives. *Bioconjugate Chem. 10*, 82–86. (b) Tsuchida, E., Komatsu, T., Matsukawa, Y., Hamamatsu, K., and Wu, J. (1999) Human serum albumin incorporating tetrakis(*o*-pivalamido)phenylporphinatoiron(II) derivative as a totally synthetic O_2-carrying hemoprotein. *Bioconjugate Chem. 10*, 797–802. (c) Komatsu, T., Matsukawa, Y., and Tsuchida, E. (2000) Kinetics of CO- and O_2-binding to human serum albumin-heme hybrid. *Bioconjugate Chem. 11*, 772–776. (d) Komatsu, T., Matsukawa, Y., and Tsuchida, E. (2002) Effect of heme structure on O_2-binding properties of human serum albumin-heme hybrids: intramolecular histidine coordination provides a stable O_2-adduct complex. *Bioconjugate Chem. 13*, 397–402. (e) Tsuchida, E., Komatsu, T., Hamamatsu, K., Matsukawa, Y., Tajima, A., Yoshizu, A., Izumi, Y., and Kobayashi, K. (2000) Exchange transfusion of albumin-heme as an artificial O_2-infusion into anesthetized rats: physiological responses, O_2-delivery and reduction of the oxidized hemin sites by red blood cells. *Bioconjugate Chem. 11*, 46–50. (f) Kobayashi, K., Komatsu, T., Iwamaru, A., Matsukawa, Y., Watanabe, M., Horinouchi, H., and Tsuchida, E. (2003) Oxygenation of hypoxia region in solid tumor by administration of human serum albumin incorporating synthetic hemes. *J. Biomed. Mater. Res. 64A*, 48–51. (g) Tsuchida, E., Komatsu, T., Matsukawa, Y., Nakagawa, A., Sakai, H., Kobayashi, K., and Suematsu, M. (2003) Human serum albumin incorporating synthetic heme: red blood cell substitute

without hypertension by nitric oxide scavenging. *J. Biomed. Mater. Res. 64A*, 257–261.
(5) Russo, S. M., Pepe, J. Y., Donohue, S., Cable E. E., Lambrecht, R. W., and Bonkovsky, H. L. (1995) Tissue distribution of zinc-mesoporphyrin in rats: relationship to inhibition of heme oxygenase. *J. Pharmacol. Exp. Ther. 272*, 766–774.
(6) Tsuchida, E., Komatsu, T., Ando, K., Kumamoto, S., and Nishide, H (1995) Synthesis and O_2-binding properties of tetraphenylporphyrinatoiron(II) derivatives bearing a proximal imidazole covalently bound at the β-pyrrolic position. *J. Chem. Soc., Perkin Trans. 2* 1995, 747–753.
(7) The synthetic details and spectroscopic data of the porphyrins can be obtained from the Supporting Information.
(8) Tsuchida, E., Komatsu, T., Arai, K., and Nishide, H. (1993) Synthesis and dioxygen-binding properties of double-sided porphyrinatoiron(II) complexes bearing covalently bound axial imidazole. *J. Chem. Soc., Dalton Trans.* 2465–2469.
(9) (a) Collman, J. P., Brauman, J. I., Collins, T. J., Iverson, B. L., Lang, G., Pettman, R. B., Sessler, J. L., and Walters, M. A. (1983) Synthesis and characterization of the "Pocket" porphyrins. *J. Am. Chem. Soc. 105*, 3038–3052. (b) Collman, J. P., Brauman, J. I., Iverson, B. L., Sessler, J. L., Morris, R. M., and Gibson, Q. H. (1983) O_2 and CO binding to iron(II) porphyrins: a comparison of the "Picket Fence" and "Pocket" porphyrins. *J. Am. Chem. Soc. 105*, 3052–3064.
(10) Tsuchida, E., Komatsu, T., and Yanagimoto, T. (2000) Molecular environment effect on O_2-binding to lipidporphyrinatoiron(II) complexes in aqueous media, *J. Porphyr. 4*, 81–87.
(11) The esff force field simulation was performed using an Insight II system (Molecular Simulations Inc.). The structure was generated by alternative minimizations and annealing dynamic calculations from 1,000 K to 100 K.
(12) Severinghaus, J. W. (1966) Blood gas calculator. *J. Appl. Physiol. 21*, 1108–1116.
(13) Sawicki, C. A., and Gibson G. H. (1977) Properties of the T State of Human Oxyhemoglobin Studied by Laser Photolysis. *J. Biol. Chem. 252*, 7538–7547.
(14) Sharma, V. S., Schmidt, M. R., and Ranney, H. M. (1976) Dissociation of CO from Carboxyhemoglobin. *J. Biol. Chem. 251*, 4267–4272.
(15) Steinmeier, R. C., and Parkhurst, L. J. (1975) Kinetic Studies on the Five Principle Components of Normal Adult Human Hemoglobin. *Biochemistry 14*, 1564–1573.

BC049859M

Heat-Resistant Oxygen-Carrying Hemoproteins Consist of Recombinant Xylanases and Synthetic Iron(II) Porphyrin

Teruyuki Komatsu,† Seiji Ishihara,‡ Eishun Tsuchida,† Hiroyuki Nishide,*,‡ Chihiro Morokuma,§ and Satoshi Nakamura§

Department of Applied Chemistry and Advanced Research Institute for Science and Engineering, Waseda University, 3-4-1 Okubo, Shinjuku-ku, Tokyo 169-8555, Japan, and Department of Bioengineering, Tokyo Institute of Technology, 4259 Nagatsuta, Midori-ku, Yokohama 226-8501, Japan

Received November 23, 2004; Revised Manuscript Received January 12, 2005

Synthetic iron(II) porphyrin (FeP) is equivalently incorporated into recombinant *Thermotoga maritima* xylanase B (TMX; family F/10 of glycoside hydrolase), producing a heat-resistant artificial hemoprotein (TMX-FeP) that can bind and release oxygen (O_2) in aqueous medium (pH 7.3, 25 °C) in the same manner as hemoglobin and myoglobin. The oxygenated species was sufficiently stable; the half-lifetime against the ferric state ($\tau_{1/2}$) was 5 h. This O_2-carrying hemoprotein showed a high degree of thermal stability over a wide range of temperatures up to 90 °C ($\tau_{1/2}$ = 5 min at 90 °C and 9 min at 75 °C). *Dictyoglomus thermophilum* xylanase B (DTX; family G/11) also incorporates FeP, and DTX-FeP showed identical O_2-binding parameters and thermostability. TMX-FeP is capable of catalyzing the β-1,4-D-xylan hydrolysis reaction. Its larger K_m value compared to that of TMX itself suggested competitive FeP binding to the active site of the host enzyme.

Introduction

The development of gene technology has provided recombinant proteins, which are structurally defined biopolymer architectures. Human serum albumin (HSA), the major plasma protein in our blood stream, is currently manufactured on an industrial scale by expression in the yeast *Pichia pastoris*.[1] In the circulatory system, HSA nonspecifically binds endogenous and exogenous compounds (e.g., fatty acids, billirubin, steroids, and hemin) and transports them to the appropriate organs.[2] We have found that synthetic iron(II) porphyrin, 2-[8-(2-methylimidazolyl)octanoyloxymethyl]-5,10,15,20-tetrakis[(α,α,α,α-*o*-pivalamido)phenyl]porphinatoiron(II) (FeP, Figure 1A), is also incorporated into recombinant HSA (rHSA), producing an entirely synthetic hemoprotein (albumin-heme; rHSA-FeP). It can reversibly coordinate oxygen (O_2) in the same manner as hemoglobin (Hb) and myoglobin (Mb).[3] The exchange transfusion of the albumin-heme solution into acute anemia rat models immediately increased the declined O_2 tension of the tissues to the basal values.[4] Varieties of modified iron(II) porphyrins (MW 680−1940) are included into rHSA, and the O_2-transporting ability can be controlled by changing their chemical structures.[5] If this host−guest chemistry can be applied to other recombinant enzymes, one may create a new field of artificial hemoproteins.

Xylanases are glycoside hydrolases that hydrolyze β-1,4 bonds in the main chain of xylan (the major component of hemicellulose in the plant cell wall). In the pulp bleaching process, the enzymatic hydrolysis of xylan at high temperature has gained importance from an environmental aspect.

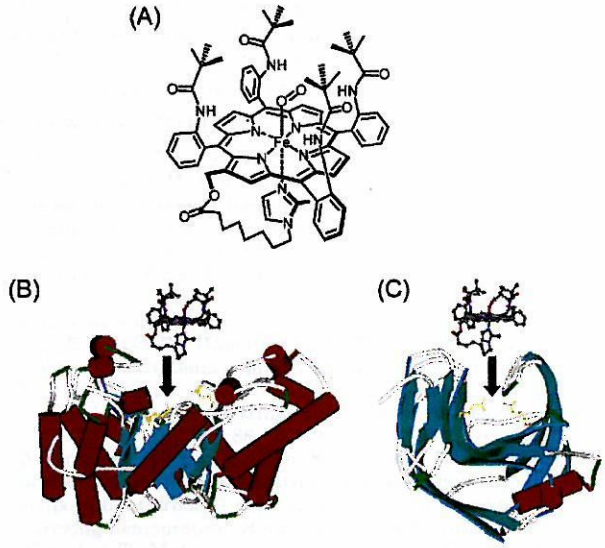

Figure 1. (A) Structure of FeP. (B) Schematic representation of family F/10 xylanase (TAX) on the basis of the 1k6a structure available at the Brookhaven Protein Data Bank, showing the overall fold. The α-helices are shown in red, β-sheets are shown in blue, and the two active sites (Glu131 and Glu237) are shown in yellow. The simulated structure of FeP, which was made by an MD simulation with Insight II (Molecular Simulations), is also displayed for the size comparison. (C) Schematic representation for family G/11 xylanase (DTX) on the basis of the 1f5j structure available at the Brookhaven Protein Data Bank. The differences in the color display are the same as described above, and the two active sites (Glu90 and Glu180) are shown in yellow. The simulated structure of FeP is also displayed for comparison.

* Corresponding author: tel +81 3-3200-2669; fax +81-3-3209-5522; e-mail nishide@waseda.jp.

† Advanced Research Institute for Science and Engineering, Waseda University.

‡ Department of Applied Chemistry, Waseda University.

§ Department of Bioengineering, Tokyo Institute of Technology.

10.1021/bm049255l CCC: $30.25
Published on Web 02/22/2005

Thermotoga maritima xylanase B (TMX, MW 39 000) shows a high degree of thermal stability even at 90 °C.[6] TMX belongs to the family F/10 xylanase, whose single polypeptide forms a unique $(\alpha/\beta)_8$ TIM-barrel fold.[7] Ramakumar and co-workers[8] elucidated the single crystal structure of the family F/10 *Thermoascus aurabtiacus* xylanase (TAX) (Figure 1B), which has a 35% sequence identity with TMX. On the other hand, the catalytic domain region of *Dictyoglomus thermophilum* xylanase B (DTX; typical family G/11 xylanase, MW 23 000) has a β-jelly roll fold.[9] The jelly roll of two highly twisted β-sheets makes a deep substrate binding cleft (Figure 1C).

More recently, we have expressed the catalytic domain regions of TMX and DTX in *Escherichia coli* and found that FeP is incorporated into their substrate binding clefts.[10] The formed xylanase-FePs showed O_2 coordination the same as Hb over a wide range of temperatures up to 90 °C. In this paper, we report the physicochemical properties, O_2-binding parameters, and enzymatic activity of these heat-resistant artificial hemoproteins.

Experimental Section

Materials and Apparatus. The catalytic domain regions of *T. maritima* xylanase B (TMX, MW 39 000) and *D. thermophilum* xylanase B (DTX, MW 23 000) were expressed in *Escherichia coli* and purified as described elsewhere.[6] 2-[8-(2-Methylimidazolyl)octanoyloxymethyl]-5,10,15,20-tetrakis[(α,α,α,α-*o*-pivalamido)phenyl]porphinatoiron(III) bromide [FeP Br^-] was prepared according to our previously reported procedures.[11] Other chemicals used were commercial high-purity grades. The water was deionized on an Advantec GS-200 system. UV−Vis absorption spectra were recorded on a Jasco V-570 spectrophotometer.

Preparation of Xylanase-FeP Hybrids. Carbon monoxide (CO) was bubbled into an EtOH solution of FeP Br^- (80 μM, 2.5 mL), and a small excess amount of ascorbic acid was added to this solution to reduce the central iron(III) of the porphyrin. The obtained ethanolic carbonylated FeP was slowly injected into the phosphate-buffered solution (25 mM, pH 7.3, 7.5 mL) of TMX or DTX (26.7 μM) under a CO atmosphere. The mixture was dialyzed with a cellulose membrane against phosphate buffer (pH 7.3) at 4 °C to remove excess EtOH and ascorbic acid. The total volume was finally adjusted to 10 mL, producing carbonyl xylanase-FeP solutions (FeP/xylanase = 1/1 (mol/mol), [FeP] = 20 μM), which were stable for more than 1 year at 4 °C without precipitation.

Physicochemical Properties. The binding constants of FeP (K^{FeP}) to xylanases were measured according to the ultrafiltration procedures described elsewhere.[12] Circular dichroism (CD) spectra were obtained on a Jasco J-725 spectropolarimeter. The xylanase concentration was 2 μM, and quartz cuvettes with a 10-mm thickness were used for the measurements over the range of 210−250 nm. The amount of FeP was determined by UV−vis absorption intensity or assay of the iron concentration by inductively coupled plasma spectrometry (ICP) on a Seiko Instruments SPS 7000A spectrometer. The isoelectric points and molecular weights were obtained on a Pharmacia Phastsystem with isoelectric focusing (IEF) in pH 3−9 Phast gel IEF 3−9 and native polyacrylamide gel electrophoresis (PAGE) in Phast gel gradient 8−25.

O_2 Coordination Equilibria and Kinetics. Light irradiation (500 W halogen lamp) of the aqueous carbonylated xylanase-FeP solutions under an O_2 atmosphere led to CO dissociation, affording the O_2 adduct complex. Upon exposure of N_2, the spectrum changed to that of the five-N-coordinated high-spin iron(II) complex with an intramolecularly coordinated proximal imidazole. O_2 coordination to FeP is expressed by

$$\mathrm{FeP} + \mathrm{O_2} \underset{k_{off}}{\overset{k_{on}}{\rightleftharpoons}} \mathrm{FeP\text{-}O_2} \qquad (K = k_{on}/k_{off}) \qquad (1)$$

The O_2-binding constant $[K = (P_{1/2})^{-1}]$ of xylanase-FeP was determined by spectral changes at various partial pressure of O_2 as in previous literature.[3b,5,13,14] The FeP concentrations of 5−20 μM were normally used for UV−vis absorption spectroscopy. The spectra were recorded within the range of 350−700 nm. The autoxidation kinetics of the xylanase-FeP(O_2) was monitored by the decay of the UV−vis absorption at 550 nm. At high temperature (75 or 90 °C), the spectral change was recorded on an Agilent 8543 spectroscopy system with an Agilent 89090A temperature controller. The temperature of the solution in the quartz cuvette was continuously monitored with an AS ONE digital thermometer IT-2100. The thermodynamic parameters for O_2 binding (ΔH and ΔS) were determined by van't Hoff plots of K in the temperature range 15−40 °C.

The O_2 association and dissociation rate constants (k_{on}, k_{off}) were measured by a competitive rebinding technique on a Unisoku TSP-600 laser flash photolysis apparatus.[3b,c,5,13,14] The absorption decays accompanying O_2 rebinding obeyed a single exponential; therefore first-order kinetics were applied to calculate the rate constants.

Enzymatic Activity of Xylanase-FeP. The xylanase activity (xylan hydrolysis reaction) was assayed by measuring the amount of reducing sugars liberated from xylan.[15] The xylanase or xylanase-FeP solution (0.418 μM, 40 μL) was mixed with the birchwood xylan (1.0 wt %, Sigma) suspension in a 100 mM Na_2CO_3−$NaHCO_3$ buffer (pH 9.0, 160 μL) and stirred at 50 °C for 10 min. After the reaction, the enzyme was inactivated by the addition of 3,5-dinitrosalicylic acid reagent (0.24 mL) and heated at 100 °C for 5 min. The obtained solution was then diluted by deionized water (2.56 mL) and used for the UV−vis spectral measurement. On the basis of the absorption intensity at 500 nm, the amount of produced xylose was calculated. This xylan hydrolysis reaction was performed with different concentrations of birchwood xylan (0.1−1.0 wt %), and the kinetic parameters [K_m and k_{cat} (V_{max}/[xylanase])] were determined by the usual Lineweaver−Burk plots.

Results and Discussion

Incorporation of FeP into Recombinant Xylanases. Preliminary UV−vis absorption spectroscopic experiments suggested that there are some binding sites for FeP in TMX

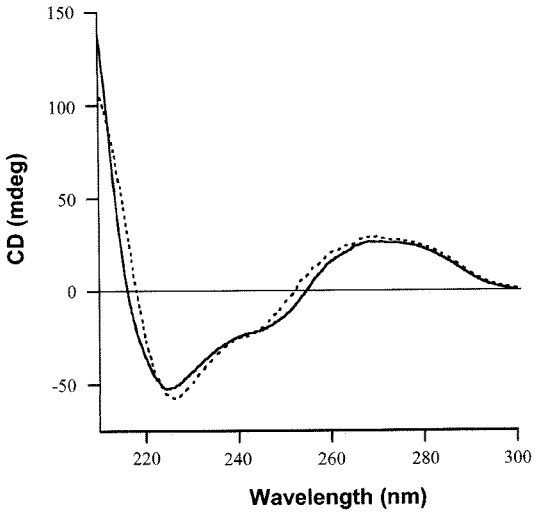

Figure 2. CD spectra of TMX (···) and TMX-FeP (—) in phosphate-buffered solution (pH 7.3, 25 mM) at 25 °C.

and DTX. The aqueous carbonyl xylanase-FeP solution prepared by FeP/xylanase = 1/1 (mol/mol) ([FeP] = 5 μM) showed a Soret band at 427 nm with absorbance of 0.62, which was almost the same as that of the well-defined rHSA-FeP with FeP/xylanase = 1/1 (mol/mol) ([FeP] = 5 μM).[3a] The absorption intensity was, however, not dependent on the increase of mixing ratio of FeP/xylanase = 2/1, 3/1, 4/1 (mol/mol) ([FeP] = 5 μM). These observations imply that the xylanase involves one major site with a high binding constant. To simplify the system, we prepared the equivalent composite, in which FeP is monomolecularly accommodated to a unique site of the protein. The obtained aqueous xylanase-FeP solutions were red-colored, homogeneous, and stable without any precipitation for over 1 year at 4 °C. The following experimental results suggest that FeP was definitely included into the host xylanase: (i) The outer aqueous phase of the dialysis during the ethanol exclusion did not show any absorbance from FeP at 427 nm. (ii) The elution band of FeP in gel-permeation chromatography (Sephadex G-25) coincided well with the xylanase band. (iii) The ICP measurement led to determine the iron concentration of FeP, which gave the accurate molar ratio of FeP/xylanase = 1:1.

The binding constants of FeP (K^{FeP}) for TMX and DTX were determined to be 2.2×10^6 and 2.9×10^6 M^{-1}. These values are in good agreement with that of FeP for rHSA (1.6×10^6 M^{-1}).[3a] Because the synthetic iron(II) porphyrin without any ionic side chain interacts with xylanase by a hydrophobic interaction, the binding constant could be similar to that for albumin. In fact, the isoelectric point (p*I* 7.0) of TMX did not change after the inclusion of FeP and its surface net charges are always identical. Furthermore, the presence of bound FeP negligibly affected the peptide CD spectrum (210–250 nm) (Figure 2). This implies that the incorporation of FeP produces no structural changes in TMX. In general, the binding of protoheme IX to the albumin molecule is accompanied by a rise to an extrinsic negative Cotton effect in the Soret band region, because it binds to an albumin through an axial ligation, allowing a high degree of immobilization.[16] In the case of the synthetic FeP, the proximal base is covalently attached at the porphyrin periphery and

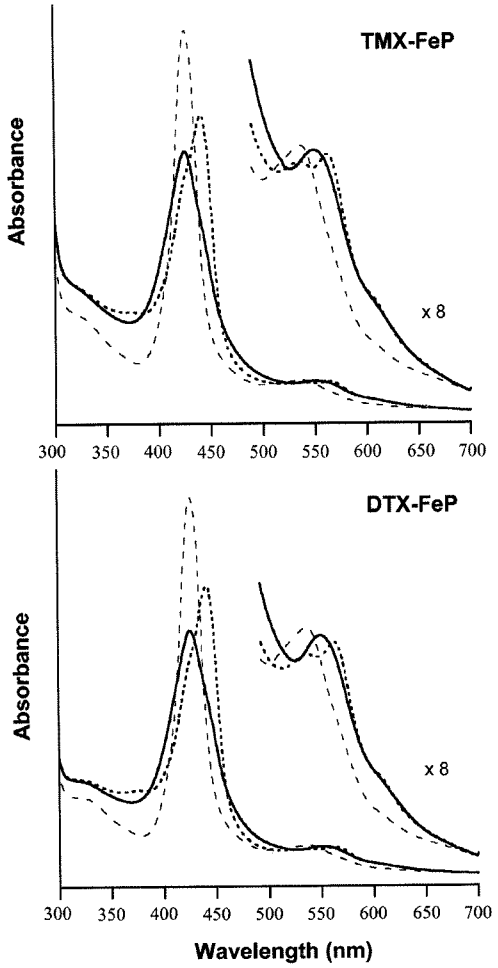

Figure 3. UV–visible absorption spectral changes of TMX-FeP and DTX-FeP in phosphate-buffered solution (pH 7.3, 25 mM) at 25 °C: (···) under an argon atmosphere; (—) under an O_2 atmosphere; (– – –) under a CO atmosphere.

intramolecularly coordinates to the iron(II) center. Actually, the induced CD was not detectable in xylanase-FeP, which is the same as that seen in the rHSA-FeP hybrid.[3a] The FeP could weakly interact with the xylanases and albumin.

O_2-Coordination Equilibrium and Kinetics. The UV–vis absorption spectrum of the aqueous solution of TMX-FeP under an N_2 atmosphere showed λ_{max} at 441, 535, and 562 nm, which indicates the formation of the typical five-N-coordinated high-spin iron(II) porphyrin complex (Figure 3).[3a,b,5] We regarded that (i) the 2-methylimidazolylalkyl arm coordinates to the central ferrous ion in a fashion similar to FeP in toluene solution and (ii) no polar amino acid residue of TMX occupies the iron(II) center in the sixth position. Upon the bubbling of O_2 gas into the solution, the UV–vis absorption spectrum immediately changed to that of the O_2 adduct complex (λ_{max} = 426, 550 nm). This oxygenation was reversibly observed and was dependent on the O_2 partial pressure. The rate of irreversible oxidation is satisfactorily slow; the half-lifetime against the ferric state ($\tau_{1/2}$) was 5 h. The addition of CO gas through the solution gave a very stable carbonyl complex with a large Soret band absorption (λ_{max} = 427, 537 nm).[3,5] The family G/11 xylanase (DTX) also incorporates FeP by the same procedure, and the formed

Table 1. O_2 Binding and Its Thermodynamic Parameters of Xylanase-FeP in Phosphate-Buffered Solution (pH 7.3) at 25 °C

	10^{-4} K (M^{-1})	$P_{1/2}$ (Torr)	10^{-7} k_{on} (M^{-1} s^{-1})	10^{-2} k_{off} (s^{-1})	ΔH (kJ mol^{-1})	ΔS (J K^{-1} mol^{-1})
TMX-FeP	2.2	27	3.2	14	−61	−111
DTX-FeP	2.6	23	3.2	12	−62	−105
rHSA-FeP[a]	4.7	13	3.2	7.2	−60	−114
FeP in toluene[b]	0.2	38	16	460	−61	−178

[a] Reference 3b. [b] Reference 11.

DTX-FeP can bind and release O_2 as well (deoxy, λ_{max} = 441, 536, 562 nm; oxy, λ_{max} = 426, 550 nm; carbonyl, λ_{max} = 427, 536 nm).

The O_2-binding constants (K) for these oxygenations could be directly determined at 25 °C. Adequate isosbestic behavior was maintained during the course of a spectrophotometric titration of O_2. We could not find a significant difference in the K and O_2 binding rate constants (k_{on}, k_{off}) of TMX-FeP and DTX-FeP (Table 1). Nevertheless, their K values are considerably higher (low $P_{1/2}$) than that of FeP itself in toluene solution by a factor of 11−13, which is kinetically due to the low O_2 dissociation rates. In Hb and Mb, the coordinated O_2 is stabilized by hydrogen bonding to the distal histidine (His-64). On the contrary, it is impossible for FeP to form such an interaction with a polar amino acid in xylanase. In the case of O_2 binding to the synthetic iron(II) porphyrin, it is widely known that changing from nonpolar to polar solvent serves to increase the equilibrium constant K by a factor of 10−40.[13] This elevation was predominantly manifested in decreased dissociation rate constants. The active-site region at the β-barrel center in the family F/10 xylanases is rich in polar and negatively charged amino acids with many of the aromatic residues.[8] DTX also has a significant proportion of polar surfaces.[9] Most probably, FeP is incorporated into the substrate binding clefts of the xylanases, and the polar microenvironment retards the dissociation of the bound O_2 and provides the high O_2-binding affinity.

Thermostability and O_2−Adduct Complex at High Temperature. In the heat-resistant family F/10 xylanases, a disulfide bond and more than 10 salt bridges between oppositely charged groups contribute to their thermal stability at elevated temperature.[8] TMX-FeP after incubation at 90 °C still showed a single band in native PAGE and the CD spectrum remained essentially unaltered (not shown). It suggests that the inclusion of FeP does not induce any changes in the S−S bonding and the ion-pair interactions of the host protein. The K^{FeP} value at high temperature could not be determined by our centrifuge procedures. However, the UV−vis absorption pattern and intensity of the carbonyl xylanase-FeP showed almost no change at 25, 75, and 90 °C, suggesting that FeP remained in the protein matrix. The stereochemistry of the iron(II) porphyrin after heating was also evaluated. In general, refluxing the toluene solution of FeP for 30 min leads to isomerization of the α,α,α,α-conformer with respect to the porphyrin ring plane in the statistical mixture of the four atropisomeric products (α,α,α,α, α,α,α,β, α,α,β,β, and α,β,α,β forms). Surprisingly, thin-layer chromatography of the $CHCl_3$ solution of FeP extracted from aqueous TMX-FeP represented only a mono spot of the α,α,α,α-isomer.

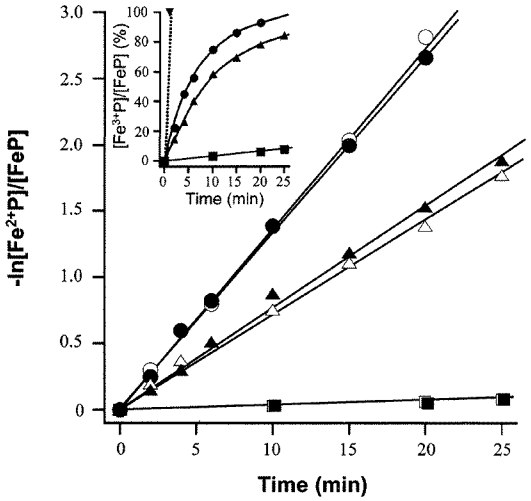

Figure 4. First-order plots for the irreversible oxidation process of oxygenated xylanase-FeP at 25, 75, and 90 °C. The oxidation kinetics was monitored by the decay of the absorption change at 550 nm based on the oxygenated FeP in phosphate-buffered solution (pH 7.3, 25 mM, $[O_2]$ = 760 Torr); TMX-FeP (● at 90 °C, ▲at 75 °C, ■ at 25 °C), DTX-FeP (○ at 90 °C, △ at 75 °C, □ at 25 °C). (Inset) Time course of the ferric content ratio of the iron porphyrin in TMX-FeP (● at 90 °C, ▲at 75 °C, ■ at 25 °C) and Hb (▼ at 90 °C, ···).

It is rather remarkable that the oxygenated xylanase-FeP exhibited heat resistance up to 90 °C. This is in contrast to the fact that the central ferrous ion of protoheme IX in Hb or FeP in water-saturated toluene was immediately oxidized within 1 min under the same conditions. Since the O_2 coordination to the iron(II) porphyrin is an exothermic reaction, the excess heating must shift the O_2 binding equilibrium to the left in eq 1. Although the slight absorption of the deoxy form at 441 nm appeared at high temperature, the dominant species was still the O_2 adduct complex. The oxidation process of the ferrous FeP in the xylanases obeyed first-order kinetics in all the temperature ranges investigated (Figure 4). The autoxidation of the oxygenated iron(II) porphyrin in homogeneous solution generally consists of two mechanisms: μ-peroxo mechanism and proton-catalyzed superoxide mechanism.[17] In natural Hb and Mb, it is clear that the former one cannot occur because polypeptide matrix prevents the approach of two heme sites. Olson and co-workers[18] have proposed that the autoxidation of oxyMb occurs through two pathways: direct dissociation of the neutral HO_2 from oxyMb at high $[O_2]$, and bimolecular reaction between O_2 and H_2O coordinated deoxyMb at low $[O_2]$. The hydrogen bonding between the bound O_2 and distal His-64 prevents both HO_2 dissociation and the bimolecular reaction, resulting in a delay of the autoxidation. In the case of the oxygenated xylanase-FeP, there is no hydrogen-bonding counterpart. The final product of the TMX-FeP

Table 2. Kinetic Parameters of Xylanase-FeP for Xylan Hydrolysis at 50 °C

	K_m (mg mL^{-1})	k_{cat} (min^{-1})	k_{cat}/K_m (min^{-1} mg^{-1} mL)
TMX	2.6	780	300
TMX-FeP	9.4	1020	109

exhibited an absorption spectrum characteristics of the ferric FeP(OH) complex (λ_{max} = 577 nm).[19] Whereas the details of the autoxidation mechanism of the oxygenated iron(II) porphyrin remain unclear, Momenteau and co-workers[20] proposed the water-driven (i.e., proton-driven) reaction on the basis of the ^{17}O NMR spectroscopic study. Consequently, it can be concluded that the water-driven reaction could govern the autoxidation of the xylanase-FeP(O_2) without μ-oxo dimer formation; the $\tau_{1/2}$ was 5 min at 90 °C and 9 min at 75 °C.

Attempts to determine their O_2-binding affinity at high temperature unfortunately failed as the lifetime of the ferrous state was not enough to allow for $P_{1/2}$ determination by the spectrophotometric technique with normal O_2 titration. Therefore, the thermodynamic parameters for O_2 binding to xylanase-FeP were determined from the temperature dependence of the K values at 15−40 °C (Table 1). ΔH and ΔS of the O_2 coordination showed almost the same values as those of rHSA-FeP.[3b]

It follows from what has been described thus far that the FeP molecule is accommodated into the cleft of the recombinant xylanases and the obtained O_2 adduct species demonstrated an unusual heat resistance; the $\tau_{1/2}$ becomes over 10-fold longer than that of Hb.

For TAX, which has a sequence similarity to TMX, the diameter of the β-barrel is 40 Å.[8] From the results of the MD simulation, the molecular dimensions of FeP were estimated to be 13 × 13 × 13 Å. Actually, FeP can fit in the cleft of the β-barrel with a depth of approximately 15 Å (Figure 1B). In DTX, the width of a deep cleft made of two β-sheet walls is 14 Å, which is also sufficiently wide to clip the encumbered iron(II) porphyrin. These findings confirmed that FeP can be included into the cleft on the rigid β-barrel of TMX or in the deep cleft between the two β-sheets of DTX. The water-driven oxidation of the central iron(II) was retarded even at high temperature and the produced O_2 adduct complexes demonstrated a significant thermal stability compared to the natural Hb.

Enzymatic Activity for Hydrolysis of Xylan. The kinetic parameters of TMX toward xylan hydrolysis are determined to be K_m = 2.6 mg mL^{-1} and k_{cat} = 780 min^{-1}, which are typical for family F/10 xylanases (Table 2).[21] TMX-FeP, the O_2-carrying xylanase, is also capable of catalyzing the xylan hydrolysis reaction. Although its k_{cat} (1020 s^{-1}) was unaltered, the K_m value (9.4 mg mL^{-1}) increased 3.6-fold larger than that of TMX. It again suggested that the FeP molecule is competitively incorporated into the substrate binding cleft of the β-barrel and affects the original enzymatic activity of the host xylanase.

Conclusion

As described in this report, the recombinant xylanases successfully incorporated the synthetic iron(II) porphyrin, giving stable artificial hemoproteins, which can form O_2 adduct complexes over a wide range of temperatures up to 90 °C. They are the first examples of the entirely synthetic heat-resistant O_2-carrying enzyme. This host−guest chemistry with a nonspecific interaction will be applied to other functional proteins, allowing us to construct a new field of artificial hemoproteins.

Acknowledgment. This work was partially supported by Grants-in-Aid for Scientific Research on Priority Area Soft Materials (13031024 and 13031072), a Grant-in-Aid for Exploratory Research (16655049) from MEXT Japan, and a Grant-in-Aid for Scientific Research (16350093) from JSPS.

References and Notes

(1) (a) Sumi, A.; Ohtani, W.; Kobayashi, K.; Ohmura, T.; Yokoyama, K.; Nishida, M.; Suyama, T. Purification and physicochemical properties of recombinant human serum albumin. In *Biotechnology of Blood Proteins*; Rivat, C., Stoltz, J.-F., Eds.; John Libbey Eurotext: Montrouge, 1993; Vol. 227, pp 293−298. (b) Ohtani, W.; Nawa, Y.; Takeshima, K.; Kamuro, H.; Kobayashi, K.; Ohmura, T. Physicochemical and immunochemical properties of recombinant human serum albumin from *Pichia pastoris*. *Anal. Biochem.* **1998**, *256*, 56−62.

(2) Peters, T., Jr. *All about albumin, biochemistry, genetics, and medical applications*; Academic Press; San Diego, CA, 1997.

(3) (a) Komatsu, T.; Hamamatsu, K.; Wu, J.; Tsuchida, E. Physicochemical properties and O_2-coordination structure of human serum albumin incorporating tetrakis(*o*-pivalamido)phenylporphinatoiron(II) derivatives. *Bioconjugate Chem.* **1999**, *10*, 82−86. (b) Tsuchida, E.; Komatsu, T.; Matsukawa, Y.; Hamamatsu, K.; Wu, J. Human serum albumin incorporating tetrakis(*o*-pivalamido)phenylporphinatoiron-(II) derivative as a totally synthetic O_2-carrying hemoprotein. *Bioconjugate Chem.* **1999**, *10*, 797−802. (c) Komatsu, T.; Matsukawa, Y.; Tsuchida, E. Kinetics of CO and O_2 binding to human serum albumin−heme hybrid. *Bioconjugate Chem.* **2000**, *11*, 772−776.

(4) Komatsu, T.; Huang, Y.; Yamamoto, H.; Horinouchi, H.; Kobayashi, K. Exchange transfusion with synthetic oxygen-carrying plasma protein "albumin-heme" into an acute anemia rat model after seventy-percent hemodilution. *J. Biomed. Mater. Res.* **2004**, *71A*, 644−651.

(5) (a) Komatsu, T.; Okada, T.; Moritake, M.; Tsuchida, E. O_2-Binding properties of double-sided porphyrinatoiron(II)s with polar substituents and their human serum albumin hybrids. *Bull. Chem. Soc. Jpn.* **2001**, *74*, 1695−1702. (b) Komatsu, T.; Matsukawa, Y.; Tsuchida, E. Effect of heme structure on O_2-binding properties of human serum albumin-heme hybrids: intramolecular histidine coordination provides a stable O_2-adduct complex. *Bioconjugate Chem.* **2002**, *13*, 397−402.

(6) (a) Morokuma, C.; Ide, M.; Yatsunami, R.; Nakamura, S. Gene cloning and expression of thermostable xylanases and characterization of recombinant proteins; *Proceedings of the 8th International SPACC Symposium*; Beijing, China, October 18−19, 2001; p 81. (b) Ihsanawati, Kumasaka, T.; Kaneko, T.; Morokuma, C.; Nakamura, S.; Tanaka, N. Crystallization and preliminary X-ray studies of xylanase 10B from *Thermotoga maritima*. *Acta Crystallogr.* **2003**, *D59*, 1659−1661.

(7) Banner, D. W.; Bloomer, A. C.; Petsko, G. A.; Phillips, D. C.; Pogson, C. I.; Wilson, I. A.; Corran, P. H.; Furth, A. J.; Milman, J. D.; Offord, R. E.; Priddle, J. D.; Waley, S. G. Structure of chicken muscle triose phosphate isomerase determined crystallographically at 2.5 Å resolution using amino acid sequence data. *Nature* **1975**, *255*, 609−614.

(8) Natesh, R.; Bhanumoorthy, P.; Vithayathil, P. J.; Sekar, K.; Ramakumar, S.; Viswamitra, M. A. Crystal structure at 1.8 Å resolution and proposed amino acid sequence of thermostable xylanase from *Thermoascus aurantiacus*. *J. Mol. Biol.* **1999**, *288*, 999−1012.

(9) McCarthy, A. A.; Morris, D. D.; Bergquist, P. L.; Baker, E. N. Structure of xynB, a highly thermostable β-1,4-xylanase from *Dictyoglomus thermophilum* Rt46B.1, at 1.8 Å resolution. *Acta Crystallogr.* **2000**, *D56*, 1367−1375.

(10) Komatsu, T.; Ishihara, S.; Tsuchida, E.; Nishide, H.; Morokuma, C.; Nakamura, S. Thermostable synthetic hemoproteins: thermophilic xylanases hybridized with dioxygen-carrying *meso*-tetrakis(*o*-pivalamidophenyl)porphinatoiron(II) derivative. *Chem. Lett.* **2003**, *32*, 108−109.

(11) Tsuchida, E.; Komatsu, T.; Ando, K.; Kumamoto, S.; Nishide, H. Synthesis and O_2-binding properties of tetraphenylporphyrinatoiron(II) derivatives bearing a proximal imidazole covalently bound at the β-pyrrolic position. *J. Chem. Soc., Perkin Trans. 2* **1995**, 747−753.

(12) Komatsu, T.; Oguro, Y.; Teramura, Y.; Takeoka, S.; Okai, J.; Anraku, M.; Otagiri, M.; Tsuchida E. Physicochemical characterization of cross-linked human serum albumin dimer and its synthetic heme hybrid as an oxygen carrier. *Biochim. Biophys. Acta* **2004**, *1675*, 21−31.

(13) Collman, J. P.; Brauman, J. I.; Iverson, B. L.; Sessler, J. L.; Morris, R. M.; Gibson, Q. H. O_2 and CO binding to iron(II) porphyrins: a comparison of the "picket fence" and "pocket" porphyrins. *J. Am. Chem. Soc.* **1983**, *105*, 3052−3064.

(14) Traylor, T. G.; Tsuchiya, S.; Campbell, D.; Mitchell, M.; Stynes, D.; Koga, N. Anthracene heme cyclophanes. Steric effects in CO, O_2, and RNC binding. *J. Am. Chem. Soc.* **1985**, *107*, 604−614.

(15) Nakamura, S.; Ishiguro, Y.; Nakai, R.; Wakabayashi, K.; Aono R.; Horikoshi, K. Purification and characterization of a thermophilic alkaline xylanase from themoalkaliphilic *Bacillus* sp. Strain TAR-1. *J. Mol. Catal.* **1995**, *B 1*, 7−15.

(16) Beaven, G. H.; Chen, S.-H.; D'Albis, A.; Gratzer, W. B. A spectroscopic study of the haemin-human-serum-albumin system. *Eur. J. Biochem.* **1974**, *41*, 539−546.

(17) Momenteau, M.; Reed, C. A. Synthetic heme dioxygen complexes. *Chem. Rev.* **1994**, *94*, 659−698.

(18) Brantley, R. E.; Smerdon, S. J.; Wilkinson, A. J.; Singleton, E. W.; Olson, J. S. The mechanism of autooxidation of myoglobin. *J. Biol. Chem.* **1993**, *268*, 6995−7010.

(19) Lexa, D.; Momenteau, M.; Saveant, J.-M.; Xu, F. Redox properties and stability of hydroxyl complexes of protected iron(III) and iron(II) porphyrins. *Inorg. Chem.* **1985**, *24*, 122−127.

(20) Gerothnassis, I. P.; Momenteau, M.; Loock, B. Hydrogen-bond stabilization of dioxygen: conformation excitation and autoxidation mechanism in hemoprotein models as revealed by oxygen-17 NMR spectroscopy. *J. Am. Chem. Soc.* **1989**, *111*, 7006−7012.

(21) Charnock, S. J.; Spurway, T. D.; Xie, H.; Beylot, M.-H.; Virden, R.; Warren, R. A. J.; Hazlewood, G.; Gilbert, H. J. The topology of the substrate binding clefts of glycosyl hydrolase family 10 xylanases are not conserved. *J. Biol. Chem.* **1998**, *273*, 32187−32199.

BM049255L

J|A|C|S
ARTICLES
Published on Web 10/20/2005

O_2 and CO Binding Properties of Artificial Hemoproteins Formed by Complexing Iron Protoporphyrin IX with Human Serum Albumin Mutants

Teruyuki Komatsu,*,† Naomi Ohmichi,† Akito Nakagawa,† Patricia A. Zunszain,‡ Stephen Curry,‡ and Eishun Tsuchida*,†

Contribution from the Advanced Research Institute for Science and Engineering, Waseda University, 3-4-1 Okubo, Shinjuku-ku, Tokyo 169-8555, Japan, and Division of Cell and Molecular Biology, Faculty of Life Sciences, Imperial College London, Huxley Building, South Kensington Campus, London SW7 2AZ, United Kingdom

Received July 18, 2005; E-mail: teruyuki@waseda.jp; eishun@waseda.jp

Abstract: The binding properties of O_2 and CO to recombinant human serum albumin (rHSA) mutants with a prosthetic heme group have been physicochemically and kinetically characterized. Iron(III) protoporphyrin IX (hemin) is bound in subdomain IB of wild-type rHSA [rHSA(wt)] with weak axial coordination by Tyr-161. The reduced ferrous rHSA(wt)−heme under an Ar atmosphere exists in an unusual mixture of four- and five-coordinate complexes and is immediately autoxidized by O_2. To confer O_2 binding capability on this naturally occurring hemoprotein, a proximal histidine was introduced into position Ile-142 or Leu-185 by site-directed mutagenesis. A single mutant (I142H) and three double mutants (I142H/Y161L, I142H/Y161F, and Y161L/L185H) were prepared. Both rHSA(I142H/Y161L)−heme and rHSA(I142H/Y161F)−heme formed ferrous five-*N*-coordinate high-spin complexes with axial ligation of His-142 under an Ar atmosphere. These artificial hemoproteins bind O_2 at room temperature. Mutation at the other side of the porphyrin, Y161L/L185H, also allowed O_2 binding to the heme. In contrast, the single mutant rHSA(I142H)−heme could not bind O_2, suggesting that removal of Y161 is necessary to confer reversible O_2 binding. Laser flash photolysis experiments showed that the kinetics of CO recombination with the rHSA(mutant)−heme were biphasic, whereas O_2 rebinding exhibited monophasic kinetics. This could be due to the two different geometries of the axial imidazole coordination arising from the two orientations of the porphyrin plane in the heme pocket. The O_2 binding affinities of the rHSA(mutant)−heme were significantly lower than those of hemoglobin and myoglobin, principally due to the high O_2 dissociation rates. Changing Leu-161 to Phe-161 at the distal side increased the association rates of both O_2 and CO, which resulted in enhanced binding affinity.

Introduction

Human serum albumin (HSA) is a versatile protein found at high concentrations (4−5 g/dL) in blood plasma and is principally characterized by its remarkable ability to bind a wide range of insoluble endogenous and exogenous compounds.[1] Physiological ligands for HSA include nonesterified fatty acids, hemin, bilirubin, bile acids, and thyroxine,[2−4] but the protein also binds a huge variety of drugs. Currently, it is of great interest to exploit the carrier properties of this shuttle protein for the development of novel therapeutic reagents for drug delivery and pharmacodynamic modulation.[5−7] Hemin [iron(III) protoporphyrin IX] released from hemoglobin (Hb) during the enucleation of red cells or through hemolysis is captured by HSA, which has a high binding constant for this ligand ($K \approx 10^8$ M^{-1}).[8] This strong affinity of HSA for hemin has stimulated efforts to develop albumin as an artificial hemoprotein which can mimic the O_2 binding capability of Hb and myoglobin (Mb).[9,10] HSA consists of a helical monomer of 66.5 kDa containing three homologous domains (I−III), each of which

† Waseda University.
‡ Imperial College London.

(1) Peters, T. *All about Albumin: Biochemistry, Genetics and Medical Applications*; Academic Press: San Diego, 1996; and references therein.
(2) (a) Kragh-Hansen, U. *Pharmacol. Rev.* **1981**, *33*, 17−53. (b) Kragh-Hansen, U. *Danish Med. Bull.* **1990**, *37*, 57−84.
(3) (a) Curry, S.; Madelkow, H.; Brick, P.; Franks, N. *Nat. Struct. Biol.* **1998**, *5*, 827−835. (b) Bhattacharya, A. A.; Grune, T.; Curry, S. *J. Mol. Biol.* **2000**, *303*, 721−732. (c) Curry, S. Plasma Albumin as a Fatty Acid Carrier. In *Adv. Mol. Cell. Biol.*; van der Vusse, G., Ed.; Elsevier: 2003; Vol. 33, pp 29−46. (d) Petitpas, I.; Petersen, C. E.; Ha, C.-E.; Bhattacharya, A. A.; Zunszain, P. A.; Ghuman, J.; Bhagavan, N. V.; Curry, S. *Proc. Natl. Acad. Sci. U.S.A.* **2003**, *100*, 6440−6445. (e) Zunszain, P. A.; Ghuman, J.; Komatsu, T.; Tsuchida, E.; Curry, S. *BMC Struct. Biol.* **2003**, *3*, 6.
(4) (a) He, X. M.; Carter, D. C. *Nature* **1992**, *358*, 209−215. (b) Carter, D. C.; Ho, J. X. *Adv. Protein Chem.* **1994**, *45*, 153−203. (c) Wardell, M.; Wang, Z.; Ho, J. X.; Robert, J.; Ruker, F.; Rubel, J.; Carter, D. C. *Biochem. Biophys. Res. Commun.* **2002**, *291*, 813−819.
(5) Beljaars, L.; Molema, G.; Schuppan, D.; Geerts, A.; De Bleser, P. J.; Weert, B.; Meijer, D. K. F.; Poelstra, K. *J. Biol. Chem.* **2000**, *275*, 12743−12751.
(6) Kurtzhals, P.; Havelund, S.; Jonassen, I.; Kiehr, B.; Larsen, U. D.; Ribel, U.; Markussen, J. *Biochem. J.* **1995**, *312*, 725−731.
(7) Sheffield, W. P. *Curr. Drug Targets Cardiovasc. Haematol. Disord.* **2001**, *1*, 1−22.
(8) Adams, P. A.; Berman, M. C. *Biochem. J.* **1980**, *191*, 95−102.
(9) (a) Komatsu, T.; Hamamatsu, K.; Wu, J.; Tsuchida, E. *Bioconjugate Chem.* **1999**, *10*, 82−86. (b) Tsuchida, E.; Komatsu, T.; Matsukawa, Y.; Hamamatsu, K.; Wu, J. *Bioconjugate Chem.* **1999**, *10*, 797−802. (c) Komatsu, T.; Matsukawa, Y.; Tsuchida, E. *Bioconjugate Chem.* **2002**, *13*, 397−402.

10.1021/ja054819u CCC: $30.25

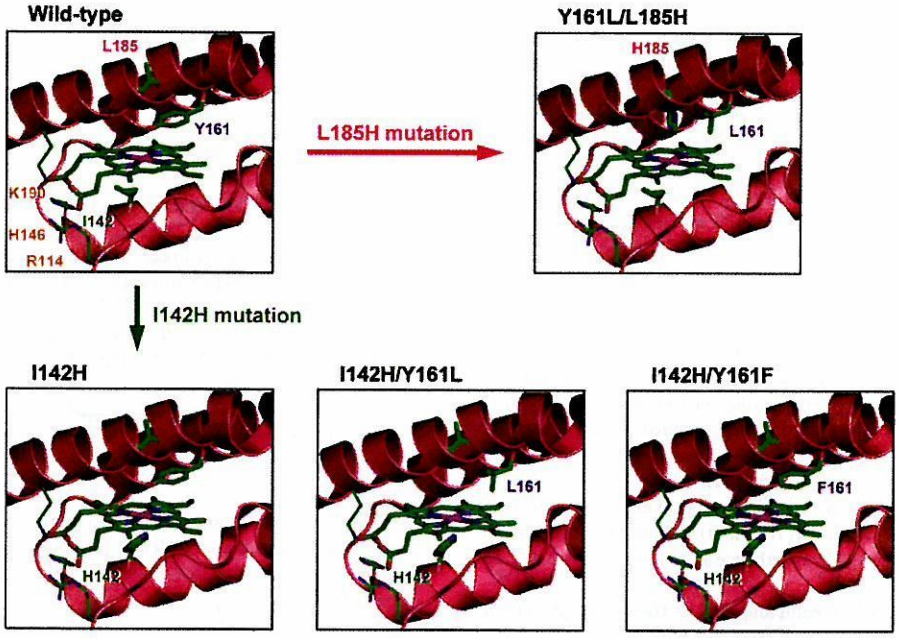

Figure 1. Structural models of the effect of site-directed mutagenesis in subdomain IB of HSA to construct a tailor-made heme pocket, which allows O_2 binding to the prosthetic Fe^{2+} protoporphyrin IX (heme) group.[12]

is composed of A and B subdomains. Crystallographic studies have revealed that hemin is bound within a narrow D-shaped hydrophobic cavity in subdomain IB with axial coordination of Tyr-161 to the central ferric ion and electrostatic interactions between the porphyrin propionates and a triad of basic amino acid residues (Arg-114, His-146, and Lys-190) (Figure 1).[3e,4c] In terms of the general hydrophobicity of this α-helical heme pocket, the subdomain IB of HSA potentially has similar features to the heme binding site of Hb or Mb. However, if one reduces the HSA−hemin to obtain the ferrous complex, it is rapidly oxidized by O_2 even at low temperature (~0 °C). This is due to the fact that HSA lacks the proximal histidine which in Hb and Mb enables the prosthetic heme group to bind O_2 and serves to regulate the O_2 binding affinity.

On the basis of the crystal structure of the HSA−hemin complex, we have used site-directed mutagenesis to introduce into the heme binding site of HSA a histidine that would be predicted to provide axial coordination to the central Fe^{2+} atom of the heme and thereby promote O_2 binding (Figure 1). An initial recombinant HSA mutant, in which Ile-142 and Tyr-161 were replaced by His and Leu, respectively [rHSA(I142H/Y161L)], has been made, and the O_2 binding capabilities of the heme complex have been partially evaluated.[11] In the present study, we have elucidated the coordination structure of the naturally occurring wild-type rHSA−heme [rHSA(wt)−heme] by UV−vis and magnetic circular dichroism (MCD) spectroscopies and characterized the unusual axial coordination of Tyr-161 to the heme. To develop HSA−heme as a synthetic O_2 carrier, we have also generated several new mutant rHSA−heme complexes. Their O_2 and CO binding properties have been characterized kinetically and compared to those of the natural Hb, Mb, and recombinant Mb (rMb) mutants. We have shown that our mutagenesis approach can create a new class of albumin-based artificial hemoproteins which would serve as an O_2 carrier.

Experimental Section

Materials and Apparatus. rHSA(wt) was kindly provided by the NIPRO Corp. (Osaka, Japan). All reagents were purchased from commercial sources as special grades and used without further purification unless otherwise noted. Iron(III) protoporphyrin IX (hemin) chloride was purchased from Fluka. Horse skeletal muscle myoglobin (Mb) was purchased from Sigma-Aldrich. The iron(III) protoporphyrin IX dimethyl ester chloride (FePPIXDME) was prepared by esterification of carboxylate side chains of hemin with acidic methanol. The UV−vis absorption spectra were recorded using an Agilent 8453 UV−visible spectrophotometer fitted with an Agilent 89090A temperature control unit.

Site-Directed Mutagenesis, Protein Expression, and Purification. Specific mutations were introduced into HSA within the context of a plasmid vector containing the entire HSA coding region (pHIL-D2 HSA) using designed primers with the QuikChange XL site-directed mutagenesis kit (Stratagene).[13] All mutations were confirmed by DNA sequencing. Each mutated pHIL-D2 HSA plasmid was linearized by NotI digestion and introduced into *Pichia pastoris GS115* by electroporation using a BioRad MicroPulser. Expressions were carried out by standard protocols (Invitrogen) with some modifications. Clones were grown upon BMGY medium [1% yeast extract, 2% peptone, 0.1 M potassium phosphate (pH 6.0), 1.34% yeast nitrogen base without amino acids, 40 ppm biotin, 1% glycerol] and transferred to BMMY medium [1% yeast extract, 2% peptone, 0.1 M potassium phosphate (pH 6.0), 1.34% yeast nitrogen base without amino acids, 40 ppm biotin, 1% methanol] for induction with methanol in baffled shaking flasks at 30 °C in a JEIOTECH SI-600R incubator at 200 rpm.

(10) Marden, M. C.; Hazard, E. S.; Leclerc, L.; Gibson, Q. H. *Biochemistry* **1989**, *28*, 4422−4426.
(11) Komatsu, T.; Ohmichi, N.; Zunszain, P. A.; Curry, S.; Tsuchida, E. *J. Am. Chem. Soc.* **2004**, *126*, 14304−14305.
(12) The pictures were produced on the basis of crystal structure coordinate of the rHSA(wt)-hemin (code: 1O9X, ref 3e) using PyMOL. DeLano, W. L. The PyMOL Molecular Graphics System 2002 DeLano Scientific, San Carlos, CA.
(13) (a) Peterson, C. E.; Ha, C.-E.; Jameson, D. M.; Bhagavan, N. V. *J. Biol. Chem.* **1996**, *271*, 19110−19117. (b) Peterson, C. E.; Ha, C.-E.; Harohalli, K.; Park, D.; Bhagavan, N. V. *Biochemistry* **1997**, *36*, 7012−7017.

The secreted rHSA was isolated as follows. The growth medium was centrifuged to harvest the culture supernatant, which was brought to 50% saturation by the addition of solid ammonium sulfate with stirring at room temperature. The mixture was then incubated at 4 °C for 1 h. The resulting precipitate was removed by centrifugation, and the supernatant fluid was brought to 95% saturation with ammonium sulfate. The precipitated protein, which contains rHSA, was collected by centrifugation and dissolved in distilled water. The brownish solution was dialyzed for 48 h at 4 °C against 100 volumes of distilled water, followed by 24 h against 100 volumes of 50 mM potassium phosphated buffer (pH 7.0). The dialysate was then loaded onto a Cibacron Blue column of Blue Sepharose 6 Fast Flow (Amersham Pharmacia Biotech) and washed with 10 bed volumes of 50 mM potassium phosphate. Elution of the rHSA(mutant) was carried out with 3 M NaCl and the eluent dialyzed against 50 mM potassium phosphate. After concentration using an ADVANTEC Q0100 ultrafilter (10 kDa Mw cutoff) in an UHP-43K ultraholder, the samples were applied to a Superdex 75 column (Amersham Pharmacia Biotech) using 50 mM potassium phosphate as the running buffer. All the purification steps were followed by SDS−PAGE analysis. Each rHSA(mutant) exhibited a single band and migrated the same distance as rHSA(wt). The protein concentration was assayed by measuring the absorbance at 280 nm ($\epsilon_{280} = 3.4 \times 10^4$ M^{-1} cm^{-1}).

Preparations of rHSA−Hemin and rHSA−Heme Complexes. The ferric rHSA(mutant)−hemin complexes were prepared according to our previously reported procedures for rHSA(wt)−hemin.[3e] Typically 5 mL of 0.1 mM rHSA(mutant) in 50 mM potassium phosphate (pH 7.0) was mixed with 0.8 mL of 0.688 mM hemin in DMSO [hemin:rHSA-(mutant) molar ratio of 1.1] and incubated overnight with rotation in the dark at room temperature. The complex was then diluted with 50 mM potassium phosphate (200 mL) and concentrated to the initial volume (5.8 mL) using an ADVANTEC Q0100 ultrafilter (10 kDa Mw cutoff). These dilution and concentration cycles were repeated to reduce the final concentration of DMSO to <0.1 vol %. The resulting samples were analyzed by a SDS−PAGE to confirm the protein integrity and concentration.

The 50 mM phosphate-buffered solution (pH 7.0) of rHSA(mutant)−hemin ([hemin] = ca. 10 μM) in a 10 mm path length optical quartz cuvette sealed with a rubber septum was purged with Ar for 40 min. A small excess amount of degassed aqueous sodium dithionate was added by microsyringe to the sample under an Ar atmosphere to reduce the central ferric ion of the hemin, generating the deoxy ferrous rHSA-(mutant)−heme complexes.

Kinetic Measurements for O_2 and CO Bindings. Kinetics studies were carried out using laser flash photolysis techniques at 22 °C, except for the determination of the CO dissociation rates. Laser flash photolysis experiments were performed using a Unisoku TSP-1000WK time-resolved spectrophotometer with a Spectron Laser Systems SL803G-10 Q-switched Nd:YAG laser, which generated a second-harmonic (532 nm) pulse of 6 ns duration (10 Hz). The probe light from a 150 W xenon arc-lamp was passed through an UV cutoff filter and an Asahi Spectra MC filter before irradiation to minimize any sample damage. Normally, fresh solutions of the deoxy rHSA(mutant)−heme were made up for each set of experiments, and the gas mixture with the desired partial pressure of O_2/CO/N_2 prepared by a KOFLOC Gasblender GB-3C was flowed into the sample cuvette for 20 min for equilibration.

In general, recombination following laser flash photolysis to hemeO$_2$ or hemeCO occurs according to eq 1 with the association rate constant (k_{on}^{L}), dissociation rate constant (k_{off}^{L}), and apparent rate constant (k_{app}) given by eq 2.[14,15] The values of k_{app} were obtained directly from the log plots of the change in absorbance (ΔA) versus time. The gas concentrations were always higher than that of the heme; therefore, the pseudo-first-order approximation can be applied throughout. For CO rebinding at high [CO], eq 2 reduces to eq 3 because $k_{on}^{CO}[CO] \gg k_{off}^{CO}$.

$$\text{hemeL} \xrightarrow{h\nu} \text{heme} \underset{k_{off}^{L}}{\overset{k_{on}^{L}}{\rightleftharpoons}} \text{hemeL} \quad [\text{L} = \text{O}_2 \text{ or CO}] \tag{1}$$

$$k_{app} = k_{on}^{L}[\text{L}] + k_{off}^{L} \tag{2}$$

$$k_{app} \approx k_{on}^{CO}[\text{CO}] \tag{3}$$

Thus, k_{on}^{CO} of the rHSA(mutant)−heme was easily calculated from k_{app}/[CO].

The O_2 association rates ($k_{on}^{O_2}$) and the O_2 binding constants [$K^{O_2} = (P_{1/2}^{O_2})^{-1}$] of the rHSA(mutant)−heme were measured using the competitive rebinding technique.[14,15] Photolysis of hemeCO in the presence of CO and O_2 gives the five-*N*-coordinate heme (deoxy state), which is first trapped as hemeO$_2$ and subsequently converted back to hemeCO (eq 4).

$$\text{hemeCO} \underset{k_{on}^{CO}}{\overset{k_{off}^{CO}}{\rightleftharpoons}} \text{heme} \underset{k_{off}^{O_2}}{\overset{k_{on}^{O_2}}{\rightleftharpoons}} \text{hemeO}_2 \tag{4}$$

The CO concentration was held constant, and the fast and slow kinetics were measured at different [O_2]. The fast process is given by eq 5, allowing the direct determination of $k_{on}^{O_2}$ from a plot of k_{app}(fast) versus [O_2].

$$k_{app}(\text{fast}) = k_{on}^{O_2}[\text{O}_2] + k_{off}^{O_2} + k_{on}^{CO}[\text{CO}] \tag{5}$$

The rate constant for the slower process, k_{app}(slow), is substituted into Traylor's eq 6 to obtain K^{O_2} [$=(P_{1/2}^{O_2})^{-1}$].[15]

$$\frac{k_{on}^{CO}[\text{CO}]}{k_{app}(\text{slow})} = K^{O_2}[\text{O}_2] + \frac{k_{on}^{CO}[\text{CO}]}{k_{off}^{O_2}} + 1 \tag{6}$$

The value of k_{on}^{CO}[CO] is constant; therefore, the plots of k_{on}^{CO}[CO]/k_{app}(slow) versus [O_2] affords K^{O_2}.

The relaxation curves that accompanied the O_2 or CO recombination were fitted to single- or double-exponentials using the Unisoku Spectroscopy & Kinetics Software. The $k_{off}^{O_2}$ values can be determined from the *y*-intercept of eq 5 or 6, but they often have large deviations. Therefore, we calculated $k_{off}^{O_2}$ from $k_{on}^{O_2}/K^{O_2}$ (both obtained from slopes).

The CO dissociation from the rHSA(mutant)−hemeCO was measured by carrying out the replacement reaction with NO.[16] A Sephadex G-25 column was equilibrated with CO-saturated potassium phosphate buffer (50 mM, pH 7.0), and the rHSA(mutant)−hemeCO solution was passed through the column to remove the dithionate. The eluent was directly connected to a optical quartz cuvette under a 10% CO (in N_2) atmosphere. The 10% NO (in N_2) equilibrated buffer was then rapidly injected into the rHSA(mutant)−hemeCO solution, and the time dependence of the decrease in absorption at 418 nm was monitored. The relaxation curves that accompanied the CO dissociation within several minutes were analyzed by fitting to double-exponentials. The CO binding constants [$K^{CO} = (P_{1/2}^{CO})^{-1}$] were calculated using k_{on}^{CO}/k_{off}^{CO}.

Magnetic Circular Dichroism (MCD). The MCD for the 50 mM potassium phosphate-buffered solutions (pH 7.0) of the rHSA(wt)−heme and rHSA(mutant)−heme series (8.0 μM) under Ar and CO atmospheres were measured using a JASCO J-820 circular dichrometer fitted with a 1.5 T electromagnet at 22 °C. The spectrum was acquired five times to improve signal-to-noise, and each data point was corrected

(14) Collman, J. P.; Brauman, J. I.; Iverson, B. L.; Sessler, J. L.; Moris, R. M.; Gibson, Q. H. *J. Am. Chem. Soc.* **1983**, *105*, 3052−3064.
(15) Traylor, T. G.; Tsuchiya, S.; Campbell, D.; Mitchel, M.; Stynes, D.; Koga, N. *J. Am. Chem. Soc.* **1985**, *107*, 604−614.
(16) Rohlfs, R.; Mathews, A. J.; Carver, T. E.; Olson, J. S.; Springer, B. A.; Egeberg, K. D.; Sliger, S. G. *J. Biol. Chem.* **1990**, *265*, 3168−3176.

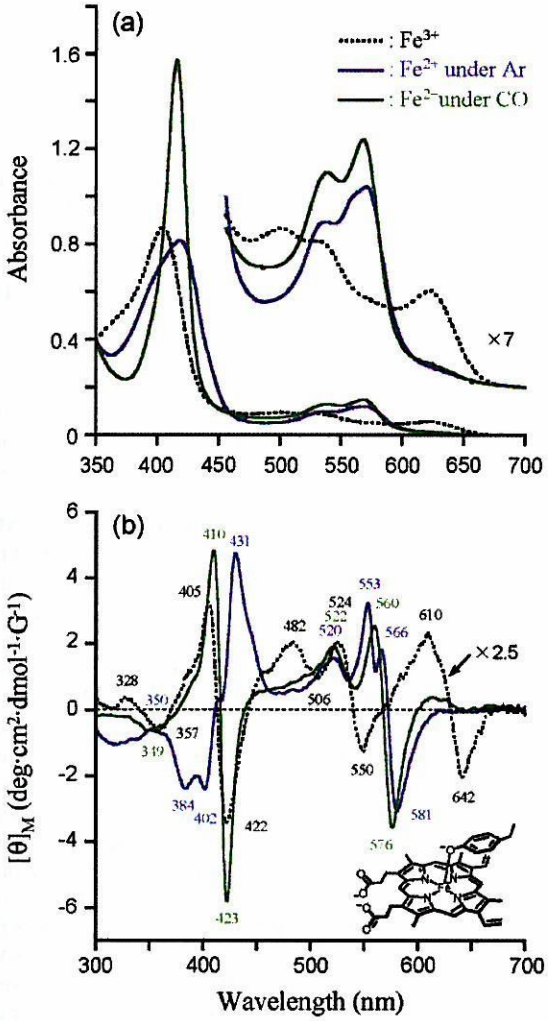

Figure 2. (a) UV−vis absorption and (b) MCD spectral changes of the rHSA(wt)-heme in 50 mM potassium phosphate buffered solution (pH 7.0, 22 °C).

by subtracting the optical rotation observed in the absence of an applied magnetic field.

Results and Discussion

Naturally Occurring rHSA(wt)−Hemin. Our crystal structure analysis revealed that hemin is bound within a D-shaped cavity in subdomain IB of rHSA(wt), where the central ferric ion is coordinated by Tyr-161, and the two propionate side chains are coordinated by a triad of basic amino acid residues (Figure 1).[3e] The UV−vis absorption spectrum of the phosphate-buffered solution (50 mM, pH 7.0) of rHSA(wt)−hemin showed a Soret band at 405 nm and the charge-transfer (CT) band of the porphyrin $p\pi$ to the Fe^{3+} $d\pi$ orbitals at 624 nm (Figure 2a). The spectral pattern and amplitudes were almost constant in the temperature range of 5−40 °C. The dominant feature of the spectrum was quite similar to those of the human or horse heart ferric H93Y recombinant Mb [rMb(H93Y)], in which the proximal histidine (His-93) was replaced with Tyr by site-directed mutagenesis (Table 1).[17,18] Adachi and co-workers showed that the ferric rMb(H93Y) formed a five-coordinate high-spin complex with a single oxygen donor of the proximal

Table 1. UV-vis Absorption Spectral Data of the rHSA(wt)-Heme, rHSA(mutant)-Heme and Other Hemoproteins

Hemoproteins	State	λ_{max} (nm) Soret	Visible
rHSA(wt)-Heme[a]	Fe^{3+}	405	501, 534, 624
	Fe^{2+}	419	538, 559(sh), 570
	Fe^{2+}CO	416	539, 568
HSA-Heme[b]	Fe^{3+}	404	498, 530, 620
	Fe^{2+}	416	534, 570
	Fe^{2+}CO	418	536, 568
Human rMb(H93Y)[c]	Fe^{3+}	402	480, 520(sh), 598
	Fe^{2+}	427	560
	Fe^{2+}CO	420	539, 567
Horse Heart rMb(H93Y)[d]	Fe^{3+}	403	487, 524, 599
	Fe^{2+}	429	556
	Fe^{2+}CO	419	539, 570
FePPIXDME(CH_3O^-)[e]	Fe^{3+}	401	476, 580(sh), 600
FePPIXDME(p-NO_2PhO^-)[f]	Fe^{3+}	402	500, 528, 621
FePPIXDME[a,g]	Fe^{3+}	400	571, 599
	Fe^{2+}	393, 414, 427, 440(sh)	535, 571
	Fe^{2+}CO	411	532, 564
rHSA(I142H)-Heme[a]	Fe^{3+}	404	501, 533, 619
	Fe^{2+}	424	530, 558
	Fe^{2+}CO	419	537, 560
rHSA(I142H/Y161L)-Heme[a]	Fe^{3+}	402	533, 620
	Fe^{2+}	426	531(sh), 559
	$Fe^{2+}O_2$	412	537, 573
	Fe^{2+}CO	419	538, 565
rHSA(I142H/Y161Y)-Heme[a]	Fe^{3+}	402	533, 620
	Fe^{2+}	425	532(sh), 559
	$Fe^{2+}O_2$	411	538, 576
	Fe^{2+}CO	419	538, 565
rHSA(Y161L/L185H)-Heme[a]	Fe^{3+}	408	528, 620
	Fe^{2+}	422	530, 558
	$Fe^{2+}O_2$	412	538, 570
	Fe^{2+}CO	419	537, 560
Mb[a,h]	Fe^{3+}	409	503, 548(sh), 632
	Fe^{2+}	434	557
	$Fe^{2+}O_2$	418	544, 581
	Fe^{2+}CO	423	541, 579

[a] In 50 mM potassium phosphate buffer (pH 7.0, 22 °C). [b] In 0.1 M phosphate buffer (pH 7.0); ref 22. [c] In 50 mM sodium phosphate buffer (pH 7.0, 20 °C); ref 17. [d] At pH 7−10, 25 °C; ref 18. [e] In CH_2Cl_2/CH_3OH = 9/1 (v/v) (25 °C); ref 21. [f] In CH_2Cl_2 (25 °C); ref 21. [g] In 0.5% Me_3CeNBr. [h] Horse muscle Mb (Sigma).

Tyr-93 by resonance Raman spectroscopy.[17b] Our absorption spectral data imply that the hemin is bound to Tyr-161 of rHSA-(wt) and forms a ferric five-coordinate high-spin complex under physiological conditions. Interestingly, the CT absorptions of the rHSA(wt)−hemin appeared at a higher wavelength (λ_{max} = 624 nm) compared to rMb(H93Y) (λ_{max} = 598−599 nm). Dawson and co-workers classified the CT bands of the oxygen-ligated hemins into two groups: the first at around 600 nm for rMb(H93Y) and the methoxide (CH_3O^-) complex of Fe^{3+} protoporphyrin IX dimethyl ester (Fe^{3+}PPIXDME), and the second at around 620 nm for p-nitrophenolate (p-NO_2PhO^-) or the acetate complex of Fe^{3+}PPIXDME, in which the nonoccupied π^* orbitals of the fifth ligand interacts with the Fe^{3+} $d\pi$ orbitals and, in turn, lowered the energy level of the CT transition (Table 1).[19] The rHSA(wt)−hemin definitely belongs to the latter group, which suggests that the axial coordination

(17) (a) Adachi, S.; Nagano, S.; Watanabe, Y.; Ishimori, K.; Morishima, I. *Biochim. Biophys. Res. Commun.* **1991**, *180*, 138−144. (b) Adachi, S.; Nagano, S.; Ishimori, K.; Watanabe, Y.; Morishima, I.; Egawa, T.; Kitagawa, T.; Makino, R. *Biochemistry* **1993**, *32*, 241−252.
(18) Hildebrand, D. P.; Burk, D. L.; Maurus, R.; Ferrer, J. C.; Brayer G. D.; Mauk, A. G. *Biochemistry* **1995**, *34*, 1997−2005.
(19) Pond, A. E.; Roach, M. P.; Sono, M.; Rux, A. H.; Franzen, S.; Hu, R.; Thomas, M. R.; Wilks, A.; Dou, Y.; Ikeda-Saito, M.; Oritz de Montellano, P. R.; Woodruff, W. H.; Boxer, S. G.; Dawson, J. H. *Biochemistry* **1999**, *38*, 7601−7608.

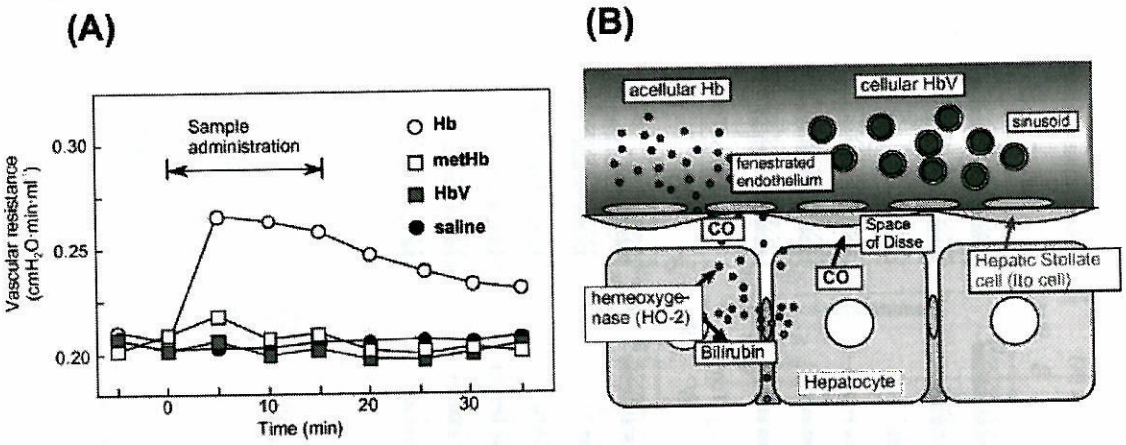

Figure 6. (A) Changes in vascular resistance during perfusion of exteriorized rat liver with HbV, Hb, metHb, or saline. (B) Schematic representation of hepatic microcirculation: the small Hb molecule extravasate across the fenestrated endothelium to reach to the space of Disse, where heme of Hb is catabolized by hemeoxygenase-2 (HO-2) and CO is released as a vasorelaxation factor. However, the excess amount of the extravasated Hb traps CO and induces vasoconstriction and the resulting higher vascular resistance. However, the larger HbV retains in the sinusoid and there is no extravasation and vasoconstriction.

molecules with a diameter of only 7 nm extravasate through the fenestrated endothelium and reach the space of Disse. However, HbV particles, which are larger than the pores, do not extravasate. Heme of extravasated Hb is excessively metabolized by hemeoxygenase-2 in hepatocyte to produce CO and bilirubin. Even though CO acts as a vasorelaxation factor in the liver, the excess amount of Hb rapidly binds CO, resulting in the vasoconstriction and an increase in vascular resistance. Furthermore, HbV (250 nm in diameter) is large enough to remain in the sinusoid, and the vascular resistance is maintained.

From these results, the optimal molecular dimension of Hb-based O_2 carriers can be proposed. The upper limitation is below the capillary diameter to prevent capillary plugging, and for sterilization by membrane filters (Fig. 7). However, smaller sizes exhibit a higher rate of vascular wall permeability with side effects such as hypertension and neurological disturbances. HbV exhibits a very low level of vascular wall permeability. Therefore, the HbV appears to be appropriate from the viewpoint of hemodynamics. However, the influence of HbV on the RES has to be clarified, because the fate of HbV is RES trapping.

Circulation persistence was measured by monitoring the concentration of radioisotope-labeled HbV in collaboration with Dr Phillips at the University of Texas at San Antonio. The circulation half-life is dose dependent, and when the dose rate was 14 ml/kg, the circulation half-life was 35 hr in rats. The circulation time in the case of the human body can be estimated to be twice as long; or about 3 days at the same dose rate. Gamma camera images of radioisotope-labeled HbV

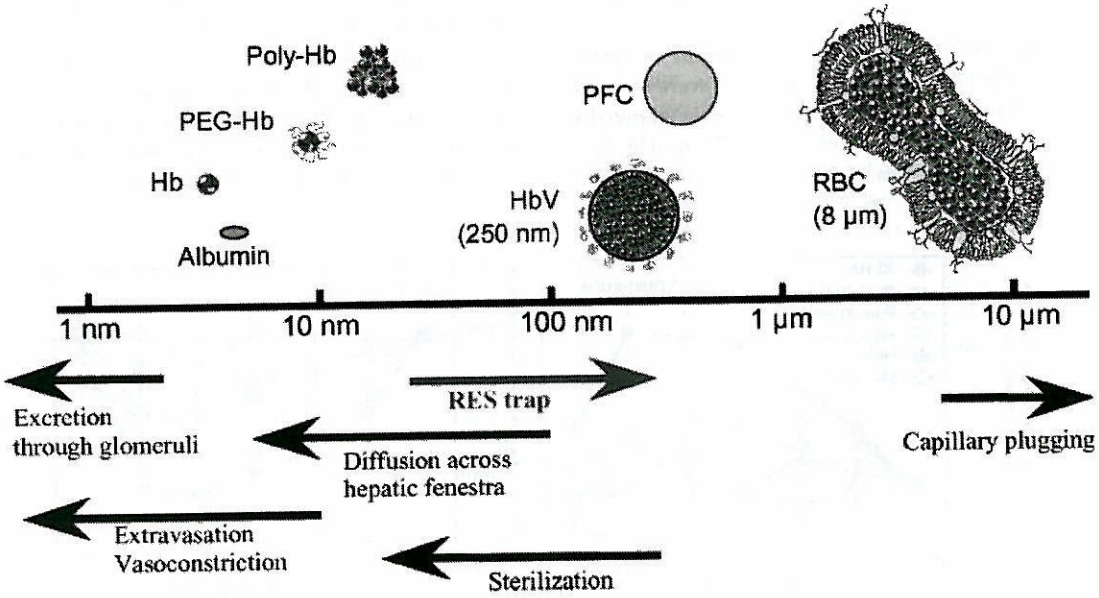

Figure 7. Optimal diameter of Hb-based oxygen carriers from the view point of physiological response and production process.

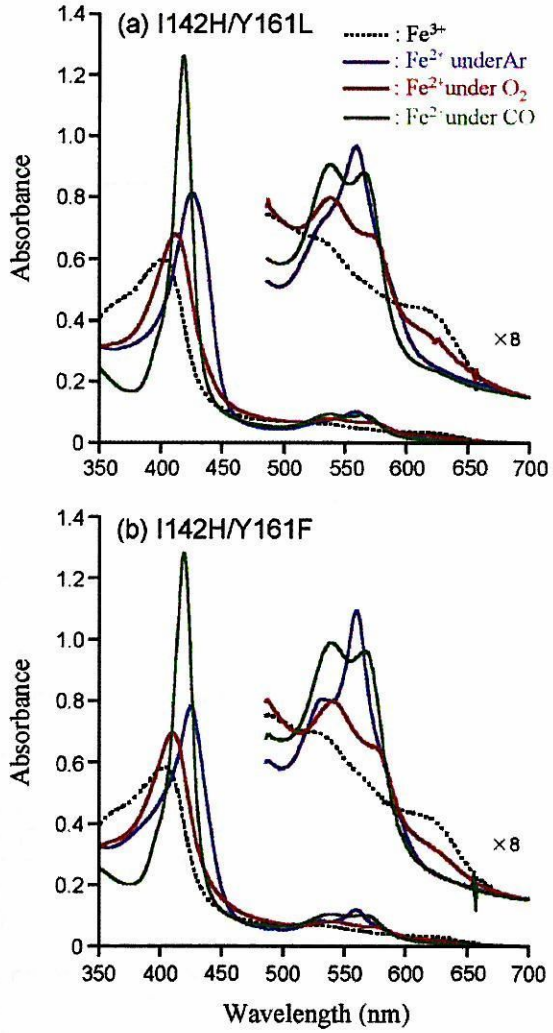

Figure 3. UV-vis absorption spectral changes of the (a) rHSA(I142H/Y161L)-heme and (b) rHSA(I142H/Y161F)-heme in 50 mM potassium phosphate buffered solution (pH 7.0, 8 °C).

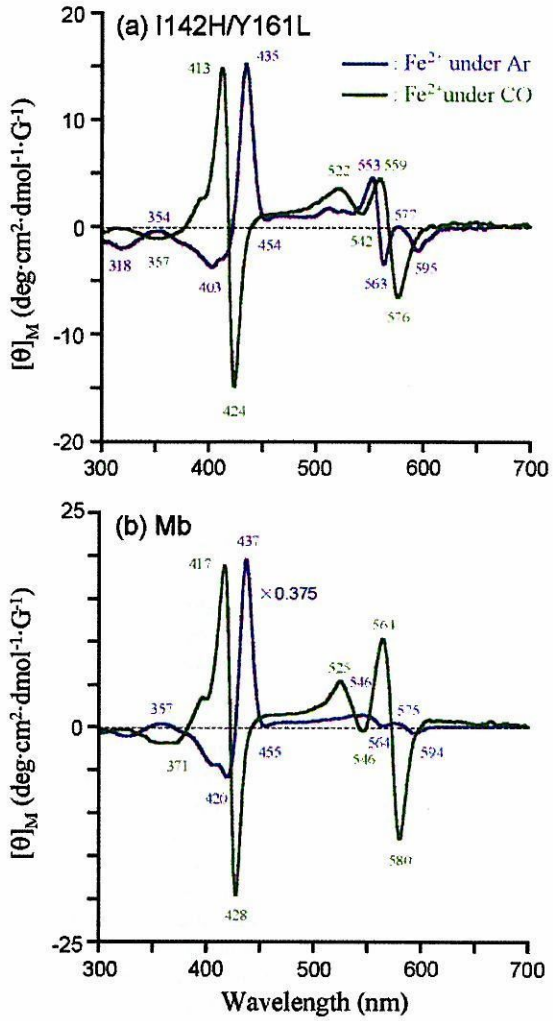

Figure 4. MCD spectral changes of the (a) rHSA(I142H/Y161L)-heme and (b) native Mb in 50 mM potassium phosphate buffered solution (pH 7.0, 22 °C).[30]

essentially the same in their general features (Figure 3 and Figure S2). The strong absorption band due to the porphyrin-to-metal CT was weakened because of the Y161L and Y161F mutations (Figure 3). Both MCD spectra showed similar S-shaped patterns in the Soret band region, which resembled that of ferric Mb (see Figure S2).[26] It is known that two water molecules are located in the heme pocket of ferric Mb.[27] One water axially coordinates to the sixth position of the central ferric ion of the hemin to produce the aquo complex, and the other one is at the rear of the pocket, hydrogen bonded to the first water. A great number of MCD studies on synthetic iron porphyrins and hemoproteins have demonstrated that the spectral shape in the Soret region can be used as a qualitative marker of the spin state and axial coordination environment.[20] Vickery and co-workers found that (i) the Soret MCD intensity of the ferric Mb with different anions at the six-coordinate position was correlated with the amount of low-spin component formed, and (ii) the shape of the band is sensitive to the nature of the sixth ligand.[26] Our MCD results suggest that both the rHSA-(I142H/Y161L)−hemin and rHSA(I142H/Y161F)−hemin are in predominantly ferric high-spin complexes having a water molecule as the sixth ligand.

O_2 and CO Binding to Ferrous rHSA(mutant)−Heme. The rHSA(mutant)−hemin was easily reduced to the ferrous complex by adding a small molar excess of aqueous sodium dithionate under an Ar atmosphere. A single broad absorption band (λ_{max} = 559 nm) in the visible region of the rHSA(I142H/Y161L)−heme and rHSA(I142H/Y161F)−heme was similar to that observed for deoxy Mb[28] or the chelated heme in DMF,[29] indicating the formation of a five-*N*-coordinate high-spin complex (Figure 3, Table 1). The spectral features and amplitude were unaltered in the temperature range of 0−25 °C. The heme therefore appears to be accommodated in the mutated heme pocket with an axial coordination involving His-142. Upon exposure of the rHSA(I142H/Y161L)−heme and rHSA(I142H/

(26) Vickery, L.; Nozawa, T.; Sauer, K. *J. Am. Chem. Soc.* **1976**, *98*, 343−350.
(27) Springer, B. A.; Sligar, S. G.; Olson, J. S.; Phillips, G. N., Jr. *Chem. Rev.* **1994**, *94*, 699−714.
(28) Antonini, E.; Brunori, M. *Hemoglobin and Myoglobin in Their Reactions with Ligands*; North-Holland Pub.: Amsterdam, 1971; p 18.
(29) Traylor, T. G.; Chang, C. K.; Geibel, J.; Berzinis, A.; Mincey, T.; Cannon, J. *J. Am. Chem. Soc.* **1979**, *101*, 6716−6731.

Y161F)−heme solutions to O_2, the UV−vis absorptions immediately changed to that of the O_2 adduct complex at 0−25 °C (Figure 3).[28,29] After flowing CO gas, these hemoproteins produced stable carbonyl complexes.

The MCD spectra of the deoxy and carbonyl rHSA(I142H/Y161L)−heme are shown in Figure 4a. The Soret MCD of the deoxy state under anaerobic conditions is dominated by an intense positive peak at 435 nm, as would be expected for the Faraday *C* terms anticipated for the high-spin Fe^{2+} porphyrin.[20a,26] On the other hand, the rHSA(I142H/Y161L)CO exhibited S-shaped MCDs which correspond to the *A* term bands for the diamagnetic Fe^{2+} porphyrin.[20a,26] These spectra are very similar to those of the high-spin deoxy Mb and low-spin MbCO measured in identical conditions (Figure 4b). Our MCD results clearly show that the central ferrous ion of the heme is coordinated by His-142 in the heme pocket and forms a five-*N*-coordinate high-spin complex under an Ar atmosphere, which converts to the low-spin diamagnetic form by the binding of CO. The rHSA(I142H/Y161F)−heme complex had the same MCD spectral features as rHSA(I142H/Y161L)−heme (data not shown).

The single mutant rHSA(I142H)−heme complex, which retains Y161, could not bind O_2. The polar phenolate residue at the top of the porphyrin plane is likely to accelerate the proton-driven oxidation of the Fe^{2+} center. This rapid autoxidation is also observed in the rMb(H64Y) mutants, in which the distal histidine (His-64) was substituted with Tyr, thus introducing a potentially anionic nucleophile near to the O_2 coordination site.[31] In contrast, replacement of Tyr-161 in rHSA(I142H)−heme by Leu or Phe enhanced the stabilization of the O_2 adduct complex. In the rHSA(Y161L/L185H)−heme, the proximal histidine coordinated to the central ferrous ion from the opposite side of the porphyrin platform also allows O_2 binding to the heme. The lifetimes for the decays of the dioxygenated rHSA(I142H/Y161L)−heme, rHSA(I142H/Y161F)−heme, and rHSA(Y161L/L185H)−heme are all 3−5 min at 20 °C.

To evaluate the kinetics of the O_2 and CO bindings to the rHSA(mutant)−heme, laser flash photolysis experiments were carried out.[14,15] The transient absorption spectra of the photodissociated product of the rHSA(I142H/Y161L)−hemeCO displayed a negative absorbance at 417 nm, due to the disappearance of the carbonyl complex, and a positive absorbance at 435 nm, which is attributed to the deoxy form (Figure 5). The transient absorption spectra in the time range from 0.1 μs to 8.0 ms with an isosbestic point at 401, 426, and 458 nm were superimposed on the static difference spectrum of the deoxy minus carbonyl compound (Figure 5, red line). They illustrate the process of reassociation of CO and are consistent with the formation of the ferrous five-*N*-coordinate high-spin complex after the laser pulse irradiation.

It is noteworthy that the absorbance decays accompanying the CO recombinations to these rHSA(mutant)-heme were composed of double-exponential profiles, which are normally not observed in Mb (Figure 6a). The ratio of the amplitude of the fast and slow phases was approximately 3:2 for the rHSA-(I142H/Y161L)-heme, 5:1 for the rHSA(I142H/Y161F)-heme and 3:1 for the rHSA(Y161L/L185H)-heme. On the other hand,

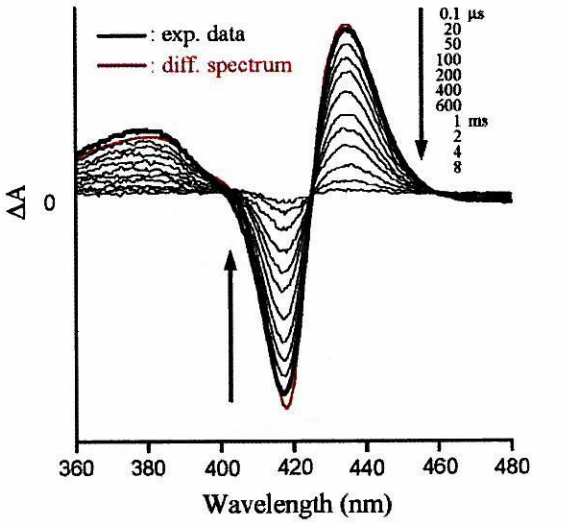

Figure 5. Transient absorption spectra of the photodissociated product of the rHSA(I142H/Y161L)-hemeCO after the laser flash photolysis at 22 °C. The red-line represents the static spectrum of deoxy minus carbonyl compound in Figure 3a.

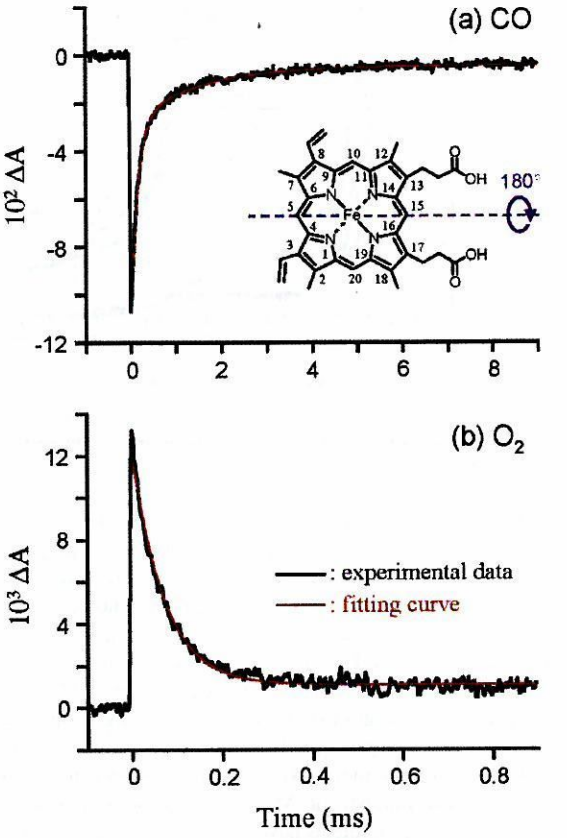

Figure 6. Absorption decay of CO rebinding to the rHSA(I142H/Y161F)-heme after the laser flash photolysis at 22 °C; the kinetics was composed of two phases and relaxation curve was fitted by double-exponentials. (b) Absorption decay of O_2 rebinding to the rHSA(I142H/Y161F)-heme after the laser flash photolysis at 22 °C; the kinetics was fitted by single-exponential relaxation curve.

the rebinding of O_2 to the rHSA(mutant)-heme followed a simple monophasic decay (Figure 6b). From numerous investigations on synthetic model hemes, it has been shown that a bending

(30) The spectra of Mb are consistent with other results reported elsewhere; refs 20, 26.
(31) Springer, B. A.; Egeberg, K. D.; Sliger S. G.; Rohlfs, R. J.; Mathews, A. J.; Olson, J. S. *J. Biol. Chem.* **1989**, *264*, 3057−3060.

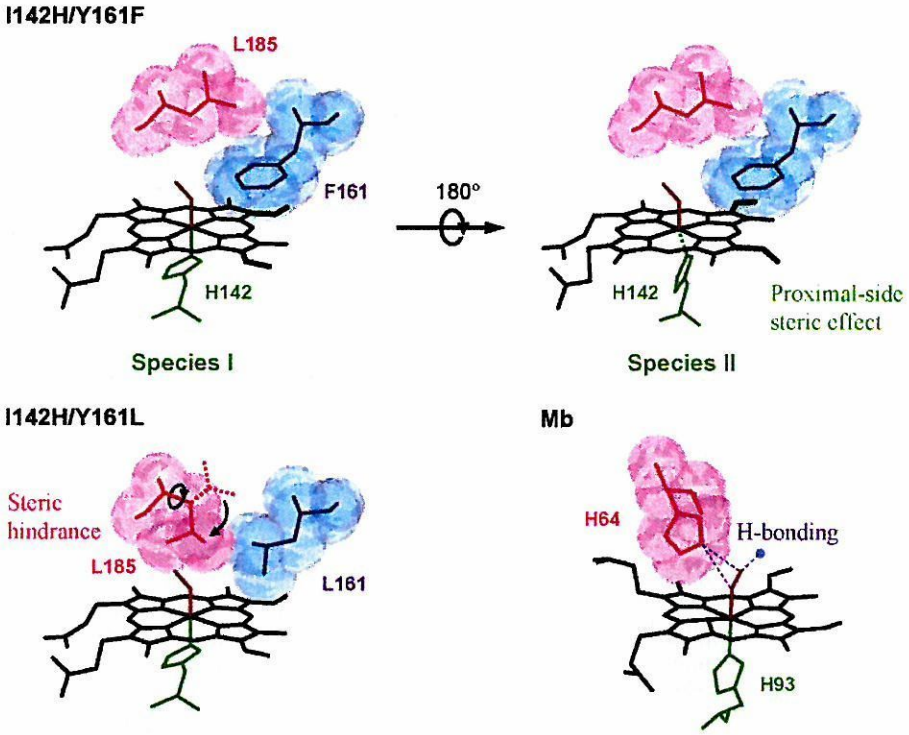

Figure 7. Structural models of the hemeO_2 sites of rHSA(I142H/Y161F)-heme and rHSA(I142L/Y161L)-heme, and comparison to Mb.[12,32]

strain in the proximal base coordination to the central Fe^{2+} atom, the "proximal-side steric effect", can both increase the dissociation rate and decrease the association rate for CO, whereas it increases the O_2 dissociation rate without greatly altering the kinetics of O_2 association.[14,15] One possible explanation is that there may be two different geometries of the axial histidine (His-142 or His-185) coordination to the central ferrous ion of the heme, each one accounting for a component of the biphasic kinetics of CO rebinding. Marden and co-workers also reported a similar two-phase kinetics in CO association with HSA-heme and interpreted it as indicating that there are two different orientations of the porphyrin ring in a single site on HSA.[10] In our case, the alternative geometries may arise because crystallographic analysis suggests that the heme molecule appears able to bind into the narrow cavity of subdomain IB in two orientation that are related by a 2-fold rotation about the 5,15-*meso* axis of the heme (180° rotational isomers). It appears that the asymmetric hydrophobic 3,8-divinyl groups at the porphyrin periphery may occupy different positions that result in a shift of the Fe^{2+} center, forming the two different geometries of the axial imidazole coordination of histidine (Figure 7).

In general, the crystal structures of natural hemoproteins have shown that the prosthetic heme group is bound in a single orientation. On the other hand, in solution, ^{1}H NMR spectra frequently exhibit two sets of heme (or hemin) resonances, which arise from alternative orientations of the porphyrin plane.[33] This orientational disorder is most readily detected in the ferric low-spin state, which shows extraordinary porphyrin 2,7,12,18-CH_3 contact shifts.[34] The amount of the minor species ranges from a few percent in Mb to 40% in insect Hb (*CTT* HbIII).[35] Reconstitution techniques have made significant contributions to clarify this molecular equilibrium; the heme in Hb and Mb can be easily removed under acidic conditions and the resulting apoprotein may be reconstituted by adding back the heme to produce the holoprotein.[36] The incorporation of hemin into apoMb is complete within 1 ms, but the initial complex does not distinguish the two possible orientations of the porphyrin ring.[34] As a result, freshly reconstituted Mb contains an equimolar 1/1 mixture of the two conformers; subsequent heme rearrangement is extremely slow (≈13 h). The influence of the heme orientation on the functional properties appears to be very dependent on the particular protein. In *CTT* HbIII, the O_2 binding affinity depends on the heme orientation.[37] On the other hand, the equilibrium and kinetic parameters for O_2 and CO binding to the reconstituted human Mb are unaffected by the slow heme rearrangement.[38,39]

Our attempts to determine the ratio of the two hemin orientations of the rHSA(I142H/Y161L)-hemin by ^{1}H NMR spectroscopy unfortunately failed. The downfield spectra of the

(32) The model of Mb was prepared on the basis of crystal structure coordinate of MbO_2 (code: 1MBO, Phillips, S. E. *J. Mol. Biol.* **1980**, *142*, 531–554.). The coordinated O_2 shows a hydrogen bond with N_ϵ(His-64) and hydrogen bond network through H_2O (light-blue circle) within the distal pocket.

(33) La Mar, G. N.; Satterlee, J. D.; de Ropp, J. S. Nuclear Magnetic Resonance of Hemoprotein. In *The Porphyrin Handbook*; Kadish, K. M., Smith, K. M., Guilard, R., Eds.; Academic Press: San Diego, 2000; Vol. 5, pp 185–298.
(34) (a) Jue, T.; Krishnamoorthi, R.; La Mar, G. N. *J. Am. Chem. Soc.* **1983**, *105*, 5701–5703. (b) La Mar, G. N.; Toi, H, Krishnamoorthi, R, *J. Am. Chem. Soc.* **1984**, *106*, 6395–6401.
(35) (a) La Mar, G. N.; Davis, N. L.; Parish, D. W.; Smith, K. M. *J. Mol. Biol.* **1983**, *168*, 887–896. (b) La Mar, G. N.; Smith, K. M.; Gersonde, K.; Sick, H.; Overcamp, M. *J. Biol. Chem.* **1980**, *255*, 66–70.
(36) Hayashi, T.; Hisaeda, Y. *Acc. Chem. Res.* **2002**, *35*, 35–43.
(37) Gersonde, K.; Sick, H.; Overkamp, M.; Smith, K. M.; Parish, D. W. *Eur. J. Biochem.* **1986**, *157*, 393–404.
(38) Light, W. R.; Rohlfs, R. J.; Palmer, G.; Olson, J. S. *J. Biol. Chem.* **1987**, *262*, 46–52.
(39) Aojula, H. S.; Wilson, M. T.; Morrison, I. G.*Biochem. J.* **1987**, *243*, 205–210.

Table 2. O_2 Binding Parameters of the rHSA(mutant)-Heme in 50 mM Potassium Phosphate Buffer Solution (pH 7.0) at 22 °C[a]

Hemoproteins	$k_{on}^{O_2}$ (μM^{-1} s^{-1})	$k_{off}^{O_2}$ ($m s^{-1}$) I	$k_{off}^{O_2}$ ($m s^{-1}$) II	$P_{1/2}^{O_2}$ (Torr) I	$P_{1/2}^{O_2}$ (Torr) II
rHSA(I142H/Y161L)-Heme	7.5	0.22	1.7	18	134
rHSA(I142H/Y161F)-Heme	20	0.10	0.99	3	31
rHSA(Y161L/L185H)-Heme	31	0.20	2.1	4	41
Hbα (R-state)[b]	33[c]	0.013[d]		0.24	
Mb[e,f]	14	0.012		0.51	
rMb(H64L)[f]	98	4.1		26	
rMb(H64F)[f]	75	10		82	
RBC[g]				8	

[a] Number I or II indicates species I or II. [b] Human Hb α-subunit. [c] In 0.1 M phosphate buffer (pH 7.0, 21.5 °C); ref 40. [d] In 50 mM phosphate buffer (pH 7.0, 20 °C); ref 41. [e] Sperm whale Mb. [f] In 0.1 M potassium phosphate buffer (pH 7.0, 20 °C); ref 16. [g] Human red cell suspension. In isotonic buffer (pH 7.4, 20 °C); ref 42.

Table 3. CO Binding Parameters of the rHSA(mutant)-Heme in 50 mM Potassium Phosphate Buffer Solution (pH 7.0) at 22 °C[a]

Hemoproteins	k_{on}^{CO} (μM^{-1} s^{-1}) I	k_{on}^{CO} (μM^{-1} s^{-1}) II	k_{off}^{CO} (s^{-1}) I	k_{off}^{CO} (s^{-1}) II	$P_{1/2}^{CO}$ (Torr) I	$P_{1/2}^{CO}$ (Torr) II
rHSA(I142H/Y161L)-Heme	2.0	0.27	0.013	0.079	0.0053	0.24
rHSA(I142H/Y161F)-Heme	6.8	0.72	0.009	0.061	0.0011	0.068
rHSA(Y161L/L185H)-Heme	3.7	0.35	0.012	0.077	0.0026	0.18
Hbα (R-state)[b]	4.6[c]		0.009[d]		0.0016[e]	
Mb[f,g]	0.51		0.019		0.030	
rMb(H64F)[g]	4.5		0.054		0.0097	

[a] Number I or II indicates species I or II. [b] Human Hb α-subunit. [c] In 50 mM potassium phosphate buffer (pH 7.0, 20 °C); ref 45. [d] In 0.1 M phosphate buffer (pH 7.0, 20 °C); ref 44. [e] Calculated from k_{on}^{CO}/k_{off}^{CO}. [f] Sperm whale Mb. [g] In 0.1 M potassium phosphate buffer (pH 7.0, 20 °C); refs 16, 48.

rHSA(I142H/Y161L)-hemin did not show sharp resonances of the four porphyrin CH_3 groups. Other trials to convert the rHSA-(I142H/Y161L)-hemin in the low-spin azide adduct complex,[33] which is much better suited for the ^1H NMR investigation, also failed even with the addition of a large excess of ligand. In any case, the amplitude ratio of the two phases observed for the CO association to rHSA(mutant)-heme was always the same, independent of time after preparation.

O_2 and CO Binding Parameters. By analyzing the CO/O_2 competitive binding following laser flash photolysis,[14,15] we obtained the association rate constants for O_2 ($k_{on}^{O_2}$) and the O_2 binding affinities [$P_{1/2}^{O_2} = (K^{O_2})^{-1}$] for the rHSA(I142H/Y161L)-heme, rHSA(I142H/Y161F)-heme and rHSA(Y161L/L185H)-heme (Table 2). From eq 6, variation in k_{on}^{CO} arising from the two geometries of the His coordination (the faster phase is defined as species I and the slower phase is defined as species II) yielded two different O_2 binding affinities. In species I, the proximal His may coordinate to the central ferrous ion without strain, whereas in species II, the ligation may involve some distortion, resulting in weaker O_2 binding (Figure 7). The absorbance decay accompanying the CO dissociation from the rHSA(mutant)-hemeCO by the replacement with NO also showed double-exponential profiles, giving two values of k_{off}^{CO} (Table 3). The proximal-side steric effect generally increases the dissociation rate for CO,[14,15] a result that is quite consistent with our interpretation that there are two orientation isomers of the heme (the larger component of k_{off}^{CO} originating from species II).

The $P_{1/2}^{O_2}$ values of the rHSA(mutant)-heme were determined to be 3−18 and 31−134 Torr for species I and II, respectively. Thus even the O_2 binding affinities of species I were 6−75-fold lower than those of native Hbα (R-state) and Mb.[16,40−42] Kinetically, these low affinities for O_2 were due to an 8−18-fold increase in the O_2 dissociation rate constants. Neutron diffraction studies of MbO_2 revealed that there is a direct hydrogen bond between the distal His-64 and the coordinated O_2 (Figure 7).[43] The high-resolution X-ray crystallographic structure of $Hb\alpha O_2$ also suggested a similar interaction in the heme pocket.[44] In both hemoproteins, the distal His stabilizes the bound O_2 by about −1.4 kcal mol^{-1} due to the hydrogen bonding. On the basis of the mutagenesis studies on sperm whale rMb, Rohlfs and co-workers demonstrated that the replacement of His-64 with apolar amino acid residues (Leu or Phe) results in loss of the hydrogen bonding, and markedly increased the O_2 dissociation rates (342−833-fold higher than Mb).[16] In the rHSA(mutant)-heme, the dioxygenated heme is buried in the core of the hydrophobic cavity without any counterpart for the hydrogen bond; thus the even small $k_{off}^{O_2}$ values for species I are greater than those of Hbα and Mb. In species II, the proximal-side steric effect could further increase the dissociation rates and cause a large decline in the O_2 binding affinity. In contrast, the binding parameters of CO to the rHSA(mutant)-heme (species I) exhibited similar values of Hbα (≤3-fold),[45,46] because the coordinated CO in Hbα does not form a hydrogen bond with the distal His-64.[47]

Comparison of the O_2 binding parameters for rHSA(I142H/Y161L)-heme and rHSA(I142H/Y161F)-heme shows that the presence of a Phe rather than Leu at position 161 results in 6-fold and 4-fold increases in the O_2 binding affinity for species I and II, respectively. This is mainly due to an increase in the O_2 association rate constant (Table 2). The same trend was observed for CO binding (3-fold increase in k_{on}^{CO}) (Table 3). The substitution of Leu-161 (102 Å^3) by Phe-161 (137 Å^3)[49] replaces an isopropyl group with a rigid benzyl group within the heme pocket. In I142H/Y161L, the small side-chain of Leu-161 may allow free rotation of the side-chain of neighboring Leu-185, thereby reducing the volume on the distal-side of the porphyrin plane (Figure 7). Actually, modeling and experimental studies suggest that His-185 in Y161L/L185H can coordinate to the central ferrous ion of the heme. On the other hand, the bulkier aromatic side-chain of Phe-161 may prevent rotation of the isopropyl group of Leu-185 and thereby provide greater room of the distal pocket; this might allow easier access to the heme Fe atom and account for the increased association rates for O_2 and CO.

Conclusion

HSA exploits weak axial coordination by Tyr-161 to bind hemin into the heme pocket. Reduction of the central ferric ion partly disrupts the Fe−O(phenolate) bond and produces unusual

(40) Gibson, Q. H. *J. Biol. Chem.* **1970**, *245*, 3285−3288.
(41) Olson, J. S.; Andersen, M. E.; Gibson, Q. H. *J. Biol. Chem.* **1971**, *246*, 5919−5923.
(42) Imai, K.; Morimoto, H.; Kotani, M.; Watari, H.; Hirata, W.; Kuroda, M. *Biochim. Biphys. Acta* **1970**, *200*, 189−197.
(43) Phillips, S. E. V.; Schoenborn, B. P. *Nature* **1981**, *292*, 81−82.
(44) Shaanan, B. *J. Mol. Biol.* **1983**, *171*, 31−59.
(45) Steinmeier, R. C.; Parkhurst, L. J. *Biochemistry* **1975**, *14*, 1564−1571.
(46) Sharma, V. S.; Schmidt, M. R.; Ranney, H. M. *J. Biol. Chem.* **1976**, *251*, 4267−4272.
(47) Hanson, J. C.; Schoenborn, B. P. *J. Mol. Biol.* **1981**, *153*, 117−146.
(48) rMb(H64L) exhibited an abnormally large CO binding affinity and k_{on}^{CO} compared to those of other mutants; ref 16.
(49) Creighton, T. E. *Proteins: Structures and Molecular Properties*; W. H. Freeman and Co.: New York, 1983; p 242.

ferrous four-coordinate intermediate-spin state hemoprotein. We have engineered mutant rHSA-heme complexes which can bind O_2 reversibly with an affinity that is only 1 order of magnitude lower than the affinity of O_2 for Hbα (R-state) and Mb. The principal modifications to the heme pocket that are required to confer reversible O_2 binding are (1) replacement of Tyr-161, the endogenous anionic nucleophile, by hydrophobic amino acid (Leu or Phe), and (2) introduction of His as a proximal base at position Ile-142 or Leu-185 (either side of the porphyrin ring plane). The transport of O_2 by the rHSA-heme could be of tremendous clinical importance not only as a red cell substitute but also as an O_2-providing therapeutic reagent. Although a number of Hb-based O_2 carriers have already been developed, the administration of these materials often elicits an acute increase in blood pressure by vasoconstriction.[50−52] This side-effect is caused by the rapid capture of the endothelial-derived relaxing factor, namely NO, by Hb that has leaked through the vascular endothelium. In contrast, our rHSA(mutant)-heme would not induce such hypertension, because the albumin carrier has low permeability through the muscle capillary pore.[53]

Our results on several mutants have also shown that modification of the distal-side of the heme pocket has a measurable effect on O_2 binding affinity (compare Leu-161 and Phe-161). To develop this promising O_2 carrier as a blood substitute, further work using a combined mutagenic and synthetic approach is required; (1) additional mutations, e.g. an introduction of a distal base which in Mb and Hbα forms a hydrogen bond with the coordinated O_2, may help to stabilize the O_2 adduct complex, and (2) small modifications to the heme structure designed to adjust its position within the pocket interior but without straining the proximal His coordination, may improve and modulate the O_2 binding ability. To aid these modifications, crystal structural analysis of rHSA(mutant)-heme complexes is now underway.

Acknowledgment. This work was supported by a Grant-in-Aid for Scientific Research (No. 16350093) from JSPS, a Grant-in-Aid for Exploratory Research (No. 16655049) from MEXT Japan, Health Science Research Grants (Regulatory Science) from MHLW Japan, and Wellcome Trust (UK). The work at Imperial College London was partially carried out as the Japan-UK Research Cooperative Program (Joint Project) of JSPS.

Supporting Information Available: UV−vis absorption and MCD spectra of FePPIXDME, MCD spectra of the ferric rHSA-(mutant)-hemin and aquo-metMb. This material is available free of charge via the Internet at http://pubs.acs.org.

JA054819U

(50) Tsuchida, E. Perspectives of Blood Substitutes. In *Blood Substitutes: Present and Future Perspectives*; Tsuchida, E., Ed.; Elsevier Science: Lausanne, 1998; pp 1−14.
(51) Winslow, R. M. *Annu. Rev. Med.* **1999**, *50*, 337−353.
(52) Squires, J. E. *Science* **2002**, *295*, 1002−1005.
(53) Tsuchida, E.; Komatsu, T.; Matsukawa, Y.; Nakagawa, A.; Sakai, H.; Kobayashi, K.; Suematsu, M. *J. Biomed. Mater. Res.* **2003**, *64A*, 257−261.

Albumin Clusters: Structurally Defined Protein Tetramer and Oxygen Carrier Including Thirty-Two Iron(II) Porphyrins

Teruyuki Komatsu,* Yukiko Oguro, Akito Nakagawa, and Eishun Tsuchida*

Advanced Research Institute for Science and Engineering, Waseda University, 3-4-1 Okubo,Shinjuku-ku, Tokyo 169-8555, Japan

Received June 30, 2005; Revised Manuscript Received August 10, 2005

Recombinant human serum albumin (rHSA) clusters have been synthesized and physicochemically characterized. Cross-linking between the Lys groups of the core albumin and a unique Cys-34 of the shell albumins with an *N*-succinimidyl-6-[3′-(2-pyridyldithio)propionamido]hexanoate produced the structurally defined rHSA trimer and tetramer. MALDI-TOF−MS showed a single peak with the triple and quadruple masses of rHSA. Their molar ellipticities and the isoelectric points (p*I* = 4.8) are all identical to those of the monomer, suggesting that the essential structures of the albumin units were intact. TEM observations demonstrated a uniform morphology of the rHSA tetramer with a diameter of 20−30 nm. The circulation half-life ($\tau_{1/2}$) of the ^{125}I-labeled rHSA tetramer in rat (5.5 h) was significantly longer than that of the monomer (2.3 h) due to the low ratio of the distribution phase (α-phase). A total of 24 and 32 molecules of the synthetic iron(II) porphyrins (FePs) are incorporated into the hydrophobic cavities of the rHSA trimer and tetramer, respectively, producing huge artificial hemoproteins. These albumin−heme clusters can reversibly bind and release O_2 under physiological conditions (37 °C, pH 7.3) and showed similar O_2-binding properties (O_2-binding affinity, association and dissociation rate constants) to those of the corresponding monomer. A large volume of O_2 can be chemically dissolved into the albumin−heme cluster solutions relative to the monomeric rHSA-FeP when the molar concentration of the albumin scaffold is identical.

Introduction

In our bloodstream, hydrophobic molecules of medium size (ex., long-chain fatty acids, bilirubin, steroids, hemin) are captured by human serum albumin (HSA, Mw: 66.5 kDa) and are allowed to circulate for a relatively long time to reach the disposal sites in the body.[1] The transporting ability of this shuttle protein contributes to maintaining the high concentration levels of the therapeutic drugs in the circulatory system.[1,2] Moreover, the albumin peptide exhibited a slow terminal clearance and catabolism, so that the conjugation of HSA with a therapeutic protein (ex., soluble CD4 and interferon-α) provides clinical benefits in permitting less frequent administrations.[3] We have found that synthetic iron(II) porphyrins (hemes) were incorporated into the hydrophobic cavities of HSA, producing an albumin−heme hybrid, which can reversibly bind and release dioxygen (O_2) under physiological conditions (pH 7.3, 37 °C).[4] This artificial hemoprotein has the capability to carry O_2 like hemoglobin (Hb) or myoglobin (Mb) and functions as a red blood cell (RBC) substitute in vivo.[5]

One of the interesting characteristics of the HSA structure is the presence of a single reactive thiol of Cys-34.[1,6] The reaction of the bifunctional reagent, 1,6-bis(maleimido)-hexane (BMH), with HSA successfully creates an intermolecular covalent bridge between the two Cys-34s.[7] A total of 16 molecules of synthetic heme were accommodated into the dimer and the obtained albumin−heme dimer solution is able to transport a large volume of O_2 compared to the human blood ([heme] = 9.2 mM) while maintaining the colloid osmotic pressure on a physiological level.[7b] Another remarkable advantage of the HSA dimer is its long circulation persistence relative to the monomer, since the 2× size of the molecule could serve to remain in the blood vessel. We now extend this approach to produce the structurally defined albumin trimer and tetramer, namely "albumin clusters". In this paper, we report, for the first time, the synthesis, physicochemical characterization, and preliminary pharmacokinetics of the albumin clusters cross-linked by *N*-succinimidyl-6-[3′-(2-pyridyldithio)propionamido]hexanoate (SPDPH), which efficiently connects an NH_2 group of Lys and an SH group of Cys. The O_2-binding properties of the albumin−heme clusters incorporating the 2-[8-{*N*-(2-methylimidazolyl)}octanoyloxymethyl]-5,10,15,20-tetrakis{α,α,α,α-*o*-(1-methylcyclohexanamido)phenyl}porphinatoiron(II) (FeP, Scheme 1), are also evaluated and compared to those of the corresponding monomer.

Experimental Section

Materials and Apparatus. An rHSA (Albrec, 25 wt %) was provided from the NIPRO Corp (Osaka, Japan). Ethanol, dithiothreitol, and 2,2′-dithiopyridine (all high-purity grades) were purchased from Kanto Chemical Co., Inc. (Tokyo) and used without further purification. *N*-Succinimidyl-6-[3′-(2-pyridyldithio)propionamido]hexanoate (SPDPH) was

* To whom correspondence should be addressed. Prof. Eishun Tsuchida, Ph.D. Tel: +81-3-5286-3120. Fax: +81-3-3205-4740. E-mail: eishun@waseda.jp (Eishun Tsuchida). E-mail: teruyuki@waseda.jp (Teruyuki Komatsu).

10.1021/bm050454u CCC: $30.25
Published on Web 10/13/2005

Scheme 1

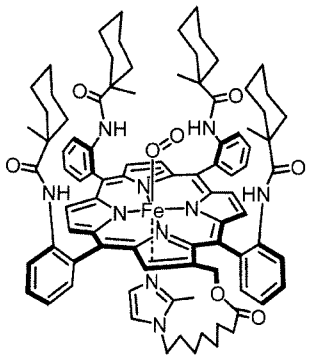

purchased from Pierce Biotechnology (Rockford, USA). 2-[8-{*N*-(2-Methylimidazolyl)}octanoyloxymethyl]-5,10,15,20-tetrakis{α,α,α,α-*o*-(1-methylcyclohexanamido)-phenyl}porphinatoiron(II) (FeP) was prepared according to our previously reported procedure.[8]

Synthesis of rHSA Clusters. Ethanolic SPDPH (20 mM, 0.75 mL) was slowly added dropwise into the rHSA solution (0.75 mM, 2.0 mL) and gently stirred for 20 min at room temperature. The reaction mixture was diluted with phosphate-buffered saline (PBS, 10 mM, pH 7.4, 25 mL) and concentrated to 2.5 mL using an ADVANTEC UHP-76K ultrafiltration system with a Q0500 076E membrane (cutoff Mw 50 kDa). This washing was repeated three times to remove the excess SPDPH, affording 3′-(2-pyridyldithio)propionamido]hexanoated albumin (PDPH−rHSA, [rHSA] = 5.15 wt %, 2 mL). The albumin concentrations were normally measured by bromcresol green (BCG) methods using a Wako AlbuminB−Test.[9] The number of PDPH chains introduced into rHSA was determined by the assay of 2-thiopyridinone (2TP) with an absorption at 343 nm [molar absorption coefficient (ϵ_{343}): 8.1×10^3 $M^{-1}cm^{-1}$]. A 15-fold molar excess of dithiothreitol (DTT, 1 M, 1.35 μL) was added to the PBS solution of PDPH−rHSA (30 μM), and the formed 2-TP was quantitatively assayed after 10 min.

On the other hand, aqueous DTT (1.0 M, 56 μL) was added to the phosphate-buffered solution (pH 7.0, 10 mM) of rHSA (0.75 mM, 20 mL), and the solution was quickly mixed by a vortex mixer, followed by incubation for 30 min at room temperature. The resultant was washed three times with PBS the same as above, yielding a mercapto−albumin (SH−rHSA, 13 mL, [rHSA] = 7.77 wt %). The mercapto ratio of the Cys-34 was confirmed as 100% using the 2,2′-ditiopyridine (2,2′-DTP) procedure.[10,11]

The SH−rHSA solution was then added to the PDPH−rHSA, and the mixture was gently stirred for 20 h at room temperature. The Native-PAGEs were performed using an Amersham Biosciences Electrophoresis Power Supply EPS 301 with a PAG Mini Daiichi 2/15 (Daiichi Pure Chemicals, Co. Ltd.). The Native-PAGE pattern of the obtained reactant showed six bands including the unreacted SH−rHSA monomer. The HPLC measurement also demonstrated the formation of the rHSA clusters with a high molecular weight. The HPLC system consisted of a Shimadzu LC-8A pump and a Shimadzu SPD-10A UV detector. A Shodex Protein KW-803 column was used with PBS (pH 7.4) as the mobile phase at 25 °C (1.0 mL min^{-1}). Peak fitting of the elution curve was done using a Hulinks PeakFit program.

The rHSA clusters were purified by gel column chromatography using a BIO-RAD EGP Combo Rec system with Superdex 200pg (Pharmacia Corp., 5 cmϕ × 40 cm) and PBS (pH 7.4) as the mobile phase (3.5 mL min^{-1}). The eluant was monitored at 280 nm and fractionated by a BIO-RAD model 2110 collector. The fraction showing the single bands for band C and D in the Native-PAGE was then carefully collected. The matrix associated laser desorption ionization time-of-flight mass spectra (MALDI-TOF−MS) were obtained using a Shimadzu AXIMA-CFR Kompact MALDI. The 10 mg mL^{-1} sinapinic acid in 40% aqueous CH_3CN was used as a matrix. The purity of the each component was checked by the HPLC measurement. The obtained yield was 10% for the rHSA trimer (band C) and 7% for the rHSA tetramer (band D).

Physicochemical Properties. The UV−vis absorption spectra were recorded on a JASCO V-570 spectrophotometer. The measurements were normally performed at 25 °C. Circular dichroism (CD) spectra were obtained using a JASCO J-725 spectropolarimeter. The concentration of the rHSA sample was 2 μM in PBS, and quartz cuvettes with a 1.0-mm thickness were used for the measurements over the range of 195−250 nm.

Transmission Electron Microscopy (TEM). An aqueous solution of the albumin cluster was mixed with 2% phosphotungstic acid (pH 7), and the droplet was placed onto a 200 mesh carbon-coated copper grid, which was hydrophilized by a JEOL HDT-400 hydrophilic treatment device prior to use. The grid was allowed to air-dry and observed in a JEOL JEM-1011 electron microscope at an accelerating voltage of 100 kV.

Circulation Lifetime in Vivo. The 125-Iodinated rHSA tetramer was prepared by our previously reported procedures.[7b] The recovered ^{125}I-albumin had a specific activity of 24.3 MBq mg^{-1} and was diluted by nonlabeled albumin tetramer before administration into anesthetized Wistar rats (ca. 250 g, male). The kinetics of the albumin clearance from the circulation was monitored by measuring the radioactivity in the plasma phase of blood taken from the lateral tail veins using an Aloka ARC 2000 Autowell Gamma Counter. Acid precipitability of the recovered radioactivity was confirmed by the TCA method.[7b,12] The rats were sacrified 8 days after the sample injection by hemorrhage. The radioactivity of the excised organs was also measured. The care and handling of the animals were in accordance with NIH guidelines.

Preparation of Albumin−Heme Clusters. The preparations of albumin−heme clusters (rHSA−FeP trimer and tetramer) were carried out by mixing the EtOH solution of carbonyl−FeP and an aqueous phosphate-buffered solution of albumin clusters according to our previously reported procedures ([FeP]/[rHSA] = 26/1 or 34/1 (mol/mol)).[4a,7b,8] The albumin concentrations were measured using the CD spectra, and the amount of FeP was determined by the assay of the iron ion concentration using inductively coupled plasma spectrometry (ICP) with a Seiko Instruments SPS 7000A spectrometer.

Magnetic Circular Dichroism (MCD). MCD spectra for the phosphate-buffered solution of the albumin−heme clusters (10 μM) under N_2, CO, and O_2 atmospheres were measured using a JASCO J-820 circular dichrometer fitted with a 1.5 T electromagnet. The CD spectra at 0 T were always used as a baseline for each condition.

O_2-Binding Equilibrium and Kinetics. O_2 binding to FeP was expressed by eq 1:

$$\mathrm{FeP} + \mathrm{O_2} \underset{k_{off}}{\overset{k_{on}}{\rightleftharpoons}} \mathrm{FeP(O_2)} \qquad (K = k_{on}/k_{off}) \qquad (1)$$

The O_2-binding affinity (gaseous pressure at half O_2 binding for heme, $P_{1/2} = 1/K$) was determined by UV−vis absorption spectral changes at various O_2 partial pressure.[4b,8,13] The appropriate O_2/N_2 gas mixture (Po_2: 0, 10, 20, 30, 80, 160, and 760 Torr) was prepared by a KOFLOC Gasblender GB-3C, and each spectrum was measured after flowing the gas for 15 min at 25 or 37 °C. FeP concentrations of 20 μM were normally used for the measurements in the range of 350−700 nm. The O_2-binding constant (K) was then calculated from the difference of the absorbance at 444 nm using Drago's equation.[4b,8] The half-lifetimes of the dioxygenated species of the albumin−heme clusters were determined by the time dependence of the absorption intensity for the O_2−adduct complex (549 nm).

The association and dissociation rate constants for O_2 (k_{on} and k_{off}) were measured by a competitive rebinding technique using a Unisoku TSP-1000WK−WIN time-resolved spectrophotometer with a Spectron Laser Systems SL803G-10 Q-switched Nd:YAG laser, which generated a second-harmonic (532 nm) pulse of 6-ns duration (10 Hz). A 150 W xenon arc-lamp was used as the monitor light source. The concentration of the albumin−heme cluster was normally 20 μM and experiments were carried out at 25 °C. The absorption decays accompanying the O_2 association obeyed three-component kinetics. We employed triple-exponentials equation to analyze the absorption decays; $\Delta A(t)$[4c]

$$\Delta A(t) = C_1 \exp(-k_1 t) + C_2 \exp(-k_2 t) + C_3 \exp(-k_3 t) \quad (2)$$

where k_1, k_2, and k_3 are apparent rate constants for the each components.

O_2-Concentration Measurements. The chemically dissolved O_2 in albumin−heme cluster solution was measured using an Ocean Photonics FOXY2000 Fiber Optic Oxygen Sensor with a USB2000 multichannels monochromator and FOXY-AL300 fiber optic sensor (Tokyo). This apparatus uses the fluorescence of a ruthenium complex to measure the partial pressure of O_2. The addition of 0.1 mL of CO to the phosphate-buffered solution of the dioxygenated rHSA−FeP cluster or monomer ([FeP]: 50 μM, 2.0 mL, [O_2]: 700 Torr) in the closed tube immediately dissociates the coordinated O_2 from FeP and increases the dissolved O_2 content in the aqueous phase.

Results and Discussion

Synthesis and Characterization of rHSA Clusters. We have shown that covalent cross-linking a unique Cys-34 of rHSA with BMH provided a defined rHSA dimer, in which

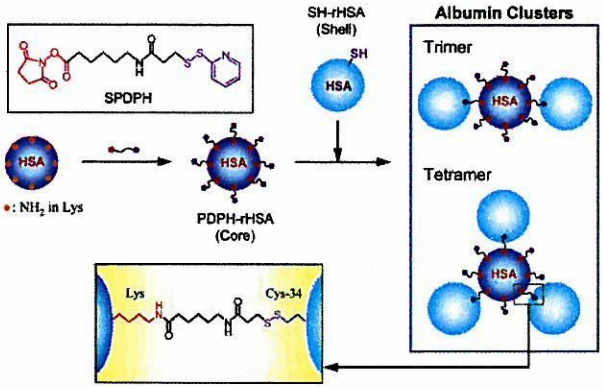

Figure 1. Synthetic scheme of albumin clusters with SPDPH.

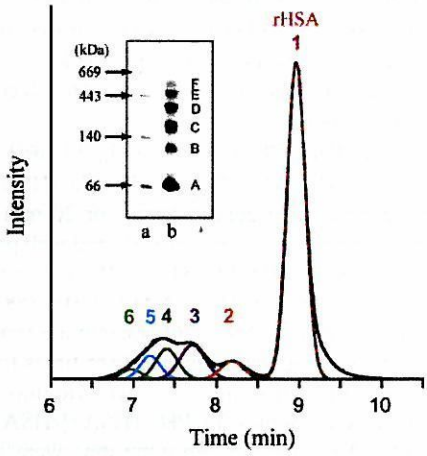

Figure 2. Native-PAGE electrophoresis and HPLC elution curve of the reaction mixture at 25 °C. In the Native-PAGE pattern, lane a, protein ladder; lane b, the reaction mixture (band A: rHSA monomer). The HPLC profile was simulated by a six-components model using a PeakFit (the dotted line, the sum of the simulated six components; peak 1, rHSA monomer).

the essential structures of the rHSA unit are intact.[7b] We now extend this approach to produce albumin clusters. Our first attempt to connect the Cys-34 of rHSAs by multi-armed maleimido(polyoxyethylene) unfortunately failed. The maleimido-terminate at the polyoxyethylene chains are likely to be too flexible to react with the small thiol on the large rHSA molecule to make albumin clusters. On the other hand, *N*-succinimidyl-6-[3′-(2-pyridyldithio)propionamido]hexanoate (SPDPH) was successfully connected to an NH_2 group of Lys and an SH group of Cys on the protein surface. Since rHSA contains 59 Lys in the globular structure, mixing a small molar excess SPDPH with rHSA immediately produced a 6-[3′-(2-pyridyldithio)propionamido]hexanoated rHSA (PDPH−rHSA; Figure 1). Assay of the pyridyldithio residues revealed that approximately 8.3 chains of PDPH were introduced into one rHSA molecule. The PDPH−rHSA acts as a core albumin for the next reaction.

Dithiothreitol (DTT) selectively reduces the mixed-disulfide of Cys-34[10,11] producing a mercapto−rHSA (SH−rHSA) as a shell albumin. After removing DTT, SH−rHSA was slowly dropwise added to the PDPH−rHSA and stirred for 20 h at room temperature (Figure 1). Native-PAGE of the reactant showed six distinct migration bands (Figure 2 inset, lane b: A−F, band A: SH−rHSA). On the basis of the

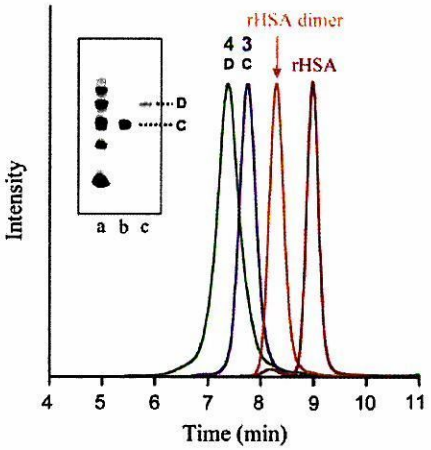

Figure 3. Native-PAGE electrophoresis and HPLC elution curves of the isolated rHSA clusters at 25 °C. In the Native-PAGE pattern, lane a, reaction mixture before purification; lane b, isolated band C; lane c, isolated band D. In the HPLC profiles, red line, rHSA monomer; orange line, rHSA dimer bridged through Cys-34 by BMH; blue line, isolated band C, which corresponds to the rHSA trimer; green line, isolated band D, which corresponds to the rHSA tetramer.

Table 1. Molecular Masses and *pI* Values of rHSA Monomer, Dimer, and Clusters

	M_w		
	obs.[a]	calcd.	p*I*
rHSA[b]	66331	66451	4.8
rHSA dimer[b,c]	132 741	133 180	4.8
band C (rHSA trimer)	200 469	201 614	4.8
band D (rHSA tetramer)	266 538	267 953	4.8

[a] Measured by MALDI-TOF−MS. [b] From ref 7b. [c] rHSA dimer bridged Cys-34 by BMH.

comparison with the protein ladder (lane a), the molecular weights of the bands B, C, and D were estimated to be ca. 130, 200, and 260 kDa, respectively. It can be postulated that they are the rHSA dimer, trimer, and tetramer. The pyridylditio terminates of the core albumin reacted with the single active Cys-34 of the shell albumin creating albumin clusters. The HPLC profile of the reaction mixture exhibited broad multiple bands in the range of 6.5−8.5 min before the rHSA peak (9.0 min; Figure 2). From the careful inspection of the elution curve by peak fitting simulation, we could divide the entire pattern into six components (peaks 1−6). Most probably, the peaks 2−6 correspond to the rHSA dimer to hexamer. Gel permeation chromatography also showed a similar elution curve. Several synthesis repetitions always gave the same patterns in Native-PAGE, HPLC, and GPC. The fractions whose Native-PAGE showed bands C and D were then corrected (Figure 3, inset lanes b and c). Their HPLC profiles exhibited a sharp peak at the exactly the same position where we predicted for peaks 3 and 4 in Figure 2.

The MALDI-TOF−MS of the components of peaks 3 (band C) and 4 (band D) showed a molecular masses at *m/z* 200 469 and 266 538, respectively, which are in good agreement with the calculated value of the rHSA trimer and tetramer (M_w = 201 614 and 267 953) within a difference of 0.5% (Table 1). We first isolated the well-defined rHSA trimer and tetramer in which the Lys groups of the core

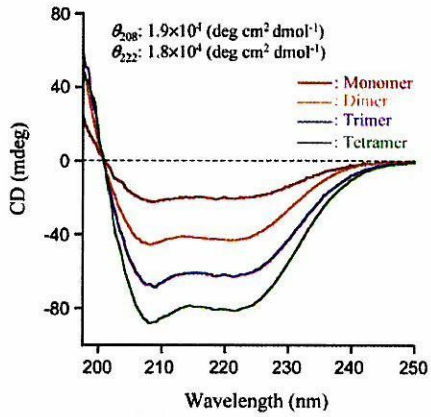

Figure 4. CD spectra of rHSA monomer, dimer bridged through Cys-34 by BMH and clusters in PBS solution (pH 7.4) at 25 °C.

albumin are covalently bridged by the Cys-34 group of the shell albumins.

The peak area evaluations for the six components in Figure 2 indicated their molar ratios in the reaction mixture; monomer (88.2%), dimer (3.1%), trimer (4.3%), tetramer (2.5%), pentamer (1.4%), and hexamer (0.5%). Because the average degree of polymerization was 3.3, we estimated the reaction ratio (X) of the PDPH−rHSA

$$\text{reacted PDPH−rHSA:unreacted (PDPH−rHSA + SH−rHSA)} = X:(1 - X) + (10 - 2.3X) = 11.8:88.2 \quad (3)$$

Thus, X was calculated to be 1.0; this means that all of the PDPH−rHSA (core albumin) participated in the reaction with the shell albumin. The formation ratio of each cluster can be estimated; dimer (26%), trimer (36%), tetramer (22%), pentamer (12%), and hexamer (4%).

The CD spectral patterns (λ_{min} = 208 and 222 nm) and the molar ellipticities at 208 and 222 nm ($[\theta]_{208} = 1.9 \times 10^4$ deg cm^2 dmol^{-1}, $[\theta]_{222} = 1.8 \times 10^4$ deg cm^2 dmol^{-1}) of the isolated rHSA trimer and tetramer were identical to those of the monomer and dimer (Figure 4).[4b,7b] Their isoelectric points (p*I* = 4.8) were also identical to that of rHSA (Table 1). These results implied that the secondary/tertiary structure, the α-helix content, and surface net charges of the rHSA units were intact after the cluster formation.

TEM of the negatively stained samples of the rHSA tetramer showed homogeneous particles with a diameter of 20−30 nm (Figure 5a,b). The appearance of the cluster solutions was unchanged for over one year and underwent no aggregation and precipitation. We postulate that one tetramer consists of four rHSA molecules bound in the trigonal pyramid form, which was drawn as a model in Figure 5c. rHSA involves a total of 59 Lys groups, and the cross-linker SPDPH can statistically bind to the surface. On the basis of the assay of the dithiopyridyl group, we found that the 8.3 functional PDPH arms are introduced into the core albumin. The shell albumins (SH−rHSAs) therefore approach the PDPH−rHSA from all directions to form a disulfide bridge with Cys-34. As a consequence, the conformation of the tetramer should become a trigonal pyramid-like structure, which is the most favorable arrangement to avoid the steric repulsion of the albumin units.

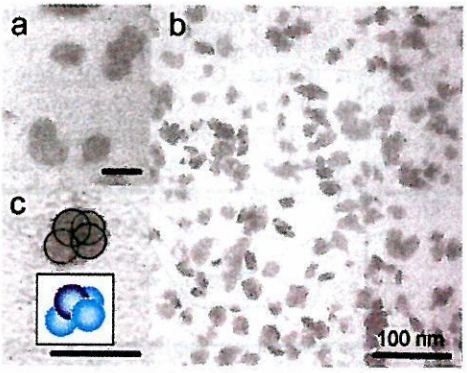

Figure 5. TEM observations of negatively stained rHSA tetramer. In panels a and c, the scale bars indicate the length of 30 nm. In panel c, the trigonal pyramid form of the rHSA tetramer is predicted from the one molecule under magnification.

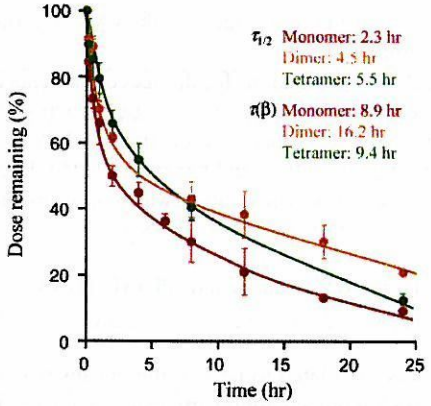

Figure 6. Plasma levels of ^{125}I−rHSA tetramer after intravenously administration to Wistar rats (rHSA amount = 1.0 mg kg^{-1}). The data for the ^{125}I−rHSA monomer and dimer were cited from our previously reported paper (ref 7b). All values are mean ± S. D. (n = 3).

Circulation Lifetime of ^{125}I-Labeled rHSA Tetramer in Rats. The rHSA tetramer labeled with ^{125}I was injected into anesthetized rats to determine the blood circulation lifetimes. Throughout the experiments, the turbidity of the plasma phase and the blood cell numbers were constant, showing no aggregation of the albumin clusters and blood cell components. The time courses of the radioactivity demonstrated two-phase kinetics and significant differences from the monomer's decay (Figure 6). The half-lifetime ($\tau_{1/2}$, time when the initial value decreased to 50%) of the rHSA tetramer was 5.5 h, which was 2.4-fold longer than that of the monomer (2.3 h).[7b] This was due to the low ratio of the distribution phase (α-phase) of the tetramer (26%), compared to the monomer and dimer, 39% and 36%, respectively. The increase in the molecular size led to retardation of the extravasation through the vascular endothelium. On the contrary, its lifetime (τ) of the disappearance phase (β-phase; 8.9 h) was shorter than the tightly bridged rHSA dimer with a sulfide bond (16.2 h); although the $\tau_{1/2}$ of the dimer is lower than the tetramer, there is a greater amount of dimer at 24 h than tetramer. The rHSA tetramer disappeared slowly after 12 h, and 10% remained at 24 h from the injection, which was almost the same amount observed in the monomer group. After 12 h, the weak disulfide bonds between the core and shell albumins may be cleaved to dissociate the monomer components and cleared from the bloodstream. Radioactivity of the trichloroacetic acid precipitates recovered up to 90% of the intensity, which means ^{125}I did not dissociate from the proteins. The tissue distributions of the rHSA tetramer were in the skin, liver, and spleen, and there were no differences to that of the rHSA monomer. Our albumin tetramer may become a unique vehicle which serves to sustain a high drug concentration particularly during the initial phase.

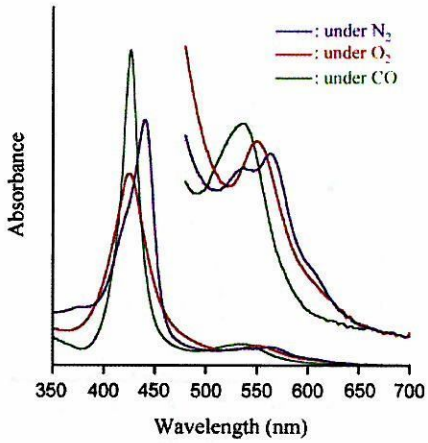

Figure 7. UV−vis absorption spectral changes of the rHSA−FeP tetramer in phosphate-buffered solution (pH 7.3) at various conditions (25 °C).

Albumin−Heme Clusters and Their O_2 Binding. Mixing the ethanolic FeP with an aqueous albumin cluster and removing the ethanol by ultrafiltration produced red-colored homogeneous albumin−heme cluster solutions. They were rather stable and stored for more than 1 year at 4 °C without any precipitation. From the quantitative assays of rHSA and FeP, the molar ratios of the FeP/rHSA were determined to be 24.2 and 31.6 for the trimer and tetramer, which are 3- and 4-fold molar excess amounts of the monomeric rHSA−FeP. We can conclude that a maximum of eight FePs were also incorporated into the rHSA unit. These albumin−heme clusters showed identical CD spectra and pI values (4.8) with the original rHSA trimer and tetramer, which implied that the FeP incorporation did not cause any structural changes in the albumin components.

The UV−vis absorption spectrum of the aqueous rHSA−FeP tetramer in an N_2 atmosphere showed the formation of a five-coordinate high-spin complex involving an axially bound 2-methylimidazolyl side-chain (λ_{max} = 444, 539, and 565 nm; Figure 7).[4b,8,13] After this solution was kept under a stream of O_2 for 5 min, the absorption spectra changed to that of a typical O_2−adduct complex (λ_{max} = 426 and 549 nm).[4b,8,13] This dioxygenation was reversibly observed and dependent on the O_2/N_2 pressure under physiological conditions (pH 7.3, 37 °C). After admitting the CO gas, the O_2−adduct complex immediately moved to the carbonyl low-spin complex (λ_{max} = 427 and 539 nm). The rHSA-FeP trimer also showed identical spectral changes under these conditions [rHSA-FeP trimer in N_2 (λ_{max} = 442, 539, and 564 nm), O_2 (λ_{max} = 423 and 547 nm), and CO atmosphere (λ_{max} = 426 and 534 nm)].

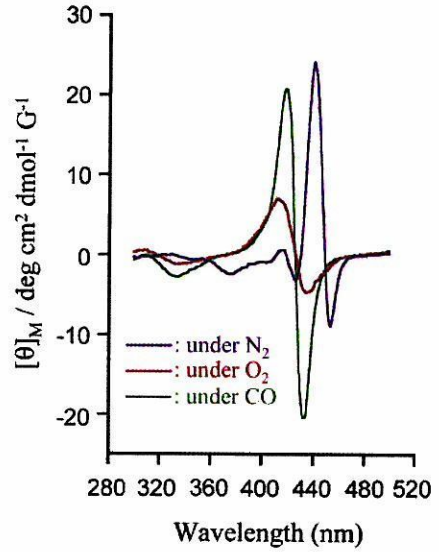

Figure 8. MCD spectral changes of the rHSA–FeP tetramer in phosphate-buffered solution (pH 7.3) at various conditions (25 °C).

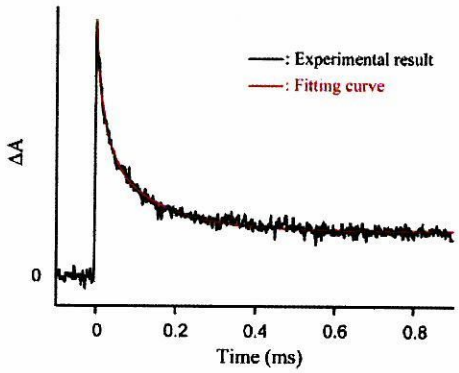

Figure 9. Absorption decay of O_2 rebinding to the rHSA–FeP cluster in phosphate-buffered solution (pH 7.3) after the laser flash photolysis at 25 °C. The kinetics was composed of three phases and relaxation curve was fitted by triple-exponentials.

MCD spectroscopy revealed the coordination structure of the FeP in the rHSA clusters. Under an N_2 atmosphere, the MCD of the rHSA-FeP tetramer resembled the well-characterized spectrum of a mono-imidazole ligated five-*N*-coordinate high-spin tetraphenylporphinatoiron(II) (Figure 8).[14] This observation indicates that the amino acid residue in the rHSA structure did not bind to the sixth position of FeP. The admission of O_2 gas changed the spectrum to an S-shaped A-term MCD in the Soret-band region, which shows the formation of an O_2–adduct complex.[14] The CO adduct is also low spin and exhibited a similar A-term MCD band with a high intensity.

The autoxidation reaction of the oxy state (λ_{max} = 549 nm) slowly occurred and the absorption intensity of 549 nm almost disappeared after 48 h, leading to the formation of the inactive Fe(III)P. The half-lives of the dioxygenated species ($\tau_{1/2}$) of the rHSA–FeP trimer and tetramer were both 7 h at 37 °C, which are almost the same as that of our previous results for the rHSA–FeP dimer ($\tau_{1/2}$ = 6 h).[7b]

O_2-Binding Kinetics and Equilibrium of Albumin–Heme Clusters. Flash photolysis experiments for the albumin–heme clusters were performed to determine the association and dissociation rate constants of O_2 (k_{on}, k_{off}). We have shown that the O_2 associations to FePs in the monomeric rHSA are affected by the molecular environments around the FeP site, for example, steric hindrance of the nearest amino acid residues.[4c] In the case of the albumin–heme clusters, there should be multiple kinetic parameters. Nevertheless, the O_2 binding profile to FeP demonstrated the same trends as the rHSA–FeP monomer. The absorption change accompanying the O_2 recombination clearly obeyed three-phases, which were fit by a triple-exponential kinetics (Figure 9). The fastest minor component (k_1) is related to a base dissociation reaction.[15] The linear relationship between the apparent rates k_2 and k_3 vs the [O_2] provided two association rate constants for the fast O_2 rebinding (k_{on}) and the slow O_2 rebinding (k'_{on}; Table 2). The k_{on} values are 4.1–7.8-fold greater than k'_{on}, and the amplitude ratios of the fast and slow phases were approximately 1/1, which implied that half of the FeP molecules in the rHSA trimer and tetramer may locate in the slow sites for the O_2 association. The O_2-binding affinity ($P_{1/2}$) of the rHSA-FeP clusters were determined to be 38 Torr at 37 °C on the basis of the UV–vis. absorption spectral changes by O_2 titration with different [O_2].[4b,8,13] The obtained $P_{1/2}$ is close to that of the rHSA–FeP monomer and human RBC (Table 2).[8,16,17] The cluster formation did not alter the O_2-binding properties of rHSA–FeP.

Table 2. O_2-Binding Parameters of rHSA-FeP Monomer, Dimer, and Clusters in Phosphate-Buffered Solution (pH 7.3) at 25 °C

	10^{-6} k_{on} (M^{-1} s^{-1})	10^{-6} K_{on} (M^{-1} s^{-1})	10^{-2} k_{off} (s^{-1})	10^{-2} K_{off} (s^{-1})	$P_{1/2}$ (Torr)[a]
rHSA-FeP[b]	46	7.3	9.8	1.6	13 (35)
rHSA-FeP dimer[c]	28	4.8	6.7	1.2	15 (38)
rHSA-FeP trimer	46	5.9	8.7	1.1	12 (38)
rHSA-FeP tetramer	53	13	11	2.7	12 (38)
Hb(T-state)α[d]	2.9		1.8		40
human RBC[e]					8 (27)

[a] At 37 °C in parenthesis. [b] From ref 8. [c] From ref 7b. [d] Hbα chain (monomer), aqueous pH 7.0–7.4, 20 °C, from ref 16. [e] From ref 17.

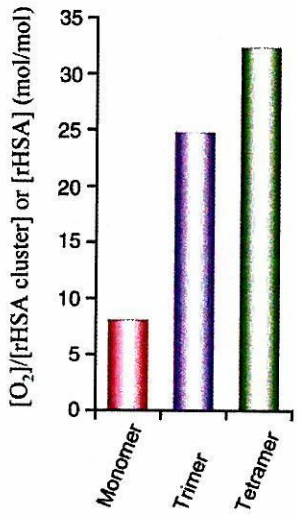

Figure 10. Molar ratio of the increased O_2 per rHSA cluster (mol/mol) after exposure of CO gas to rHSA–FeP cluster solutions (25 °C).

O_2 Concentration in Albumin−Heme Cluster Solution. The addition of small amounts of CO to the aqueous solutions of the dioxygenated rHSA−FeP clusters ([FeP] = 50 μM) in closed tubes dissociates the coordinated O_2, which immediately diffuses in the medium. In all cases, the O_2 concentrations increased 0.05 mM after the CO exposure. The UV−vis absorption spectra of the solutions changed to that of the carbonyl complex. The molar ratio of the chemically bound O_2 per albumin vehicle ([rHSA cluster] or [rHSA]) (mol/mol) showed that the albumin−heme clusters bind a large volume of O_2 relative to the monomer (Figure 10). The rHSA-FeP tetramer solution ([rHSA tetramer] = 0.75 mM, [heme] = 24 mM) could probably transport a 2.6-fold greater volume of O_2 compared to human blood ([heme] = 9.2 mM) while maintaining the colloid osmotic pressure on a physiological level.

Conclusions

The structurally defined albumin clusters prepared using a unique SH group of Cys-34 reported here provide the following characteristics.

(i) Essential properties of the rHSA units (the secondary/tertiary structure, surface net charges) were intact after the cluster formation. Our albumin clusters behave as a gigantic serum albumin.

(ii) The tetramer showed a longer half-life (5.5 h) in the bloodstream of rats compared to that of the monomer due to the low ratio of the α-phase (26%). However, it slowly disappeared after 12 h and was 10% of the basal value at 24 h after the injection.

(iii) The rHSA unit in the clusters can incorporate a maximum of eight FeP molecules, that is, the trimer and tetramer contain 24 and 32 active O_2-binding heme sites, which are 6- and 8-fold greater than that of the native tetrameric Hb, respectively. The obtained albumin−heme clusters become huge artificial hemoproteins with molecular weights of 235 and 313 kDa and can reversibly bind O_2 under physiological conditions.

(iv) The albumin−heme tetramer has the capability to transport a 4-fold larger volume of O_2 compared to the corresponding monomer when the albumin vehicle molar concentrations were identical. It implies that the albumin−heme clusters potentially become novel RBC substitutes having a 2.6-fold higher O_2 transporting ability than human blood.

This method of creating albumin clusters should lead to generating defined protein polymers and a new series of functional biomaterials. The preparations of the starburst rHSA dendrimer and linear string of rHSA pearls are now in progress.

Acknowledgment. This work was partially supported by a Grant-in-Aid for Scientific Research (No. 16350093) from JSPS, and a Grant-in-Aid for Exploratory Research (No. 16655049) from MEXT Japan, and a Health Science Research Grant (Regulatory Science, B5-551) from MHLW Japan. Prof. Dr. Koichi Kobayashi (Keio University) and Mr. Hisashi Yamamoto (NIPRO Corp.) are greatly acknowledged for the animal experiments.

References and Notes

(1) Peters, T., Jr. *All about albumin, biochemistry, genetics, and medical applications*; Academic Press: San Diego, CA, 1997; and reference therein.
(2) (a) Kragh-Hansen, U. *Pharmacol. Rev.* **1981**, *33*, 17−53. (b) Kragh-Hansen, U. *Danish Med. Bull.* **1990**, *37*, 57−84.
(3) Sheffield, W. P. *Curr. Drug Targets Cardiovasc. Haematol. Disord.* **2001**, *1*, 1−22.
(4) (a) Komatsu, T.; Hamamatsu, K.; Wu, J.; Tsuchida, E. *Bioconjugate Chem.* **1999**, *10*, 82−86. (b) Tsuchida, E.; Komatsu, T.; Matsukawa, Y.; Hamamatsu, K.; Wu, J. *Bioconjugate Chem.* **1999**, *10*, 797−802. (c) Komatsu, T.; Matsukawa, Y.; Tsuchida, E. *Bioconjugate Chem.* **2000**, *11*, 772−776.
(5) Tsuchida, E.; Komatsu, T.; Matsukawa, Y.; Nakagawa, A.; Sakai, H.; Kobayashi, K.; Suematsu, M. *J. Biomed. Mater. Res.* **2003**, *64A*, 257−261.
(6) Carter, D. C.; Ho, J. X. *Adv. Protein Chem.* **1994**, *45*, 153−203.
(7) (a) Komatsu, T.; Hamamatsu, K.; Tsuchida, E. *Macromolecules* **1999**, *32*, 8388−8391. (b) Komatsu, T.; Oguro, Y.; Teramura, Y.; Takeoka, S.; Okai, J.; Anraku, M.; Otagiri, M.; Tsuchida, E. *Biochim. Biophys. Acta* **2004**, *1675*, 21−31.
(8) Komatsu, T.; Matsukawa, Y.; Tsuchida, E. *Bioconjugate Chem.* **2002**, *13*, 397−402.
(9) Doumas, B. T.; Watson, W. A.; Biggs, H. G. *Clin. Chim. Acta* **1971**, *31*, 87−96.
(10) Grassetti, D. R.; Murray, J. F., Jr. *Arch. Biochem. Biophys.* **1967**, *119*, 41−49.
(11) Pedersen, A. O.; Jacobsen, J. *Eur. J. Biochem.* **1980**, *106*, 291−295.
(12) Watanabe, H.; Yamasaki, K.; Kragh-Hansen, U.; Tanase, S.; Harada, K.; Suenaga, A.; Otagiri, M. *Pharm. Res.* **2001**, *18*, 1775−1781.
(13) Collman, J. P.; Brauman, J. I.; Iverson, B. L.; Sessler, J. L.; Morris, R. M.; Gibson, Q. H. *J. Am. Chem. Soc.* **1983**, *105*, 3052−3064.
(14) (a) Collman, J. P.; Brauman, J. I.; Doxsee, K. M.; Halbert, T. R.; Bunnenberg, E.; Linder, R. E.; LaMar, G. N.; Guadio, J. D.; Lang, G.; Spartalian, K. *J. Am. Chem. Soc.* **1980**, *102*, 4182−4192. (b) Collman, J. P.; Basolo, F.; Bunnenberg, E.; Collins, T. C.; Dawson, J. H.; Ellis, P. E., Jr.; Marrocco, M. L.; Moscowitz, A.; Sessler, J. L.; Szymanski, T. *J. Am. Chem. Soc.* **1981**, *103*, 5636−5648.
(15) Geibel, J.; Cannon, J.; Campbell, D.; Traylor, T. G. *J. Am. Chem. Soc.* **1978**, *100*, 3575−3585.
(16) Sawicki, C. A.; Gibson, Q. H. *J. Biol. Chem. Soc.* **1977**, *252*, 7538−7547.
(17) Severinghous, J. W. *J. Appl. Physiol.* **1966**, *21*, 1108−1116.

BM050454U

Human Serum Albumin Hybrid Incorporating Tailed Porphyrinatoiron(II) in the α,α,α,β-Conformer as an O_2-Binding Site

Akito Nakagawa, Teruyuki Komatsu,* Makoto Iizuka, and Eishun Tsuchida*

Advanced Research Institute for Science and Engineering, Waseda University, 3-4-1 Okubo, Shinjuku-ku, Tokyo 169-8555 Japan. Received June 1, 2005; Revised Manuscript Received October 30, 2005

We have found that recombinant human serum albumin (HSA) incorporating tailed porphyrinatoiron(II) in the α,α,α,β-conformer can reversibly bind and release O_2 under physiological conditions (pH 7.3, 37 °C) like hemoglobin and myoglobin. β-2-Methylimidazolyl-tailed porphyrinatoirons (**6a**, **6b**) are synthesized via four steps from the atropisomers of tetrakis(*o*-aminophenyl)porphyrin. The stereochemistry of the α,α,α,β-conformer has been determined by NMR spectroscopy. **6a** and **6b** form stable O_2-adduct complexes in toluene solution at room temperature. The association rate constants of O_2 are 3.1- and 1.9-fold lower than those of the corresponding α,α,α,α-conformers (**1a**, **1b**), indicating that the three substituents (cyclohexanamide or pivalamide groups) are close to each other on the porphyrin platform and construct a narrow encumbrance around the O_2-coordination site. Although **6a** and **6b** are incorporated into the hydrophobic domains of HSA to produce the albumin–heme hybrid, only HSA-**6a** can bind O_2 in aqueous medium. The cyclohexanamide fences are necessary for the tailed porphyrinatoiron to form a stable O_2-adduct complex under physiological conditions. The O_2-binding affinity ($P_{1/2}$) of HSA-**6a** is 45 Torr (37 °C), and the O_2 transporting efficiency between lungs and muscle tissues in the human body is estimated to be identical to that of human red blood cells. The HSA-**6a** solution will become one of the most promising materials for red blood cell substitutes, which can be manufactured on an industrial scale.

INTRODUCTION

To reproduce the O_2-binding ability of hemoglobin (Hb) and myoglobin (Mb), numerous numbers of model hemes have been synthesized over the past decades (*1*). These continuous approaches, aimed at understanding the precise mechanism of the O_2-binding reaction, have been mostly accomplished in organic solvents, and tetrakis(phenyl)porphyrin (TPP) was widely used as a molecular scaffold. We have also synthesized tetrakis-{α,α,α,α-*o*-(1-methylcyclohexanamido)phenyl}porphinatoiron-(II) bearing a covalently linked proximal imidazole (**1a**, Figure 1)[1] that forms a stable O_2-adduct complex in toluene solution at ambient temperature (*2*). The four cyclohexanamide fences on the distal-side (α-side) of the porphyrin plane are bulky enough to prevent μ-oxo dimer formation, and the 2-methylimidazolyl arm intramolecularly coordinated to the Fe^{2+} center from the proximal-side (β-side) modulates the O_2-binding affinity.

Some substantial efforts have been directed to prepare an artificial O_2 carrier involving a synthetic heme under physiological conditions (pH 7.3, 37 °C), which may become a red blood cell substitute (*1a*, *3*). We have successfully incorporated **1a** into the hydrophobic domains of recombinant human serum albumin (HSA) and found that the albumin–heme hybrid (HSA–**1a**) could reversibly absorb O_2 in aqueous medium (*1a*, *2*, *4*). This red-colored albumin solution showed a long shelf life of over two years without precipitation. More recently, exchange transfusion experiments with HSA–**1a** into anesthetized rats demonstrated that it effectively rescitates the hemorrhagic shock state and transports O_2 to the muscle tissues (*5*). We are now developing this albumin–heme hybrid as an entirely synthetic red blood cell substitute that can be extensively used in a variety of medical situations (*6*).

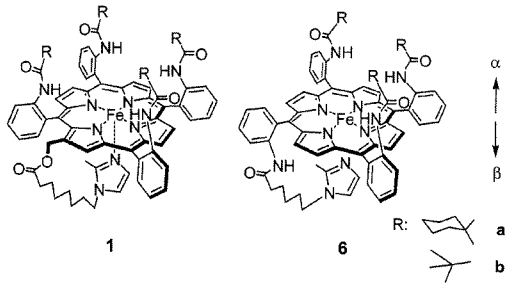

Figure 1. Structures of porphyrinatoiron derivatives in the α,α,α,α-conformer and α,α,α,β-conformer (tailed porphyrinatoiron).

The only disadvantage of this synthetic heme **1a** is that a great deal of labor is required to make the α,α,α,α (α^4)-conformer and to introduce the imidazolylalkyl arm at the porphyrin periphery via the Vilsmeier reaction (*2*). The starting material, tetrakis(α,α,α,α-*o*-aminophenyl)porphyrin (TAPP), is in a statistical mixture of the four possible atrop isomers (α,α,α,α, α,α,α,β, α,β,α,β, α,α,β,β; the ratio is 1:4:2:1), and the variable α^4-conformer used to be isolated by Lindsey's procedure with a silica gel column separation (*7*). The number of total steps for the synthesis of **1a** is, therefore, eight from TAPP.

In this study, we first incorporated a "tailed porphyrinatoiron" with the $\alpha^3\beta$-conformer as an O_2-binding site of the albumin–heme. A series of tailed porphyrins as the model compound of Hb and Mb were synthesized by Collman and co-worker (*8*). There are two advantages of the tailed porphyrin: (i) the statistical content of the $\alpha^3\beta$-conformer of TAPP is maximum

* Corresponding authors: (E.T.) Tel: +81-3-5286-3120. Fax: +81-3-3205-4740. E-mail: eishun@waseda.jp. (T.K.) E-mail: teruyuki@waseda.jp.

[1] Abbreviations: **1a**: 2-[8-{*N*-(2-methyl-1-imidazolyl)octanoyloxy]-methyl]-5,10,15,20-tetrakis{(α,α,α,α-o-(1-methylcyclohexanamido)-phenyl}porphinatoiron; **1b**: 2-[8-{*N*-(2-methyl-1-imidazolyl)octanoyl oxymethyl]-5,10,15,20-tetrakis{α,α,α,α-*o*-(pivalamido)phenyl}porphinatoiron; **6a**: 5,10,15-Tris {α,α,α-*o*-(1-methylcyclohexanamido)-phenyl}-20-mono[β-*o*-[6-{*N*-(2-methyl-1-imidazolyl)}hexanamido]phenyl]-porphinatoiron; **6b**: 5,10,15-Tris(α,α,α-*o*-(pivalamido)phenyl)-20-mono[β-*o*-[6-{*N*-(2-methyl-1-imidazolyl)}hexyramido]phenyl]-porphinatoiron.

10.1021/bc050154+ CCC: $33.50
Published on Web 12/21/2005

Scheme 1. Synthesis of Tailed Porphyrinatoirons

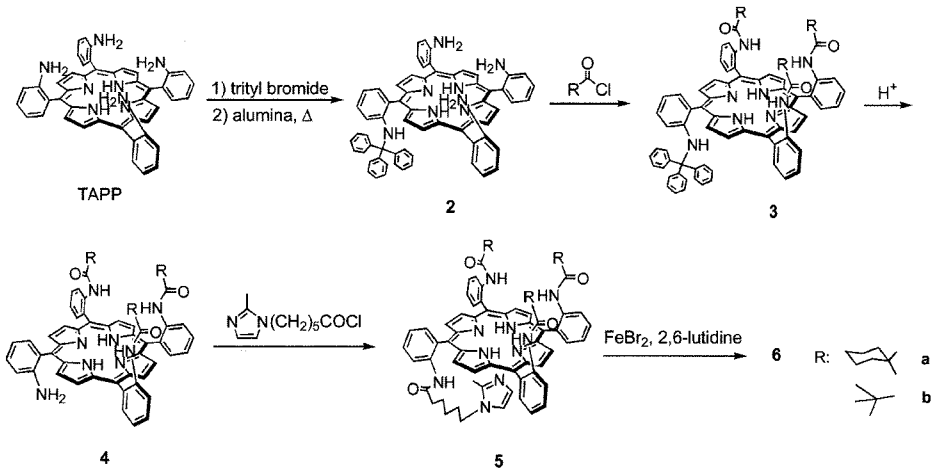

(50%), and (ii) there is no need to modify the porphyrin ring because the proximal base is attached to the fourth β-*o*-NH_2 group of the phenyl ring. This convenient synthetic procedure is a great advantage for the industrial scale-up of the manufacturing of the albumin–heme solution. However, we were not certain of the stability of the O_2-adduct complex of the tailed porphyrinatoiron(II) in an aqueous medium. It has been postulated that the four substituents were essential for preventing an unfavorable proton-driven oxidation of the central ferrous ion of the Fe^{2+}TPP derivatives in water (*1a*, *3*).

First, we describe the synthesis and stereochemistry of the 2-methylimidazole-tailed porphyrinatoirons (**6a**, **6b**) and compare their O_2-binding properties in toluene solution. The effects of the substituents on the O_2-binding parameters are discussed. Furthermore, the O_2-binding property of the albumin–heme hybrid including the tailed porphyrinatiron(II) **6a** has been characterized under physiological conditions. The 5 wt % albumin–heme solution involving the easily prepared **6a** could be the most promising artificial O_2 carrier suitable for mass production.

EXPERIMENTAL SECTION

Synthesis of Tailed Porphyrinatoirons. Experimental details of the synthesis and spectra (^{1}H NMR, IR, UV–Vis, HR-MS) are supplied as Supporting Information.

Reduction of Ferric Complex to Ferrous Complex in Toluene. Reduction to the porphyrinatoiron(II) was carried out using toluene-aq $Na_2S_2O_4$ in a heterogeneous two-phase system under an N_2 atmosphere as previously reported (*9*). After separation of the two phases, the organic layer containing the ferrous complex was transferred to a 1-cm quartz cuvette under an N_2 atmosphere. The UV–Vis absorption spectra were recorded by a JASCO V-570 spectrophotometer.

Preparation of Albumin–Heme Hybrid. The HSA (Albrec, 25 wt %) was obtained from the NIPRO Corp. (Osaka). Aqueous ascorbic acid (15 mM, 20 μL) was added to an ethanol solution of the porphyrinatoiron(III) derivative (37.5 μM, 4 mL) under CO. After complete reduction of the central ferric ion, the UV–Vis absorption spectrum showed the formation of the six-coordinated carbonyl complex. This ethanol solution was slowly injected into the phosphate buffered solution (pH 7.3, 8 mL) of HSA (9.38 μM) through a Teflon tube under a pressure of CO stream. The mixture was dialyzed using a cellulose membrane against phosphate buffer (pH 7.3) for 2 and 15 h at 4 °C. The ethanol concentration should be reduced to less than 100 ppm. Finally, the total volume was adjusted to 15 mL, thus producing the carbonyl albumin–heme solution (heme/HSA = 4 (mol/mol), [Fe]: 20 μM). The water was deionized using an ADVANTEC GS-200 system.

O_2-Coordination Equilibria and Kinetics. The O_2-binding affinity ($P_{1/2}$) of the porphyrinaoitron(II) in organic solvents or their albumin–hemes in aqueous solution were determined by the spectral changes at various partial pressures of O_2 in previous reports (*2*, *10*). The heme concentrations of 20 μM were normally used for the UV–Vis absorption spectroscopy. The spectra were recorded within the range of 350–700 nm. The O_2-association and -dissociation rate constants (k_{on}, k_{off}) were measured by a competitive rebinding technique (*11*, *12*) using a Unisoku TSP-1000WK-WIN time-resolved spectrophotometer with a Spectron Laser system SL803G-10 Q-switched Nd:YAG laser, which generated a 532 nm pulse of 6-ns duration (10 Hz).

Magnetic Circular Dichroism (MCD). The MCD for the phosphate buffered solutions (pH 7.3) of HSA–**6a** (20 μM) under N_2, O_2, and CO atmospheres were measured using a JASCO J-820 circular dichrometer fitted with a 1.5 T electromagnet at 25 °C. The accumulation times were normally five, and each spectra were subtracted by ones without the electromagnetic as a baseline.

RESULTS AND DISCUSSION

Synthesis of Tailed Porphyrinatoiron. The tailed porphyrinatoirons, **6a** and **6b**, can be synthesized via four reaction steps from TAPP with 6-{*N*-(2-methyl-1-imidazolyl}hexanoic acid (Scheme 1), and their structures were determined by IR, UV, mass and NMR (^{1}H NMR, H–H COSY, Nuclear Overhauser effect (NOE) experiment) spectroscopies. First, TAPP was monotritylated using tritylbromide at room temperature. Statistically, six atrop isomers of the monotritylated compound are formed. Collman and co-workers reported the superior synthesis of tris(α,α,α-aminopheny)-mono(β-tritylaminophenyl)porphyrin (**2**) using the alumina absorption technique in the dark (*13*). We isolated two major components from the reaction mixture according to the procedure with the R_f values (chloroform/ethyl acetate = 1:1 (v:v)) of 0.75 (compound **A**) and 0.90 (compound **B**). The coupling reaction of compound **A** with pivaloyl chloride gave a single product, tris(pivalamido)phenyl-monotritylphenyl-porphyrin (compound **A1**). On the other hand, the same coupling reaction of compound **B** provided two products (compounds **B1** and **B2**) with R_f values (chloroform/ethyl acetate = 2:1 (v/v)) of 0.68 and 0.62, respectively. The mass spectra of the above three compounds exactly demonstrated the same value (calcd. for $C_{78}H_{73}N_8O_3$: 1169.5806), indicating that **A1**, **B1**, and **B2** are atrop isomers. In ^{1}H NMR spectra of **A1** and **B1**, the peaks derived from the CH_3 protons in the pivalamide groups were

Scheme 2. Atropisomers of 2 and Their Pivalamide Derivatives

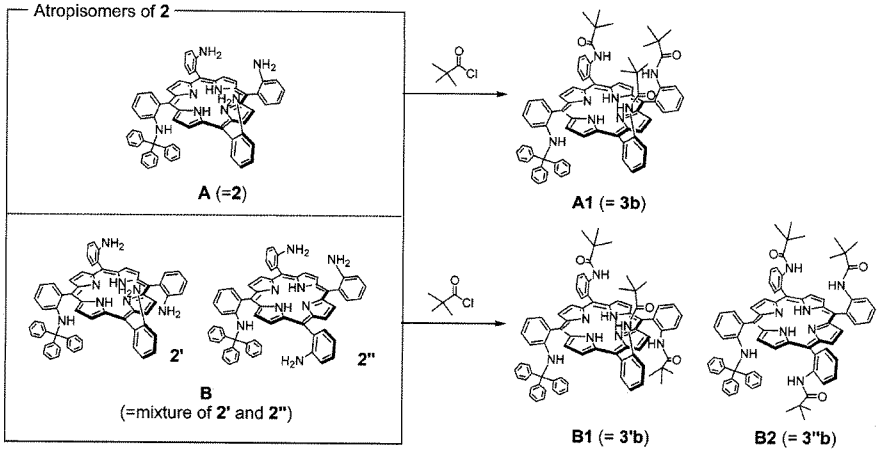

clearly separated into two peaks, and the patterns resembled those of the other $\alpha^3\beta$-structured TAPP derivatives (*14*, *15*) (see Figures ESI1−ESI3, Supporting Information). The differences in the chemical shift between the two peaks were 0.12 (**A1**) and 0.15 (**B1**) ppm, respectively. The CH_3 peaks of **B2** were also splited, but the peak separation was rather small, 0.01 ppm.

To clarify the stereochemistry of these atrop isomers and the geometry of the substituents, we employed the NOE differential spectra (*16*) (see Figures ESI1−ESI3, Supporting Information). In porphyrin **A1**, three pivalamide groups are directed toward the same side and a trityl group is directed only toward the other side, which means **A1** is the target compound **3b**. In **B1**, one of the pivalamide groups is in the same plane with the trityl group, but they do not interact with each other. This result suggests the formation of the $\alpha,\beta,\alpha,\beta$-conformer **3'b**. In **B2**, at least one pivalamide group is on the same side with the trityl group. In this case, there are four atrop isomers expected, but we concluded **B2** would be the $\alpha,\alpha,\beta,\beta$-structure (**3"b**) because the parent compound **B** was less polar than compound **A** in the $\alpha^3\beta$-conformer. In summary (Scheme 2), (i) compound **A** is porphyrin **2** in the $\alpha^3\beta$-conformer, (ii) compound **B** is a mixture of **2'** ($\alpha,\beta,\alpha,\beta$-conformer) and **2"** ($\alpha,\alpha,\beta,\beta$-conformer). Our attempts to perform the same NOE experiment on **3a** unfortunately failed because it was difficult to saturate only the peak of the 1-methyl group at the bottom of cyclohexane ring. The coupling reaction of **2** with 1-methylcyclohexanoyl chloride gave the desired **3a** (yield: 53%).

After detritylation under acidic conditions, 6-(2-methylimidazole-1-yl)hexanoic acid chloride was reacted with the β-*o*-NH_2 group of **4**. Iron insertions of these free base porphyrins were performed with an excess of $FeBr_2$ with 2,6-lutidine as the base. The total yields of **6a** and **6b** were 15 and 10% from the atrop-isomeric mixture of TAPP. All these compounds are now available in gram quantities.

During the synthesis of the tailed porphyrinatoiron, we are always careful to prevent the atrop isomerizations of the products. The bulky pivalamide or 1-methylcyclohexanamide substituted phenyl rings did not rotate with respect to the porphyrin plane by the ambient light and heating even at 100 °C in toluene for 2 h (*8*). However, the same heating of the detritylated porphyrin **4** afforded two components, the unchanged original **4** and the new one with a lower R_f value. They both showed identical molecular weights. The newly appearing compound is suspected to be the porphyrin **4'** in the α^4-conformer. Tritylation of **4'** again by the same procedure for TAPP with tritylbromide did not proceed at all due to the steric hindrance of the fence groups next to the NH_2 group.

Table 1. Absorption Maxima (λ_{max}) of Tailed Porphyrinatoiron(II) in Toluene

	λ_{max}		
	under N_2	under O_2	under CO
6a	438, 535, 558	426, 550	424, 535
6b	435, 535, 555	422, 546	421, 534
1a	441, 539, 558	424, 552	425, 534
1b[a]	439, 535, 561	422, 550	422, 534

[a] Reference 10b.

Table 2. O_2-Binding Parameters of Tailed Porphyrinatoiron(II) in Toluene at 25°C

	k_{on} ($M^{-1}\,s^{-1}$)	k_{off} (s^{-1})	$P_{1/2}$ (Torr)
6a	5.8×10^7	5.1×10^4	67
6b	8.6×10^7	5.6×10^4	50
1a[a]	1.8×10^8	4.7×10^4	20
1b[a]	1.6×10^8	7.9×10^4	38

[a] Reference 2.

O_2-Binding Properties of Tailed Porphyrinatoiron(II) in Toluene Solution. UV−Vis absorption spectra of ferrous **6a** and **6b** in toluene solution under an N_2 atmosphere were very similar to those of the five-N-coordinate complexes of **1a** and **1b** (Table 1). This indicates that **6a** and **6b** are also five-N-coordinate high-spin Fe^{2+} complex with an intramolecularly coordinated imidazole tail. Upon bubbling of O_2 gas into these solutions, the absorption spectra immediately changed to that of the well-characterized O_2 adduct complex of the Fe^{2+}TPP derivative. After passing the CO gas, the spectral pattern was converted to the typical carbonyl complex. There is no significant difference in the λ_{max} values of **6a**, **6b**, **1a**, and **1b** within 6 nm.

The binding affinities ($P_{1/2}$), association and dissociation rate constants (k_{on}, k_{off}) of O_2 to the tailed porphyrinatoiron(II)s, **6a** and **6b**, were determined (Table 2). We thought that the reduction of the fence numbers on the porphyrin ring plane from four to three unfastens the steric hindrance around the O_2-coordination site and enhanced the association rate constant of O_2. It is generally recognized that the k_{on} value increases with the relaxing distal steric encumbrance (*1*, *11*, *12*, *15*). However, the reverse was the case. In contrast to our assumption, the k_{on} values of the tailed porphyrinatoirons, **6a** and **6b**, were 3.1- and 1.9-fold lower than the corresponding α^4-conformers (**1a** and **1b**), respectively, while their k_{off} values were nearly the same. This result suggests that the steric hindrances for the O_2 association to **6a** and **6b** are greater than those of **1a** and **1b**. Most probably, three fences on the amide bonds in the $\alpha^3\beta$-

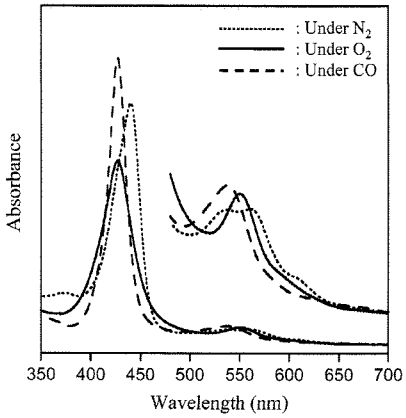

Figure 2. UV−Vis absorption spectral change of HSA−**6a** hybrid in phosphate buffered solution (pH 7.3).

Table 3. Absorption Maxima (λ_{max}) of HSA−Tailed Porphinatoiron (II) Hybrid in Phosphate Buffered Solution (pH 7.3)

	λ_{max}		
	under N_2	under O_2	under CO
HSA-**6a**	440, 536, 559	427, 550	427, 539
HSA-**6b**	—	—	424, 537
HSA-**1a**[a]	445, 543, 567	428, 555	429, 545
HSA-**1b**[a]	443, 542, 567	426, 552	427, 539

[a] Reference 2.

conformer can easily move on the porphyrin platform compared to the crowded four fences of the α^4-conformer. These flexible geometries of the substituents, if anything, narrowed the encumbrance around the O_2-coordination site relative to the α^4 arrangement.

O_2-Binding Properties of HSA-Tailed Porphyrinatoiron in Aqueous Medium. The tailed porphyrinatoirons, **6a** and **6b**, in the $\alpha^3\beta$-conformer could be incorporated into hydrophobic domains of HSA, providing the corresponding albumin−heme hybrids. Their maximum binding numbers to HSA were determined to be approximately 8 (mol/mol), which is identical to those of **1a** and **1b** (*2*, *10a*). It is known that HSA binds porphyrin derivatives and their binding sites largely depend on the chemical structures, hydrophobicity, and electrostaticity. Crystal structure analysis of HSA complexed with natural Fe^{3+} protoporphyrin IX, namely, hemin, revealed that hemin is accommodated into subdomain IB of HSA (*17*). On the other hand, hematoporphyrin is incorporated into subdomain IIIA (*18*), and tetrakis(*p*-sulfonatophenyl)porphyrin binds to subdomain IIA or IIIA (*19*). On the basis of the competitive binding inhibition, we supposed that the some of the binding sites of **1a** are subdomains IB, IIA, and IIIB (*10a*). Attempts to crystallize HSA−**6a** hybrid are now underway, but the porphyrin **6a** dissociated from albumin during the crystallization process due to the relatively low binding constants of **6a** to HSA (10^6–10^4 M^{-1}) and coexistence of poly(ethylene glycol) in the media. We suspect that the binding sites of **6a** and **6b** are the same places of **1a**. The isoelectric point (*p*I = 4.8) and circular dichroism spectral patterns of HSA−**6a** and HSA−**6b** were similar to those of HSA itself, indicating that the surface and conformation of albumin were unaltered after bindings of the tailed porphyrinatoirons.

UV−Vis absorption spectra of the freshly prepared ferrous HSA−**6a** showed λ_{max} values at 424 and 537 nm (Figure 2, Table 3). This spectrum was almost identical to that of the CO coordinated low-spin **6a** in toluene solution, implying that the incorporated tailed porphyrinatoiron(II) is still the CO adduct complex in HSA. Light irradiation to this aqueous HSA−**6a** using a 500-W halogen lamp under an O_2 atmosphere leads to

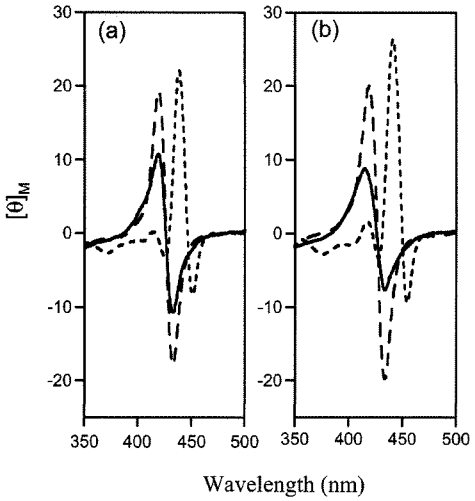

Figure 3. MCD spectral changes of (a) HSA−**6a** and (b) HSA−**1a** hybrids in phosphate buffered solution (pH 7.3). Solid line: under O_2; dotted line: under N_2; dashed line: under CO.

Table 4. O_2-Binding Parameters of HSA−Tailed Porphinatoiron (II) Hybrid in Phosphate Buffered Solution (pH 7.3) at 25°C

	k_{on} (M^{-1} s^{-1})		k_{off} (s^{-1})		
	fast	slow	fast	slow	$P_{1/2}$ (Torr)[a]
HSA−**6a**	2.9×10^7	4.4×10^6	1.1×10^3	1.6×10^2	22 (45)[b]
HSA−**1a**[c]	4.6×10^7	7.3×10^6	9.8×10^2	1.6×10^2	13 (35)[b]

[a] $P_{1/2} = (k_{on}/k_{off})^{-1}$. [b] At 37 °C in parentheses. [c] Reference 2.

CO dissociation, giving a typical spectral pattern of the O_2 adduct complex. Upon exposure of the dioxygenated HSA−**6a** to N_2, the absorption spectrum changed to that of the five-N-coordinated ferrous complex with an intramolecularly coordinated axial imidazole. This O_2 binding and releasing were found to be reversible.

In contrast, the ferrous HSA−**6b** was irreversibly oxidized during the CO dissociation process under an O_2 atmosphere. We concluded that the bulky and hydrophobic substituent like the 1-methylcyclohexanamide fences are necessary for the tailed porphyrinatoiron(II) in the $\alpha^3\beta$-conformer to form a stable O_2 adduct complex under physiological conditions (pH 7.3, 37 °C).

The magnetic circular dichloisim (MCD) spectra of HSA−**6a** showed almost the same pattern as those of HSA−**1b** (Figure 3) (*20*). Under an N_2 atmosphere, the MCD spectrum of HSA−**6a** showed the formation of the five-coordinate ferrous high-spin complex of **6a** with the intramolecular coordinated proximal imidazole. This result showed no ligation of the amino acid residues of the protein, e.g., histidine, tyrosine, cysteine, to the sixth coordination site of the heme. The bulky fences on the porphyrin plane could prevent access of the neighboring peptide residues to the sixth coordination site of **6a**. Upon exposure of this solution to O_2, the spectrum immediately changed and showed an S-shaped A-term MCD in the Soret region, which indicates a transformation to the ferrous low-spin complex (*8*, *21*). The CO adduct complex of HSA−**6a** also exhibited a similar A-term MCD band in the same region with a much stronger intensity. The wavelength where the value of $[\theta]_M$ is zero for the O_2 and CO adduct complex coincided well with the absorption maxima in their corresponding UV−Vis spectra.

The $P_{1/2}$ of the HSA−**6a** was determined by measuring the UV−Vis absorption spectral changes during the O_2 titration. The laser flash photolysis experiments provided the k_{on} and k_{off} values of the O_2 binding to HSA−**6a** (Table 4). The absorption decays accompanying the O_2 recombination were composed of two-phases of the first-order kinetics. The curve was fitted by

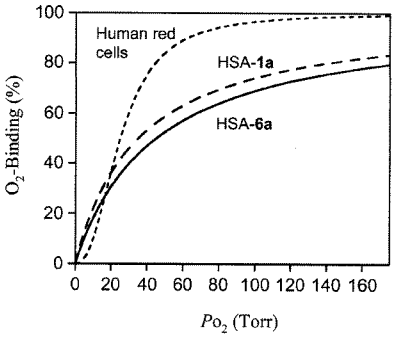

Figure 4. O_2-binding equilibrium curve of HSA−**6a** under physiological conditions (pH 7.3, 37 °C).

a double exponential equation, which was assigned to the fast and slow rebindings [k_{on}(fast) and k_{on}(slow)] of O_2. The k_{on}(fast) values were 7 times greater than k_{on}(slow), and the concentration ratio of the fast and slow reactions was 2:1. This is presumably because the O_2 association to **6a** in HSA is influenced by the molecular microenvironment in the hydrophobic domains (steric hindrance of the amino acid residue and difference in polarity). This behavior was similarly observed in HSA−**1a** and HSA−**1b** (*2*, *22*). The k_{on} values of HSA−**6a** are again 1.6−1.7-fold lower than those of HSA−**1a** in aqueous medium as observed in toluene solution. This is also caused by the narrow encumbrance on the porphyrin ring plane constructed by the three 1-methlcyclohexanamide fences of **6a**.

The HSA−**6a** did not show a cooperative O_2-binding profile like Hb; the Hill coefficient was 1.0 (Figure 4). Although the O_2-binding affinity of HSA−**6a** at 37 °C is relatively low ($P_{1/2}$ value (45 Torr) is high) compared to those of HSA−**1a** (35 Torr) and human red blood cells (28 Torr), the O_2-transporting efficiency of HSA−**6a** between the lungs (Po_2: 110 Torr) and muscle tissues (Po_2: 40 Torr) is estimated to be 22%, which is identical to human red blood cells and HSA−**1a**.

CONCLUSIONS

Tailed porphyrinatoirons have been first employed as an O_2-binding site of the synthetic hemoprotein, albumin−heme. **6a** and **6b** with a *β-o*-(2-methylimidazolyl)hexyramide tail have been easily synthesized via four steps from the TAPP scaffold compared to the eight steps of **1a**. The stereochemistry of the $\alpha^3\beta$-conformer was confirmed by NOE experiments. The association rates of O_2 were slower than for the corresponding α^4-conformers, which indicates that three substituents are close to the porphyrin platform and narrowed the encumbrance space around the O_2-coordination site. As an active site for the albumin−heme hybrid, **6a** was effective, but **6b** was rapidly oxidized. It can be concluded that bulky and hydrophobic substituents like the 1-methylcyclohexanamide fences are necessary for obtaining a stable O_2 adduct complex. The O_2 transporting ability of the HSA−**6a** was almost the same as human red blood cells. Currently, since HSA is manufactured on a large scale by yeast expression (*23*), the 5 wt % albumin−heme solution involving **6a** as O_2 binding site is the most promising material as a red blood cell substitute and O_2-carrying therapeutic reagent, which would be mass produced on an industrial scale.

ACKNOWLEDGMENT

This work was partially supported by Grant-in-Aid for Scientific Research (No. 16350093) from JSPS, Grantin-Aid for Exploratory Research (No. 16655049) from MEXT Japan, and Health Science Research Grants (Regulatory Science) from MHLW Japan.

Supporting Information Available: Synthetic procedure of the tailed porphyrinatoirons (**6a**, **6b**); ^{1}H NMR and NOE differential spectra of compounds **A1**, **B1**, and **B2**. These materials are available free of charge via the Internet at http://pubs.acs.org.

LITERATURE CITED

(1) (a) Collman, J. P., Boulatov, R., Sunderland, C. J., and Fu, L. (2004) Functional analogues of cytochrome *c* oxidase, myoglobin, and hemoglobin. *Chem. Rev. 104*, 561−588. (b) Momenteau, M., and Reed, C. A. (1994) Synthetic heme-dioxygen complexes. *Chem. Rev. 94*, 659−698 and references therein.

(2) Komatsu, T., Matsukawa, Y., and Tsuchida E. (2002) Effect of heme structure on O_2-binding properties of human serum albumin-heme hybrids: Intramolecular histidine coordination provides a stable O_2-adduct complex. *Bioconjugate Chem. 13*, 397−402.

(3) Komatsu, T., Moritake, M., Nakagawa, A., and Tsuchida, E. (2002) Self-organized lipid-porphyrin bilayer membranes in vesicular form: Nanostructure, photophysical properties and dioxygen coordination. *Chem. Eur. J. 8*, 5469−5480.

(4) Komatsu, T., Oguro, Y., Teramura, Y., Takeoka, S., Okai, J., Anraku, M., Otagiri, M., and Tsuchida, E. (2004) Physicochemical characterization of cross-linked human serum albumin dimer and its synthetic heme hybrid as an oxygen carrier. *Biochim. Biophys. Acta 1675*, 21−31.

(5) (a) Huang, Y., Komatsu, T., Yamamoto, H., Horinouchi, H., Kobayashi, K., and Tsuchida, E. (2004) Safety evaluation of an artificial O_2 carrier as a red blood cell substitute by blood biochemical tests and histopathology observations, *ASAIO J. 50*, 525−529. (b) Komatsu, T., Huang, Y., Yamamoto, H., Horinouchi, H., Kobayashi, K., and Tsuchida, E. (2004) Exchange transfusion with synthetic oxygen-carrying plasma protein "albumin-heme" into an acute anemia rat model after seventy-percent hemodilution. *J. Biomed. Mater. Res. 71A*, 644−651. (c) Huang, Y., Komatsu, T., Yamamoto, H., Horinouchi, H., Kobayashi. K., and Tsuchida, E. (2004) Exchange transfusion with entirely synthetic red-cell substitute albumin-heme into rats: physiological responses and blood biochemical tests. *J. Biomed. Mater. Res. 71A*, 63−69.

(6) Kobayashi, K., Komatsu, T., Iwamaru, A., Matsukawa, Y., Horinouchi, H., Watanabe, M., and Tsuchida, E. (2002) Oxygenation of hypoxic region in solid tumor by administration of human serum albumin incorporating synthetic hemes. *J. Biomed. Mater. Res. 64A*, 48−51.

(7) Lindsey, J. (1980) Increased yield of a desired isomer by equilibriums displacement on binding to silica gel, applied to meso-tetrakis(o-aminophenyl)porphyrin. *J. Org. Chem. 45*, 5215−5215.

(8) Collman, J. P., Brauman, J. I., Doxsee, K. M., Halbert, T. R., Bunnenberg, E., Linder, R. E., LaMar, G. N., Gaudio, J. D., Lang, G., and Spartalian, K. (1980) Synthesis and characterization of "tailed picket fence" porphyrins. *J. Am. Chem. Soc. 102*, 4182−4192.

(9) Tsuchida, E., Hasegawa, E., Komatsu, T., Nakata, T., Nakao, K., and Nishide, H. (1991) Synthesis and coordination behaviors of new double-sided porphyrinatoiron(II) complexes: effect of the pocket size for imidazole on dioxygen binding. *Bull. Chem. Soc. Jpn. 64*, 888−894.

(10) (a) Komatsu, T., Hamamatsu, K., Wu, J., and Tsuchida, E. (1999) Physicochemical properties and O_2-coordination structure of human serum albumin incorporating tetrakis-(*o*-pivalamido)phenylporphyrinatoiron(II) derivatives. *Bioconjugate Chem. 10*, 82−86. (b) Tsuchida, E., Komatsu, T., Kumamoto, S., Ando, K., and Nishide, H. (1995) Synthesis and O_2-binding properties of tetraphenylporphyrinatoiron(II) derivatives bearing a proximal imidazole covalently bound at the β-pyrrolic position. *J. Chem. Soc., Perkin Trans. 2*. 747−753.

(11) Collman, J. P., Brauman, J. I., Iverson, B. L., Sessler, J. L., Morris, R. M., and Gibson, Q. H. (1983) O_2 and CO binding to iron(II) porphyrins: A comparison of the "picket fence" and "pocket" porphyrins. *J. Am. Chem. Soc. 105*, 3052−3064.

(12) Traylor, T. G., Tsuchiya, S., Campbell, D., Mitchell, M., Stynes, D., and Koga, N. (1985) Anthracene heme cyclophanes. Steric Effects in CO, O_2 and RNC Binding. *J. Am. Chem. Soc. 107*, 604−614.

(13) Collman, J. P., Broring, M., Fu, L., Rapta, M., Schwenninger, R., and Straumanis, A. (1998) Novel protecting strategy for the synthesis of porphyrins with different distal and proximal superstructures. *J. Org. Chem. 63*, 8082−8083.

(14) Inaba, Y., and Kobuke, Y. (2004) Synthesis of a complementary dimer from mono(imidazolyl)-substituted cobalt(II) porphyrin as a new artificial T-form hemoglobin. *Tetrahedron 60*, 3097−3107.

(15) Wuenschell, G. E., Tetreau, C., Lavalette, D., and Reed, C. A. (1992) Hydrogen-bonded oxyhemoglobin models with substituted picket-fence porphyrins: the model compound equivalent of site-directed mutagenesis. *J. Am. Chem. Soc. 114*, 3346−3355.

(16) Collman, J. P., Sunderland, C. J., and Boulatov, R. (2002) Biomimetic studies of terminal oxidases: trisimidazole picket metalloporphyrins. *Inorg. Chem. 41*, 2282−2291.

(17) Zunszain, P. A., Ghuman, J., Komatsu, T., Tsuchida, E., and Curry, S. (2003) Crystal structural analysis of human serum albumin complexes with hemin and fatty acid, *BMC Struct. Biol. 3*, 6.

(18) Cohen, S., and Margalit, R. (1990) Binding of porphyrin to human serum albumin, structure−activity relationship. *Biochem. J. 270*, 325−330.

(19) Andrade, S. M., and Costa, S. M. B. (2002) Spectroscopic studies on the interaction of a water soluble porphyrin and two drug carrier proteins. *Biophys. J. 82*, 1607−1619.

(20) Tsuchida, E., Nakagawa, A., and Komatsu, T. (2003) Coordination structure of active site in synthetic hemoprotein (albumin-heme) with dioxygen and carbon monoxide. *Macromol. Symp. 195*, 275−280.

(21) (a) Collman, J. P., Brauman, J. I., Collins, T. J., Iverson, B. L., Lang, G., Pettman, R. B., Sessler, J. L., and Walters, M. A. (1983) Synthesis and characterization of the "pocket" porphyrins. *J. Am. Chem. Soc. 105*, 3038−3052. (b) Collman, J. P., Basolo, F., Bunnenberg, E., Collins, T. C., Dawson, J. H., Ellis, P. E., Marrocco, M. L., Moscowitz, A., Sessler, J. L., and Szymanski, T. (1981) Use of magnetic circular dichroism to determine axial ligation for some sterically encumbered iron(II) porphyrin complexes. *J. Am. Chem. Soc. 103*, 5636−5648.

(22) Komatsu, T., Matsukawa, Y., and Tsuchida, E. (2000) Kinetics of CO and O_2 binding to human serum albumin-heme hybrid. *Bioconjugate Chem. 11*, 772−776.

(23) Sumi, A., Ohtani, W., Kobayashi, K., Ohmura, T., Yokoyama, K., Nishida, M., and Suyama, T. (1993) Purification and physicochemical properties of recombinant human serum albumin. *Biotechnology of Blood Proteins* (Rivat, C., Stoltz, J.-F., Eds.) Vol. 227, pp 293−298, John Libbey Eurotext, Montrouge.

BC050154+

Poly(ethylene glycol)-Conjugated Human Serum Albumin Including Iron Porphyrins: Surface Modification Improves the O_2-Transporting Ability

Yubin Huang,[†] Teruyuki Komatsu,[†,*] Rong-Min Wang,[†,‡] Akito Nakagawa,[†] and Eishun Tsuchida[†,*]

Advanced Research Institute for Science and Engineering, Waseda University, 3-4-1 Okubo, Shinjuku-ku, Tokyo 169-8555 Japan, and Key Laboratory of Polymer Materials of Gansu Province, Institute of Polymer, Northwest Normal University, Lanzhou 730070, China. Received November 3, 2005; Revised Manuscript Received February 10, 2006

Artificial O_2-carrying hemoprotein composed of human serum albumin including tetrakis(*o*-amidophenyl)-porphinatoiron(II) (Fe4P or Fe3P) [HSA−FeXP] has been modified by maleimide- or succinimide-terminated poly(ethylene glycol) (PEG), and the formed PEG bioconjugates have been physicochemically characterized. 2-Iminothiolane (IMT) reacted with the amino groups of Lys to create active thiol groups, which bind to α-maleimide-ω-methoxy PEG [Mw: 2-kDa (PEG_{M2}), 5-kDa (PEG_{M5})]. On the other hand, α-succinimidyl-ω-methoxy PEG [Mw: 2-kDa (PEG_{S2}), 5-kDa (PEG_{S5})] directly binds to Lys residues. MALDI-TOF MS of the PEG-conjugated HSA−FeXP showed distinct molecular ion peaks, which provide an accurate number of the PEG chains. In the case of PEG_{MY}(HSA−FeXP), the spectroscopic assay of the thiol groups also provided the mean of the binding numbers of the polymers, and the degree of the modification was controlled by the ratio of [IMT]/[HSA]. The viscosity and colloid osmotic pressures of the 2-kDa PEG conjugates (phosphate-buffered saline solution, [HSA] = 5 g dL^{-1}) were almost the same as that of the nonmodified one, whereas the 5-kDa PEG binding increased the rheological parameters. The presence of flexible polymers on the HSA surface retarded the association reaction of O_2 to FeXP and stabilized the oxygenated complex. Furthermore, PEG_{MY}(HSA−FeXP) exhibited a long circulation lifetime of FeXP in rats (13−16 h). On the basis of these results, it can be concluded that the surface modification of HSA−FeXP by PEG has improved its comprehensive O_2-transporting ability. In particular the PEG_{MY}(HSA−FeXP) solution could be a promising material for entirely synthetic O_2-carrying plasma expander as a red cell substitute.

INTRODUCTION

Poly(ethylene glycol) (PEG) is commonly used for the surface modification of peptides, proteins, enzymes, and liposome to confer several potential beneficial effects: not only a longer plasma half-life and nonimmunogenicity but also a solubility in organic solvents and extreme thermostability (*1*−*4*). To develop an artificial O_2 carrier, substantial efforts have been directed to the preparation of PEG-conjugated hemoglobin (Hb) over the past decades (*5*−*8*), and the optimized PEG−Hbs are currently being tested in clinical trials. Human serum albumin (HSA) is a versatile protein, which is found in our blood plasma at a high concentration (4−5 g dL^{-1}) (*9*). We have reported that HSA including tetrakis(*o*-amidophenyl)porphinatoiron(II) (Fe3P or Fe4P, Chart 1) [HSA−FeXP] can reversibly bind and release O_2 under physiological condition (pH 7.4, 37 °C) in a fashion similar to Hb (*10*). The administration of this synthetic O_2 carrier into anesthetized rats has proved its safety and O_2-transporting efficacy (*11*). Nevertheless, there is only one defect in that the FeXP molecule easily dissociates from HSA when infused into animals. This is due to the fact that FeXP is noncovalently bound to the hydrophobic cavity of albumin with binding constants (*K*) of 10^4−10^6 (M^{-1}). Natural heme, namely protoporphinatoiron IX, is also incorporated into HSA and shows a 10^2−10^4-fold higher *K* compared to FeXP (*12*); however, it is released from HSA during blood circulation with a half-life of 2.5−3.6 h (*13*, *14*). Under these circumstances,

Chart 1. Structures of O_2-Adduct Complexes of Tetrakis-(*o*-amidophenyl)porphinatoiron(II)

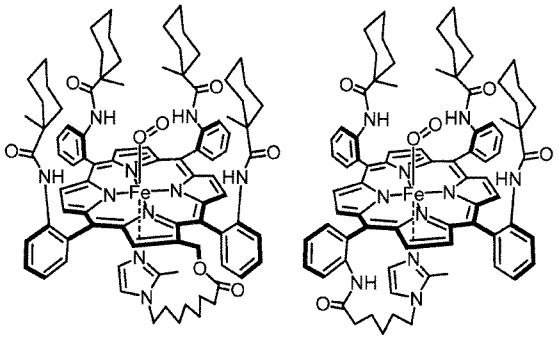

Fe4P Fe3P

we postulated that the surface modification of HSA−FeXP by PEG could help to prolong the circulation life of FeXP and thereby retain its O_2-transporting ability for a long period. Although HSA is a very common plasma protein, its PEG conjugation chemistry has not yet been studied in detail. It is known that a huge variety of drugs are incorporated into specific sites of HSA (*9*). The PEG modification should prevent the rapid release of these drugs from the HSA scaffold and contribute to raising their potential therapeutic efficacies.

In the present study, we have systematically prepared several PEG-conjugated HSA−FeXPs and characterized their physicochemical properties. The surface modification by PEG affects the viscosity and colloid osmotic pressure of the solution, O_2-binding behavior of the parent HSA−FeXP, and circulatory lifetime of FeXP. The PEG-conjugated HSA−FeXP could be

* Corresponding authors: (E.T.) Tel: +81-3-5286-3120, Fax: +81-3-3205-4740, E-mail: eishun@waseda.jp. (T.K.) E-mail: teruyuki@waseda.jp; eishun@waseda.jp.

† Waseda University.

‡ Northwest Normal University.

10.1021/bc050315+ CCC: $33.50
Published on Web 02/22/2006

of extreme medical importance as a red cell substitute or O_2-therapeutic reagent.

EXPERIMENTAL PROCEDURES

Materials and Apparatus. All reagents were purchased from commercial sources as special grades and used without further purification. 2-Iminothiolane hydrochloride (IMT) was purchased from Wako Pure Chemical Industries, Ltd. (Osaka, Japan). α-[3-(3-Maleimido-1-oxopropyl)amino]propyl-ω-methoxy PEG [averaged Mw: 2333 (Sunbright ME-020MA, PEG_{M2}), averaged Mw: 5207 (Sunbright MEMAL-50H, PEG_{M5})] and α-succinimidyloxyglutaryl-ω-methoxy PEG [averaged Mw: 2325 (Sunbright MEGC-20HS, PEG_{S2}), averaged Mw: 5261 (Sunbright MEGC-50HS, PEG_{S5})] were purchased from NOF Corp. (Tokyo, Japan). 2-{8-(2-Methylimidazolyl-1-yl)-octanoyloxymethyl}-5,10,15,20-tetrakis{α,α,α,α-*o*-(1-methylcyclohexanamido)phenyl}porphinatoiron(III) chloride (Fe4P) and 5,10,15-tris{α,α,α-*o*-(1-methylcyclohexanamido)-phenyl}-20-mono-[β-*o*-{6-(2-methylimidazolyl) hexanamido}-phenyl]porphinatoiron(III) chloride (Fe3P) were synthesized using previously reported procedures (*10d,e*). Recombinant HSA was provided by the NIPRO Corp. (Osaka, Japan). The UV−vis absorption spectra were recorded using an Agilent 8453 UV−visible spectrophotometer fitted with an Agilent 89090A temperature control unit. The water was deionized using Millipore Elix and Simpli Lab-UV.

Preparation of PEG-Conjugated HSA−FeXP. The HSA−FeXP solutions (X = 3, 4, [HSA]: 5 g dL^{-1}, [FeXP]/[HSA]= 4 (mol/mol), pH 7.4) were prepared as described elsewhere (*10b,d*).

PEG_{MY}(HSA−FeXP): The modification of HSA−FeXP by α-maleimide-ω-methoxy PEG_{M2} was, for instance, carried out as follows. IMT (72 mg, 0.54 mmol) was slowly added to the HSA−FeXP solution (48 mL, [HSA]: 5 g dL^{-1}, [Fe4P] = 3 mM, pH 7.4) ([IMT]/[HSA] = 15/1, mol/mol) and gently stirred at room temperature in the dark. After 3 h, PEG_{M2} (1.44 g, [PEG_{M2}]/[HSA]:20/1, mol/mol) was added to the mixture, which was continually stirred for another 2 h. The resultant solution was ultrafiltered and washed by at least a 600 mL of phosphate-buffered saline (PBS) solution (pH 7.4) to remove any unreacted IMT and PEG_{M2} using the ADVANTEC UHP-76K holder with a Q0500 076E membrane (cutoff Mw: 50 kDa). The volume was finally condensed to 48 mL and sterilized by a DISMIC 0.45 μm filter, producing the PEG_{M2}(HSA−FeXP) solution. The FeXP concentration was determined by the assay of the iron ion by inductively coupled plasma (ICP) spectrometry using a Seiko Instruments SPS 7000A Spectrometer. The HSA concentration was calculated from the intensity of the circular dichroism spectrum at 208 nm, because the molar ellipticity of HSA (1.9×10^4 deg cm^2 $dmol^{-1}$) was unaltered after the PEG conjugation. Circular dichroism (CD) spectra were obtained using a JASCO J-725 spectropolarimeter. The concentration of the HSA sample was 0.15 μM in PBS, and quartz cuvettes with a 10-mm thickness were used for the measurements over the range of 195−250 nm. The PEG_{M2}(HSA−Fe3P) and PEG_{M5}-(HSA−Fe4P) solutions were also prepared by the same procedure. The product was sealed in a glass bottle under CO pressure and stored at 4 °C.

PEG_{SY}(HSA−Fe4P): The surface modification of HSA−Fe4P by α-succinimidyl-ω-methoxy PEG_{S2} was carried out as follows. PEG_{S2} (0.72 g, 0.36 mmol) was directly added to the HSA−Fe4P solution ([HSA]: 5 g dL^{-1}, [Fe4P] = 3 mM, pH 7.4) ([PEG_{S2}]/[HSA]:10/1, mol/mol), and the mixture was stirred at room temperature for 2 h. The resultant solution was ultrafiltered, condensed (48 mL), and sterilized as described above, producing the PEG_{S2}(HSA−Fe4P) solution. Using PEG_{S5} instead of PEG_{S2}, PEG_{S5}(HSA− Fe4P) was obtained. The Fe4P and HSA concentrations were determined by the same procedures for PEG_{MY}(HSA−FeXP).

Matrix-Associated Laser Desorption Ionization Time-of-Flight Mass Spectra (MALDI-TOF MS). The MALDI-TOF MS were obtained using a Shimadzu/Kratos AXIMA-CFR S/W Version 2, which was calibrated by BSA (Sigma A-0281) and HSA (Sigma A-3782). The specimens were prepared by mixing the aqueous sample solution (10 μM, 1 μL) and matrix (10 mg mL^{-1} sinapinic acid in 40% aqueous CH_3CN, 1 μL) on the measuring plate and air-drying.

Determination of Mean of PEG_{MY} Chains per Protein by Assay of Thiol Groups. The active thiol groups on the protein surface can be assayed by the disulfide exchange reaction with 2,2′-dithiopyridine (2,2′-DTP) to produce 2-thiopyridinone (2-TP) with an absorption at 343 nm (molar absorption coefficient (ϵ_{343}): 8.1×10^3 M^{-1} cm^{-1}) (*15*). Quantitative spectroscopic measurements conveniently provide the thiol concentration. The parent HSA−FeXP showed a small absorption band in this range, which should be subtracted from the spectrum after the disulfide exchange reaction. The difference in the thiol groups per HSA−FeXP before and after the PEG_{MY} modification corresponds to the mean of the PEG_{MY} chains on the protein surface.

Solution Properties. The viscosity and density of the PEG-conjugated HSA−FeXP solution (PBS, pH 7.4) were obtained using an Anton Paar DSC 300 capillary viscometer at 37 °C. The colloid osmotic pressures of the solutions (PBS, pH 7.4) were measured by a WESCOR 4420 Colloid Osmometer at 25 °C. A membrane filter with a 30 kDa cutoff was used.

O_2-Binding Parameters. O_2-binding to PEG-conjugated HSA−FeXP was expressed by eq 1,

$$\text{PEG(HSA−FeXP)} + O_2 \underset{k_{off}}{\overset{k_{on}}{\rightleftharpoons}} \text{PEG(HSA−FeXPO}_2\text{)} \quad (1)$$

where $K = k_{on}/k_{off}$. The O_2-binding affinity (gaseous pressure at half O_2 binding for FeXP, $P_{1/2} = 1/K$) was determined by spectral changes at various partial pressures of O_2/N_2 as previously reported (*10b,d*). The FeXP concentrations of 10−20 μM were normally used for the UV−vis absorption spectroscopy. The spectra were recorded within the range of 350−700 nm. The half-lifetime of the O_2-adduct complex was determined by the time dependence of the absorption intensity at 550 nm (O_2-adduct species). The association and dissociation rate constants for O_2 (k_{on}, k_{off}) were measured by a competitive rebinding technique using a Unisoku TSP-1000WK laser flash photolysis as reported in a previous paper (*16*).

Circulation Lifetime in Vivo. The animal investigations were carried out using twenty male Wistar rats (297 ± 29 g). All animal handling and care were in accordance with the NIH guidelines. The protocol details were approved by the Animal Care and Use Committee of Keio University. The PEG-conjugated HSA−FeXP solution (20% volume of the circulatory blood) was intravenously injected into rats from the tail vein (1 mL/min) under an inhalation anesthesia with diethyl ether (n = 4 each). Blood was taken from the tail vein at 3, 30 min, 1, 2, 4, 8, 16 h, 1, 2, 3 days (10 time points) after the infusion and then centrifuged to isolate the serum, which was colored brown by the presence of the sample. The animals were sacrificed after the experiments by hemorrhage. The FeXP concentration was measured by an iron ion assay using ICP spectrometry as described above.

RESULTS AND DISCUSSION

Synthesis of PEG-Conjugated HSA−FeXP. The HSA−FeXP molecules were conjugated with PEG having a terminal reactive chain-end, maleimide-PEG or succinimide-PEG, at

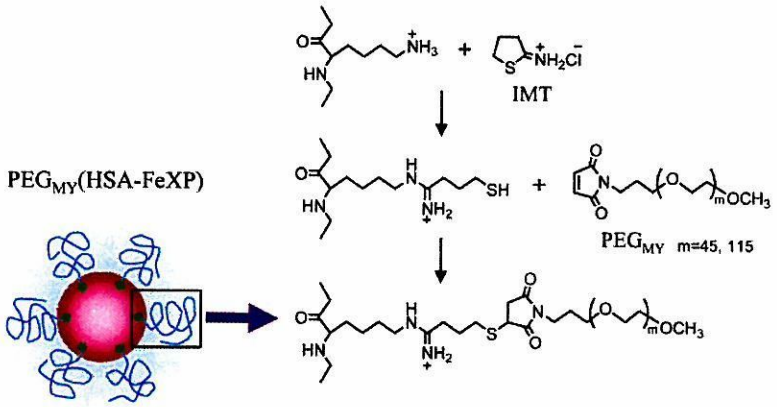

Figure 1. Two-step reaction schemes of IMT and maleimide-PEG (PEG$_{MY}$) with HSA−FeXP.

ambient temperature. Thiolation regent, IMT, quantitatively reacted with the amino groups of Lys to create active thiol groups, which bind to the α-maleimide-ω-methoxy PEG (PEG$_{M2}$ or PEG$_{M5}$) (Figure 1). The two-step reaction is reproducible and did not form any toxic side-product. On the other hand, the α-succinimidyl-ω-methoxy PEG (PEG$_{S2}$ or PEG$_{S5}$) directly binds to the amino groups of Lys. The gel permeation chromatogram (Sephacryl 200HR) of the well-washed PEG conjugate exhibited a single band, so that we did not need any further chromatographic purification.

The MALDI-TOF MS of PEG$_{M5}$(HSA−Fe4P), as prepared under the condition of [IMT]/[HSA−Fe4P] = 15/1 (mol/mol), showed five distinct ion peaks at 85, 90, 95, 101, and 106 kDa (Figure 2a). No unreacted HSA−FeXP was observed at all. The difference in each mass was 5.25 kDa, which implies that HSA−Fe4P is covalently bound to PEG$_{M5}$ and the individual peaks are attributed to PEG$_{M5}$(HSA−Fe4P) having a different number of PEG chains. Here, we have to be cautious whether these mass values involve a molecular weight of Fe4P, because our previous MALDI-TOF MS experiments of HSA−Fe4P demonstrated a single peak of HSA (Mw: 66.5 kDa); the incorporated Fe4P dissociated from the albumin during the ionization process (*10a*). In this study, we found that the mean of the surface PEG chains on HSA−FeXP is conveniently determined by a spectroscopic assay of the HSA scaffold and thiol groups. In general, the concentration of HSA is measured by the absorption at 280 nm or bromcresol green method (*17*), but they are probably obstructed by the surface modification. We then employed a CD measurement to determine the HSA concentration. The comparison of the CD spectra of HSA and PEG−HSA solutions revealed that the molecular ellipcity of albumin (ϵ_{208} = 1.9 × 10^4 deg cm^2 dmol^{-1}) is unaltered even after the PEG binding. Moreover, the presence of FeXP does not disturb the CD in the range of 190−250 nm. Therefore, the HSA concentration of PEG modified HSA−FeXP was quantitatively determined by its CD intensity at 208 nm. On the other hand, the active thiol groups on proteins are generally assayed by a disulfide exchange reaction with 2,2′-DTP (*15*). The combination of these two methodologies allows us to estimate the number of thiols on HSA−FeXP. The mean of the thiol groups was 6.7 per protein after the thiolation by IMT ([IMT]/[HSA−Fe4P] = 15 mol/mol) and decreased to 0.6 after the reaction with 20-fold excess moles of PEG$_{M5}$ (Table 1). These results suggested that the mean of 6.1 reactive thiols was conjugated with PEG$_{M5}$. The averaged molecular weight of this PEG$_{M5}$(HSA−FeXP) calculated from the intensity of the MS peak was 95 kDa. If one subtracts the total mass of the six PEG$_{M5}$ chains (5 kDa × 6 = 30 kDa) from 95 kDa, the difference of 65 kDa equals that

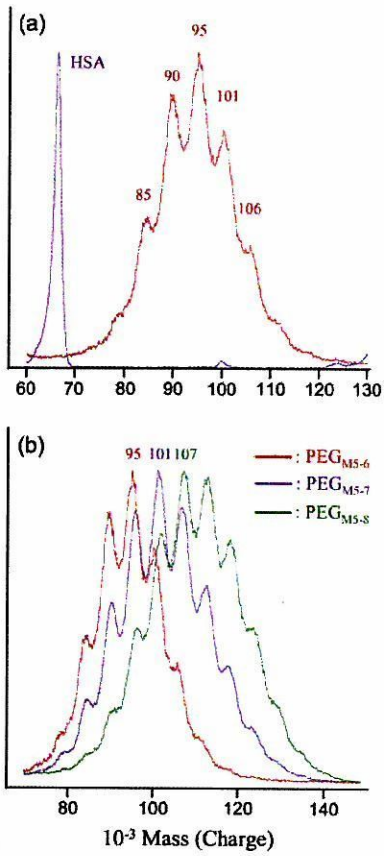

Figure 2. MALDI-TOF MS of (a) HSA and PEG$_{M5-6}$(HSA−Fe4P) and (b) PEG$_{M5}$(HSA−Fe4P) prepared in different [IMT]/[HSA−Fe4P] ratios of 15 (red), 20 (blue), and 30 (green) (mol/mol).

of HSA without Fe4P. Therefore, we concluded that all the mass ion peaks observed in the MALDI-TOF MS did not include the molecular weight of FeXP.

The number of the meleimide-PEG$_{M5}$ chains on HSA−Fe4P were modulated by the mixing ratio of [IMT]/[HSA−Fe4P] (mol/mol). The maximum peak of PEG$_{M5}$(HSA−Fe4P) in the MALDI-TOF MS significantly shifted to the higher molecular region (95 → 101 → 107 kDa) by increasing the IMT (Figure 2b). It is quite remarkable that the distributions of the entire spectral pattern were always identical. The averaged binding number of the PEG$_{M5}$ chains per HSA estimated from the intensity of the mass peak was consistent with the number determined from the assay of the thiol groups (Table 1).

Table 1. The Mean of Thiol Groups per HSA−Fe4P Molecule and Binding Number of the PEG Chains

PEG	[IMT]/[HSA−Fe4P] mol/mol	thiol groups per HSA after IMT addition (A)	thiol groups per HSA after PEG binding (B)	decreased thiol groups (B − A)[a]	averaged PEG number from MS
PEG_{M2}	10	5.6	0.5	5.1	4.6
	15	6.6	0.9	5.7	5.7
	20	8.3	1.1	7.2	6.6
PEG_{M5}	15	6.7	0.6	6.1	5.9
	20	8.0	0.9	7.1	7.2
	30	9.3	1.1	8.2	8.3

[a] This number corresponds to the binding numbers of PEG_{MY} on the protein surface.

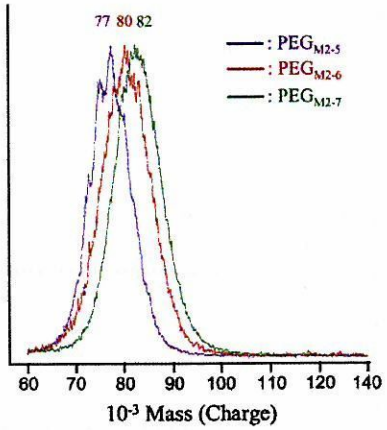

Figure 3. MALDI-TOF MS of PEG_{M2}(HSA−Fe4P) prepared in different [IMT]/[HSA−Fe4P] ratios of 10 (blue), 15 (red), and 20 (green) (mol/mol).

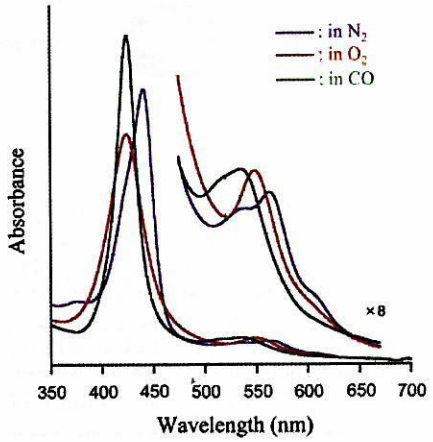

Figure 4. UV-vis absorption spectral change of PEG_{M2-6}(HSA−Fe4P) in PBS solution (pH 7.4).

Table 2. Solution Properties of PEG-Conjugated HSA−FeXP Solutions at 37 °C (pH 7.4, [FeXP] = 3 mM)

PEG	density (g/cm^3)	viscosity (cP)	COP (mmHg)
PEG_{M2-5}(HSA−Fe4P)	1.01	1.08	22
PEG_{M2-6}(HSA−Fe4P)	1.01	1.14	27
PEG_{M2-7}(HSA−Fe4P)	1.01	1.17	28
PEG_{M2-6}(HSA−Fe3P)	1.01	1.14	26
PEG_{M5-6}(HSA−Fe4P)	1.01	2.34	65
PEG_{S2-6}(HSA−Fe4P)	1.01	1.14	22
PEG_{S5-6}(HSA−Fe4P)	1.01	2.30	45
HSA−Fe4P	1.01	1.05	21
HSA	1.01	1.00	21

On the contrary, PEG_{M2}(HSA−Fe4P) demonstrated only one broad peak, because the difference in each mass is relatively close compared to the PEG_{M5} conjugate. The peak maxima of PEG_{M2}(HSA−Fe4P) also shifted to the higher region, dependent on the [IMT]/[HSA−Fe4P] ratio (Figure 3, Table 1).

The succinimide-PEG modified HSA−Fe4P showed the same MALDI-TOF MS patterns as PEG_{MY}(HSA−Fe4P) (data not shown). The number of 5-kDa PEG_{S5} chains per protein increased from 4 → 5 → 6 by elevating the ratio of [PEG_{S5}]/[HSA−Fe4P] (mol/mol): 10 → 20 → 30, respectively. However, the introduced 2-kDa PEG_{S2} number was always 6 in the range of [PEG_{S2}]/[HSA−Fe4P] 10−20. The stoichiometry of the PEG_{S2} binding could not be controlled. This is probably due to the hydrolysis of the succinimidyl end group in aqueous media. The concentration assays of [HSA] by CD and [FeXP] by ICP measurements showed that the initial FeXP/HSA ratio, 4/1 (mol/mol), were constant after the PEG conjugation.

Solution Properties. The viscosity and colloid osmotic pressure (COP) of the 2-kDa PEG-conjugates, PEG_{M2}(HSA−FeXP) and PEG_{S2}(HSA−Fe4P) (PBS solution, [HSA] = 5 g dL^{-1}, pH 7.4), were almost the same as those of the nonmodified HSA−FeXP independent of the number of the PEG chains (Table 2). In contrast, the 5-kDa PEG-conjugate solutions, PEG_{M5}(HSA−FeXP) and PEG_{S5}(HSA−Fe4P), showed a high viscosity (2.30−2.34, at a shear rate of 230 s^{-1}) and hyperoncotic property (45−65 mmHg) in comparison to those of HSA−Fe4P and HSA. From the viewpoint of the design of a blood alternative, it has to achieve a COP similar to that of human blood. However, to increase the effectiveness as a plasma expander, the COP should be higher than the physiological level (*18*). Similar approaches have been utilized for hypertonic saline−dextran formulations.

On the other hand, maintenance of the viscosity has recently been proposed as an important mechanism to preserve shear forces in the microcirculation which prevents loss of the functional capillary density (*19*). The latest PEG-Hb product has been designed to approach that of human whole blood (*7*). Anyway, the COP and viscosity of our PEG-conjugated HSA−FeXP can be adjustable to some extent based on the length of the PEG chains (2-kDa, 5-kDa) on the molecular surface.

O_2-Binding Properties. The UV−vis absorption spectrum of the PEG_{M2}(HSA−Fe4P) solution under an N_2 atmosphere showed λ_{max} at 441, 537, 563 nm (Figure 4), which indicates the formation of the ferrous five-N-coordinate high-spin complex of Fe4P with an intramolecular coordinated 2-methylimidazolyl-group (*10b,c, 20*). The other amino acid residue of HSA did not bind to the sixth-coordinate position of the central ferrous ion. Upon flowing O_2 gas through this solution, the spectral pattern shifted to that of the well-defined O_2-adduct complex of the tetrakis(phenyl)porphinatoiron(II) derivatives (λ_{max}: 424, 550 nm) (*10b,c, 20*). This oxygenation was reversibly observed, dependent on the O_2-partial pressure. After exposure of this solution to CO, PEG_{M2}(HSA−Fe4P) produced a very stable CO-adduct complex (λ_{max}: 425, 535 nm). The all maleimide- and succinimide-PEG-conjugated HSA−FeXP solutions showed similar UV−vis absorption spectra under N_2, O_2, and CO atmospheres. These spectral changes were completely the same as that observed in the nonmodified HSA−Fe4P.

Table 3. O_2-Binding Parameters of PEG-Conjugated HSA−FeXP Solution at 25 °C (pH 7.4)

system	k_{on} ($\mu M^{-1} s^{-1}$) fast	k_{on} ($\mu M^{-1} s^{-1}$) slow	k_{off} (ms^{-1}) fast	k_{off} (ms^{-1}) slow	$P_{1/2}$ (Torr)	$\tau_{1/2}$ (h) at 37 °C
PEG_{M2-5}(HSA−Fe4P)	11	5.8	0.16	0.08	38 (11)	13
PEG_{M2-6}(HSA−Fe4P)	12	4.6	0.17	0.07	32 (11)	12
PEG_{M2-7}(HSA−Fe4P)	9.3	4.7	0.16	0.08	35 (13)	12
PEG_{M2-6}(HSA−Fe3P)	15	4.2	0.52	0.14	41 (26)	8
PEG_{M5-6}(HSA−Fe4P)	12	6.2	0.17	0.09	31 (11)	16
PEG_{S2-6}(HSA−Fe4P)	10	4.3	0.14	0.06	36 (11)	13
PEG_{S5-6}(HSA−Fe4P)	12	5.5	0.25	0.11	32 (16)	18
HSA−Fe4P	31	7.3	0.53	0.13	34 (13)	9
HSA−Fe3P	29	4.4	1.1	0.16	45 (22)	4

The time course of the absorption decay after laser flash photolysis determined the association rate constants of the O_2binding to the PEG-conjugated HSA−FeXP (k_{on}). We have previously reported that the O_2-binding reaction to HSA−FeXP was significantly affected by the microenvironment around FeXP in the protein (e.g., steric hindrance of the amino acid residue and difference in polarity) (*10c−e*). As a result, the binding process of O_2 was observed as the sum of the two single-exponentials, giving fast and slow association rate constants [k_{on}(fast) and k_{on}(slow)]. This unique property of HSA−FeXP has been unaltered after the surface modification by PEG, and all kinetics accompanying the O_2 recombinations consisted of two phases (Table 3). Interestingly, their k_{on}(fast) values were 1.9−3.3-fold lower than those of the corresponding HSA−FeXP, independent of the molecular weight (2-kDa or 5-kDa) and the linkage structure of the PEG. The differences observed in the slow phase were smaller. It may be considered that the presence of flexible polymers on the protein surface retarded the diffusion of the O_2 molecule.

The O_2-binding affinities ($P_{1/2} = K(O_2)^{-1}$) of the PEG-modified HSA−FeXP series were determined by measuring the UV−vis absorption spectral changes by O_2/N_2 titration (Table 3). All the PEG conjugates showed almost the same $P_{1/2}$ values relative to that of the original HSA−FeXP, indicating that the O_2-binding equilibria were not influenced by the presence of PEGs. In contrast, the surface modification by PEG delayed the proton-driven oxidation of the $FeXPO_2$ species and prolonged the half-lifetime of the O_2-adduct complex [$\tau_{1/2}(O_2)$]. The PEG_{M5-6}(HSA−Fe4P)O_2 complex showed the longest $\tau_{1/2}(O_2)$ of 16 h at 37 °C, which is greater than those of HSA−Fe4P and natural hemoprotein, myoglobin ($\tau_{1/2}(O_2)$: 12 h at pH 7, 35 °C) (*21*). Basic polymer PEG conjugation might change the local proton concentration of the HSA interior compared to the outer aqueous solution. Actually, it was shown that the surface PEG modification of hemoproteins has modulated the redox behavior of the active heme site (*1*, *2*, *22*).

Circulation Lifetime in Bloodstream of Rats. The circulation persistence of FeXP in the bloodstream after the administration of PEG_{MY-6}(HSA−FeXP) or PEG_{SY-6}(HSA−Fe4P) solution in rats is shown in Figure 5. The concentration decays of the PEG_{MY}(HSA−FeXP) series showed single exponentials, and the half-lifetimes ($\tau_{1/2}$) were 12.9−15.8 h, independent of the molecular weight of the polymers and FeXP structures. These values are much longer than those of the corresponding nonmodified HSA−FeXP (0.6−3.2 h) (*23*). The surface modification by PEG significantly prevented the rapid clearance of the incorporated FeXP and contributed to increasing the O_2-transporting efficacy.

On the contrary, the PEG_{SY}(HSA−Fe4P) series showed biphasic kinetics and a $\tau_{1/2}$ value of 1.5−2.1 h. We have postulated two reasons for this short circulation lifetime. The first reason is the charges of the Lys residues. The maleimide-PEG connects to Lys through the ring-opened IMT, which maintains the positive charge of Lys; therefore, PEG_{MY}(HSA−FeXP) could preserve the total electrostatic potential of albumin. In contrast, the succinimide-PEG directly binds to the amino group of Lys to form the amide bond, thereby reducing the positive charge and alters the surface electrostatic potential. This changing of the molecular charge may influence the rapid clearance of the incorporated FeXP.

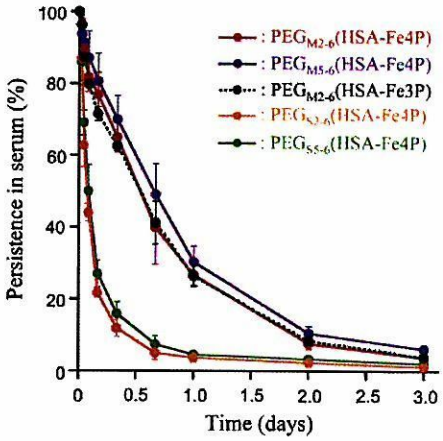

Figure 5. Persistence of FeXP in serum after administration of PEG-conjugated HSA−FeXP into Wistar rats. All values are mean ± SD (n = 4).

The second probability is the binding sites of the PEG chains. As shown in Table 1, the difference in the thiol number per protein before and after the reaction with maleimide-PEG was 0.5−1.1. This means that the binding position of PEG_{MY} is governed by the reaction place of IMT, which is small enough to statistically attach 59 Lys in HSA. Thus, the molecular surface of HSA−FeXP is uniformly covered by PEG_{MY}. On the other hand, the attaching sites of succinimide-PEG are presumably heterogeneous, because PEG_{SY} could only bind the accessible amino group of Lys due to the bulkiness of the long polymer. The incorporated Fe4P molecules might be more easily released from the PEG_{SY}-modified HSA in the circulatory system.

CONCLUSIONS

The surface modification of the albumin-based synthetic hemoprotein, HSA−FeXP, by PEG (Mw 2-kDa or 5-kDa) has improved its comprehensive O_2-transporting ability. The PEG conjugation decreased the O_2-association rate constant but retarded the irreversible oxidation of the central ferrous ion, thereby increasing the stability of the O_2-adduct complex. The 5-kDa PEG conjugation increased the viscosity and COP; however, the 2-kDa PEG conjugation did not change these rheological parameters. The linkage form of the PEG chain dramatically affects the circulation persistence of FeXP. In particular, the maleimide-PEG_{MY} conjugates showed a 6−8-fold longer lifetime compared to the succinimide-PEG_{SY} analogues. This is not dependent on the molecular weight of the polymer chains. In summary, the PEG_{MY}(HSA−FeXP) solution is the most promising candidate as an entirely synthetic O_2-carrying plasma expander for a red cell substitute.

Furthermore, we have recently found that water evaporation of the PEG_{MY}(HSA−FeXP) solution produced a red-colored thin film. Its UV−vis absorption spectrum reversibly changed from the deoxy state under an N_2 atmosphere to the oxy state by exposure to O_2 gas. This PEG_{MY}(HSA−FeXP) film was redissolved in nonaqeuous organic solvents, ethanol, chloroform, etc., and the reversible O_2 binding was again observed. The detailed study of the oxygenations of PEG_{MY}(HSA−FeXP) in a cast film and organic solvent are now underway.

ACKNOWLEDGMENT

This work was partially supported by a Grant-in-Aid for Scientific Research (No. 16350093) from JSPS, a Grant-in-Aid for Exploratory Research (No. 16655049) from MEXT Japan, and Health Science Research Grants (Regulatory Science) from MHLW Japan. Prof. Koichi Kobayashi, Dr. Hirohisa Horinouchi (Keio University), and Mr. Hisashi Yamamoto (NIPRO Corp.) are greatly appreciated for their cooperation with the animal experiments.

LITERATURE CITED

(1) (a) Harris, J. M., Ed. (1992) *Poly(ethylene glycol) Chemistry: Biotechnical and Biomedical Applications*, Plenum Press, New York; (b) Veronese, F. M., Harris, J. M. (2002) Introduction and overview of peptide and protein PEGylation. *Adv. Drug Delivery Rev. 54*, 453−456. (c) Roberts, M. J., Bentley, M. D., Harris, J. M. (2002) Chemistry for peptide and protein PEGylation. *Adv. Drug Delivery Rev. 54*, 459−476.

(2) Veronese, F. M. (2001) Peptide and protein PEGylation: a review of problems and solutions. *Biomaterials 22*, 405−417.

(3) Nucci, M. L., Shorr, R., and Abuchowski, A. (1991) The therapeutic value of poly(ethylene glycol) modified proteins. *Adv. Drug Delivery Rev. 6*, 133−151.

(4) Kawahara, N. Y., and Ohno, H. (1997) Induced thermostability of poly(ethylene oxide)-modified hemoglobin in glycols. *Bioconjugate Chem. 8*, 643−648.

(5) Yabuki, A., Yamaji, K., Ohki, H., and Iwashita, Y. (1990) Characterization of a pyridoxalated hemoglobin-polyoxyethylene conjugate as a physiologic oxygen carrier. *Transfusion 30*, 516−520.

(6) Talarico, T. L., Guise, K. J., and Stacey, C. J. (2000) Chemical characterization of pyridoxalated hemoglobin polyoxyethylene conjugate. *Biochim. Biophys. Acta 1476*, 53−65.

(7) Vandegriff, K. M., Malavalli, A., Wooldbridge, J., Lohman, J., and Winslow, R. M. (2003) MP4, a new nonvasoactive PEG-Hb conjugate. *Transfusion 43*, 509−516.

(8) Manjula, B. M., Tsai, A., Upadhya, R., Perumalsamy, K., Smith, P. K., Malavalli, A., Vandegriff, K., Winslow, R. M., Intaglietta, M., Prabhakaran, M., Friedman, J. M., and Acharya, A. S. (2003) Site-specific PEGylation of hemoglobin at Cys-93(β): correlation between the colligative properties of the PEGylated protein and the length of the conjugated PEG chain. *Bioconjugate Chem. 14*, 464−472.

(9) Peters, T. (1996) *All about Albumin: Biochemistry, Genetics and Medical Applications*, Academic Press, San Diego.

(10) (a) Komatsu, T., Hamamatsu, K., Wu, J., and Tsuchida, E. (1999) Physicochemical properties and O_2-coordination structure of human serum albumin incorporating tetrakis-(*o*-pivalamido)phenylporphyrinatoiron(II) derivatives. *Bioconjugate Chem. 10*, 82−86. (b) Tsuchida, E., Komatsu, T., Matsukawa, Y., Hamamastu, K., and Wu, J. (1999) Human serum albumin incorporating tetrakis(*o*-pivalamido)phenylporphinatoiron(II) derivative as a totally synthetic O_2-carrying hemoprotein. *Bioconjugate Chem. 10*, 797−802. (c) Komatsu, T., Matsukawa, Y., and Tsuchida, E. (2000) Kinetics of CO and O_2 binding to human serum albumin-heme hybrid. *Bioconjugate Chem. 11*, 772−776. (d) Komatsu, T., Matsukawa, and Y., Tsuchida E. (2002) Effect of heme structure on O_2-binding properties of human serum albumin-heme hybrids: Intramolecular histidine coordination provides a stable O_2-adduct complex. *Bioconjugate Chem. 13*, 397−402. (e) Nakagawa, A., Komatsu, T., Iizuka, M., and Tsuchida, E. (2006) Human serum albumin hybrid incorporating tailed porphyrinatoiron(II) in $\alpha,\alpha,\alpha,\beta$-conformer as an O_2 binding site. *Bioconjugate Chem. 17*, 146−151.

(11) (a) Komatsu, T., Huang, Y., Yamamoto, H., Horinouchi, H., Kobayashi. K., and Tsuchida, E. (2004) Exchange transfusion with synthetic oxygen-carrying plasma protein "albumin-heme" into an acute anemia rat model after seventy-percent hemodilution. *J. Biomed. Mater. Res. 71A*, 644−651. (b) Huang, Y., Komatsu, T., Yamamoto, H., Horinouchi, H., Kobayashi. K., and Tsuchida, E. (2004) Exchange transfusion with entirely synthetic red-cell substitute albumin-heme into rats: physiological responses and blood biochemical tests. *J. Biomed. Mater. Res. 71A*, 63−69.

(12) Adams, P. A., and Berman, M. C. (1980) Kinetics and mechanism of the interaction between human serum albumin and monomeric hemin. *Biochem. J. 191*, 95−102.

(13) Russo, S. M., Pepe, J. A., Donohue, S., Cable, E. E., Lambrecht, R. W., and Bonkovsky, H. L. (1995) Tissue distribution of zinc-mesoporphyrin in rats: relationship to inhibition of heme oxygenase. *J. Pharmacol. Exp. Ther. 272*, 766−774.

(14) Komatsu, T., Huang, Y., and Tsuchida, E. (2005) paper in preparation.

(15) Pedersen, A. O., and Jacobsen, J. (1980) Reactivity of the thiol group in human and bovine albumin at pH 3−9, as measured by exchange with 2,2′-dithiodipyridine. *Eur. J. Biochem. 106*, 291−295.

(16) Komatsu, T., Ohmichi, N., Nakagawa, A., Zunszain, P. A., Curry, S., and Tschida, E. (2005) O_2 and CO binding properties of artificial hemoproteins formed by complexing iron protoporphyrin IX with human serum albumin mutants. *J. Am. Chem. Soc. 127*, 15933−15942.

(17) Doumas, B. T., Watson, W. A., and Biggs, H. G. (1971) Albumin standards and measurement of serum albumin with bromcresol green. *Clin. Chim. Acta 31*, 87−96.

(18) Vandegriff, K. D., McCarthy, M., Rohlfs, R., and Winslow, R. M. (1997) Colloid osmotic properties of modified hemoglobins: chemically cross-linked versus polyethylene glycol surface-conjugated. *Biophys. J. 69*, 23−30.

(19) Tsai, A. G., Friesenecker, B., and McCarthy, M. (1998) Plasma viscosity regulates capillary perfusion during extreme hemodilution in hamster skinfold model. *Am. J. Physiol. 275*, H2170−80.

(20) Tsuchida, E., Komatsu, T., Kumamoto, S., Ando, K., and Nishide, H. (1995) Synthesis and O_2−Binding properties of tetraphenylporphyrinatoiron(II) derivatives bearing a proximal imidazole covalently bound at the β-pyrrolic position. *J. Chem. Soc., Perkin Trans. 2* 747−753.

(21) Sugawara, Y., Shikama, K. (1980) Autoxidation of native oxymyoglobin. *Eur. J. Biochem. 110*, 241−246.

(22) Ohno, H. and Tsukuda, T (1992) Electron-transfer reaction of polyethylene oxide-modified myoglobin in polyethylene oxide oligomera. *J. Electroanal. Chem. 341*, 137−149.

(23) Tsuchida, E., T. Komatsu, T., Hamamatsu, K., Matsukawa, Y., Tajima, A.; Yoshizu, A., Izumi, Y., and Kobayashi, K. (2000) Exchange transfusion of albumin-heme as an artificial O_2-infusion into anesthetized rats: physiological responses, O_2-delivery and reduction of the oxidized hemin sites by red blood cells. *Bioconjugate Chem. 11*, 46−50.

BC050315+

Available online at www.sciencedirect.com
SCIENCE DIRECT®
Biomaterials 27 (2006) 4477–4483
Biomaterials
www.elsevier.com/locate/biomaterials

PEGylated albumin-heme as an oxygen-carrying plasma expander: Exchange transfusion into acute anemia rat model

Yubin Huang[a], Teruyuki Komatsu[a], Hisashi Yamamoto[b,c], Hirohisa Horinouchi[c], Koichi Kobayashi[c], Eishun Tsuchida[a,*]

[a]*Advanced Research Institute for Science and Engineering, Waseda University, 3-4-1 Okubo, Shinjuku-ku, Tokyo 169 8555, Japan*
[b]*Pharmaceutical Research Center, NIPRO Corp., 3023 Noji-cho, Kusatsu-shi, Shiga 525 0055, Japan*
[c]*Department of General Thoracic Surgery, School of Medicine, Keio University, 35 Shinanomachi, Shinjuku-ku, Tokyo 160 8582, Japan*

Received 11 January 2006; accepted 5 April 2006
Available online 4 May 2006

Abstract

Poly(ethylene glycol) (PEG) conjugated recombinant human serum albumin (HSA) incorporating the synthetic iron-porphyrin (FeP) [PEGylated albumin-heme, PEG(HSA–FeP)] is a unique albumin-based oxygen carrier as a red blood cell (RBC) substitute. The physiological responses to an exchange transfusion with PEG(HSA–FeP) into an acute anemia rat model were investigated. After a 65% isovolemic hemodilution with HSA, a 30% volume of the circulatory blood was withdrawn, affording a hemorrhaged state. The circulation parameters, blood parameters, renal cortical oxygen partial pressure [PtO_2(R)], and muscle tissue oxygen partial pressure [PtO_2(M)] were continuously monitored. The intravenous infusion of PEG(HSA–FeP) restored the reduced levels of the mean arterial pressure, heart rate, respiration rate, mixed venous PO_2, and arterial PCO_2. The increased arterial PO_2 and pH also returned to their basal values. These effects were almost to the same extent as those observed after the administration of the RBC suspension. The relatively low recovery in PtO_2(R) and PtO_2(M) might be due to the Langmuir-type oxygen binding profile of PEG(HSA–FeP) (Hill coefficient: 1.0). All the animals survived during the experiments. In contrast, those injected with HSA died within 41 min. The PEG(HSA–FeP) solution is an oxygen-carrying plasma expander which can be used as a resuscitative fluid for hemorrhagic shock.

Keywords: Albumin; Biomimetic material; Blood; In vivo test; Oxygenation; Poly(ethylene glycol)

1. Introduction

Human hemoglobin (Hb)-based oxygen carriers as a blood replacement composition have been vigorously developed in the past decade [1–3], e.g., polymerized Hb [4], polymer-conjugated Hb [5], and phospholipid vesicle encapsulated Hb [6,7]. Some of them have already been used in clinical Phase II/III trials. The most superior property of these materials is certainly "no blood type". One can administer these materials into patients who need a blood transfusion without cross matching and typing before use. This saves time and facilities, allowing instant transfusion, which is tremendously useful in an emergency. On the other hand, the largest concern of the Hb-products is the source of the human Hb, which is regulated by the availability of donated human blood.

Based on this background, poly(ethylene glycol) (PEG) conjugated human serum albumin (HSA) incorporating 2-[8-{*N*-(2-methylimidazolyl)}octanoyloxymethyl]-5,10,15,20-tetrakis{α,α,α,α-*o*-(1-methylcyclohexanamido)phenyl}porphinatoiron(II) (FeP, Chart 1) [PEGylated albumin-heme, PEG(HSA–FeP)] has been developed as a unique albumin-based oxygen carrier [8]. Recombinant HSA is now manufactured on an industrial scale (one million vials per year) [9] and the batch production of the synthetic FeP has also been established [10]. The oxygen binding affinity (oxygen pressure where 50% of heme is oxygenated) of PEG(HSA–FeP) (P_{50}) was adjusted to 32 Torr (at 37 °C) that is similar to the 28 Torr of human RBC, and the solution properties are almost the same as those of HSA itself. The surface modification with PEG significantly improved not only the

*Corresponding author. Tel.: +81 3 5286 3120; fax: +81 3 3205 4740.
E-mail address: eishun@waseda.jp (E. Tsuchida).

0142-9612/$ - see front matter © 2006 Elsevier Ltd. All rights reserved.
doi:10.1016/j.biomaterials.2006.04.008

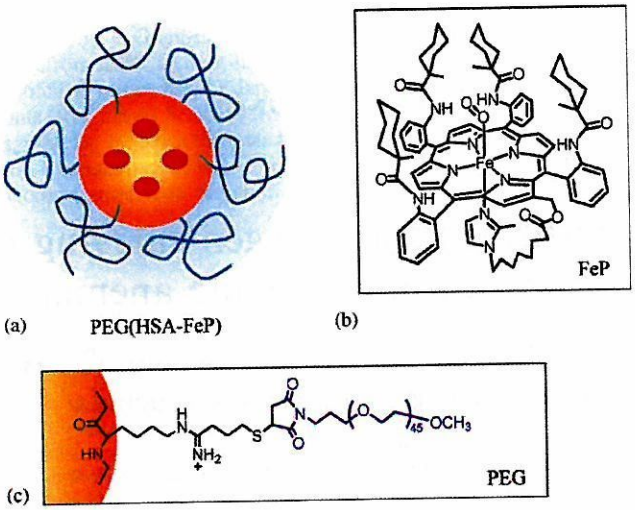

Chart 1. (a) Schematic illustration of PEGylated albumin-heme [PEG(HSA–FeP)], (b) chemical structure of FeP, and (c) binding form of PEG to the lysine group of HSA.

circulation lifetime of FeP in vivo, but also the stability of the oxygenated complex [8]. The PEG(HSA–FeP) solution would be of extreme medical importance as a new type of oxygen-carrying plasma expander.

We now report for the first time the systemic evaluations of the physiological responses to an exchange transfusion with PEG(HSA–FeP) into an acute anemia rat model. The animals were first placed in a 65 vol% hemodilution with HSA and then underwent a 30 vol% blood replacement with PEG(HSA–FeP). The circulation parameters, blood parameters, the oxygen deliveries to the renal cortex and the muscle tissue were monitored and compared to the HSA group and RBC group for 120 min after the infusion.

2. Materials and methods

2.1. Preparation of PEG(HSA–FeP) solution

The 5 g/dL HSA solution was prepared by dilution of recombinant HSA [Albrec®, 25 wt%, NIPRO Corp. (Osaka)] with a saline (Otsuka Pharmaceutical Co., Ltd.). The PEG(HSA–FeP) was prepared according to our previously reported procedure [8] (phosphate buffer saline solution, pH = 7.4, [HSA] = 5 g/dL, [FeP] = 3 mM (FeP/HSA = 4 mol/mol), Mw of PEG = 2333 Da, averaged number of PEG per HSA–FeP = 6, oxygen-binding affinity (P_{50}) = 32 Torr (37 °C), density = 1.01 g/cm^3, colloid osmotic pressure = 27 mmHg, viscosity = 1.14 cP).

2.2. Extreme hemodilution and exchange transfusion

The investigations were carried out with 15 male Wistar rats (288 ± 18 g). The methods of operation were described elsewhere in detail [11].

The animals were under an inhalation anesthesia with sevoflurane; its concentration was kept at 1.5% during the experiment. First, a 65% hemodilution was carried out using 5 g/dL HSA. The blood withdrawal via the common carotid artery (2 mL) and the HSA infusion from the femoral vein (2 mL) (each 1 mL/min) were repeated for eight cycles. After 10 min, a 30% volume of the circulatory blood was withdrawn, and the identical volume of PEG(HSA–FeP) was injected ($n = 5$) (1 mL/min). As negative or positive-control group, the 5 g/dL HSA solution (HSA group, $n = 5$) or the washed RBC suspension (RBC group, $n = 5$) was infused to the similarly operated rats in hemorrhage. The washed RBC suspension was prepared as follows. The fresh withdrawn whole rat blood in the heparinized tube was centrifuged and the plasma layer was discarded. The 5 g/dL HSA was added to the tube and centrifuged again. Then, the supernatant was discarded and 5 g/dL HSA was added to adjust the Hb concentration to 5 g/dL ([heme] = 3 mM).

The blood samples from the artery (0.3 mL) and vein (0.2 mL) were collected at the following seven time-points: (1) before the 65% hemodilution, (2) immediately after the hemodilution, (3) 10 min after the hemodiluation, (4) immediately after the 30% bleeding, (5) immediately after the sample infusion, (6) 60 min, and (7) 120 min after the infusion. Mean arterial pressure (MAP) and heart rate (HR) were recorded by a Polygraph System (NIHON KODEN LEG-1000 Ver. 01-02 or PEG-1000 Ver. 01-01) at the following eleven time-points; (1) before the 65% hemodilution, (2) immediately after the hemodilution, (3) 10 min after the hemodilution, (4) immediately after the 30% bleeding, (5) immediately after the sample infusion, (6) 5 min, (7) 15 min, (8) 30 min, (9) 60 min, (10) 90 min, and (11) 120 min after the sample infusion. Collected blood sample was applied to a blood gas system (Radio Meter Trading ABL555) to measure the oxygen pressure (PaO_2), carbon dioxide pressure ($PaCO_2$) and pH of the arterial blood, and the oxygen pressure (PvO_2) and lactate of the venous blood. Renal cortical oxygen partial pressure [PtO_2(R)] and muscle tissue oxygen partial pressure [PtO_2(M)] were monitored by a tissue oxygen pressure monitor (Inter Medical PO_2-100 DW) using a polarographic oxygen-electrode (Intermedical POE-10 N and POE-40PS) inserted into the left renal cortex and muscle in the abdomen.

The animals were sacrificed after the experiments by venesection. All animal handling and care were in accordance with the NIH guidelines. The protocol details were approved by the Animal Care and Use Committee of Keio University.

2.3. Statistical analysis

All data were represented by mean ± standard deviation (SD). Statistical analyses ware performed using the Tukey–Kramer multiple comparison test for three groups, and by repeated measures analysis of variance followed by paired t-test. The software used was a StatView (SAS Institute, Inc.). Values of $p < 0.05$ were considered significant.

3. Results

3.1. Survival time

The changes in the hematocrit (Hct) clearly demonstrated a good accordance with the 65% hemodilution and 30% shock resuscitation (Fig. 1(a)). Isovolemic hemodilution with HSA reduced the Hct to 13–15%; this value is below the threshold at which the organism becomes oxygen supply limited [12,13]. Under an extreme hemodilution, the effect of the RBC substitute is magnified upon introduction into the circulation.

The intravenous infusion of HSA did not make any improvement on the appearance of the animals. All the rats died within 41 min; the average survival time was 17.9 ± 14.0 min (Fig. 1(b)). In contrast, after the transfusion of PEG(HSA–FeP) or washed RBC, all the animals survived over 120 min. In the glass capillaries for the Hct determinations of the PEG(HSA–FeP) group, the supernatant after centrifugation (12 kG, 5 min) was colored red by the homogeneously dispersed sample. This indicates that PEG(HSA–FeP) has a good solubility with the blood components without aggregation.

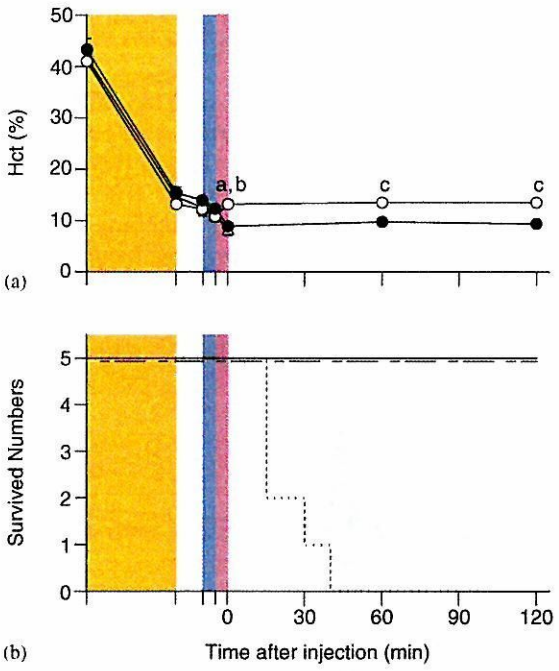

Fig. 1. Effect of PEG(HSA–FeP) solution on (a) Hct in anesthetized rats subjected to hemodilution and hemorrhage, and (b) the changes of their survived numbers. In (a), each value represents the mean ± SD of 5 rats [●; PEG(HSA–FeP) group, ○; RBC group, and △; HSA group]. $^{a}p < 0.05$ versus HSA group (Tukey–Kramer test), $^{b}p < 0.05$ versus PEG(HSA–FeP) group (Tukey–Kramer test), and $^{c}p < 0.05$ versus PEG(HAS–FeP) group (unpaired t-test). In (b), solid line; PEG(HSA–FeP) group, broken and dotted line; RBC group, and dotted line; HSA group. The yellow, blue, and pink areas indicate the periods of 65% hemodilution, 30% bleeding, and sample infusion, respectively.

3.2. Circulation parameters (MAP, HR, and respiration rate)

The MAP decreased to 70–73 mmHg [72–74% of the basal value (b.v.)] after the 65% hemodilution, and further dropped to 28–29 mmHg (28–29% of the b.v.) by the 30% bleeding in all groups (Fig. 2(a)). The injection of PEG(HSA–FeP) or RBC significantly increased the lowered values to 70 or 73 mmHg, that corresponds to 85% or 98% of the levels before the bleedings. On the other hand, no recovery was observed in the HSA group.

The HR and respiration rate decreased to 332–356 beats/min (86–91% of the b.v.) and 51–57 time/min (80–93% of the b.v.) by the 30% bleeding (Fig. 2(b), (c)). Both parameters returned to their initial levels by the infusion of PEG(HSA–FeP). The degree of the recovery was almost the same as those of the RBC transfusion.

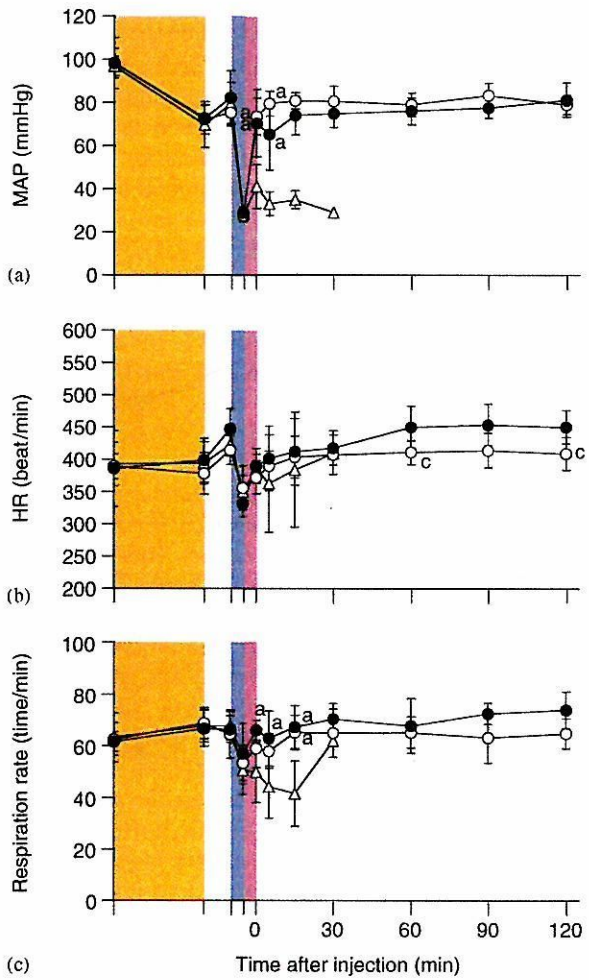

Fig. 2. Effect of PEG(HSA–FeP) solutions on (a) MAP, (b) HR, and (c) respiration rate in anesthetized rats subjected to hemodilution and hemorrhage. Each value represents the mean ± SD of 5 rats [●; PEG(HSA–FeP) group, ○; whole blood group, and △; HSA group]. The yellow, blue, and pink areas indicate the periods of 65% hemodilution, 30% bleeding, and sample infusion, respectively. $^{a}p < 0.05$ versus HSA group (Tukey–Kramer test) and $^{c}p < 0.05$ versus PEG(HAS–FeP) group (unpaired t-test).

3.3. Blood parameters [PaO_2, PvO_2, $PaCO_2$, and pH]

The PaO_2 increased to 96–118 mmHg (120–140% of the b.v.) after the 65% hemodilution, and became further elevated to 131–137 mmHg (156–167% of the b.v.) after the 30% bleeding (Fig. 3(a)). It was not changed by the injection of HSA, however, the administration of RBC immediately restored the PaO_2 to 97 mmHg (118% of the b.v.), and kept the level constant throughout the measurement. The injection of PEG(HSA–FeP) also showed a similar restoration like that of RBC.

The PvO_2 decreased to 32–35 mmHg (59–67% of the b.v.) after the 30% bleeding (Fig. 3(b)). Although the administration of HSA did not improve the low value, the infusion of PEG(HSA–FeP) or RBC increased the PvO_2 to 49 or 52 mmHg (91% or 95% of the the b.v.).

The $PaCO_2$ dropped to 23–26 mmHg (59–66% of the b.v.) after the 30% bleeding (Fig. 3(c)). The injection of HSA did not recover the low level, while the administration of PEG(HSA–FeP) or RBC increased the $PaCO_2$ to 31 mmHg, and it reached 35 mmHg after 1 h.

The pH of 7.43–7.45 was increased to 7.53–7.56 after the 30% bleeding. The administration of PEG(HSA–FeP) or RBC quickly decreased the high pH to the initial value before the hemodilution (Fig. 3(d)).

3.4. Tissue oxygen partial pressure [$PtO_2(R)$ and $PtO_2(M)$]

The PtO_2(R) decreased to 8–10 mmHg (51–59% of the b.v.) after the 65% hemodilution, and further declined to 3–5 mmHg (17–28% of the b.v.) after the 30% bleeding (Fig. 4(a)). The administration of HSA showed no improvement, however, the injection of PEG(rHSA–FeP) or RBC immediately increased the PtO_2(R) to 8–9 mmHg (84–97% of the values before the bleeding). In the RBC group, the PtO_2(R) became somewhat higher and reached

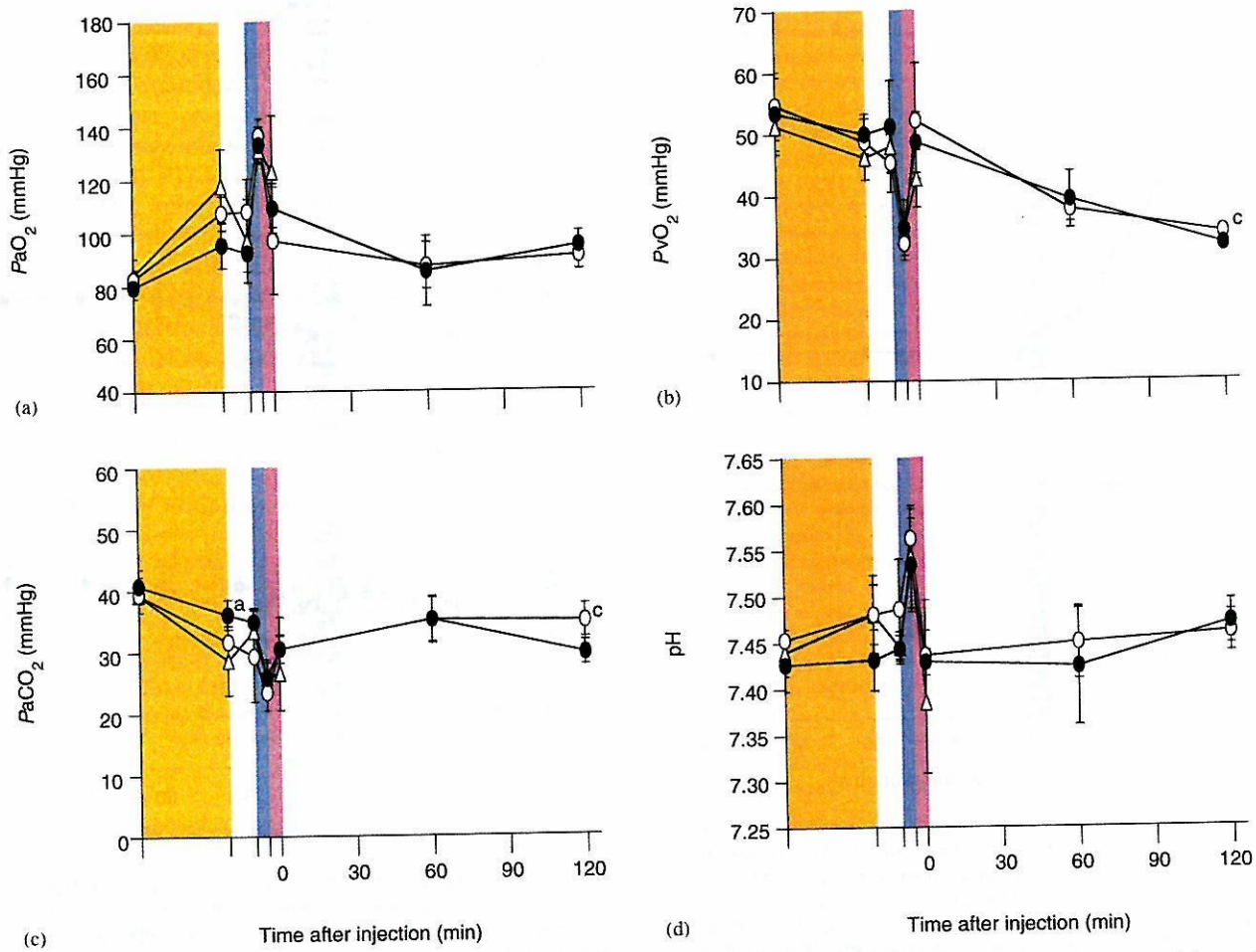

Fig. 3. Effect of PEG(HSA–FeP) solutions on (a) PaO_2, (b) PvO_2, (c) $PaCO_2$, and (d) pH in anesthetized rats subjected to hemodilution and hemorrhage. Each value represents the mean ± SD of 5 rats [●; PEG(HSA–FeP) group, ○; whole blood group, and △; HSA group]. The yellow, blue, and pink areas indicate the periods of 65% hemodilution, 30% bleeding, and sample infusion, respectively. $^{a}p<0.05$ versus HSA group (Tukey–Kramer test) and $^{c}p<0.05$ versus PEG(HAS–FeP) group (Unpaired t-test).

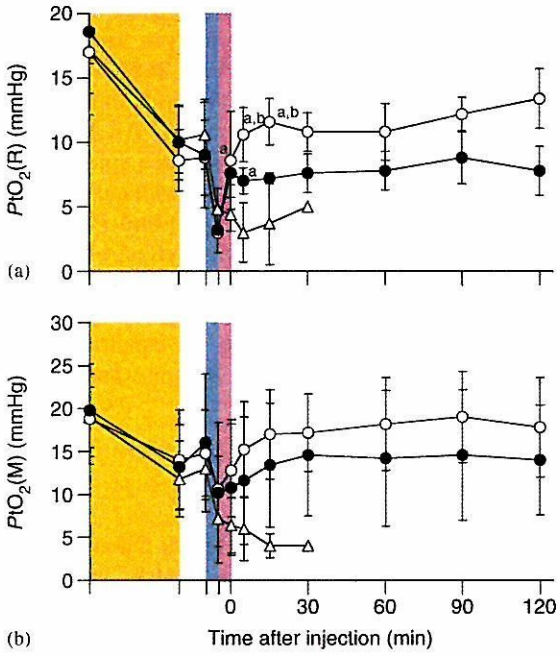

Fig. 4. Effect of PEG(HSA–FeP) solutions on (a) PtO_2(R) and (b) PtO_2(M) in anesthetized rats subjected to hemodilution and hemorrhage. Each value represents the mean ± SD of 5 rats [●; PEG(HSA-FeP) group, ○; whole blood group, and △; HSA group]. The yellow, blue, and pink areas indicate the periods of 65% hemodilution, 30% bleeding, and sample infusion, respectively. $^{a}p<0.05$ versus HSA group (Tukey–Kramer test) and $^{b}p<0.05$ versus PEG(HSA–FeP) group (Tukey–Kramer test).

11 mmHg after 15 min. They both remained constant by the end of the measurements.

The PtO_2(M) decreased to 7–11 mmHg (38–56% of the b.v.) by the 30% bleeding (Fig. 4(b)). The administration of the RBC gradually increased the PtO_2(M) to 17 mmHg (90% of the b.v.) for 15 min, and maintained this level. The transfusion of PEG(HSA–FeP) also slowly increased the PtO_2(M) to 15 mmHg (74% of the b.v.) for 30 min, and the value was stable throughout the experiment.

4. Discussion

4.1. Acute anemia

The isvolemic 65% hemodilution with HSA reduced the Hb concentration, leading to a decrease in the oxygen supply to the tissue. Hypoxia in vital organs and muscle tissues were clearly shown by the declines of MAP, PtO_2(R), and PtO_2(M). The initial response to compensate for this acute anemia is generally an increase in the rate or depth of respiration (hyperventilation); both result in an elevation of the PaO_2 level. In fact, the PaO_2 was increased to 120–140% of the b.v. just after the 65% hemodilution. Since the respiration rate was not changed, we theorized that the increase of depth of respiration is the major factor for the high PaO_2.

4.2. Hemorrhagic shock

During the hemorrhagic shock by the 30% bleeding, significant decreases in the MAP, PvO_2, PtO_2(R), and PtO_2(M) were observed by the loss of the circulation blood volume. The HR and respiration rate also decreased. On the contrary, PaO_2 was increased to about 160% of the b.v., because the RBC has to increase its oxygen saturation. The $PaCO_2$ decreased to about 62% of the b.v. and the pH increased to 7.55. A respiratory alkalosis probably overcomes the metabolic acidosis. The lactate also increased (data not shown), which could be due to the anaerobic metabolism in the peripheral circulation systems.

4.3. Responses to infusion of PEG(HSA–FeP)

The injection of the sample solutions increased the blood volume and improved the circulatory flows. The lactate was washed out from the tissues and into the circulatory system, which decreased the pH to the initial level of 7.43 in all groups. The administration of HSA did not restore any parameters, leading to death within 41 min. In contrast, the infusion of PEG(HSA–FeP) or RBC kept all the rats alive until the end of the measurement.

The circulation half lifetime of FeP (τ_{50}) after the administration of PEG(HSA–FeP) (20% top loading) in anesthetized rats has been determined to be 14 h [8]. The surface modification by PEG significantly prevented the rapid clearance of the incorporated FeP and contributed to increasing the oxygen-transporting efficacy. In this experimental setup, over 80% of the material remained in the bloodstream 120 min after the injection. It is almost the same level as those observed in the 20% top-loading test.

After the injection of PEG(HSA–FeP), the animals showed significant and quick recoveries in MAP, HR, respiration rate, PaO_2, PvO_2, $PaCO_2$, and pH, the same as seen in the RBC group. These results definitely show the oxygen-transporting capability of the PEG(HSA–FeP) solution as a resuscitative fluid. The PvO_2 is a crucial parameter to evaluate the oxygen saturation in blood. The complete restoring of PvO_2 to the level before the bleeding implies a sufficient oxygen supply by PEG(HSA–FeP). The hyperventilation by hypoxia was also depressed and PaO_2 returned to the b.v.

Among the vital organs, renal perfusion is first impaired due to redistribution of the systemic blood flow, so that the PtO_2(R) is a sensitive parameter to the subtle change in the blood circulation and oxygen delivery. The increase in PtO_2(R) by the transfusion of PEG(HSA–FeP) or RBC was very quick, because the oxygen is preferentially supplied to the vital organs. On the other hand, the PtO_2(M) was gradually elevated for 30 min with the stabilization of the blood circulation.

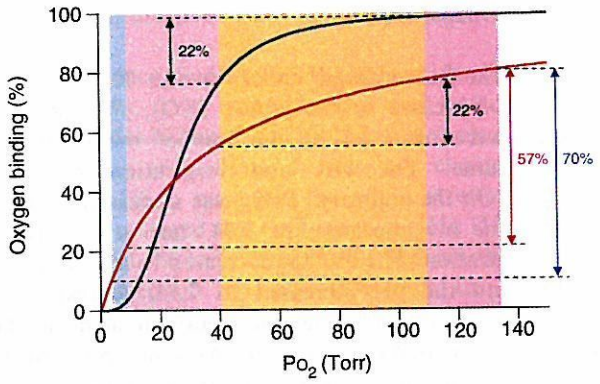

Fig. 5. Oxygen equilibrium curves of PEG(HSA–FeP) (red line) and human RBC (blue line) at 37 °C. The yellow-colored area represents the difference between 110 mmHg at lungs and 40 mmHg at muscle tissues in human. The pink-colored area corresponds to the difference between 134 mmHg of PaO_2 and 9.3 mmHg of PtO_2(M) in hemorrhagic shock state after the 30% bleeding. The left edge of the blue-colored area indicates 3.7 mmHg of PtO_2(R) at the hemorrhagic shock state. The values represented in percent indicate the OTEs.

4.4. Oxygenation of the tissues by PEG(HSA–FeP)

All the physiological responses showed that PEG (HSA–FeP) has the capability to transport oxygen throughout the body. Nevertheless, the restoration effect by PEG(HSA–FeP) in PtO_2(R) and PtO_2(M) was slightly weak compared to that observed in the RBC group. The infusion volume and heme concentration ([heme] = 3 mM) were exactly the same. The oxygen transporting efficiency (OTE) of PEG(HSA–FeP) between the lungs (PO_2 = 110 Torr) and muscle tissues (PO_2 = 40 Torr) (22%) is also identical to the human RBC (Fig. 5) [10]. Therefore, we theorized that the relatively low oxygenation of the renal cortex is due to a Langmuir-type absorption of the oxygen binding of PEG(HSA–FeP); the Hill's coefficient (n) is 1.0. It is well known that human RBC has an allosteric effect on the oxygen-binding equilibrium (n = 3.0) [14]. If the oxygen partial pressure of the peripheral tissue dramatically decreased, a significant difference would appear in the OTEs of PEG(HSA–FeP) and RBC. For instance, in this experimental set up, the 30% blood-bleeding induced extreme low-oxygen partial pressures in the renal cortex (3.7 mmHg) and muscle tissue (9.3 mmHg), and also the high PaO_2 of 134 mmHg. In this situation, the RBC shows maximum OTE of 94–99%, because of the allosteric effect on the oxygen binding to Hb. On the contrary, PEG(HSA–FeP) demonstrated a 57–70% OTE (Fig. 5). This would provide an insufficient oxygen supply to the renal cortex and muscle tissues to some degree, even though the increased PtO_2(R) and PtO_2(M) after the infusion of PEG(HSA–FeP) remained constant for 120 min during the experiment period.

5. Conclusions

The administration of the PEGylated albumin-heme solution into the acute anemia rat model showed a significant efficacy on (i) resuscitation of hemorrhagic shock, (ii) improving the blood circulation, and (iii) oxygen delivery throughout the body. The overall restoration ability of PEG(HSA–FeP) occurred to almost the same extent as that of the RBC suspension. All the systemic responses imply that the PEG(HSA–FeP) solution can be used as an valuable oxygen-carrying plasma expander. The relatively low improvement in PtO_2(R) and PtO_2(M) may be due to the absence of the allosteric effect of the oxygen binding to FeP (n = 1.0). It is also of great interest to design a cooperative oxygen-binding system using a synthetic molecule. This may be an essential issue for constructing the next generation albumin-based artificial RBC substitutes.

Acknowledgements

This work was supported by Health Science Research Grants (Regulatory Science) of the MHLW Japan, Grant-in-Aid for Scientific Research (No. 16350093) from JSPS, and Grant-in-Aid for Exploratory Research (No. 16655049) from MEXT Japan.

References

[1] Riess JG. Oxygen carriers ("blood substitute")—raison d'etre, chemistry, and some physiology. Chem Rev 2001;101:2797–919.
[2] Squires JE. Artificial blood. Science 2002;295:1002–5.
[3] Winslow R. Blood substitutes. London: Elsevier; 2005.
[4] Gould SA, Moore EE, Moore FA, Haenel JB, Burch JM, Sehgal H, et al. The clinical utility of human polymerized hemoglobins as a blood substitute following acute trauma and urgent surgery. In: Tsuchida E, editor. Blood substitutes. Present and future perspectives. Amsterdam: Elsevier; 1998. p. 41–54.
[5] Vandergriff KD, Malavalli A, Wooldrige J, Lohman J, Winslow RM. MP4, a new nonvasoactive PEG-Hb conjugate. Transfusion 2003;43: 509–16.
[6] Sakai H, Hara H, Yuasa M, Tsai AG, Takeoka S, Tsuchida E, et al. Molecular dimensions of Hb-based O_2 carriers determine constriction of resistance arteries and hypertension. Am J Phisiol Heart Circ Physiol 2000;279:H908–15.
[7] Sakai H, Horinouchi H, Masada Y, Takeoka S, Ikeda E, Takaori M, et al. Metabolism of hemoglobin-vesicles (artificial oxygen carriers) and their influence on organic functions in a rat model. Biomaterials 2003;25:4317–25.
[8] Huang Y, Komatsu T, Wang RM, Nakagawa A, Tsuchida E. Poly(ethylene glycol)-conjugated human serum albumin including iron porphyrins: surface modification improves the O_2-transporting ability. Bioconjugate Chem 2006;17:393–8.
[9] Sumi A, Ohtani W, Kobayashi K, Ohmura T, Yokoyama K, Nishida M, et al. Purification and physicochemical properties of recombinant human serum albumin. In: Rivat C, Stoltz J-F, editors. Biotechnology of blood proteins, vol. 227. Montrouge: John Libbey Eurotext; 1993. p. 293–8.
[10] Komatsu T, Matsukawa Y, Tsuchida E. Effect of heme structure on O_2-binding properties of human serum albumin–heme hybrids: intramolecular histidine coordination provides a stable O_2-adduct complex. Bioconjugate Chem 2002;13:397–402.
[11] Komatsu T, Yamamoto H, Huang Y, Horinouchi H, Kobayashi K, Tsuchida E. Exchange transfusion with synthetic oxygen-carrying plasma protein "albumin-heme" into an acute anemia rat model

after seventy-percent hemodilution. J Biomed Mater Res 2003;71A: 644–51.

[12] Tsai AG, Vandegriff KD, Intaglietta M, Winslow RM. Targeted O_2 delivery by low-P_{50} hemoglobin: a new basis for O_2 therapeutics. Am J Physiol Heart Circ Physiol 2003;285:H1411–9.

[13] Cabrales P, Tsai AG, Intaglietta M. Microvascular pressure and functional capillary density in extreme hemodilution with low and high plasma viscosity expander. Am J Physiol Heart Circ Physiol 2004;287:H363–73.

[14] Antonini E, Brunori M. Hemoglobin and myoglobin in their reactions with ligands. In: Neuberger A, Tatum EL, editors. North-Holland research monographs. Frontiers of biology, vol. 21. Amsterdam: North-Holland Publisher Co.; 1971. p. 153–87.

J|A|C|S
ARTICLES
Published on Web 11/30/2006

Photosensitized Reduction of Water to Hydrogen Using Human Serum Albumin Complexed with Zinc−Protoporphyrin IX

Teruyuki Komatsu,*,†,‡ Rong-Min Wang,†,§ Patricia A. Zunszain,¶ Stephen Curry,¶ and Eishun Tsuchida*,†

Contribution from the Advanced Research Institute for Science and Engineering, Waseda University, 3-4-1 Okubo, Shinjuku-ku, Tokyo 169-8555, Japan, PRESTO, Japan Science and Technology Agency (JST), 4-1-8 Honcho, Kawaguchi-shi, Saitama 332-0012, Japan, Key Laboratory of Polymer Materials of Gansu Province, Northwest Normal University, Lanzhou 730070, China, and Biophysics Section, Division of Cell and Molecular Biology, Faculty of Natural Sciences, Imperial College London, South Kensington Campus, London SW7 2AZ, United Kingdom

Received August 5, 2006; E-mail: teruyuki@waseda.jp; eishun@waseda.jp

Abstract: We present the photophysical properties of complexes of recombinant human serum albumin (rHSA) with Zn(II)−protoporphyrin IX (ZnPP) and their activities in the photosensitized reduction of water to hydrogen (H_2) using methyl viologen (MV^{2+}) as an electron relay. The ZnPP is bound in subdomain IB of wild-type rHSA [rHSA(wt)] by an axial coordination of Tyr-161 and, in the rHSA(I142H/Y161L) mutant [rHSA(His)], by a His-142 coordination. Both the rHSA(wt)−ZnPP and rHSA(His)−ZnPP complexes showed a long-lived photoexcited triplet state with lifetimes (τ_T) of 11 and 2.5 ms, respectively. The accommodation of ZnPP into the protein matrix efficiently eliminated the collisional triplet self-quenching process. The addition of a water-soluble electron acceptor, MV^{2+}, resulted in a significant decrease in the triplet lifetime. The transition absorption spectrum revealed the oxidative quenching of rHSA−^{3}ZnPP* by MV^{2+}. The quenching rate constant (k_q) and backward electron transfer rate constant (k_b) were determined to be 1.4×10^7 and 4.7×10^8 M^{-1} s^{-1} for rHSA(wt)−ZnPP. In the presence of the colloidal PVA−Pt as a catalyst and triethanolamine (TEOA) as a sacrificial electron donor, the photosensitized reduction of water to H_2 takes place. The efficiency of the photoproduction of H_2 was greater than that of the system using the well-known organic chromophore, tetrakis(1-methylpyridinium-4-yl)porphinatozinc(II) ($ZnTMPyP^{4+}$), under the same conditions.

Introduction

The photosensitized reduction of water to molecular H_2, which is a clean-burning fuel free of CO_2 emission, has attracted considerable attention during the past decade. In order to trigger this reaction by visible light, organic chromophores are extensively used as photosensitizers, such as ruthenium tris(bipyridyl) complexes and zinc−porphyrins.[1,2] The classical, but effective system, appears to consist of water-soluble, positively charged tetrakis(1-methylpyridinium-4-yl)porphinatozinc(II) ($ZnTMPyP^{4+}$), methyl viologen (MV^{2+}), a colloidal Pt catalyst, and sacrificial electron donor.[1a,2] Instead of the synthetic $ZnTMPyP^{4+}$, if one can use the most prominent porphyrin in nature, namely, protoporphyrin IX, it would have a significant impact not only on pure chemistry but also on solar energy conversion. However, the Zn(II) complex of protoporphyrin IX (ZnPP) is relatively insoluble in water (<pH 9), and it is therefore difficult to employ ZnPP in order to construct a practical catalyst system in aqueous media.

Human serum albumin (HSA), the most abundant plasma protein in our bloodstream, acts as a transporter for a range of insoluble endogenous and exogenous compounds, such as fatty acids, bilirubin, thyroxine, hemin [Fe(III)−protoporphyrin IX], and a variety of drugs.[3,4] This heart-shaped monomer protein contains three homologous domains (I−III), each of which is composed of A and B subdomains.[4,5] Recent X-ray crystallographic studies have revealed that hemin is bound within a narrow hydrophobic D-shaped cavity in subdomain IB of HSA with an axial coordination of Tyr-161 to the central ferric

† Waseda University.
‡ JST.
§ Northwest Normal University.
¶ Imperial College London.

(1) (a) Kalyanasundaram, K.; Grätzel, M. *Helv. Chim. Acta* **1980**, *63*, 478−485. (b) Kalyanasundaram, K. *Coord. Chem. Rev.* **1982**, *46*, 159−244.
(2) (a) Harriman, A.; Porter, G.; Richoux, M.-C. *J. Chem. Soc., Faraday Trans. 2* **1981**, *77*, 833−844. (b) Richoux, M.-C.; Harriman, A. *J. Chem. Soc., Faraday Trans. 1* **1982**, *78*, 1873−1885. (c) Harriman, A.; Porter, G.; Richoux, M.-C. *Coord. Chem. Rev.* **1982**, *44*, 83−126.
(3) Peters, T. *All about Albumin: Biochemistry, Genetics and Medical Applications*; Academic Press: San Diego, CA, 1996.
(4) (a) Curry, S.; Madelkow, H.; Brick, P.; Franks, N. *Nat. Struct. Biol.* **1998**, *5*, 827−835. (b) Petitpas, I.; Petersen, C. E.; Ha, C.-E.; Bhattacharya, A. A.; Zunszain, P. A.; Ghuman, J.; Bhagavan, N. V.; Curry, S. *Proc. Natl. Acad. Sci. U.S.A.* **2003**, *100*, 6440−6445. (c) Ghuman, J.; Zunszain, P. A.; Petitpas, I.; Bhattacharya, A. A.; Otagiri, M.; Curry, S. *J. Mol. Biol.* **2005**, *353*, 38−52.
(5) (a) He, X. M.; Carter, D. C. *Nature* **1992**, *358*, 209−215. (b) Carter, D. C.; Ho, J. X. *Adv. Protein Chem.* **1994**, *45*, 153−203.

10.1021/ja0656806 CCC: $33.50

ion.[6,7] Furthermore, we have demonstrated that site-directed mutagenesis to introduce a proximal histidine into position Ile-142 and to replace Tyr-161 by Leu at the heme-binding site [rHSA(I142H/Y161L); rHSA(His)] confers a reversible dioxygen binding capability to the prosthetic heme group in a fashion similar to hemoglobin.[8]

In this paper, we report for the first time the photophysical properties of rHSA complexes with a ZnPP [rHSA(wt)−ZnPP, rHSA(His)−ZnPP] and their photoinduced electron transfer to MV^{2+} and highlight their activities for the photosensitized reduction of water to H_2 in the presence of colloidal PVA−Pt as a catalyst and triethanolamine (TEOA) as a sacrificial regent.

Experimental Section

Materials and Apparatus. All reagents were purchased from commercial sources as special grades and used without further purification. The rHSA(wt) and rHSA(I142H/Y161L) mutant [rHSA-(His)] were prepared according to our previously reported procedures.[7,8] Zinc(II)−protoporphyrin IX (ZnPP) was purchased from Sigma-Aldrich. 5,10,15,20-Tetrakis(1-methylpyridinium-4-yl)porphinatozinc(II) tetrachloride ($ZnTMPyP^{4+}$) was synthesized by insertion of the central zinc-(II) into 5,10,15,20-tetrakis(1-methylpyridinium-4-yl)porphin tetra-*p*-toluenesulfonate (Sigma-Aldrich) using $Zn(AcO)_2$ followed by exchanging the counteranions with chlorides using a Bio-Rad AG 1-X8 resin (100−200 mesh) chloride form with CH_3CN/H_2O (1/1). The UV−vis absorption spectra were recorded using an Agilent 8453 UV−visible spectrophotometer with an Agilent 89090A temperature control unit. The fluorescence spectra were obtained from a HITACHI F-4500 spectrofluorometer. Water was deionized using a Millipore Elix and Simpli Lab-UV.

Preparation of rHSA(wt)−ZnPP and rHSA(His)−ZnPP. Typically, 5 mL of a potassium phosphate buffered solution (pH 7.0, 50 mM) of rHSA(wt) (0.1 mM) was mixed with 0.8 mL of 0.625 mM ZnPP in DMSO (ZnPP:rHSA molar ratio of 1:1) and incubated for 12 h with rotation in the dark at room temperature. The complex was then diluted with 50 mM potassium phosphate and concentrated to the initial volume using a Vivaspin 20 centrifuge filter (10 kDa MW cutoff) at 4000*g* using a Beckman Coulter Allegra X-15R centrifuge. These dilution/concentration cycles were repeated to reduce the DMSO concentration to <0.1 vol %. The phosphate buffered solution (pH 7.0, 10 mM) of rHSA(wt)−ZnPP ([ZnPP] = 10 μM) in a 10 mm path length optical quartz cuvette sealed with a rubber septum was degassed and purged with Ar prior to use. The rHSA(His)−ZnPP solution was prepared by the same procedure.

Excited State Lifetimes. The singlet lifetimes of rHSA−ZnPP were measured using a HORIBA NAES-500 nanosecond fluorometer with a N_2 lamp (excitation side: an Asahi spectra MZ0560 multicavity filter (λ = 560 ± 2 nm), emission side: a HOYA R-620 sharp cut filter). The samples (5 μM) were held in a quartz cuvette (optical path length = 10 mm), and the experiments were carried out at 25 °C.

The transient absorption spectra and triplet lifetime measurements were carried out using a Unisoku TSP-1000WK time-resolved spectrophotometer with a Spectron Laser Systems SL803G-10 Q-switched Nd:YAG laser, which generated a second-harmonic (532 nm) pulse of 6 ns duration (10 Hz).[8b]

Photoreduction of MV^{2+}. Steady-state irradiations were carried out using an Oriel 450 W xenon arc lamp model 66021 in conjunction with an Asahi Spectra MZ0550 multicavity filter (550 ± 2 nm). The filtered light (1.61 $mWcm^{-2}$) was used to irradiate the potassium phosphate buffered solution (pH 5.4, 50 mM) of rHSA−ZnPP (10 μM, 3.5 mL) including MV^{2+} (2 mM) and TEOA (0.19 M) as it was gently stirred in a 10 mm path length quartz cuvette under an Ar atmosphere at 25 °C. The distance between the cuvette and the light source was 12 cm.

The overall quantum efficiency (Φ) of the photoreduction of MV^{2+} was calculated as the ratio (numbers of $MV^{+\bullet}$ molecules produced)/(numbers of photons absorbed); the denominator was determined by the change in the power of the transmitted light, measured by an Advantest Q8230 photo power meter with a Q82313 silicon photodiode sensor, which was placed after the quartz cuvette.

Hydrogen Evolution from Water. Colloidal PVA−Pt was prepared as follows. An aqueous H_2PtCl_6 solution (66 mM, 1 mL) was added dropwise to an $EtOH/H_2O$ (1/1) solution (100 mL) of poly(vinyl alcohol) (PVA, 271 mg, average degree of polymerization = 500, Wako Pure Chemical Industries) with vigorous stirring, and the mixture was refluxed for 1.5 h. After being cooled to room temperature, a dark brown PVP−Pt colloid solution was obtained. To remove the EtOH and produce the aqueous colloidal PVP−Pt, the solution was evaporated using a rotary evaporator at 50 °C. The concentration was assayed based on the Pt ion by inductively coupled plasma (ICP) spectrometry using a Seiko Instruments SPS 7000A spectrometer; [Pt−PVA] = 3.55 mM. The diameter of the colloidal Pt was determined to be approximately 3.0 ± 0.7 nm using transmission electron microscopy observations on a JEOL JEM 1011 transmission electron microscope.

The phosphate buffered solution (pH 5.4, 50 mM, 3.5 mL) of the mixture of rHSA−ZnPP (10 μM), MV^{2+} (2 mM), TEOA (0.19 M), and a colloidal PVA−Pt (20 μM) in a quartz cuvette (optical path length = 10 mm) connected to a 40 mL glass chamber was degassed by Ar. Steady-state irradiations were carried out at 25 °C using a 450 W xenon arc lamp in conjunction with a HOYA HA30 heat absorption filter (330−700 nm) to eliminate the UV light and excess heating. The distance between the cuvette and light source was 12 cm. After a designated period, 100 μL of the gas above the solution was removed by a gastight syringe and applied to a Shimadzu GC-8APT gas chromatograph with a TCD detector to measure the amount of H_2. The column used was a Shinwa Chemical Industries Shincarbon ST.

Results and Discussion

Photophysical Properties of rHSA−ZnPP Complexes. The rHSA(wt)−ZnPP and rHSA(His)−ZnPP complexes were prepared essentially as described previously for HSA−hemin complexes.[8] The gel permeation chromatogram (Superdex 75g) of the pink-colored proteins exhibited only a single elution peak, indicating that ZnPP is perfectly incorporated into rHSA. No precipitation was observable for over a year at 4 °C. Our crystal structure analysis and spectroscopy experiments revealed that hemin is bound within a D-shaped hydrophobic cavity in subdomain IB of rHSA(wt) with a relatively weak axial coordination by Ty-161.[7,8] In the genetically engineered rHSA-(His) mutant, hemin is in the ferric high-spin complex with an axial His-142 coordination and a water molecule as the sixth ligand.[8b]

The UV−vis absorption spectra of the phosphate buffered solution (pH 7.0, 10 mM) of rHSA(wt)−ZnPP showed a Soret band at 420 nm and the Q-bands at 547 and 585 nm (Figure 1A), which are very similar to those for the toluene solution of Zn(II)−protoporphyrin IX dimethylester (ZnPPDME) with 5 vol % ethanol (Figure 1B). The aqueous rHSA(His)−ZnPP solution exhibited the same spectral features of ZnPPDME-coordinated 1-methylimidazole (1-MIm) in toluene. The bandwidth at half-height of the Soret band [$\Delta\lambda_{1/2}$ = 21 nm for rHSA(wt)−ZnPP or 19 nm for rHSA(His)−ZnPP] was identical to that observed

(6) Wardell, M.; Wang, Z.; Ho, J. X.; Robert, J.; Ruker, F.; Rubel, J.; Carter, D. C. *Biochem. Biophys. Res. Commun.* **2002**, *291*, 813−819.
(7) Zunszain, P. A.; Ghuman, J.; Komatsu, T.; Tsuchida, E.; Curry, S. *BMC Struct. Biol.* **2003**, *3*, 6.
(8) (a) Komatsu, T.; Ohmichi, N.; Zunszain, P. A.; Curry, S.; Tsuchida, E. *J. Am. Chem. Soc.* **2004**, *126*, 14304−14305. (b) Komatsu, T.; Ohmichi, N.; Nakagawa, A.; Zunszain, P. A.; Curry, S.; Tsuchida, E. *J. Am. Chem. Soc.* **2005**, *127*, 15933−15942.

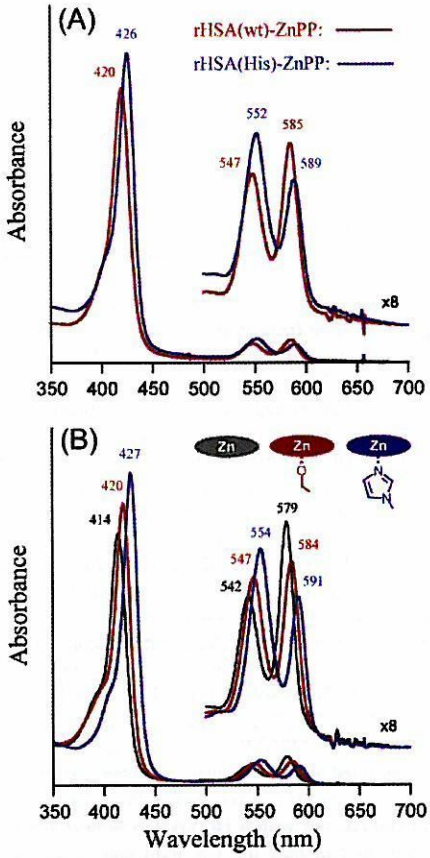

Figure 1. (A) UV−vis absorption spectra of rHSA(wt)−ZnPP and rHSA-(His)−ZnPP (10 μM) in potassium phosphate buffered solution (pH 7.0, 10 mM) at 25 °C. (B) UV−vis absorption spectra of ZnPPDME (10 μM) in toluene solution with EtOH (5 vol %) or 1-methylimidazole (5 mM) at 25 °C.

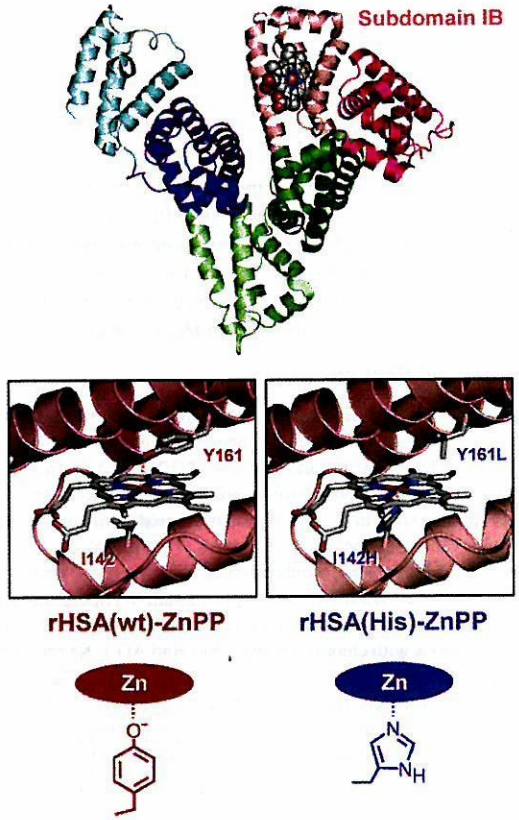

Figure 2. Structure models of rHSA complexed with ZnPP in subdomain IB (light red area).[9] In rHSA(wt), Tyr-161 axially coordinates to the central zinc ion of ZnPP. In rHSA(His), His-142 coordinates to the central zinc of ZnPP.

in the toluene solution. Since inhomogeneities of the porphyrin binding to rHSA would lead to a broadening of all the absorption spectra, the observed sharp and intense absorption bands of rHSA−ZnPP are consistent with a single binding site for the porphyrin chromophore. In fact, prosthetic heme groups in natural hemoproteins mostly show sharp absorption spectra. The fluorescence spectroscopy of rHSA(wt)−ZnPP and rHSA(His)−ZnPP also gave the same pattern of ZnPPDME with EtOH and 1-MIm, respectively (Figure S1). All these results imply that ZnPP is bound in subdomain IB of rHSA(wt) by the axial coordination of Tyr-161 and in rHSA(His) by the His-142 coordination (Figure 2). It is noteworthy that ZnPP can be monomolecularly dissolved in water at pH 5−8 by complexing it with rHSA at concentrations up to 3 mM.

The transient absorption spectrum of the degassed solution of rHSA(wt)−ZnPP upon laser flash photolysis at 532 nm showed the typical triplet−triplet (T−T) absorption of ZnPP (λ_{max} = 457, 673, 746 nm) (Figure S2).[10] The time course of the absorbance decay followed a single exponential kinetics with a triplet lifetime (τ_T) of 11 ms (Figure S3), which is considerably longer than that of $ZnTMPyP^{4+}$ (0.81 ms).[2a] The decay profile of the photoexcited ZnPP triplet is independent of the rHSA-(wt)−ZnPP concentration. In general, the triplet kinetics of a metalloporphyrin solution at a comparable concentration is dominated by the bimolecular exchange process.[11] In our case, (i) the ZnPP chromophore is held in a fixed position within the heme pocket of rHSA with a proximal base coordination, and (ii) the surface potential of rHSA is always negative at the neutral pH region because of its low isoelectric point of 4.8. Thus, the shielding of ZnPP by the negatively charged protein matrix appears to prevent a direct encounter between the excited triplets, and thereby inhibits a bimolecular T−T annihilation process. The same behavior was observed in Zn-substituted myoglobin.[12,13] The τ_T of rHSA(His)−ZnPP (2.5 ms) was one-fourth of the value observed for rHSA(wt)−ZnPP; the Tyr-161 coordination is clearly better at promoting the triplet state compared to the proximal His-142.

Photoinduced Electron Transfer to MV^{2+}. We investigated the photoinduced electron transfer reaction from rHSA−ZnPP to the water-soluble cationic acceptor, MV^{2+}. The addition of MV^{2+} resulted in a significant decrease in the triplet lifetime of rHSA(wt)−ZnPP. The transient absorption spectrum at 100 ns after the laser flash photolysis showed the same pattern as that without MV^{2+} (Figure 3A), while the spectrum after 200

(9) The picture was produced on the basis of crystal structure coordinate of the rHSA(wt)−hemin (code: 1O9X, ref 7) using PyMOL. DeLano, W. L. *The PyMOL Molecular Graphics System*; DeLano Scientific: San Carlos, CA, 2006.

(10) Aono, S.; Nemoto, S.; Okura, I. *Bull. Chem. Soc. Jpn.* **1992**, *65*, 591−593.

(11) Pekkarinen, L.; Linschitz, H. *J. Am. Chem. Soc.* **1960**, *82*, 2407−2411.

(12) Tsukahara, K.; Asami, S.; Okada, M.; Sakurai, T. *Bull. Chem. Soc. Jpn.* **1994**, *67*, 421−431.

(13) Zemel, H.; Hoffman, B. M. *J. Am. Chem. Soc.* **1981**, *103*, 1192−1201.

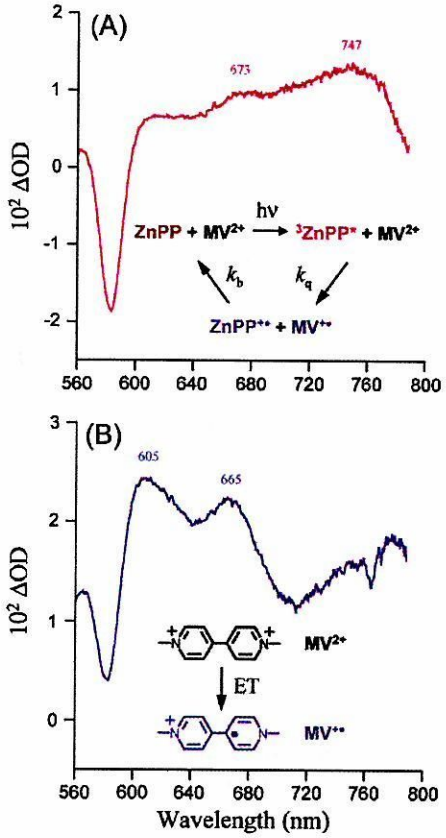

Figure 3. Transient absorption spectra of rHSA(wt)−ZnPP (10 μM) with MV^{2+} (1 mM) in phosphate buffered solution (pH 7.0, 10 mM) after the laser flash photolysis (λ = 532 nm) under argon atmosphere at 25 °C. (A) Spectrum after 100 ns, and (B) spectrum after 200 μs.

μs exhibited a very different shape with new peaks at 605 and 665 nm (Figure 3B). The intensity of these bands increased with the bleaching of the T−T absorption of ^{3}ZnPP*, indicating the oxidative quenching of rHSA(wt)−^{3}ZnPP* by MV^{2+}. The peak at 605 nm is characteristic of the one-electron-reduced MV^{2+} ($MV^{+\bullet}$), and the peak at 665 nm originates from the π-cation radicals of ZnPP ($ZnPP^{+\bullet}$).[1a,2,10,14] Concentration of MV^{2+} as high as 2 mM showed no influence on either the grand state absorption spectrum or the lifetime of the lowest-energy excited singlet state of rHSA(wt)−ZnPP (τ_S = 2.44 ns).[15] We conclude that there is no singlet reaction and that any observed photochemistry is attributed to the triplet pathway.

The triplet lifetime of rHSA(wt)−^{3}ZnPP* decreased linearly with the increasing MV^{2+} concentration to yield the Stern−Volmer constant (K_{SV}) of 1.5 × 10^5 M^{-1} (Figure 4).[16] The quenching rate constant (k_q) was determined to be 1.4 × 10^7 M^{-1} s^{-1}, indicating that it is almost diffusion controlled (Table 1). The charge-separated radical ions were reasonably long-lived and decayed via second-order kinetics. The rate constant of the thermal backward electron transfer (k_b) was 4.7 × 10^8 M^{-1} s^{-1}.[12] This can also be attributed to diffusional recombination. Similar kinetic parameters of rHSA(His)−ZnPP with MV^{2+}

(14) Liang, N.; Mauk, A. G.; Pielak, G. J.; Johnson, J. A.; Smith, M.; Hoffman, B. M. *Science* **1988**, *240*, 311−313.
(15) The τ_S of rHSA(wt)−ZnPP was 2.44 ns in the absence of MV^{2+} and 2.46 ns in the presence of 2 mM MV^{2+}.
(16) $\tau_T^0/\tau_T = K_{SV}[MV^{2+}]$ (τ_T^0 and τ_T represent triplet lifetimes in the absence and presence of MV^{2+}).

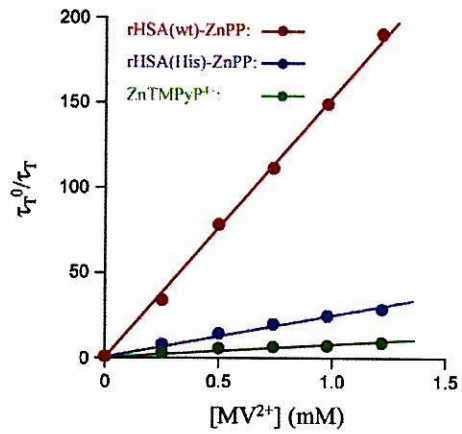

Figure 4. Stern−Volmer plots of triplet state quenching for rHSA−ZnPP (10 μM) with MV^{2+} in phosphate buffered solution (pH 7.0, 10 mM) at 25 °C.

Table 1. Rate Constants for Photoinduced Electron Transfer Reaction of rHSA−ZnPP to MV^{2+} in Phosphate Buffered Solution (pH 7.0, 10 mM) at 25 °C

Zn−porphyrin	k_q (M^{-1} s^{-1})	k_b (M^{-1} s^{-1})
rHSA(wt)−ZnPP	1.4 × 10^7	4.7 × 10^8
rHSA(His)−ZnPP	1.1 × 10^7	6.8 × 10^8
Zn−myoglobin[a]	2.7 × 10^7	4.0 × 10^7
$ZnTMPyP^{4+}$	9.3 × 10^6	9.8 × 10^8
	1.8 × 10^7 [b]	3.7 × 10^8 [b]
	2.0 × 10^6 [c]	

[a] From refs 10 and 12. [b] Ionic strength of the media was high (0.05); ref 2a. [c] From ref 1a.

imply the same mechanism of the quenching. Both the rHSA(wt)−ZnPP and rHSA(His)−ZnPP showed a higher k_q and lower k_b relative to $ZnTMPyP^{4+}$ under the same conditions (Table 1).

The probability of quenching the triplet state by a particular concentration of MV^{2+} (ϕ_q) is expressed as $k_q[MV^{2+}]/((\tau_T^0)^{-1} + k_q[MV^{2+}])$.[2a] Even in the case of 1 mM MV^{2+}, ϕ_q is nearly 1.0; the photoexcited rHSA(wt)−^{3}ZnPP* was almost completely quenched by MV^{2+}.

Upon steady-state light irradiation (550 ± 2 nm) of the phosphate buffered solution (pH 5.4, 50 mM) of rHSA(wt)−ZnPP (10 μM) in the presence of MV^{2+} (2 mM) and TEOA (0.19 M), the color of the solution turned blue due to the accumulation of the $MV^{+\bullet}$ (λ_{max} = 605 nm). The reaction mechanism involves the electron transfer from rHSA(wt)−^{3}ZnPP* to MV^{2+}, followed by the reduction of rHSA(wt)−$ZnPP^{+\bullet}$ by TEOA. The intensity of the Soret band did not diminish, indicating no photodegradation of the ZnPP sensitizer. This is in rather sharp contrast to the fact that ZnPPDME in toluene (10 μM) was bleached with a half-life of ca. 10 min under the same conditions. The solution of rHSA(wt)−ZnPP absorbed 8.9 × 10^{16} photons for the initial 60 s, and 5.3 × 10^{15} molecules of $MV^{+\bullet}$ were produced; the overall quantum efficiency was calculated to be 5.9% [rHSA(His)−ZnPP = 5.6%].

Hydrogen Evolution from Water. Reduced MV^{2+} is well-known to drive the reduction of water to H_2 in the presence of a colloidal Pt catalyst. It should be possible to exploit the rHSA−ZnPP sensitizer for the light-induced H_2 evolution from water (Scheme 1). Colloidal PVA−Pt (20 μM) was then coupled

Scheme 1. Diagram of Photoinduced Reduction of Water Using rHSA–ZnPP as Sensitizer in Conjunction of MV^{2+} as Electron Relay, TEOA as Sacrificial Reagent, and Colloidal PVA–Pt as Catalyst

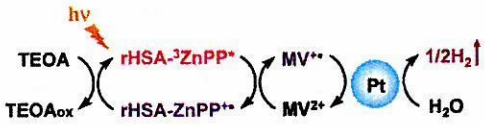

with the above phosphate buffered solution (pH 5.4, 50 mM) of the mixture consisting of rHSA(wt)–ZnPP (10 μM), MV^{2+} (2 mM), and TEOA (0.19 M). The coexistence of PVA–Pt and TEOA did not cause any λ_{max} shift in the UV–vis absorption of rHSA–ZnP, suggesting that the protein structure and the five-coordinate complex form of ZnPP in rHSA were unaltered. Upon exposure of this solution to a 450 W xenon arc lamp with an HA30 heat absorption filter (330–700 nm), the photogeneration of H_2 was observed without a decrease in activity during the experimental period (Figure 5). The volume of H_2 produced from a 3.5 mL solution of the complex following 6 h illumination with 57 turnovers was 0.044 mL. The rHSA(His)–ZnPP also exhibited an identical activity for the photosensitized reduction of water to H_2. We could not detect H_2 at the same experiments performed without the PVA–Pt catalyst or without TEOA. It is quite remarkable that the efficiency of the H_2 evolution using our rHSA–ZnPP is 25–30% greater than that of the system using $ZnTMPyP^{4+}$.

Conclusion

It is likely that the intense visible solar spectrum and long triplet lifetimes of rHSA(wt)–ZnPP and rHSA(His)–ZnPP are responsible for the excellent photoreduction of water to H_2 by these complexes. This astonishing result for the blood protein sensitizer including natural protoporphyrin IX will serve as a trigger to create a new field in artificial photosynthetic chemistry and innovative solar energy conversion. Currently, rHSA(wt) is manufactured in an industrial scale,[17] which allows us to use this zinc–protein photosensitizer in practical applications.

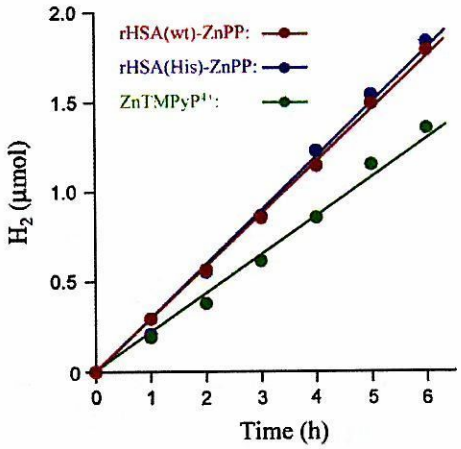

Figure 5. Time dependence of the H_2 production from water in the phosphate buffered solution (pH 5.4, 50 mM) of rHSA–ZnPP (10 μM), MV^{2+} (2 mM), TEOA (0.19 M), and colloidal PVA–Pt (20 μM) at 25 °C upon exposure to a 450 W xenon arc lamp with HA30 filter (330–700 nm).

Further research to optimize solute concentrations, catalyst preparation, and crystal structure analyses of the new rHSA–ZnPP series is now underway.

Acknowledgment. This work was supported by PRESTO, JST, Grant-in-Aid for Scientific Research from JSPS, and the Wellcome Trust (UK). The work at Imperial College London was partially carried out as the Japan–UK Research Cooperative Program (Joint Project) of JSPS.

Supporting Information Available: Fluorescence spectra, transient absorption spectra, and triplet absorption decay of rHSA(wt)–ZnPP and/or rHSA(His)–ZnPP. This material is available free of charge via the Internet at http://pubs.acs.org.

JA0656806

(17) Kobayashi, K. *Biologicals* **2006**, *34*, 55–59.

meso-Tetrakis(α,α,α,α-*o*-amidophenyl)porphinatoiron(II) Bearing a Proximal Histidyl Group at the β-Pyrrolic Position via an Acyl Bond: Synthesis and O_2 Coordination in Aqueous Media

Akito Nakagawa,[1] Teruyuki Komatsu,*[1,2] and Eishun Tsuchida*[1]
[1]*Advanced Research Institute for Science and Engineering, Waseda University, 3-4-1 Okubo, Shinjuku-ku, Tokyo 169-8555*
[2]*PRESTO, Japan Science and Technology Agency (JST)*

(Received February 16, 2007; CL-070182; E-mail: teruyuki@waseda.jp, eishun@waseda.jp)

meso-Tetrakis(α,α,α,α-*o*-(1-methylcyclohexanamido)phenyl)porphinatoiron(III) bearing a proximal histidyl group at the β-pyrrolic position via an acyl bond (**4c**) has been synthesized. Human serum albumin (HSA) incorporating the ferrous complex (**4d**) formed a stable O_2 adduct under physiological conditions (pH 7.4, 37 °C). Although an electron-withdrawing acyl group is attached to the porphyrin periphery, the O_2-binding affinity of HSA-**4d** was slightly higher than that of a similar analogue with a histidyl–alkylene group (**2d**).

In the active centers of hemoproteins, a basic amino acid residue, axially coordinated to the prosthetic heme group, namely the proximal base, plays a crucial role in controlling their biological functions, for example, histidine in hemoglobin (Hb) and cysteine in cytochrome P450. To mimic the versatile performances of the hemoproteins, numerous porphyrin derivatives have been synthesized over the past decades.[1,2] The most important factor in the molecular design of these compounds is how to confer the proximal base into the porphyrin structure by a covalent bond.

We successfully introduced a histidyl–alkylene group to the β-pyrrolic position of *meso*-tetrakis(α,α,α,α-*o*-(1-methylcyclohexanamido)phenyl)porphine (**1a**) using the Vilsmeier reaction.[3] Human serum albumin (HSA) incorporating the ferrous complex (**2d**) can reversibly bind and release O_2 under physiological conditions (pH 7.4, 37 °C) in a fashion similar to Hb and myoglobin.[3b] The advantage of this strategy is to confer the proximal histidine to the porphyrin periphery in the last step of the synthesis.[3,4] However, the preparation processes are still labor-intensive: (1) formylation of the porphyrin, followed by (2) demetallation of copper, (3) reduction of –CHO to $-CH_2OH$, (4) connection with glutaric acid, and (5) binding of terminal histidine.[3,4] If the axial base can be introduced into the superstructured porphyrin in a few steps, it will lead to creating a new field in the hemoprotein model chemistry.

In this communication, we report for the first time, the one-step introduction of the 4-carboxybutanoyl group into the β-pyrrolic position of *meso*-tetrakis(α,α,α,α-*o*-(1-methylcyclohexanamido)phenyl)porphyrin, which is easily converted into the hisitidine-linked porphyrin (**4a**) by other two processes. The O_2-binding property of the HSA hybrid incorporating the ferrous complex (**4d**) was then investigated in aqueous media.

The copper(II) complex of the parent porphyrin (**1b**) was synthesized according to our previously reported procedure.[3] We have found that the 4-carboxybutanoyl group is introduced by the Friedel–Crafts reaction using glutaric anhydride and aluminium chloride ($AlCl_3$) (Scheme 1). The progress of the reaction was monitored by the red shift of the absorption maxima

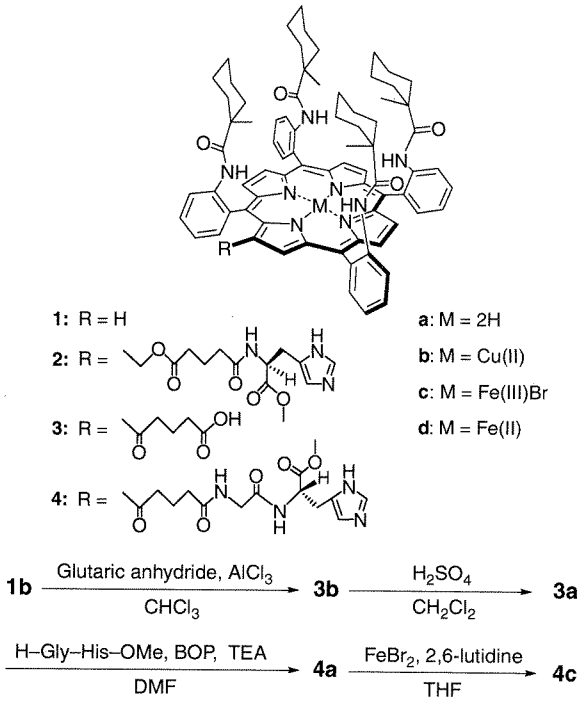

Scheme 1. Synthesis route of **4c**.

of the porphyrin and change in the R_f value during TLC. The brownish-red colored **3b** was purified by column chromatography and demetallated by H_2SO_4. The glycyl-*O*-methyl-L-histidine[5] was then coupled using benzotriazol-1-yl-oxytris(dimethylamino)phosphonium hexafluorophosphate (BOP). Finally, an iron insertion was carried out using $FeBr_2$ and 2,6-lutidine in anhydrous THF. The analytical data of all compounds described here were satisfactorily obtained (see Supporting Information).[6] The bathochromic shifts (3–7 nm) observed in the UV–vis absorption spectrum of **4a** compared to **2a** were due to the electron-withdrawing acyl group at the β-pyrrolic position.[6]

The ferric porphyrin (**4c**) in toluene was converted into the ferrous complex (**4d**) by reduction in a heterogeneous two-phase system (toluene/aq. $Na_2S_2O_4$) under an argon atmosphere.[4] The UV–vis absorption spectrum of the orange solution showed the formation of a five-N-coordinate high-spin complex (λ_{max}: 440, 544, 564 nm).[3,4,7] Upon exposure to O_2 or CO, the spectral pattern immediately changed to those of the O_2 adduct complex (λ_{max}: 429, 551 nm) or carbonyl complex (λ_{max}: 429, 544 nm).

The aqueous solution of the HSA-**4d** hybrid [in phosphate-buffered saline (PBS) solution (pH 7.4), [HSA]/[**4d**] = 1/4

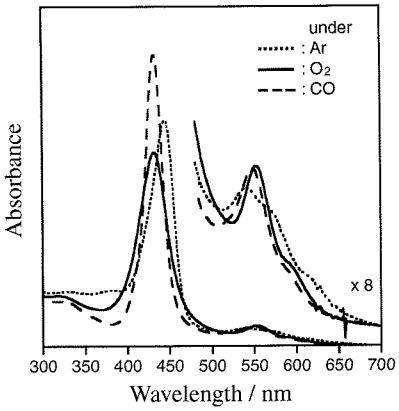

Figure 1. UV–vis absorption spectral changes of HSA-**4d** in PBS solution (pH 7.4) at 37 °C.

Table 1. O_2 binding parameters of HSA-porphinatoiron(II) in PBS solution (pH 7.4) at 25 °C[a]

Porphinatoiron(II)	$P_{1/2}$ /Torr	$k_{on}/\mu M^{-1}\,s^{-1}$		k_{off}/s^{-1}	
		fast	slow	fast	slow
2d[b]	1 (3)	54	8.8	89	14
4d	0.8 (2)	34	4.5	45	5.9

[a]The values in parenthesis are measured at 37 °C. [b]Ref 3b.

(mol/mol)] was prepared by a previously reported method.[3b] The UV–vis absorption spectrum of this aqueous solution under an argon atmosphere showed that **4d** formed a five-N-coordinate high-spin complex with an intramolecularly coordinated axial histidine (Figure 1). Upon exposure of HSA-**4d** to O_2, the absorption spectrum changed to that of the O_2 adduct complex. After reacting with the CO gas, a stable carbonyl complex was produced. The absorption maxima of HSA-**4d** showed 1–3 nm bathochromic shifts compared to those of the HSA-**2d** (Table S1).[3b,6]

The O_2-binding affinity of HSA-**4d** ($P_{1/2}$ = 0.8 Torr) determined by the spectral changes at the different O_2 partial pressures was slightly higher than that of HSA-**2d** (Table 1). This is in significant contrast to the fact that the substitutions of two 3,8-vinyl groups of the imidazole-bound protoporphinatoiron(II) by acetyl groups decreased the O_2-binding affinity by 1/4–1/6 due to the reduction of the electron density in the porphyrin plane.[8,9] Our result suggested that (1) the reduced basicity of the porphyrin core by the introduction of one acyl group did not influence the O_2-binding equilibrium very much, and (2) that there is another structural factor that increases the O_2-binding affinity of the porphyrin.

To determine the association and dissociation rate constants for O_2 (k_{on}, k_{off}) to HSA-**4d**, the laser flash photolysis experiments were carried out.[3b,10,11] The absorption decay accompanying the O_2 recombination was composed of two phases of first-order kinetics, producing the fast and slow rebinding constants [k_{on}(fast) and k_{on}(slow)]. The k_{on}(fast) value was 7.6-fold higher than k_{on}(slow), and the molar concentration ratio of the two reactions was 3:1. The O_2 association to **4d** in the protein scaffold might be influenced by the microenvironment around the coordination site. This behavior was similarly observed in HSA-**2d**.[3b] The characteristics of the O_2 binding to **4d** was kinetically the low k_{off} values (approximately 1/2) compared to **2d**.

The structures of the ferrous complexes were then simulated.[12] It is remarkable that the porphyrin plane of **2d** in the five-coordinate high-spin complex was significantly domed compared to that of **4d** (Figure S1).[6] On the other hand, their O_2 adduct complexes showed similar structures having the flat porphyrin macrocycles. The difference in the five-coordinate species could be caused by the spacer moiety between the histidine and porphyrin. The rigid (histidyl-glycyl)carbonylbutanoyl group of **4d** presumably produces a favorable geometry to fix the proximal imidazole at the central iron(II) of the porphyrin, which could result in the relatively low dissociation rate constant of O_2.

In conclusion, we could successfully introduce the proximal histidyl group at the β-pyrrolic position of the *meso*-(tetrakis-*o*-amidophenyl)porphine via an acyl bond in two steps. The O_2 binding affinity was slightly higher than that of the imidazolyl–alkylene analogue, which might be due to the rigid structure of the spacer moiety between the histidine and porphyrin ring. This strategy would be useful to confer the proximal base to the superstructured porphyrin without any change in the activity, which allows us to create a new class of model heme compounds.

This work was supported by a Grant-in-Aid for Young Scientists (B) (No. 18750156) and for Scientific Research (No. 16350093) from JSPS, PRESTO from JST, and Health Science Research Grants from MHLW, Japan.

References and Notes

1 M. Momenteau, C. A. Reed, *Chem. Rev.* **1994**, *94*, 659, and references therein.
2 a) J. P. Collman, L. Fu, *Acc. Chem. Res.* **1999**, *32*, 455. b) J. P. Collman, R. Boulatov, C. J. Sunderland, *Chem. Rev.* **2004**, *104*, 561.
3 a) T. Komatsu, Y. Matsukawa, K. Miyatake, E. Tsuchida, *Chem. Lett.* **2001**, 668. b) T. Komatsu, Y. Matsukawa, E. Tsuchida, *Bioconjugate Chem.* **2002**, *13*, 397.
4 E. Tsuchida, T. Komatsu, S. Kumamoto, K. Ando, H. Nishide, *J. Chem. Soc., Perkin Trans. 2* **1995**, 747.
5 E. Monzani, L. Linati, L. Casella, L. D. Gioia, M. Favretto, M. Gullotti, F. Chillemi, *Inorg. Chem. Acta* **1998**, *273*, 339.
6 Supporting Information is available electronically on the CSJ-Journal Web site, http://www.csj.jp/journals/chem-lett/index.html.
7 J. P. Collman, J. I. Brauman, T. J. Collins, B. L. Iverson, G. Lang, R. B. Pettman, J. L. Sessler, M. A. Walters, *J. Am. Chem. Soc.* **1983**, *105*, 3038.
8 A. Nakagawa, N. Ohmichi, T. Komatsu, E. Tsuchida, *Org. Biomol. Chem.* **2004**, *2*, 3108.
9 T. G. Traylor, D. K. White, D. H. Campbell, A. P. Berzinis, *J. Am. Chem. Soc.* **1981**, *103*, 4932.
10 J. P. Collman, J. I. Brauman, B. L. Iverson, J. L. Sessler, R. M. Morris, Q. H. Gibson, *J. Am. Chem. Soc.* **1983**, *105*, 3052.
11 T. G. Traylor, S. Tsuchiya, D. Campbell, M. Mitchell, D. Stynes, N. Koga, *J. Am. Chem. Soc.* **1985**, *107*, 604.
12 The esff forcefield simulation was performed using an Insight II system (Molecular Simulation Inc.). The structure was generated by alternative minimizations and annealing dynamic calculations from 1000 to 100 K.

Published on the web (Advance View) April 14, 2007; doi:10.1246/cl.2007.640

Induced Long-Range Attractive Potentials of Human Serum Albumin by Ligand Binding

Takaaki Sato,[1,2,*] Teruyuki Komatsu,[2,3] Akito Nakagawa,[2] and Eishun Tsuchida[2,†]

[1]*Division of Pure and Applied Physics, Faculty of Science and Engineering, Waseda University, 3-4-1 Okubo, Shinjuku-ku, Tokyo 169-8555, Japan*

[2]*Advanced Research Institute for Science and Engineering, Waseda University, 3-4-1 Okubo, Shinjuku-ku, Tokyo 169-8555, Japan*

[3]*PRESTO, Japan Science and Technology Agency (JST), 4-1-8 Honcho, Kawaguchi-shi, Saitama 332-0012, Japan*

(Received 9 July 2006; published 15 May 2007)

Small-angle x-ray scattering and dielectric spectroscopy investigation on the solutions of recombinant human serum albumin and its heme hybrid revealed that heme incorporation induces a specific long-range attractive potential between protein molecules. This is evidenced by the enhanced forward intensity upon heme binding, despite no hindrance to rotatory Brownian motion, unbiased colloid osmotic pressure, and discontiguous nearest-neighbor distance, confirming monodispersity of the proteins. The heme-induced potential may play a trigger role in recognition of the ligand-filled human serum albumins in the circulatory system.

DOI: 10.1103/PhysRevLett.98.208101 PACS numbers: 87.14.Ee, 61.10.Eq, 83.80.Lz

Human serum albumin (HSA) is the most abundant plasma protein in our bloodstream, whose primary functions are transportation of hydrophobic molecules and adjustment of colloid osmotic pressure (COP) of blood [1]. Owing to its nonspecific ligand-binding capability, HSA has served many potential medical applications. Information on HSA-ligand interactions and their structural basis have recently been available by x-ray crystal structure analysis [2–5]. Such approaches have provided a structural foundation to create functional protein-ligand complexes. One of the promising materials is the rHSA-heme hybrid that can transport oxygen as hemoglobin does [6–9]. The material is currently investigated in preclinical tests as an artificial blood substitute [8]. Recent manifold interests in protein crystallography, critical phenomena, and disease processes have attracted increasing attention to interparticle interactions in globular protein solutions [10–15]. However, the fundamental problems like an influence of the ligand-binding upon protein-protein interactions remain elusive.

We investigated solutions of recombinant HSA (rHSA) (MW 66.5 kDa) and its heme hybrid [rHSA-heme; rHSA incorporating four iron-porphyrins (synthetic hemes)] [7]. Using small-angle x-ray scattering (SAXS), we scrutinized spatial correlations of these proteins in a 0.15M phosphate buffer saline (PBS) solution to fulfil ionic strength and pH close to physiological conditions and those in water to minimize ionic strength. The PBS solution of rHSA-heme (heme/rHSA = 4, mol/mol) was prepared according to our previously reported procedures [7]. The deionization of the protein sample was performed by several cycles of centrifugation/dilution with pure water using a Millipore Amicon Ultra to give aqueous solution of rHSA-heme. The solutions were passed through a 0.22 μm filter before all measurements. The deep red-colored, transparent solution of rHSA-heme can long be stored without precipitation or liquid-liquid phase separation. It has been confirmed that isoelectric point (pI), solution viscosity, and COP for rHSA-heme under the physiological environment are identical to those of rHSA.

All SAXS experiments were carried out by using a SAXSess camera (Anton Paar) in the q range of 0.072–5 nm^{-1}. A model-independent collimation-correction procedure was made via an indirect Fourier transformation (IFT) routine and/or based on a Lake algorithm. We also performed dielectric relaxation spectroscopy (DRS) experiments on aqueous rHSA and rHSA-heme solutions in the frequency range of $0.0005 \leq \nu/\mathrm{GHz} \leq 20$ using time domain reflectometry [16].

Figure 1 shows SAXS experiments on a concentration series of rHSA in PBS solution at 25 °C. The normalized scattered intensities $I(q)/c$, where $I(q)$ is the scattered intensity at scattering vector q and c the protein concentration, exhibit a decreasing forward intensity $I(q \to 0)/c$ with increasing c [Fig. 1(a)]. HSA carries a net negative charge of about 18 electronic charges at pH 7.4 [1]. Since the long-range electrostatic repulsion between rHSAs is efficiently screened in the PBS solutions, the suppressed forward intensity is mainly attributed to the decreased osmotic compressibility due to the increased particle number density. Lowering c results in the convergence of $I(q)/c$ to the intrinsic form factor $P(q)$ of rHSA, achieving the structure factor $S(q) \sim 1 (c \to 0)$.

The pair-distance distribution functions $p(r)$ of rHSA [Fig. 1(b)] in solution are obtained using generalized indirect Fourier transformation (GIFT) technique [17], for which we approximated $S(q)$ assuming a Yukawa potential and the Rogers-Young closure. The procedure confirms the existence of oblatelike particles having the maximum diameter of $D_{\max} \sim 8.0$–8.5 nm at all c. All features of $p(r)$ highly resemble those calculated from x-ray crystallography data on HSA (Protein Data Bank code 1UOR) [3].

Figure 2(a) presents variation of $I(q)$ of rHSA solutions, depending on the presence and absence of the heme incorporation and ionic strength of solvents. The more pronounced decrease of the forward intensity and the sig-

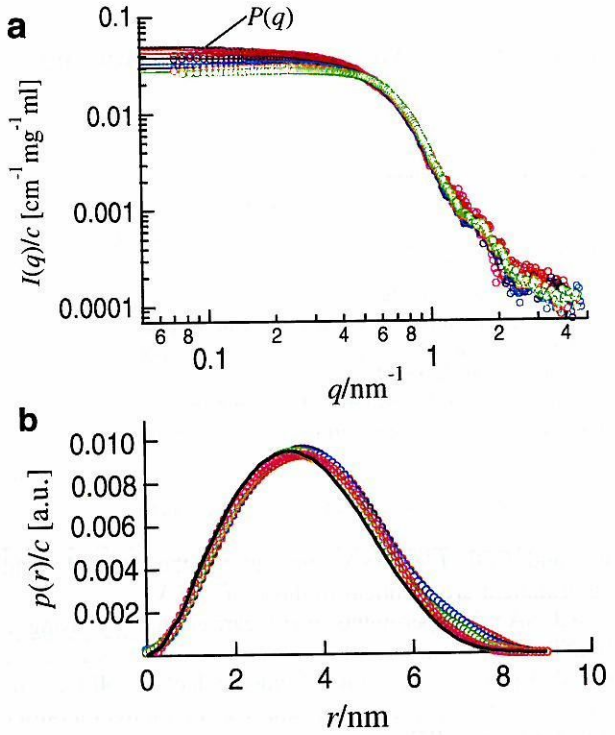

FIG. 1 (color online). (a) The normalized x-ray scattered intensities, $I(q)/c$, and (b) the pair-distance distribution functions, $p(r)$, of rHSA in 0.15M PBS solutions in $3.0 \leq c/\mathrm{mg\,ml^{-1}} \leq 50$. The black solid curve shown in (b) represents $p(r)$ calculated from the crystallography data on HSA [3].

nificant low-q shift of the monomer-monomer correlation peak position for aqueous rHSA reflect the only weakly screened, thus stronger electrostatic repulsions between the rHSA molecules. Importantly, we observed that heme-incorporated samples exhibit an enhanced forward intensity, which indicates that heme incorporation significantly enhances particle density fluctuations on a large length scale.

Further insights into the spatial correlations between the proteins are gained from the effective structure factors $S^{\mathrm{eff}}(q)$ [11] [Fig. 2(b)]. We extracted $S^{\mathrm{eff}}(q)$ by dividing $I(q)/c$ by $P(q)$ obtained from a dilute rHSA PBS solution. We confirmed that for rHSA-heme, lowering c from 10 to 3.5 mg ml^{-1}, leads to a significantly weaker relative low-q intensity, $I(q)/c$, as shown in Fig. 2. In terms of $S^{\mathrm{eff}}(q)$, rHSA under physiological condition still preserves the nature of a repulsively interacting charged colloid but behaves nearly as a hard sphere. If we apply a Yukawa potential model to $S^{\mathrm{eff}}(q)$ with *a priori* input of the solvent ionic strength, the effective protein charge of 18 ± 2 is obtained, being consistent with Ref. [1]. Solutions of rHSA-heme exhibit a similar low-q upturn in $S^{\mathrm{eff}}(q)$, independent of ionic strength. The observation suggests the emergence of a long-range attractive interaction [12,13] between the heme-incorporated rHSA molecules. However, this assignment is only valid when the monodispersity assumption of the protein is fulfilled. In the following, we carefully verify this interpretation, providing convincing evidence for monodispersity of rHSA-heme.

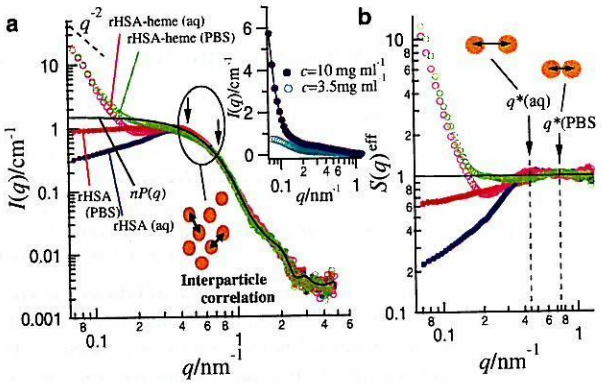

FIG. 2 (color online). (a) Variation of $I(q)$ and (b) the effective structure factors $S^{\mathrm{eff}}(q)$ for rHSA and rHSA-heme in aqueous and 0.15M PBS solutions of a fixed concentration $c = 30\ \mathrm{mg\,ml^{-1}}$. In the inset, the low-$q$ intensities for $c = 3.5\ \mathrm{mg\,ml^{-1}}$ and $c = 10\ \mathrm{mg\,ml^{-1}}$ are compared. Arrows on $S^{\mathrm{eff}}(q)$ highlight the monomer-monomer correlation peak positions q^*.

The peak in $S^{\mathrm{eff}}(q)$ arises from protein-protein positional correlations [Fig. 2(b)]. The mean nearest-neighbor distance d^* among the proteins is approximated as $\sim 2\pi/q^*$, where q^* is the scattering vector corresponding to the peak position of $S^{\mathrm{eff}}(q)$. Importantly, q^* is essentially independent before and after heme binding, but it simply depends on the solvent ionic strength related to the screening of the long-range electrostatic repulsion. In Fig. 3, we display a concentration series of $S^{\mathrm{eff}}(q)$ for rHSA and rHSA-heme solutions at different ionic strength. For aqueous rHSA and rHSA-heme, increasing c shifts q^* to higher values, holding a relation $q^* \propto n^{1/3}$ [Fig. 3(e)], where n is the particle number density. The finding clearly shows that both aqueous rHSA and rHSA-heme exhibit a typical feature of charged colloids at low ionic strength, maximizing d^*.

The identical COP (18 mmHg at $c = 50\ \mathrm{mg\,ml^{-1}}$) between the solutions of rHSA-heme and rHSA despite a half value for covalently dimerized rHSA at the same volume fraction [6] also rules out irreversible aggregate formation in rHSA-heme solutions. A simple model calculation demonstrates that a compact aggregate having several tens of aggregation number can never explain the observed low-q feature. No further enhancement of the low-q rise upon screening of the electrostatic repulsion excludes a strong short-range attraction as its origin.

Figure 4 presents complex dielectric spectra of rHSA and rHSA-heme solutions at various c. The relaxation time $\tau_{\mathrm{water}} \sim 8.3$ ps for the high-frequency process common for all solutions reflects the time scale of cooperative rearrangement of the hydrogen-bond network of bulk water [16,18,19]. Besides, the low-frequency relaxation, as-

signed to the rotational diffusion of the proteins [19,20], gives an excellent measure of dimer or higher aggregate formation. The identical relaxation times before and after heme binding, $\tau_{\mathrm{rHSA}} \sim 52$–$58$ ns, provides identical effective molar volume for rHSA and rHSA-heme, $V^{\mathrm{eff}} = 4.7 \times 10^4\ \mathrm{cm^3\,mol^{-1}}$ $(c \to 0)$, according to the Stokes-Einstein-Debye equation, which is very close to the anticipated value of $4.9 \times 10^4\ \mathrm{cm^3\,mol^{-1}}$ from the molecular mass and specific volume of HSA. This reveals that the freedom of the rotational diffusive motion of the protein is not significantly affected by the heme incorporation.

We point out that in contrast to HSA, well-investigated aqueous lysozyme solutions [11–14,21,22] are already in aggregation regime; even at very low ionic strength, most of lysozyme molecules stick together due to its highly adhesive nature, which is demonstrated by the appearance of the low-q subpeak in $S^{\mathrm{eff}}(q)$ and d^* coinciding with the diameter of the protein molecule. Although there arose a controversy as to whether the low-q rise for lysozyme solutions is due to a long-range attraction (LRA) [13,21] or large aggregate formation [22], as for rHSA-heme, the simultaneous observations of the low-q rise in $S^{\mathrm{eff}}(q)$ with a host of evidence for monodispersity of the protein, such as d^* far exceeding the contact distance, no additional frictional force on the rotational diffusive motions, identical molecular volume with rHSA, and unbiased COP, provide a plausible argument for the emergence of a LRA. Note that any kind of protein aggregation requires the direct contact between the monomers. Generally, when the repulsion is so strong as to make the particles apart, the low-q rise can be explained only by a LRA [12].

The theoretical $S(q)$ analysis based on a two Yukawa potential model [13] has shown that the relatively longer attraction range than the repulsion one is necessary to produce the so-called zero-q peak in $S(q)$. The more pronounced low-q decrease in $S^{\mathrm{eff}}(q)$ for aqueous rHSA is clearly taken over by the deeper dip in $S^{\mathrm{eff}}(q)$ for aqueous rHSA-heme, which indicates that the electrostatic repulsion is still active in rHSA-heme solutions and the attraction range is greater than the range of the weakly screened electrostatic repulsion.

For further quantitative description, we tested a two Yukawa model [12,13] for $S^{\mathrm{eff}}(q)$ of rHSA-heme. When the attraction range is very long, the model produces a downward convex low-q rise and a huge zero-q intensity reaching more than $\sim$1000 even at small c. However, $S(q)$ starts to rise at $q \leq 0.1\ \mathrm{nm^{-1}}$, whereas we observed the onset around $q = 0.2\ \mathrm{nm^{-1}}$. The real expression for a LRA and its potential shape are still not very clear, but the formalism of the potential should significantly affect the low-q shape of $S(q)$. If the system exhibits more slowly decaying attractive potential than the Yukawa decay at small-r, the onset of the low-q rise is expected to shift to higher-q values than that predicted by the Yukawa LRA model.

It is important to recognize that isotropic interaction is not self-evident for any kind of protein system because proteins have irregular shape and inhomogeneously distributed patches by nature. However, until now, almost all experimental and theoretical works on the interactions proteins have been performed based on mean spherical approximation (MSA) and an isotropic interaction assumption [10–15,23]. The recent theoretical work of Bianchi *et al.* [24] revealed that particles interacting with an anisotropic attractive potential can enhance anomalous density fluctuations or gel-network formation even at very low volume fractions. This also implies that anisotropic potentials caused by a site-specific interaction or inhomogeneous distributions of charge or hydrophobic patches may generate unexpectedly drastic effects on the spatial correlations of proteins, where the inherent limitation of small-angle scattering technique lies in the fact that such anisotropic interactions are reduced into one-dimensional $S(q)$. Nevertheless, carefully confirmed monodispersity of rHSA-heme leads us to conclude that our present interpretation based on a LRA is still broadly correct, even if the actual situation is much more complicated, where anisotropic interactions may affect the spatial correlation of the proteins.

Compared to the well-developed short-range attraction and long-range electrostatic repulsion [11,13,23], the general understanding of a LRA of proteins in solution

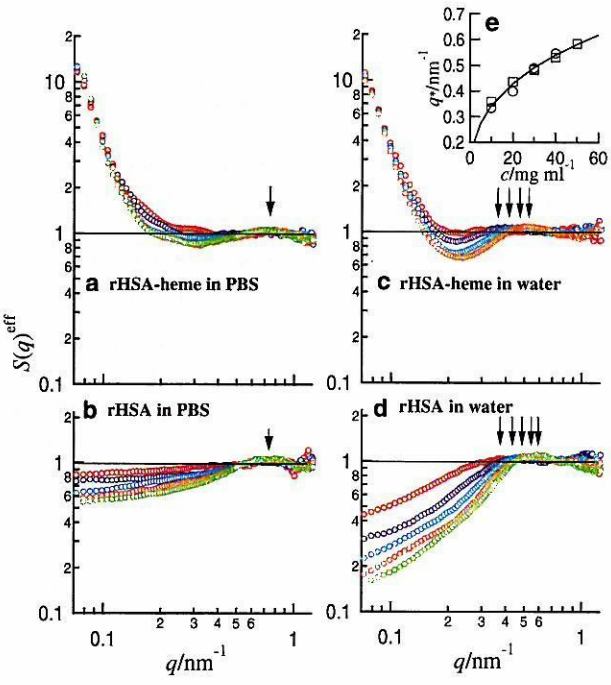

FIG. 3 (color online). Effects of concentration, ionic strength, and heme binding on $S^{\mathrm{eff}}(q)$. (a) rHSA-heme and (b) rHSA in 0.15M PBS solutions and (c) rHSA-heme and (d) rHSA in aqueous solutions in $10 \leq c/\mathrm{mg\,ml^{-1}} \leq 50$ (an increment of 10 mg ml^{-1}). (e) The protein-protein correlation peak position q^* in $S^{\mathrm{eff}}(q)$ for aqueous rHSA (□) and rHSA-heme (○) as a function of c.

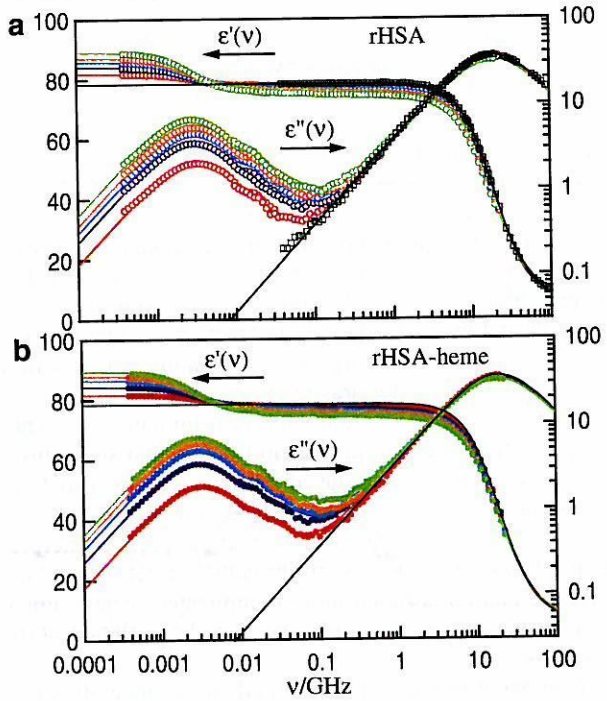

FIG. 4 (color online). Complex dielectric spectra of aqueous solutions of (a) rHSA and (b) rHSA-heme in $10 \leq c/\mathrm{mg\,ml^{-1}} \leq 50$ (an increment of 10 mg ml^{-1} from the bottom) at 25 °C.

[12,13,15] is at an incipient stage. Judging from unbiased $p\mathrm{I}(= 4.9)$ and polarization fluctuation amplitudes for rHSA-heme, net charges and their distributions are unlikely to be modified by heme binding, whereas how the occupation of the ligand-binding site allosterically affects the electrostatic interaction of the protein is unclear. The physical origin of a LRA might be entoropic driven, possibly due to modulated hydrophobic patches and their inhomogeneous distributions.

HSA binds heme; the rHSA-heme hybrid takes advantage of this naturally occurring process. In the human body, heme released from methemoglobin is immediately captured by hemopexin or HSA acting as scavengers, and it is efficiently transported to the liver for methabolism [25,26]. Since the emergence of the collective nature of HSAs while preserving the monodispersity could be an efficient way to give the ligand-filled HSA molecules a sort of marker, our data suggest that the heme-bound or -unbound HSAs may be recognized in the bloodstream in terms of the presence and absence of the LRA. Therefore, the optimization of the interparticle potential will be a key to the control of distribution, circulation persistence, and metabolism of functional ligands for medical applications.

This work was partly supported by MEXT, the Grant in Aid for Young Scientists (B) (No. 18740264), and by JSPS, the Grant in Aid for Scientific Research (B) (No. 16350093). T. S. acknowledges the 21st century COE program at Waseda University funded by MEXT. The authors appreciate the strong support of the late Professor Hironobu Kunieda for SAXS measurements and thank Professor Sow-Hsin Chen and Dr. Yun Liu for providing the MATLAB code for two Yukawa model [13].

*Email address: takaaki.sato@waseda.jp
†Email address: eishun@waseda.jp

[1] T. Peters, *All About Albumin: Biochemistry, Genetics, and Medical Applications* (Academic, New York, 1996).
[2] P. A. Zunszain *et al.*, BMC Struct. Biol. **3**, 6 (2003).
[3] X. M. He and D. C. Carter, Nature (London) **358**, 209 (1992).
[4] S. Curry *et al.*, Nat. Struct. Biol. **5**, 827 (1998).
[5] J. Ghuman *et al.*, J. Mol. Biol. **353**, 38 (2005).
[6] T. Komatsu *et al.*, Macromolecules **32**, 8388 (1999).
[7] T. Komatsu, Y. Matsukawa, and E. Tsuchida, Bioconjugate Chemistry **13**, 397 (2002).
[8] T. Komatsu *et al.*, J. Biomed. Mater. Res. **71A**, 644 (2004).
[9] T. Komatsu *et al.*, J. Am. Chem. Soc. **127**, 15 933 (2005).
[10] A. Tardieu *et al.*, J. Cryst. Growth **196**, 193 (1999).
[11] A. Stradner *et al.*, Nature (London) **432**, 492 (2004).
[12] Y. Liu *et al.*, Phys. Rev. Lett. **95**, 118102 (2005).
[13] Y. Liu, W. R. Chen, and S. H. Chen, J. Chem. Phys. **122**, 044507 (2005).
[14] M. Malfois, F. Bonnete, L. Belloni, and A. Tardieu, J. Chem. Phys. **105**, 3290 (1996).
[15] M. G. Noro, N. Kern, and D. Frenkel, Europhys. Lett. **48**, 332 (1999).
[16] T. Sato and R. Buchner, J. Phys. Chem. A **108**, 5007 (2004).
[17] G. Fritz, A. Bergmann, and O. Glatter, J. Chem. Phys. **113**, 9733 (2000).
[18] T. Fukasawa *et al.*, Phys. Rev. Lett. **95**, 197802 (2005).
[19] N. Nandi, K. Bhattacharyya, and B. Bagchi, Chem. Rev. **100**, 2013 (2000).
[20] Y. Hayashi *et al.*, Biophys. J. **79**, 1023 (2000).
[21] Y. Liu *et al.*, Phys. Rev. Lett. **96**, 219802 (2006).
[22] A. Stradner, F. Cardinaux, and P. Schurtenberger, Phys. Rev. Lett. **96**, 219801 (2006).
[23] F. Sciortino *et al.*, Phys. Rev. Lett. **93**, 055701 (2004).
[24] E. Bianchi *et al.*, Phys. Rev. Lett. **97**, 168301 (2006).
[25] V. Jeney, J. W. Eaton, and G. Balla *et al.*, Blood **100**, 879 (2002).
[26] E. Tolosano and F. Altruda, DNA and Cell Biology **21**, 297 (2002).

O_2-Binding Albumin Thin Films: Solid Membranes of Poly(ethylene glycol)-Conjugated Human Serum Albumin Incorporating Iron Porphyrin

Akito Nakagawa,[†] Teruyuki Komatsu,[†,‡,*] Yubin Huang,[†] Gang Lu,[†] and Eishun Tsuchida[†,*]

Research Institute for Science and Engineering, Waseda University, 3-4-1 Okubo, Shinjuku-ku, Tokyo 169-8555 Japan, and PRESTO, Japan Science and Technology Agency (JST), 4-1-8 Honcho, Kawaguchi-shi, Saitama 332-0012, Japan.
Received March 14, 2007; Revised Manuscript Received July 7, 2007

Poly(ethylene glycol) (PEG)-conjugated human serum albumin (HSA) incorporating the tetrakis(α,α,α,α-*o*-amidophenyl)porphinatoiron(II) derivative (FeP) [PEG(HSA−FeP)] is a unique plasma protein-based O_2 carrier as a red blood cell substitute. The aqueous solution of PEG(HSA−FeP) [mw of PEG: 2-kDa (PEG_2) or 5-kDa (PEG_5)] was evaporated on a glass surface to produce a red-colored solid membrane. Scanning electron microscopy observations revealed that the PEG_2(HSA−FeP) membrane consisted of two parts: (i) a surface layer made of a fibrous component (10 μm thickness), and (ii) a bottom layer of an amorphous phase (5 μm thickness). The condensed solution provided a thick membrane (70 μm), which also has the amorphous bottom layer. On the other hand, the PEG_5(HSA−FeP) produced homogeneous membrane made of the fibrous component. The FeP active sites in the solid membrane formed very stable O_2-adduct complexes at 37 °C with a half-lifetime of 40 h. The O_2-binding affinity of the PEG_2(HSA−FeP) membrane ($P_{1/2}$ = 40 Torr, 25 °C) was 4-fold lower than that in aqueous solution, which is kinetically due to the low association rate constant. The membrane was soluble again in water and organic solvents (ethanol and chloroform) without deformation of the secondary structure of the protein. The addition of hyaluronic acid gave a free-standing flexible thin film, and it can also bind and release O_2 as well. These O_2-carrying albumin membranes with a micrometer-thickness would be of significant medical importance for a variety of clinical treatments.

INTRODUCTION

Covalently surface-modified proteins with poly(ethylene glycol) (PEG) show a number of unique properties that make them of interest in a range of practical applications (*1*−*6*). The most beneficial effect of the PEG conjugation from a biological aspect is to confer a nonimmunogenicity to the proteins, rendering them invisible in the body (*7*−*10*). Several classes of protein drugs, such as enzymes and cytokines, have already been approved by the FDA (*4*, *5*), and one of the expected compounds is a PEG-conjugated hemoglobin (PEG-Hb) for use as artificial blood (*11*, *12*). The optimized product has completed a phase I trial and is currently undergoing a phase II safety study (*13*). Second, the PEG modification allows the proteins to be soluble in nonaqueous solvents (benzene, ethanol, and chloroform, etc.) (*14*−*16*). In organic solutions, the proteins exhibited new characteristics, for example, a high thermal stability and a different substrate selectivity. Third, the aqueous PEGylated proteins can be dried on a flat surface to produce solid membranes without any loss of their original activities. However, only limited characterization has been performed on the PEG-conjugated proteins in the solid state.

Recombinant human serum albumin (HSA) incorporating the tetrakis{α,α,α,α-*o*-(1-methylcyclohexanamido)phenyl}-porphinatoiron(II) derivative (FeP, Figure 1) (HSA−FeP) is a unique plasma protein-based O_2 carrier (*17*, *18*). This entirely synthetic hemoprotein can reversibly bind and release O_2 under physiological conditions (pH 7.4, 37 °C) in a fashion similar to Hb. It has also been demonstrated that the surface decoration of HSA−FeP by PEG improved its circulation persistence in the bloodstream (*19*). The PEG(HSA−FeP) is now the most promising material for an entirely synthetic red blood cell substitute.

We have recently found that the aqueous PEG(HSA−FeP) solution cast on the glass surface produces a very smooth solid membrane. The spectroscopic measurements revealed that a reversible O_2 binding to FeP took place in the red-colored membrane. We now report our new findings on the layered film structures of the PEG-conjugated artificial hemoprotein and their O_2-binding behavior.

EXPERIMENTAL PROCEDURES

Materials and Apparatus. All reagents were purchased from commercial sources as special grades and used without further purification. 2-{8-(2-Methylimidazolyl-1-yl)octanoyloxymethyl}-5,10,15,20-tetrakis{α,α,α,α-o-(1-methylcyclohexanamido)-phenyl}porphinatoiron(II) (FeP) was synthesized according to our previously reported procedures (*17*, *20*). Recombinant HSA was provided by the NIPRO Corp. (Osaka, Japan). 2-Iminothiolane hydrochloride (IMT) was purchased from Wako Pure Chemical Industries, Ltd. (Osaka, Japan). α-[3-(3-Maleimido-1-oxopropyl)amino]propyl-ω-methoxy PEG [averaged mw: 2333, Sunbright ME-020MA, PEG_2, and averaged mw: 5207, Sunbright MEMAL-50H, PEG_5) was purchased from the NOF Corp. (Tokyo, Japan). Hyaluronic acid sodium salt (HA, mw: 1.9−2.7 × 10^3 kDa) was a gift from Shiseido Co., Ltd. (Tokyo, Japan). The water was deionized using Millipore Elix and Simpli Lab-UV. The UV−vis absorption spectra were recorded using an Agilent 8453 UV−visible spectrophotometer fitted with an Agilent 89090A temperature control unit. The circular dichroism (CD) spectra were obtained using a JASCO J-820 spectropolarimeter over the range of 200−250 nm.

* Corresponding author. (E.T.) Tel: +81-3-5286-3120, fax: +81-3-3205-4740, e-mail: eishun@waseda.jp. (T.K.) E-mail: teruyuki@waseda.jp.
† Waseda University.
‡ Japan Science and Technology Agency.

10.1021/bc070086m CCC: $37.00
Published on Web 08/16/2007

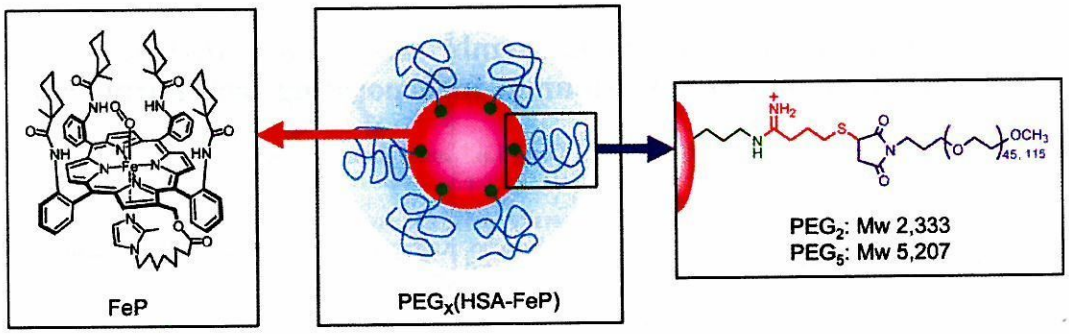

Figure 1. Structure of the PEG$_X$(HSA−FeP) molecule.

Preparation of PEG$_X$(HSA−FeP) Solid Membranes. The phosphate-buffered saline (PBS) solutions of PEG$_X$(HSA−FeP) (X = 2 or 5) were prepared with IMT and PEG$_X$ (pH 7.4, [HSA] = 5 wt %, FeP/HSA = 4/1 (mol/mol)) according to our previously reported methods (*19*). The binding number of the PEG$_X$ chain on the HSA−FeP surface was determined by the MALDI-TOF MS spectra (*19*). The PBS solution was dialyzed using a Spectra/Por 1 regenerated cellulose dialysis membrane (MWCO: 6−8 kDa, Spectrum Labratories, Inc.) against the pure water to remove any included electrolytes. The obtained aqueous solution of PEG$_X$(HSA−FeP) (CO adduct complex, 0.5 mL) was spread on a glass plate [30 × 40 mm, thickness: 0.12−0.17 mm, Matsunami Glass Ind., Ltd. (Osaka, Japan)] and evaporated at an ambient temperature in the dark for 12 h, which produced a red-colored transparent solid membrane.

For the scanning electron microscopy measurements, the samples on the glass plate were sputtered with Pd−Pt using a Hitachi E-1030 ion sputter. The SEM observations were performed using a Hitachi S-4500S field emitted scanning electron microscope.

Furthermore, 0.5 mL of an aqueous solution of hyaluronic acid (HA, 0.2, 0.4, 0.6, 0.8, 1.0 wt %) was added to the PEG$_2$-(HSA−FeP) solution (CO adduct complex, 0.5 mL, [HSA] = 5 wt %). The mixture was poured into a poly(styrene) balance dish (44 × 44 × 15 mm) and dried at room temperature in the dark. After 12 h, the formed membrane was gently peeled off and characterized.

The water content of the solid membrane was measured by thermogravimetric-differential thermal analysis using a Rigaku TG8120 instrument at a hearing rate of 10 °C/min.

O_2-Binding Parameters. The O_2 binding to PEG$_X$(HSA−FeP) is expressed by eq 1,

$$\text{PEG}_X(\text{HSA}-\text{FeP}) + \text{O}_2 \underset{k_{\text{off}}}{\overset{k_{\text{on}}}{\rightleftharpoons}} \text{PEG}_X(\text{HSA}-\text{FeP}(\text{O}_2)) \quad (1)$$

where the O_2 binding equilibrium constant $K = k_{on}/k_{off}$.

The PEG$_X$(HSA−FeP) membrane or PEG$_2$(HSA−FeP)/HA hybrid membrane on the glass plate was placed in a 1-cm quartz cuvette for the spectral measurements, which was sealed tightly with a rubber septa. The O_2-binding affinity (gaseous partial pressure at which 50% of FeP was dioxygenated, $P_{1/2} = 1/K$) was determined by the spectral changes at various O_2/N_2 pressures (*17*, *19*, *20*). The UV−vis absorption spectra were recorded within the range of 350−700 nm. The half-lifetime of the autooxidation of the FeP(O_2) complex was determined by the time-course of the absorption change at 426 nm. The association and dissociation rate constants for O_2 (k_{on}, k_{off}) to the PEG$_X$(HSA−FeP) membrane or PEG$_2$(HSA−FeP)/HA hybrid membrane were measured by a competitive rebinding technique using a Unisoku TSP-1000WK laser flash photolysis instrument (*17*, *19*, *20*).

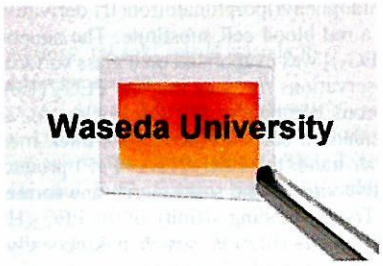

Figure 2. Photograph of the PEG$_2$(HSA−FeP) solid membrane on the glass plate.

RESULTS AND DISCUSSION

Structure of PEG$_X$(HSA−FeP) Membrane. The PEGylation of HSA−FeP (FeP/HSA = 4/1 (mol/mol)) was readily accomplished under mild conditions using the commercially available IMT and maleimide-terminated PEG (*19*). The average number of the PEG chain on the HSA−FeP surface was modulated to 6.0; the viscosity and colloid osmotic pressure of the PBS solution of this molecule ([HSA] = 5 wt %) satisfied the clinical requirements of a red blood cell substitute (*19*). The solution was subsequently desalted by dialysis against pure water and spread on the glass plate. After drying overnight at room temperature, a red-colored transparent solid membrane was formed (Figure 2). The HSA−FeP without the PEG modification did not produce such a homogeneous thin film, only affording a brittle membrane with many cracks.

Scanning electron microscopy observations of the PEG$_2$-(HSA−FeP) membrane showed a uniform thickness of 15 μm and a very smooth surface [Figure 3a,b)]. From a careful inspection of the side-view, we found that the membrane consists of two parts: (i) the surface layer with a thickness of 10 μm made of a highly oriented fibrous component, and (ii) the bottom layer with a thickness of 5 μm made of an amorphous phase (Figure 3b). Cutting the glass plate with a lateral force, the PEG$_2$-(HSA−FeP) membrane was extended and produced long fibers with a width of 350 nm (Figure 3c). The condensed solution ([HSA] = 15 wt %) provided a thick membrane with a thickness of 70 μm, which also has the amorphous bottom layer of 5 μm (Figure 3d). Interestingly, the membrane prepared on the poly-(styrene) dish was mainly composed of the amorphous layer; the surface fibrous phase was less than 20% (Figure 3e). On the other hand, water evaporation of the PEG$_5$(HSA−FeP) solution ([HSA] = 5 wt %) on the glass surface provided a homogeneous membrane, which is made of the fibrous component. The precise mechanism of the fiber formation during the water evaporation process is still not clear, but our results show that the structure of the PEG$_X$(HSA−FeP) membrane is very dependent on the surface feature of the substrate and the chain length of the PEG.

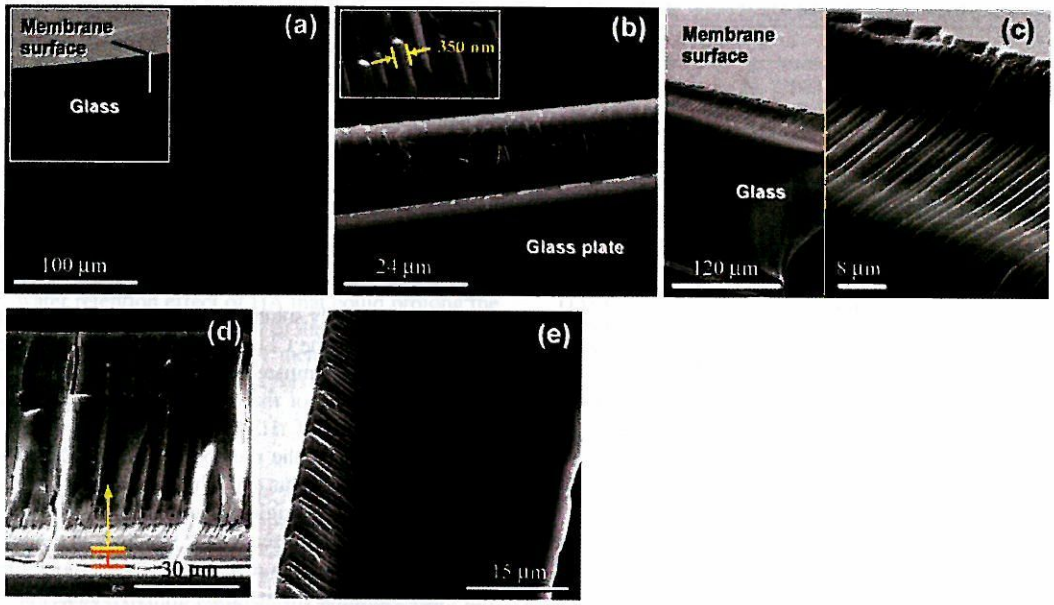

Figure 3. SEM images of the PEG_2(HSA−FeP) membrane on the glass plate. (a) Top-view of the very smooth surface without any crack. (b) Side-view of the membrane section, showing a surface layer made of fibrous component and a bottom layer made of an amorphous phase. (c) Extended nanofiber structure of the surface layer. (d) Thick membrane with a 5 μm amorphous bottom layer (indicated by orange bars) on the glass surface. (e) Membrane prepared on the poly(styrene) surface.

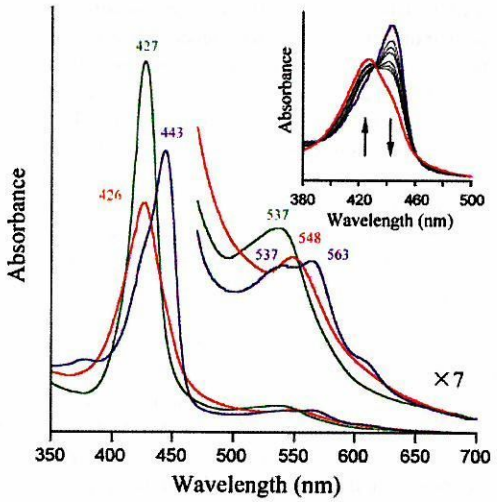

Figure 4. UV−vis absorption spectral changes of the PEG_2(HSA−FeP) membrane on the glass plate at 25 °C (blue line: under N_2, red line: under O_2, green line: under CO). The inset shows the spectral changes at various O_2-partial pressures (P_{O_2}: 0, 10, 19, 30, 76, 114, 152, 760 Torr from blue to red line).

O_2-Binding Properties. The UV−vis absorption spectrum of the PEG_X(HSA−FeP) membrane showed an absorption maxima (λ_{max}) at 427 and 537 nm, indicating the formation of the CO-coordinate low-spin state of FeP (Figure 4) (*17, 19*−21). This suggested that the ferrous carbonyl complex was retained during the water evaporation for 12 h at an ambient temperature. Light irradiation to the membrane using a 500-W halogen lamp under a 100% O_2 for 20 min led to the CO dissociation and O_2-adduct complex formation of FeP (λ_{max}: 426, 548 nm). By flowing N_2 to the membrane in the quartz cuvette, the UV−vis absorption spectrum shifted to that of a high-spin ferrous complex with an intramolecularly coordinated 2-methylimidazolyl group (λ_{max}: 443, 537, 563 nm). These spectral changes were repeatedly observed and found dependent on the O_2-partial pressure (0 Torr ↔ 760 Torr), which demonstrated that the reversible dioxygenation of FeP took place in the membrane. The half-lifetime of the autoxidation ($\tau_{1/2}$) of the FeP(O_2) to Fe^{3+}P was 40 h at 37 °C, which is 3-fold longer than the value in the PBS solution.

The O_2-binding affinity of the PEG_2(HSA−FeP) membrane ($P_{1/2}$ = 40 Torr, 25 °C) determined from the UV−vis absorption spectral changes at various O_2/N_2 pressures (Figure 4 inset) was 4-fold lower (high $P_{1/2}$) than that of the monomeric PEG_2(HSA−FeP) in water (Table 1). Since the O_2 coordination to the Fe porphyrin is an exothermic reaction, the O_2-binding affinity of the membrane decreased at 37 °C ($P_{1/2}$ = 61 Torr). In contrast, PEG_5(HSA−FeP) membrane showed the identical O_2-bidnig affinity to that in aqueous PBS solution ($P_{1/2}$ = 11 Torr, 25 °C).

In order to elucidate the O_2-binding kinetics of the PEG_X-(HSA−FeP) membrane, flash photolysis experiments were carried out. The time course of the absorption change after the laser pulse irradiation to the PEG_2(HSA−FeP) membrane in the quartz cuvette exhibited two first-order kinetics. We previously reported that the binding processes of O_2 to HSA−FeP and PEG_X(HSA−FeP) in aqueous media were fitted to a double-exponential expression, giving two different association rate constants for the fast and slow reactions (k_{on} and k'_{on}) (*19, 22*). It has been interpreted that the O_2 recombination to FeP in the protein could be affected by the each nanoscopic environment around the accommodation site, for example, a steric hindrance of the amino acid residue and difference in polarity. The k'_{on} was used to be approximately one-third of the k_{on} (*17, 19, 22*). Nevertheless, the ratio of k'_{on}/k_{on} observed in the PEG_2-(HSA−FeP) membrane was less than one-tenth (Table 1). We then theorized that this can be attributed to the O_2 diffusion in the two parts of the membrane. In the major surface layer of the fibrous component, the diffusion of the O_2 could be slower than in water, and it could be much slower in the amorphous bottom phase. The following results support our assumption. (i) The thickness ratio of the two layers (10 μm/5 μm = 2.0) corresponds well to the molar ratio of the k_{on} and k'_{on} (= 2.1). (ii) The absorption decay accompanied with the O_2 rebinding

Table 1. O_2-Binding Parameters of Solid Membranes of PEG_X(HSA−FeP) at 25 °C

system	k_{on} (Torr^{-1} s^{-1})	k'_{on} (Torr^{-1} s^{-1})	k_{off} (s^{-1})	k'_{off} (s^{-1})	$P_{1/2}$ (Torr)[a]
PEG_2(HSA−FeP) solution[b]	20	7.5	1.7×10^2	70	11 [32]
PEG_5(HSA−FeP) solution[b]	20	10	1.7×10^2	90	11 [31]
PEG_2(HSA−FeP) membrane	5.7	0.54	2.3×10^2	22	40 [61]
PEG_5(HSA−FeP) membrane	3.1		34		11 [33]
PEG_2(HSA−FeP)/HA membrane	4.3	0.22	1.4×10^2	7	32 [60]
Hb solution (T-state)[c]	4.8		1.8×10^2		40
Hb/maltose membrane[d]	1.2×10^{-13}		8.3×10^{-11}		760

[a] At 37 °C in brackets [ ]. [b] In PBS solution (pH 7.4), ref 19. [c] In 50 mM potassium phosphate buffer (pH 7.0) at 20 °C, ref 24. [d] Reference 23.

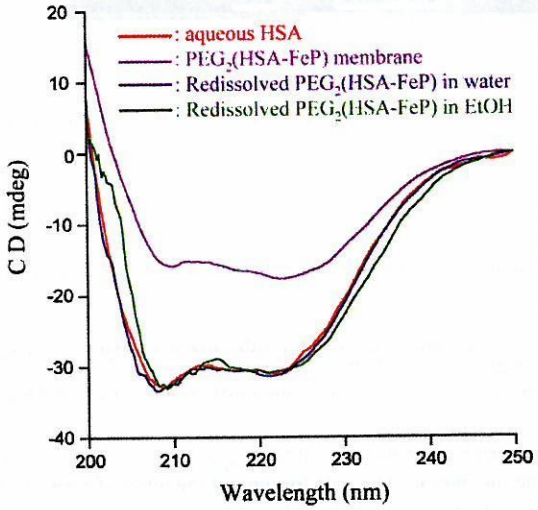

Figure 5. CD spectra of PEG_2(HSA−FeP) at various conditions at 25 °C.

to the PEG_5(HSA−FeP) membrane, which consists of the homogeneous fibrous layer, was fitted by single exponential, giving only one association rate constant k_{on}.

The low O_2-binding affinity of the solid membrane of PEG_2-(HSA−FeP) compared to that in the PBS solution is kinetically due to the low association rate constants (Table 1). Even though this result was in significant contrast to the fact that the similar solid membrane of human Hb with maltose (Hb/maltose = 6/4, wt/wt) could not bind O_2 under the same conditions, its O_2-binding affinity was extremely low ($P_{1/2}$ = 760 Torr) (*23*). Since the quaternary structure of Hb was restrained in the solid form, its tense-state conformation cannot change to a relaxed-state with a high O_2-binidng affinity (*24*). In the PEG_X(HSA−FeP) membrane, the protein scaffold was solidified by a bulk water evaporation; however, it would not dramatically influence the dioxygenation of FeP, because the O_2-binding equilibrium is not synchronized with the quaternary structure of the HSA matrix.

PEG_X(HSA−FeP) in Organic Solutions. We have found that the PEG modification enables HSA−FeP to dissolve in organic solvents. The red-colored PEG_X(HSA−FeP) membrane was homogeneously soluble not only in water but also in ethanol and chloroform. The CD spectrum of the membrane showed a different pattern compared to that in aqueous media (Figure 5). The intensity ratio of the double minimum peaks at 208 and 222 nm (I_{208}/I_{222}) of rHSA or PEG_X(HSA−FeP) is normally 1.1 (*25*, *26*), while the membrane showed 0.9. Interestingly, the redissolved aqueous and ethanol solutions both showed the same spectra as the original aqueous HSA. This result implies that the change of the secondary structure in the protein in the solid and liquid states is reversible. The ethanolic PEG_X(HSA−FeP) also exhibited the same absorption changes upon exposure to O_2 and N_2. These organic solutions can also be cast on a glass surface to form identical PEG_X(HSA−FeP) membranes.

PEG_2(HSA−FeP) Membrane with Hyaluronic Acid. An attempt to isolate the PEG_X(HSA−FeP) membrane from the glass surface unfortunately failed, because it was rather fragile, when peeled off. We then added a supporting polymer to the protein solution and prepared the solid membrane on a glass plate or a poly(styrene) dish. Hyaluronic acid (HA), which is known as a glycosaminoglycan component of connective tissues, hyaline body and extracellular matrix, was selected as the biocompatible polymer support (*27*). We also expected that the high water retention capability of HA may have a positive effect on retarding the proton-driven oxidation of the FeP(O_2) complex. Water evaporation of the PEG_2(HSA−FeP)/HA mixture [0.5 mL/0.5 mL, total [HSA] = 2.5 wt %, total [HA] = 0.2 wt %] on the glass plate or poly(styrene) dish produced the red-colored uniform solid membranes. It could not be isolated from the glass plate but was easily peeled off from the poly(styrene) surface, providing a free-standing thin film of the PEG_2(HSA−FeP)/HA hybrid [Figure 6a]. The formation of the flexible film was quite dependent on the HA content. When the total concentration of HA is 0.2−0.5 wt %, we could readily obtain the membrane from the plastic surface. The SEM observations of the film showed that it was made of a homogeneous layer with a relatively coarse structure (Figure 6b). In contrast, the film cast on the glass plate consists of the two-layered form: a major course phase and bottom dense phase (Figure 6c). This implies

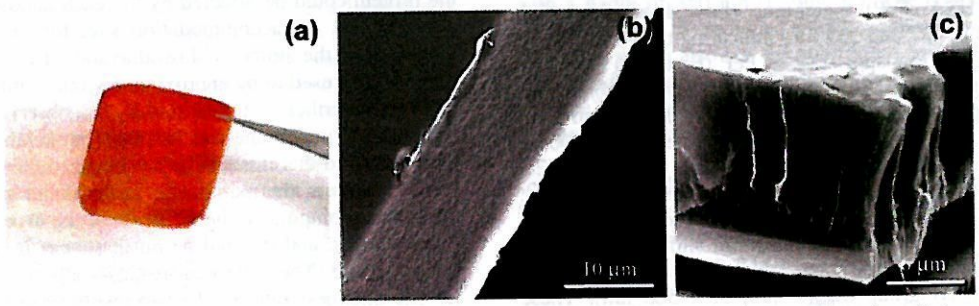

Figure 6. PEG_2(HSA−FeP)/HA membrane. (a) Photograph of the free-standing flexible film, which is prepared on the poly(styrene) surface. (b) SEM of the isolated film. (c) SEM of the membrane prepared on the glass surface.

that the membrane structure of the PEG_2(HSA−FeP)/HA is also influenced by the surface properties of the substrate.

The UV−vis absorption spectral pattern reversibly changed from that of the five-N-coordinate high-spin ferrous complex under an N_2 atmosphere (λ_{max}: 445, 540, 566 nm) to that of the O_2-adduct complex under an O_2 atmosphere (λ_{max}: 426, 545 nm). The O_2-binding parameters of the PEG_2(HSA−FeP)/HA membrane showed a tendency similar to the PEG_2(HSA−FeP) film; the low O_2-binding affinity ($P_{1/2}$ = 32 Torr, 25 °C) is mainly due to the slow association rate constant (Table 1). The half-life of the O_2-adduct complex was 40 h at 37 °C; we could not see any water retention effect of HA that could prolong the stability of FeP(O_2). The water content of the PEG_2(HSA−FeP) membrane and PEG_2(HSA−FeP)/HA membrane were determined by the differential thermal analyses to be 6.5 wt % and 6.6 wt %, respectively.

CONCLUSIONS

The stable solid membranes of a PEGylated artificial hemoprotein have been prepared, and their O_2-binding properties were physicochemically characterized in relation to the layer morphology. The red-colored thin film is soluble again in water and organic solvents (ethanol, chloroform) without any deformation of the secondary structure of the protein. The addition of hyaluronic acid as the polymer support gave the free-standing flexible film. These O_2-binding albumin membranes are a red blood cell substitute with a micrometer-thickness that can be preserved anywhere (e.g., on a shelf and in an ambulance) and reproduced as a saline solution at anytime (e.g., at the scene of a disaster). Furthermore, it would be of great medical importance for a variety of clinical treatments, such as O_2-enriched coating agents for medical devices or artificial organs and an O_2-transporting adhesive plaster for wound healing.

ACKNOWLEDGMENT

This work was partially supported by a Grant-in-Aid for Scientific Research (No. 16350093, No. 18750156) from JSPS, PRESTO, and from JST, and Health Science Research Grants from MHLW, Japan.

LITERATURE CITED

(1) Harris, J. M., Martin, N. E., and Modi, M. (2001) Pegylation—a novel process for modifying pharmacokinetics. *Clin. Pharmacokinet. 40*, 539−551.

(2) Veronese, F. M., and Harris, J. M. (2002) Introduction and overview of peptide and protein PEGylation. *Adv. Drug Delivery Rev. 54*, 453−456.

(3) Roberts, M. J., Bentley, M. D., and Harris, J. M. (2002) Chemistry for peptide and protein PEGylation. *Adv. Drug Delivery Rev. 54*, 459−476.

(4) Veronese, F. M. (2001) Peptide and protein PEGylation: a review of problems and solutions. *Biomaterials 22*, 405−417.

(5) Veronese, F. M., and Pasut, G. (2005) PEGylation, successful approach to drug delivery. *Drug Discovery Today 10*, 1451−1455.

(6) Nucci, M. L., Shorr, R., and Abuchowski, A. (1991) The therapeutic value of poly(ethylene glycol) modified proteins. *Adv. Drug Delivery Rev. 6*, 133−151.

(7) Abuchowski, A., van Es, T., Palzuk, N. C., and Davis, F. F. (1977) Alteration of immunological properties of bovine serum albumin by covalently attachment of polyethylene glycol. *J. Biol. Chem. 252*, 3578−3581.

(8) Abuchowski, A., McCoy, J. R., Palczuk, N. C., van Es, T., and Davis, F. F. (1977) Effect of covalently attachment of polyethylene glycol on immunogenicity and circulating life of bovine liver catalase. *J. Biol. Chem. 252*, 3582−3586.

(9) He, X. H., Shaw, P. C., and Tam, S. C. (1999) Reducing the immunogenicity and improving the in vivo activity of trichosanthin by site-directed PEGylation. *Life Sci. 65*, 355−368.

(10) Hinds, K. D., and Kim, S. W. (2002) Effects of PEG conjugation on insulin properties. *Adv. Drug Delivery Rev. 54*, 505−530.

(11) Vandegriff, K. M., Malavalli, A., Wooldbridge, J., Lohman, J., and Winslow, R. M. (2003) MP4, a new nonvasoactive PEG-Hb conjugate. *Transfusion 43*, 509−516.

(12) Manjula, B. M., Tsai, A., Upadhya, R., Perumalsamy, K., Smith, P. K., Malavalli, A., Vandegriff, K., Winslow, R. M., Intaglietta, M., Prabhakaran, M., Friedman, J. M., and Acharya, A. S. (2003) Site-specific PEGylation of hemoglobin at Cys-93(β): correlation between the colligative properties of the PEGylated protein and the length of the conjugated PEG chain. *Bioconjugate Chem. 14*, 464−472.

(13) Olofsson, C., Ahl, T., Johansson, T., Larsson, S., Nellgard, P., Ponzer, S., Fagrell, B., Przybelski, R., Keipert, P., Winslow, N., and Winslow, R. M. (2006) A multicenter clinical study of the safety and activity of maleimide-polyethylene glycol-modified hemoglobin (hemospan) in patients undergoing major orthopedic surgery. *Anesthesiology 105*, 1153−1163.

(14) Takahashi, K., Ajima, A., Yoshimoto, T., and Inada, Y. (1984) Polyethylene glycol-modified catalase exhibits unexpectedly high activity in benzene. *Biochem. Biophys. Res. Commun. 125*, 761−766.

(15) Kawahara, N. Y., and Ohno, H. (1997) Induced thermostability of poly(ethylene oxide)-modified hemoglobin in glycols. *Bioconjugate Chem. 8*, 643−648.

(16) Wiwatchaiwong, S., Nakamura, N., and Ohno, H. (2006) Spectroscopic characterization and electrochemistry of poly(ethylene oxide)-modified myoglobin in organic solvents. *Biotechnol. Prog. 22*, 1276−1281.

(17) Komatsu, T., Matsukawa, Y., and Tsuchida, E. (2002) Effect of heme structure on O_2-binding properties of human serum albumin−heme hybrids: intramolecular histidine coordination provides a stable O_2-adduct complex. *Bioconjugate Chem. 13*, 397−402.

(18) Komatsu, T., Yamamoto, H., Huang, Y., Horinouchi, H., Kobayashi, K., and Tsuchida, E. (2004) Exchange transfusion with synthetic oxygen-carrying plasma protein "albumin-heme" into an acute anemia rat model after seventy-percent hemodilution. *J. Biomed. Mater. Res. A 71A*, 644−651.

(19) Huang, Y., Komatsu, T., Wang, R.-M., Nakagawa, A., and Tsuchida, E. (2006) Poly(ethylene glycol)-conjugated human serum albumin including iron porphyrins: surface modification improves the O_2-transporting ability. *Bioconjugate Chem. 17*, 393−398.

(20) Tsuchida, E., Komatsu, T., Kumamoto, S., Ando, K., and Nishide, H. (1995) Synthesis and O_2-Binding properties of tetraphenylporphyrinatoiron(II) derivatives bearing a proximal imidazole covalently bound at the β-pyrrolic position. *J. Chem. Soc., Perkin Trans. 2*, 747−753.

(21) Collman, J. P., Brauman, J. I., Iverson, B. L., Sessler, J. L., Morris, R. M., and Gibson, Q. H. (1983) O_2 and CO binding to iron(II) porphyrins: a comparison of the "picket fence" and "pocket" porphyrins. *J. Am. Chem. Soc. 105*, 3052−3064.

(22) Komatsu, T., Matsukawa, Y., and Tsuchida, E. (2000) Kinetics of CO and O_2 binding to human serum albumin−heme hybrid. *Bioconjugate Chem. 11*, 772−776.

(23) Chung, J. E., Sakai, H., Takeoka, S., Nishide, H., and Tsuchida, E. (1995) Coordination behavior of O_2 and CO in a solid film consisting of hemoglobin and maltose. *Bull. Chem. Soc. Jpn. 68*, 1006−1011.

(24) Sawicki, C. A., and Ginson, Q. H. (1977) Properties of the T state of human oxyhemoglobin studied by laser photolysis. *J. Biol. Chem. 252*, 7538−7547.

(25) Nakajou, K., Watanabe, H., Kragh-Hansen, U., Maruyama, T., and Otagiri, M. (2003) The effect of glycation on the surface on the structure, function and biological fate of human serum albumin as revealed by recombinant mutants. *Biochim. Biophys. Acta 1623*, 88−97.

(26) Peters, T. (1996) *All about albumin: biochemistry, genetics and medical applications*; Academic Press, San Diego.

(27) Goa, K. L., and Benfield, P. (1994) Hyaluronic-acid −a review of its pharmacology and use as a surgical and in ophthalmology, and its therapeutic potential in joint disease and wound-healing. *Drugs 47*, 536−566.

BC070086M

J|A|C|S
ARTICLES
Published on Web 08/18/2007

Genetic Engineering of the Heme Pocket in Human Serum Albumin: Modulation of O_2 Binding of Iron Protoporphyrin IX by Variation of Distal Amino Acids

Teruyuki Komatsu,*,†,‡ Akito Nakagawa,† Patricia A. Zunszain,‖ Stephen Curry,‖ and Eishun Tsuchida*,†

Contribution from the Research Institute for Science and Engineering, Waseda University, 3-4-1 Okubo, Shinjuku-ku, Tokyo 169-8555, Japan, PRESTO, Japan Science and Technology Agency, 4-1-8 Honcho, Kawagichi-shi, Saitama 332-0012, Japan, and Division of Cell and Molecular Biology, Faculty of Natural Sciences, Imperial College London, South Kensington Campus, London SW7 2AZ, United Kingdom

Received June 8, 2007; E-mail: teruyuki@waseda.jp; eishun@waseda.jp

Abstract: Complexing an iron protoporphyrin IX into a genetically engineered heme pocket of recombinant human serum albumin (rHSA) generates an artificial hemoprotein, which can bind O_2 in much the same way as hemoglobin (Hb). We previously demonstrated a pair of mutations that are required to enable the prosthetic heme group to bind O_2 reversibly: (i) Ile-142 → His, which is axially coordinated to the central Fe^{2+} ion of the heme, and (ii) Tyr-161 → Phe or Leu, which makes the sixth coordinate position available for ligand interactions [I142H/Y161F (HF) or I142H/Y161L (HL)]. Here we describe additional new mutations designed to manipulate the architecture of the heme pocket in rHSA−heme complexes by specifically altering distal amino acids. We show that introduction of a third mutation on the distal side of the heme (at position Leu-185, Leu-182, or Arg-186) can modulate the O_2 binding equilibrium. The coordination structures and ligand (O_2 and CO) binding properties of nine rHSA(triple mutant)−heme complexes have been physicochemically and kinetically characterized. Several substitutions were severely detrimental to O_2 binding: for example, Gln-185, His-185, and His-182 all generated a weak six-coordinate heme, while the rHSA(HF/R186H)−heme complex possessed a typical bis-histidyl hemochrome that was immediately autoxidized by O_2. In marked contrast, HSA(HL/L185N)−heme showed very high O_2 binding affinity ($P_{1/2}^{O_2}$ 1 Torr, 22 °C), which is 18-fold greater than that of the original double mutant rHSA(HL)−heme and very close to the affinities exhibited by myoglobin and the high-affinity form of Hb. Introduction of Asn at position 185 enhances O_2 binding primarily by reducing the O_2 dissociation rate constant. Replacement of polar Arg-186 with Leu or Phe increased the hydrophobicity of the distal environment, yielded a complex with reduced O_2 binding affinity ($P_{1/2}^{O_2}$ 9−10 Torr, 22 °C), which nevertheless is almost the same as that of human red blood cells and therefore better tuned to a role in O_2 transport.

Introduction

In the human circulatory system, iron(III) protoporphyrin IX (hemin) released from methemoglobin (metHb) is captured by a specific glycoprotein, hemopexin (Hpx, 60 kDa), which binds it with very high affinity ($>10^{13}$ M^{-1}).[1,2] Nevertheless, due to the extremely low abundance of Hpx in the blood stream (~17 μM), human serum albumin (HSA, 66.5 kDa, 640 μM) acts as a depot of hemin under pathological conditions of trauma and severe hemolysis.[3] HSA is the most prominent plasma protein and has a remarkable ability to bind a broad range of insoluble endogenous and exogenous compounds, such as fatty acids, hemin, bilirubin, bile acids, thyroxine, and a wide variety of drugs.[4,5] This heart-shaped carrier protein is composed of three structurally similar domains (I−III), each of which contains two subdomains (A and B).[6,7] Recent crystallographic studies revealed that the hemin is bound within a narrow D-shaped hydrophobic cavity in subdomain IB (Figure 1a).[8,9] The central iron atom is weakly coordinated by Tyr-161 and the porphyrin propionate side chains interact with a triad of basic amino acid

† Waseda University.
‡ JST.
‖ Imperial College London.

(1) (a) Muller-Eberhard, U; Grizzuti, K. *Biochemistry* **1971**, *10*, 2062−2066. (b) Muller-Eberhard, U.; Morgan, W. T. *Ann. N.Y. Acad. Sci.* **1975**, *244*, 624−650.
(2) Paoli, M.; Anderson, B. F.; Baker, H. M.; Morgan, W. T.; Smith, A.; Baker, E. N. *Nat. Struct. Biol.* **1999**, *6*, 926−931.
(3) Tolosano, E.; Altruda, F. *DNA Cell Biol.* **2002**, *21*, 297−306.
(4) Peters, T. *All about Albumin: Biochemistry, Genetics and Medical Applications*; Academic Press: San Diego, CA, 1996; and references therein.
(5) (a) Kragh-Hansen, U. *Pharmacol. Rev.* **1981**, *33*, 17−53. (b) Kragh-Hansen, U. *Danish Med. Bull.* **1990**, *37*, 57−84.
(6) (a) He, X. M.; Carter, D. C. *Nature* **1992**, *358*, 209−215. (b) Carter, D. C.; Ho, J. X. *Adv. Protein Chem.* **1994**, *45*, 153−203.
(7) (a) Curry, S.; Madelkow, H.; Brick, P.; Franks, N. *Nat. Struct. Biol.* **1998**, *5*, 827−835. (b) Bhattacharya, A. A.; Grune, T.; Curry, S. *J. Mol. Biol.* **2000**, *303*, 721−732.
(8) Wardell, M.; Wang, Z.; Ho, J. X.; Robert, J.; Ruker, F.; Rubel, J.; Carter, D. C. *Biochem. Biophys. Res. Commun.* **2002**, *291*, 813−819.
(9) Zunszain, P. A.; Ghuman, J.; Komatsu, T.; Tsuchida, E.; Curry, S. *BMC Struct. Biol.* **2003**, *3*, 6.

10.1021/ja074179q CCC: $37.00

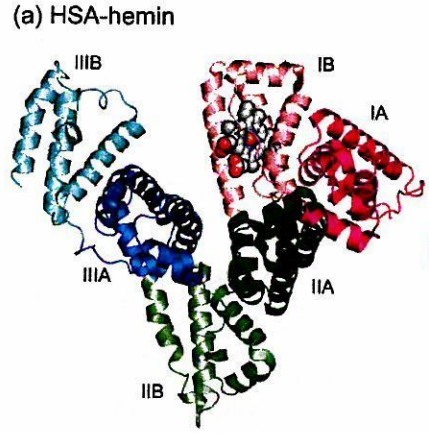

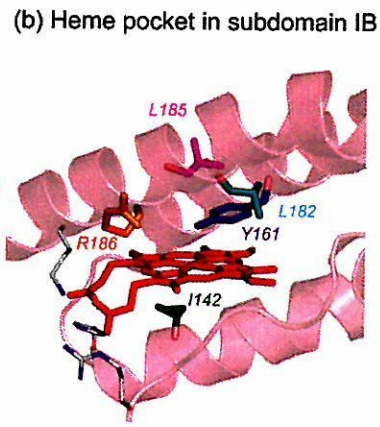

	Positions 142	161	182	185	186
Wild type (wt)	I	Y	L	L	R
I142H/Y161F (HF)	H	F	L	L	R
I142H/Y161L (HL)	H	L	L	L	R
HF/L185N	H	F	L	N	R
HL/L185N	H	L	L	N	R
HF/L185Q	H	F	L	Q	R
HL/L185Q	H	L	L	Q	R
HF/L185H	H	F	L	H	R
HL/L182H	H	L	H	L	R
HF/R186H	H	F	L	L	H
HL/R186L	H	L	L	L	L
HL/R186F	H	L	L	L	F

Figure 1. (a) Crystal structure of HSA−hemin complex (1O9X) from ref 9. Hemin is shown in a space-filling representation. (b) Heme pocket structure in subdomain IB and positions of amino acids where site-specific mutations were introduced. The essential double mutations to confer O_2 binding capability to the heme group are I142H and Y161F (or Y161L). Abbreviations of the triple mutants are shown in the table.

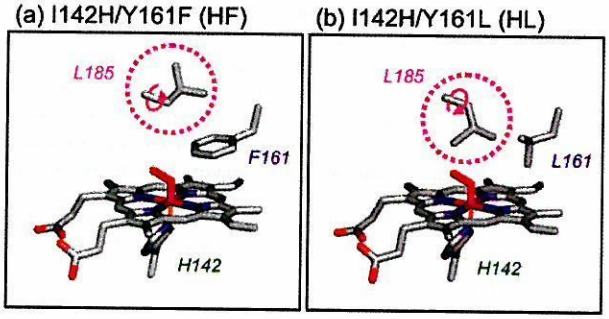

Figure 2. Structural models of the heme pocket in dioxygenated (a) rHSA-(HF)−heme and (b) rHSA(HL)−heme: distal-side steric effect of Leu-185 on O_2 and CO association.[20]

residues at the entrance (Arg-114, His-146, and Lys-190) (Figure 1b). In terms of the general hydrophobicity of the α-helical heme pocket, subdomain IB of HSA has broadly similar features to the globin-wrapping heme in Hb and myoglobin (Mb). If the HSA-based O_2 carrier is realized, it has the potential of acting not only as a red blood cell (RBC) substitute but also as an O_2-providing therapeutic reagent. However, the reduced ferrous HSA−heme would be immediately autoxidized by O_2, because HSA lacks the proximal histidine that in Hb and Mb allows the prosthetic heme group to bind O_2.[10] On the basis of the detailed structure of the heme binding site of HSA, we introduced a His into the Leu-142 position by site-directed mutagenesis that provides axial coordination to the central Fe^{2+} atom of the heme, and we replaced the coordinated Tyr-161 by Phe or Leu, neither of which can interact with the Fe^{2+} ion (Figure 2).[11] This mutagenic approach produced the recombinant HSA(I142H/Y161F)−heme [rHSA(HF)−heme] and HSA(I142H/Y161L)−heme [rHSA(HL)−heme] complexes; these artificial hemoproteins can bind and release O_2 at room temperature, although the O_2 binding affinity of rHSA−heme is at least an order of magnitude lower than that of Hb(α) (R-state).[11] To develop this promising O_2-carrying plasma protein as a blood substitute, further work is required to regulate the O_2 binding affinity suitable for Hb, Mb, and human RBC.

In Hb and Mb, His-64 on the distal side of the heme has been conserved during evolution and plays an important role for tuning their ligand affinities. A neutron diffraction study of MbO_2 clearly showed that the N−H bond of the distal His-64 is restrained from optimal alignment for strong hydrogen bonding with the coordinated O_2.[12] Olson et al.[13a] reported that the substitution of Gly for His-64 in Mb and Hb(α) caused a significant decrease in the O_2 binding affinity due to an ~100-fold increase in the O_2 dissociation rate constant. A number of systematic investigations of site-directed mutants of Hb and Mb have shown that the overall polarity and packing of the distal residues are key factors in regulating the rate and equilibrium constants for ligand bindings.[13]

In addition to mutagenic analyses of heme binding sites on proteins, the value of using synthetic iron porphyrins as Hb and Mb active-site models has also been amply demonstrated.[14,15] Tetrakis(α,α,α,α-*o*-pivalamido)phenylporphinato-iron(II) "picket-fence porphyrin" of Collman et al.[16] was a pioneering molecule, which forms an O_2 adduct complex at room temperature that is quite stable and shows a high O_2 binding affinity. The polar secondary amide groups in the four fences were believed to contribute to the high O_2 affinity. Moementeau and Lavalette[17] first demonstrated the distal polarity effect on the O_2 binding to the "hanging-base porphyrins". The presence of the amide groups in the strapped handle over the porphyrin macrocycle yielded a 9-fold higher O_2 binding affinity compared to the ether-bond analogue; it was due to an 8-fold reduction in the dissociation rate constant. This polarity effect of the substituent

(10) Monzani, E.; Bonafè, B.; Fallarini, A.; Redaelli, C.; Casella, L.; Minchiotti, L.; Galliano, M. *Biochim. Biophys. Acta.* **2001**, *1547*, 302−312.
(11) (a) Komatsu, T.; Ohmichi, N.; Zunszain, P. A.; Curry, S.; Tsuchida, E. *J. Am. Chem. Soc.* **2004**, *126*, 14304−14305. (b) Komatsu, T.; Ohmichi, N.; Nakagawa, A.; Zunszain, P. A.; Curry, S.; Tsuchida, E. *J. Am. Chem. Soc.* **2005**, *127*, 15933−15942.
(12) Phillips, S. E. V.; Schoenborn, B. P. *Nature* **1981**, *292*, 81−82.
(13) (a) Olson, J. S.; Mathews, A. J.; Rohlfs, R. J.; Springer, B. A.; Egeberg, K. D.; Sligar, S. G.; Tame, J.; Renaud, J.-P.; Nagai, K. *Nature* **1988**, *336*, 265−266. (b) Rohlfs, R.; Mathews, A. J.; Carver, T. E.; Olson, J. S.; Springer, B. A.; Egeberg, K. D.; Sligar, S. G. *J. Biol. Chem.* **1990**, *265*, 3168−3176. (c) Springer B. A.; Sligar, S. G.; Olson, J. S.; Phillips, G. N., Jr. *Chem. Rev.* **1994**, *94*, 699−714.
(14) Momenteau, M.; Reed, C. A. *Chem. Rev.* **1994**, *94*, 659−698.
(15) Collman, J. P.; Fu, L. *Acc. Chem. Res.* **1999**, *32*, 455−463.
(16) (a) Collman, J. P.; Gagne, R. R.; Halbert, T. R.; Marchou, J.-C.; Reed. C. A. *J. Am. Chem. Soc.* **1973**, *95*, 7869−7870. (b) Collman, J. P.; Gagne, R. R.; Reed, C. A.; Halbert, T. R.; Lang, G.; Robinson, W. T. *J. Am. Chem. Soc.* **1975**, *97*, 1427−1439. (c) Collman, J. P.; Brauman, J. I.; Iverson, B. L.; Sessler, J. L.; Morris, R. M.; Gibson, Q. H. *J. Am. Chem. Soc.* **1983**, *105*, 3052−3064.
(17) Momenteau, M.; Lavalette, D. *J. Chem. Soc., Chem. Commun.* **1982**, 341−343.

was also well illustrated by our "double-sided porphyrins" having ester fences with a 23-fold lower O_2 binding affinity relative to the picket-fence porphyrin.[18]

In view of these investigations, we reasoned that systematic variation of the steric hindrance and local polarity of the heme pocket in subdomain IB of HSA would allow us to modulate the O_2 binding affinity of rHSA−heme. In this study, we designed and generated nine rHSA(triple mutant)−heme complexes, in which the specific third mutation was introduced into three different positions near the O_2 binding site. The effects of the engineered distal amino acids on the O_2 and CO binding properties of the prosthetic heme group have been physicochemically and kinetically characterized. We now present a new chemistry of albumin-based artificial hemoproteins that would serve as an entirely synthetic O_2 carrier with a controllable ligand binding affinity.

Experimental Section

Materials and Apparatus. All materials were reagent-grade and were used as purchased without further purification. Iron(III) protoporphyrin IX (hemin) chloride was purchased from Fluka. UV−vis absorption spectra were obtained on an Agilent 8453 UV−visible spectrophotometer equipped with an Agilent 89090A temperature control unit. Kinetic measurements for the O_2 and CO bindings were carried out on a Unisoku TSP-1000WK time-resolved spectrophotometer with a Spectron Laser Systems SL803G-10 Q-switched Nd:YAG laser, which generated a second-harmonic (532 nm) pulse of 6-ns duration (10 Hz).[11b] A 150 W xenon arc lamp was used as the probe light source. The gas mixture with the desired partial pressure of O_2/CO/N_2 was prepared by a Kofloc Gasblender GB-3C. MCD spectra were measured by a Jasco J-820 circular dichrometer.

Preparations of rHSA Triple Mutants and Their Heme Complexes. The designed rHSA triple mutants were prepared according to our previously reported techniques.[11] The third mutation (L185N, L185Q, L185H, L182H, R186H, R186L, or R186F) was introduced into the HSA coding region in a plasmid vector encoding the double mutants [rHSA(I142H/Y161F) [rHSA(HF)] or rHSA(I142H/Y161L) [rHSA(HL)]][11] by use of the Stratagene QuikChange mutagenesis kit. All mutations were confirmed by DNA sequencing. The plasmid was then digested by *Not*I and introduced into yeast (*Pichia pastoris* GS115) by electroporation. The expression protocols and media formulations were as previously described.[11b] Briefly, the clones were grown in BMGY medium and transferred to BMMY medium for induction with methanol in baffled shaking flasks at 30 °C, 200 rpm. The obtained proteins were harvested from the growth medium by precipitation with ammonium sulfate and purified by a Cibacron Blue column of Blue Sepharose 6 Fast Flow (Amersham Pharmacia Biotech). The rHSA triple mutants were finally subjected to gel filtration on an ÄKTA Prime Plus FPLC system with a Superdex 75 preparative-grade column (Amersham Pharmacia Biotech). The protein concentration was assayed by measuring the absorbance at 280 nm ($\epsilon_{280} = 3.4 \times 10^4$ M^{-1} cm^{-1}) and by SDS−PAGE.

The ferric rHSA(mutant)−hemin complexes [hemin:rHSA(mutant) molar ratio of 1:1] were prepared by established procedures.[9,11] The resulting samples were analyzed by SDS−PAGE to confirm a pure preparation. The 50 mM phosphate buffered solution (pH 7.0, 3 mL) of rHSA(mutant)−hemin ([hemin] = 10 μM) in a 10-mm path length optical quartz cuvette sealed with a rubber septum was purged with Ar for 40 min. A small excess amount of degassed aqueous sodium dithionate was added by a microsyringe to the sample under an Ar atmosphere to reduce the central ferric ion of the hemin, to give the ferrous rHSA(mutant)−heme complexes.

O_2 and CO Binding Parameters. The O_2 or CO recombination with the heme after nanosecond laser flash photolysis of hemeO_2 or hemeCO occurs according to eq 1 with the association rate constant (k_{on}^{L}) and dissociation rate constant (k_{off}^{L}):[11,16c,19]

$$\text{hemeL} \xrightarrow{h\nu} \text{heme} \underset{k_{off}^{L}}{\overset{k_{on}^{L}}{\rightleftharpoons}} \text{hemeL} \qquad (1)$$

where L = O_2 or CO. The CO association rate (k_{on}^{CO}) was simply measured by following the absorption at 425 nm after laser pulse irradiation to rHSA(mutant)−hemeCO at 22 °C.[11] The O_2 association rate constant ($k_{on}^{O_2}$) and O_2 binding equilibrium constant K^{O_2} [= $(P_{1/2}^{O_2})^{-1}$] can be determined by a competitive rebinding technique by use of gas mixtures with different partial pressures of O_2/CO/N_2 at 22 °C.[11,16c,19] The relaxation curves that accompanied the O_2 or CO recombination were analyzed by single- or double-exponential profiles with Unisoku Spectroscopy & Kinetics software. The O_2 dissociation rate ($k_{off}^{O_2}$) was calculated from $k_{on}^{O_2}/K^{O_2}$.

The CO dissociation rate constant (k_{off}^{CO}) was measured by displacement with NO for rHSA(mutant)−hemeCO at 22 °C.[11b] The time course of the UV−vis absorption change that accompanied the CO dissociation was fitted to two single exponentials. The CO binding constants [K^{CO} = $(P_{1/2}^{CO})^{-1}$] were calculated from k_{on}^{CO}/k_{off}^{CO}. Fresh solutions of rHSA(mutant)−heme were normally made up for each set of experiments.

Magnetic Circular Dichroism Spectroscopy. MCD for the 50 mM potassium phosphate buffered solutions (pH 7.0) of rHSA(mutant)−hemin or −heme complex (10 μM) were measured under Ar and CO atmospheres with a 1.5 or 1.65 T electromagnet at 22 °C.

Results and Discussion

Design of Distal Pocket with Asn, Gln, and His. We recently compared the O_2 and CO binding properties of the rHSA(double mutant)−heme complexes [rHSA(HF)−heme and rHSA(HL)−heme] and found evidence for a noteworthy distal-side steric effect on ligand binding.[11b] The rHSA(HF)−heme complex binds O_2 and CO about 4−6 times more tightly than rHSA(HL)−heme, primarily because of enhanced association rate constants. Structurally, this affect appears to be due to the concerted effects of the residues at positions 161 and 185 on ligand binding. In the rHSA(HF)−heme complex, the bulky aromatic side chain of Phe-161 is presumed to prevent rotation of the neighboring Leu-185, thereby providing easy access to the O_2 binding site in the distal pocket (Figure 2a). In contrast, the substitution of Phe-161 by the smaller Leu-161 may allow rotation of the isopropyl group of Leu-185, which reduces the volume of the distal side (Figure 2b) and hinders association of O_2 and CO ligands with the heme iron atom. On the basis of these findings, we reasoned that other modifications of the heme pocket architecture would allow us to further modulate its O_2 binding properties.

One approach to enhancing the O_2 binding affinities of rHSA(HF)−heme and rHSA(HL)−heme would be to introduce a histidine into an appropriate position on the distal side of the heme. The N_ϵ atom of His may act as a proton donor to form an H-bond with the coordinated O_2. However, another important requirement in this molecular design is to prevent the formation

(18) (a) Komatsu, T.; Hasegawa, E.; Nishide, H.; Tsuchida, E. *J. Chem. Soc., Chem. Commun.* **1990**, 66−68. (b) Tsuchida, E.; Komatsu, T.; Arai, K.; Nishide, H. *J. Chem. Soc., Dalton Trans.* **1993**, 2465−2469.

(19) Traylor, T. G.; Tsuchiya, S.; Campbell, D.; Mitchel, M.; Stynes, D.; Koga, N. *J. Am. Chem. Soc.* **1985**, *107*, 604−614.

(20) The pictures were produced on the basis of crystal structure coordinatex of rHSA(wt)−hemin (1O9X, ref 9) by use of PyMOL: DeLano, W. L. The PyMOL Molecular Graphics System; DeLano Scientific: San Carlos, CA, 2002.

of a six-coordinate low-spin ferrous complex. The bis-histidyl hemochromes are normally autoxidized by O_2 via an outer-sphere mechanism as well as by inner-sphere pathways involving the metal-coordinated O_2.[21−23] The distal amino acid must therefore be located relatively far (>4 Å) from the central iron.

Our modeling experiments suggested that the favorable position for the distal His insertion was Leu-185, which is in the final helix in subdomain IB and forms part of the top of the distal pocket (Figure 1). Leu-182 and Arg-186 were also considered likely to be good candidate positions for the introduction of an amide-containing side chain designed to stabilize O_2 binding (see below). In elegant studies on Mb, Rohlfs and co-workers showed that Gln, which has a primary amide group potential to form an H-bond, was able to substitute effectively for the stabilizing role of the distal histidine (His-64).[13b,c] Thus, we decided to vary the polarity of the distal side of the heme in rHSA(HF) and rHSA(HL) by replacing Leu-185 with Asn, Gln, and His by site-directed mutagenesis. The Asn residue should behave similarly to Gln, although a rMb-(H64N) mutant has never been reported. The His-185 mutation was only done for rHSA(HF), because His-185 could be long enough to bind to the sixth coordinate position of the heme if allowed the greater freedom of movement that would occur in the rHSA(HL) background. As a result, five triple mutants [rHSA(HF/L185N), rHSA(HL/L185N), rHSA(HF/L185Q), rHSA-(HL/L185Q), and rHSA(HF/L185H)] were cloned and their hemin complexes were prepared.

Ferric States of L185N, L185Q, and L185H Mutants. The site-specific mutations with Asn, Gln, and His were successfully introduced into the Leu-185 position of rHSA(HF) or rHSA-(HL), and the proteins were purified to homogeneity as determined by SDS−PAGE. The rHSA(mutant)−hemin complexes produced from these proteins were stable for several months at 4 °C without precipitation.

The UV−vis absorption spectra of the five rHSA(triple mutant)−hemin complexes are essentially the same regarding their general features (Figure 3, Table 1). When analyzed by MCD spectroscopy to evaluate the redox state, spin state, and axial ligand environment, all the ferric rHSA(triple mutant)−hemins showed a characteristic MCD with similar S-shaped patterns in the Soret band region, though their intensities were dependent on the nature of the distal amino acid (Figure 4). Vickery et al.[24] previously reported that the Soret MCD intensity of the ferric Mb with different anions at the sixth coordinate position was correlated with the amount of low-spin component. rHSA(HL)−hemin showed almost the same band as ferric Mb, in which one water axially coordinates to the sixth position of the hemin to produce the aquo complex.[11,24,25] In contrast, rHSA-(HF/L185H)−hemin showed 3-fold greater intensity at 405 nm. This is probably caused by the coexistence of a low-spin six-coordinate hemin. Introduction of Asn or Gln at position 185

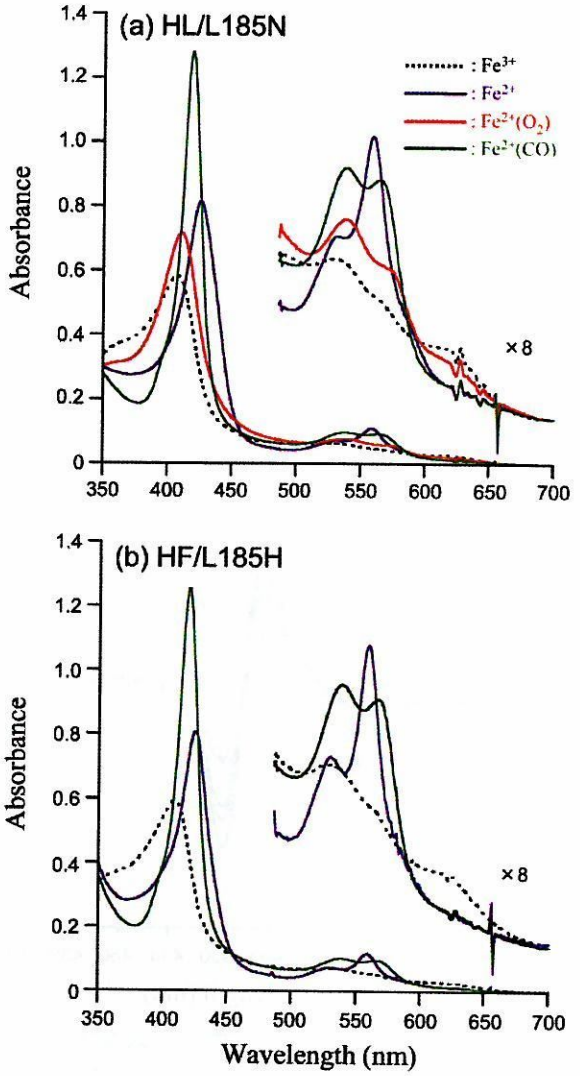

Figure 3. UV−vis absorption spectral changes of (a) rHSA(HL/L185N)−heme and (b) rHSA(HF/L185H)−heme complexes in 50 mM potassium phosphate buffered solution (pH 7.0, 22 °C).

gave intermediate effects, though mutants with Q185 yielding a slightly more intense peak at 405 nm. Overall, our MCD results for these five rHSA(triple mutant)−hemin complexes imply that the introduction of the distal nitrogenous residue at the 185 position tends to increase the ferric low-spin nature.

Ferrous States of L185N, L185Q, and L185H Mutants and O_2 Binding. rHSA(triple mutant)−hemins were easily reduced to form the ferrous complexes by adding a small excess of aqueous sodium dithionate under an Ar atmosphere. rHSA(HF/L185N)−heme, rHSA(HL/L185N)−heme, and rHSA(HL/L185Q)−heme each showed a visible absorption band at 558−559 nm with a small shoulder at 530 nm (Figure 3a; Figure S1, Supporting Information), that was similar to the spectra observed for rHSA(HF)−heme, rHSA(HL)−heme,[11b] deoxyMb,[27] and synthetic chelated protoheme.[26] The spectral patterns clearly indicated the formation of a five-N-coordinate high-spin complex. In contrast, in the spectra of rHSA(HF/L185Q)−heme and

(21) Chu, M. M. L.; Castro, C. E.; Hathaway, G. M. *Biochemistry* **1978**, *17*, 481−486.
(22) Tsuchida, E.; Nishide, H.; Sato, Y.; Kaneda, M. *Bull. Chem. Soc. Jpn.* **1982**, *55*, 1890−1895.
(23) Uno, T.; Sakamoto, R.; Tomisugi, Y.; Ishikawa, Y.; Wilkinson, A. *Biochemistry* **2003**, *42*, 10191−10199.
(24) Vickery, L.; Nozawa, T.; Sauer, K. *J. Am. Chem. Soc.* **1976**, *98*, 343−350.
(25) Collman, J. P.; Basolo, F.; Bunnenberg, E.; Collins, T. J.; Dawson, J. H.; Ellis, P. E., Jr.; Marrocco, M. L.; Moscowitz, A.; Sessler, J. L.; Szymanski, T. *J. Am. Chem. Soc.* **1981**, *103*, 5636−5648.
(26) Traylor, T. G.; Chang, C. K.; Geibel, J.; Berzinis, A.; Mincey, T.; Cannon, J. *J. Am. Chem. Soc.* **1979**, *101*, 6716−6731.
(27) Antonini, E.; Brunori, M. *Hemoglobin and Myoglobin in Their Reactions with Ligands*; North-Holland: Amsterdam, 1971; p 18.

Table 1. UV−vis Absorption Spectral Data of rHSA(mutant)−Heme Complexes[a]

hemoproteins	λ_{max} (nm)			
	Fe^{3+}	Fe^{2+}	$Fe^{2+}O_2$	$Fe^{2+}CO$
rHSA(HF)−heme[b]	402, 533, 620	425, 532(sh), 559	411, 538, 576	419, 538, 565
rHSA(HL)−heme[b]	402, 533, 620	426, 531(sh), 559	412, 537, 573	419, 538, 565
rHSA(HF/L185N)−heme	406, 528, 618	425, 530(sh), 559	411, 540, 575	419, 539, 566
rHSA(HL/L185N)−heme	407, 530, 620	425, 530(sh), 559	411, 537, 575	419, 537, 564
rHSA(HF/L185Q)−heme	406, 530, 620	424, 528, 558		419, 538, 566
rHSA(HL/L185Q)−heme	406, 530, 620	425, 530(sh), 558	411, 537, 574[c]	419, 537, 566
rHSA(HF/L185H)−heme	407, 528, 620	424, 528, 558		419, 538, 566
rHSA(HL/L182H)−heme	410, 532, 624	425, 530, 559		419, 539, 567
rHSA(HF/R186H)−heme	411, 533, 565	424, 529, 560		420, 539, 568
rHSA(HL/R186L)−heme	406, 530, 620	426, 531(sh), 559	411, 539, 576	419, 539, 567
rHSA(HL/R186F)−heme	405, 532, 621	426, 531(sh), 559	410, 535, 571	419, 538, 568
Mb[d]	409, 503, 548(sh), 632	434, 557	418, 544, 581	423, 541, 579
chelated heme[e]	408, 540, 565	427, 530, 558	414, 543, 575	420, 540, 569

[a] In 50 mM potassium phosphate buffered solution (pH 7.0) at 22 °C. [b] Reference 11b. [c] At 5 °C. [d] Horse muscle myoglobin (Sigma); ref 11b. [e] In DMF/H_2O (7/3) at 15 °C; ref 26.

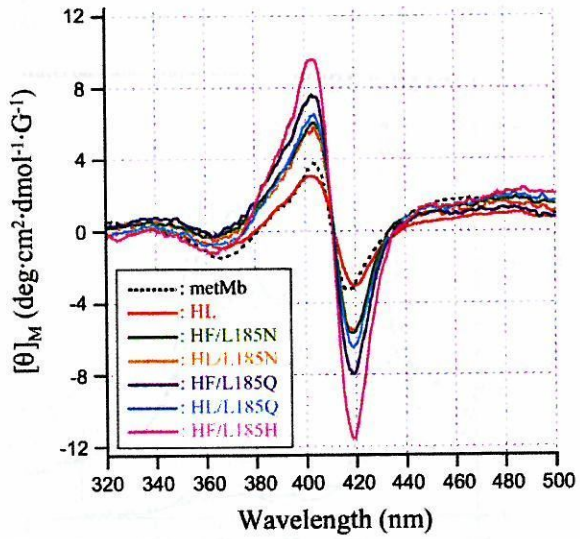

Figure 4. MCD spectra of rHSA(185-mutant)−hemin complexes in 50 mM potassium phosphate buffered solution (pH 7.0, 22 °C).

rHSA(HF/L185H)−heme, the β band at 528 nm appeared relatively sharp (Figure 3b), which suggests partial formation of a six-coordinate heme complex. This is consistent with the finding that the ferric state of these two mutant complexes had the highest peaks in the MCD.

The Soret MCD spectra of ferrous rHSA(HF/L185N)−heme, rHSA(HL/L185N)−heme, and rHSA(HL/L185Q)−heme under Ar atmosphere are dominated by an intense positive peak at 433 nm and a small trough at 402 nm as expected for the Faraday *C*-terms for high-spin ferrous porphyrins like deoxyMb (Figure 5a).[24,25] In contrast to these three mutant complexes, rHSA(HF/L185Q)−heme and rHSA(HF/L185H)−heme show weaker intensity in the Soret band region and greater intensity in the visible region (Figure 5b).

On the basis of all the UV−vis absorption and MCD spectral results, we concluded that the reduced ferrous heme is axially coordinated by His-142 at the core of the heme pocket in rHSA-(mutant) and forms a five-N-coordinate high-spin ferrous complex under an Ar atmosphere in the case of HF/L185N, HL/L185N, and HL/L185Q mutants (Figure 6a,b,d). In addition to the His-142 ligation, Gln-185 and His-185 partially interact with the sixth coordinate position of the central Fe^{2+} ion of the

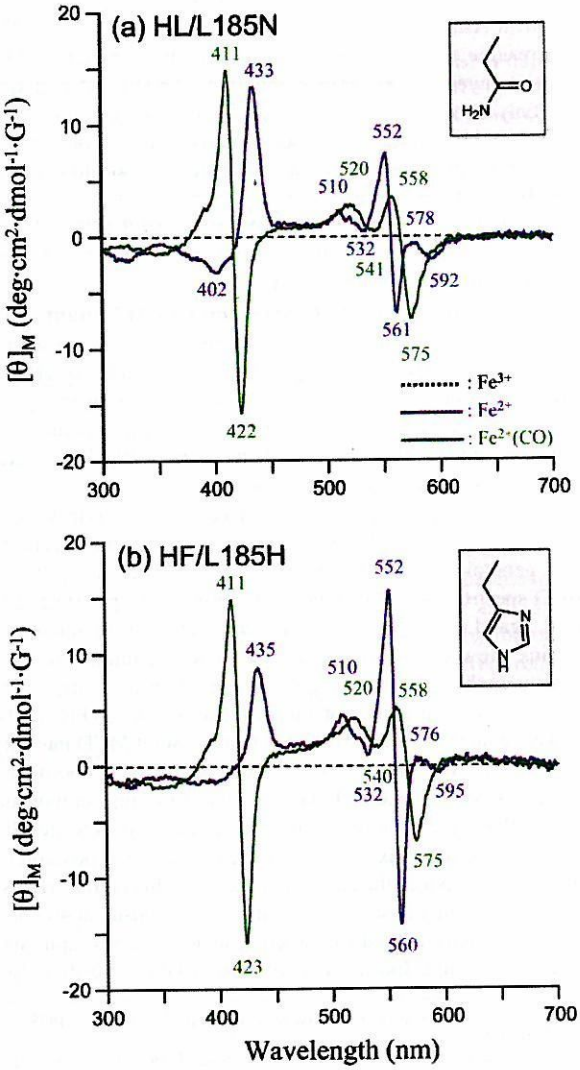

Figure 5. MCD spectral changes of (a) rHSA(HL/L185N)−heme and (b) rHSA(HF/L185H)−heme complexes in 50 mM potassium phosphate buffered solution (pH 7.0, 22 °C).

heme in the HF/L185Q and HF/L185H mutants in spite of the bulky aromatic ring of Phe-161 (Figure 6c,e). We postulated that rHSA(HL/L185Q)−heme would also form a six-coordinate

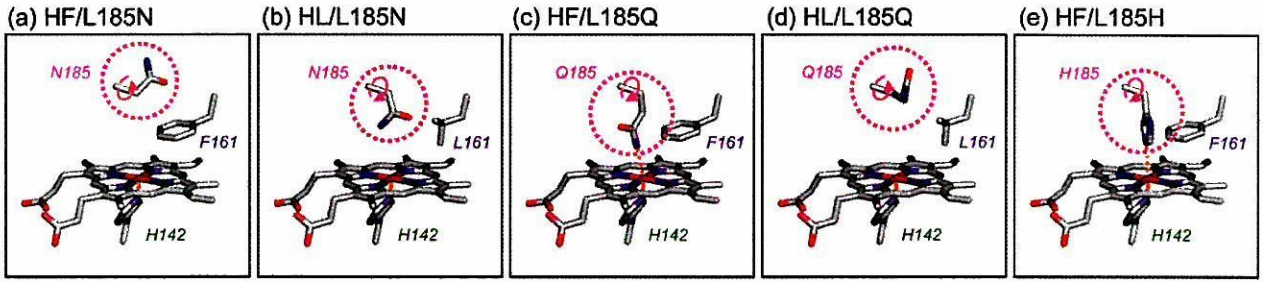

Figure 6. Structural models of the heme pocket in rHSA(triple mutant)−heme complexes: distal-side effects of engineered amino acids at position 185.

low-spin complex, because the small Leu-161 should allow additional room for rotation of Gln-185. However, it yielded a five-coordinate high-spin ferrous complex (Figure S1). This suggests that the flexible Gln-185 may interact with neighboring amino acids (Figure 6d) and underscores the difficulty in accurately predicting the impact of amino acid substitutions.

Upon exposure of the rHSA(HF/L185N)−heme and rHSA-(HL/L185N)−heme solutions to O_2, the UV−vis absorptions immediately changed to that of the O_2 adduct complex at 22 °C (Figure 3a, Table 1).[11,26,27] However, the rHSA(HL/L185Q)−heme complex bound O_2 only at 5 °C (Figure S1a) and was observed to autoxidize rapidly at 22 °C. This rapid oxidation may suggest that the distal side of the heme has an open structure, which allows easy access of water to the heme, thereby facilitating autoxidation.[28] The rHSA(HF/L185Q)−heme and rHSA(HF/L185H)−heme complexes, both of which exhibit side-chain interactions with the sixth coordinate position of the heme, were immediately oxidized by O_2 even at low temperature (5 °C).

After introduction of CO gas, all the hemoproteins produced stable carbonyl complexes with identical absorption spectral patterns (Figures 3 and S1a, Table 1).[11,26,27] In every case the carbonyl rHSA(triple mutant)−heme complexes exhibited the same S-shaped MCDs, which correspond to the *A*-term bands for the diamagnetic low-spin protoheme with CO and axial His coordinations (Figures 5 and S1b).[24,25] This result implies that in the carbonyl complexes the Asn-185 and Gln-185 residues do not act as a proximal base instead of His-142.

O_2 and CO Binding Parameters of L185N Mutants. By use of laser flash photolysis, analysis of the kinetics of ligand binding to the double mutants rHSA(HF)−heme and rHSA-(HL)−heme revealed that the asymmetric iron protoporphyrin IX molecule is accommodated in subdomain IB in two different orientations (180° rotational isomers).[11] As a result, there exist two geometries of the axial His-142 coordination to the central Fe^{2+} ion of the heme (species I and II). In species I, the proximal His coordinates to the heme without strain, while in species II, the ligation involves some distortion, resulting in weaker O_2 binding. The bending strain in the proximal His−Fe^{2+} bond in species II increases the dissociation rate constant and decreases the association rate for CO, whereas it increases the O_2 dissociation rate without changing the kinetics of the O_2 association.[16c,19] Consequently, the entire absorption decay accompanying the CO recombination with rHSA(HF)−heme or rHSA(HL)−heme was composed of two single exponentials, but the rebinding process of O_2 followed a simple monophasic decay. In rHSA(triple mutant)−hemes, this alternative geometry of the heme plane would also arise in the same manner.

We again used laser flash photolysis to characterize the O_2 and CO binding properties of the rHSA(triple mutant)−heme complexes. As expected, the binding behavior of O_2 for rHSA-(HF/L185N)−heme and rHSA(HL/L185N)−heme was broadly similar to that of the double mutants. However, detailed analysis reveals that the absorption decay accompanied by O_2 rebinding to the heme was composed of two very similar phases (Figure S2, Supporting Information). Numerous investigations of the synthetic iron porphyrins have demonstrated that the "distal-side steric effect" is the only factor that influences the association rate constant for O_2.[16c,19] The double-exponential profiles for O_2 association are therefore likely to indicate that there are two distinct conformations of the distal Asn-185 above the heme. The amplitude ratio of the two phases was approximately 1:1 for rHSA(HL/L185N)−heme, suggesting that half of the Asn residue may turn toward the inside of the heme pocket and the other turns to the outside (Figure 6b). These two conformers of the distal Asn-185 residue also influence the association rate for CO. If we were to take this minimal effect into account, the CO rebinding process would have to be analyzed as four phases. However, (i) it would be too complicated to comprehend the fundamental aspects of the ligand binding properties of rHSA(triple mutant)−heme, and (ii) the observed distal-side effect is less significant compared to the major proximal-side steric effect in this system. Hence, the absorbance decays after laser pulse irradiation to rHSA(HF/L185N)−hemeCO and rHSA(HL/L185N)−hemeCO were fitted by biphasic kinetics. The ratio of the amplitude of the dominant fast phase (species I) and minor slow phase (species II) was approximately 7:3 for rHSA(HF/L185N)−heme and 3:2 for rHSA(HL/L185N)−heme. These values were within the same range observed in the rHSA(double mutant)−heme complexes.[11] Concomitantly, the O_2 association rate of rHSA(HF/L185N)−heme or rHSA(HL/L185N)−heme was determined as one value by weighted averaging of the $k_{on}^{O_2}$ values for the two phases (Table 2).

In general, k_{off}^{CO} is a simple indicator of the bending strain in the proximal His coordination to the central Fe^{2+} ion.[16c,19] rHSA(HF)−heme, rHSA(HL)−heme, rHSA(HF/L185N)−heme, and rHSA(HL/L185N)−heme exhibited similar k_{off}^{CO} values in species I (0.008−0.013 s^{-1}) and they are identical to that of Hb(α) (R-state) (0.009 s^{-1}) (Table 3).[29] This result indicated that the axial His-142 ligation to the heme in these artificial hemoproteins has the same features as that of Hb.

(28) Brantley, R. E., Jr.; Smerdon, S. J.; Wilkinson, A. J.; Singleton, E. W.; Olson, J. S. *J. Biol. Chem.* **1993**, *268*, 6995−7010.

(29) Sharma, V. S.; Schmidt, M. R.; Ranney, H. M. *J. Biol. Chem.* **1976**, *251*, 4267−4272.

Table 2. O_2 Binding Parameters of rHSA(mutant)−Heme Complexes[a]

hemoproteins	$k_{on}^{O_2}$ (μM^{-1} s^{-1})	$k_{off}^{O_2}$ (ms^{-1}) I	$k_{off}^{O_2}$ (ms^{-1}) II	$P_{1/2}^{O_2}$ (Torr) I	$P_{1/2}^{O_2}$ (Torr) II
rHSA(HF)−heme[b]	20	0.10	0.99	3	31
rHSA(HL)−heme[b]	7.5	0.22	1.70	18	134
rHSA(HF/L185N)−heme	26	0.10	1.03	2	24
rHSA(HL/L185N)−heme	14	0.02	0.29	1	14
rHSA(HL/R186L)−heme	25	0.41	8.59	10	209
rHSA(HL/R186F)−heme	21	0.29	7.01	9	203
Hb(α) (R-state)[c]	33[d]	0.013[e]		0.24	
Mb[f]	14	0.012		0.51	
RBC[g]				8	

[a] In 50 mM potassium phosphate buffered solution (pH 7.0) at 22 °C. I or II indicates species I or II. [b] Reference 11. [c] Human hemoglobin α-subunit. [d] In 0.1 M phosphate buffer (pH 7.0, 21.5 °C); ref 30. [e] In 10 mM phosphate buffer (pH 7.0, 20 °C); ref 31. [f] Sperm whale myoglobin, in 0.1 M potassium phosphate buffer (pH 7.0, 20 °C); ref 13b. [g] Human red cell suspension, in isotonic buffer (pH 7.4, 20 °C); ref 32.

Table 3. CO Binding Parameters of rHSA(mutant)−Heme Complexes[a]

hemoproteins	k_{on}^{CO} (μM^{-1} s^{-1}) I	k_{on}^{CO} (μM^{-1} s^{-1}) II	k_{off}^{CO} (s^{-1}) I	k_{off}^{CO} (s^{-1}) II	$P_{1/2}^{CO}$ (Torr) I	$P_{1/2}^{CO}$ (Torr) II
rHSA(HF)−heme[b]	6.8	0.72	0.009	0.061	0.0011	0.068
rHSA(HL)−heme[b]	2.0	0.27	0.013	0.079	0.0053	0.240
rHSA(HF/L185N)−heme	7.7	1.09	0.008	0.043	0.0008	0.032
rHSA(HL/L185N)−heme	6.8	1.60	0.008	0.039	0.0010	0.020
rHSA(HL/R186L)−heme	5.0	0.57	0.011	0.165	0.0018	0.234
rHSA(HL/R186F)−heme	7.9	1.12	0.010	0.148	0.0010	0.107
Hb(α) (R-state)[c]	4.6[d]		0.009[e]		0.0016[f]	
Mb[g]	0.51		0.019		0.030	

[a] In 50 mM potassium phosphate buffered solution (pH 7.0) at 22 °C. I or II indicates species I or II. [b] Reference 11. [c] Human hemoglobin α-subunit. [d] In 50 mM potassium phosphate buffer (pH 7.0, 20 °C); ref 33. [e] In 0.1 M phosphate buffer (pH 7.0, 20 °C); ref 29. [f] Calculated from $(k_{on}^{CO}/k_{off}^{CO})^{-1}$. [g] Sperm whale myoglobin, in 0.1 M potassium phosphate buffer (pH 7.0, 20 °C); ref 13b.

Effect of Asn-185 Residue on O_2 Binding Affinity. The O_2 and CO binding parameters for the rHSA(HF)−heme and rHSA(HF/L185N)−heme complexes did not show any significant differences. The bulky benzyl side chain of Phe-161 may retard rotation of the polar amide group of Asn-185 and thereby maintain the polarity and size of the distal pocket (Figure 6a). In contrast, there are marked differences in the comparison of the O_2 and CO binding parameters for rHSA(HL)−heme and rHSA(HL/L185N)−heme. First, the presence of Asn rather than Leu at position 185 resulted in 2- and 3−6-fold increases in the association rate constants for O_2 and CO, respectively. As described above, the kinetics of O_2 binding to rHSA(HL/L185N)−heme actually consist of two phases. The Asn may partly rotate upward, which provides a somewhat greater space for the distal pocket. This presumably increases the association rate constants. Second, Asn-185 induced 18- and 10-fold increases in the O_2 binding affinity for species I and II, respectively (Table 2); these increases were predominantly due to the 6−11-fold diminution of the $k_{off}^{O_2}$ values. This corresponds to a free energy difference of −1.8 kcal mol^{-1} at 22 °C that may be attributable to a H-bond interaction with the bound O_2. This is consistent with the observation that, in HbO_2 and MbO_2, the distal His-64 stabilizes the coordinated O_2 by −0.6∼−1.4 kcal mol^{-1} due to the H-bonding.[13] Unfortunately, attempts to measure the stretching frequency of the bound O_2 molecule in rHSA(HL/L185N)−heme by infrared spectroscopy failed because the O_2 adduct complex was not sufficiently stable. Nevertheless, it is noteworthy that the high O_2 binding affinity ($P_{1/2}^{O_2}$ 1 Torr) for rHSA(HL/L185N)−heme is now close to that of natural Hb(α) (0.24 Torr)[30,31] and Mb (0.5 Torr)[13] (Table 2).

Replacement of L182 or R186 by His. Leu-182 and Arg-186 were also considered to be good candidates for introduction of the distal His, so we prepared the rHSA(HL/L182H) and rHSA(HF/R186H) triple mutants (Figure 1). Modeling trials demonstrated that neither of these introduced histidines is coplanar with the Fe−O−O moiety. Rather, they are positioned off to the side, so that there may be an oblique interaction with the coordinated O_2 and the heme center.

The rHSA(HL/L182H)−hemin complex and its reduced form showed spectra similar to those of rHSA(HF/L185H)−heme. In contrast, the color of the ferric rHSA(HF/R186H)−hemin solution was bright red, and the UV−vis absorption spectrum clearly showed the formation of a bis-histidine-coordinated low-spin ferric complex (Figure 7a).[22,26] The MCD intensity of the S-shaped curve in the Soret band region (Figure 8) was higher than that observed with rHSA(HF/L185H)−hemin (Figure 4). The chemical reduction of the Fe^{3+} complex results in very sharp β, α bands in the visible absorption spectrum (529, 560 nm) (Figure 7a). In MCD, we observed the loss of the strong *C*-terms in the Soret band and the appearance of intense *A*-terms corresponding to the α band (Figure 7b). They all resembled those of the typical bis-histidyl hemochrome, for example, cytochrome b_5,[34] soluble guanylcyclase,[35a] and bis-imidazole-bound protoheme,[22,26,35b] as well as Hpx.[1b] It can be concluded that rHSA(HF/R186H)−heme produced a strong six-coordinate low-spin ferrous complex under an Ar atmosphere. Unfortunately, the ferrous forms of both rHSA(HF/R186H)−heme and rHSA(HL/L182H)−heme were readily autoxidized upon the addition of O_2 gas. It is known that bis-histidyl hemochromes are rapidly oxidized by O_2 via an outer-sphere mechanism.[21] We have demonstrated that this also applies to our artificial hemoprotein, the rHSA(mutant)−heme system.

O_2 and CO Binding Parameters for R186L and R186F Mutants. We have clearly shown that the O_2 binding equilibrium and kinetics of rHSA−heme complexes may be significantly enhanced by site-directed mutagenesis. In fact, the O_2 binding affinity of the rHSA(HL/L185N)−heme complex (1 Torr) was shown to be similar to those of Mb and the high-affinity R-state of Hb(α). However, for saline solutions of artificial rHSA−heme complexes to provide effective lung-to-tissue O_2 transport in vivo, the affinity should be reduced to render it more similar to the affinity of human RBC ($P_{1/2}^{O_2}$ 8 Torr).[32] This requires an O_2 binding affinity that is intermediate between the values observed for rHSA(HL)−heme and rHSA(HL/L185N)−heme.

Both site-directed mutagenesis and synthetic porphyrin approaches have previously shown that an effective way to diminish the O_2 binding affinity of the heme is to introduce a

(30) Gibson, Q. H. *J. Biol. Chem.* **1970**, *245*, 3285−3288.
(31) Olson, J. S.; Andersen, M. E.; Gibson, Q. H. *J. Biol. Chem.* **1971**, *246*, 5919−5923.
(32) Imai, K.; Morimoto, H.; Kotani, M.; Watari, H.; Hirata, W.; Kuroda, M. *Biochim. Biphys. Acta.* **1970**, *200*, 189−197.
(33) Steinmeier, R. C.; Parkhurst, L. J. *Biochemistry* **1975**, *14*, 1564−1571.
(34) Vickery, L.; Salmon, A.; Sauer, K. *Biochim. Biophys. Acta.* **1975**, *386*, 87−98.
(35) (a) Burstyn, J. N.; Yu, A. E.; Dierks, E. A.; Hawkins, B. K.; Dawson, J. H. *Biochemistry* **1995**, *34*, 5896−5903. (b) Svastits, E. W.; Dawson, J. H. *Inorg. Chim. Acta.* **1986**, *123*, 83−86.

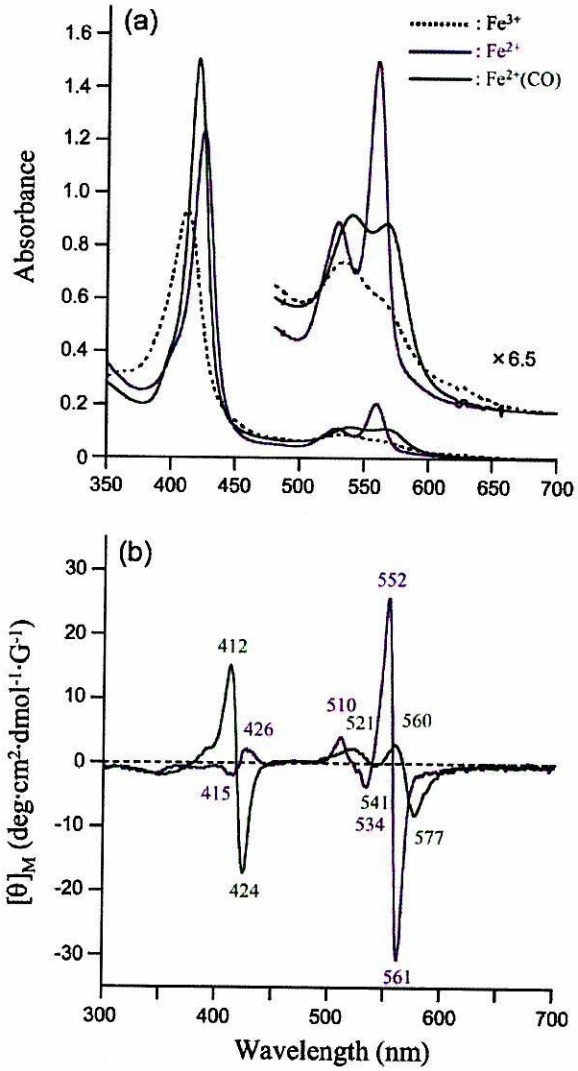

Figure 7. (a) UV−vis and (b) MCD spectral changes of rHSA(HF/R186H)−heme complex in 50 mM potassium phosphate buffered solution (pH 7.0, 22 °C).

hydrophobic amino acid (or substituent) around the O_2 binding site.[13,14,17−19] We expected that increasing the hydrophobicity of the distal side of the heme pocket by insertion of a nonpolar residue would reduce the O_2 binding affinity of the rHSA−heme complex. The most suitable position for this introduction could be at Arg-186, which is the entrance of the heme pocket and is rather close to the central Fe^{2+} ion.

Thus, we designed new triple mutants rHSA(HL/R186L) and rHSA(HL/R186F) in an effort to prepare rHSA-based artificial hemoproteins having the same O_2 binding affinity as human RBC (Figure 9). An important structural factor in these mutants is Y161L, which is likely to allow rotation of the isopropyl group of Leu-185 above the O_2 coordination site.

MCD spectra in the Soret band region of ferric rHSA(HL/R186L)−hemin and rHSA(HL/R186F)−hemin both showed very low intensity, essentially the same as that observed for rHSA(HL)−hemin (Figure 8). The reduced ferrous form demonstrated the characteristic UV−vis absorption and MCD spectra of the five-N-coordinate high-spin complex under an Ar atmosphere (Table 1; Figure S3, Supporting Information).

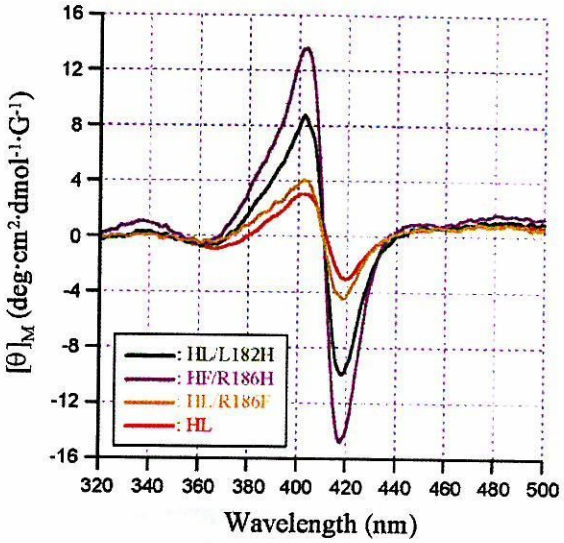

Figure 8. MCD spectra of rHSA(182-mutant)−hemin and rHSA(186-mutant)−hemin complexes in 50 mM potassium phosphate buffered solution (pH 7.0, 22 °C).

Upon bubbling of O_2 gas through the solutions, the spectral patterns were shifted to that of the O_2 adduct complex. The distinct features of all the spectra were quite similar to those of rHSA(HL)−heme.

Following laser flash photolysis, the absorption decays associated with O_2 recombination with rHSA(HL/R186L)−heme and rHSA(HL/R186F)−heme were monophasic, which suggests that the distal space in the pocket is uniform, in contrast to the L185N mutants. The kinetics for CO rebinding were still composed of double exponentials, consistent with the existence of two different geometries of the axial His-142 coordination to the central Fe^{2+} ion of the heme.

We previously showed that rHSA(HF) binds O_2 with significantly higher affinity than rHSA(HL) and reasoned that the presence of Leu rather than Phe at position 161 allowed a downward rotation of the adjacent L185 side chain that restricted access to the O_2 binding site on the heme group and reduced the affinity by a factor of 6 (Table 2).[11b] Strikingly, however, insertion of Leu or Phe at position 186 in the presence of Leu-161 [as in rHSA(HL/R186L)−heme and rHSA(HL/R186F)−heme complexes] yielded $k_{on}^{O_2}$ and k_{on}^{CO} values that were 3−4-fold higher than those of rHSA(HL)−heme. The presence of a hydrophobic residue at position 186 may restrict the mobility of Leu-185 and thereby enhance access to the O_2 binding site (Figure 9).

Overall, the O_2 and CO binding parameters of rHSA(HL/R186L)−heme and rHSA(HL/R186F)−heme were more similar to those of rHSA(HF)−heme. In species I, for example, the k_{off}^{CO} values were almost identical, which again implies unhindered axial coordination structures of His-142 to the heme; as a result, the CO binding affinities of these triple mutants ($P_{1/2}^{CO}$ 0.0010−0.0018 Torr) were close to that of the rHSA(HF)−heme complex. In contrast, the O_2 dissociation rate constants of rHSA(HL/R186L)−heme and rHSA(HL/R186F)−heme were 3−4-fold higher than found for rHSA(HF)−heme, which modestly reduced the O_2 binding affinities (higher $P_{1/2}^{O_2}$). This could be due to the increase in the hydrophobicity in the distal pocket. Crucially, the O_2 binding affinities of rHSA(HL/

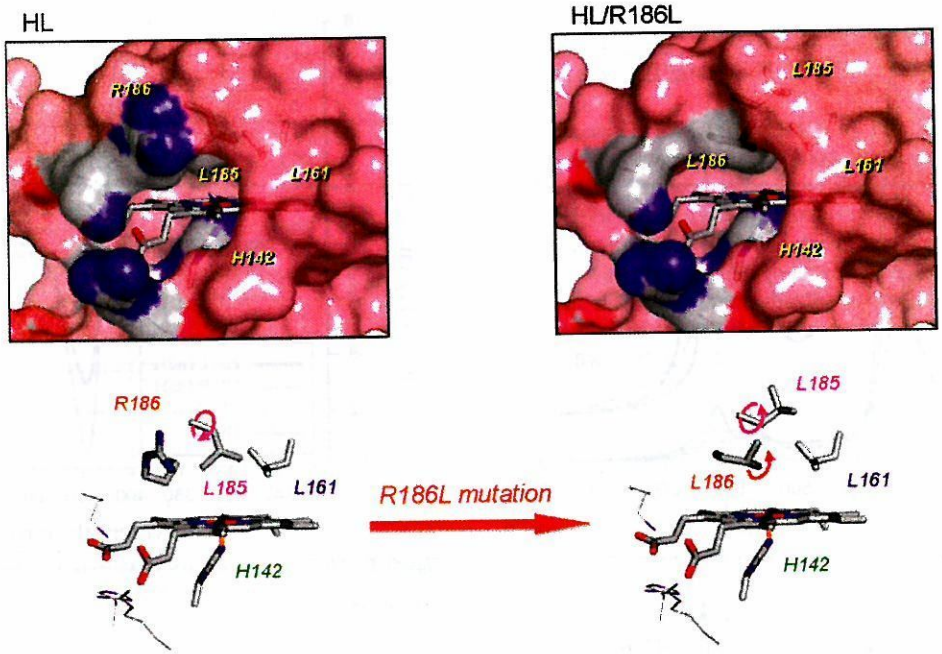

Figure 9. Structural models of rHSA(HL)−heme and rHSA(HL/R186L)−heme complexes. Introduction of R186L mutation may induce upward rotation of the L185 residue.

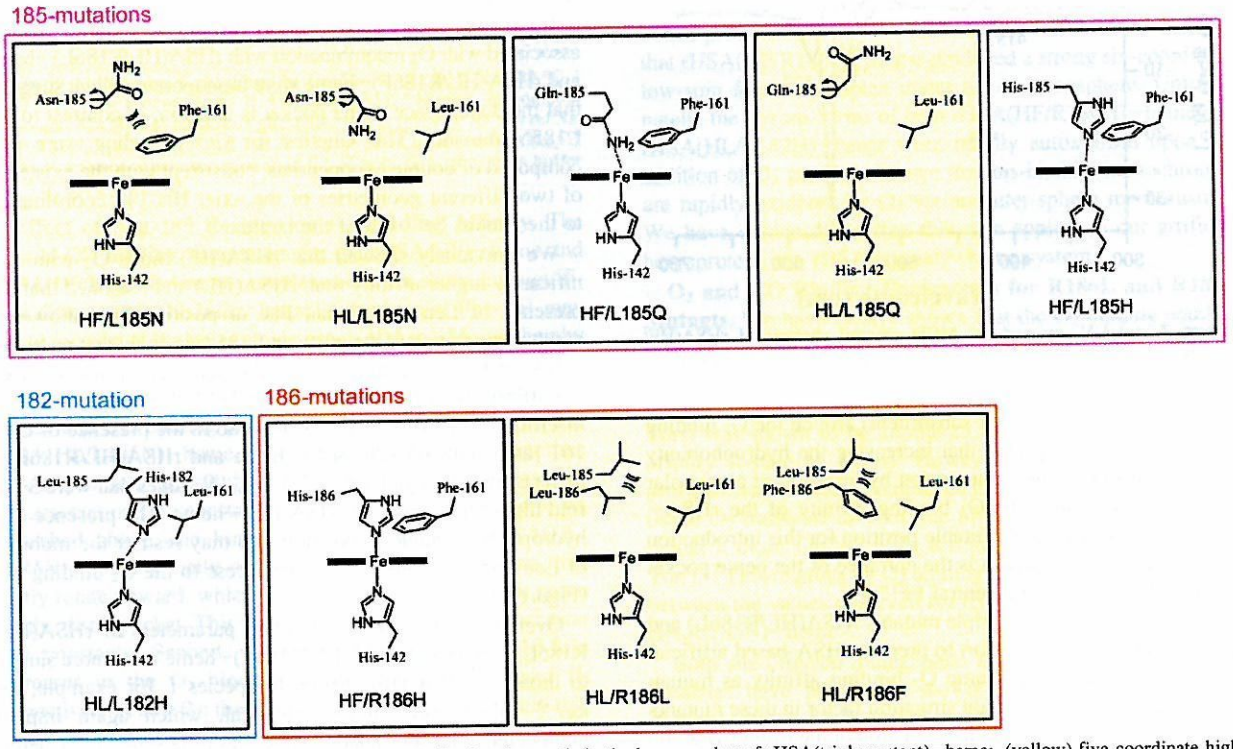

Figure 10. Schematic illustrations of the engineered distal amino acids in the heme pocket of rHSA(triple mutant)−heme: (yellow) five-coordinate high-spin ferrous complex; (blue) five-coordinate high-spin complex including six-coordinate low-spin ferrous complex; (pink) six-coordinate low-spin ferrous complex.

R186L)−heme ($P_{1/2}^{O_2}$ 10 Torr) and rHSA(HL/R186F)−heme ($P_{1/2}^{O_2}$ 9 Torr) are essentially indistinguishable from that of human RBC ($P_{1/2}^{O_2}$ 8 Torr). These results show that there are several different combinations of mutations that can confer the RBC-like O_2 binding affinity to the prosthetic heme group. Another possibility, yet to be explored, is that insertion of a proximal His into the 186 position would construct a distal pocket on the opposite side of the porphyrin plane (the Ile-142 side), that would provide somewhat different O_2 binding properties of the heme.

Conclusions

Transport of O_2 by rHSA−heme complexes could be of great clinical importance, not only as a blood alternative but also as an O_2-providing therapeutic fluid. Such a synthetic compound has the potential advantage of not having to be matched to the recipient's blood type; moreover, it could be prepared in controlled facilities without viral contamination.

We have previously demonstrated that rHSA−heme complexes can be engineered to bind O_2 reversibly;[11] however, these complexes did not display optimal O_2 binding affinities. By use of structure-based mutagenesis of HSA combined with chemical modification of the synthetic iron−porphyrin, we have attempted to modify the heme pocket architecture so as to refine the O_2 binding properties of rHSA−heme complexes. By focusing on modifications on the distal side of the heme binding pocket in rHSA, we have successfully engineered distinct rHSA(triple mutant)−heme complexes with a broad range of O_2 binding affinities. Schematic illustrations of the engineered distal amino acids in the heme pocket of the different rHSA mutants are shown in Figure 10. These include mutants such as rHSA(HL/L185N) with affinities that mimic the high affinity of Hb(α) ($P_{1/2}^{O_2}$ 0.24 Torr) and others [e.g., rHSA(HL/R186L)] with affinities similar to that of human RBC ($P_{1/2}^{O_2}$ 8 Torr).

The highest affinity mutants rHSA(HL/L185N) and rHSA(HF/L185N) both contain Asn-185, which has a short amide side chain that significantly enhances the O_2 binding affinity, particularly when the neighboring amino acid is Leu-161. The N−H bond of the Asn-185 may face the terminal oxygen atom of the Fe−O_2 moiety, providing an amide dipole that stabilizes the O_2 binding to the heme. This interpretation is consistent with the findings of Chang et al.,[36] who first demonstrated that the dipole−dipole interaction between the Fe−O_2 and amide group can produce kinetic and thermodynamic control of the dioxygenation of the model hemes. In contrast, introduction of the larger Gln and His side chains at position 185 partly provided a six-coordinate heme character and therefore did not stabilize O_2 binding.

In a different approach, substitution of the polar Arg-186 at the entrance of the heme pocket with Leu or Phe caused a useful reduction in the O_2 binding affinity, yielding $P_{1/2}^{O_2}$ values that are very close to that of the human RBC and therefore well adapted for O_2 transport in vivo (Table 2). The impact of these substitutions may be due to their interaction with the adjacent residue, L185, which results in enhanced access to the O_2 binding site.

(36) Chang, C. K.; Ward, B.; Young, R.; Kondylis, M. P. *J. Macromol. Sci., Chem.* **1988**, *A25*, 1307−1326.

Other mutations were deleterious to O_2 binding but nevertheless produced complexes that might have other uses. For example, rHSA(HF/R186H)−heme formed a typical bis-histidyl Fe^{3+} or Fe^{2+} complex. In the circulation, free hemin is known to participate in the Fenton reaction to produce the highly toxic hydroxyl radical. However, it is sequestered by Hpx, in which the bis-histidyl coordination tightly fixes the hemin with the highest binding affinity of any known protein.[1,2] In the same manner, rHSA(HF/R186H) has a bis-histidine clamp for hemin and might conceivably be exploited as an antioxidant reagent to protect the body from oxidative damage after blood heme overload.

On the other hand, it would be of great importance to study the NO binding property of rHSA(mutant)−heme for practical medical applications. Some of the Hb-based blood substitutes leak through the vascular endothelium and capture the endothelial-derived relaxing factor, NO, that elicits an acute increase in blood pressure by vasoconstriction.[37] Our rHSA(mutant)−heme would bind NO in the same way as Hb, but it would not induce such hypertension, because the albumin carrier has low permeability through the muscle capillary pore.[38]

Ultimately, to fully understand the structural basis of the effects of the various mutations on O_2 binding, it will be necessary to examine the structural details of the heme binding pocket. Crystal structural analysis of the rHSA(mutant)−heme complexes is now underway. Structural information should enhance our ability to design mutations that will further optimize the O_2 binding properties of these complexes.

Acknowledgment. This work was supported by PRESTO "Control of Structure and Functions", JST, Grant-in-Aid for Scientific Research (16350093) from JSPS, and by Health Science Research Grants (Regulatory Science) from MHLW Japan. The work at Imperial College London was partially carried out as the Japan−U.K. Research Cooperative Program (Joint Project) of JSPS.

Supporting Information Available: UV−Visible absorption and MCD spectra of rHSA(HL/L185Q)−heme, absorption decay of O_2 rebinding to rHSA(HL/L185N)−heme after laser flash photolysis, and MCD spectra of rHSA(HL/R186F)−heme complex. This material is available free of charge via the Internet at http://pubs.acs.org.

JA074179Q

(37) Squires, J. E. *Science* **2002**, *295*, 1002−1005.
(38) Tsuchida, E.; Komatsu, T.; Matsukawa, Y.; Nakagawa, A.; Sakai, H.; Kobayashi, K.; Suematsu, M. *J. Biomed. Mater. Res.* **2003**, *64A*, 257−261.

POLYMERS FOR ADVANCED TECHNOLOGIES
Polym. Adv. Technol. 2005; **16**: 73–83
Published online 7 January 2005 in Wiley InterScience (www.interscience.wiley.com). DOI: 10.1002/pat.559

PAT

Oxygen infusions (hemoglobin-vesicles and albumin-hemes) based on nano-molecular sciences†

Eishun Tsuchida[1]*, Hiromi Sakai[1], Teruyuki Komatsu[1], Shinji Takeoka[1], Yubin Huang[1], Keitaro Sou[1], Akito Nakagawa[1], Yuji Teramura[1] and Koichi Kobayashi[2]

[1]Advanced Research Institute for Science & Engineering, Waseda University, Tokyo 169-8555, Japan
[2]Department of Surgery, School of Medicine, Keio University, Tokyo 160-8582, Japan

Since the discovery of a red-colored saline solution of a heme derivative that reversibly binds and releases oxygen (1983), significant efforts have been made to realize an oxygen infusion as a red cell substitute based on the sciences of both molecular assembling phenomena and macromolecular metal complexes. The authors have specified that hemoglobin (Hb)-vesicles (HbV) and recombinant human serum albumin-hemes (rHSA-heme) would be the best systems that meet the clinical requirements. (A) Hb is rigorously purified from outdated, donated red cells via pasteurization and ultrafiltration, to completely remove blood type antigen and pathogen. The HbV encapsulates thus purified concentrated Hb solution with a phospholipid bimolecular membrane (diameter, 250 nmø), and its solution properties can be adjusted comparable with blood. Surface modification of HbV with a water-soluble polymer ensures stable dispersion state and storage over a year at 20°C. *In vivo* tests have clarified the efficacy for extreme hemodilution and resuscitation from hemorrhagic shock, and safety in terms of biodistribution, metabolism in reticuloendothelial system (RES), clinical chemistry, blood coagulation, etc. The HbV does not induce vasoconstriction thus maintains blood flow and tissue oxygenation. (B) rHSA is now manufactured in Japan as a plasma-expander. The rHSA can incorporate eight heme derivatives (axial base substituted hemes) as oxygen binding sites, and the resulting rHSA-heme is a totally synthetic O_2-carrier. Hb binds endothelium-derived relaxation factor, NO, and induces vasoconstriction. The rHSA-heme binds NO as Hb does, however, it does not induce vasoconstriction due to its low pI (4.8) and the resulting low permeability across the vascular wall (1/100 of Hb). A 5%-albumin solution possesses a physiologic oncotic pressure. Therefore, to increase the O_2-transporting capacity, albumin dimer is effective. Albumin dimer can incorporate totally 16 hemes with a regulated oncotic pressure. The rHSA-heme is effective not only as a red cell substitute but also for oxygen therapeutics (e.g. oxygenation for tumor). Significant efforts have been made to produce HbV and rHSA-heme with a facility of Good Manufacturing Practice (GMP) standard, and to start preclinical and finally clinical trials.

KEYWORDS: oxygen infusion; blood substitutes; surface modification; water-soluble polymers; biomaterials

INTRODUCTION

For human beings to survive, it is necessary to continuously deliver O_2 that is needed for the respiration of all tissue cells. Blood, a so-called moving internal-organ, reversibly binds and releases O_2 under physiological conditions. From this point of view, realization of red blood cell (RBC) substitutes, or O_2-infusions, would contribute significantly to human health and welfare. In this research field, the basic sciences for macromolecular complexes, molecular assemblies, and nano-molecular sciences play fundamental roles. The authors have systematically studied the metal complexes (synthetic heme derivatives) embedded into a hydrophobic cluster in aqueous medium, and clarified that the electronic processes of the active sites are controlled by the surrounding molecular environment. As a result, the reaction activity is observed as cooperative phenomena with the properties of the molecular atmosphere. In other words, the development of our O_2-infusion has been based on "the regulation of the electronic process on macromolecular metal complexes".[1,2]

To reproduce the O_2-binding ability of RBCs, that is, the development of a synthetic O_2-carrier that does not need hemoglobin (Hb), was the starting point of the idea for this study. In general, central ferric iron of a heme is immediately oxidized by O_2 in water, preventing the O_2 coordination process from being observed. Therefore, the electron transfer

*Correspondence to: E. Tsuchida, Professor, Advanced Research Institute for Science and Engineering, Waseda University, Tokyo 169-8555, Japan.
E-mail: eishun@waseda.jp
†Selected paper presented at the 7th International Symposium on Polymers for Advanced Technologies, 21–24 September 2003, Fort Lauderdale, Florida, USA.

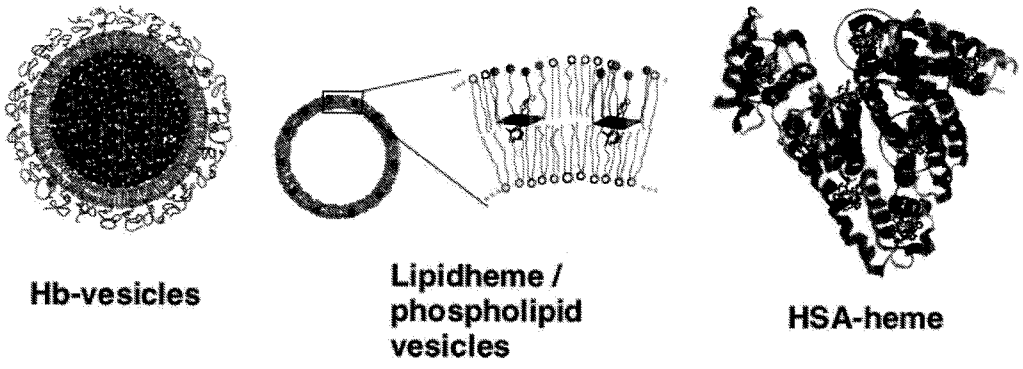

Figure 1. Schematic representation of lipidheme-vesicle, hemoglobin-vesicle, and albumin-heme.

must be prevented. Fortunately, the formation of the O_2-adduct complex could be detected but for only several nano-seconds by utilizing the molecular atmosphere and controlling the electron density in the iron center. Based on this finding, the authors succeeded in reversible and stable O_2-coordination in 1983 and preparing phospholipid vesicles embedded amphiphilic-heme, known as lipidheme/phospholipids vesicles (Fig. 1).[3–5] This was the first example of reversible O_2-binding taking place under physiological conditions. For example, human blood can dissolve about 27 ml of O_2 per dl, however a 10 mM lipidheme-phospholipid vesicle solution can dissolve 29 ml of O_2 per dl. This material is suitable for "O_2-infusion". Thus over hundred types of heme derivatives have been synthesized, and recently new lipidheme bearing phospholipid groups have been synthesized, which completes self-organization in water to form stable vesicles.[6]

In 1985, Dr Sekiguchi at Hokkaido Red Cross Blood Center proposed Waseda group to consider the utilization of Hb in outdated RBCs. Thus the research of Hb-vesicles (HbV) based on molecular assembly technologies was started. In the latter 1990s, a mass-production system for recombinant human serum albumin (rHSA) was established and then albumin-heme hybrids (rHSA-heme) using its non-specific binding ability was prepared, which is now considered to be a promising synthetic material. Based on the effective integration of nano-molecular science and technologies for functional materials developed by Waseda University, and the outstanding evaluation system of safety and efficacy developed by Keio University using animal experiments, strong progress on the research of the O_2-infusion project has been made. In the near future, mass production and clinical tests of O_2-infusion will be started by the pharmaceutical industry.

DEVELOPMENT OF Hb-BASED O_2-CARRIERS AND THE CHARACTERISTICS OF HbV

Historically, the first attempt of Hb-based O_2-carrier in this area was to simply use stroma-free Hb (Fig. 2). However, several problems became apparent, including dissociation into

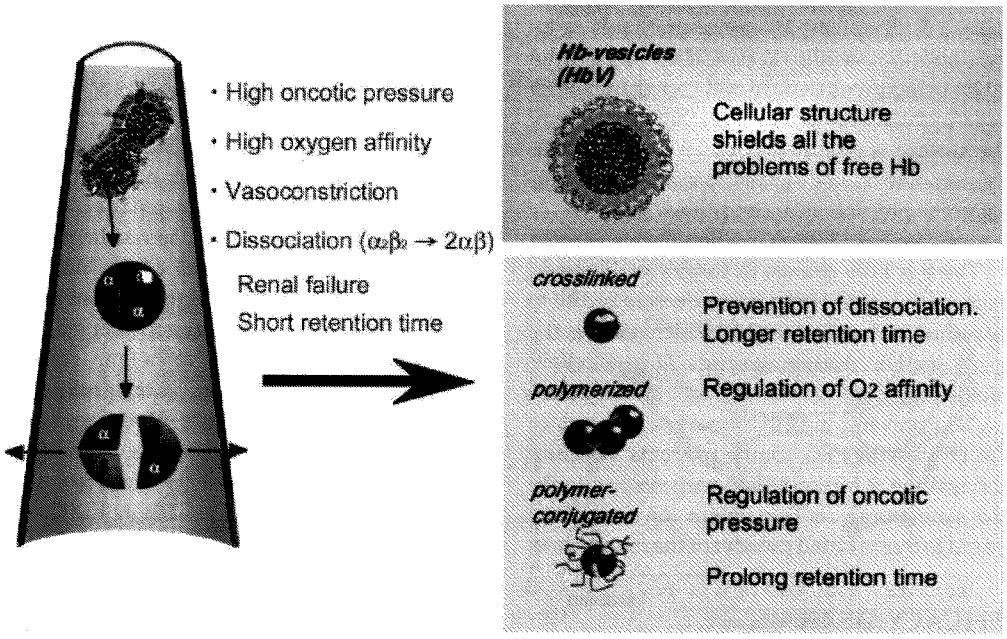

Figure 2. Approaches to solve the problems of utilization of Hb as an O_2-carrier, chemical modification or encapsulation of Hb.

dimers that have a short circulation time, renal toxicity, high oncotic pressure and high O_2-affinity. Since the 1970s, various approaches were developed to overcome these problems.[7,8] This includes intra-molecular crosslinking, polymerization and polymer-conjugation. However, in some cases the significantly different structure in comparison with RBCs resulted in side effects such as vasoconstriction.[9]

Another idea is to encapsulate Hb with a lipid bilayer membrane to solve all the problems of molecular Hb.[10] RBCs have a biconcave structure with a diameter of about 8000 nm. RBCs can deform to a parachute-like configuration to pass through narrow capillaries. The possibility of infection and blood-type mismatching, and short shelf life are the main problems. The idea of Hb encapsulation with a polymer membrane mimicking the structure of RBC is originated from Dr Chang at McGill University.[7] After that, the encapsulation of Hb within a phospholipid vesicle was studied by Dr Djordjevich at the University of Illinois in the 1970s.[11] However, it was not so easy to make HbV with a regulated diameter and adequate O_2-transport capacity, the authors made a breakthrough in routinely producing HbV by using fundamental knowledge of macromolecular and supramolecular sciences.[12–19] Several liters of HbV are routinely prepared in a completely sterile condition. Hb is purified from outdated RBCs, and concentrated to 40 g/dl. Virus removal is performed using a combination of pasteurization at 60° and filtration with a virus removal filter. The Hb encapsulation with phospholipids bilayer membrane and size regulation was performed with an extrusion method. The vesicular surface is modified with polyethylene glycol (PEG) chains. The suspension of Hb-vesicles is deoxygenated at the final stage.

The particle diameter of HbV is regulated to about 250 nm, therefore, the bottle of HbV is turbid. One vesicle contains about 30,000 Hb molecules so that it does not show oncotic pressure. There is no chemical modification of Hb. O_2-affinity is controllable with an appropriate amount of allosteric effectors, pyridoxal 5-phosphate. Hb concentration is regulated to 10 g/dl, and the weight ratio of Hb to total lipid approaches 2.0 by using an ultra pure and concentrated Hb solution of 40 g/dl, which is covered with a thin lipid bilayer membrane. The surface is modified with 0.3 mol% of PEG-lipid. Viscosity, osmolarity, and oncotic pressure are regulated according to the physiological conditions.

HbV can be stored for over 2 years in a liquid state at room temperature.[17] There is little change in turbidity, diameter, and P_{50}. Methemoglobin (MetHb) content decreases due to the presence of reductant inside the HbV, which reduces the trace amount of metHb during storage. This excellent stability is obtained by deoxygenation and PEG-modification. Deoxygenation prevents metHb formation. The surface modification of HbV, with PEG chains prevents vesicular aggregation and leakage of Hb and other reagents inside the vesicles. Liquid state storage is convenient for emergency infusion compared to freeze-dried powder or the frozen state.

IN VIVO EFFICACY OF HbV

The efficacy of HbV has been confirmed mainly with isovolemic hemodilution and resuscitation from hemorrhagic shock.[20–28] In this review two important cases are described. One is isovolemic hemodilution with 90% blood exchange in a rat model. The other is resuscitation from hemorrhagic shock in a hamster model.

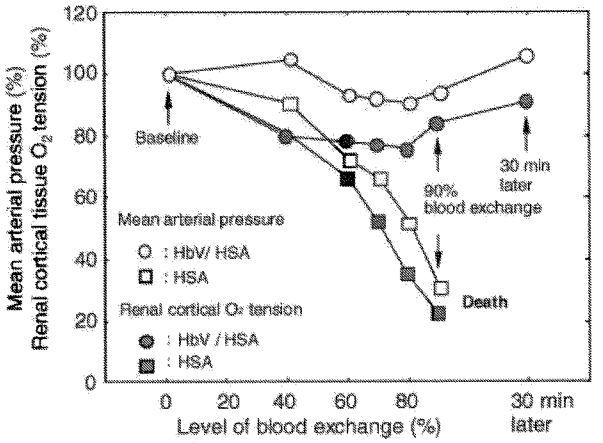

Figure 3. Ninety per cent exchange-transfusion with HbV suspended in HSA (HbV/HSA), or HSA alone. Mean arterial pressure and renal cortical oxygen tension were monitored.

To confirm the O_2-transporting ability of HbV, extreme hemodilution was performed with HbV suspended in human serum albumin (HSA)[21,23] (Fig. 3). The final level of blood exchange reached 90%. Needle-type O_2 electrodes were inserted into the renal cortex, and the blood flow rate in the abdominal aorta was measured with the pulsed Doppler method. Hemodilution with albumin alone resulted in significant reductions in mean arterial pressure and renal cortical O_2 tension, and finally all the rats died of anemia. However, hemodilution with HbV, suspended in HSA sustained both blood pressure and renal cortical O_2 tension, and all the rats survived. These results clearly demonstrate that HbV has sufficient O_2 transporting capability.

To observe the microcirculatory response to the infusion of Hb products, intravital microscopy was used equipped with all the units to measure blood flow rates, vascular diameter, O_2 tension, and so on, in collaboration with Dr Intaglietta at the University of California, San Diego. The hamster dorsal-skin fold preparation allows observation of blood vessels from small arteries down to capillaries. The HbV suspension, as a resuscitative fluid for hemorrhagic-shocked hamsters was evaluated.[26] About 50% of the blood was withdrawn, and the blood pressure was maintained at around 40 mmHg for 1 hr, and the hamsters either received HbV suspended in HSA (HbV/HSA), HSA alone, or shed blood (Fig. 4). Immediately after infusion, all the groups showed increases in mean arterial pressure. However, only the albumin infusion resulted in incomplete recovery. However, the HbV/HSA group showed the same recovery with the shed autologous blood infusion. During the shock period, all the groups showed significant hyperventilation that was evident from the significant increase in arterial O_2 tension. Simultaneously, base excess and pH decreased significantly. Immediately after resuscitation, all the groups tended to recover. However, only the HSA group showed sustained hyperventilation. Base excess for the HSA group remained at a

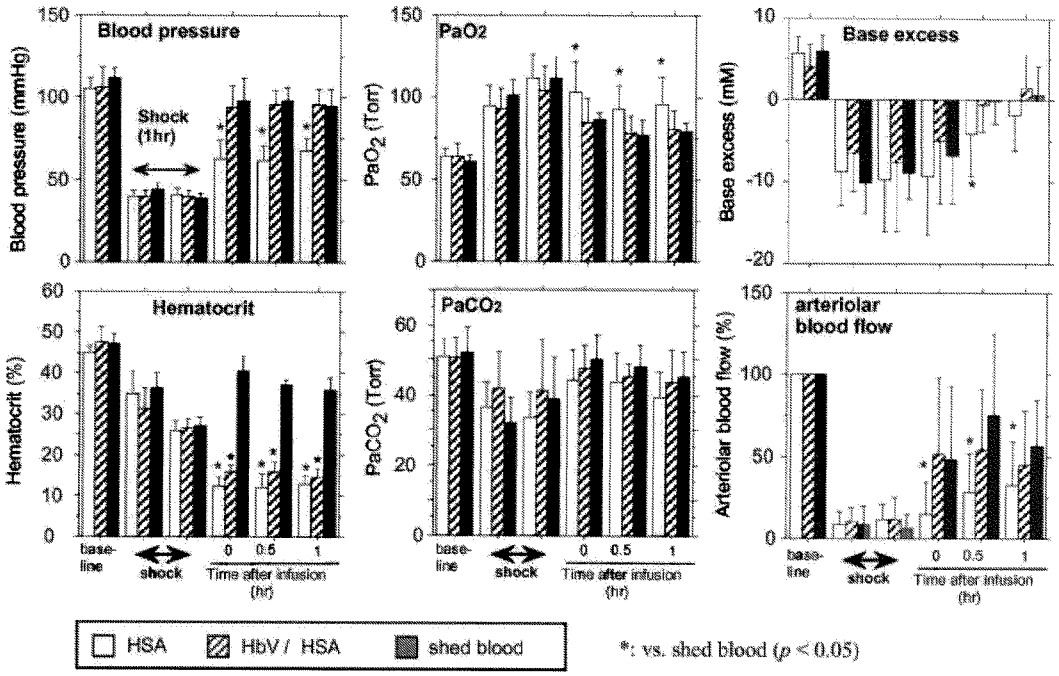

Figure 4. Resuscitation from hemorrhagic shock with HbV suspended in HSA (HbV/HSA) in hamster dorsal skinfold model. Mean ± SD.

significantly lower value 1 hr after resuscitation. Blood flow decreased significantly in arterioles to 11% of basal value during shock. The HbV/HSA and shed autologous blood groups immediately showed significant increases in blood flow rate after resuscitation, while the albumin group showed the lowest recovery.

SAFETY EVALUATION OF HbV

The safety profile of HbV such as cardiovascular responses, pharmacokinetics, influence on RES, influence on clinical measurements and daily repeated infusions were further examined.[29–37]

The microvascular responses to the infusion of intramolecularly crosslinked Hb (XLHb) and HbV were studied using conscious hamsters. XLHb (7 nm in diameter) showed a significant increase in hypertension equal to 35 mmHg, and simultaneous vasoconstriction of the resistance artery equal to 75% of the baseline levels[30] (Fig. 5). However, HbV with diameter of 250 nm showed minimal changes. The small acellular XLHb is homogeneously dispersed in the plasma, and it diffuses through the endothelium layer of the vascular wall and reaches the smooth muscle. XLHb traps nitric oxide (NO) as an endothelium-derived relaxation factor, and induces vasoconstriction, and hypertension. However, the large HbV stay in the lumen and does not induce vasoconstriction. Several mechanisms are proposed for Hb-induced vasoconstriction. These include NO-binding, excess O_2 supply, reduced shear stress, or the presence of Hb recognition site on the endothelium. But it is clear that Hb-encapsulation shields against the side effects of acellular Hbs.

Professor Suematsu at Keio University has revealed the effects of Hb-based O_2 carriers in hepatic microcirculation[29,32] (Fig. 6). On the vascular wall of the sinusoid in hepatic microcirculation, there are many pores, called fenestration, with a diameter of about 100 nm. The small Hb

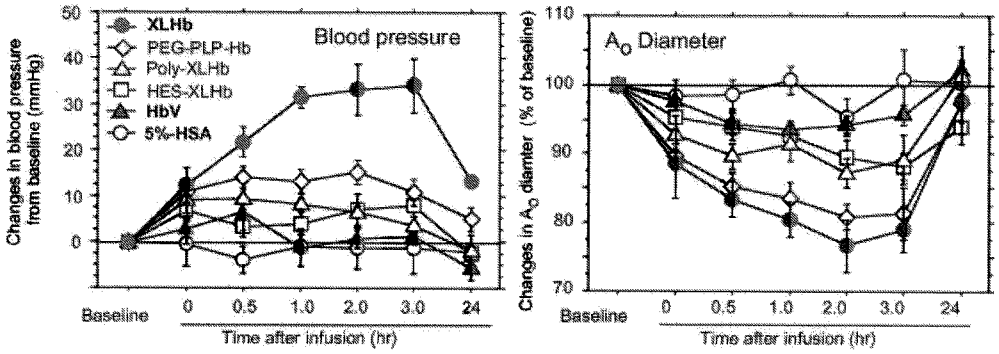

Figure 5. Changes in mean arterial pressure and the diameters of the resistance artery in hamster dorsal skin microcirculation after the bolus infusion of Hb-based O_2-carriers. Mean ± SD.

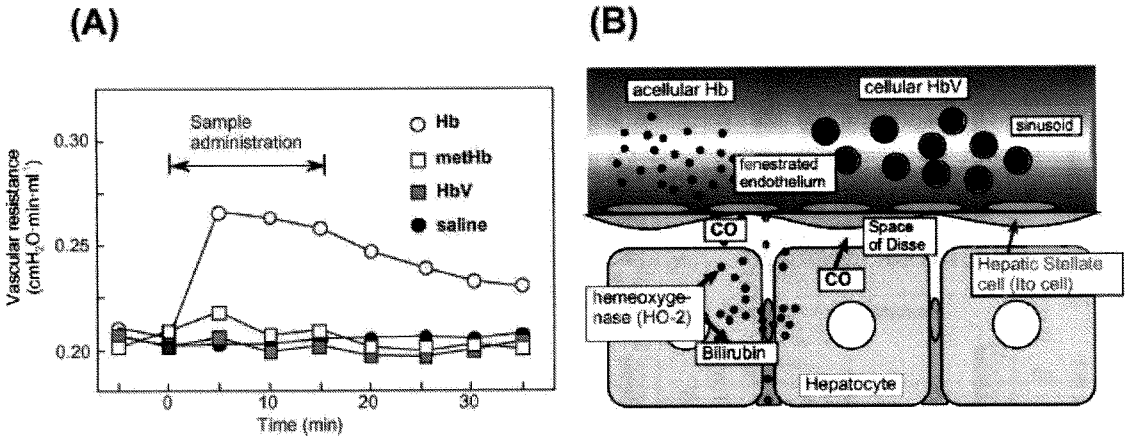

Figure 6. (A) Changes in vascular resistance during perfusion of exteriorized rat liver with HbV, Hb, metHb, or saline. (B) Schematic representation of hepatic microcirculation: the small Hb molecule extravasate across the fenestrated endothelium to reach to the space of Disse, where heme of Hb is catabolized by hemeoxygenase-2 (HO-2) and CO is released as a vasorelaxation factor. However, the excess amount of the extravasated Hb traps CO and induces vasoconstriction and the resulting higher vascular resistance. However, the larger HbV retains in the sinusoid and there is no extravasation and vasoconstriction.

molecules with a diameter of only 7 nm extravasate through the fenestrated endothelium and reach the space of Disse. However, HbV particles, which are larger than the pores, do not extravasate. Heme of extravasated Hb is excessively metabolized by hemeoxygenase-2 in hepatocyte to produce CO and bilirubin. Even though CO acts as a vasorelaxation factor in the liver, the excess amount of Hb rapidly binds CO, resulting in the vasoconstriction and an increase in vascular resistance. Furthermore, HbV (250 nm in diameter) is large enough to remain in the sinusoid, and the vascular resistance is maintained.

From these results, the optimal molecular dimension of Hb-based O_2 carriers can be proposed. The upper limitation is below the capillary diameter to prevent capillary plugging, and for sterilization by membrane filters (Fig. 7). However, smaller sizes exhibit a higher rate of vascular wall permeability with side effects such as hypertension and neurological disturbances. HbV exhibits a very low level of vascular wall permeability. Therefore, the HbV appears to be appropriate from the viewpoint of hemodynamics. However, the influence of HbV on the RES has to be clarified, because the fate of HbV is RES trapping.

Circulation persistence was measured by monitoring the concentration of radioisotope-labeled HbV in collaboration with Dr Phillips at the University of Texas at San Antonio. The circulation half-life is dose dependent, and when the dose rate was 14 ml/kg, the circulation half-life was 35 hr in rats. The circulation time in the case of the human body can be estimated to be twice as long; or about 3 days at the same dose rate. Gamma camera images of radioisotope-labeled HbV

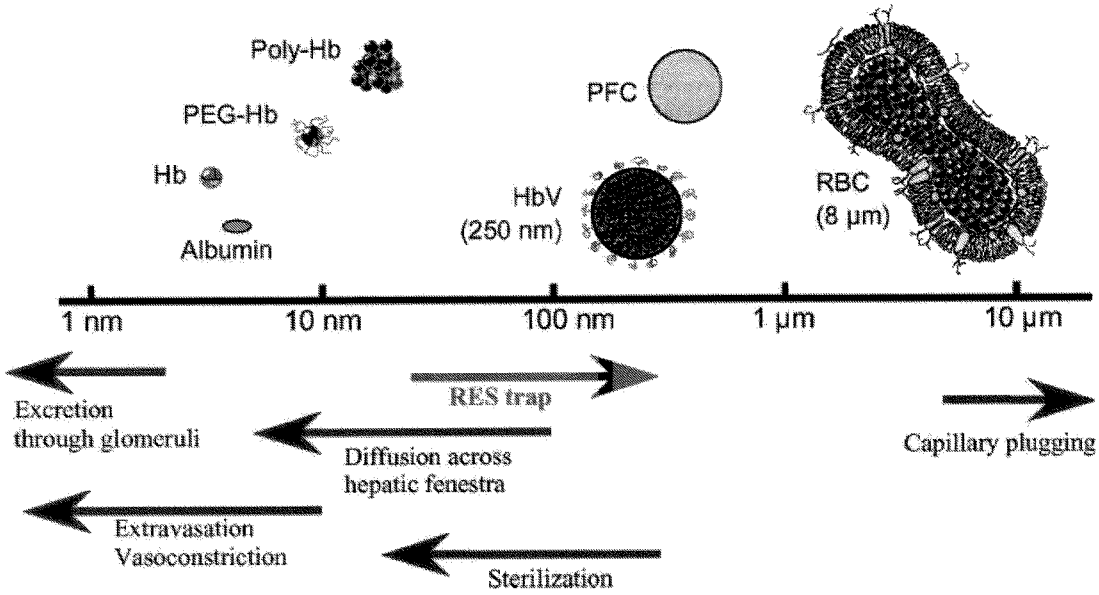

Figure 7. Optimal diameter of Hb-based oxygen carriers from the view point of physiological response and production process.

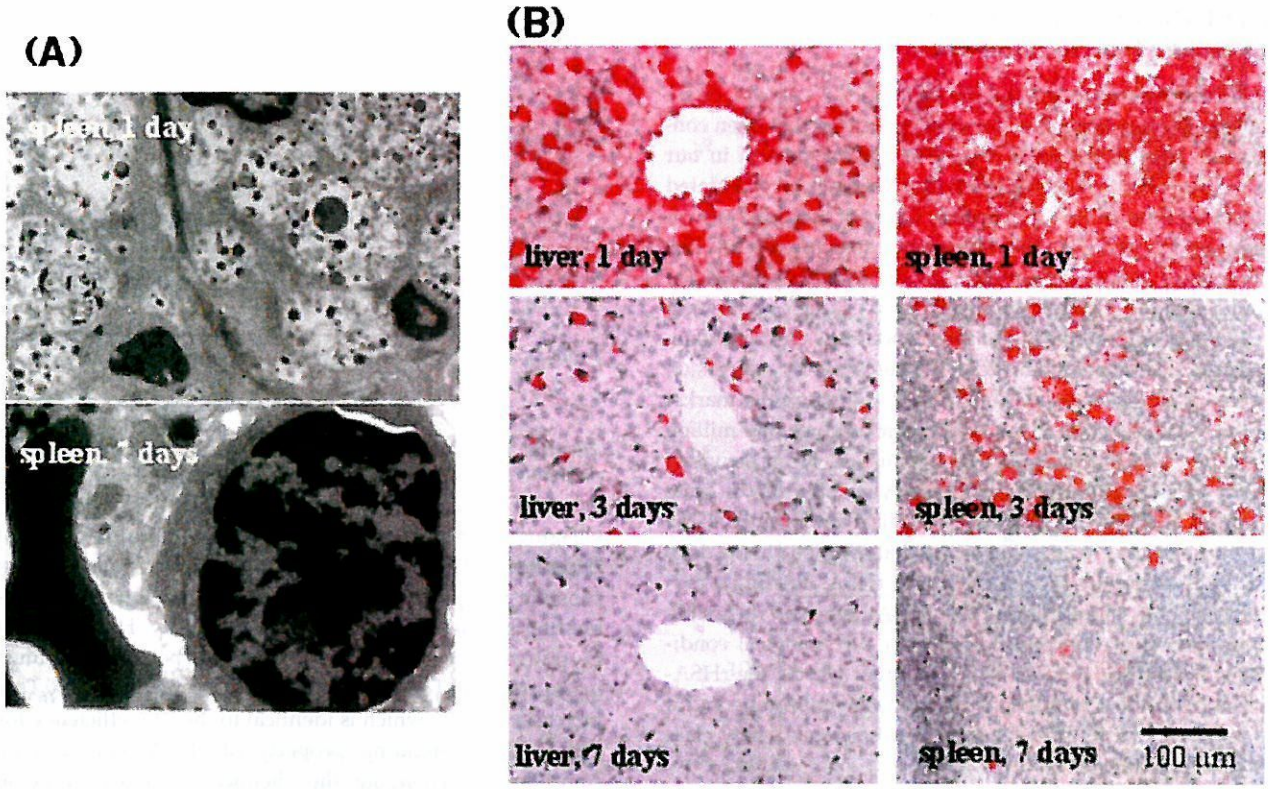

Figure 8. (A) TEM of rat spleen 1 day after the infusion of HbV (20 ml/kg) and after 7 days. Black dots are HbV particles captured in phagosomes in the spleen macrophages, and they disappeared at 7 days. (B) Staining with anti-human Hb antibody showed the presence of HbV in spleen and liver. HbV particles disappeared within 7 days.

showed the time course of biodistribution. After HbV finished playing its role in O_2-transport, a total of 35% of HbV are finally distributed mainly in the liver, spleen and bone marrow. The transmission electron microscopy (TEM) of the spleen 1 day after infusion of HbV clearly demonstrated the presence of HbV particles in macrophages, where HbV particles that appear as black dots are captured by the phagosomes[34] (Fig. 8). RBCs and HbV contain a lot of ferric ion with a high electron density, so that they show strong contrast in TEM. However, after 7 days, the HbV structure cannot be observed. There were no abnormalities in the tissues and no irreversible damages to the organs. A polyclonal anti-human Hb antibody was used as the marker of Hb in the HbV. This antibody does not recognize rat Hb. The red colored parts indicate the presence of Hb in HbV, and they have almost disappeared after 7 days in both the spleen and liver. Therefore, this shows that HbV can be metabolized quite promptly.

One issue of the Hb-based O_2-carriers is that they have a significant influence on clinical laboratory tests. They remain in the plasma phase in hematocrit capillaries after centrifugation of blood samples, and interfere with the colorimetric and turbidimetric measurements. However, HbV can be simply removed from blood plasma either by ultracentrifugation or centrifugation in the presence of a high-molecular-weight dextran to enhance precipitation. A very clear supernatant for accurate analyses can be obtained.[35] This is one advantage of HbV in comparison with acellular Hb solutions. Accordingly, the influence on organ functions by serum clinical laboratory tests after the bolus infusion of HbV at a dose rate of 20 ml/kg was examined. Albumin, alanine aminotransferase, aspartate aminotransferase, and lactate dehydrogenase, which reflect the liver function, moves their values within normal range.[36] Concentrations of bilirubin and ferric ion are maintained at a low level. The concentration of lipids transiently changed. In particular, the cholesterols increased significantly. And phospholipids slightly increased, however, they returned to the original level after 7 days. These results indicate that the membrane components of HbV, once they reappear from RES, are metabolized on the physiological pathway.

A test of daily repeated infusion is required to evaluate the safety of a new drug. The daily repeated infusion of HbV in Wistar rats at a dose rate of 10 ml/kg/day for 14 days, everyday was tested.[37] The total infusion volume (140 ml/kg) was 2.5 times as much as the volume of the whole blood (56 ml/kg), however, all rats tolerated it well and survived. The body weight showed a monotonous but slightly depressed increase in comparison with the saline. However, after 2 weeks there was no significant difference with the saline control group. All the rats seemed very healthy and active. Histopathological examination 1 day after the final infusion of HbV showed significant accumulation of HbV in spleen macrophages, and liver Kupffer cells, and they mostly disappeared after 14 days. There were no irreversible other morphological abnormalities, and the serum clinical chemistry indicated transient but reversible increases in lipid components. AST and ALT were within the normal range. From these results the authors are confident with the safety of HbV.

DESIGN AND PHYSICOCHEMICAL PROPERTIES OF rHSA-HEME

In this study research on totally synthetic O_2-carriers, or so-called albumin-heme that does not require Hb has been conducted. HSA is the most abundant plasma protein in our blood stream, but its crystal structure has not been elucidated for a long time. In 1998, Dr Stephen Curry of the Imperial College London first elucidated the crystal structure of the HSA complexed with seven molecules of myristic acids.[38] He found that the dynamic conformational changes of albumin take place by the binding of fatty acid. However, in Japan, rHSA is now manufactured on a large scale by expression in the yeast *Pichia pastoris*, and it will appear on the market soon.[39] A large-scale plant, which can produce one million vials per year, has been already established. From the viewpoint of clinical application, O_2-carrying albumin is quite exciting and may be of extreme medical importance. With this background, it has been found that synthetic heme derivative is efficiently incorporated into rHSA, creating a red-colored rHSA-heme hybrid. This rHSA-heme can reversibly bind and release O_2 molecules under physiological conditions in the same manner as Hb. In other words, the rHSA-heme hybrid is a synthetic O_2-carrying hemoprotein, and it is believed that its saline solution will become a new class of RBC substitute.[40–51]

Figure 9 summarizes the structure of the rHSA-heme molecule. The maximal binding numbers of heme to one albumin are eight, and the magnitude of the binding constants ranged from 10^6 to 10^4 (M^{-1}). The isoelectric point of rHSA-heme was found to be 4.8, independent of the binding numbers of heme. This value is exactly the same as that of albumin itself. Furthermore, the viscosity and density did not change after the incorporation of heme molecules, and the obtained solution showed a long shelf life of almost 2 years at room temperature. Since the O_2-binding sites of rHSA-heme are iron-porphyrin, the color of the solution changed in a similar way to Hb. Upon addition of O_2 gas through this solution, the visible absorption pattern immediately changed to that of the O_2-adduct complex. Moreover, after bubbling carbon monoxide gas, rHSA-heme formed a very stable carbonyl complex.

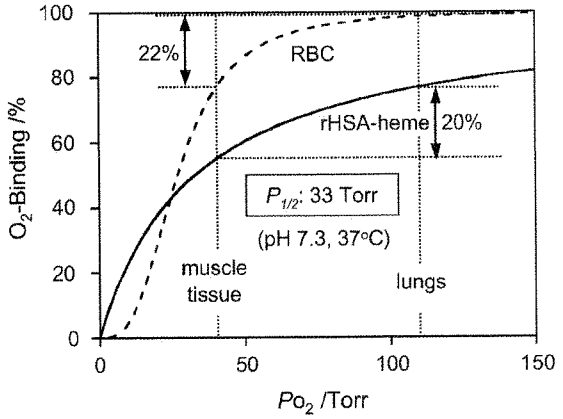

Figure 10. O_2-binding equilibrium curve of albumin-heme.

Figure 10 shows the O_2-binding equilibrium curve of rHSA-heme. The O_2-binding affinity of rHSA-heme is always constant independent of the number of heme, and the O_2-binding profile does not show cooperativity. However, the O_2-transporting efficiency of rHSA-heme between the lungs measuring 110 Torr and muscle tissue measuring 40 Torr increases to 22%, which is identical to the 22% efficiency for RBCs. The O_2-binding property of rHSA-heme can be controlled by changing the chemical structure of heme derivatives incorporated. More recently, it has been found that a protoheme derivative is also incorporated into albumin and can bind and release O_2 as well.[52]

IN VIVO SAFETY AND EFFICACY OF rHSA-HEME

Based on these findings, it can be said that rHSA-heme can become an entirely synthetic O_2-carrier, and satisfy the initial clinical requirements for a RBC substitute. However, there is another problem to solve before this material can be used as an O_2-carrier in the circulatory system. This problem is NO scavenging. Of course, rHSA-heme can bind NO, and it may be anticipated that the injection of rHSA-heme also induce hypertensive action. The authors have evaluated the

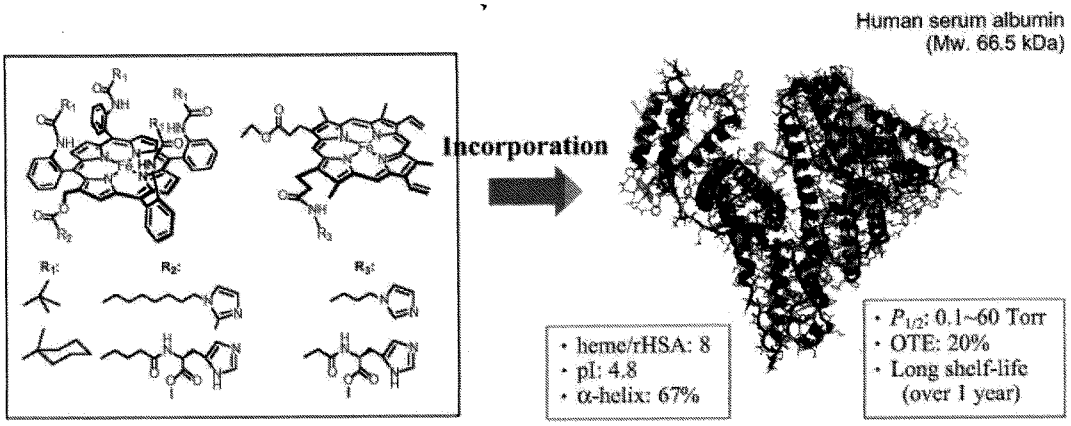

Figure 9. Structure of the albumin-heme molecule.

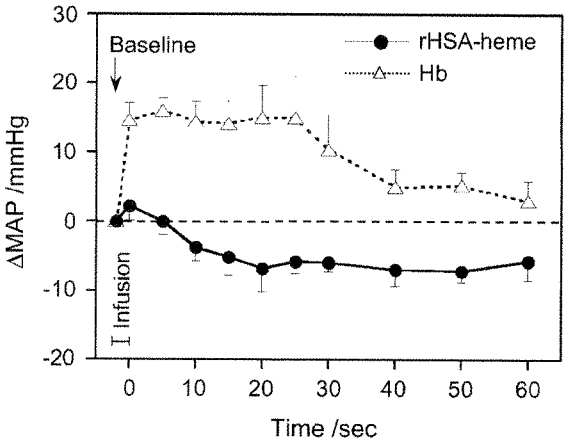

Figure 11. Change of MAP after the administration of rHSA-heme solution in the anesthetized rats ($n=5$). All data are shown as changes from the basal values (ΔMAP) just before the infusion and expressed as mean ± SE. Basal value is 90.1 ± 3.0 mmHg.

efficacy and safety of this rHSA-heme solution with animal experiments.

As described earlier, small Hb molecules extravasate through the vascular endothelium and react with NO, thus inducing vasoconstriction and acute increases in systemic blood pressure. Contrary to the expectations, the observation of the intestinal microcirculation after the infusion of rHSA-heme into an anesthetized rat revealed that the diameters of the venules and arterioles were not deformed at all.[53] Indeed, only a small change in the mean arterial pressure was observed after the administration of the rHSA-heme solution (Fig. 11). In contrast, the infusion of Hb elicited an acute increase in blood pressure. Why does rHSA-heme not induce vasoconstriction or hypertension? The answer probably lies in the negatively charged molecular surface of albumin. One of the unique characteristics of serum albumin is its low permeability through the muscle capillary pore, which is less than 1/100 that for Hb due to the electrostatic repulsion between the albumin surface and the glomerular basement membrane around the endothelial cells.

Thus the authors are now evaluating the O_2-transporting ability of this rHSA-heme molecule in the circulatory system with further animal experiments.[54] First, the physiological responses to exchange transfusion with rHSA-heme solution into rats after 70% hemodilution and 40% hemorrhage was determined (Fig. 12). The declined mean arterial pressure and blood flow after a 70% exchange with albumin and further 40% bleeding of blood showed a significant recovery of up to 90% of the baseline values by the infusion of the rHSA-heme solution. However, all rats in the control group only injected with albumin died within 30 min. Furthermore, muscle tissue O_2-tension significantly increased. These responses indicate the *in vivo* O_2-delivery of the rHSA-heme solution.

More recently, HSA dimer, which can incorporate 16 hemes in its hydrophobic domain has been synthesized.[55] The human serum rHSA-heme dimer solution dissolves 1.3-times more O_2 compared to that of RBC and keeps its colloid osmotic pressure at the same level as the physiological value.

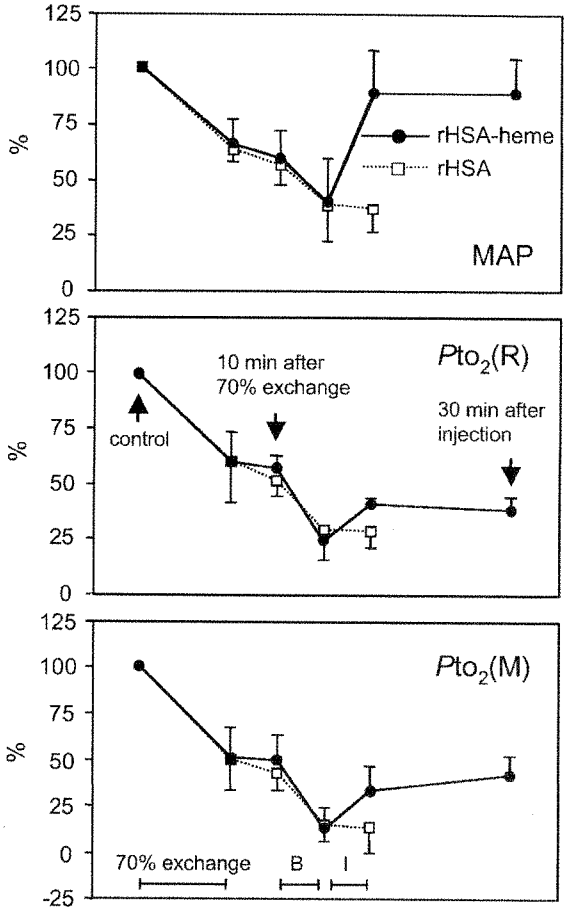

Figure 12. Change of (a) MAP and (b) O_2-tension in renal cortex during the 70% hemodilution with 5 wt% rHSA and further 40% exchange transfusion with rHSA-heme in anesthetized rats ($n=5$). All data are shown as changes from the basal values and expressed as mean ± SE.

POTENTIAL APPLICATIONS OF ARTIFICIAL O_2 CARRIERS

As described earlier the primary application of artificial O_2-carriers would be the resuscitative fluid for hemorrhage. Since some of the characteristics of artificial O_2-carriers overwhelm those of donated blood, there are many potential applications other than blood substitutes.

Tumor oxygenation

Unlike vessels in normal tissues, the development of a vasculature in a tumor lacks regulation and is hence, highly heterogeneous. Consequently, areas of hypoxia are quite common in tumors. In these hypoxic regions, it can be added that tumor cells acquire resistance to treatments such as chemotherapy and radiation. The rHSA-heme was injected into the responsible artery that supplies circulation to an implanted tumor (Fig. 13).[56] O_2-tension of the tumor rises immediately after intra-arterial infusion of albumin heme up to 2.4 times that of the baseline value. The findings in animals indicate that tumor tissue O_2-levels can be elevated by the administration of artificial O_2-carriers due to the

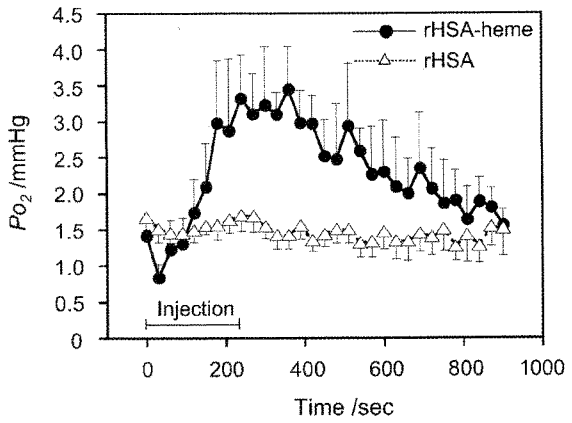

Figure 13. Changes in the O_2 tension of the hypoxic region of the ascites hepatoma LY80 solid tumor after the administration of the O_2 saturated rHSA-heme or rHSA solutions in the anesthetized rats ($n=4$ each). All data are shown as changes from the basal values (P_{O_2}) just before the infusion and expressed as mean ± SE.

difference in O_2-transporting properties from RBCs. Whether this increase in tissue O_2 can potentiate cancer treatment is currently under investigation.

Oxygenation of ischemic tissue

Tissue ischemia can ensue from impairment of peripheral perfusion due to a variety of diseases such as arteriosclerosis obliterans, diabetes, and Burger's disease. The key event in the progression of ischemic diseases is the inability of red cells to flow through the capillaries, beyond which point ulceration and gangrene formation become imminent. It is believed that this critical phase can be avoided or delayed by the application of artificial O_2-carriers, which can be designed to flow even through these damaged capillaries.[27,28]

Organ preservation

One of the most important agenda in transplantation medicine is long-term organ preservation and circumvention of ischemia reperfusion injuries. It is believed that artificial O_2-carriers can be applied as a perfusate for donor tissue in order to overcome these problems. In particular, its O_2 carrying capacity has the potential to significantly extend the preservation period. This will make it easier to transport organs. Also, utilizing the extra time, it may be possible in the future to perform additional organ tests for better compatibility, or even perform genetic modifications during this period. It is believed that through these applications, the concept of organ preservation can be expanded to culture organs, and furthermore to include the preservation of cells derived from donor tissues.

Extracorporeal circulation

Extracorporeal circulation is quite common in cardiac surgery. Improvements are being made in the priming solutions but red cells are often still required to fill the device circuit, particularly in compromised cases and in children.[57] It is believed that the use of artificial O_2-carriers in the priming solution can decrease or completely eliminate the need for a transfusion in such cases, and hence reduce the incidence of infection or graft-versus-host disease (GVHD).

Liquid ventilation for acute lung injury

For patients who present acute lung injury or acute respiratory distress syndrome (ARDS), gas exchange in the lung exhibits severe deterioration and sometimes even the newest mechanical ventilation method fails to establish adequate oxygenation of the blood. In this type of critical case, liquid ventilation using an artificial O_2-carrier can establish optimal oxygenation of the blood and may reproduce the integrity of lung parenchyma.[58] Briefly explained, oxygenated liquid ventilation fluid is administered into the lung through trachea and O_2 molecules are transferred through diseased alveolus by diffusion and oxygenate the blood. Currently, this method is thought to be effective for patients with congenital diaphragmatic herniation. Efficacy for adult acute lung injuries is now under investigation. Perfluorochemicals are the main fluid used for clinical use, however, aqueous artificial O_2-carriers may have the potential to be used for liquid ventilation.

FUTURE SCOPE

The research field of the red cell substitutes is moving forward very rapidly, and the paradigm in this field is expanding from red cell substitutes to "O_2 therapeutics". Significant efforts have been made to produce HbV and albumin-heme with a facility of GMP standard, and to start preclinical and finally clinical trials. We look forward to the day that our research will play an effective role in treating patients.

Acknowledgements

This work has been supported by The Ministry of Education, Culture, Sports, Science and Technology and The Ministry of Health, Labor and Welfare.

REFERENCES

1. Tsuchida E (ed.). *Macromolecular Complexes, Dynamic Interactions and Electronic Processes*. VCH: New York, 1991.
2. Ciardelli F, Tsuchida E. Wöhrle D (eds). *Macromolecule-metal Complexes*. VCH: New York, 1996.
3. Matsushita Y, Hasegawa E, Eshima K, Tsuchida E. Synthesis of amphiphilic porphinatoiron complexes having phosphocholine groups. *Chem. Lett.* 1983; 1387–1389.
4. Tsuchida E. Liposome-embedded iron-porphyrins as an artificial oxygen carrier. *Ann. New York Acad. Sci.* 1985; **446**: 429–442.
5. Tsuchida E, Nishide H. Hemoglobin model—artificial oxygen carrier composed of porphinatoiron complexes. *Top. Curr. Chem.* 1986; **132**: 63–99.
6. Komatsu T, Moritake M, Nakagawa A, Tsuchida E. Self-organized lipid-porphyrin bilayer membranes in vesicular form: nanostructure, photophysical properties and dioxygen coordination. *Chem. Eur. J.* 2002; **8**: 5469–5480.
7. Chang TMS. *Blood Substitutes: Principles, Methods, Products, and Clinical Trials*. Karger: Basel, 1997.
8. Riess JG. Oxygen carriers ("blood substitutes")-raison d'etre, chemistry, and some physiology. *Chem. Rev.* 2001; **101**: 2797–2919.
9. Sloan EP, Koenigsberg M, Gens D, Cipolle M, Runge J, Mallory MN, Rodman G Jr. Diaspirin cross-linked hemoglobin (DCLHb) in the treatment of severe traumatic hemorrhagic shock. *JAMA* 1999; **282**: 1857–1864.

10. Tsuchida E. *Blood Substitutes: Present and Future Perspectives*. Elsevier: Amsterdam, 1998.
11. Djordjevich L, Mayoral J, Miller IF, Ivankovich AD. Cardiorespiratory effects of exchange transfusions with synthetic erythrocytes in rats. *Crit. Care Med.* 1987; **15**: 318–323.
12. Takeoka S, Ohgushi T, Yokohama H, Sakai H, Nishide H, Tsuchida E. Preparation conditions of human hemoglobin vesicles covered with lipid membrane. *Artif. Organs Today* 1993; **3**: 129–136.
13. Sakai H, Takeoka S, Yokohama H, Seino Y, Nishide H, Tsuchida E. Purification of concentrated Hb using organic solvent and heat treatment. *Protein Expression Purif.* 1993; **4**: 563–569.
14. Takeoka S, Ohgushi T, Terase K, Ohmori T, Tsuchida E. Layer-controlled hemoglobin vesicles by interaction of hemoglobin with a phospholipid assembly. *Langmuir* 1996; **12**: 1755–1759.
15. Naito Y, Fukutomi I, Masada Y, Sakai H, Takeoka S, Tsuchida E, Abe H, Hirayama J, Ikebuchi K, Ikeda H. Virus removal from hemoglobin solution using Planova membrane. *J. Artif. Organs* 2002; **5**: 141–145.
16. Fukutomi I, Sakai H, Takeoka S, Nishide H, Tsuchida E, Sakai K. Carbonylation of oxyhemoglobin solution using a membrane oxygenator. *J. Artif. Organs* 2002; **5**: 102–107.
17. Sou K, Endo T, Takeoka S, Tsuchida E. Poly(ethylene glycol)-modification of the phospholipid vesicles by using the spontaneous incorporation of poly(ethylene glycol)-lipid into the vesicles. *Bioconjugate Chem.* 2000; **11**: 372–379.
18. Sakai H, Tomiyama K, Sou K, Takeoka S, Tsuchida E. Poly(ethyleneglycol)-conjugation and deoxygenation enable long term preservation of hemoglobin vesicles as oxygen carriers. *Bioconjugate Chem.* 2000; **11**: 425–432.
19. Sou K, Naito Y, Endo T, Takeoka S, Tsuchida E. Effective encapsulation of proteins into size-controlled phospholipid vesicles using the freeze–thawing and extrusion. *Biotechnol. Prog.* 2003; **19**: 1547–1552.
20. Izumi Y, Sakai H, Hamada K, Takeoka S, Yamahata T, Kato R, Nishide H, Tsuchida E, Kobayashi K. Physiologic responses to exchange transfusion with hemoglobin vesicles as an artificial oxygen carrier in anesthetized rats: changes in mean arterial pressure and renal cortical tissue oxygen tension. *Crit. Care Med.* 1996; **24**: 1869–1873.
21. Izumi Y, Sakai H, Kose T, Hamada K, Takeoka S, Yoshizu A, Horinouchi H, Kato R, Nishide H, Tsuchida E, Kobayashi K. Evaluation of the capabilities of a hemoglobin vesicle as an artificial oxygen carrier in a rat exchange transfusion model. *ASAIO J.* 1997; **43**: 289–297.
22. Kobayashi K, Izumi Y, Yoshizu A, Horinouchi H, Park SI, Sakai H, Takeoka S, Nishide H, Tsuchida E. The oxygen carrying capability of hemoglobin vesicles evaluated in rat exchange transfusion models. *Artif. Cells Blood Substitues Immobilization Biotechnol.* 1997; **25**: 357–366.
23. Sakai H, Takeoka S, Park SI, Kose T, Nishide H, Izumi Y, Yoshizu A, Kobayashi K, Tsuchida E. Surface modification of hemoglobin vesicles with poly(ethyleneglycol) and effects on aggregation, viscosity, and blood flow during 90% exchange transfusion in anesthetized rats. *Bioconjugate Chem.* 1997; **8**: 23–30.
24. Sakai H, Tsai AG, Kerger H, Park SI, Takeoka S, Nishide H, Tsuchida E, Intaglietta M. Subcutaneous microvascular responses to hemodilution with a red cell substitute consisting of polyethyleneglycol-modified vesicles encapsulating hemoglobin. *J. Biomed. Mater. Res.* 1998; **40**: 66–78.
25. Sakai H, Tsai AG, Rohlfs RJ, Hara H, Takeoka S, Tsuchida E, Intaglietta M. Microvascular responses to hemodilution with Hb-vesicles as red cell substitutes: influences of O_2 affinity. *Am. J. Physiol.* 1999; **276**: H553–H562.
26. Sakai H, Takeoka S, Wettstein R, Tsai AG, Intaglietta M, Tsuchida E. Systemic and microvascular responses to the hemorrhagic shock and resuscitation with Hb-vesicles. *Am. J. Physiol. Heart Circ. Physiol.* 2002; **283**: H1191–H1199.
27. Erni D, Wettstein R, Schramm S, Contaldo C, Sakai H, Takeoka S, Tsuchida E, Leunig M, Banic A. Normovolemic hemodilution with hemoglobin-vesicle solution attenuates hypoxia in ischemic hamster flap tissue. *Am. J. Physiol. Heart Circ. Physiol.* 2003; **284**: H1702–H1709.
28. Contaldo C, Schramm S, Wettstein R, Sakai H, Takeoka S, Tsuchida E, Leunig M, Banic A, Erni D. Improved oxygenation in ischemic hamster flap tissue is correlated with increasing hemodilution with Hb vesicles and their O_2 affinity. *Am. J. Physiol. Heart Circ. Physiol.* 2003; **285**: H1140–H1147.
29. Goda N, Suzuki K, Naito M, Takeoka S, Tsuchida E, Ishimura Y, Tamatani T, Suematsu M. Distribution of heme oxygenase isoform in rat liver: topographic basis for carbon monoxide-mediated micorvascular relaxation. *J. Clin. Invest.* 1998; **101**: 604–612.
30. Sakai H, Hara H, Yuasa M, Tsai AG, Takeoka S, Tsuchida E, Intaglietta M. Molecular dimensions of Hb-based O_2 carriers determine constriction of resistance arteries and hypertension in conscious hamster model. *Am. J. Physiol. Heart Circ. Physiol.* 2000; **279**: H908–H915.
31. Wakamoto S, Fujihara M, Abe H, Sakai H, Takeoka S, Tsuchida E, Ikeda H, Ikebuchi K. Effects of PEG-modified hemoglobin vesicles on agonist induced platelet aggregation and RANTES release *in vitro*. *Artif. Cells Blood Substitues Immobilization Biotechnol.* 2001; **29**: 191–201.
32. Kyokane T, Norimizu S, Taniai H, Yamaguchi T, Takeoka S, Tsuchida E, Naito M, Nimura Y, Ishimura Y, Suematsu M. Carbon monoxide from heme catabolism protects against hepatobiliary dysfunction in endotoxin-treated rat liver. *Gastroenterology* 2001; **120**: 1227–1240.
33. Ito T, Fujihara M, Abe H, Yamaguchi M, Wakamoto S, Takeoka S, Sakai H, Tsuchida E, Ikeda H, Ikebuchi K. Effects of poly(ethyleneglycol)-modified hemoglobin vesicles on *N*-formyl-methionyl-leucyl-phenylalanine induced responses of polymorphonuclear neutrophils *in vitro*. *Artif. Cells Blood Substitues Immobilization Biotechnol.* 2001; **29**: 427–438.
34. Sakai H, Horinouchi H, Tomiyama K, Ikeda E, Takeoka S, Kobayashi K, Tsuchida E. Hemoglobin-vesicles as oxygen carriers: influence on phagocytic activity and histopathological changes in reticuloendothelial systems. *Am. J. Pathol.* 2001; **159**: 1079–1088.
35. Sakai H, Tomiyama K, Masada Y, Takeoka S, Horinouchi H, Kobayashi K, Tsuchida E. Pretreatment of serum containing Hb-vesicles (oxygen carriers) to avoid their interference in laboratory tests. *Clin. Chem. Lab. Med.* 2003; **41**: 222–231.
36. Sakai H, Horinouchi H, Masada Y, Takeoka S, Kobayashi K, Tsuchida E. Metabolism of hemoglobin-vesicles (artificial oxygen carriers) and their influence on organ functions in a rat model. *Biomaterials* 2004; **25**: 4317–4325.
37. Sakai H, Masada Y, Horinouchi H, Ikeda E, Sou K, Takeoka S, Suematsu M, Kobayashi K, Tsuchida E. Physiologic capacity of reticuloendothelial system for degradation of homoglobin-vesicles (artificial oxygen carriers) after massive intravenous doses by daily repeated infusions for 14 days. *J. Pharmacol. Exp. Ther.* 2004; **311**: 874–884.
38. Curry S, Mandelkow H, Brick P, Franks N. Crystal structure of human serum albumin complexes with fatty acid reveals an asymmetric distribution of binding sites. *Nature Struct. Biol.* 1998; **5**: 827–835.
39. Sumi A, Ohtani W, Kobayashi K, Ohmura T, Yokoyama K, Nishida M, Suyama T. Purification and physicochemical properties of recombinant human serum albumin. In *Biotechnology of Blood Proteins*, Rivat C, Stoltz JF (eds). John Libbey Eurotext: Montrouge, 1993; vol. 227, 293–298.
40. Komatsu T, Ando K, Kawai N, Nishide H, Tsuchida E. O_2-transport albumin: a new hybrid-haemoprotein incorporating tetraphenylporphinatoiron(II) derivative. *Chem. Lett.* 1995; 813–814.
41. Tsuchida E, Ando K, Maejima H, Kawai N, Komatsu T, Takeoka S, Nishide H. Properties of oxygen binding by albumin-tetraphenylporphyrinatoiron(II) derivative complexes. *Bioconjugate Chem.* 1997; **8**: 534–538.
42. Wu J, Komatsu T, Tsuchida E. Resonance raman studies of O_2-binding to *ortho*-substituted tetraphenyl- and tetranaphthyl-porphinatoiron(II) derivatives with a covalently linked axial imidazole. *J. Chem. Soc., Dalton Trans.* 1998; 2503–2506.
43. Komatsu T, Hamamatsu K, Wu J, Tsuchida E. Physicochemical properties and O_2-coordination structure of human serum albumin incorporating tetrakis(*o*-pivalamido)phenylporphinatoiron(II) serivatives. *Bioconjugate Chem.* 1999; **10**: 82–86.
44. Tsuchida E, Komatsu T, Mastukawa Y, Hamamatsu K, Wu J. Human serum albumin incorporating tetrakis(*o*-pivalamido)phenylporphinatoiron(II) derivative as a totally

synthetic O_2-carrying hemoprotein. *Bioconjugate Chem.* 1999; **10**: 797–802.
45. Komatsu T, Matsukawa Y, Tsuchida E. Kinetics of CO and O_2 binding to human serum albumin-heme hybrid. *Bioconjugate Chem.* 2000; **11**: 772–776.
46. Komatsu T, Matsukawa Y, Tsuchida E. Reaction of nitric oxide with synthetic hemoprotein, human serum albumin incorporating tetraphenylporphinatoiron(II) derivatives. *Bioconjugate Chem.* 2001; **12**: 71–75.
47. Nakagawa A, Komatsu T, Tsuchida E. Photoreduction of autooxidized albumin-heme hybrid in saline solution: revival of its O_2-binding ability. *Bioconjugate Chem.* 2001; **12**: 648–652.
48. Komatsu T, Okada T, Moritake M, Tsuchida E. O_2-Binding properties of double-sided porphyrinatoiron(II)s with polar substituents and their human serum albumin hybrids. *Bull. Chem. Soc. Jpn* 2001; **74**: 1695–1702.
49. Wu Y, Komatsu T, Tsuchida E. Electrochemical studies of albumin-heme hybrid in aqueous media by modified electrode. *Inorg. Chim. Acta* 2001; **322**: 120–124.
50. Komatsu T, Matsukawa Y, Tsuchida E. Effect of heme structure on O_2-binding properties of human serum albumin-heme hybrids: intramolecular histidine coordination provides a stable O_2-adduct complex. *Bioconjugate Chem.* 2003; **13**: 397–402.
51. Tsuchida E, Komatsu T, Yanagimoto T, Sakai H. Preservation stability and *in vivo* administration of albumin-heme hybrid solution as an entirely synthetic O_2-carrier. *Polym. Adv. Technol.* 2002; **13**: 845–850.
52. Nakagawa A, Komatsu T, Ohmichi N, Tsuchida E. Synthetic dioxygen-carrying hemoprotein: human serum albumin including iron(II) complex of protoporphyrin IX with an axially coordinated histidylglycyl-propionate. *Chem. Lett.* 2003; **32**: 504–505.
53. Tsuchida E, Komatsu T, Matsukawa Y, Nakagawa A, Sakai H, Kobayashi K, Suematsu M. Human serum albumin incorporating synthetic heme: red blood cell substitute without hypertension by nitric oxide scavenging. *J. Biomed. Mater. Res.* 2003; **64A**: 257–261.
54. Tsuchida E, Komatsu T, Hamamatsu K, Matsukawa Y, Tajima A, Yoshizu A, Izumi Y, Kobayashi K. Exchange transfusion of albumin-heme as an artificial O_2-infusion into anesthetized rats: physiological responses, O_2-delivery and reduction of the oxidized hemin sites by red blood cells. *Bioconjugate Chem.* 2000; **11**: 46–50.
55. Komatsu T, Hamamatsu K, Tsuchida E. Cross-linked human serum albumin dimers incorporating sixteen (tetraphenylporphinato)iron(II) derivatives: synthesis, characterization, and O_2-binding property. *Macromolecules* 1999; **32**: 8388–8391.
56. Kobayashi K, Komatsu T, Iwamaru A, Matsukawa Y, Horinouchi H, Watanabe M, Tsuchida E. Oxygenation of hypoxic region in solid tumor by administration of human serum albumin incorporating synthetic hemes. *J. Biomed. Mater. Res.* 2003; **64A**: 48–51.
57. Kobayashi K, Izumi Y, Yamahata T, Sakai H, Takeoka S, Nishide H, Tsuchida E. Efficacy of synthetic oxygen-carrying substances. In *Int. Congr. Ser. 1995, 1102 (Shock: from Molecular and Cellular Level to Whole Body)*. Elsevier: Amsterdam, 1996; 305–310.
58. Horinouchi H, Tajima A, Kobayashi K. Liuid ventilation using artificial oxygen carrier. *Artif. Blood* 2001; **9**: 2–5 (in Japanese).

Oxygen-Carrying Plasma Hemoprotein Including Synthetic Heme

Teruyuki Komatsu and Eishun Tsuchida

Summary. Recombinant human serum albumin (rHSA) incorporating tetraphenylporphyrinatoiron(II) derivative with four pivaloylamino substituents (FepivP), albumin-heme, is an entirely synthetic hemoprotein that can reversibly bind and release O_2 under physiological conditions. We have recently found that replacing the substituent groups of FepivP with more hydrophobic 1-methylcyclohexanoylamino groups, affording FecycP, substantially stabilizes the formed O_2–adduct complex. The O_2- and CO-binding abilities and blood compatibility of this new rHSA-heme hybrid (rHSA-FecycP) have been investigated by spectroscopy. The maximum number of FecycP binding to one albumin was determined to be eight. Because the isoelectric point and circular dichroism (CD) spectral pattern were identical to those of rHSA itself, the two-dimensional structure of the host albumin could be unchanged after the incorporation of FecycP. Laser-flash photolysis experiments gave the association and dissociation rate constants for O_2 and CO (k_{on}, k_{off}). The rebinding kinetics of these gaseous ligands consists of multiple exponentials. We conjectured that the O_2- and CO-binding reactions are affected by the molecular environment around each of the active heme sites. rHSA-FecycP showed almost the same O_2-binding affinity($P_{1/2}^{O_2}$ 34 torr at 37°C) and thermodynamic parameters (ΔH, ΔS) for the oxygenation as rHSA-FepivP. In contrast, the half-life of the O_2-adduct complex (9 h, 37°C) became significantly longer than that of rHSA-FepivP (by a factor of 4.5), which is close to that of myoglobin. The obtained red solution was stable and demonstrated a long shelf life (>2 years) at room temperature. The equivalent mixture of rHSA-FecycP and whole blood exhibited no coagulation or precipitation, indicating its high blood compatibility.

Advanced Research Institute for Science and Engineering, Waseda University, 3-4-1 Okubo, Shinjuku-ku, Tokyo 169-8555, Japan

Key words. Human serum albumin, Albumin-heme, Synthetic hemoprotein, Oxygen-binding ability, Red blood cell substitute

Introduction

Human serum albumin (HSA) used for clinical treatment in Japan amounted to 1.9 million l (in terms of a blood source) in 2002 [1]. Most was administered to hemorrhagic shocked patients as a resuscitation fluid. If HSA can transport oxygen (O_2) like red blood cells, it could be of extreme medical importance not only as a blood replacement but also as an O_2 therapeutic agent.

In our circulatory system, free hemin, an iron(III) complex of protoporphyrin IX dissociated from methemoglobin, is potentially toxic because it may (1) intercalate phospholipid membranes, (2) be a major source of iron for bacterial pathogens, and (3) catalyze the formation of free radicals. Hemopexin has high affinity for binding protein with hemin, having the highest binding constant of any known protein ($K > 10^{12}\,M^{-1}$), but it releases it into liver cells via specific surface receptors [2]. Crystal structure analysis of the hemopexin-hemin complex revealed that the hemin is tightly bound by double histidine coordinations to the central ferric ion and multiple hydrogen bondings with the amino acid residues [3]. Nevertheless, the concentration of hemopexin in the plasma is rather low (<17 μM). HSA may also provide reserve binding capacity of hemin in various conditions (e.g., trauma, inflammation, hemolysis). In fact, HSA binds hemin with a relatively high affinity ($K = 10^8\,M^{-1}$) [4]. We have determined the single crystal structure of the HSA-hemin-myristate complex with a resolution of 3.2 Å [5]. Hemin is accommodated into the narrow D-shaped pocket in subdomain IB; and proximal coordination with Tyr-161 and three hydrogen bondings with basic amino acids contribute to maintaining the assembly. Addition of a sodium dithionate into this solution under an N_2 atmosphere reduced the central ferric ion to the ferrous state, although exposure to O_2 gas immediately oxidized the iron(II) center (T. Komatsu, N. Ohmichi, E. Tsuchida, unpublished data, 2004).

We have found that tetraphenylporphyrinatoiron(II) derivative with four pivaloylamino substituents (FepivP) (Fig. 1) was also incorporated into HSA, and the obtained albumin-heme (HSA-FepivP) can reversibly bind and release O_2 under physiological conditions in the same manner as hemoglobin (Hb) and myoglobin (Mb) [6–12]. Because recombinant HSA (rHSA) was manufactured on a large scale by expression in *Pichia pastoris* [13], rHSA-heme hybrid has become entirely synthetic and absolutely free of infectious pathogens. Our animal experiments have also demonstrated that rHSA-heme works as an "oxygen-carrying plasma hemoprotein" in the bloodstream [14; T. Komatsu et al., unpublished data, 2004].

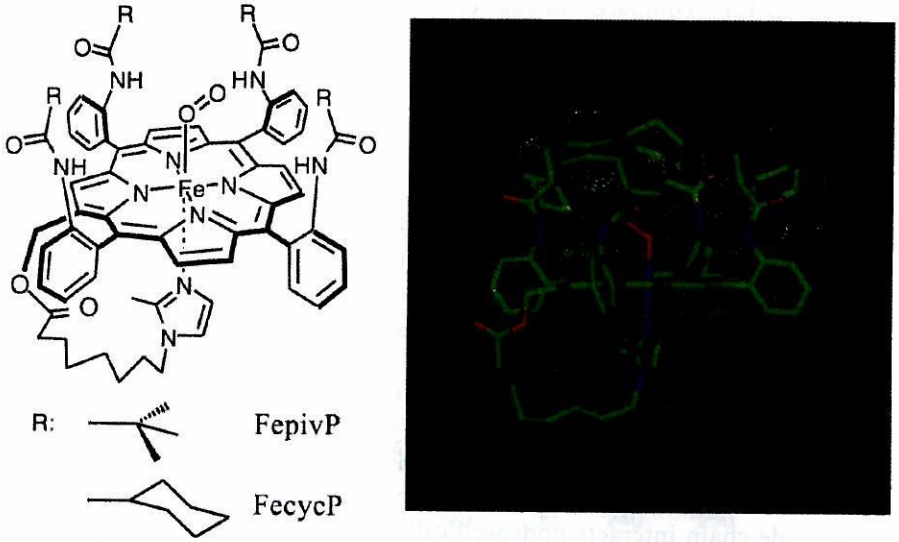

FIG. 1. Structures of the new tetraphenylporphyrinatoiron(II) derivative with more hydrophobic 1-methylcyclohexanoylamino groups on the porphyrin ring plane (FecycP) and pivaloylamino substituents (FepivP), and the simulated structure of oxygenated FecycP. The extensible systematic forcefield (ESFF) simulation was performed using an Insight II system (Molecular Simulations, San Diego, CA, USA). The structure was generated by alternative minimization and annealing dynamic calculations from 1000 K to 100 K. The dielectric constant was fixed at 2.38 D, corresponding to the toluene solution. The *dotted surface* represents the van der Waals radius

Half of the Hb-based O_2 carrier in advanced clinical trials still exhibited vasoconstriction, which increased blood pressure and decreased cardiac output [15–19]. The precise mechanism of this hypertension is controversial, but many investigators suspect that the Hb molecules penetrate the vascular endothelium and bind the endothelial-derived relaxing factor (EDRF), namely nitric oxide [20–27]. Others believe that excessive delivery of O_2 to arteriolar vascular walls induces autoregulatory vasoconstriction [28–33]. Interestingly, rHSA-heme does not induce such a vasopressor effect [34]. The electrostatic repulsion between the albumin surface and glomerular basement membrane around the endothelial cell retards rapid leakage of the rHSA-heme molecule and quick scavenging of NO. Albumin-heme is now recognized to be one of the most promising materials as a new class of red blood cell substitute.

To improve the O_2-binding ability of rHSA-FepivP, we have synthesized new tetraphenylporphyrinatoiron(II) derivative with more hydrophobic 1-methylcyclohexanoylamino groups on the porphyrin ring plane (FecycP) (Fig. 1) [35]. rHSA-FecycP forms a significantly stable O_2-adduct complex with

a long half-life compared to that of FepivP (by a factor of 4.5). We herein report the O_2- and CO-binding abilities of this entirely synthetic albumin-based O_2 carrier.

Incorporation of Heme into rHSA

Based on quantitative analysis of the absorption intensity for the Soret band of aqueous rHSA-FecycP, the maximum number of FecycP binding to an rHSA was determined to be eight using a molar extinction coefficient [35]. FecycP is accommodated into certain domains of rHSA with binding constants of 10^6–$10^4\,M^{-1}$.

The isoelectric points (*p*I) of the obtained rHSA-FecycP hybrid (FecycP/rHSA = 1–8 mol/mol) were 4.8, exactly the same as those of rHSA. Fatty acid binding, for example, induced a reduction in the *p*I value due to partial neutralization of the surface charge. The FecycP molecule without any ionic side chain interacts nonspecifically with a hydrophobic subdomain of rHSA, so its surface charge distributions are unaltered. Consequently, the essential biological roles as serum albumin [i.e., control of colloid osmotic pressure (COP) and plasma expansion] are essentially sustained after the incorporation of FecycP.

The secondary and tertiary structures of rHSA and the deformation upon FecycP binding were measured by circular dichroism (CD) spectroscopy. The spectral pattern showed typical double-minimum negative peaks in the ultraviolet (UV) region independent of the number of FecycP molecular bound (Fig. 2). The estimated α-helix content was approximately 67%, suggesting that the FecycP association did not cause any high-ordered structural change in the host albumin. Moreover, rHSA-FecycP showed no induced CD in the Soret region (400–500 nm). The hemin binding to the serum albumin is accompanied by a rise in the extrinsic negative Cotton effect in the Soret region because it binds to albumin through axial coordination, allowing a large degree of immobilization [36,37]. We concluded that hydrophobic interaction is the major molecular force of FecycP binding, and its incorporation does not induce any changes in the highly ordered structure or in the surface net charges of rHSA.

O_2-Binding Property of rHSA-Heme

The UV-visible absorption spectrum of the aqueous rHSA hybrid that included carbonyl FecycP showed the formation of the typical CO-coordinated low-spin tetraphenylporphyrinatoiron(II) derivative (λ_{max}: 429, 545 nm). Light irradiation of this solution under an O_2 atmosphere led to

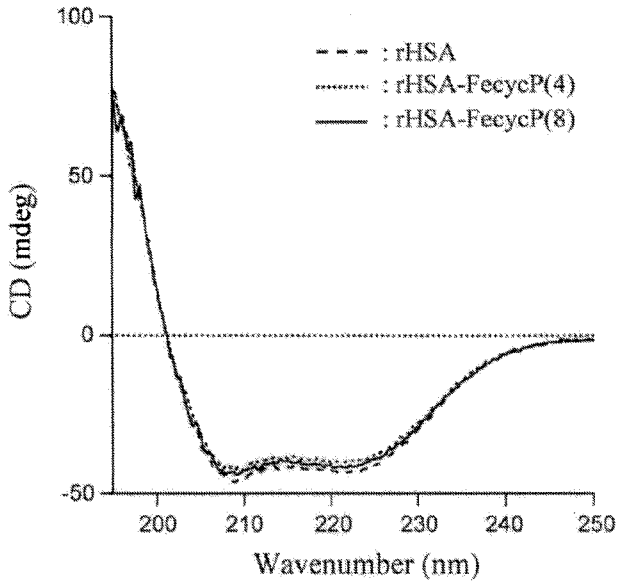

FIG. 2. Circular dichroism (*CD*) spectra of recombinant human serum albumin (*rHSA*) and rHSA-FecycP in water at 25°C

CO dissociation, giving the O_2-adduct complex (λ_{max}: 428, 555 nm). Upon exposure of the oxygenated rHSA-FecycP to N_2, the UV-visible absorption pattern changed to that of the five-*N*-coordinated high-spin iron(II) complex with an intramolecularly coordinated proximal imidazole (λ_{max}: 445, 543, 567 nm). This oxygenation was reversibly dependent on the O_2 partial pressure and sufficiently stable under physiological conditions (37°C, pH 7.4) (Fig. 3). The rate of irreversible oxidation is satisfactorily slow (vide infra).

The O_2 coordination to FecycP in human serum albumin is expressed by Eq. 1.

$$\mathrm{FeP} + \mathrm{O_2} \underset{k_{off}^{O_2}}{\overset{k_{on}^{O_2}}{\rightleftharpoons}} \mathrm{FeP\text{-}O_2} \qquad (1)$$

$$\left[P_{1/2}^{O_2} = \left(K^{O_2}\right)^{-1} = k_{on}^{O_2} / k_{off}^{O_2}\right]$$

The O_2 association and O_2-dissociation rate constants ($k_{on}^{O_2}$, $k_{off}^{O_2}$) were explored by laser flash photolysis (Table 1) [9,35,38–40]. The detailed kinetic evaluation of rHSA-FecycP gave the following results.

1. The absorption decays accompanying O_2 recombination were composed of three phases of first-order kinetics; the curves were fit by a triple-exponential equation [9]. The minor (<10%) and fastest component was

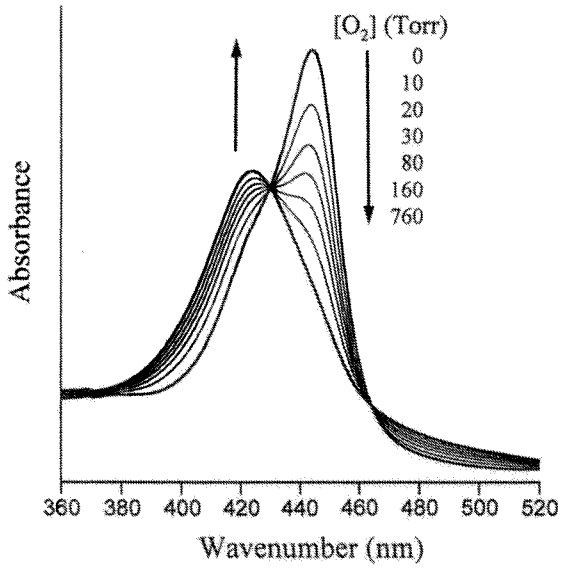

FIG. 3. Ultraviolet-visible. Absorption spectral changes of rHSA-FecycP(4) dependent on the O_2 partial pressure in phosphate-buffered solution (pH 7.3) at 37°C. The number in parenthesis is molar ratio of FecycP and rHSA

TABLE 1. O_2 association and dissociation rate constants for rHSA-FecycP in phosphate-buffered solution (pH 7.3) at 25°C

	$k_{on}[M^{-1}s^{-1}]$		$k_{off}[s^{-1}]$	
Substance	Fast	Slow	Fast	Slow
rHSA-FecycP(8)	4.6×10^7	7.3×10^6	9.8×10^2	1.6×10^2
rHSA-FepivP(8)[a]	3.4×10^7	9.5×10^6	7.5×10^2	2.0×10^2
Hb (T-state)α[b]	2.9×10^6		1.8×10^2	

rHSA, recombinant human serum albumin; FecycP, tetraphenylporphyrinatoiron(II) derivative with 1-methyl cyclohexanoylamino groups; FepivP, tetraphenyl porphyrinatoiron (II) with pivaloyamino substitute; Hb, hemoglobin.
[a]Ref. [9].
[b]pH 7, 20°C; Ref. [40].
The numbers in parenthesis is molar ratio of porphyrin and rHSA.

independent of the O_2 concentrations. It should be correlated with a base elimination [41].

2. Based on careful inspection of the two slower phases, the association rate constants for the fast and slow rebinding [k_{on}(fast) and k_{on}(slow)] of O_2 were calculated. The k_{on}(fast) values are four- to fivefold higher than the k_{on}(slow) volues.
3. The concentration ratios of the fast and slow reactions were 2:1 to 3:1.

Based on these findings, we can conclude that the O_2 association with FecycP in the hydrophobic domains of rHSA is influenced by the molecular

TABLE 2. O_2-binding equilibrium parameters and half-lifetime of rHSA-FecycP in phosphate-buffered solution (pH 7.3)

Substance	$P_{1/2}$(torr)[a]	ΔH[kJ mol^{-1}]	ΔS[J $K^{-1}mol^{-1}$]	$\tau_{1/2}$[h][a]
rHSA-FecycP(4)	34	−59	−108	9
rHSA-FecycP(8)	35	−59	−107	9
rHSA-FepivP(4)[b]	36	−60	−114	2
rHSA-FepivP(8)[b]	33	−60	−112	2
Red cells[c]	27			
Hbα	40[d]	−57 to −65[e]	−116 to −133[e]	35[f]
Mb[d]	40[d]	−57 to −65[e]	−116 to −133[e]	12[g]

[a] At 37°C.
[b] Ref. [8].
[c] pH 7.4; ref. [42].
[d] T-state, pH 7, 20°C; ref. [40].
[e] pH 7.4; ref. [43].
[f] At 37°C, pH 7.2; ref. [44].
[g] At 35°C, pH 7.0; ref. [45].
The number in parenthesis is molar ratio of porphyrin and rHSA.

microenvironment around each O_2 coordination site (e.g., steric hindrance of the amino acid residue and difference in polarity).

The O_2-binding affinity for such oxygenation could be directly determined. Adequate isosbestic behavior was maintained during the course of a spectrophotometric titration of O_2 (Fig. 3). According to the kinetic experiments, the $P_{1/2}$ values were divided into two components using our previously reported equation [9]. The calculated $P_{1/2}$ for the fast and slow phases were identical in each case (Table 2). The thermodynamic parameters (ΔH, ΔS) of oxygenation were also measured by the van't Hoff plots of the K^{O_2} values (Fig. 4) [8]. The $P_{1/2}{}^{O_2}$, ΔH, and ΔS values for oxygenation of rHSA-FecycP resembled those of Hb and Mb [8,40,42–45]. Moreover, we could not find significant differences in these parameters for rHSA-FepivP and rHSA-FecycP. This result indicates that the substituent structure on the porphyrin plane does not cause any substantial change in the O_2 equilibria and kinetics of rHSA-heme.

Stability of O_2-Adduct Complex of Albumin-Heme

Accompanying the autooxidation of the central iron(II), the absorption band (λ_{max} 555 nm) slowly disappeared at 37°C, leading to formation of the inactive ferric porphyrin. The effect of the heme structure on the half-life of the O_2-adduct complex against the ferric state ($\tau_{1/2}$) was marked. The rHSA-FecycP had a $\tau_{1/2}$ of 9 h, which is 4.5-fold longer than that of rHSA-FepivP and close to that of the Mb (12 h at 37°C) [46].

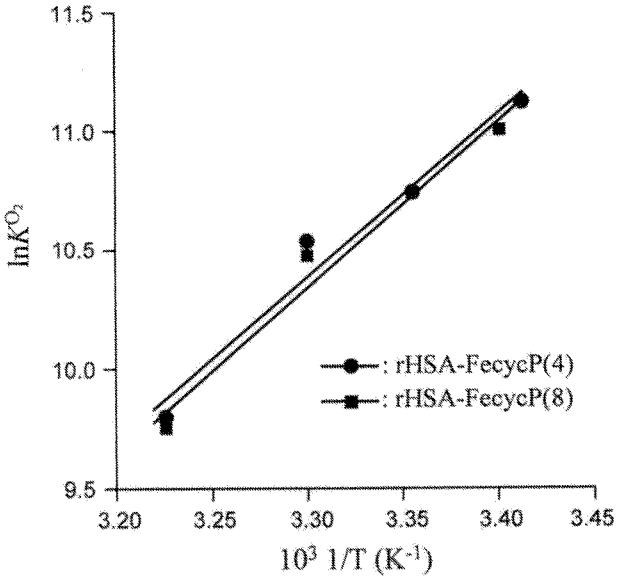

FIG. 4. Van't Hoff plots of O_2-binding affinity of rHSA-FecycP in phosphate-buffered solution (pH 7.3)

CO-Binding Property of rHSA-Heme

Upon addition of CO gas through the deoxy or oxy state of the rHSA-FecycP solution, the spectrum immediately exhibited formation of the carbonyl complex. The CO-binding affinity ($P_{1/2}^{CO}$) of rHSA-FecycP became 2.5-fold higher than that of rHSA-FepivP (Table 3) [9,47,48]. Kinetically, this is due to the low CO dissociation rate constant, k_{off}^{CO}. More recently, CO/O_2 discrimination of Hb and Mb has not been based mainly on distal steric constraints in the heme pocket; the emphasis has shifted to polar interactions in the binding pocket [49,50]. That is, a polar environment could favor the highly polarized coordinated Fe-O_2 unit over the apolar Fe-CO moiety. In FecycP, the hydrophobic cavity around the central ferrous ion probably contributes to the rise in CO-binding affinity. This interpretation is in good agreement with assumptions by other investigators.

Blood Compatibility

The red rHSA-FecycP solution showed a long shelf life (>2 years) at temperatures of 4°–37°C without any aggregation or precipitation. The solution properties also satisfied physiological requirements. The specific gravity was 1.013 (FecycP/rHSA = 1–8 mol/mol). The viscosity of 1.2 cP (at a high shear

TABLE 3. CO-binding parameters of rHSA-FecycP in phosphate-buffered solution (pH 7.3) at 25°C

Substance	$P_{1/2}^{CO}$(torr)	$k_{on}(M^{-1}s^{-1})$	
		Fast	Slow
rHSA-FecycP(8)	0.04	5.9×10^6	8.9×10^5
rHSA-FepivP(8)	0.10	4.9×10^6	6.7×10^5
Hb (T-state)α[a]	0.30	2.2×10^5	

[a] Aqueous, pH 7.0–7.4, 20°C; refs. [47, 48].
The number in parenthesis is molar ratio of porphyrin and rHSA.

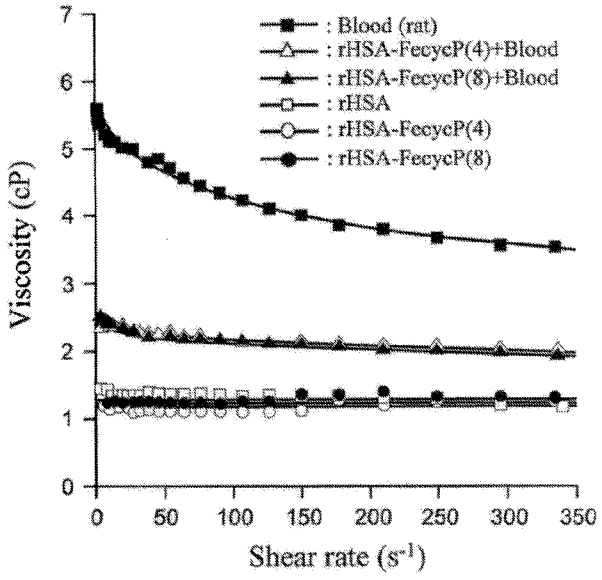

FIG. 5. Viscosity of rHSA-FecycP solution with whole blood at 37°C

rate of 230 s^{-1}) was much lower than that of whole blood (4.0 cP) and exhibited Newtonian-type shear rate dependence similar to that of rHSA itself (Fig. 5). Furthermore, the viscosity of the mixed dispersion with freshly drawn blood (1:1, v/v) showed 2.0 cP (at 230 s^{-1}), indicating that rHSA-FecycP had good compatibility with blood. Optical microscopic observations also revealed that the homogeneous morphology of the red blood cells was not affected by mixing with whole blood (not shown).

Conclusions

Human serum albumin incorporating synthetic heme formed an O_2-adduct complex under physiological conditions. In particular, oxygenated rHSA-FecycP showed high stability compared to the previous rHSA-FepivP, and its half-life reached a value similar to that of the native Mb. It has been also found

that another rHSA-heme complex incorporating an FecycP analogue with a histidyl base at the porphyrin periphery had an extremely long half-life of the oxygenated complex (25 h) under the same conditions (in this case the O_2-binding affinity is quite high) [35]. rHSA–FecycP with a $P_{1/2}$ value (34 torr at 37°C) similar to that of red blood cells is now the most promising material to be used as an artificial O_2 carrier. Exchange transfusion with rHSA-FecycP into anesthetized beagles to evaluate its clinical safety and efficacy is now under investigation.

Acknowledgments. This work was partially supported by Health Science Research Grants from MHLW, Grant-in-Aid for Scientific Research (No. 16350093) from JSPS, and Grant-in-Aid for Exploratory Research (No. 16655049) from MEXT. The authors are grateful to NIPRO Corp. for their supporting the oxygen-infusion project. We also thank Mr. Seiji Ishihara (Waseda University) for his skilful physicochemical experiment.

References

1. Homepage of Ministry of Health, Labor, and Welfare, Japan (2003) (http://www.mhlw.go.jp/shingi/2003/06/s0627-12.html)
2. Tolosano E, Altruda F (2002) Hemopexin: structure, function, and regulation. DNA Cell Biol 21:297–306
3. Paoli M, Anderson BF, Baler HM, et al (1999) Crystal structure of hemopexin reveals a novel high-affinity heme site formed between two β-propeller domains. Nat Struct Biol 6:926–931
4. Adams PA, Berman MC (1980) Kinetics and mechanism of the interaction between human serum albumin and monomeric heamin. Biochem J 191:95–102
5. Zunszain PA, Ghuman J, Komatsu T, et al (2003) Crystal structural analysis of human serum albumin complexed with hemin and fatty acid. BMC Struct Biol 3:6
6. Komatsu T, Hamamatsu K, Wu J, et al (1999) Physicochemical properties and O_2-coordination structure of human serum albumin incorporating tetrakis(*o*-pivamido)phenylporphyrinatoiron(II) derivatives. Bioconjug Chem 10:82–86
7. Komatsu T, Hamamatsu K, Tsuchida E (1999) Cross-linked human serum albumin dimers incorporating sixteen (tetraphenylporphinato)iron(II) derivatives: synthesis, characterization, and O_2-binding property. Macromolecules 32:8388–8391
8. Tsuchida E, Komatsu T, Mastukawa, et al (1999) Human serum albumin incorporating tetrakis(*o*-pivalamido)phenylporphinato-iron(II) derivative as a totally synthetic O_2-carrying hemoprotein. Bioconjug Chem 10:797–802
9. Komatsu T, Matsukawa Y, Tsuchida E (2000) Kinetics of CO and O_2 binding to human serum albumin-heme hybrid. Bioconjug Chem 11:772–776
10. Komatsu T, Matsukawa Y, Tsuchida E (2001) Reaction of nitric oxide with synthetic hemoprotein, human serum albumin incorporating tetraphenylporphyrinatoiron(II) derivatives. Bioconjug Chem 12:71–75
11. Komatsu T, Okada T, Moritake M, et al (2001) O_2-binding properties of double-sided porphyrinatoiron(II)s with polar substituents and their human serum albumin hybrids. Bull Chem Soc Jpn 74:1695–1702

12. Huang Y, Komatsu T, Nakagawa A, et al (2003) Compatibility in vitro of albumin-heme (O_2 carrier) with blood cell components. J Biomed Mater Res 66A:292–297
13. Sumi A, Ohtani W, Kobayashi K, et al (1993) Purification and physicochemical properties of recombinant human serum albumin. Biotechnol Blood Proteins 227:293–298
14. Tsuchida E, Komatsu T, Hamamatsu K, et al (2000) Exchange transfusion of albumin-heme as an artificial O_2-infusion into anesthetized rats: physiological responses, O_2-delivery and reduction of the oxidized hemin sites by red blood cells. Bioconjug Chem 11:46–50
15. Chang TMS (1997) Recent and future developments in modified hemoglobin and microencapsulated hemoglobin as red blood cell substitutes. Artif Cells Blood Substit Immobil Biotechnol 25:1–24
16. Tsuchida E (1998) Perspectives of blood substitutes. In: Tsuchida E (ed) Blood substitutes: present and future perspectives. Elsevier Science, Lausanne, pp 1–14
17. Winslow RM (1998) The role of blood substitutes in emerging healthcare systems. In: Tsuchida E (ed) Blood substitutes: present and future perspectives. Elsevier Science, Lausanne, pp 15–32
18. Winslow RM (1999) New transfusion strategies: red cell substitutes. Annu Rev Med 50:337–353
19. Squires JE (2002) Artificial blood. Science 295:1002–1005
20. Keipert P, Chang T (1998) Pyridoxylated-polyhemoglobin solution: a low viscosity oxygen-delivery blood replacement fluid with normal oncotic pressure and long term storage feasibility. Biomater Artif Cells 16:185–196
21. Keipert PE, Gonzales A, Gomez CL, et al (1993) Acute changes in systemic blood pressure and urine output of conscious rats following exchange transfusion with diaspirin-crosslinked hemoglobin solution. Transfusion 33:701–708
22. Hess JR, MacDonald VW, Brinkley WW (1993) Synthetic and pulmonary hypertension after resuscitation with cell-free hemoglobin. J Appl Physiol 74:1769–1778
23. Schultz SC, Grady B, Cole F, et al (1993) A role for endothelin and nitric oxide in the pressor response to diaspirin cross-linked hemoglobin. J Lab Clin Med 122:301–308
24. Thompson A, McGarry AE, Valeri CR, et al (1994) Stroma-free hemoglobin increases blood pressure and GFR in the hypotensive rat: role of nitric oxide. J Appl Physiol 77:2348–2354
25. Sharma AC, Singh G, Gulati A (1995) Role of NO mechanism in cardiovascular effects of diaspirin cross-linked hemoglobin in anesthetized rats. Am J Physiol 269:H1379–H1399
26. Moisan S, Drapeau G, Burhop KE, et al (1998) Mechanism of the acute pressor effect and bradycardia elicited by disapirin crosslinked hemoglobin in anesthetized rats. Can J Physiol Pharmacol 76:434–442
27. Abassi Z, Kotob S, Pieruzzi F, et al (1997) Effects of polymerization on the hypertensive action of diaspirin cross-linked hemoglobin in rats. J Lab Clin Med 129:603–610
28. Guyton AC, Ross JM, Carrier O, et al (1964) Evidence for tissue oxygen demand as the major factor causing autoregulation. Circ Res 14:1–60
29. Johnson PC (1986) Autoregulation of blood flow. Circ Res 59:483–495
30. Vandegriff KD, Winslow RM (1995) A theoretical analysis of oxygen transport: a new strategy for the design of hemoglobin-based red cell substitutes. In: Winslow RM, Vandegriff KD, Intaglietta M (eds). Blood substitutes: physiological basis of efficiency. Birkhäuser, Boston, pp 143–154
31. Tsai AG, Kerger H, Intaglietta M (1995) Microcirculatory consequences of blood substitution with αα-hemoglobin. In: Winslow RM, Vandegriff KD, Intaglietta M (eds) Blood substitutes: physiological basis of efficiency. Birkhäuser, Boston, pp 155–174

32. Rohlfs RJ, Bruner E, Chiu A, et al (1998) Arterial blood pressure responses to cell-free hemoglobin solutions and the reaction with nitric oxide. J Biol Chem 273:12128–12134
33. Winslow RM (2000) αα-Crosslinked hemoglobin: was failure predicted by preclinical testing? Vox Sang 79:1–20
34. Tsuchida E, Komatsu T, Matsukawa Y, et al (2003) Human serum albumin incorporating synthetic heme: red blood cell substitute without hypertension by nitric oxide scavenging. J Biomed Mater Res 64A:257–261
35. Komatsu T, Matsukawa Y, Tsuchida E (2002) Effect of heme structure on O_2-binding properties of human serum albumin-heme hybrids: intramolecular histidine coordination provides a stable O_2-adduct complex. Bioconjug Chem 13:397–402
36. Beaven H, Chen CH, D'Albis A, et al (1974) A spectroscopic studies of the haemin-human-serum-albumin system. Eur J Biochem 41:539–546
37. Casella L, Gullotti M, Ploi S, et al (1993) Haem-protein interactions: the binding of haem complexes to serum albumin. Gazz Chim Itali 123:149–154
38. Traylor TG, Tsuchiya S, Campbell D, et al (1985) Anthracene heme cyclophanes: steric effects in CO, O_2, and RNC binding. J Am Chem Soc 107:604–614
39. Collman JP, Brauman JI, Iverson BL, et al (1983) O_2 and CO binding to iron(II) porphyrins: a comparison of the "picket fence" and "pocket" porphyrins. J Am Chem Soc 105:3052–3064
40. Sawicki CA, Gibson QH (1977) Properties of the T state of human oxyhemoglobin stideid by laser flash photolysis. J Biol Chem 252:7538–7547
41. Geibel J, Cannon J, Campbell D, et al (1978) Model compounds for R-state and T-state hemoglobins. J Am Chem Soc 100:3575–3585
42. Severinghaus JW (1966) Blood gas calculator. J Appl Physiol 21:1108–1116
43. Imai K, Yonetani T (1975) Thermodynamical studies of oxygen equilibrium of hemoglobin. J Biol Chem 250:7093–7098
44. Sugawara Y, Shikama K (1980) Autoxidation of native oxymyoglobin. Eur J Biochem 110:241–246
45. Mansouri A, Winterhalter H (1973) Nonequivalence of chains in hemoglobin oxidation. Biochemistry 12:4946–4949
46. Sugawara Y, Shikama K (1980) Autoxidation of native oxymyoglobin. Eur J Biochem 110:241–246
47. Steinmeier RC, Parkhurst LJ (1975) Kinetic studies on the five principle components of normal adult human hemoglobin. Biochemistry 14:1564–1573
48. Sharma VS, Schmidt MR, Ranney HM (1976) Dissociation of CO from carboxyhemoglobin. J Biol Chem 251:4267–4272
49. Springer BA, Sligar SG, Olson JS, et al (1994) Mechanism of ligand recognition in myoglobin. Chem Rev 94:699–714
50. Matsuura M, Tani F, Naruta Y (2002) Formation and characterization of carbon monoxide adducts of iron "twin coronet" porphyrins: extremely low CO affinity and a strong negative polar effect on bound CO. J Am Chem Soc 124:1941–1950

Chapter 46

Albumin-Heme: A Synthetic Heme-Based Oxygen Carrier

Teruyuki Komatsu, Yubin Huang, Hisashi Yamamoto*†, Hirohisa Horinouchi†, Koichi Kobayashi† and Eishun Tsuchida

Advanced Research Institute for Science and Engineering, Waseda University, Shinjuku-ku, Tokyo, Japan

**Pharmaceutical Research Centre, NIPRO corp., Kusatsu-shi, Shiga, Japan*

†Department of General Thoracic Surgery, School of Medicine, Keio University, Shinjuku-ku, Tokyo, Japan

INTRODUCTION

The risk of transmission of viral illness by transfused blood has become extremely low and the transfusion of donor blood is currently a routine procedure. However, this level of safety has been achieved at great cost, and hepatitis virus or unknown pathogens cannot be completely excluded by the NAT system. Furthermore, the transfusion of donor blood requires cross-matching and compatibility tests to avoid a hemolytic reaction in the recipient, and the purified red blood cells (RBC) need to be stored in the refrigerator at 4°C. These requirements limit the availability of blood in a disaster or emergency. Against this background, several types of hemoglobin (Hb)-based oxygen carriers (HBOCs) have been studied as potential RBC substitutes or O_2 therapeutic reagents (Chang, 1997;Tsuchida, 1998; Winslow, 1999; Squires, 2002; Greenburg and Kim, 2004). Unfortunately, these materials do not fulfill all the requirements of blood replacement compositions. The first concern is the source of human Hb, which is limited by the availability of outdated human blood. Animal blood raises concerns about the transmission of animal pathogens, as Hb products potentially carry risks due to the biological origin of the raw materials. The second problem of the HBOCs (i.e., modified Hb) is the high colloid osmotic pressure (Keipert and Chang, 1988) and its vasoconstriction effect (Schultz *et al.*, 1993; Abassi *et al.*, 1997; Moisan *et al.*, 1998). About 50 per cent of the products in advanced clinical trials still increase blood pressure and decrease cardiac output (Squires, 2002). The precise mechanism of this hypertension is controversial, but many researchers suspect that the Hb molecules penetrate the vascular endothelium and capture the endothelial-derived relaxing factor (EDRF), namely NO. Others believe that the excessive delivery of oxygen to arteriolar vascular walls induces autoregulatory vasoconstriction (Guyton *et al.*, 1964; Tsai *et al.*, 1995; Rohlfs *et al.*, 1998; Winslow, 2000).

RATIONALE FOR ALBUMIN-HEME

In our circulatory system, free hemin (iron(III) complex of protoporphyrin IX dissociated from metHb) is captured by hemopexin, which is a unique protein having an extremely high binding constant of hemin ($K > 10^{12}\,M^{-1}$) (Tolosano and Altruda, 2002). Crystal structure analysis of the hemopexin–hemin complex has revealed that the hemin is tightly bound by double histidine

Blood Substitutes, edited by Robert M. Winslow.
ISBN-13: 978-0-12-759760-7 ISBN-10: 0-12-759760-3

coordinations to the central ferric ion and multiple hydrogen bondings with the amino acid residue (Paoli *et al.*, 1999). Nevertheless, the concentration of hemopexin in the plasma is rather low (<17 μM) and human serum albumin (HSA) may provide a reserve binding capacity of hemin in various conditions, for instance trauma, inflammation, hemolysis etc. In fact, HSA binds hemin with a relatively high affinity ($K > 10^8 M^{-1}$) (Adams and Berman, 1980). If HSA can transport O_2 like Hb, it would be of extreme medical importance not only as a blood replacement composition but also as an O_2 therapeutic reagent.

We have found that a series of super-structured heme derivatives with a covalently linked proximal-base were incorporated into HSA, and the obtained red-colored albumin–heme hybrids (Figure 46.1) can reversibly bind and release O_2 under physiological conditions in the same manner as Hb and myoglobin (Mb) (Komatsu *et al.*, 1999, 2000, 2001a, 2002; Tsuchida *et al.*, 1999; Nakagawa *et al.*, 2004). Since recombinant HSA (rHSA) is manufactured on a large scale by yeast expression, the rHSA–heme hybrid has become entirely synthetic hemoprotein and absolutely free of infectious pathogens. Our recent animal experiments demonstrated that rHSA-heme actually works as an oxygen-carrying plasma protein in the bloodstream (Tsuchida *et al.*, 2000; Komatsu *et al.*, 2004). Although the NO-binding affinity of rHSA-heme is higher than that of Hb (Komatsu *et al.*, 2001b), it does not induce an unfavorable vasopressor effect at all

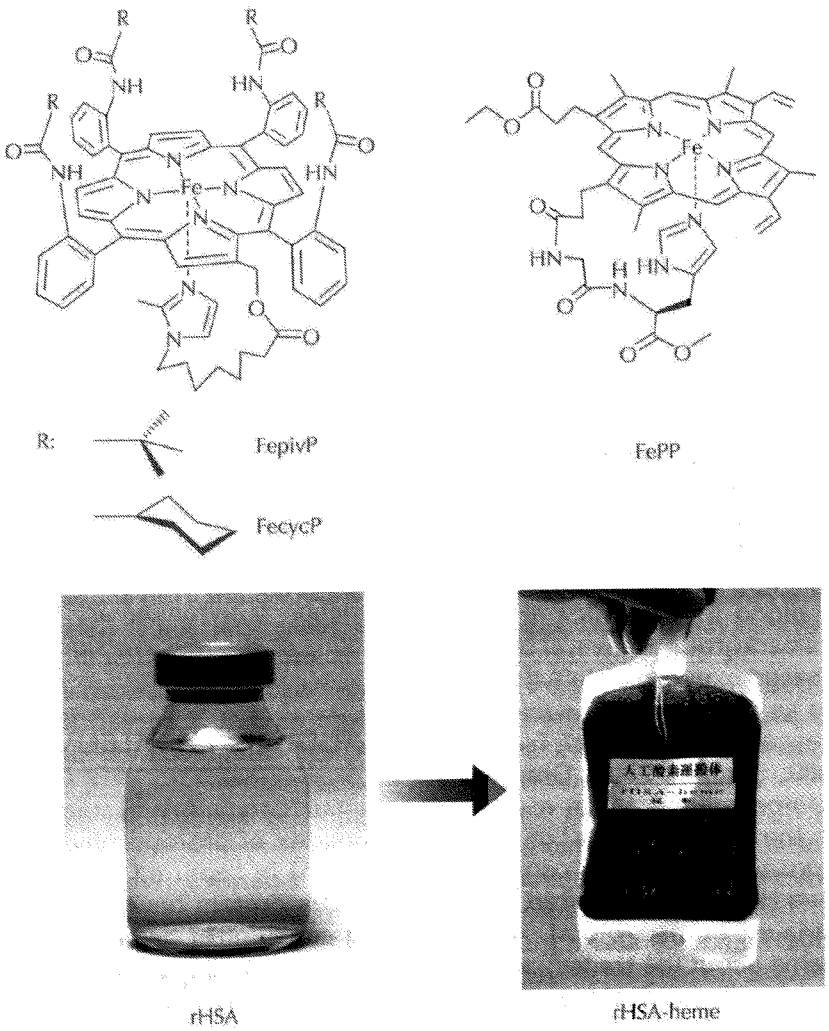

Figure 46.1 Super-structured heme derivatives for the albumin-heme hybrids and the red-colored rHSA-heme solution ([rHSA] = 5 g/dl). See color plate 23.

(Tuschida *et al.*, 2003). We suspect that the electrostatic repulsion between the albumin surface and glomerular basement membrane around the endothelial cell retards the rapid leakage of the rHSA-heme molecule and quick scavenging of NO. The albumin-heme is now recognized to be a promising material for a new class of RBC substitutes. In this chapter, we describe the O_2-transporting efficacy and preclinical safety of this synthetic heme-based O_2-carrier.

OXYGEN BINDING AND PHYSICOCHEMICAL CHARACTERISTICS

From the 30 super-structured heme compounds that were all synthesized by the authors, we found that oxygenated rHSA-FecycP showed a high stability against the autoxidation; its half-time against the ferric form *in vitro* (9 h at 37°C) was close to that of the native Mb (Komatsu *et al.*, 2002). We selected rHSA-FecycP with a similar *P*50 value (34 mmHg at 37°C) to that of RBCs as the most suitable material for an artificial O_2-carrier. The physicochemical characteristics and shelf-life of the rHSA-heme solution ([rHSA], 5 g/dl; heme/rHSA, 4 (mol/mol); isoelectric point, 4.8; COP, 18 mmHg; viscosity, 1.1–1.2 cPs; shelf-life greater than 2 years) had already been reported elsewhere (Komatsu *et al.*, 1999, 2002; Tsuchida *et al.*, 2002).

BLOOD COMPATIBILITY *IN VITRO*

The viscosity of the rHSA-heme solution (1.2 cPs at a high shear rate of 230 s^{-1}) was much lower than that of whole blood (4.0 cPs) and exhibited Newtonian type shear rate dependence just like rHSA itself. After mixing the rHSA-heme solution into whole blood at 10–44 per cent of the volume, the heme concentration in the plasma phase remained constant for 6 hours at 37°C, and no significant time dependence was observed in the numbers of RBCs, white blood cells and platelets (Huang *et al.*, 2003). The microscopic observations clearly showed that the shapes of the RBC had not been deformed during the measurement period. These results suggest that the rHSA-heme has no effect on the morphology of the blood cell components *in vitro*. With respect to the blood coagulation parameters (prothrombin time and activated partial thromboplastin time), the coexistence of rHSA-heme has only a negligibly small influence. Moreover, it was also shown that the rHSA-heme solution has no influence on the complement factors (CH50, SC5b-9) and platelet activation. Although more functional assay is necessary to establish firmly the biocompatibility of rHSA-heme with whole blood, we can conclude that it has a good compatibility with blood cells.

IN VIVO EFFECTS

Blood pressure effects

The administration of extracellular HBOCs often elicits an acute increase in blood pressure by vasoconstriction. At the beginning of this study, our concern was that the small rHSA-heme molecules (8 × 3 nm) injected into the blood vessels would be eliminated from the circulation, and contribute to the significant consumption of NO in the interstitial space between the endothelium and vascular smooth muscle. In fact, rHSA-heme strongly binds NO; the NO-binding affinity ($P50^{NO} = 1.8 \times 10^{-8}$ mmHg) is nine-fold higher than that of the Hb, and is high enough to react with 1 μM NO in the wall of the vasculator (Komatsu *et al.*, 2001b). In order to clarify the hemodynamic behavior after the administration of this entirely synthetic O_2-carrying hemoprotein, we tested a top-load dose of the rHSA-heme solution in anesthetized rats (Tsuchida *et al.*, 2003). Contrary to our expectations, only a negligibly small change in the mean arterial pressure (MAP) was observed after the administration of the rHSA-heme solution (5 g/dl, 300 mg/kg; Figure 46.2a). If anything, the difference from the baseline (ΔMAP) slowly decreased to −6.8 ± 3.4 mmHg within 20 minutes and remained constant during the monitoring period. The response was completely the same as that observed following infusion with an equivalent volume of rHSA (5 g/dl) in this experimental set-up. In contrast, the administration of extracellular Hb solution elicited an acute increase in blood pressure (ΔMAP 16 ± 1.9 mmHg), which followed a graduated decrease throughout the 60-minute period of observation (Tsuchida *et al.*, 2003). Why does rHSA-heme not induce the hypertension? The answer probably lies in the negatively charged molecular surface of the albumin vehicle. One of the unique characteristics of serum albumin is its low permeability through the muscle capillary

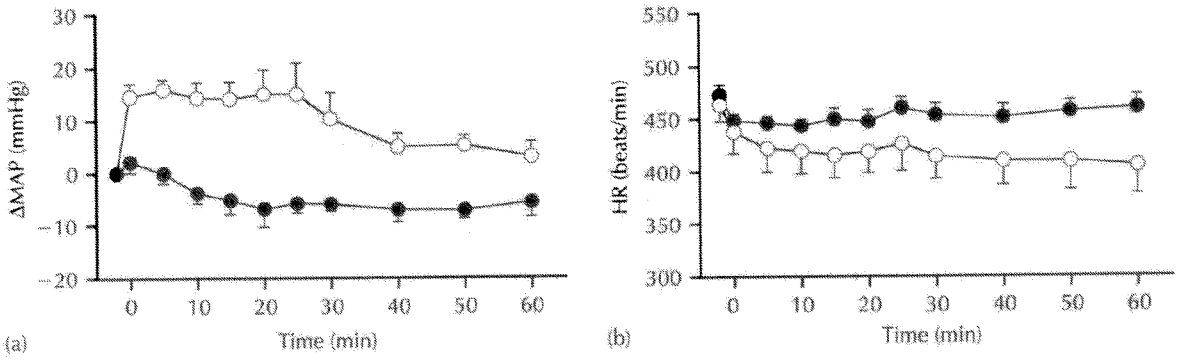

Figure 46.2 Changes of (a) MAP and (b) HR in anesthetized rats before and after infusion of rHSA-heme solution (n = 5) (●, rHSA-heme group; ○, Hb group). MAP is represented as change from the basal value (ΔMAP) just before the infusion with mean ± SEM (n = 5) (basal value is 90.1 ± 3.0 mmHg). HR was shown as mean ± SEM (n = 5) (Tsuchida, 2003).

pore, which is less than 1/100 that for Hb due to the electrostatic repulsion between the albumin surface and the glomerular basement membrane around the endothelial cells. In the blood vessels, rHSA-heme presumably circulates for a longer time compared to Hb without extravasation. The heart rate (HR) responses after the rHSA-heme injection were also negligibly small (Figure 46.2b). Visualization of the intestinal microcirculatory changes clearly showed that the widths of the venule and arteriole are fairly constant (Tsuchida *et al.*, 2003).

Hemodilution

The physiological responses to a 30 per cent exchange transfusion with rHSA-heme solution after 70 per cent hemodilution with 5 g/dl rHSA were investigated using anesthetized rats (Komatsu *et al.*, 2004). First, the isovolemic 70 per cent hemodilution was carried out using 5-g/dl rHSA solution. The blood withdrawal via the common carotid artery (2 ml) and the rHSA infusion from the femoral vein (2 ml) (each 1 ml/min) were repeated for nine cycles until Hct was reduced to 13.6 per cent (32 per cent of the initial Hct value of 42.6 per cent). After 10 minutes, a 30 per cent volume of the circulatory blood was withdrawn, producing a severe hemorrhagic shock state. The same volume of the samples was then intravenously injected. As negative or positive control groups, the rats were infused with the 5-g/dl rHSA solution (rHSA group) or the shed rat blood ([heme] = 5.3 mM, whole blood group). The circulation parameters, blood parameters, renal cortical PO_2 (PtO_2(R)) and muscle tissue PO_2 (PtO_2(M)) were carefully monitored for 60 minutes after the injection.

Following administration of the 5-g/dl rHSA solution, the MAP, HR, respiration rate, PtO_2(R), PtO_2(M), arterial blood O_2 pressure (PaO_2), venous blood O_2 pressure (PvO_2), and arterial blood CO_2-pressure ($PaCO_2$) did not recover, leading to death within 32 minutes (Figure 46.3). By contrast, the infusion of whole blood improved these values, except for PtO_2(M), to their initial levels. In the rHSA-heme group, the animals survived over 60 minutes after the infusion, and the HR, respiration rate, PtO_2(R) and PvO_2 showed similar recoveries to those as observed in the whole blood group (Komatsu *et al.*, 2004). MAP, PtO_2(M), PaO_2, pH and PCO_2 also significantly recovered. We are certain that the albumin-heme solution has the potential to resuscitate hemorrhagic shock, stabilize the blood circulation, and transport oxygen throughout the body.

PRECLINICAL SAFETY

In order to evaluate the preclinical safety of this synthetic O_2 carrier, we performed a 20 per cent exchange transfusion with rHSA-heme into anesthetized rats and measured the time courses of the circulation parameters (MAP, HR, respiration rate) and blood parameters (PaO_2, PvO_2, pH, blood cell numbers) for 6 hours, which is adequate time to identify acute toxicity (Huang *et al.*, 2004a). After stabilization of the animals' condition, the

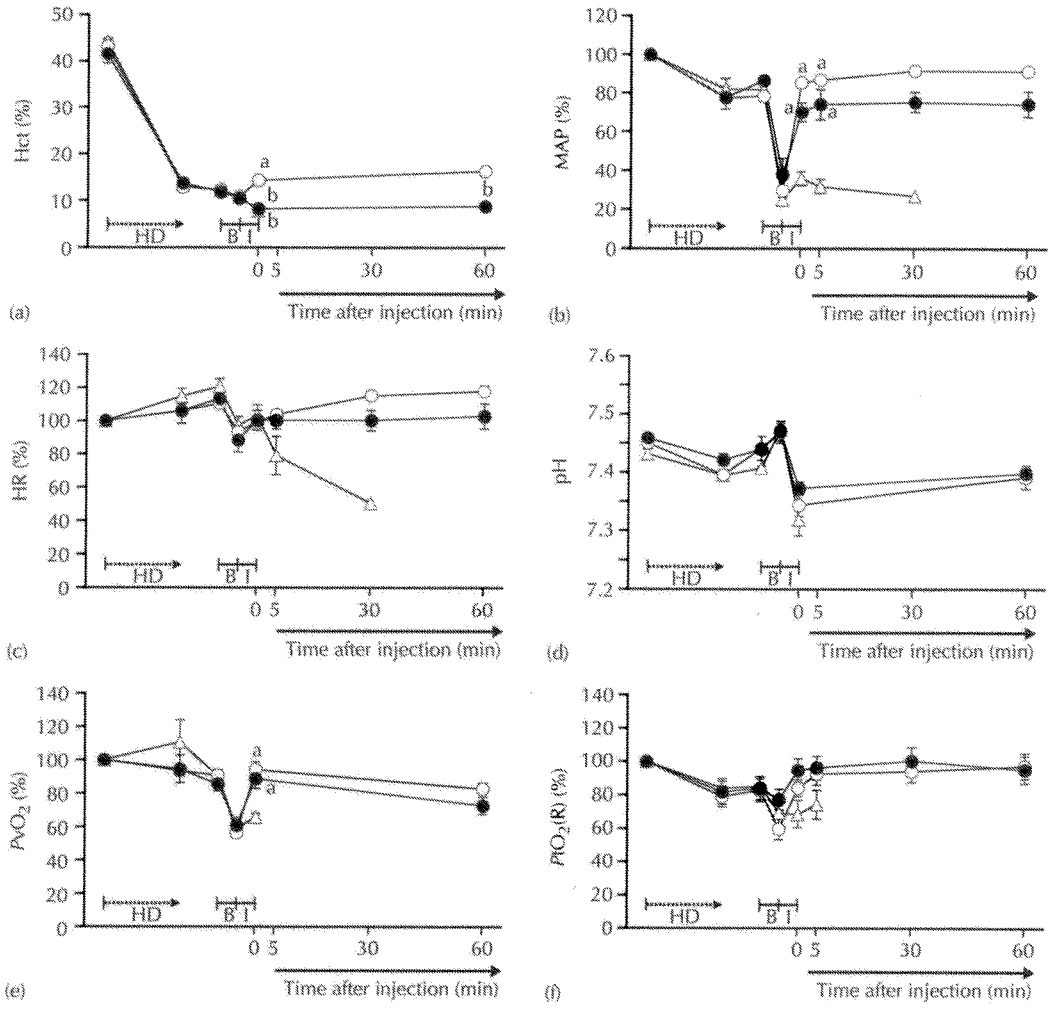

Figure 46.3 Time courses of (a) Hct, (b) MAP, (c) HR, (d) pH, (e) PvO_2 and (f) PtO_2(R) in anesthetized rats after 70 per cent hemodilution with rHSA and 30 per cent exchange transfusion with rHSA-heme solution (n = 6) (●, rHSA-heme group; ○, whole blood group; △, rHSA group). MAP, HR, PvO_2 and PtO_2(R) are represented as percentage ratios of the basal values with mean ± SEM. Hct, HR and pH were shown as mean ± SEM. HD, hemodilution; B, bleeding; I, sample injection. $^aP < 0.05$ versus rHSA group. $^bP < 0.05$ versus whole blood group (Komatsu, 2004).

20 per cent exchange transfusion was performed by 1 ml blood withdrawal via the common carotid artery and 1 ml rHSA-heme infusion from the femoral vein (each 1 ml/min) with four repeating cycles.

The appearance of all the animals showed absolutely no change for 6 hours after the exchange transfusion. The physiological responses of the blood circulation, gas equilibria and blood cell numbers in the rHSA-heme group were almost the same as those of the control group (surgery treatments without infusion) and rHSA groups (Figure 46.4; Huang *et al.*, 2004a). MAP and HR did remain constant after the injection of the rHSA-heme, suggesting again that the albumin-based O_2 carrier does not induce the vasoconstriction. It is also noteworthy that autoxidation of the ferrous rHSA-heme to the ferric state was retarded in the bloodstream; the half-time of the oxygenated rHSA-heme *in vivo* was approximately four-fold longer than that *in vitro* (Tsuchida *et al.*, 2000). It was found that autoxidated rHSA-hemin was certainly reduced in the whole blood suspension. A physiological concentration of ascorbic acid continuously provided by RBC probably re-reduces the ferric hemin, leading to the apparent long lifetime of the oxygenated species.

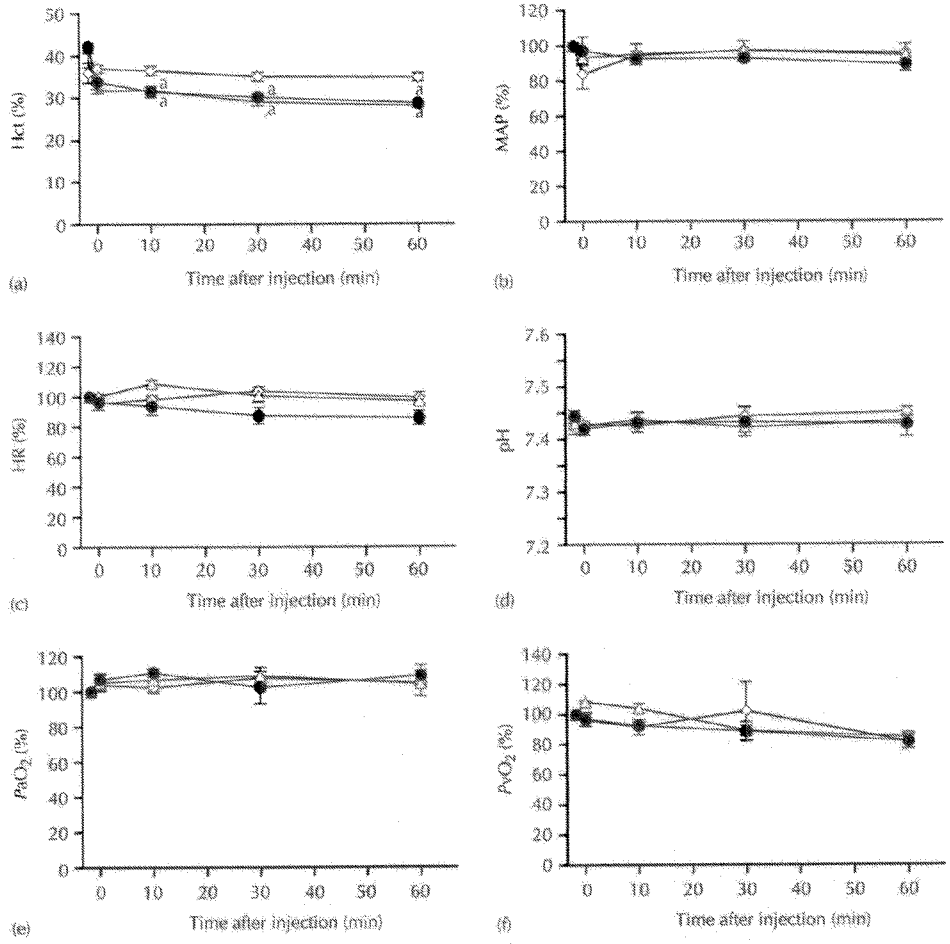

Figure 46.4 Time courses of (a) Hct, (b) MAP, (c) HR, (d) pH, (e) PaO_2 and (f) PvO_2 in anesthetized rats after 20 per cent exchange transfusion with rHSA-heme or rHSA solution (n = 6) (◇, control group (only surgery treatments without infusion); △, rHSA group; ■, rHSA-heme group). MAP, HR, PaO_2 and PvO_2 are represented as percentage ratios of the basal values with mean ± SEM. Hct, HR and pH are shown as mean ± SEM. (Huang, 2004a).

Furthermore, 20 per cent exchange transfusions with rHSA-heme into anesthetized rats were followed by blood biochemical tests of the withdrawn plasma and histopathology observations of the vital organs for 7 days (Huang *et al.*, 2004b).

In the albumin-heme group, a total of 30 analytes showed almost the same values, by blood biochemical tests, as those observed in the reference rHSA group, implying that there was no significant toxicity caused by the exchange transfusion with rHSA-heme (Huang *et al.*, 2004b). Histopathology observations implied that the administration of rHSA-heme did not produce any negative side effects on the vital organs. All these results showed the preclinical safety of the rHSA-heme solution.

FUTURE RESEARCH

As described in this chapter, results have shown O_2-transporting efficacy and initial clinical safety of the rHSA-heme solution that allow us to undergo further advanced preclinical testing of this synthetic O_2 carrying plasma protein. Exchange transfusion with rHSA-heme into beagles is now under investigation.

Furthermore, rHSA-heme as a monomolecular O_2 carrier was tested for its ability to increase O_2 tension in the hypoxia of the solid tumor rat model. By the direct administration of the rHSA-heme solution (10 ml/kg) into the ascites hepatoma LY80 tumor on the femur, the O_2 tension of the hypoxic region immediately increased

to 3.45 ± 1.43 mmHg, which corresponds to a 2.4-fold increase compared to that of the baseline value (Kobayashi *et al.*, 2003). These high O_2 levels continued for 300 s after the infusion. While more research is required to consider how rHSA-heme behaves in the tumor blood vessel and is related to the increase in the O_2 partial pressure, the present results obviously indicate that rHSA-heme led to increased O_2 release in the hypoxic region in the solid tumor. Experiments regarding combined treatment with the rHSA-heme administration and radiation therapy are currently underway.

ACKNOWLEDGMENTS

This work was partially supported by Grant-in-Aid for Scientific Research (No. 16350093) from JSPS, Grant-in-Aid for Exploratory Research (No. 16655049) from MEXT Japan, and Health Science Research Grants (Regulatory Science) from MHLW Japan. The authors are grateful to NIPRO Corp. for their support of the oxygen-infusion project.

EDITOR'S SUMMARY

Albumin-heme is a unique product – an oxygen transporter that is totally synthetic. By this approach, human serum albumin is produced in a recombinant yeast system, and then synthetic heme is coordinated to its surface. Up to 8 heme groups per molecule have been incorporated so far.

Albumin-heme has been prepared to have a *P*50 similar to that of red blood cells, but the oxygen binding is not cooperative. It avidly binds NO, but is not hypertensive in preliminary animal tests. It appears to be as stable with regard to oxidation as native human hemoglobin. A number of early preclinical tests have been performed, including biocompatibility and effects on coagulation, and no significant toxic effects have been noted.

While it is still early in the development of albumin-heme as a therapeutic agent for use in humans, and the cost of production is likely to be high, it is an intriguing product that could find use in specialized applications such as oxygenating tumors to increase the effects of radio- or chemotherapy.

REFERENCES

Abassi, Z., Kotob, S., Pieruzzi, F. *et al.* (1997). Effects of polymerization on the hypertensive action of diaspirin cross-linked hemoglobin in rats. *J. Lab. Clin. Med.*, **129**, 603–610.

Adams, P. A. and Berman, M. C. (1980). Kinetics and mechanism of the interaction between human serum albumin and monomeric heamin. *Biochem. J.*, **191**, 95–102.

Chang, T. M. S. (1997). Recent and future developments in modified hemoglobin and microencapsulated hemoglobin as red blood cell substitutes. *Artif. Cells Blood Subst. Immob. Biotech.*, **25**, 1–24.

Greenburg, A. G. and Kim, H. M. (2004). Hemoglobin-based oxygen carriers. *Crit. Care Med.*, **8**, S61–64.

Guyton, A. C., Ross, J. M., Carrier, O. and Walker, J. R. (1964). Evidence for tissue oxygen demand as the major factor causing autoregulation. *Circ. Res.*, **14**, 1–60.

Huang, Y., Komatsu, T., Nakagawa, A. *et al.* (2003). Compatibility *in vitro* of albumin-heme (O_2 carrier) with blood cell components. *J. Biomed. Mater. Res.*, **66A**, 292–297.

Huang, Y., Komatsu, T., Yamamoto, H. *et al.* (2004a). Exchange transfusion with entirely synthetic red-cell substitute albumin-heme into rats: physiological responses and blood biochemical tests. *J. Biomed. Mater. Res.*, **71A**, 63–69.

Huang, Y., Komatsu, T., Yamamoto, H. *et al.* (2004b). Safety evaluation of artificial O_2-carrier as red cell substitute 'albumin-heme' by blood biochemical tests and histopathology observations. *Am. Soc. Artif. Int. Organs J.*, **50**, 525–529.

Keipert, P. and Chang, T. (1988). Pyridoxylated-polyhemoglobin solution: a low viscosity oxygen-delivery blood replacement fluid with normal oncotic pressure and long term storage feasibility. *J. Biomat. Artif. Cells Artif. Organs*, **16**, 185–196.

Kobayashi, K., Komatsu, T., Iwamaru, A. *et al.* (2003). Oxygenation of hypoxia region in solid tumor by administration of human serum albumin incorporating synthetic hemes. *J. Biomed. Mater. Res.*, **64A**, 48–51.

Komatsu, T., Hamamatsu, K., Wu, J. and Tsuchida, E. (1999). Physicochemical properties and O_2-coordination structure of human serum albumin incorporating tetrakis(*o*-pivamido)phenylporphyrinatoiron (II) derivatives. ***Bioconjug. Chem.*, 10,** 82–86.

Komatsu, T., Matsukawa, Y. and Tsuchida, E. (2000). Kinetics of CO- and O_2-binding to human serum albumin-heme hybrid. *Bioconjug. Chem.*, **11,** 772–776.

Komatsu, T., Okada, T., Moritake, M. and Tsuchida, E. (2001a). O_2-Binding properties of double-sided porphyrinatoiron(II)s with polar substituents and their human serum albumin hybrids. *Bull. Chem. Soc. Jpn.*, **74,** 1695–1702.

Komatsu, T., Matsukawa, Y. and Tsuchida, E. (2001b). Reaction of nitric oxide with synthetic hemoprotein, human serum albumin incorporating tetraphenylporphinatoiron(II) derivatives. *Bioconjug. Chem.*, **12,** 71–75.

Komatsu, T., Matsukawa, Y. and Tsuchida, E. (2002). Effect of heme structure on O_2-binding properties of human serum albumin-heme hybrids: intramolecular histidine coordination provides a stable O_2-adduct complex. *Bioconjug. Chem.*, **13,** 397–402.

Komatsu, T., Yamamoto, H., Huang, Y. *et al.* (2004). Exchange transfusion with synthetic oxygen-carrying plasma protein 'albumin-heme' into acute anemia rat model after 70% hemodilution. *J. Biomed. Mater. Res.*, **71A,** 644–651.

Moisan, S., Drapeau, G., Burhop, K. E. and Rioux, F. (1998). Mechanism of the acute pressor effect and bradycardia elicited by disapirin crosslinked hemoglobin in anesthetized rats. *Can. J. Physiol. Pharmacol.*, **76,** 434–442.

Nakagawa, A., Ohmichi, N., Komatsu, T. and Tsuchida, E. (2004). Synthesis of protoheme derivatives with a covalently linked proximal-base and their human serum albumin hybrids as artificial hemoprotein. *Org. Biomol. Chem.*, **2,** 3108–3312.

Paoli, M., Anderson, B. F. and Baler, H. M. *et al.* (1999). Crystal structure of hemopexin reveals a novel high-affinity heme site formed between two β-propeller domains. *Nat. Struct. Biol.*, **6,** 926–931.

Rohlfs, R. J., Bruner, E., Chiu, A. *et al.* (1998). Arterial blood pressure responses to cell-free hemoglobin solutions and the reaction with nitric oxide. *J. Biol. Chem.*, **273,** 12128–12134.

Schultz, S. C., Grady, B., Cole, F. *et al.* (1993). A role for endothelin and nitric oxide in the pressor response to diaspirin cross-linked hemoglobin. *J. Lab. Clin. Med.*, **122,** 301–308.

Squires, J. E. (2002). Artificial blood. *Science,* **295,** 1002–1005.

Tolosano, E. and Altruda, F. (2002). Hemopexin: structure, function, and regulation DNA. *Cell Biol.*, **21,** 297–306.

Tsai, A. G., Kerger, H. and Intaglietta, M. (1995). Microcirculatory consequences of blood substitution with $\alpha\alpha$-hemoglobin. In: R. M. Winslow, K. D. Vandegriff and M. Intaglietta (eds), *Blood Substitutes: Physiological Basis of Efficiency,* pp. 155–174. Birkhäuser, Boston.

Tsuchida, E. (1998). Perspectives of blood substitutes. In: E. Tsuchida (ed.), *Blood Substitutes: Present and Future Perspectives,* pp. 1–14. Elsevier Science, Lausanne.

Tsuchida, E., Komatsu, T., Matsukawa, Y. *et al.* (1999). Human serum albumin incorporating tetrakis (*o*-pivalamido)phenylporphinatoiron(II) derivative as a totally synthetic O_2-carrying hemoprotein. *Bioconjug. Chem.*, **10,** 797–802.

Tsuchida, E., Komatsu, T., Hamamatsu, K. *et al.* (2000). Exchange transfusion of albumin-heme as an artificial O_2-infusion into anesthetized rats: physiological responses, O_2-delivery and reduction of the oxidized hemin sites by red blood cells. *Bioconjug. Chem.*, **11,** 46–50.

Tsuchida, E., Komatsu, T., Yanagimoto, T. and Sakai, H. (2002). Preservation stability and *in vivo* administration of albumin-heme hybrid solution as an entirely synthetic O_2-carrier. *Polymer Adv. Technol.*, **13,** 845–850.

Tsuchida, E., Komatsu, T., Matsukawa, Y. *et al.* (2003). Human serum albumin incorporating synthetic heme: red blood cell substitute without hypertension by nitric oxide scavenging. *J. Biomed. Mater. Res.*, **64A,** 257–261.

Winslow, R. M. (1999). New transfusion strategies: red cell substitutes. *Annu. Rev. Med.*, **50,** 337–353.

Winslow, R. M. (2000). $\alpha\alpha$-crosslinked hemoglobin: was failure predicted by preclinical testing? *Vox Sang.*, **79,** 1–20.

Human plasma protein modified to bind oxygen reversibly

Albumin engineered for artificial blood

A modified version of human serum albumin (HSA) that binds oxygen has been created by British and Japanese researchers. The work marks a first step towards a new form of artificial blood.

HSA is the most abundant plasma protein in human blood. It naturally binds with haem, an iron-containing porphyrin group that is a central component of haemoglobin, to produce a complex that can be oxidised. Chemists and structural biologists from Waseda University, Tokyo, and Imperial College London have developed a version of this HSA–haem complex that can reversibly bind oxygen, rather than react with it.

After studying the crystal structure of the complex, the researchers experimented with different versions produced by introducing modified plasmids into the yeast *Pichia pastoris*. Replacing a specific tyrosine residue in the HSA–haem complex with a hydrophobic amino acid such as leucine or phenylalanine and introducing histidine as a proximal base led to effective oxygen binding. This modified complex could reversibly bind oxygen with an affinity only one order of magnitude less than that of haemoglobin.

Artificial blood based on HSA-haem will not induce high blood pressure

ISTOCKPHOTOS

Previous candidates for artificial blood are based on haemoglobin and liable to induce high blood pressure. This would not happen with an artificial blood based on the HSA–haem complex, say the researchers, because of an electrostatic repulsion between HSA and blood vessel walls.

Much work remains, admits Stephen Curry, reader in structural biology at Imperial. 'The lifetime of oxygen binding at the HSA–haem complex is still too short for practical use,' he told *Chemistry World*. 'At present we are trying to engineer additional mutations in the protein in order to enhance the oxygen binding properties still further.'

Jon Evans

Reference

T Komatsu *et al*, *J. Am. Chem. Soc.*, 2005, **127**, 15933

Chemistry World, December **2005**, p. 18 (Royal Society of Chemistry)

Close window

Imperial College London

where science is leading

text size T T T T

Show more news

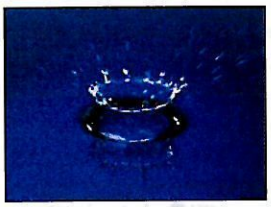

GENETICALLY ENGINEERED BLOOD PROTEIN CAN BE USED TO PRODUCE HYDROGEN GAS FROM WATER

Scientists combine two molecules that occur naturally in blood to engineer molecular complex that uses solar energy to produce hydrogen gas from water - *News Release*

Date 01 Dec 2006
Category All
Contact Laura Gallagher

Imperial College London News Release

For immediate release
Friday 1 December 2006

Scientists have combined two molecules that occur naturally in blood to engineer a molecular complex that uses solar energy to produce hydrogen gas from water, says research published today in the Journal of the American Chemical Society.

This molecular complex can use energy from the sun to create hydrogen gas, providing an alternative to electrolysis, the method typically used to split water into its constituent parts. The breakthrough may pave the way for the development of novel ways of creating hydrogen gas for use as fuel in the future.

Proteins occurring in the blood have been used to make a molecule that splits water in oxygen and hydrogen

Professors Tsuchida and Komatsu from Waseda University, Japan, in collaboration with Imperial College London, synthesised a large molecular complex from albumin, a protein molecule that is found at high levels in blood serum, and porphyrin, a molecule which is used to carry oxygen around the body and gives blood its deep red colour. Porphyrin molecules are normally found combined with metals, and in their natural state in the blood they have an iron atom at their centre. The scientists modified the porphyrin molecule to swap the iron for a zinc atom in the middle, which completely changed the chemistry and characteristics of the molecule.

This modified porphyrin molecule was then combined with albumin; with the albumin molecule itself being modified by genetic engineering to enhance the efficiency of the process. The resulting molecular complex was proven to be sensitive to light, and can capture light energy in a way that allows hydrogen gas to be produced from water molecules.

Dr Stephen Curry, a structural biologist from Imperial College London's Division of Cell and Molecular Biology who participated in the research explains: "This work has shown that it is possible to manipulate molecules and proteins that occur naturally in the human body by changing one small detail of their make-up, such as the type of metal at the heart of a porphyrin molecule, as we did in this study.

"It's very exciting to prove that we can use these biological structures as a conduit to harness solar energy to produce hydrogen gas from water. In the long term, these synthetic molecules may provide a more environmentally friendly way of producing hydrogen gas, which can be used as a 'green' fuel."

For further information please contact:

Laura Gallagher
Imperial College London Press Office
Tel: +44 (0)20 759 46702
Mob: +44 (0)7803 886248
Email: l.gallagher@imperial.ac.uk

Notes to Editors:

1. "Photosensitised reduction of water to hydrogen using human serum albumin complexed with zinc protoporphyrin IX", Journal of the American Chemical Society

Teruyuki Komatsu (1, 2), Rong-Min Wang (1, 3), Patricia A Zunszain (4), Stephen Curry (4), Eishun Tsuchida (1).

(1) Advanced Research Institute for Science and Engineering, Waseda University, 3-4-1 Okubo, Shinjuku-ku, Tokyo 169-8555, Japan
(2) Japan Science and Technology Agency, 4-1-8 Honcho, Kawaguchi-shi, Saitama 332-0012, Japan
(3) Gansu Key Laboratory of Polymer Materials, Northwest Normal University, Lanzhou 730070, China
(4) Biophysics Section, Division of Cell and Molecular Biology, Faculty of Natural Sciences, Imperial College London, South Kensington Campus, London SW7 2AZ, UK

Published online at http://pubs.acs.org/journals/jacsat/

2. Consistently rated in the top three UK university institutions, Imperial College London is a world leading science-based university whose reputation for excellence in teaching and research attracts students (11,500) and staff (6,000) of the highest international quality. Innovative research at the College explores the interface between science, medicine, engineering and management and delivers practical solutions that enhance the quality of life and the environment - underpinned by a dynamic enterprise culture. Website: www.imperial.ac.uk

spektrumdirekt
Die Wissenschaftszeitung im Internet
19. Dezember 2006

ENERGIEGEWINNUNG

Grüner Treibstoff - blutrot

Proteine aus unseren Adern produzieren den Energieträger Wasserstoff

Kein Labor der Welt kann nachahmen, was jede Balkonpflanze nebenbei erledigt: Energie aus Sonnenlicht in Energievorrat für den Eigenbedarf umwandeln. Nun soll bald eine rote Alternative den Prozess rund um das grüne Chlorophyll simulieren - und Lichtfang mit der Hilfe von Blut eine hoffnungsvolle Route zur sauberen Energie werden.

Blut ist auch für das Forscherteam um Stephen Curry vom Imperial College London, Eishun Tsuchida von der Waseda-Universität in Tokio und seinen Kollegen Teruyuki Komatsu ein ganz besonderer Saft - allerdings aus nicht ganz alltäglichen Gründen. Eigentlich stand nur Grundlagenforschung über die Chemie seiner Inhaltsstoffe an. Doch Komatsu verfiel der verführerischen Idee, daraus lichthungrige Energiequelle zu bauen. Eine transsilvanisch anmutende Zukunftsvision, mehr nicht? Eine realistische Perspektive, meinen die Wissenschaftler aus Großbritannien, Japan und China: Sie bastelten mit den Proteinen Albumin und Porphyrin einen Molekülkomplex, der Lichtenergie einfängt und damit dem Wasser seinen Wasserstoff abzwackt.

Die beiden Proteine zirkulieren in großen Mengen durch unsere Adern und übernehmen dabei wichtige Aufgaben. Albumin gleicht einem molekularen Schwamm: Es regelt den Wasserhaushalt in den Blutgefäßen und schleust wasserunlösliche Stoffe durch unseren Kreislauf. Porphyrin dagegen kutschiert gewöhnlich den Sauerstoff durch unsere Gefäße.

Komatsu kam nun auf die Idee, das Sauerstoff transportierende Porphyrin in ihrem Sinne umzumodeln. Dazu ersetzten die Forscher zuerst das typische Eisen-Atom im Herzen des Moleküls - es verleiht ihm die schnittige rote Farbe - durch ein Zink-Atom und stellten damit seinen chemischen Charakter auf den Kopf. Damit nicht genug, schnallten sie zur Krönung dem umgebauten Transporter noch das chemisch leicht modifizierte Albumin auf.

Ihr so radikal getuntes Sauerstoff-Taxi zeigt die von Komatsu vorhergesagten Talente: Aktiviert durch Licht reduziert der Molekülkomplex in Windeseile ein H aus dem H_2O zu elementarem Wasserstoff, der aus dem Gemisch entweicht. Zurück bleiben Hydroxid-Ionen. Dabei arbeitet das Team von Albumin und Porphyrin als Rädelsführer einer Bande von Reaktionspartnern: Es bezieht aus dem Licht seine Energie, um einem benachbarten Statisten, dem "TEOA" (Triethanolamin), ein Elektron zu entreißen. Das gibt es sofort weiter an einen Mittelsmann, "MV2+" (Methyl-Viologen), der damit schließlich Wasserstoff aus dem Wasser erlöst: Über dem Gemisch entsteht - genug Licht vorausgesetzt – eine stetig wachsende H_2-Blase. Die rote Energiealternative ersetzt damit zugleich die Solarzelle und den Elektrolyseapparat, der im herkömmlichen Verfahren via Elektrizität das "Knallgas"-Gemisch aus Wasserstoff und Sauerstoff, Nahrung für die Brennstoffzelle, herstellt.

Die Idee zu ähnlichen Verfahren ist nicht neu. Allerdings kamen als Reagenzien bislang nur schwer zu produzierende Riesenmoleküle zum Einsatz - und die waren auch noch nach Minuten unbrauchbar und damit zur Energiegewinnung ungeeignet. Die Allianz der beiden Blutmoleküle Albumin und Porphyrin dagegen produzierte im Labor für Stunden emsig den begehrten Wasserstoff - und bringt damit eine neue Perspektive für die Forschung an erneuerbaren Energien. Allerdings muss das Gemisch regelmäßig mit neuem TEOA aufgefrischt werden. Außerdem zerstört das Licht nach einiger Zeit das Porphyrin.

Für Stephen Curry zeigt der lichthungrige Blutbestandteil aber mustergültig das große Potenzial, das Naturstoffe mittels kleiner Manipulationen frei setzen können: "Es ist sehr spannend, dass wir biologische Strukturen nutzen können, um Sonnenenergie einzufangen und damit Wasserstoff herzustellen." Bleibt noch die Frage, ob zur Energiedeckung per Bluteiweiß ein steter menschlicher Aderlass nötig wird. Zur Beruhigung: Schon heute können die benötigten Moleküle Albumin und Porphyrin auch ohne Menschenblut besorgt werden. Für die Albumingewinnung pflanzt man, ähnlich wie bei der Herstellung von Blutgerinnungspräparaten, Mikroorganismen die Gensequenzen zu seiner Produktion ein. Das Porphyrin wird dagegen wirklich aus Blut extrahiert - allerdings aus dem von Rindern.

Sicherlich, so Curry, müsse die Produktion der Proteine billiger und die Lebensdauer des Porphyrins länger werden. "Langfristig können diese synthetischen Moleküle jedoch den Weg zu einer umweltfreundlicheren Produktion von Wasserstoff ebnen, der den grünen Treibstoff liefert." Dann hieße es allerdings Rinderblut für Öl - was manchen Freunden erneuerbarer Energien nicht unbedingt schmecken dürfte.

Christoph Ulhaas

QUELLEN:
Journal of the American Chemical Society 128: 16297-16301 (2006), Abstract

Link:
http://www.wissenschaft-online.de/sixcms/detail.php?id=860332

日経バイオテク Biotechnology Japan

2007年06月15日

日本血液代替物学会、早大、血液由来のヘモグロビンを使わない次世代人工酸素運搬体を提案

2007年6月14日、慶応大学で日本血液代替物学会年次大会が開催され、人工血液研究の最前線と題するシンポジウムの中で、早稲田大学理工学術院の小松晃之准教授は、アルブミンにヘムを結合させたアルブミン-ヘムについて報告した。

ヘムは2価の鉄を中心に持つポルフィリン化合物。ヘモグロビンは4つのヘムを持つ分子量6万4000のたんぱく質だ。現在、オキシジェニックス（東京・港、大村孝男社長）やテルモが人工酸素運搬体を開発しているが（関連記事1、関連記事2）、これらは日本赤十字社から提供された期限切れの赤血球製剤から精製したヘモグロビンをリポソームに封入して作ったもの。血液型に関係なく利用でき、長期間保存できるなどの利点があるが、ヘモグロビンの安定性の問題や、赤血球製剤からヘモグロビンを精製する過程で病原体が混入する可能性がゼロにはならない、などの課題がある。

一方、アルブミンについては、三菱ウェルファーマや化学及血清療法研究所が遺伝子組み換え技術で製造されたものを医薬品として開発しており、血液由来ではないものがもうすぐ実用化されようとしている。

小松准教授らはアルブミンが脂肪酸と結合することに着目し、アルブミンと結合するヘムを30種類程度化学合成した。ヘムによって酸素親和性が高いものから低いものまでさまざまあり、「用途に応じて使い分けられる」と小松准教授は説明した。ヘムを解離しにくいようにアルブミン-ヘムの表面をPEGで修飾したものを作成し、貧血状態にしたラットに投与した結果、赤血球を投与したのと同様の効果が得られた。これらのことから、血液由来の成分を全く使わない完全合成のアルブミン-ヘムを次世代の人工酸素運搬体として利用できる可能性を示した。さらに小松准教授は、アルブミンのアミノ酸を遺伝子組換えにより3つだけ改変すれば、天然のヘムでも結合し酸素を運搬できるようになることを明らかにした。

小松准教授は、「アルブミン-ヘムは、たんぱく質製剤として利用されているアルブミンを酸素の運搬に使おうというもので、ヘモグロビンを封入したリポソームとはコンセプトが違う。また、リポソームの直径は200nmから250nmだが、アルブミンは8nm程度なので、脳梗塞などの虚血部位への酸素供給など、用途も広がる」と語った。ちなみに、小松准教授はアルブミン-ヘムの適応として、出血ショックの蘇生液、救急車内での酸素供給液、虚血部位への酸素供給液のほか、移植用臓器の灌流液、体外循環回路の補填液などを挙げている。また、天然のヘムを利用しても、「ヘモグロビンを利用する場合と違って感染因子が入り込む可能性はほとんどない」（小松准教授）とのことだ。（橋本宗明）